MASSACHUSETTS INSTITUTE OF TECHNOLOGY

RADIATION LABORATORY SERIES

LOUIS N. RIDENOUR, *Editor-in-Chief*

MICROWAVE DUPLEXERS

MASSACHUSETTS INSTITUTE OF TECHNOLOGY

RADIATION LABORATORY SERIES

---

1. RADAR SYSTEM ENGINEERING—*Ridenour*
2. RADAR AIDS TO NAVIGATION—*Hall*
3. RADAR BEACONS—*Roberts*
4. LORAN—*Pierce, McKenzie, and Woodward*
5. PULSE GENERATORS—*Glasoe and Lebacqz*
6. MICROWAVE MAGNETRONS—*Collins*
7. KLYSTRONS AND MICROWAVE TRIODES—*Hamilton, Knipp, and Kuper*
8. PRINCIPLES OF MICROWAVE CIRCUITS—*Montgomery, Dicke, and Purcell*
9. MICROWAVE TRANSMISSION CIRCUITS—*Ragan*
10. WAVEGUIDE HANDBOOK—*Marcuvitz*
11. TECHNIQUE OF MICROWAVE MEASUREMENTS—*Montgomery*
12. MICROWAVE ANTENNA THEORY AND DESIGN—*Silver*
13. PROPAGATION OF SHORT RADIO WAVES—*Kerr*
14. MICROWAVE DUPLEXERS—*Smullin and Montgomery*
15. CRYSTAL RECTIFIERS—*Torrey and Whitmer*
16. MICROWAVE MIXERS—*Pound*
17. COMPONENTS HANDBOOK—*Blackburn*
18. VACUUM TUBE AMPLIFIERS—*Valley and Wallman*
19. WAVEFORMS—*Chance, Hughes, MacNichol, Sayre, and Williams*
20. ELECTRONIC TIME MEASUREMENTS—*Chance, Hulsizer, MacNichol, and Williams*
21. ELECTRONIC INSTRUMENTS—*Greenwood, MacRae, Reed, and Holdam*
22. CATHODE RAY TUBE DISPLAYS—*Soller, Starr, and Valley*
23. MICROWAVE RECEIVERS—*Van Voorhis*
24. THRESHOLD SIGNALS—*Lawson and Uhlenbeck*
25. THEORY OF SERVOMECHANISMS—*James, Nichols, and Phillips*
26. RADAR SCANNERS AND RADOMES—*Cady, Karelitz, and Turner*
27. COMPUTING MECHANISMS AND LINKAGES—*Svoboda*
28. INDEX—*Linford*

MICROWAVE DUPLEXERS

Edited by

LOUIS D. SMULLIN

RESEARCH LABORATORY OF ELECTRONICS
MASSACHUSETTS INSTITUTE OF TECHNOLOGY

CAROL G. MONTGOMERY

ASSOCIATE PROFESSOR OF PHYSICS
YALE UNIVERSITY

OFFICE OF SCIENTIFIC RESEARCH AND DEVELOPMENT
NATIONAL DEFENSE RESEARCH COMMITTEE

FIRST EDITION
SECOND IMPRESSION

NEW YORK · TORONTO · LONDON
McGRAW-HILL BOOK COMPANY, INC.
1948

MICROWAVE DUPLEXERS

THE MAPLE PRESS COMPANY, YORK, PA.

MICROWAVE DUPLEXERS

EDITORIAL STAFF

CAROL G. MONTGOMERY
LOUIS D. SMULLIN

CONTRIBUTING AUTHORS

W. C. CALDWELL
H. K. FARR
H. A. LEITER
C. G. MONTGOMERY
L. D. SMULLIN
C. W. ZABEL

Foreword

THE tremendous research and development effort that went into the development of radar and related techniques during World War II resulted not only in hundreds of radar sets for military (and some for possible peacetime) use but also in a great body of information and new techniques in the electronics and high-frequency fields. Because this basic material may be of great value to science and engineering, it seemed most important to publish it as soon as security permitted.

The Radiation Laboratory of MIT, which operated under the supervision of the National Defense Research Committee, undertook the great task of preparing these volumes. The work described herein, however, is the collective result of work done at many laboratories, Army, Navy, university, and industrial, both in this country and in England, Canada, and other Dominions.

The Radiation Laboratory, once its proposals were approved and finances provided by the Office of Scientific Research and Development, chose Louis N. Ridenour as Editor-in-Chief to lead and direct the entire project. An editorial staff was then selected of those best qualified for this type of task. Finally the authors for the various volumes or chapters or sections were chosen from among those experts who were intimately familiar with the various fields, and who were able and willing to write the summaries of them. This entire staff agreed to remain at work at MIT for six months or more after the work of the Radiation Laboratory was complete. These volumes stand as a monument to this group.

These volumes serve as a memorial to the unnamed hundreds and thousands of other scientists, engineers, and others who actually carried on the research, development, and engineering work the results of which are herein described. There were so many involved in this work and they worked so closely together even though often in widely separated laboratories that it is impossible to name or even to know those who contributed to a particular idea or development. Only certain ones who wrote reports or articles have even been mentioned. But to all those who contributed in any way to this great cooperative development enterprise, both in this country and in England, these volumes are dedicated.

L. A. DuBRIDGE.

Preface

THIS volume of the Radiation Laboratory Series is concerned with the theoretical and practical aspects of the design of duplexing circuits for use in microwave radar equipments, and of the gas-filled switching tubes (TR and ATR tubes) used in these duplexers. For a clearer picture of the equipment with which a duplexer must work the reader is referred to the following volumes of this series: Vol. 16 "Microwave Mixers," Vol. 9 "Microwave Transmission Circuits," Vol. 23 "Microwave Receivers," and Vol. 6 "Microwave Magnetrons."

The work upon which this book is based was done under the urgency of war commitments, and the main goal was always the production of a particular tube or duplexer circuit before a certain target date. As a result, many corners were cut and many intuitive steps were taken without clearly understood reasons, and there are today many gaps in our knowledge of the phenomena involved. This applies with particular emphasis to the problem of the high-frequency gas discharge. It is our belief that the material presented here fairly represents the present state of the art.

Besides the authors of the individual sections of this book, we wish to mention the following Radiation Laboratory personnel who actively participated in the design, study, and testing of the various tubes and duplexers discussed here. These people are: I. H. Dearnley, C. W. Jones, T. Kê, F. L. McMillan, Jr., H. Margenau, C. Y. Meng, C. S. Pearsall, J. Reed, F. Rosebury, and Norma Wolf.

Much work was done outside the Radiation Laboratory on these problems. The outstanding contributors were M. D. Fiske at the General Electric Research Laboratories, H. J. McCarthy of the Sylvania Electric Products Co., A. L. Samuel of the Bell Telephone Laboratories, and S. Krasik and D. Alpert of the Westinghouse Research Laboratories.

The editors wish to acknowledge the work of C. W. Jones in the collection of data and photographs and in the organization of Chapter 9. The preparation of the manuscript was greatly facilitated by the efforts of Gwenyth Johnson, Janet M. Jackson, and Anne Whalen. V. Josephson and his group produced all of the illustrations.

The publishers have agreed that ten years after the date on which each volume of this series is issued, the copyright thereon shall be relinquished, and the work shall become part of the public domain.

THE AUTHORS.

CAMBRIDGE, MASS.,
June 25, 1946.

Contents

CHAPTER 1

INTRODUCTION

By C. G. Montgomery

1·1. Microwave Radar.—The importance of the military applications of *ra*dio *d*irection *a*nd *r*ange, or radar, in the last war is common knowledge. For the detection of enemy ships and aircraft, for precise bombing at night or through overcast, and for the control of night fighters of raiding squadrons, radar has been unexcelled. At the beginning of the war there were only a few long-wave radar equipments; at the end of the hostilities many thousands of radar sets were in operation. Almost all of this equipment was developed during the war and most of it operated in the microwave region. Although no definite boundaries are established, the microwave region that has been developed extends from frequencies of about 1000 Mc/sec or wavelengths of 30 cm to frequencies near 30,000 Mc/sec or wavelengths near 1 cm. The microwave region is characterized by the fact that the components used for the generation and for the transmission of waves of these high frequencies have dimensions that are comparable with the wavelength, and the form of the microwave circuits is greatly influenced by this fact.

An important part of a microwave radar is the duplexer. In order to appreciate fully the problems involved in the development and design of duplexers and duplexing components, it is necessary to have in mind the parameters that describe the performance of a radar system and the orders of magnitude of the various quantities involved. A radar set operates by the detection of the energy reflected from a distant target. A short pulse of energy is sent out by the radar transmitter, and the pulse strikes a reflecting object that scatters it. The scattered wave, still in the form of a short pulse, although very much reduced in amplitude, is picked up by the radar receiver. The range of the target object is obtained from the length of time between the transmission of the high-power pulse and the reception of the weak reflected pulse. The direction of the target is obtained by measuring the direction in which the radar antenna is pointed when a signal of maximum intensity is being received.

The relation between the power P_T in the transmitted pulse and the power P_R in the received echo signal is known as the radar equation, which is,

$$P_R = P_T \cdot \frac{G}{4\pi R^2} \cdot \sigma \cdot \frac{A}{4\pi R^2}. \tag{1}$$

The power P_T is not radiated uniformly in all directions by the radar antenna, but is concentrated in a narrow beam by an amount that is measured by the antenna gain G of the transmitting antenna. The product of the first two factors of Eq. (1) is thus the power crossing a unit area at a distance R from the antenna. The target is characterized by the scattering cross section σ, and the receiving antenna by the absorbing cross section or effective area A. The magnitude of the received power as given by Eq. (1) is not explicitly dependent upon the wavelength λ of the radiation. It depends on λ implicitly through the quantities G and σ. For targets that have dimensions large compared with λ, σ is independent of λ.

The maximum range at which a target can be detected is obtained from Eq. (1) if the value for P_R corresponding to the minimum detectable signal is inserted. In order to avoid confusion of the signal with the thermal noise that is inevitably present in any electrical circuit, the signal power must be greater than some minimum value. The noise power in an electrical circuit is proportional to the bandwidth Δf of the circuit. For an ideal circuit that has no other sources of noise except temperature fluctuations, the noise power is $kT\Delta f$. The bandwidth of the radar receiver must be large enough so that the short pulses are sufficiently sharp for accurate range determination. If the length of the pulse is 1 μsec, a common value, Δf is usually about 2Mc/sec, and $kT\Delta f$ is 8×10^{-15} watt. An actual receiver, of course, has other sources of noise; it is not ideal. The magnitude of the smallest signal that can be recognized is dependent on a great many variables, and a discussion of these would lead too far afield. A representative value for the smallest signal power would be $100kT\Delta f$, or 8×10^{-13} watt. Values of the other quantities in Eq. (1) which are typical are $P_T = 10^6$ watts, $G = 1000$, $A = 10$ ft^2. If σ is 10^3 ft^2, the value for a medium bomber, then the maximum value of R is found to be 3×10^5 ft or 50 nautical miles. It is evident that the most effective radar equipment has the highest possible transmitter power, the most sensitive receiver, and the largest antennas for transmission and reception.

1·2. Radar Components.—At microwave frequencies, the high-power transmitter is a magnetron. A magnetron tube has a cylindrical cathode capable of the emission of large currents. Around the cathode there is a ring of closely coupled resonant cavities that form the "tank" circuit of the oscillator. There is an axial magnetic field of several thousand gauss supplied by a permanent magnet. A high-voltage pulse is applied between the cathode and the resonant cavities, and a bunched rotating space charge is set up which takes energy from the d-c field and delivers radio-frequency energy to the cavities. Useful power is extracted from the ring of cavities by a coupling loop or series waveguide circuit and is

made available in the microwave transmission line. The value of one megawatt chosen for P_T in the previous section is a value near the upper limit of the practical range for magnetron oscillators near a wavelength of 10 cm. At shorter wavelengths, the attainable power decreases and, in fact, is roughly proprotional to the wavelength.

The microwave transmission line is usually a rigid coaxial line, for wavelengths above 10 cm and for low powers at 10 cm. The diameter of the coaxial line must be small enough to prevent the propagation of higher transmission modes along it. Consequently, difficulties of construction and voltage breakdown at high power levels make it necessary to use waveguide, usually of rectangular cross section, for high powers and short wavelengths. Coaxial line may be used in the 10-cm region for powers up to about 100 kw; above this level, waveguide 1½ by 3 in. OD, is employed. For smaller wavelengths, waveguide is used exclusively.

The sensitive receiver that is necessary for good radar performance is a superheterodyne receiver with a silicon crystal converter. The received echo signal is mixed with a microwave local-oscillator signal without any amplification, and an intermediate frequency signal in the neighborhood of 30 Mc/sec is produced. The signal is amplified, rectified by a diode, further amplified by a wideband video-frequency amplifier, and applied to one or more cathode-ray tubes that are watched by the radar operator. The proper sweep voltages are also applied to the cathode-ray tubes in order that the range and direction of the target may be read off the tubes. The sensitive converter crystal is easily damaged by overload. The large difference in power level between the transmitted and reflected pulses (180 db in the example given) makes the important problem of protecting the crystal a difficult one.

Microwave antennas have forms that are characteristic of the short wavelength. The dimensions of the antenna are large compared with the wavelength and it is possible to obtain high gain and narrow beamwidth with an antenna that is not too large. Microwave antennas are designed on optical principles. Large converging mirrors or, more rarely, lenses, are used to focus the signal and divert it down the small transmission line to the receiver. The effective area A of the antenna is related to the beam width Θ and to the wavelength; approximately,

$$\Theta \approx \frac{\lambda}{\sqrt{A}}. \tag{2}$$

For A equal to 10 ft² and λ equal to $\frac{1}{8}$ ft or about 10 cm, Θ is about 6 degrees. The quantity Θ is the resolving power of the radar system in angle. The accuracy of a determination of direction may be about

$\Theta/10$. *The gain of the receiving antenna is approximately*

$$G \approx \frac{4\pi}{\Theta^2}, \tag{3}$$

or about 1000 for the example cited. The receiving and transmitting antennas have equal values of gain and consequently equal areas.

A radar antenna, to be able to search a volume of space for a target, must scan or be pointed to cover the angle subtended by that volume. If the transmitting and receiving antennas are separate, both of them must be scanned together. It is evident that there are many advantages to be gained by the use of a single antenna for both reception and transmission. A switch must be provided to connect the antenna to the transmitter or to the receiver, and this switch is called the duplexer.

1·3. Microwave Duplexers.—The requirements of a radar duplexing switch are easily stated:

1. During the period of transmission the switch must connect the antenna to the transmitter and disconnect it from the receiver.
2. The receiver must be thoroughly isolated from the transmitter during the emission of the high-power pulse to avoid damage of the sensitive converter elements.
3. After transmission, the switch must rapidly disconnect the transmitter and connect the receiver to the antenna. If targets close to the radar are to be seen, the action of the switch must be extremely fast.
4. The switch should absorb little power, either during transmission or during reception.

A radar duplexer is thus the microwave equivalent of a fast, double-pole double-throw switch, with low loss. Since the times involved are measured in microseconds, no mechanical switch is possible, and electronic devices must be used. The electronic tubes that have been developed for this purpose take forms similar to spark gaps where high-current microwave discharges furnish low-impedance paths. A duplexer usually contains two switching tubes connected in a microwave circuit with three terminal transmission lines, one each for the transmitter, the receiver, and the antenna. One tube is called the transmit-receive tube or TR tube; the other is called the anti-transmit-receive tube or ATR tube. The names are neither particularly appropriate nor descriptive, but they have received common acceptance and will be used throughout this book. The TR tube has the primary function of disconnecting the receiver, the ATR tube of disconnecting the transmitter.

The commonly accepted meaning of duplex operation is operation that permits the simultaneous passage of signals in both directions along

a transmission line. In the narrow sense, it is improper to apply the term to the switching operation in a radar equipment, since the transmitted and received pulses are not simultaneous. Strictly simultaneous operation must involve a 3-db loss in each direction (this is demonstrated in Chap. 8), and such a loss is too large to be tolerated for radar purposes. Although it is possible to build microwave duplexers for continuous-wave operation, little attention has been given to the practical development of such devices.

1·4. Duplexing Tubes.—The design and development of a radar duplexer involves two major problems which are related to each other. The tubes for the duplexer must be designed, engineered, and produced, and the microwave circuits in which the tubes are used must be developed. A tube for a duplexer must operate properly under two very different conditions: when a gas discharge is passing through the tube and the tube is a nonlinear device, and when the tube is exposed to low power levels and behaves linearly. The design of a TR tube to have the desired low-level properties is similar to the design of many other microwave components. A knowledge of the behavior of cavities and methods of coupling to them is necessary. Measurements, such as those described in Chap. 9, must be made of the reflected and transmitted power through the switch. The dimensions and tolerances of the switch must be determined to a great extent by experiment, although theoretical calculations are important since they make it possible to hold the number of experiments that must be done to a minimum. The operation of linear microwave devices is well understood. Chapters 2, 3, and 4 of this book are devoted to the linear behavior of duplexing tubes.

On the other hand, the operation of a switching tube at high power levels is not so easy to understand. Although the phenomena occurring in discharges of electricity through gases have been known for a long time and have been the subject of countless investigations, many problems remain to be solved. In fact, a principal result of the many investigations is that the extreme complexity of even the simplest forms of discharge has been emphasized. The fact that the discharges encountered in radar duplexers are excited by high-frequency voltages in a frequency range where very little fundamental investigation has been done renders it difficult to predict the behavior by extrapolation from past experience. The design procedure has therefore been almost completely empirical. The urgency of the military needs was great, and satisfactory solutions were the primary goal of the investigations rather than an understanding of the phenomena involved. Chapters 5 and 6 are devoted to the high-level behavior of duplexing tubes.

An important consideration in the design of a microwave tube is the ease with which it can be manufactured. Microwave tubes must be made

of metal in order that no energy may be lost by radiation. The envelope of a microwave tube is often a portion of the walls of a resonant cavity, and is therefore an important circuit element. The construction is fundamentally different from that of low-frequency tubes where the circuit elements are inside an envelope that has only the function of retaining the vacuum. The development of new microwave tubes must therefore be paralleled by the development of new techniques of construction. Nearly all duplexer tubes involve constructional features that were developed during the war. Thus the first TR tubes employed copper-glass disk seals; integral-cavity tubes were possible only after the development of Kovar-glass seals in the form of windows for resonant cavities; and bandpass TR tubes and broadband ATR tubes were concurrently developed with the large resonant Fernico-glass window. Close cooperation was necessary at all times between the tube manufacturers and the designers of components for radar equipment.

An additional complication to be overcome in the successful design of a duplexing tube arises from the fact that a gas must fill the tube. A high-frequency discharge in a gas makes it extremely active chemically. For good performance the gas filling must remain unchanged in composition and pressure during several hundred hours of operation.

1·5. Microwave Circuits.—The switching tubes must be incorporated in a microwave circuit to produce a complete duplexer. The circuit itself is linear, and the nonlinear duplexing tubes can be regarded for many purposes as simple knife switches that are opened or closed by the gas discharge. One of the important developments during the war has been the extension of the concepts of the conventional network theory, applicable at low frequencies, to microwave frequencies and to the propagation of microwave power in waveguides. This generalization has been made rigorously and it will be adopted without explanation in the succeeding chapters. A more complete explanation of the basic principles involved is given in other volumes of the series.[1]

The practical aspect of the generalization is that the familiar concepts of impedance, of impedance-matching, and of insertion loss, and the transmission-line equations may be used with confidence. Thus transmission through a cavity with two coupling lines may be regarded as equivalent to transmission through a length of transmission line almost short-circuited at each end by a high shunt susceptance. The power transfer from a generator connected to one coupling line to a load connected to the other coupling line may be computed from well-known relations. An obstacle in a waveguide which is thin in the direction along the axis of the guide is equivalent to a shunt susceptance, and the

[1] Vols. 8, 9 and 10.

scattered wave from the obstacle can be accurately described by circuit equations.

Duplexing circuits can be divided into two classes, branched circuits and balanced circuits. The branched circuits are simple in principle and are widely used. A T-shaped junction in waveguide or coaxial line with three arms, called a T-junction, is provided with switches in the two arms that are connected to the transmitter and to the receiver. The third arm is connected to the antenna. During transmission one switch is open and the other closed; during reception the reverse is true. The chief design problem in a branched duplexer is that of minimizing the losses over a broad band of frequencies. In Chap. 7 the methods of design are discussed. Some practical branched duplexers are described in Chap. 8.

Balanced duplexing circuits are more complicated and involve the combination of two magic T's and two TR tubes. A magic T is the microwave analogue of a balanced bridge circuit at low frequencies. It may have any of a number of different forms in waveguide or coaxial line. Although balanced circuits have been developed only recently, they show great promise for the future. Balanced circuits are described in Chap. 8.

Although the duplexers that are described here were designed with a highly specialized application in mind, there is much to be learned from a study of the development. A good duplexer can result only from a careful combination of the most advanced techniques in three fields: linear microwave circuits of the most highly developed type must be combined with a knowledge of the properties of electrical discharges in gases at microwave frequencies and with the best techniques of construction of microwave vacuum tubes.

CHAPTER 2

LINEAR THEORY OF HIGH-Q TR TUBES

By Louis D. Smullin

2·1. Linear Behavior of the TR Tube.—The TR tube is a switch which is used to short-circuit the receiver during the transmitting period, and it also allows echoes to pass to the receiver when the transmitter is off. An ideal TR tube would present a perfect short circuit during the transmitting period and would cause no loss of the received signal. These functions could be performed by a simple knife switch but the speed and frequency of operation which are needed are far beyond the possibilities of any mechanical switch. Typical operating requirements are represented by a repetition rate of 2000 cycles per second, with the transition from either open to short circuit or short to open circuit taking place in less than 10^{-7} sec. Such high-speed performance can be attained by using a spark gap for the switch. In some installations these spark gaps have taken the form of very simple air spark gaps; in others, the gaps have been placed in low-pressure atmospheres to reduce the breakdown and the sustaining voltages of the discharge.

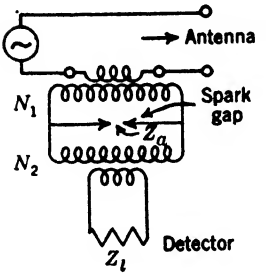

Fig. 2·1.—Duplexing circuit with spark gap and ideal transformer.

From the point of view of transmitter efficiency, it is desirable to make the discharge appear as a very low impedance in series with the line. Similarly, to get best receiver protection, the voltage stepdown ratio from the gap to the receiver line should be as large as possible. Figure 2·1 indicates how such a circuit would appear if ideal transformers were used. During the fired condition the arc or discharge impedance Z_a will transform to the terminals in the antenna line as Z_a/N_1^2. The leakage power to the receiver load will be $(V_a/N_2)^2/Z_l$ where V_a is the voltage drop across the discharge. During the receiving condition the receiver impedance will appear to be $Z_l(N_2/N_1)^2$ at the antenna-line terminals.

Except at comparatively low frequencies, it is difficult if not impossible to construct an "ideal" transformer or even one which is approximately "ideal." However, it is fairly simple to make resonant transformers. These may take the form of either lumped-constant or distributed-constant networks. The lumped-constant circuits are made of conventional

inductors and capacitors suitable for the desired frequency range. The distributed-constant circuits usually take the form of a cavity or transmission-line resonator. Such resonators may have unloaded Q's of several thousand, whereas ordinary LC-circuits have maximum Q's of the order of several hundred.

Although in the microwave region the use of lumped-constant elements and circuits in the usual sense is impractical, it will be informative first to discuss the TR tubes as if such construction were possible. Then in succeeding sections, cavity resonators and their equivalent circuits, high-Q TR tubes and their characteristics, and bandpass TR tubes will be discussed.

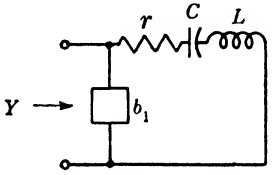

FIG. 2·2.—Series LC-circuit.

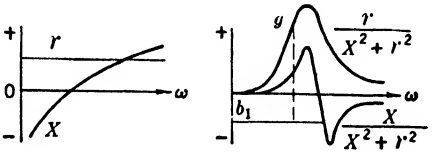

FIG. 2·3.—Frequency dependence of circuit parameters of Fig. 2·2.

2·2. Lumped-constant Resonant Transformers.—The circuit of Fig. 2·2 has a number of interesting properties. As shown, it consists of a series LC-circuit with internal losses represented by the resistance r, shunted by a susceptance b_1. The input susceptance is

$$Y = \frac{r}{X^2 + r^2} + j\left(b_1 - \frac{X}{X^2 + r^2}\right), \tag{1}$$

where $X = (\omega L - 1/\omega C)$. If resonance is defined as the frequency at which the imaginary part of Y is zero, then

$$X = \frac{\frac{1}{b_1} \pm \sqrt{\frac{1}{b_1^2} - 4r^2}}{2}, \tag{2}$$

and for $rb_1 < \frac{1}{8}$,

$$X \approx \frac{1}{b_1}.$$

Then, at resonance,

$$Y \approx rb_1^2. \tag{3}$$

Thus, this is a resonant impedance transformer, since by varying b_1 and adjusting the LC-circuit to make $\mathrm{Im}(Y) = 0$, the input conductance $\mathrm{Re}(Y)$ can be made to vary over a wide range. Figure 2·3 illustrates graphically what is involved. The $\mathrm{Re}(Y) = g$ moves up and down the curve as b_1 is varied.

Similarly, let us consider the circuit of Fig. 2·4 where an output circuit consisting of the shunt susceptance b_2 and the load conductance g_2 has been added. The input admittance Y when the circuit is tuned to resonance [$\mathrm{Im}(Y) = 0$] is

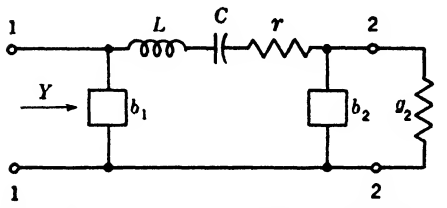

FIG. 2·4.—Resonant impedance transformer with output circuit.

$$\mathrm{Re}(Y) = g \approx rb_1^2 + g_2\left(\frac{b_1}{b_2}\right)^2, \quad (4)$$

where $(r + g_2/b_2^2)b_1 < \frac{1}{8}$ and $b_2^2 \gg g_2^2$. Equation (4) could also represent an ideal transformer circuit with voltage stepup and stepdown ratios of b_1 and b_2, respectively.

Let us now examine the frequency response of the circuit of Fig. 2·4 in the vicinity of resonance.

$$\mathrm{Im}(Y) = b = b_1 - \frac{X + X'}{(r + r')^2 + (X + X')^2}, \quad (5)$$

where $X' = -b_2/(g_2^2 + b_2^2)$ and $r' = g_2/(g_2^2 + b_2^2)$. If this is restricted to the region where $b_2^2 \gg g_2^2$, then

$$b = b_1 - \frac{1}{X - 1/b_2}. \quad (6)$$

At resonance, $b = 0$, and

$$X_0 = -\frac{1}{b_0} = \frac{1}{b_1} + \frac{1}{b_2} = \frac{b_1 + b_2}{b_1 b_2}. \quad (7)$$

The Q of a simple series-resonant circuit is given by

$$Q_{\text{series}} = \frac{\omega L}{R} = \frac{1}{\omega CR}. \quad (8)$$

A parallel-resonant circuit having L, C, and G all in shunt is described by

$$Q_{\text{shunt}} = \frac{\omega C}{G} = \frac{1}{\omega LG}. \quad (9)$$

In the circuits under discussion there is obviously neither a simple series- nor a parallel-resonant circuit at the input terminals. Near resonance, the behavior of the susceptance curve is at least similar to that in a parallel-resonant circuit. However, since it is not obvious just what particular L, C, or G should be used to get an expression for the Q of the circuit, further investigation into the nature of the quantity defined by Q should be made.

It is possible to define Q in a number of ways all of which are equivalent. The amplitude of oscillation of a freely oscillating system

will decrease exponentially with a time constant equal to $2Q/\omega$, where Q is defined as in Eqs. (8) or (9). Alternatively, Q may be defined as 2π times the ratio of the energy stored to the energy dissipated per cycle. In the parallel circuit, oscillating with a frequency $\omega/2\pi$ and amplitude V, the energy stored per cycle is $\frac{1}{2}CV^2$. The energy dissipated per cycle is $2\pi GV^2/2\omega$, and $Q = \omega C/G$, as before. Finally, the frequency variation of the susceptance or reactance of an oscillating circuit around its natural or resonant frequency can be studied. The parallel-resonant circuit of Fig. 2·5 has an admittance

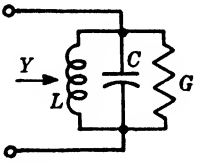

FIG. 2·5. — Parallel-resonant circuit.

$$Y = G + j\left(\omega C - \frac{1}{\omega L}\right) = G + j\omega C\left(1 - \frac{\omega_0^2}{\omega^2}\right), \tag{10}$$

where $\omega_0^2 = (LC)^{-1}$. By using Eq. (9) and the approximation that

$$(\omega_0 - \omega) \ll \omega,$$

$$Y \approx G + j2QG\frac{\Delta\omega}{\omega_0}. \tag{11}$$

Let $\mathrm{Im}(Y) = b$; then from Eq. (10), at resonance,

$$\frac{db}{d(\ln\omega)} = \frac{\omega db}{d\omega} = 2\omega C = 2QG, \tag{12}$$

or

$$Q = \frac{\omega}{2G}\frac{db}{d\omega}. \tag{13}$$

With Eq. (13) as a basis, an equivalent definition of Q may be set up for the more complex circuit of Fig. 2·4. If the derivative of Eq. (6) with respect to $\ln\omega$ is taken, then

$$\frac{db}{d(\ln\omega)} = \frac{\omega db}{d\omega} = b_1 + \frac{(\omega b_0' b_2 + b_0 b_2)(b_0 + b_2) - b_0 b_2(\omega b_0' + b_2)}{(b_0 + b_2)^2}, \tag{14}$$

where

$$\frac{\omega db_1}{d\omega} = |b_1| = b_1, \qquad \frac{\omega db_2}{d\omega} = |b_2| = b_2,$$

and

$$\omega b_0' = \omega\frac{db_0}{d\omega} = \frac{-\omega_0}{\Delta\omega}\frac{b_0 b_2^2}{(b_1 + b_2)^2}. \tag{15}$$

Then by the use of Eq. (7) for b_0, and

$$\frac{\omega_0}{\Delta\omega} = -\left(\frac{2b_0}{\omega C}\right),$$

$$\frac{\omega db}{d\omega} \approx |b_1| + \frac{2b_1^2}{\omega C} \approx \frac{2b_1^2}{\omega C}. \tag{16}$$

The Q of the circuit is defined by Eq. (13) where the total conductance $G = Y_0 + rb_1^2 + g_2 (b_1/b_2)^2$, and

$$Q = \frac{1}{\omega C \left(\frac{Y_0}{b_1^2} + r + \frac{g_2}{b_2^2} \right)}, \tag{17}$$

where Y_0 is the conductance of the line or generator connected to the circuit at terminals 1-1.

Equation (17) may be rewritten

$$\frac{1}{Q} = \omega C \left(\frac{Y_0}{b_1^2} + r + \frac{g_2}{b_2^2} \right) = \frac{1}{Q_{in}} + \frac{1}{Q_0} + \frac{1}{Q_{out}}, \tag{18}$$

thus defining the "input," "output," and "unloaded" Q's. On this basis,

$$\frac{1}{Q_{L1}} = \frac{1}{Q_{in}} + \frac{1}{Q_0},$$

$$\frac{1}{Q_{L2}} = \frac{1}{Q_{in}} + \frac{1}{Q_0} + \frac{1}{Q_{out}},$$

where the subscripts indicate that the resonant circuit is loaded by the generator only (Q_{L1}), or by the generator and a load (Q_{L2}).

Next, let us consider what happens if the capacitor C in Fig. 2·4 is short-circuited. This would correspond to the placing of a spark gap across C which would break down upon the application of sufficient voltage and which would require zero sustaining voltage, Fig. 2·6. The resistance r may be neglected since the circuit is no longer resonant. The ratio of the power delivered to g_2 to the available power from the generator will be determined. The input admittance to the circuit is

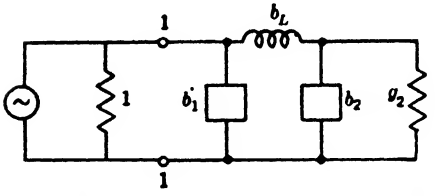

FIG. 2·6.—Circuit of Fig. 2·4 with the capacitance short-circuited.

$$Y = jb_1 + \frac{(g_2 + jb_2)(-jb_L)}{g_2 + j(b_2 - b_L)}. \tag{19}$$

For b_1 and b_2 large

$$Y \approx g_2 \left(\frac{b_L}{b_2} \right)^2 - jb_L + jb_1. \tag{20}$$

The power absorbed in g_2 is

$$P = \frac{g_2 \left(\frac{b_L}{b_2} \right)^2}{\left[1 + g_2 \left(\frac{b_L}{b_2} \right)^2 \right]^2 + [b_1 - b_L]^2} \approx \frac{g_2 b_L^2}{b_1^2 b_2^2}. \tag{21}$$

This power is known as the *direct-coupled* leakage power to distinguish it from the leakage power due to the voltage drop across the discharge. The direct-coupling attenuation D expressed in decibels is 10 $\log_{10}$ of the ratio of P of Eq. (21) to the maximum power available;

$$D = 10 \log_{10} \frac{b_1^2 b_2^2}{4 g_2 b_L^2} \, db. \tag{22}$$

As a last example, the insertion loss of the circuit in Fig. 2·4 will be calculated, with the assumption of a current generator with unit internal admittance. At resonance, the input conductance of the circuit is given by Eq. (4). The power transferred to the load is

$$P = \frac{g_2 \left(\frac{b_1}{b_2}\right)^2}{\left[1 + g_2 \left(\frac{b_1}{b_2}\right)^2 + r b_1^2\right]^2}. \tag{23}$$

The insertion loss expressed as the ratio of the actual to the available power is the reciprocal of the transmission,

$$T^{-1} = \frac{\left[1 + g_2 \left(\frac{b_1}{b_2}\right)^2 + r b_1^2\right]^2}{4 g_2 \left(\frac{b_1}{b_2}\right)^2}. \tag{24}$$

Thus, Eqs. (4), (18), (22), and (20) indicate that the impedance transformation ratio, Q_{L2}, insertion loss, and direct-coupling attenuation all increase with the square of the coupling susceptances. It is, therefore, necessary in any practical design to compromise between maximum tolerable insertion loss and minimum transformation ratio.

2·3. Cavity Resonators.—The circuit analyzed in Sec. 2·1 is a thoroughly practical circuit and can be used with little modification up to frequencies of the order of 100 Mc/sec. At higher frequencies, radiation losses from open-wire circuits become excessive, and at the same time it becomes practical to use resonant transmission lines or cavities instead of conventional LC-circuits. Although it is difficult to obtain a Q of more than a few hundred with lumped constants, it is not difficult to achieve an unloaded Q of 2000 to 10,000, and practical designs exist for resonators with Q's of 50,000 or more. As a result, it is possible to use large transformation ratios without paying the penalty of excessively large insertion losses.

Most microwave TR tubes ($\lambda < 50$ cm) use some form of resonant cavity as a voltage and impedance transformer. The low-Q resonant irises used in bandpass TR tubes constitute a transitional group between

lumped-constant and distributed-constant circuits and will be discussed in Chap. 3. The remainder of this chapter will deal with the linear properties of high-Q TR tubes and with detailed descriptions of various tubes.

Resonant cavities have been discussed by a number of authors, and complete mathematical analyses exist for a large number of different geometrical shapes and modes of oscillation which give the resonant frequency Q and equivalent shunt or series resistance. In the following sections, a knowledge of microwave circuitry will be presumed, and, primarily on the basis of transmission line analysis, the relation between various cavity parameters and the functions of the TR tube will be indicated. Because the methods of handling lumped-constant circuits are so highly perfected and widely understood, equivalent lumped-constant circuits will be developed for TR-tube resonant cavities.

In the design of a TR-tube cavity, a number of factors must be considered simultaneously. The mode of oscillation and the shape of the cavity must be such that it is convenient to place a short spark gap at a point of maximum voltage, so that when the gap fires the direct-coupling attenuation will be a maximum. For instance, it would be difficult to satisfy these conditions in the TE_{011}-mode of oscillation. The ratio between the gap voltage and the exciting voltage should be large. Since the loaded Q and the stepup ratio vary by the same factors in a given cavity design, and since extremely large values of Q are undesirable because of instability in tuning, a compromise must be made between the two.

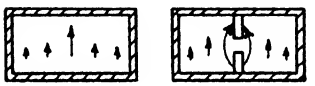

(a) (b)

FIG. 2·7.—Cross sections of cavities.

Although the actual shapes of most TR cavities are fairly complicated, they can be considered as modifications of a cavity made of a resonant length of rectangular waveguide operating in the TE_{01}-mode and coupled through large shunt susceptances to the load and generator, Fig. 2·7*a*. In order to reduce the breakdown voltage to a low enough value to be used, a pair of posts are placed across the cavity at a point of maximum voltage to form a spark gap, Fig. 2·7*b*. The posts add a shunt capacitance across the cavity which causes the resonant frequency to be lower than if there were no posts present.

Impedance Transformation.—Let us consider the resonant mode of a length of lossless transmission line of characteristic admittance Y_0 short-circuited at the far end and shunted by a comparatively large susceptance B_1 at the point *a-a*, Fig. 2.8. The input susceptance will be

$$Y_i = jB_1 - jY_0 \cot \frac{2\pi l}{\lambda}, \tag{25}$$

where l is the length of the line. For simplicity it is assumed that the guide wavelength is equal to the air wavelength. By adjusting either B_1 or l the input susceptance can be made zero at any given wavelength.

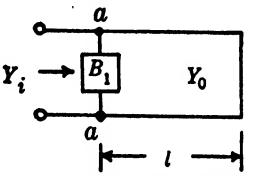

FIG. 2·8.—Transmission line with shunt susceptance.

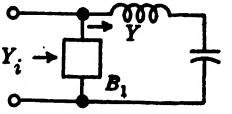

FIG. 2·9.—Equivalent circuit of Fig. 2·8 near resonance.

If B_1 is large, Y_i will be zero for $2\pi l/\lambda \approx (n\pi \pm \epsilon)$ where ϵ is small. The *impedance* of a short-circuited transmission line is

$$Z = jZ_0 \tan \frac{2\pi l}{\lambda}, \tag{26}$$

and if $2\pi l/\lambda = n\pi \pm \epsilon$,

$$Z \approx jZ_0\epsilon = jZ_0 \frac{2\pi l}{\lambda_0} \frac{\Delta\lambda}{\lambda_0}. \tag{27}$$

In other words, the reactance of a short-circuited length of line varies linearly around zero with wavelength. This, of course, is just like the variation in reactance of a series LC-circuit near resonance; and for small values of $\Delta\lambda/\lambda_0$, a short-circuited length of transmission line can be accurately represented by a series-resonant circuit. Thus, an equivalent circuit for Fig. 2·8 can be drawn in as shown Fig. 2·9. The frequency response of the circuit may be analyzed as in Fig. 2·10 where it has been assumed that B_1 is an inductive susceptance. The frequency for which the input susceptance Y_i is zero will fall to the left or to the right of the pole, depending upon whether B_1 is an inductive or a capacitive susceptance. In the vicinity of f_0, if B is large, the susceptance will vary nearly linearly through zero, which is similar to the variation of a simple parallel-resonant circuit.

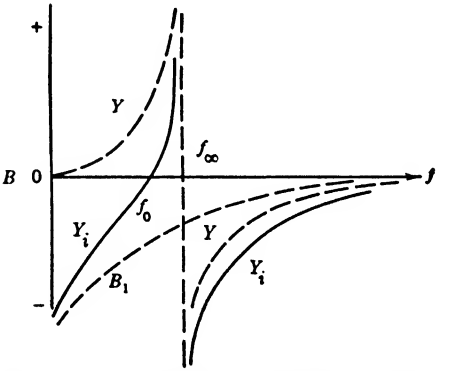

FIG. 2·10.—Frequency response of circuit of Fig. 2·9.

The circuit of Fig. 2·8 is a two-terminal network, and as such can be used only as a shunt or series element. This is useful for ATR tubes and further applications are discussed in Chap. 4. For a TR tube a four-terminal network through which power is transmitted is required. This

may be accomplished by coupling the cavity to an output load by a susceptance B_2, Fig. 2·11*a*.

The input susceptance Y_i may be written as

$$Y_i = jB_1 + Y_0 \frac{(G_2 + jB_2) + jY_0 \tan \beta l}{Y_0 + j(G_2 + jB_2) \tan \beta l}$$
$$\approx jB_1 + Y_0 \frac{G_2 Y_0(1 + \tan^2 \beta l) + jB_2(Y_0 - Y_0 \tan^2 \beta l - B_2 \tan \beta l)}{(Y_0 - B_2 \tan \beta l)^2 + (G_2 \tan \beta l)^2}, \quad (28)$$

where $\beta = 2\pi/\lambda$. If the imaginary part is set equal to zero the solution for $\tan \beta l$, where B_1 and B_2 are large compared with Y_0, is

$$\tan \beta l \approx Y_0 \frac{B_1 + B_2}{B_1 B_2}. \quad (29)$$

The real part of $Y_i = G + jB$, with B_1 and $B_2 \gg Y_0$, is

$$G = Y_0 \frac{G_2 Y_0(1 + \tan^2 \beta l)}{(Y_0 - B_2 \tan \beta l)^2 + (G_2 \tan \beta l)^2} \approx G_2 \left(\frac{B_1}{B_2}\right)^2. \quad (30)$$

Equations (29) and (30) are to be compared with Eqs. (7) and (4) which give the identical results for the lumped-constant circuit. Alternatively, a more exact equivalent circuit can be drawn by using the equivalent π-section for a length of line,[1] Fig. 2·11*b*, and the same relations will be found at resonance.

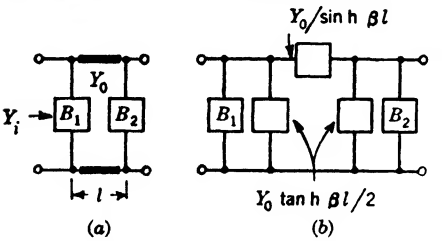

FIG. 2·11.—Transmission line with two coupling susceptances.

Cavity Losses.—The calculations thus far have neglected the power dissipated within the cavity itself. If the cavity is not too lossy, the net effect of dissipation in the walls can be represented by a lumped resistance shunted across the cavity at the point of maximum voltage. It can be defined as

$$\frac{1}{G_{sh}} = R_{sh} = \frac{(\text{voltage})^2}{2\pi \times \text{energy lost per sec}}, \quad (31)$$

where

$$\text{Energy lost per sec} = \frac{\delta f}{8} \int |B|^2 d\sigma \quad (32)$$

and δ is the skin depth, f thre fequency, and B the magnetic field at the surface of the cavity. The voltage is the line integral of the electric field, which by Stoke's theorem is

$$\int E \cdot ds_1 = -\frac{1}{c} \int B' \cdot d\sigma_1 = -j \frac{2\pi f}{c} \int B \cdot d\sigma_1, \quad (33)$$

[1] Guillemin, *Communications Networks*, Wiley, New York, 1935.

where ds_1 is an element of length and $d\sigma_1$ an element of area in the cross section of the cavity. The path of integration usually chosen for this integral is one that gives a maximum of voltage without using an extreme path. If Eqs. (31), (32), and (33) are combined,

$$R_{sh} = 16\pi^2 \frac{\left[\int B \cdot d\sigma_1\right]^2}{\lambda^2 \int B^2 |d\sigma|} \frac{\lambda c}{\delta}, \qquad \text{emu.} \tag{34}$$

Equation (34) is the equivalent shunt resistance that would have to be placed across the resonator along the particular path of integration in order to produce the same effect as the dissipation in the cavity walls. It should be pointed out that since the "inductive" and "capacitive" elements are hopelessly intermingled, the equivalent series resistance R_s, if calculated by a similar procedure, will be related to the shunt resistance by $R_s = R_{sh}/A$, where A may be larger than Q^2 by as much as a factor of 2.[1]

This method of calculating R_{sh} has been applied to most of the simpler geometric shapes and to most of the modes of oscillation. The cavities of TR tubes are usually so complicated geometrically that the method becomes extremely complicated, and all design work is based on experimentally determined values of a quantity proportional to R_{sh}. Such values are obtained by measuring the input conductance of a cavity at resonance ($B = 0$). It is, therefore, of interest to see how this measured conductance varies with the coupling to the cavity.

Let us refer again to the simple line cavity of Fig. 2·11, and calculate the input admittance Y_i. The assumption now is that the transmission line forming the cavity has a propagation factor $\gamma = \alpha + j\beta$ where the attenuation constant α is small. Then

$$\frac{Y}{Y_0} = \frac{g_2 + jb_2 + \tanh \gamma l}{1 + (g_2 + jb_2) \tanh \gamma l}, \tag{35}$$

where $g_2 = G_2/Y_0$, and $b_2 = B_2/Y_0$. Expanding $\tanh \gamma l$,

$$\tanh \gamma l = \frac{e^{2\alpha l}e^{j\beta l} - e^{-j\beta l}}{e^{2\alpha l}e^{j\beta l} + e^{-j\beta l}} \approx \frac{(1 + 2\alpha l)e^{j\beta l} - e^{-j\beta l}}{(1 + 2\alpha l)e^{j\beta l} + e^{-j\beta l}} \approx \frac{\alpha l}{\cos^2 \theta} + j \tan \theta, \tag{36}$$

where $\theta = \beta l$. If B_1 and $B_2 \gg Y_0$, and $\alpha l \ll 1$, the cavity will be nearly a half wavelength long. If this is so,

$$\begin{aligned} \tanh \gamma l &\approx \alpha l + j\epsilon, \\ \beta l &= \pi + \epsilon. \end{aligned} \tag{37}$$

[1] W. W. Hansen, Lecture Series at Radiation Laboratory, RL Report T-2.

The substitution of Eq. (37) into Eq. (35) gives

$$\frac{Y}{Y_0} = \frac{[g_2 + \alpha l + j(\epsilon + b_2)][1 + g_2\alpha l - b_2\epsilon - j(g_2\epsilon + b_2\alpha l)]}{(1 + g_2\alpha l - \epsilon b_2)^2 + (g_2\epsilon + b_2\alpha l)^2}. \quad (38)$$

For resonance, the imaginary part of Eq. (38) must equal $-b_1$. To satisfy this, it is found that, if $\alpha l \ll b_2 \gg g_2$

$$\epsilon = \frac{b_1 + b_2}{b_1 b_2}.$$

Finally, the solution for the real part is

$$\frac{G_i}{Y_0} = \left(\frac{b_1}{b_2}\right)^2 g_2 + b_1^2 \alpha l. \quad (39)$$

Thus, at the input terminals, there is a total conductance composed of the load conductance transformed through two coupling susceptances and a quantity that may be variously interpreted as the shunt conductance or the series resistance of the cavity transformed through the input coupling. The form of this equation is identical with that of Eq. (4) for the lumped-constant circuit.

Finally, let us find the conductance at the center of the cavity. At resonance, the imaginary part of the admittance is zero and Eq. (37) can be written as

$$\tanh \gamma \frac{l}{2} = \frac{2\alpha l}{\epsilon^2} - j\frac{2}{\epsilon},$$

$$\frac{\beta l}{2} = \frac{\pi}{2} + \frac{\epsilon}{2}.$$

If this is put back into Eq. (35), it is found that at resonance the conductance at the center of the cavity looking toward the output terminal is

$$\frac{G}{Y_0} = \frac{\alpha l}{2} + \frac{g_2}{b_2^2}. \quad (40)$$

The total conductance at the center, including both input and output terminals and assuming a matched generator is

$$\frac{G}{Y_0} = \alpha l + \frac{1}{b_1^2} + \frac{g_2}{b_2^2}. \quad (41)$$

Thus, the quantity αl can be defined as the shunt conductance of the cavity, and the total conductance-loading of the cavity is the simple sum of the external and cavity conductances, each transformed by a constant appropriate to the reference plane chosen.

Equation (39) asserts that at its resonant frequency, the cavity and its load may be replaced by an equivalent conductance. If this con-

ductance G_i is equal to the generator conductance Y_0, the power delivered by the generator is a maximum since the reflection coefficient

$$\Gamma = \frac{Y_0 - G_i}{Y_0 + G_i}$$

is zero. However, G_i is the sum of the transformed cavity and load conductances; and it is the power delivered to the load that is of interest. The net power flow into the cavity and its load is given by

$$P = P_{\text{inc}}(1 - \Gamma^2). \tag{42}$$

The fraction of this power delivered to the load conductance is

$$P_l = P\left[\frac{g_2\left(\frac{b_1}{b_2}\right)^2}{g_2\left(\frac{b_1}{b_2}\right)^2 + g_c b_1^2}\right]^2,$$

and the insertion loss in decibels is given by

$$L = 10 \log_{10} \frac{\left[1 + b_1^2 g_c + g_2\left(\frac{b_1}{b_2}\right)^2\right]^2}{4g_2\left(\frac{b_1}{b_2}\right)^2}. \tag{44}$$

This equation is identical in form with that of Eq. (24) for the lumped-constant circuit.

Calculation of Q.—As has been indicated at the beginning of this section, the calculation of Q_0 for a cavity of simple design, such as a right cylinder, is a straightforward procedure, and formulas are available for a number of different designs.[1] These have been derived by calculating the ratio of the energy stored to the energy dissipated per cycle. However, the quantity of direct interest is not this ratio but the rate of change of input admittance with frequency (or alternatively, the variation of insertion loss with frequency). Therefore, let Q be defined in the same way as before,

$$Q = \frac{\omega}{2G}\frac{db}{d\omega}. \tag{13}$$

The problem, therefore, is to determine $\omega db/d\omega$.

For convenience, variables are changed from ω to $k = 2\pi/\lambda = \omega/c$. This is done because in microwave experiments wavelength is the variable that can be measured conveniently. It can be shown that the derivative of the input admittance of a section of transmission line

[1] Vol. 11, Chap. 5, and the references there cited.

terminated in an admittance Y_{out} is

$$\frac{1}{1+(jY_{in})^2}\frac{dY_{in}}{d(\ln k)} = jKl\left(\frac{k}{K}\right)^2 + \frac{1}{1+(jY_{out})^2}\frac{dY_{out}}{d(\ln k)}, \tag{45}$$

where $K = 2\pi/\lambda_g$ and λ_g is the wavelength in the transmission line under consideration, and all admittances have been normalized with respect to Y_0.[1] *For waveguide of a high-pass type, λ_g and λ are related by*

$$\lambda_g = \frac{\lambda}{\sqrt{1-\left(\frac{\lambda}{\lambda_c}\right)^2}}, \tag{46}$$

where λ_c is the cutoff wavelength. Two other useful relations are

$$k\,dk = K\,dK \tag{47}$$

and

$$\frac{d\lambda_g}{d\lambda} = \left(\frac{\lambda_g}{\lambda}\right)^3. \tag{48}$$

It can be seen from Fig. 2·11*a* that $Y_{out} = g_2 + jb_2$ and at resonance $Y_{in} = g - jb_1$ (the reference plane is just to the right of b_1); hence

$$\frac{dY_{out}}{d(\ln k)} = jb_2,$$

and

$$\frac{dY_{in}}{d(\ln k)} = jKl\left(\frac{k}{K}\right)^2(1-g^2+b_1^2+2jgb_1) + \frac{jb_2(1-g^2+b_1^2+2jgb_1)}{1-g_2^2+b_2^2-2jg_2b_2}. \tag{49}$$

If 1, g, and g_2 are small compared with b_1 and b_2,

$$\left.\begin{aligned}\frac{d\mathrm{Re}(Y_{in})}{d(\ln k)} &\approx -2gb_1Kl\left(\frac{k}{K}\right)^2\\ \frac{d\mathrm{Im}(Y_{in})}{d(\ln k)} &\approx b_1^2Kl\left(\frac{k}{K}\right)^2\end{aligned}\right\}. \tag{50}$$

If the relationships $g = g_2\left(\frac{b_1}{b_2}\right)^2 + g_cb_1^2$ and

$$Kl = \tan^{-1}\frac{b_1+b_2}{b_1b_2} \approx \frac{b_1+b_2}{b_1b_2} + n\pi,$$

and $Y_i = Y_{in} + jb_1$ are substituted into Eq. (50),

$$\left.\begin{aligned}\frac{d\mathrm{Re}(Y_i)}{d(\ln k)} &\approx -2\left[g_2\left(\frac{b_1}{b_2}\right)^2 + g_cb_1^2\right]b_1n\pi\left(\frac{k}{K}\right)^2\\ \frac{d\mathrm{Im}(Y_i)}{d(\ln k)} &\approx b_1^2n\pi\left(\frac{k}{K}\right)^2\end{aligned}\right\}, \tag{51}$$

[1] "Wave Guide Handbook Supplement," RL Report No 41-1/23/45.

where n is the number of electrical half wavelengths most nearly equal to the length of the cavity.

To determine Q, Eq. (13) is used, and for the loaded Q

$$Q_{L2} = \frac{1}{2G}\frac{d\mathrm{Im}(Y_i)}{d(\ln k)} = -\frac{b_1^2 n\pi}{2\left[1 + g_2\left(\frac{b_1}{b_2}\right)^2 + g_c b_1^2\right]}\left(\frac{k}{K}\right)^2,$$

$$Q_{L2} = \frac{n\pi}{2}\left[\frac{1}{b_1^2} + \frac{g_2}{b_2^2} + g_c\right]^{-1}\left(\frac{k}{K}\right)^2. \tag{52}$$

This expression is completely analogous to the corresponding one for the lumped-constant circuit, Eq. (17).

If the coupling susceptances are large, then Eqs. (51) indicate that the conductance will change slowly with frequency, relative to the rate at which the susceptance changes. Therefore, it is usual to approximate a resonant cavity by a simple parallel-resonant circuit with a constant conductance equal to the actual value of the circuit at resonance, and to choose L and C to give the same Q as the actual circuit. In ordinary cavities this approximation is sufficiently accurate to predict the performance at frequencies different from the resonant frequency by $\Delta\omega/\omega = 3/Q$, despite the fact that the admittance has a pole at a frequency relatively close to the resonant frequency instead of at infinity.

Voltage Transformation Ratio.—The voltage transformation ratio of a resonant cavity used for a TR tube is of considerable importance since it is one of the factors that determine the amount of leakage power reaching the crystal detector. Two transformation ratios are of interest. The first ratio refers to the behavior of the resonant cavity and is the ratio between a voltage applied to its terminals and the voltage across the gap *before a spark has formed.* The second is the ratio of the voltage drop of the discharge maintained across the gap to the voltage appearing across the load. Although both of these quantities have to do with leakage power, they are functions of the linear properties of the cavity and, therefore, will be discussed here.

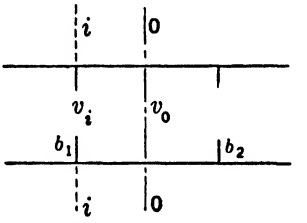

FIG 2·12.—Resonant line with susceptances b_1 and b_2.

Let us consider the case of a simple section of resonant line with no spark-gap posts, Fig. 2·12. At the plane i-i, the power flowing to the right is $v_i^2 G_i$; similarly, at the plane 0-0 the power flowing to the right is $v_0^2 G_0$. If there are no losses between the two planes, the two quantities

must be equal. If Eq. (39) is used for G_i,

$$P_i = v_i^2 \left[G_2 \left(\frac{b_1}{b_2} \right)^2 + b_1^2 \alpha l Y_0 \right]. \tag{53}$$

If the cavity losses are assumed to be negligible ($\alpha l = 0$) then

$$P_i = v_i^2 G_2 \left(\frac{b_1}{b_2} \right)^2 = P_0 = \frac{v_0^2 G_2}{b_2^2},$$

and

$$\frac{v_0}{v_i} = b_1, \tag{54}$$

which is the voltage stepup ratio from plane i-i to plane 0-0.

Consider how cavity dissipation affects this ratio. Practical design considerations generally require that at the input terminals to the cavity the apparent shunt conductance be of the order of one-third the load conductance. This amounts to about a 30 per cent power loss in the cavity and, therefore, P_i will be about 15 per cent greater than P_0 because of loss through the first half of the cavity.

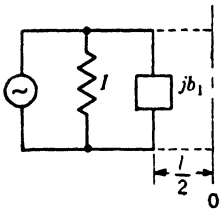

FIG. 2·13.—Equivalent circuit of half of line in Fig. 2·12.

If the center of the cavity 0-0 is chosen as the reference plane, Thévenin's theorem may be used to replace the actual generator to the left of i-i by an equivalent one at 0-0. The equivalent generator has an internal admittance Y' obtained by open-circuiting the actual current generator and observing the admittance seen looking to the left from 0-0. The intensity of the new current source equals the current flowing through a short circuit across 0-0.

Equation (40) gives the equivalent generator admittance

$$g = \frac{\alpha l}{2} + \frac{1}{b_1^2} = \frac{g_c}{2} + \frac{1}{b_1^2}.$$

To obtain the short-circuit current through 0-0, the various incident and reflected waves are added, Fig. 2·13. If the *current* reflection coefficient $\Gamma_I = (Y - Y_0)/(Y + Y_0)$, then the total current at 0-0 can be shown to be $|I_0| = I/b_1$ for b_1 large. Now, the voltage at the input terminals is the current I divided by the total conductance or

$$v_i = \frac{I}{1 + g_c b_1^2 + g_2 \left(\frac{b_1}{b_2} \right)^2}.$$

The voltage at the center of the cavity is found in a similar manner,

$$v_0 = \frac{I}{b_1} \frac{1}{\frac{1}{b_1^2} + \frac{g_c}{2} + \frac{g_c}{2} + \frac{g_2}{b_2^2}},$$

and

$$\frac{v_0}{v_i} = b_1, \tag{54}$$

which is the same result that was obtained when cavity dissipation was neglected. Thus, it is seen that the voltage stepup is proportional to the *square root* of the input Q (similarly the voltage stepdown is proportional to the square root of the output Q). This could have been anticipated on a conservation-of-energy basis, since the admittance transformation is proportional to the external Q.

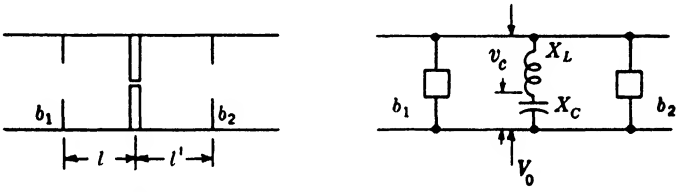

(a) (b)

FIG. 2·14.—Cavity with capacitive posts and equivalent circuit.

A practical TR tube will differ from this cavity in that it will have a pair of posts across the guide at a voltage maximum to form a small spark gap, Fig. 2·14*a*. The gap, of course, adds a capacitive load across the cavity. However, more detailed examination indicates that there is an inductive reactance in each of the posts forming the gap and, therefore, the equivalent circuit is similar to that of Fig. 2·14*b*. The net susceptance across the center of the cavity is

$$jb_0 = -j(X_L - X_C)^{-1}.$$

In a similar manner it can be shown that the voltage stepup ratio from the external terminals to the center of the cavity is proportional to the corresponding external Q. However, the voltage across the gap v_c is greater than the cavity voltage V_0 by a factor

$$\frac{v_c}{V_0} = \frac{X_C}{X_C - X_L} = \frac{b_L}{b_L - b_C}, \tag{55}$$

and the total transformation ratio is

$$\frac{v_c}{v_i} = b_1 \frac{b_L}{b_L - b_C}. \tag{56}$$

The Q of such a cavity can be shown to be

$$Q_{L2} \approx \frac{2\left(\frac{b_0^2}{4}+1\right) Kl \left(\frac{k}{K}\right)^2 + b_0}{\left(\frac{1}{b_1^2}+\frac{g_2}{b_1^2}+g_c\right)}, \tag{57}$$

where $Kl = \tan^{-1}\frac{2}{b_0} \approx \frac{\pi}{2} - \frac{b_0}{2}$ if b_1 and $b_2 \gg b_0$.

Direct-coupling Attenuation.—During the transmitting period there is a discharge across the gap which for all practical purposes may be con-

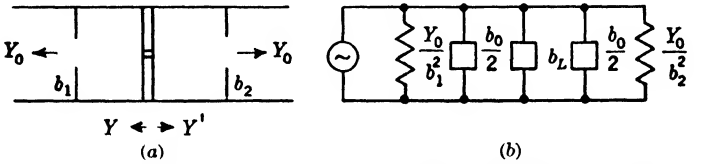

FIG. 2·15.—Cavity with short-circuited post and equivalent circuit.

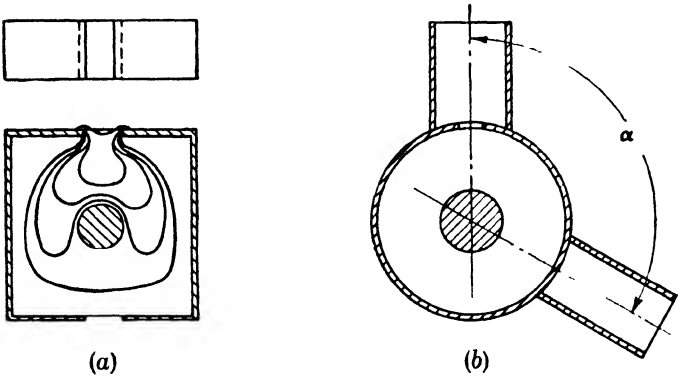

FIG. 2·16.—(*a*) Magnetic field in a cavity with short-circuited post. (*b*) Cylindrical cavity with two output lines.

sidered to have zero dynamic impedance. Since the discharge only short-circuits the capacitor X_C in Fig. 2·14, the total susceptance across the guide is not infinite, but is equal to $-jb_L$. As a result, the attenuation between the input and the output terminals will be large, but finite. To calculate the attenuation, all voltages and admittances are referred to the center of the cavity, Fig. 2·15*a*. Toward the left from the post, there is an admittance $Y = 1/b_1^2 - jb_0/2$, and toward the right $Y' = g_2/b_2^2 - jb_0/2$ and, therefore, the circuit is that of Fig. 2·15*b*. The ratio of the power delivered to the load, g_2/b_2^2, to the available power is

$$\frac{P}{P_{max}} \approx \frac{4g_2}{b_1^2 b_2^2 (b_0 + b_L)^2}. \tag{58}$$

Thus, the direct-coupled power is inversely proportional to the product

of the external Q's, and it also varies inversely with the square of the post susceptance b_L.

A qualitative but useful concept of direct-coupling attenuation assumes that the cavity short-circuited by the post, Fig. 2·16*a*, may be thought of as two waveguides in parallel that are beyond cutoff at the operating frequency. The incident power is exponentially attenuated between the input and output terminals of the cavity, and the attenuation increases with the diameter of the center post. This, of course, is simply a restatement of the fact that the attenuation increases with the post susceptance. If a cylindrical cavity is considered, Fig. 2·16*b*, it becomes apparent that the attenuation decreases rapidly as the angle α between the input and the output lines is made less than 180°.

2·4. Comparison of Loop-coupled and Iris-coupled Cavities.—In the analysis of resonant cavities thus far, it has been assumed that the external cavities have been connected to the resonant structure by *direct* inductive or capacitive coupling. That is, it has been assumed that there is no mutual reactance between the couplings and the resonant circuit. The equivalent circuit assumed may be either the simple one in Sec. 2·1 or the more exact one shown in Fig. 2·11*b*. A better representation of the TR tube is shown in Fig. 2·17 where b_1 and b_2 are the coupling susceptances, b_0 is the equivalent capacitive susceptance of the gap and posts across the cavity, g_c is the shunt conductance of the cavity. If $b_l = b_1 b_0/(2b_1 \times b_0)$, and b_l' is similarly defined for b_2 and if b_1 and b_2 are large,

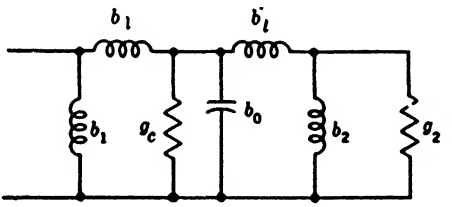

FIG. 2·17.—Equivalent circuit of TR tube including losses.

$$\left.\begin{aligned} b_l &\approx \frac{b_0}{2}\left(1 + \frac{b_0}{2b_1}\right) \\ b_l' &\approx \frac{b_0}{2}\left(1 + \frac{b_0}{2b_2}\right) \end{aligned}\right\}. \tag{59}$$

All these calculations and equivalent circuits are based on the assumption that no mutual couplings exist between b_1 and b_2 and the rest of the circuit. This condition is satisfied if thin inductive or capacitive irises are used for b_1 and b_2, Fig. 2·18*a*.[1] However, coupling to a cavity can be done equally well by means of a loop linking the magnetic field of the cavity, Fig. 2·18*b*. If this is done, it is necessary to consider the mutual coupling between loop and cavity, and the equivalent circuit may be

[1] For equivalent circuits of various obstacles in waveguides, see "Wave Guide Handbook," RL Report No. 43-2/7/44, and Vol. 10 of this series.

drawn as in Fig. 2·19. It has been shown by W. W. Hansen[1] that the transformed conductance seen at the input terminals varies inversely with the square of the mutual conductances M_1 and M_2 for b_1 and b_2 large,

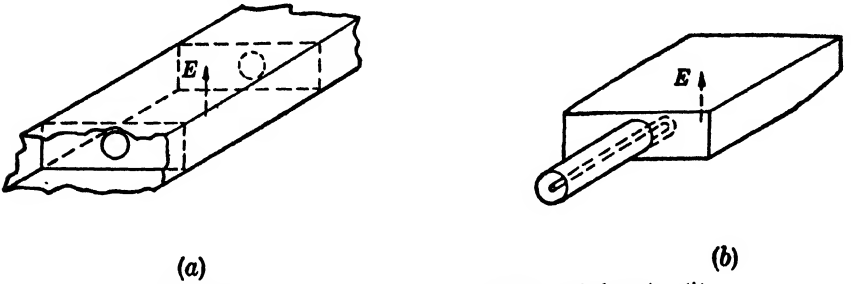

FIG. 2·18.—Iris-coupled cavity (*a*) and loop-coupled cavity (*b*).

($b_1 = 1/\omega L_1$). The mutual inductance is proportional to the loop area and at resonance

$$G_i = G_c(A/\Sigma_i)^2 + G_2(\Sigma_o/\Sigma_i)^2 \tag{60}$$

where G_i is the input conductance, A is the area of the cavity in a plane parallel to the E vector, Σ_i and Σ_o are the areas of the input and output loops, and G_c is the cavity shunt conductance.

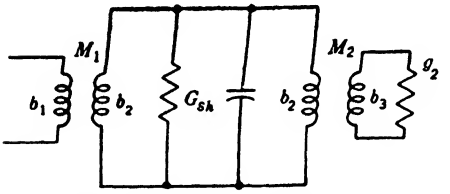

FIG. 2·19.—Equivalent circuit of loop-coupled cavity.

In a similar manner, expressions for Q and direct coupling which are completely analogous to those for the iris-coupled cavity can be derived.

Although a detailed discussion of methods for coupling to cavities will be reserved for a later section, it is of interest to make a simple

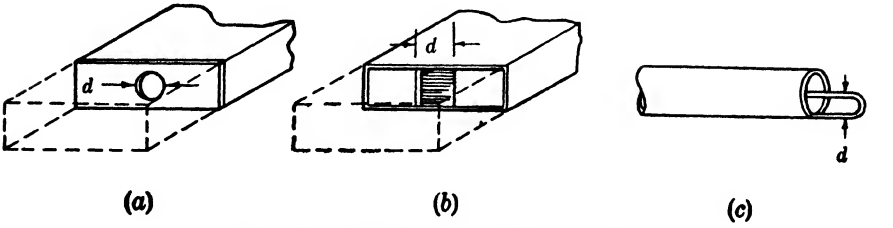

FIG. 2·20.—Methods of coupling to a cavity.

comparison between loop and iris coupling. There are three cases to be considered:

1. If the coupling iris is a small circular hole in a thin plate, Fig. 2·20*a*, the susceptance is inductive and varies nearly as d^{-3}.

[1] W. W. Hansen, *J. App. Phys.*, **9**, 654 to 663 (1938).

2. If the iris is symmetrical, of the type shown in Fig. 2·20*b*, the susceptance is inductive and varies nearly as d^{-2}.
3. If the coupling is a small loop, Fig. 2·20*c*, the inductance is proportional to its length and the susceptance, then, varies as d^{-1}.

The admittance transformation ratio N in these three cases may be tabulated as in Table 2·1.

TABLE 2·1.—ADMITTANCE TRANSFORMATION RATIO N FOR THREE CASES

Coupling	N varies as
Circular iris	b^2, d^{-6}
Symmetrical inductive iris	b^2, d^{-4}
Small loop	b^4, d^{-4}

It should be pointed out that these variations are for small loops or irises. For irises it is further assumed that the metal plate is very thin. As the opening of the iris or the length of the loop is made larger, the rate of change of b with d becomes slower. The rates indicated in the last column may be deceptive because, although the tolerance on the circular iris is the most severe, a round hole may be made to much closer tolerances than is possible with the other structures.

A symmetrical inductive iris is more difficult to make to accurate tolerances; but most difficult of all is the loop which is made of fairly thick wire, to give it rigidity, but is bent on a radius which is only a few times the thickness of the wire. Despite this difficulty, it was possible to make coupling loops for 10-cm TR tubes in which the admittance transformation ratio was held to a tolerance of about ± 10 per cent.

2·5. Methods of Tuning.—It is usually required that a given TR tube operate anywhere within a band of frequencies that is wide compared with its bandwidth ($\Delta\omega \gg \omega/Q$). The resonant circuit, therefore, must be made tunable. From a consideration of Fig. 2·17 it is seen that variation of either the gap capacitance or the cavity inductance changes the resonant frequency. It is not desirable to tune by varying the coupling susceptances since the insertion loss and leakage power change rapidly while the tuning rate remains very slow.

Variation of the gap capacitance is a convenient method of tuning if the mechanical design of the tube permits a mechanical motion to be transmitted into the low-pressure region where the spark gap is located. Several TR tubes have been designed with such a tuning system. The high-frequency end of the tuning range is generally limited by the leakage power, which increases with the gap length. It is usually possible in this way to get a tuning range of 10 to 15 per cent and still maintain satisfactory leakage power levels.

The inductance of the circuit may be changed by a variety of mechanical schemes. Basically, what is desired is to change the magnetic field strength in a given region, and thus change the energy storage or the

inductance. A vane across a waveguide acts as an inductive lumped susceptance, Fig. 2·21, because it causes a local concentration of the magnetic field. Thus, the cavity can be made tunable as shown in Fig. 2·22. Sliding irises which continually make good contact with the

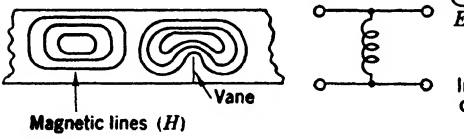

FIG. 2·21.—Waveguide with inductive vane.

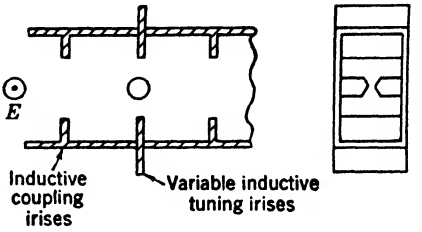

FIG. 2·22.—Variable inductive irises for tuning a cavity.

top and the bottom of the guide present a design problem which is mechanically very difficult. Figure 2·23 shows an equivalent scheme commonly used with cell-type TR tubes. In tubes of this type the gap and low-pressure region are confined within a glass envelope whose diameter is small compared with the cavity diameter. A metal slug,

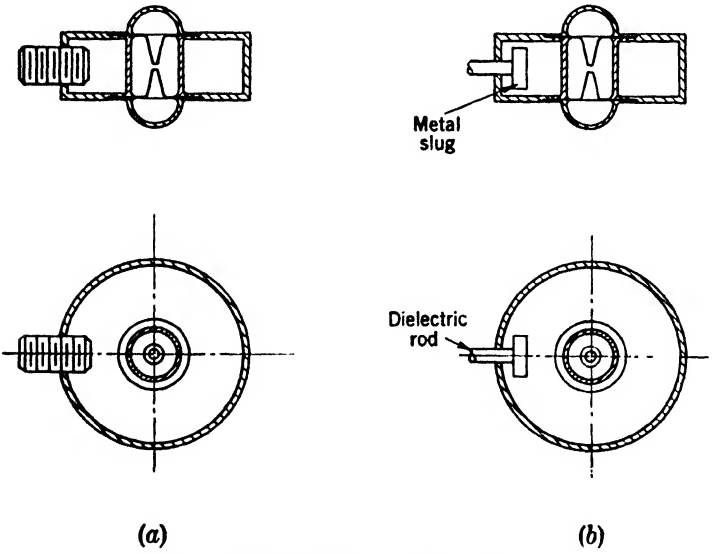

FIG. 2·23.—Metal slugs for tuning a TR cavity.

usually a screw, is pushed into the cavity. This adds a lumped inductance in parallel with the rest of the circuit, and the frequency *increases as the slug is pushed into the cavity.* A change in the cavity diameter has an equivalent effect, and in fact, the slug may be considered simply as a partial change in the equivalent cavity diameter.

A third method of tuning involves changing the total circuit capacitance by means of a metal slug that can be moved in and out radially, but which is insulated from the cavity, Fig. 2·23*b*. Although the geometric capacitance of the slug does not vary with position, the electric field varies from a maximum at the center to zero at the outside of the cavity. The displacement currents flowing through the capacitance between the slug and cavity increase as the slug is moved toward the center. *Moving the capacitive slug toward the center decreases the resonant frequency of the cavity.*

A method that is markedly different from those just described employs an auxiliary cavity tuned by one of these methods, and coupled to the main TR cavity in such a way as to act as a variable susceptance in parallel with it. The susceptance can take on positive or negative values as the auxiliary cavity is tuned to higher or lower frequencies than the incident frequency. In general, this scheme introduces a certain amount of excess loss into the circuit. It has the advantage, however, that a precise tuning mechanism may be built into it which may be calibrated. This is not generally possible in the TR cavity. The two cavities may be butted together and coupled by an iris, or they may be joined by a transmission line about $\lambda/2$ long and coupled either by loops or by irises.

2·6. Equivalent-circuit Calculations. *Insertion Loss.*—In previous sections it was shown that a resonant cavity could be represented to a good approximation by an equivalent parallel-resonant circuit. The plane of reference is arbitrary; but it is generally convenient to refer all admittances to the input terminals. This is indicated in Fig. 2·24 where all admittances have been normalized with respect to Y_0, $g_c' = g_c b_1^2$ is the apparent cavity conductance, $g_L = g_2(b_1/b_2)^2$ is the apparent load conductance, and b is the input susceptance. On the basis of this simple circuit, a number of useful relationships involving Q, insertion loss, and input standing-wave ratio may be derived.

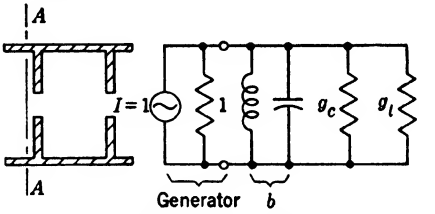

FIG. 2·24.—Cavity and equivalent circuit referred to terminals AA.

The *transmission* T of the circuit is the ratio of the power dissipated in g_L to the power available from the generator. The *insertion loss* L will be defined as $-10 \log_{10} T$,

$$T = \frac{4g_L}{(1 + g_L + g_c')^2 + b^2}, \tag{61}$$

where the generator is assumed to have unit internal conductance.

Cavity Q.—In Sec. 2·2 an expression for Q was derived. Equation (52) may be rewritten in the following forms:

$$\left.\begin{aligned} Q_0 &= \frac{1}{2g_c'}\frac{db}{d(\ln k)} \\ Q_{L1} &= \frac{1}{2(g_c'+1)}\frac{db}{d(\ln k)} = Q_0\frac{g_c'}{g_c'+1} \\ Q_{L2} &= \frac{1}{2(g_c'+1+g_L)}\frac{db}{d(\ln k)} = Q_0\frac{g_c'}{g_c'+1+g_L} \end{aligned}\right\}, \tag{62}$$

where Q_0 is the unloaded Q of the cavity; Q_{L1} is the Q of the cavity loaded only at its input terminals by a matched generator; and Q_{L2} is the Q of the cavity loaded at both the input and output terminals.

The standing wave set up in a transmission line by a discontinuity is equal to the sum of the incident and the reflected waves. The ratio of the maximum voltage to the minimum voltage of the standing wave is the *standing-wave ratio* r, and is defined by

$$r = \frac{1+|\Gamma|}{1-|\Gamma|}, \tag{63}$$

where Γ is the voltage reflection coefficient. For the cavity whose input admittance is

$$\left.\begin{aligned} Y &= (g_L + g_c') + jb, \\ \Gamma &= \frac{Y_0 - Y}{Y_0 + Y} = \frac{1-[(g_L+g_c')+jb]}{1+[(g_L+g_c')+jb]}, \\ |\Gamma| &= \frac{\sqrt{(1-g_L-g_c')^2+b^2}}{\sqrt{(1+g_L+g_c')^2+b^2}}. \end{aligned}\right\} \tag{64}$$

If this is substituted into Eq. (63),

$$r = \frac{\sqrt{(1+g_L+g_c')^2+b^2}+\sqrt{(1-g_L-g_c')^2+b^2}}{\sqrt{(1+g_L+g_c')^2+b^2}-\sqrt{(1-g_L-g_c')^2+b^2}}. \tag{65}$$

Examination of Eq. (61) indicates that the power to the load g_L falls to half its maximum value when $|b| = (1+g_L+g_c)$, and for this condition the standing-wave ratio will be

$$r_{1/2} = \frac{(1+g_L+g_c')+\sqrt{1+(g_L+g_c')^2}}{(1+g_L+g_c')-\sqrt{1+(g_L+g_c')^2}}. \tag{66}$$

If the input standing-wave ratio at resonance is

$$r_0 = \beta^{-1} = \frac{1}{(g_L+g_c')},$$

then

$$r_{\frac{1}{2}} = \frac{1 + \beta + \sqrt{1 + \beta^2}}{1 + \beta - \sqrt{1 + \beta^2}}. \tag{67}$$

It should be noted that a substitution of $1/\beta$ for β results in the identical equation.

Similarly, Eq. (65) may be solved for b, and

$$b = \sqrt{\beta \frac{r^2 + 1}{r} - \beta^2 - 1}. \tag{68}$$

Figure 2·25 is a plot of the standing-wave ratio against frequency, measured at the input of a typical TR cavity with no output loading. A curve of b, calculated from the data by means of Eq. (67) s superimposed. The curve of b is a straight line over the range considered, which is what would be obtained from a simple parallel-resonant circuit.

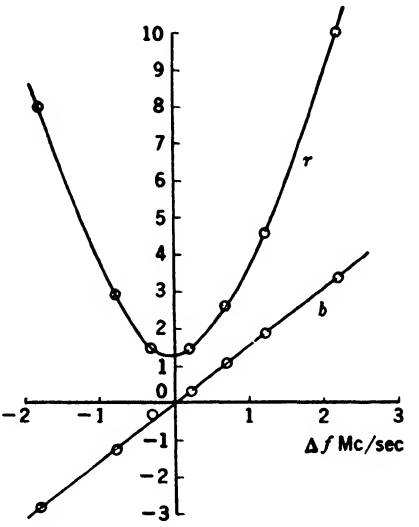

FIG. 2·25.—Input standing-wave ratio r, and susceptance b for a 1B27 TR cavity; $\beta = g'_c = 1.30$, $f_0 = 3260$ Mc/sec, $Q_0 = \frac{1}{2g'_c}\omega\frac{db}{dw} = 1910$.

Optimum Coupling.—Maximum power is delivered to the load g_L for a given g'_c when $g_L = 1 + g'_c$. Similarly, a reduction in g'_c results in an increase in T. It is generally necessary, however, to make the best possible compromise between leakage power and insertion loss.

Leakage power will be discussed in detail in Chap. 5; however, it has already been seen that the direct-coupled power varies inversely as the product of the input and output Q's for a given tube and cavity, and it will be seen later that the arc leakage power and spike leakage energy are substantially independent of the input Q, but vary inversely with the output Q.

It is important to choose the best operating point for a certain specified insertion loss that will give usable values of direct-coupled and arc leakage power, and spike leakage energy. Figure 2·26 is a plot of insertion loss L in db vs. g_L for various values of g'_c. It is obvious that there are an infinite number of combinations of g_L and g'_c that will give the same loss. Since the arc leakage power and spike energy increase with increasing g_L, only values of $g_L \leqq (1 + g'_c)$ will be chosen.

Let us investigate the conditions that give maximum direct-coupling attenuation for a given value of L. In Eq. (61) let $b = 0$ and substitute the following quantities: $g'_c = N_1 g_c$, $g_L = N_1/N_2$. Then solve for the product N_1N_2 which is proportional to the direct-coupling attenuation,

$$N_1N_2 = \frac{N_1^2}{\frac{2}{T} - 1 - N_1 g_c \pm 2\sqrt{\frac{1}{T^2} - \frac{1}{T} - \frac{N_1 g_c}{T}}}. \tag{69}$$

If the derivative $d(N_1N_2)/dN_1$ is set equal to zero, a solution for the points

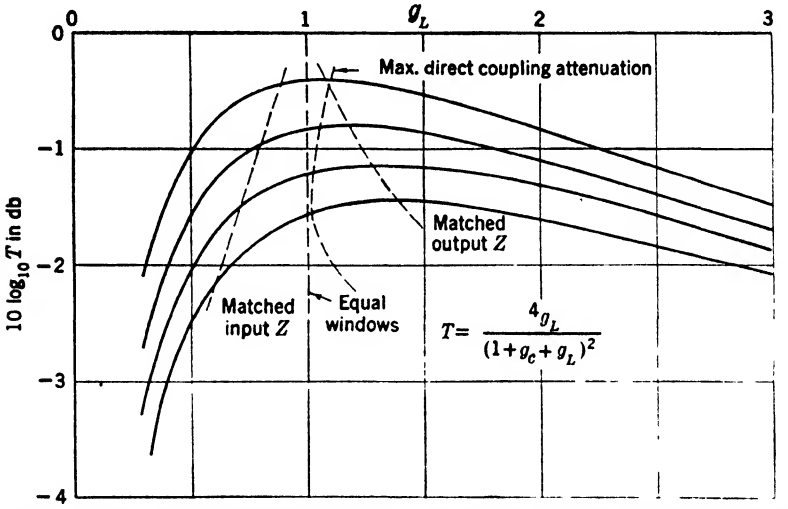

FIG. 2·26.—Plot of insertion loss in decibels as a function of g_L for various values of g'_c.

of maximum or minimum direct-coupling attenuation for a given value of low-level transmission may be obtained,

$$\frac{d(N_1N_2)}{dN_1} = N_1^2 + N_1^2\frac{5}{g_c} + N_1\frac{4}{g_c^2}\left(2 - \frac{1}{T}\right) + \frac{4}{g_c^2}\left(1 - \frac{1}{T}\right) = 0. \tag{70}$$

The roots of this equation are most easily found by assuming specific values of T, and then using Horner's method or some similar approximation. Only positive, real roots are of interest. Investigation shows that these roots do indeed correspond to a maximum value of N_1N_2, and, therefore, represent maximum attenuation. These solutions are plotted in Fig. 2·26 superimposed on the loss contours as the locus of points giving maximum direct-coupling attenuation. For values of $g'_c > 0.1$, the optimum coupling condition lies somewhere between "equal" coupling ($N_1 = N_2$), and "matched-output" coupling ($g_L = 1 + g'_c$ or $N_2 = 1 + N_1 g_c$).

For best performance in the receiving period it is desirable to use a "matched-output" coupling since variations in the load conductance g_L cause the least change of T in this region. This is important because of the comparatively large variations that are found in the admittance of crystal detectors. The conductance spread may be as large as 4 to 1 (from $g_x = Y_0/2$ to $2Y_0$), even after the crystal mount has been designed to minimize this spread. In Table 2·2 the insertion loss L in decibels and relative leakage power are listed corresponding to a crystal conductance $g_x = Y_0/2,\ Y_0,\ 2Y_0$. The leakage power has been separated into direct-coupled power, and gas (flat or spike) leakage power. The latter is simply proportional to N_2^{-1} while the former is proportional to $(N_1N_2)^{-1}$.

TABLE 2·2.—COMPARISON OF INSERTION LOSS, GAS LEAKAGE POWER, AND DIRECT-COUPLED POWER FOR THREE DIFFERENT COUPLING CONDITIONS
All adjusted to $L = -1.25$ db for $g_x = 1$

	Insertion loss db			Gas leakage power			Direct-coupled power		
$\frac{g_x}{Y_0}$	Matched input	Equal coupling	Matched output	Matched input	Equal coupling	Matched output	Matched input	Equal coupling	Matched output
0.5	−2.46	−2.14	−1.76	0.375	0.5	0.666	0.57	0.5	0.58
1	−1.25	−1.25	−1.25	0.75	1	1.33	1.15	1	1.16
2	−1.0	−1.06	−1 76	1.5	2	2.66	2.3	2	2.32

Examination of Table 2.2 indicates that the direct-coupled power is a rather insensitive function of the particular coupling. The insertion loss undergoes the largest excursions with matched-input coupling. Conversely, the leakage power is smallest for matched-input and largest

TABLE 2·3.—SUMMARY OF FORMULAS FOR COUPLING THROUGH A TR CAVITY

	Matched input	Equal coupling	Matched output
Input standing-wave ratio	1	$1 + g_c' = 2\left(\frac{1}{\sqrt{T}} - 1\right)$	$1 + 2g_c'$
T	$1 - g_c' = 1 - 2\rho$	$\left(1 + \frac{g_c'}{2}\right)^{-2} = (1 - \rho)^2$	$(1 + g_c')^{-1} = 1 - 2\rho$
$\rho = \frac{Q_{L2}}{Q_0}$	$\frac{g_c'}{2} = \frac{1 - T}{2}$	$\frac{g_c'}{2 + g_c'} = 1 - \sqrt{T}$	$\frac{g_c'}{2(1 + g_c')} = \frac{1 - T}{2}$
$\frac{Q_{L1}}{Q_0}$	$\frac{g_c'}{1 + g_c'} = \frac{1 - T}{2 - T}$	$\frac{g_c'}{1 + g_c'} = \frac{2(1 - \sqrt{T})}{2 - \sqrt{T}}$	$\frac{g_c'}{1 + g_c'} = 1 - T$

for matched-output coupling. Equal coupling has the advantage of ease of mechanical construction if the line to the receiver is of the same type as the transmitter line (same size coaxial line or waveguide), since the tube can be made symmetrical.

Special Cases.—A few special formulas may be derived for the three couplings just described and the results are shown in Table 2·3.

2·7. Electromagnetic Calculations of Cavities.—Although the basic phenomena of the resonant cavity are extremely simple, the exact calculation of the resonant frequency Q voltage-stepup ratio, and equivalent shunt conductance becomes very difficult when practical shapes of cavities must be analyzed. Fairly straightforward methods of analyzing cylindrical, spherical, and similar cavities have been derived by a number of authors.[1,2] For TR cavities or klystron cavities (rhumbatrons), the fields can no longer be expressed by simple functions, but must be compounded out of a sum of many different modes, so adjusted as to satisfy the boundary conditions that tangential **E** is zero at the metal walls.

At the present time, an exact solution has not been obtained for the cylindrical cavity with conical posts. Extremely accurate calculations have been made, however, in which the posts were assumed to be right circular cylinders, and where suitable means of estimating the equivalent diameter of the cylinder were determined.[3,4,5] By these means it has been possible to calculate the resonant frequency with an error of less than 1 per cent.

The mathematical techniques used in these calculations will not be discussed here since they are long and involved. The solutions obtained, however, give the resonant frequency in terms of an effective parallel L and C, where the C is a function of the static capacitance of the post, and L is associated with the energy storage in the annular ring between the posts and the outer walls.

A more recent and advanced method in the art of treating cylindrical resonant cavities has been used by N. Marcuvitz of the Radiation Laboratory. This method[6] considers the cavity as composed of several radial transmission lines of various impedances (heights) and lengths (radii). Although this method has not been applied to TR cavities, its use would

[1] W. W. Hansen, *Jour. App. Physics* **9**, 654 (1938); **10**, 38 (1939).

[2] S. A. Schelkunoff, *Electromagnetic Waves*, Van Nostrand, N. Y., 1943.

[3] H. A. Bethe, R. E. Marshak, J. Schwinger, "Theoretical Results on the TR Box," NDRC Report D1-116, Jan. 20, 1943.

[4] H. A. Bethe, R. E. Marshak, J. Schwinger, "Theory of the TR Box," NDRC Report 14-128, May 14, 1943.

[5] J. Schwinger, "Theoretical Treatment of a Cylindrical TR Box," RL Group Report 43-8/26/42.

[6] Vol. 8, Chap. 8.

result in great mathematical simplification, when radial-transmission-line charts become available.

The coupling between the cavity and an external load or source of power may take any of several forms. It may be a small hole in the wall of the cavity, a loop, or a capacitive probe. The first two, the hole and the loop, are used almost exclusively in TR cavities. The small hole or iris is equivalent to the large shunt inductive susceptances in the equivalent circuits of Secs. 2·1 and 2·2; the loop has been briefly described in Sec. 2·3.

The calculation of the power flow through an iris involves the matching of three fields: the unperturbed field in the cavity, the unperturbed field in the waveguide or space into which the iris allows power to flow, and the field in the immediate vicinity of the iris. Here again, the mathematical complications grow roughly exponentially with the size of the hole. If the hole is very small, then it can be assumed that the field in the cavity and waveguide are completely undisturbed by the presence of the hole, except in its immediate vicinity. Furthermore, it can be assumed that the tangential **H** will be constant in magnitude and phase over the entire window. With these limiting assumptions, it has been possible to calculate correctly the loading and frequency shift caused by inductive irises in TR cavities.[1,2,3,4]

Loop coupling, although basically very simple, is complicated by the finite thickness of the wire and the standing wave along the loop. As a result, no accurate solutions exist for this problem.

2·8. Cell-type TR Tubes. *Tube Types.*—The cell-type TR tube is a unit consisting of a spark gap in a low-pressure gaseous atmosphere, enclosed in a glass envelope. Electrodes are brought out through the glass for connecting to an external cavity, which in combination with the TR tube is a resonant circuit. The tube is placed in the cavity so that there is a maximum voltage across the gap.

One of the earliest 10-cm microwave TR tubes is shown in Fig. 2·27. It was developed by J. L. Lawson at the Radiation Laboratory, and consisted of a spark gap in a small glass tube which plugged into a cavity. The leakage power of this tube was undoubtedly high, and because of the small gas volume its life was short; however, it had only to protect a grounded-grid-triode first detector, which it did. The first "modern"

[1] H. A. Bethe, "Lumped Constants for Small Irises," RL Report 43-22, Mar. 22, 1943.

[2] H. A. Bethe, "Theory of Side Windows in Waveguides," RL Report 199, Apr. 4, 1943

[3] H. A. Bethe, "Excitation of Cavities through Windows," RL Report 202, Apr. 9, 1943.

[4] H. A. Bethe, "Theory of Diffraction by Small Holes," RL Report 128, Jan. 23, 1942.

microwave TR tube was the so-called soft Sutton tube developed by the simple expedient of admitting gas into a Sutton reflex klystron tube and using it, cavity and all, as a TR tube. One cavity and three tubes were used to tune the three bands 9.1 cm ± 1 per cent, 10 cm ± 1 per cent, and 10.7 cm ± 1 per cent. The tubes were identical except that they were pretuned by varying the gap spacing before they were evacuated.

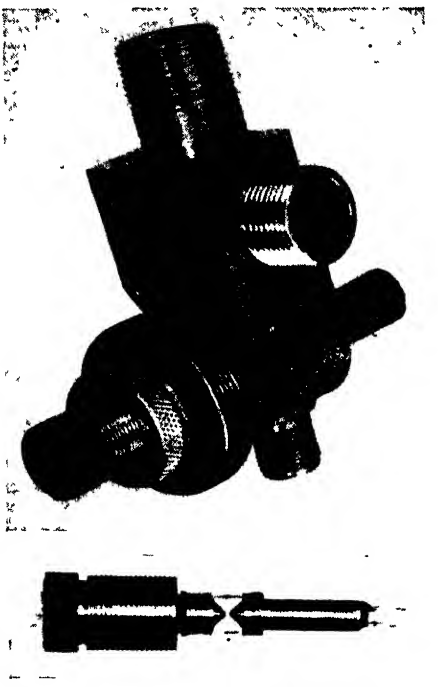

FIG. 2·27.—Early 10-cm TR tube.

The 721A TR tube and later the 724A tube, were engineered by a group under A. L. Samuel at the Bell Telephone Laboratories.[1] These two tubes are used in the 9-cm to 11-cm and 3.1-cm to 3.5-cm bands respectively, and, together with the 1B27 tube developed cooperatively by the Radiation Laboratory and Sylvania Electrical Products Company, are the most widely used microwave cell-type TR tubes. They are illustrated in Fig. 2·28. The spark gap is formed between the small ends of two copper cones. The cones are drawn from thin copper sheet and have circular flanges at their bases. A cylinder of low-loss glass separates the two flanges. In order to make a butt seal between the glass and the copper, it is necessary to balance the strains by simultaneously sealing glass cylinders to the backs of the flanges, as in Fig. 2·29. After the disk seals have been made, the keep-alive electrode is sealed in at one end, the tube is pretuned and evacuated, and the other end is sealed off.

Two other microwave cell-type TR tubes that have been used at longer wavelengths (about 25 cm) are the 1B23 tube and the 1B40 tube. The spark gap in the 1B23 tube, Fig. 2·30, is between the *inside of the cone* and the wire electrode. The 1B40 tube is different from any of the other tubes in this group, in that it has no r-f electrodes within the glass envelope. It is used with a cavity such as that shown in Fig. 2·31, and an *electrodeless* discharge is struck between the two cylinders of the

[1] Samuel, McCrae, and Mumford, "Gas Discharge TR Switch," BTL MM-42-140-26, Apr 17, 1942.

external cavity. Although this simplifies the design, the leakage power of this tube is very large and is tolerable only in certain special applica-

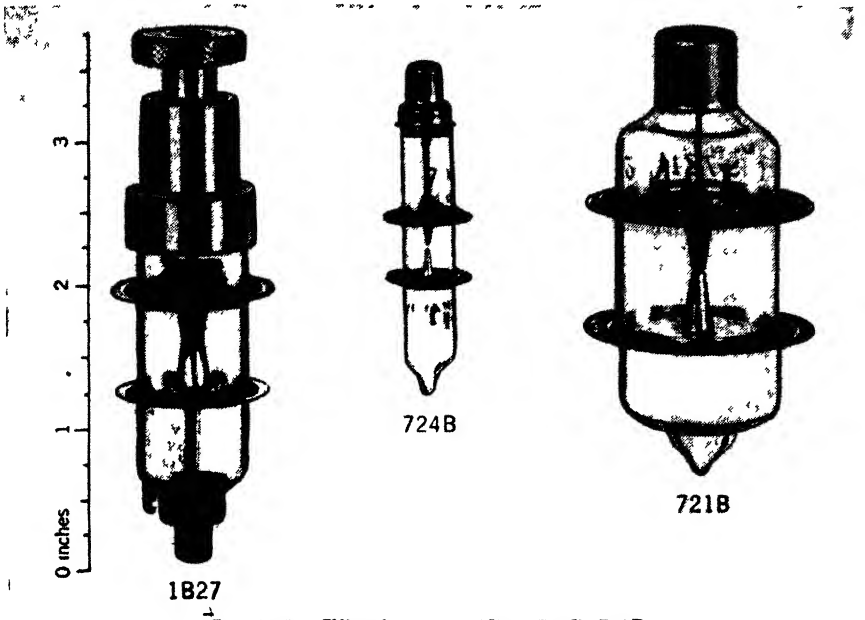

FIG. 2·28 TR tubes types 1B27, 724B, 721B.

tions. The construction is very simple for it involves only Kovar-glass seals

The cell-type TR tubes have the advantage that they may be used in a variety of circuits and cavities, and over a wide range of frequencies. With suitable cavities the 1B27 tube has been used at wavelengths ranging from 8 cm to 13 cm. The 721B, 724B, 1B23, and 1B40 tubes are *fixed-tuned* tubes By varying the spacing each is adjusted to resonate at a specified frequency in a cavity of standard dimensions. Once the tube is sealed off, no further adjustments of gap spacing can be made, and the complete TR assembly is tuned by inductive or capacitive slugs in the external cavity as described in Sec. 2·5. The 1B27 is a tunable tube. The gap spacing may be varied by means of a differential screw mechanism that moves one of the cones in or out. The cone is sealed, of

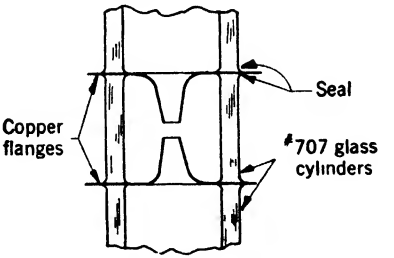

FIG. 2·29 — First stage in assembling cell-type TR tube Glass cylinders are sealed simultaneously to both sides of the flanges

course, to maintain a low-pressure region around the gap. In a given cavity, it is possible to tune the 1B27 tube from 10 to 15 per cent.

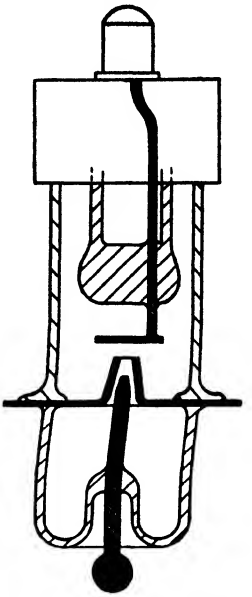

FIG. 2·30.—1B23 TR tube.

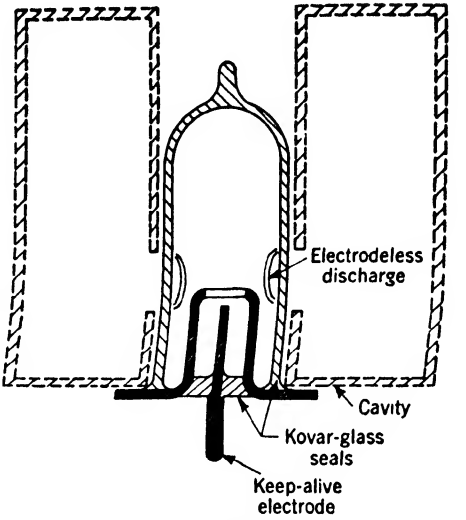

FIG. 2·31.—1B40 TR tube.

The critical dimensions of the 721B, 724B, and 1B27 tubes are shown in Fig. 2·32. These dimensions are the glass diameter, the distance between flanges, the cone angle, the gap spacing, the cone diameter, and the flange diameters. Table 2·4 gives the dimensions of these three tubes.

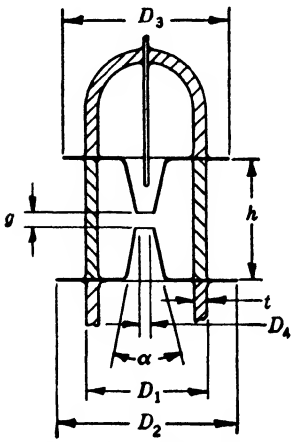

FIG. 2·32.—Critical dimensions of 721B, 724B, and 1B27 tubes given in Table 2·4.

The use of high-Q cavities with large admittance transformation ratios requires that the losses in the cavity be held to a minimum. The glass cylinder between the disks of the TR tube is in a region of moderately high field. The dielectric loss in the glass can make a considerable contribution to the effective shunt conductance g_c of the cavity. Corning 707 glass has the lowest dielectric loss of any of the common glasses. Only fused quartz and Corning "Vicor" 709 glass, which is about 90 per cent quartz, have lower losses. These, however, cannot be sealed to copper because of their high melting points and low coefficients of expansion. In Table 2·5

TABLE 2·4.—CRITICAL DIMENSIONS OF CELL-TYPE TR TUBES AS INDICATED IN FIG. 2·32

Dimensions are in Inches

Dimensions	721B	724B	1B27
D_1	$1\frac{1}{8}$	0.372	$\frac{3}{4} \pm \frac{1}{32}$
D_2	$1\frac{1}{2} \pm \frac{1}{64}$	0 622 max. 0 615 min.	1.062
D_3	$1\frac{1}{2} \pm \frac{1}{64}$	0 622 max. 0 615 min.	1.000
D_4	0 075	0 020	0 125
g	0.030	0 030	0 002 to 0 035
α	18°	18°	18°
h	0 825	0 410	0.670
t	0 030	0 030	0 030

the complex dielectric constant $\epsilon = \epsilon' + j\epsilon''$ is given for Corning 707 glass and 705 glass.

TABLE 2·5.—COMPLEX DIELECTRIC CONSTANT OF 707 AND 705 GLASSES

λ	707 glass		705 glass	
	ϵ'	ϵ''/ϵ'	ϵ'	ϵ''/ϵ'
25 cm	4 0	0 0019	4 72	0 0047
10 cm	4 0	0 0019	4 72	0 0052
3 2 cm	3 99	0 0021	4 71	0 0061

The copper flanges extending beyond the glass are made thin so that they can be deformed by the clamping rings of the cavity, and can also be pressed tightly against the cavity shoulder without breaking the glass seal. This allows the resistance of the contact between the flanges and the cavity to be held to a minimum.

Cavities and Tuning.—The TR cavity most commonly used in the 3-cm and 10-cm bands is illustrated in Fig. 2·33. It is cylindrical, and operates in what may be described as a modified TE_{010}-mode. There is no variation of the field with angle, and except in the vicinity of the posts, there is no variation of E between the top and the bottom of the cavity.

For a given tube, the height h of the cavity is usually maintained constant, and the diameter D is varied to make cavities for various tuning ranges. To permit the tube to be connected into the cavity, the cavity is split into two halves along a diametral plane. Since the lines of current flow are radial on the top and bottom faces, the break between the two

halves of the cavity does not cut any current lines, and therefore there are no losses from radiation or from poor contacts.

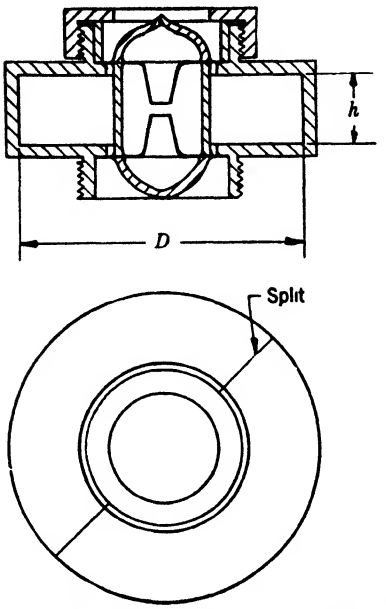

FIG. 2·33.—TR cavity for cell-type TR tubes.

Since the current flow in the top and bottom faces is radial, an intimate contact must be made between the tube flanges and the cavity in order to hold to a minimum the I^2R losses at the joint. This is done by exerting enough pressure to deform the flange and cause it to flow against the cavity. Figure 2·34 shows the details of two such arrangements. In Fig. 2·34*a* the clamping ring *A* is drawn down against the flange by six screws spaced around the circumference. This makes an excellent contact, but it is difficult to replace tubes quickly in such a cavity. Figure 2·34*b* shows an alternative method wherein a clamping nut *B* forces a ring *C* against a neoprene gasket *D*, which in turn presses against the tube flange. The gasket, by virtue of its flexibility, forces the flange to make good contact with the cavity despite any high spots on the cavity or misalignment between the ring and the cavity. The screw-clamping mechanism is commonly used on the 1B27 and 724B TR tubes,

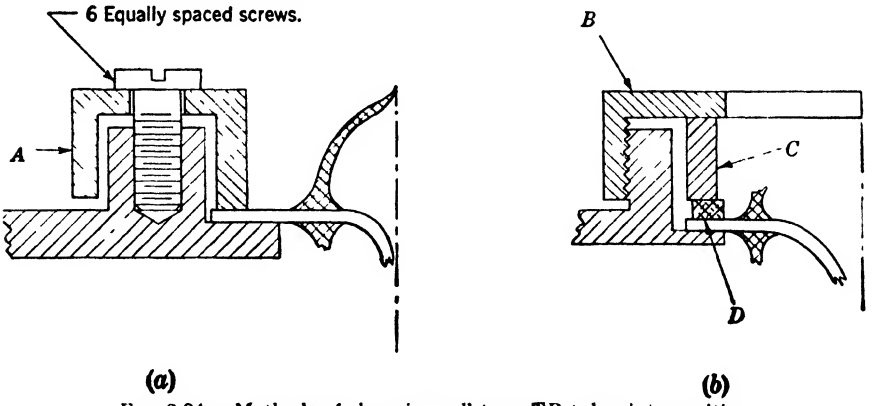

FIG. 2·34.—Methods of clamping cell-type TR tubes into cavities.

except that it has been found unnecessary to use the gasket on the 724B, presumably because of the small flange diameter. In the 1B27 tube (or

the 721B), failure to use the gasket may result in an increase of insertion loss of 1 or 2 db.

The fixed-tuned tubes (721B, 724B and 1B23) can each be characterized by a curve which gives the resonant wavelength as a function of cavity diameter. Figures 2·35 and 2·36 show these curves for the tubes, 721B and 724B. Figures 2·37 and 2·38 show a typical cavity and a tuning curve for the 1B23 tube. The curves are nominal, and production tubes lie within a band less than ±0.5 per cent around the average curve. The tubes are all pretuned in a standard cavity by changing the gap spacing before the tube is sealed off until resonance is obtained at a standard frequency. This means that if the cone diameter or glass thickness (for instance) varies from tube to tube, although

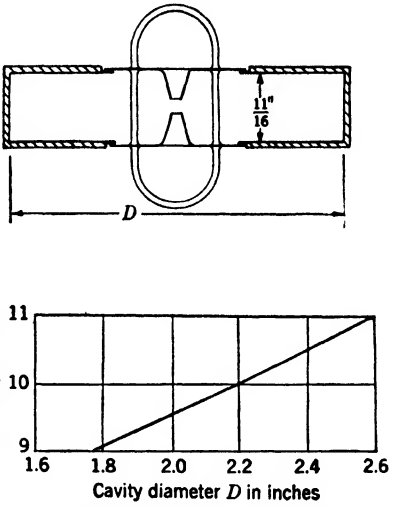

FIG. 2·35.—Tuning characteristics of 721B TR tube as a function of cavity diameter. The cavity is loop-coupled to a loaded Q of 300.

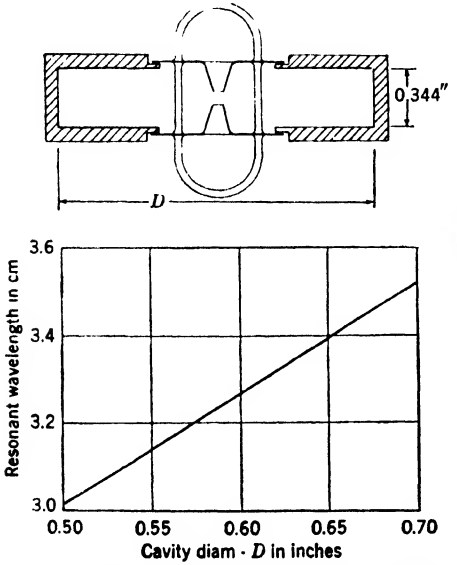

FIG. 2·36.—Tuning characteristics of 724B TR tube as a function of cavity diameter. The cavity is iris-coupled to a Q_{L_2} of 200.

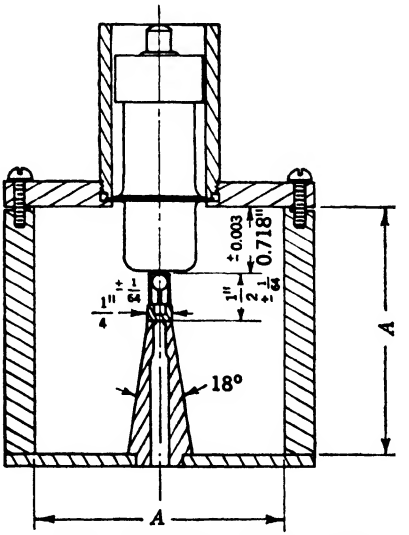

FIG. 2·37.—Cavity for 1B23 TR tubes.

the tuning will be correct at the standard frequency, for diameters larger or smaller than the standard cavity the slope of the λ vs. D curve will vary and the spread will increase.

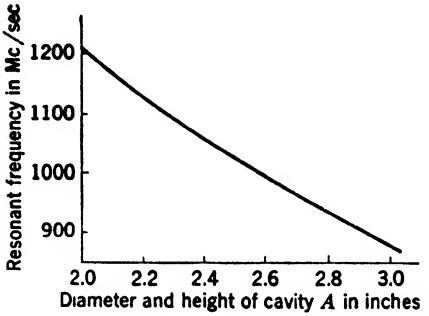

FIG 2·38.—Tuning curve for 1B23 TR tube for cavity shown in Fig. 2·37. (*Data are from Western Electric Co*)

Figure 2·39 shows the tuning effect of inductive tuning plugs on the resonant wavelength of cavities of various diameters. Two plugs, diametrically opposite, are inserted equal distances for these curves. The mechanical design of inductive tuning plugs is difficult. Figure 2·40 shows two possible constructions. The tuning screw in Fig. 2·40*a* is required to make good contact only somewhere near the cavity wall, as indicated. Its tuning range, however, is small. If the $\frac{3}{4}$-in. screws shown in Fig. 2·39 were replaced by $\frac{5}{8}$-in. screws, the tuning range ($\Delta\lambda/\lambda$) would be only about 2 to 3 per cent, as compared with the 10 to 15 per cent obtained with the large screws. The screw shown in Fig. 2·40*b* completely fills the space between the top and the bottom of the cavity, and the tuning ranges indicated are obtained. To be effective, however, the screw must make a good electrical contact with the cavity at its *inner end*, as shown in the drawing. This is a difficult condition to satisfy. The threads in the cavity wall only span about 15° to 20° and they lack precision for, in order to facilitate production, they are tapped rather than machine cut. Furthermore, because the threads must be silver-plated, it is not possible to specify a tight fit because the plating jams the threads, and makes it difficult or even impossible to turn the screws by hand. As a result, when the lock nut is loosened, the resonant wavelength of the cavity may jump back and forth erratically as the contact changes, and, therefore, make it very

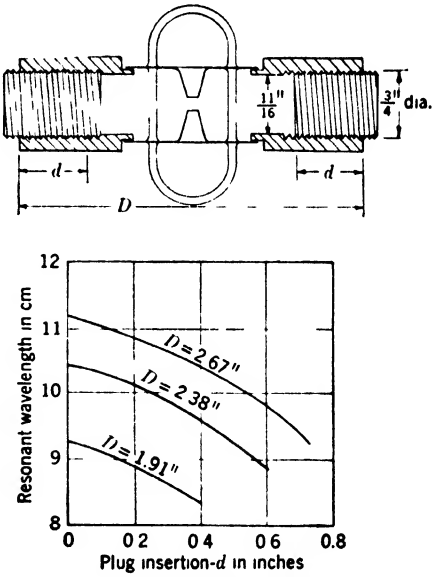

FIG. 2·39.—Tuning characteristics of 721B TR tube as a function of plug insertion, $Q_{L2} = 300$.

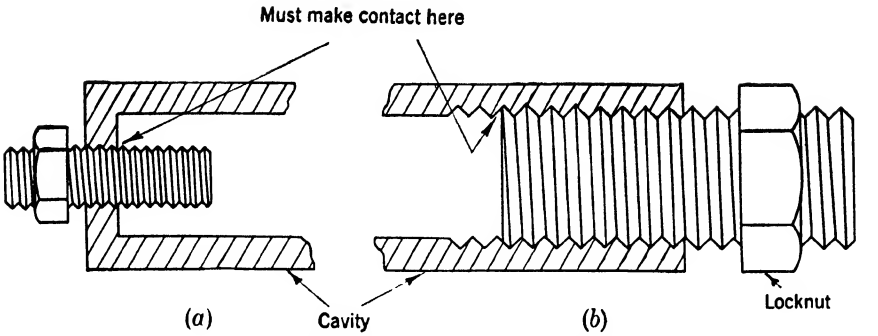

FIG. 2·40.—Inductive tuning screws.

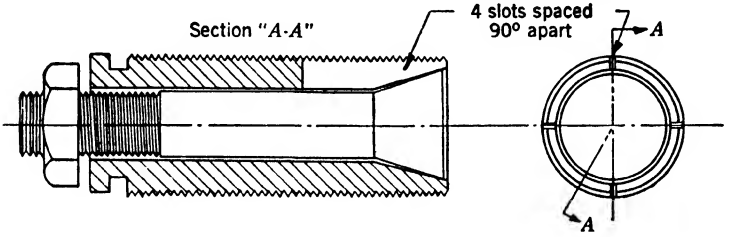

FIG. 2·41. Expanding inductive tuning screw.

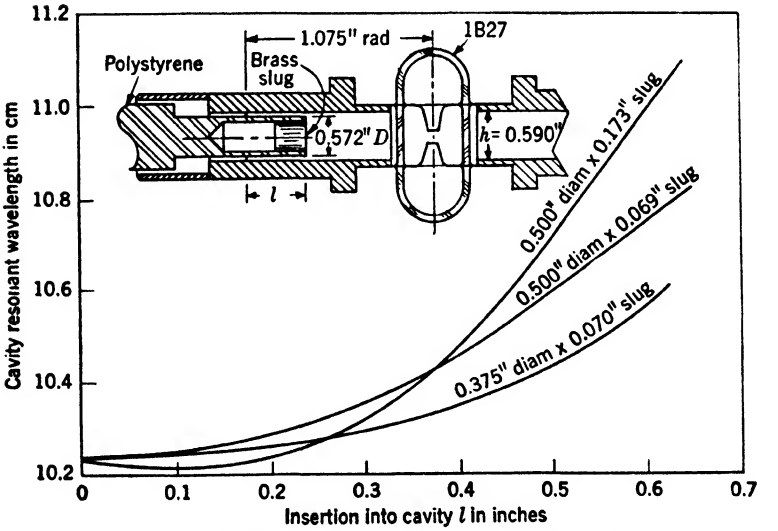

FIG. 2·42.—Capacitive tuning slug in 2.15-in. diameter 1B27 cavity.

difficult to tune the cavity to a new wavelength. These effects become worse as the radial travel of the tuning screw increases. In 10-cm tubes these effects are pronounced, whereas in 3-cm tubes they are hardly noticeable.

In order to overcome this contact trouble, a number of schemes have been considered. It is possible to use spring loading, but in order to maintain constant pressure on the screw, the spring must be several times as long as the maximum travel of the screw. This makes the cavity assembly very large and bulky. Figure 2·41 shows an expanding tuning screw that has been used successfully. It allows a continuously variable pressure to be exerted between the end of the screw and the cavity, and thus permits the operator to loosen it to the point where it can just be turned by hand and still maintain a good contact during rotation.

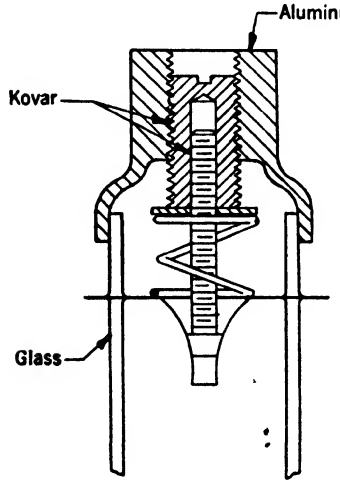

FIG. 2·43.

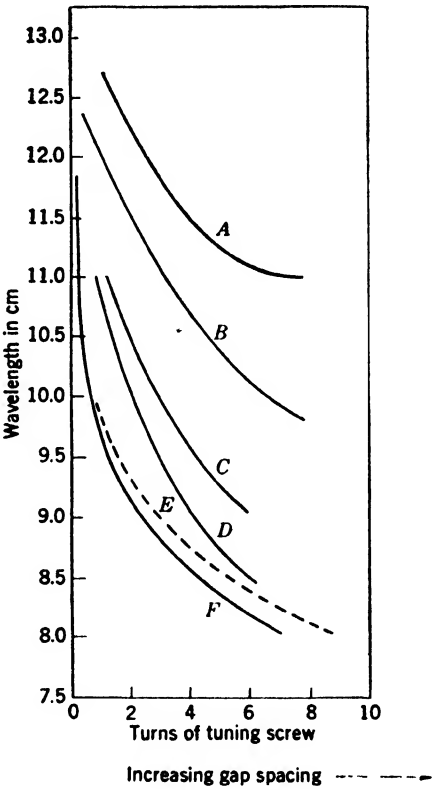

FIG. 2·44.

FIG. 2·43.—Differential tuning-screw mechanism for 1B27 TR tube.

FIG. 2·44.—Tuning range of 1B27 TR tube in various cavities: Curve *A*, coaxial cavity; Curve *B*, cavity 2.150″ ID on 1½″ × 3″ waveguide; Curve *C*, 1.800″ ID cavity loop-coupled to ⅞″ coaxial line; Curve *D*, 1.550″ ID cavity loop-coupled to ⅞″ coaxial line; Curve *E*, 1.400″ ID ATR cavity on 1½″ × 3″ guide; Curve *F* 1.400″ ID cavity on 1½″ × 3″ guide.

Figure 2·42 indicates the tuning ranges which can be obtained with a capacitive tuning slug. Since no electrical contacts are involved, the tuning is very smooth. No measurements of the loss introduced by the

currents in the slug, or by the presence of the polystyrene sleeve around the slug have been made, but casual observations indicate that they are not excessive.

Capacitive tuning slugs have found very little use thus far, partly because of the mechanical-design difficulties associated with getting a smooth driving mechanism on the polystyrene rod, and partly because of the advent of the TR tube which has an adjustable gap.

These tuning difficulties are avoided in the 1B27 tube, which is tuned by varying the gap spacing with the mechanism shown in Fig. 2·43. The aluminum shell which carries the tuning mechanism is cemented to the glass cylinder sealed to the back of one of the disks. Smooth

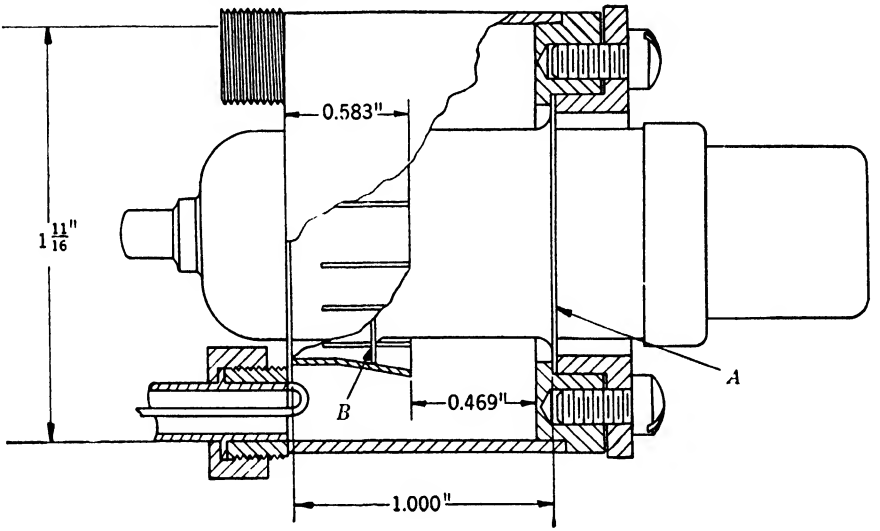

FIG. 2·45.—TR tube in coaxial cavity.

tuning, without the necessity of using lock nuts to secure a given setting, is obtained over a range of 10 to 15 per cent in a given cavity. Figure 2·44 shows the tuning characteristics of the 1B27 tube in cavities of various diameters D. Examination of the curves shows that the cavity diameter required to tune to a wavelength of 13 cm would be about 2.5 in. However, in certain lightweight airborne radar equipment, the space and weight allotted to a TR cavity to tune to 13 cm were extremely small. The cavity shown in Fig. 2·45 was designed for this application. It may be considered either as a capacitance-loaded coaxial cavity or as a folded TE_{010}-cavity. It is only $1\frac{1}{16}$ in. ID by 1 in. long, but it tunes over the range indicated in Fig. 2·44 according to the Curve A. It is almost impossible to fabricate such a cavity as a split unit, with the parting line always parallel to the current flow. It was therefore decided to make the cavity a "plug-in" type. The two flanges on the 1B27 tube

have a difference in diameter of $\frac{1}{16}$ in. This allows the tube to be inserted from the end A, Fig. 2·45, and have its large flange clamped at this end by a suitable ring, while the smaller flange is forced into the spring fingers at B. If these fingers are properly tempered they will deform the tube flange and make a good contact. A tube can be inserted into a cavity of this type only a few times before its small flange is permanently deformed and will no longer make a good contact. This is objectionable for laboratory use; but where the life of the complete equipment is only two or three times that of a TR tube, this is not a serious defect.

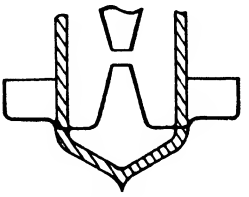

FIG. 2·46.— Modified flange for use in plug-in cavity.

The unloaded Q of the coaxial cavity is only about one half that of the conventional cavity. As a result, either higher leakage power for a given insertion loss compared with a TE_{010}-cavity, or more insertion loss for a given leakage power must be accepted. In high-performance equipments, this definitely rules out the coaxial cavity; but where weight and size are of paramount importance, the loss in performance (about $1\frac{1}{2}$ db) can be accepted.

An improved design for a plug-in tube has been reported by the British. In this design the small disk on the TR tube is formed as shown in Fig. 2·46. The bent-over small disk is stronger than the straight type and presents a greater area to the contact fingers.

2·9. Tuning Temperature Compensation.—Military radar equipment must operate at maximum efficiency under a great variety of conditions. In particular, airborne equipment must be subjected to temperatures ranging from −55°C to 100°C. This imposes the first requirement on components—they must not break or otherwise fail because of extreme temperatures. The next requirement imposed is that every component must *function electrically* over a temperature range from about −15°C to 100°C. There is no clear limit on the low-temperature point; this limit is estimated by assuming that the average *temperature rise* within an operating radar equipment is 40°C over the external ambient temperature.

The characteristics of a TR tube which are temperature sensitive, are tuning, leakage power, and recovery time. The leakage power and the recovery time will be discussed in Chap. 5. Except at the start of the operation, it is undesirable and often impossible to tune the TR tube in an aircraft. This initial tuneup usually occurs on the ground where the temperature may be widely different from the temperature under which the plane operates when aloft. The change of temperature changes the resonant frequency of both the TR cavity and the transmitter. It is required, of course, that the two frequencies either remain constant or change by the same amount.

The magnetron transmitter used at microwave frequencies is in almost all cases of all-copper construction. As its temperature changes, therefore, it expands in all dimensions by an amount determined by the coefficient of expansion of the metal. If all the linear dimensions of a resonant structure are multiplied by a constant, its resonant wavelength is multiplied by the same factor; therefore a copper magnetron changes frequency at a rate of 16 parts per million per °C—the frequency decreases as the temperature increases.

For ease of machining, cavities for cell TR tubes are usually made of brass. The temperature coefficient of brass is not much different from that of copper, varying from about 17 to 20 parts per million per °C. The glass cylinder between the copper disks has a much lower coefficient of expansion (3.1×10^{-6}/°C) than copper, and, therefore, the distance between the flanges is practically independent of temperature. The copper cones, of course, expand with temperature and, therefore, the gap between them decreases. Since the external cavity expands at about the same rate as a copper cavity, and the gap *decreases* with increasing temperature and thus increases the capacitance loading, the resonant frequency of the TR tube decreases faster with increasing temperature than does the resonant frequency of the magnetron.

The problem involved may be stated in the following way. Let the height of the cavity be h, the length of the posts l, the gap length δ, the coefficient of expansion of the cavity α_c, and that of the glass α_g. Then at some temperature t_0,

$$\delta_0 = h - 2l. \tag{71}$$

At any other temperature $t_0 + \Delta t$, if the cavity were all copper

$$\delta' = (1 + \alpha_c \Delta t)(h - 2l). \tag{72}$$

For this same temperature, the gap in the TR cavity is

$$\delta'' = (1 + \alpha_g \Delta t)h - 2(1 + \alpha_c \Delta t)l. \tag{73}$$

The difference between the two,

$$\delta' - \delta'' = h(\alpha_c - \alpha_g)\Delta t, \tag{74}$$

is the amount by which the cones in the cell TR tube must be pulled apart at $(t_0 + \Delta t)$ in order to tune this tube to the same frequency as that of an all-copper cavity at this temperature.

In the 721B and 724B TR tubes the gap spacing is compensated by proper shaping of the disk between the base of the cone and the inside of the glass. This is a purely empirical process, but it is known that almost any temperature-tuning curve which is desired can be obtained by giving the disk the appropriate initial curvature. The 1B27 TR tube has one of its cones exposed to the atmosphere and connected to a

tuning-screw mechanism, Fig. 2·43. The temperature coefficient of this tuning mechanism may be used to make the proper correction to the cavity. Let the length of the screw (from the cone to the first thread in the housing) be l_s and its coefficient be α_s; the length of the housing from the glass to the first thread be l_h and its coefficient α_h; and use the same quantities for the glass cylinder l_g and α_g. The motion of the end

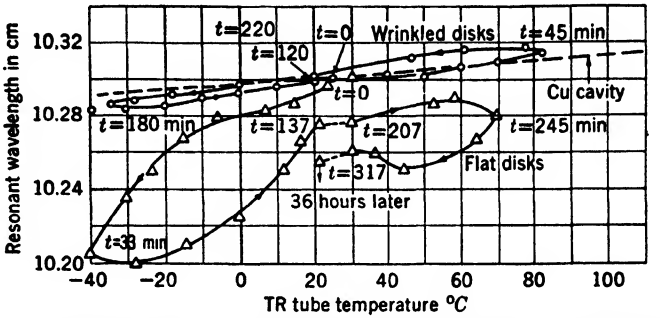

FIG. 2·47.—Tuning-temperature characteristics of 721A TR tube. A comparison is made of flat and wrinkled disks, measured in a brass cavity.

of the screw relative to the disk (assuming the copper is easily deformed) is

$$\Delta = (l_g\alpha_g + l_h\alpha_h - l_s\alpha_s)\Delta t. \tag{75}$$

If Δ is positive and equal to $\delta' - \delta''$, as given by Eq. (74), the cavity will be properly compensated. The housing shell of the 1B27 tube must be light since it is cemented to the glass. This automatically restricts the choice of material to some grade of aluminum with an α of about 23×10^{-6}/°C. The length may be varied within reasonable limits, but it is basically restricted by mechanical considerations. Since Δ in Eq. (75) must be positive, $\alpha_s < \alpha_h$. Kovar with an α of only 5×10^{-6}/°C is a suitable material for the screw. After a reasonable mechanical arrangement of the tuning mechanism has been made, even if the tuning-temperature curve which results is either over- or undercompensated, it can be corrected by proper shaping of the disk which carries the stationary cone.

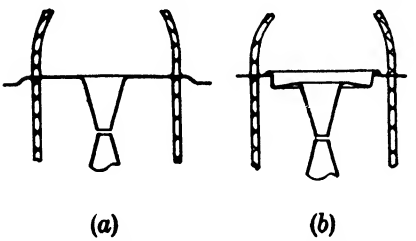

FIG. 2·48.—Comparison of plain (*a*) and temperature-compensated (*b*) TR-tube cones.

Figure 2·47 shows the difference in temperature-tuning characteristics between a flat disk and a disk which has a wrinkle, Fig. 2·48. The wrinkled disk, in addition to giving almost the same tuning slope as an all-copper cavity, has almost no hysteresis, whereas the flat disk has

both a very large tuning-temperature slope and hysteresis. If the disk were perfectly flat between the seals, it could equally well buckle *in* or *out* with an increase in temperature. On the other hand, if it has an initial concave curvature (seen from the gap), it tends to become even more concave at higher temperatures, and thus pulls the gap apart and gives the proper sign to the slope of the tuning curve. If the disk is simply bowed the cones move in the desired direction, but there is considerable hysteresis in the motion. The wrinkled disk shown in Fig. 2·48 overcomes this objection and gives the performance shown in Fig. 2·47.

Figure 2·49 shows the temperature-tuning curves of a 1B27 TR tube in a brass cavity tuned to several different frequencies. The couplings to a 1B27 cavity are normally adjusted to make Q_{L2} about 350. Under these conditions the bandwidth (to half-power transmission) is 9 Mc/sec at $\lambda_0 = 9.5$ cm. Comparison of the tube characteristics with that of a copper cavity at a temperature rise of 60°C above the initial tuning temperature indicates that the TR and magnetron cavities will differ in frequency by about 2 to 4 Mc/sec. The detuning losses are of the order of 0.7 to 2.3 db.

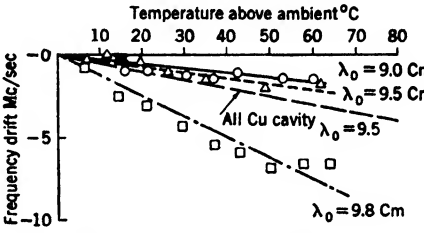

FIG. 2·49.- Tuning-temperature curve of 1B27 TR tube.

2·10. Cavity Couplings.—Thus far in the equivalent-circuit calculations the couplings to a cavity have been characterized by a susceptance in the case of the iris, or by a reactance and mutual inductance in the case of a loop. In practice these quantities are almost never measured directly, and are only of academic interest to the engineer. Once a particular TR tube and external cavity have been chosen, then only the couplings remain to be adjusted in order to get the desired insertion loss in the desired manner (equal coupling, matched input, and so forth). Thus, in order to adjust the coupling to the proper value it is necessary to measure the input admittance at resonance, first with no load to determine the value of g_c' and then with the proper output load to determine $(g_c' + g_L)$. These two measurements, plus a measurement of Q, completely specify the low-level properties of the cavity. These measurements are not enough, however, to determine the coupling susceptances b_1 or b_2.

Equation (76) is the expression for the Q of an iris-coupled cavity

$$Q_{L2} = A\left(\frac{1}{b_1^2} + \frac{g_2}{b_2^2} + g_c\right)^{-1}. \tag{76}$$

It is possible to measure Q_{L1} or Q_{L2} directly and then to compute Q_0;

however, no measurements made at the external terminals (input or output) can define the magnitudes of b_1 and b_2 unless either g_c or A is known. The shape and capacitive loading of the cavity determine the constant, A. In particularly simple cases, as for a cavity made of a resonant length of rectangular waveguide, the iris susceptance may be found in various handbooks,[1] or computed from the length of the cavity and its propagation constant. In principle, this can still be done in cavities of even more complicated shape, but the mathematical complications are

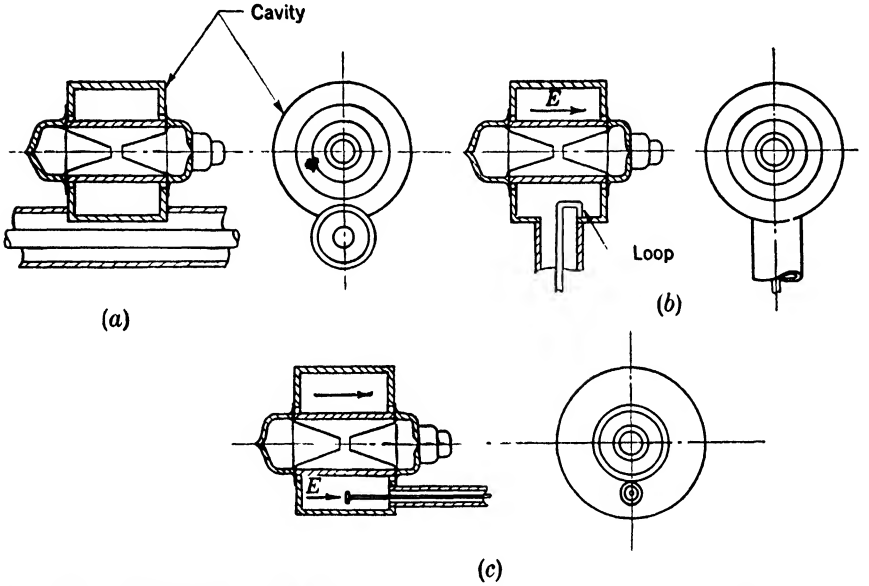

FIG. 2·50.—Methods of coupling a cavity to a coaxial line; (*a*) series (iris) coupling, (*b*) loop coupling, (*c*) capacitive (probe) coupling.

so great as to discourage such computations. As a result, the data available consist of curves of the apparent shunt conductance g_c' *of a given TR cavity coupled to transmission lines of a given type* as a function of the dimensions of the iris or loop.

The frequency of operation and the type of set under consideration determine whether a TR cavity is to be coupled to a coaxial or to a waveguide transmission line. Figure 2·50 illustrates three methods of coupling a cavity to a coaxial line. Figure 2·50*a* shows series, or iris, coupling in which the outer conductor is cut so that the transmission-line current is interrupted by the cavity. Figure 2·50*b* shows a loop-coupled cavity in which the current in the loop sets up a magnetic field that couples to that of the cavity. Figure 2·50*c* is a capacitance-coupled cavity in which

[1] "Waveguide Handbook," RL Report 43-2/7/44 and "Waveguide Handbook Supplement," RL Report No. 41-1/23/45; also Vol. 10, Radiation Laboratory Series.

the probe acts as an antenna and the voltage drop along it excites the E field in the cavity. The first two are fairly common methods of coupling; but the last one has never been used on any microwave TR cavities, since the electric field in the outer portions of the cavity, where a probe can be inserted, is so weak that it is difficult to obtain sufficiently tight coupling.

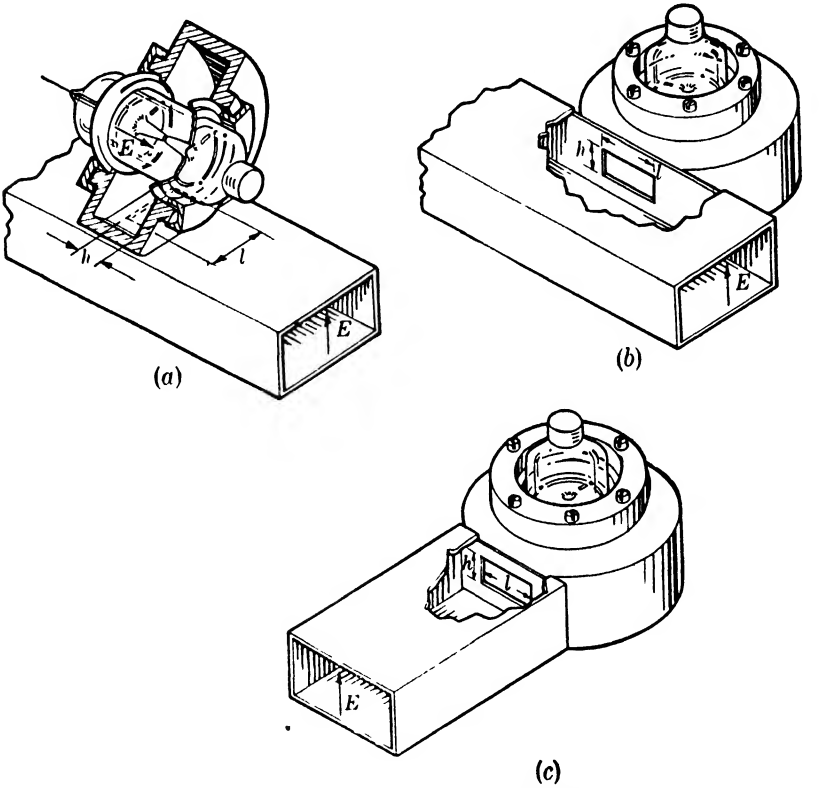

FIG. 2·51.—Methods of coupling a TR cavity to a rectangular waveguide; (*a*) series coupling, (*b*) shunt coupling, (*c*) feed-through coupling.

Figure 2·51 shows three common methods of coupling TR cavities to rectangular waveguides. Figure 2·51*a* shows series coupling in which the cavity is mounted on the broad face of the waveguide, so that the coupling hole interrupts the longitudinal line current. Figure 2·51*b* illustrates the so-called shunt coupling in which the cavity is mounted on the narrow face of the guide so that the coupling hole interrupts the vertical currents in the wall.[1] Figure 2·51*c* is the so-called "feed-

[1] For a more complete discussion of the meaning of "series" and "shunt" connections to waveguides, see Chap. 7 of this volume.

through" coupling in which the cavity is mounted on the end of the waveguide and, therefore, the coupling is of the type discussed in Sec. 2·2.

At 10 cm, the couplings illustrated in Figs. 2·50*a* and *b* and Figs. 2·51*b* and *c* have found the widest use. At 3 cm, coaxial lines, because of their comparatively high attenuation are never used as main transmission lines, and the 724 TR tube has been used exclusively with the couplings shown in Fig. 2·51*a* and *b*.

An iris cut into a cavity as shown in Fig. 2·51 acts as an inductive susceptance if its height is equal to the height h of the cavity. If the cavity were made of a section of waveguide of the type discussed in Sec. 2·2, the irises could be made either capacitive or inductive by bringing the irises in from the top and bottom, or from the sides. The susceptance resulting from a given opening δ between the irises is much greater for an inductive than for a capacitive iris. For this reason larger openings and less critical mechanical tolerances are allowable with inductive irises. Figure 2·52 is a comparison of the reflection coefficient of symmetrical capacitive and inductive irises $\frac{1}{32}$ in. thick in waveguide 1 in. by 0.5 in. by 50-mil wall at $\lambda = 3.2$ cm.[1]

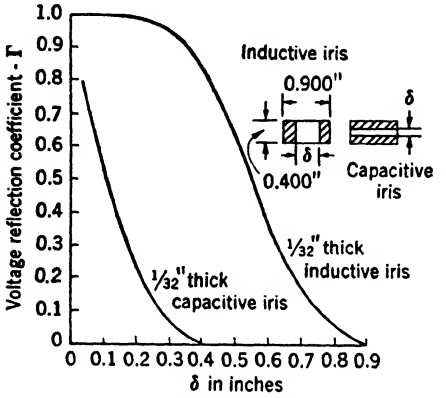

FIG. 2·52.—Reflection coefficient of inductive and capacitive irises in waveguide 0.400 in. by 0.900 in. at $\lambda = 3.2$ cm.

The coupling iris between a circular TE_{010}-cavity and a waveguide (as seen in Fig. 2·51*a*) which is made by slicing off a segment of the cavity, is rectangular. Its height h is always equal to that of the cavity, while its length l is determined by the distance from the center at which the slice is made. The length of the hole for any practical TR-cavity coupling is less than a half wavelength; it is of the order of $\lambda/4$, and, therefore, it acts as an inductive susceptance whose magnitude varies inversely with l. The actual susceptance of the hole varies not only with its length, but also with its thickness. An iris of zero thickness appears as a pure shunt susceptance across the guide. If the thickness $t \neq 0$, then the equivalent circuit is that shown in Fig. 2·53.[2]

Figure 2·54 is a plot of the variation of B_a and B_b as a function of t with $d = 0.375$ in., $a = 0.900$ in., and $b = 0.400$ in. at $\lambda = 3.20$ cm.

[1] "Waveguide Handbook Supplement," RL Report No. 41-1/23/45.

[2] "Waveguide Handbook Supplement." The discussion and examples will be for round holes, but the general application to rectangular or elliptical holes is valid.

Let us now examine the input susceptance to this network terminated in a conductance g,

$$Y = -jb_a + \frac{(g - jb_a)(-jb_b)}{g - j(b_a + b_b)}$$
$$= -jb_a + b_b \frac{gb_b - j(g^2 + b_a^2 + b_a b_b)}{g + (b_a + b_b)^2}.$$

For $t = 0$, $b_b = \infty$, and $b_a = -2.3$, $Y = g - j\,4.6$; but at $t = 0.020$ in., $b_b = -28$, and $b_a = -2.7$, $Y = 0.83g - j5.13$. Thus, the apparent

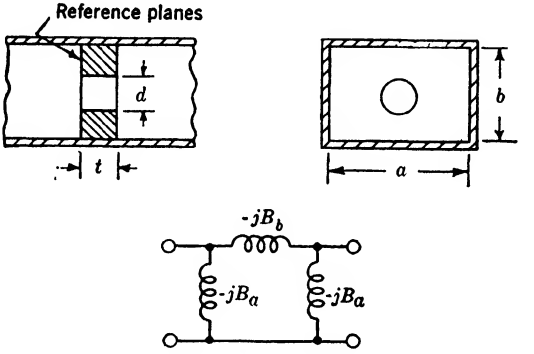

FIG. 2·53. –Equivalent circuit of thick iris.

susceptance has been increased by about 10 per cent, and the conductance transformation through the hole is about 1.2; therefore the diameter of the

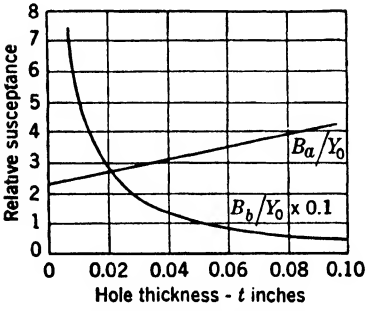

FIG. 2·54.—Variation of series and shunt susceptances of a 0.375-in. hole in a diaphragm across a waveguide 0.400 in. by 0.900 in. at λ 3.2 cm.

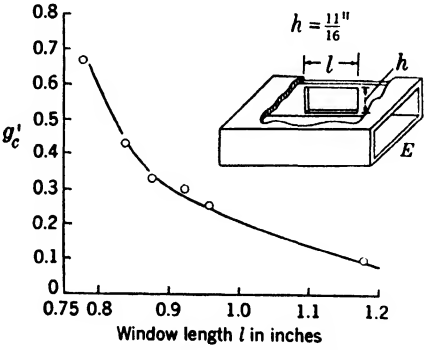

FIG. 2·55.—Conductance of 721 TR cavity, 2.67-in. ID, shunt-coupled to 1½ in. by 3 in. waveguide as a function of window length l, λ = 10.7 cm, Q_0 = 2500.

hole required to produce a certain coupling to a cavity must be increased with increasing thickness of the hole.

For several different coupling schemes the following curves show the variation in equivalent cavity conductance with the variation in size

of the coupling window. Figure 2·55 shows the variation for a 721A TR cavity, 2.67-in. ID, coupled to the narrow side of 1½-in. by 3-in. waveguide at $\lambda = 10.7$ cm. The thickness of the iris was that of the guide wall, 0.080 in. Figure 2·56 shows the coupling of the same cavity to a 1⅝-in. coaxial line by means of an iris; the equivalent cavity conductance g_c is plotted against the chord l of the intersecting circles. Figure 2·57 illustrates a 721A cavity iris-coupled to a ⅞-in.

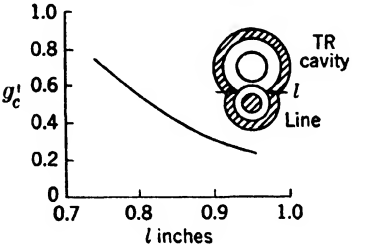

FIG. 2·56.—Conductance of a 721 TR cavity, 2.67-in. ID, iris-coupled to 1⅝-in. by ⅝-in. diameter coaxial line. $\lambda = 10.7$ cm, $Q_0 = 2500$.

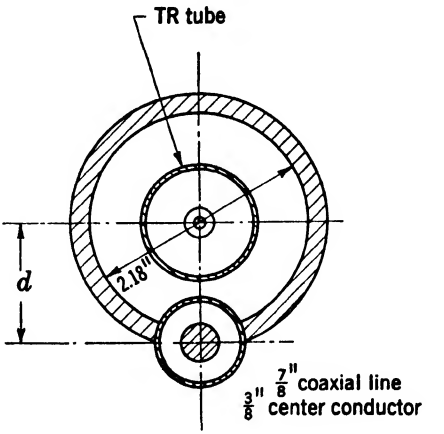

FIG. 2·57.—Dimensions of 721 TR cavity, iris-coupled to coaxial line; $d = 1.439''$ for $g'_c = 0.30$; $d = 1.219''$ for $g'_c = 0.10$; $Q_0 = 2500$.

coaxial line, measured at $\lambda = 9.4$ cm. Figure 2·58 gives g'_c vs. l, at 8.5 cm and 10.7 cm, for 1B27 cavities coupled to the narrow side of a 1½-in. by 3-in. waveguide.

Figure 2·59 shows the effect of placing a sheet $\frac{1}{32}$ in. thick of dielectric ($\epsilon' \approx 3.5$) over the iris of a 1B27 TR cavity; it also shows the frequency sensitivity of the coupling. Within the accuracy of the experiment, the curves are straight lines and thus indicate that the effective coupling susceptance of the iris increases as the square root of the wavelength, since $g'_c = b_1^2 g_c$. This is unexpected, since it would have been predicted that an inductive susceptance would vary directly with wavelength.

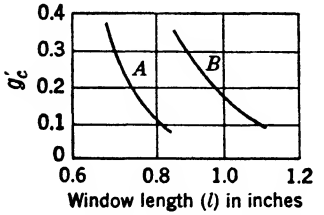

FIG. 2·58.—Transformed cavity conductance g'_c vs. coupling-window length l in 1B27 cavities on narrow side of 1½-in. by 3-in. waveguide. Curve A is for $\lambda = 8.5$ cm, cavity diameter of 1.40", window thickness of 0.040"; Curve B is for $\lambda = 10.7$ cm, cavity diameter 2.15", window thickness 0.080"; $Q_0 = 3000$.

In Secs. 2·1 and 2·2 it has been seen that the coupling susceptances cause the loaded cavity to resonate at a frequency different from that of the unloaded cavity. Inductive irises cause the loaded cavity to resonate at a *lower* frequency than the unloaded cavity. Capacitive irises or loop couplings cause the loaded cavity to resonate at a *higher*

frequency than the unloaded cavity. Figure 2·60 indicates the change in resonant wavelength of a 721A cavity as a function of the orientation of the loops. When the plane of the loop is at 90° to the magnetic field, the coupling is a minimum. The frequency shift is of the order of $\frac{1}{2}$ per cent when Q_{L2} is 250 and Q_0 is 2500. Measurements on a 724A-tube cavity coupled for matched input with inductive irises give the

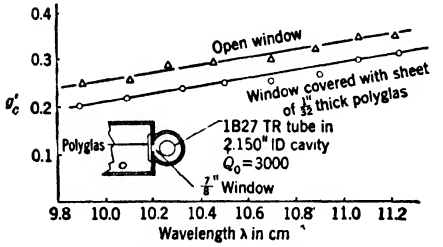

FIG. 2·59.—Frequency sensitivity of iris coupling to cavity on end of 1½-in. by 3-in. waveguide and effect of polyglas sheet placed over the iris.

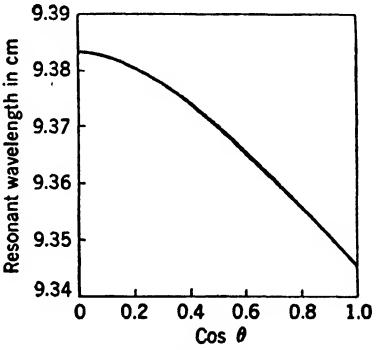

FIG. 2·60.—Effect of loop coupling on cavity resonant wavelength for a 721A TR tube; cavity 1.875" diameter coupled to a 72-ohm coaxial line by a loop $\frac{3}{8}$ in. by $\frac{1}{4}$ in. made of $\frac{1}{16}$-in. wire. The angle of orientation is θ.

results tabulated below, where l_1 and l_2 are the lengths of the input and output windows. The wavelength shift is about $1\frac{2}{3}$ per cent from the lowest to the highest loaded Q; the *wavelength increases* with increased loading.

TABLE 2·6.—MEASUREMENTS ON 724A-TUBE CAVITY COUPLED FOR MATCHED INPUT WITH INDUCTIVE IRISES

l_1, in.	l_2, in.	λ, cm	Q_{L2}
0.23	0.216	3.13	320
0.275	0.244	3.205	178
0.315	0.275	3.23	133

2·11. Direct-coupling Attenuation.—Direct-coupling attenuation was discussed in Secs. 2·2 and 2·7, where it was shown that the attenuation is proportional to the product of the input and output Q's and to $(b_0 + b_L)^2$ where b_L is the susceptance of the post across the cavity and b_0 is the susceptance of the cavity inductance.

The order of magnitude of this attenuation in 10-cm TR tubes loaded to $Q_{L2} = 300$ is 60 db. However, if the TR tube is connected as shown in Fig. 2·61 and its impedance is very small compared with the line

impedance, then the ratio of the available power to the direct-coupled power is 4 times as great as if the TR tube were connected directly across the generator terminals. Thus, because the critical quantity is the leakage power when the TR tube is used as in Fig. 2·61, it is customary to use this new definition for direct-coupling attenuation (leakage power/transmitter power) and the value of 60 db quoted above should now read 66 db.

The direct-coupled leakage power with 10^6 watts transmitted is 0.25 watts if the attenuation is 66 db. Experience has shown that 10-cm silicon crystal detectors withstand pulses of 5 to 10 watts for short times, but they show a steady slow deterioration at leakage powers of the order of 0.15 to 0.2 watt. It thus becomes apparent that TR tubes for high-power radar sets need direct-coupling attenuation greater than 66 db.

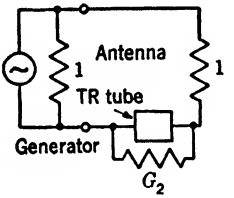

FIG. 2·61.—TR tube connection for direct-coupling attenuation.

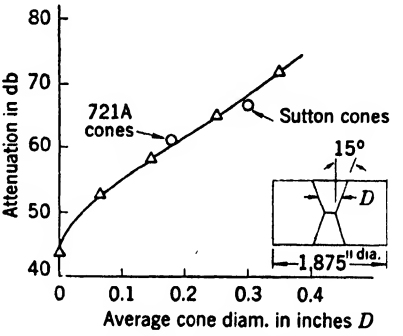

FIG. 2·62.—Direct-coupling attenuation as a function of mean post diameter.

R. L. McCreery has made a series of measurements of the attenuation through a 721A cavity and through a Sutton-tube cavity.[1] Figure 2·62 is a curve of the attenuation, in a cavity of 1.875-in. diameter with two conical posts short-circuited across the gap, against the average diameter D. The cavity was coupled to give a value of Q_{L1} of 320 when the gap between the posts was adjusted to produce resonance at $\lambda = 9.1$ cm; the insertion loss was about 1 db. The attenuation measured is the insertion loss of the cavity, and the direct-coupling attenuation in a system would be 6 db greater.

Although it would appear that the TR-tube cones should be made large in order to get optimum performance, it must be recalled that the use of a larger post has one of two effects: (1) If the gap capacitance and, therefore, cavity diameter are to be kept constant, the gap length must be increased, and this increases the arc leakage power (see Chap. 5); (2) If the gap length is kept constant, the capacitance is increased, and the cavity diameter must be decreased to resonate at a given frequency; this

[1] R. L. McCreery, "Direct Coupling in the TR Box," RL Report No. 352, Nov. 3, 1942.

seriously restricts the high-frequency tuning range. A compromise between the two must be effected, and historically, the 721A, which was already in production at the time of these measurements, seemed to be a reasonable compromise.

Measurements of high-level leakage power as a function of transmitter-power level have been made on 721A TR tubes in a number of different cavities.[1] Figure 2·63 is a plot of such data. Table 2·7 compares the direct-coupling attenuation through 721A TR cavities coupled in several ways. Values are corrected to $Q_0 = 2000$, $L = -1.5$ db, matched input.

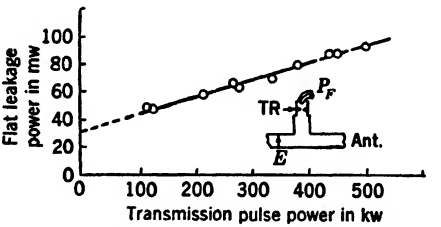

FIG. 2·63.—Direct-coupling attenuation through 721A TR cavity on waveguide E-plane T; $\lambda = 10.7$ cm, $Q_0 = 2000$, $L = -1.54$ db. The slope of the curve gives a value of the direct coupling attenuation of 68.8 db.

TABLE 2·7.—DIRECT-COUPLING ATTENUATION THROUGH 721A TR CAVITIES CORRECTED TO $Q_0 = 2000$, $L = -1.5$ DB, $g_c' + g_L = 1$

Original conditions				Corrected db attenuation	Method of coupling
λ	Q_0	db L	$g_c' + g_L$		
10.22	2550	0.95	1	66.9	Iris on $\frac{1}{8}$" coaxial
10.22	2463	1.15	1	68	Shunt T on $\frac{1}{8}$" coaxial
10.75	2000	1.54	1	68.6	E-plane waveguide T
10.75	2200	1.54	1	68.6	E-plane waveguide T
10.75	2160	2.2	1	66.8	Shunt T on $\frac{1}{8}$" coaxial
10.75	2180	2.14	1	66.8	Shunt T on $\frac{1}{8}$" coaxial
10.8	2000	0.74		67	Iris on $\frac{1}{8}$" coaxial
10.8	2000	0.74		67.7	Iris on $\frac{1}{8}$" coaxial
10.8	2065	1.34	1	68.4	E-plane waveguide T
10.8	2065	1.34	1	69	E-plane waveguide T

In the course of a series of measurements of leakage power through a 721A TR tube, it was observed that the leakage power measured was dependent upon the insertion of the inductive tuning slugs if they completely filled the cavity ($\frac{3}{4}$-in. screws in an $\frac{11}{16}$-in.-high cavity); but smaller tuning screws ($\frac{5}{8}$-in. dia.) had no effect on the leakage power.

Figure 2·64 illustrates a cavity that was developed for the 721 ATR tube for use at line powers of the order of 500 kw or greater. It is larger in diameter than the usual cavity used to tune over the range from

[1] L. D. Smullin, "Measurements of 721A TR-Tube Leakage Power," RL Report No. 249, Mar. 9, 1943.

10.3 to 11.1 cm (3.25 in. compared with 2.67 in.) but four tuning slugs, two of which are fixed, are used to tune over this same range. The effectiveness of this arrangement is indicated in Fig. 2·65 which compares the leakage power through the large cavity with the standard cavity. The quantity plotted is the average rectified crystal current produced by the leakage power. Since the duty factor is 1/2000, the peak rectified current is of the order of 10 ma or greater. The degree of saturation of the crystal is indicated by the curve of leakage power through the 2.67-in. cavity, with plugs clear out, against line power. The leakage power through the large cavity is plotted against plug insertion for a constant line power of 690 kw. It can be seen that the leakage power at wavelengths between

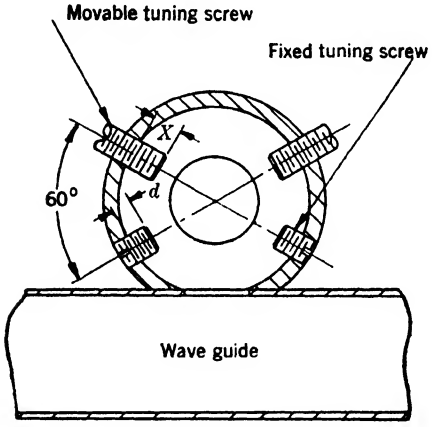

FIG. 2·64.—Large cavity for 721A TR tube.

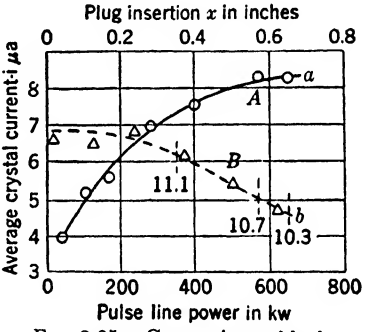

FIG. 2·65.—Comparison of leakage power through 2.67-in.- and 3.25-in.-diameter cavities. Curve *A* shows i vs. p for 2.67-in. cavity at $\lambda = 11.1$ cm; Curve *B* show i vs. x at 690 kw.

11.1 and 10.3 cm is well below that of the smaller cavity with no tuning plugs at the same power level. Since the small cavity had a measured direct-coupling attenuation of 66 db, and the large cavity, when tuned to 10.7 cm and with a line power of 690 kw, had a leakage power corresponding to that through the smaller one at a line power of 110 kw, its direct-coupling attenuation is greater by 7.9 db, or is equal to about 74 db.

Harmonics.—The transmission characteristics of the fired TR cavity at frequencies higher than the fundamental or carrier frequency of the transmitter are of considerable importance. Sideband frequencies for microsecond pulses are restricted to a relatively few megacycles per second above or below the carrier, and are attenuated to the same extent as the carrier in passing through the fired cavity. Harmonics, however, are not necessarily attenuated to the same extent. Since the two "waveguides" around the short-circuited center post of the TR cavity are no

longer small compared with $\lambda/2$ for the second or third harmonics, it would be expected that there would be relatively little direct-coupling attenuation at these higher frequencies.

Unfortunately, no quantitative data are available to illustrate this. When the cavity is coupled to a waveguide, there is no way of determining in what modes the harmonics are propagating, since they may choose any or all of four or five different modes depending upon the shape of the exciting feed and upon various obstacles in the guide. It is therefore dangerous to synthesize the operating conditions by feeding in signals at these harmonic frequencies and measuring the attenuation directly because these synthesized conditions may be different from actual operating conditions by as much as 10 db.

Tests made on a 1B27 TR cavity normally tuned to 10.7 cm in a 2.15-in. ID cavity indicated as little as 6-db attenuation at a wavelength of 5 cm. If these measurements are typical, the pulsed magnetron is an exceptionally good oscillator, since measurements of actual harmonic leakage power[1] have given maximum values of a few tenths of a watt when the pulse power at the nominal frequency was 50 kw.

If the harmonic leakage power becomes excessive, there is little that can be done to the cavity to reduce this power. Crystal mixers for high-power 10-cm radar sets usually have harmonic-suppressor chokes built into them. About 10 to 20 db of protection can be obtained in this way. Difficulty with harmonic burnout of crystals has been encountered only in the highest-power sets, where it has been remedied by the use of a pre-TR tube (see Chap. 4).

2·12. Integral-cavity TR Tubes.—The cell TR tubes discussed in Sec. 2·10 are comparatively inexpensive to manufacture, and they have the advantage of being adaptable for use in a variety of different cavities and circuits. As the frequency increases, the tube becomes smaller; but, because of the requirements for strength, the thickness of the glass cylinder separating the two disks remains constant and, consequently, occupies an increasingly larger fraction of the volume of the cavity. This results in dielectric losses which increase rapidly as frequency increases. A further consequence of the presence of the glass is that it adds a proportionately greater capacitive loading to the cavity at higher frequencies, and thus forces the spark-gap capacitance to be reduced by increasing the gap for a given cavity diameter. Or if the gap is kept constant, the cavity diameter must be reduced to keep the resonant frequency constant, thus increasing the copper losses. In any case, a cell tube is practically out of the question for use in the 1.25-cm region; and in the 3-cm band it is just usable, Q_0 being about 1500 or less.

[1] B. Cork, "Transmission of Higher Harmonics through a TR Cavity," RL Report No. 361, Jan. 11, 1943.

Since the excess loss results mainly from the presence of the glass in a region of high electric fields, the obvious step is either to remove the glass entirely, or to place it where the field is weak, that is at the outer diameter of the cavity. Figure 2·66 shows an early 3-cm TR tube built by Wm. Preston of the Radiation Laboratory early in 1942. It consists of a resonant length of waveguide with a spark gap at the center, and the coupling irises covered by glass windows. At the time this tube was made, it was not possible to seal the flat windows into the cavity and therefore, it was necessary to wax them in place. As a result, when the 724A cell TR tube was developed, further work on this tube was dropped.

As interest in the 1.25-cm band developed, it became obvious that a cell tube would be quite impractical. A group at the Westinghouse Research Laboratories, under the direction of S. Krasik and D. Alpert,

FIG. 2·66.—Old 3-cm TR tube.

developed an integral cavity by a new technique.[1] The glass was sealed directly to a Kovar ring, and the combination then soldered to the copper cavity. At the time the tube was first demonstrated there were no 1.25-cm radar sets ready for production; but 3-cm sets were experiencing considerable difficulty with the 724A TR tube in the form of crystal burnout, short tube life, and frequent tube breakage. It was, therefore, requested that a similar integral-cavity tube be developed for 3 cm. The Westinghouse group made such a tube, and J. B. Wiesner and F. L. McMillan of the Radiation Laboratory perfected leakage-power characteristics. This tube was the 1B24 and was put into production by the Westinghouse Electric Co. at Bloomfield, N. J., and the Sylvania Electric Products Co. at Salem, Mass. The 1.25-cm tube was developed at a slower pace under the joint efforts of the Westinghouse Research group and C. W. Zabel, at the Radiation Laboratory. Its production

[1] D. Alpert, "Kovar to Glass Disc Seals, Some Applications in Micro-Wave Equipment, TR Box Group Report No. 1," Research Report SR 198, Westinghouse Research Laboratories.

form is known as the 1B26 and was made by Westinghouse and Sylvania. Figure 2·67 shows these two tubes.

At the request of the Navy Bureau of Ships, H. J. McCarthy of Sylvania made a similar tube, the 1B50, to operate in the 4-cm region.

Before entering into a detailed description of these three tubes, the general characteristics which favor the use of the integral-cavity over the cell TR tube will be discussed. At the highest frequencies glass losses become excessive in the cell tube. The 724 has a Q_0 of about 1500, whereas that of the 1B24 is 3000 or more. Because the glass diameter of the 724 tube is not very much smaller than the cavity

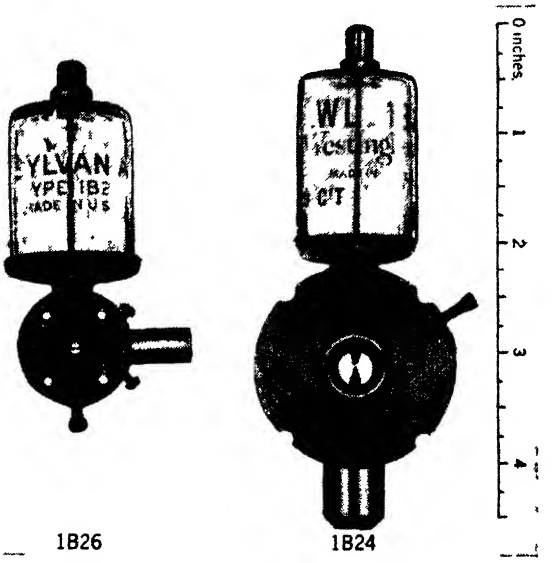

FIG 2 67.—1B24 and 1B26 TR tubes

diameter, there is little room for inductive tuning screws and the maximum tuning range obtainable in an ordinary cavity is 2 to 3 per cent. A double-mode cavity that can be tuned over a 12 per cent band has been designed for use as an ATR switch (see Chap. 4) but it was never applied to a TR switch.

The integral-cavity tubes are capacitance-tuned. This is done by varying the gap spacing by means of a differential screw which acts on the back of one of the cones, as in the 1B27. The resulting tuning range is of the order of 10 to 15 per cent of the nominal frequency.

The 724 tube is not very large, and the cavity into which it must fit has a number of small parts all of which must be assembled at once. Under extreme conditions of military service, even the simplest repair job becomes an intolerable burden, and complicated tasks are either poorly executed or not performed at all. It was felt that the use of an

integral-cavity tube, mounted in some simple manner between two waveguide choke connectors, would greatly improve the ease of maintenance of the radar equipment, and that the ultimate in TR design would be achieved when it would be possible for a "chambermaid with boxing gloves" to change tubes *in the field successfully. A final advantage of the integral-cavity tube is that it is possible to add an external gas reservoir to it in order to increase its life.* This is hardly possible in the cell tube because of the way it is clamped into its cavity.

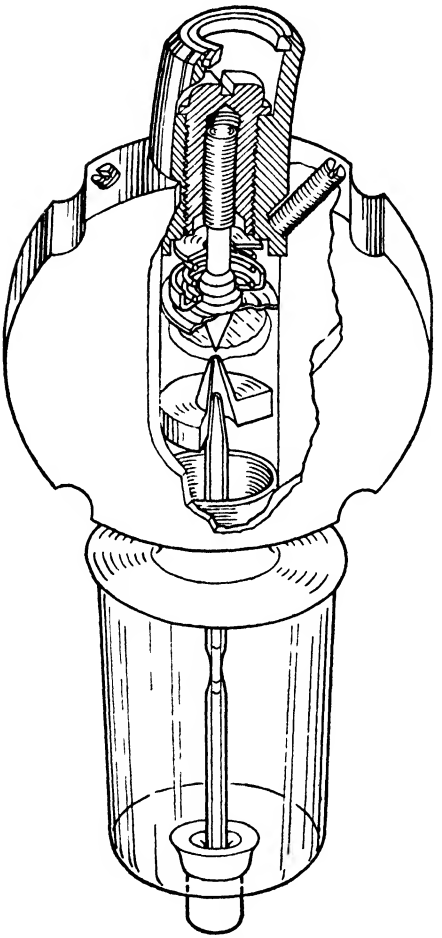

FIG. 2·68.—Cut-away view of the 1B24 tube.

The fact that Q_0 is higher for an integral-cavity TR tube permits looser coupling (larger coupling susceptances) with a consequent increase of the transformation ratio so that *for a given insertion loss*, if all other factors are equal, the high-level leakage power will be smaller than that from a cell TR tube.

To offset these advantages there is the obvious fact that the integral-cavity tube is more complicated and more expensive to make. The cavity for the cell tube is a permanent part of the duplexer, and is not thrown away whenever a tube is replaced; but the entire cavity and tuning mechanism of the integral-cavity tube are scrapped each time a tube is discarded. Although this would be an important economic consideration in normal peace-time undertakings, the life of the 1B24 integral-cavity tube is several times that of the 724, and therefore, the cost *per hour* of operation of the two are roughly equal.

Figure 2·68 is a cut-away view of the 1B24 tube, which shows the tuning mechanism, cavity, coupling window, keep-alive electrode, and gas reservoir. The 1B26, except for a 90° change of position of the reservoir, is a scaled-down version of the 1B24. The cavity is made out

of an oxygen-free, high-conductivity (OFHC) copper or selenium copper block, with the cones silver-soldered in place as shown, and the windows set into the face. The block itself has both faces parallel and they are of the proper diameter to act as the cover for a waveguide choke connector.

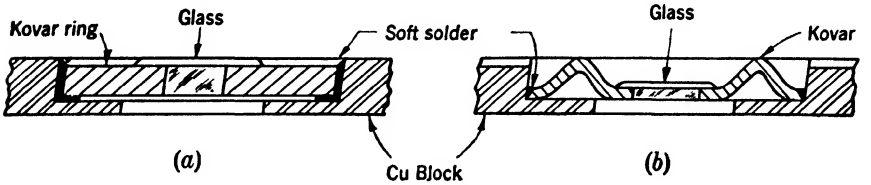

FIG. 2·69.—Methods of sealing glass windows into copper blocks.

The windows are glass disks sealed into Kovar rings which are in turn soft-soldered to the block. The original windows were made as shown in Fig. 2·69*a*. The Kovar disk was flat. As a result, it soon became apparent that when the copper cooled, after soldering, it contracted enough either to squeeze the Kovar and thus crack the glass, or else to cause the solder to flow beyond its elastic limit with the result that when the tube was warmed up again the solder cracked and allowed the tube to leak. The wrinkled Kovar disk shown in Fig. 2·69*b* allows the outer diameter of the Kovar to be squeezed without cracking the glass, and the bevel on the edge, with solder confined to the top as shown, prevents the type of solder leak just described.

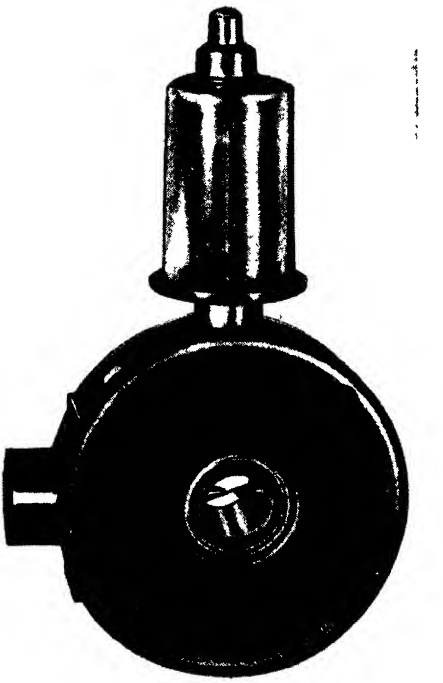

FIG. 2·70.—1B50 integral-cavity TR tube

The windows are made by sealing glass disks to the oxidized Kovar ring in an induction heating coil. A eutectic soft solder, 67 per cent tin and 33 per cent lead, with a melting point of 180°C, or a pure tin solder, is used to solder the Kovar to the copper. This is the final assembly operation on the tube before final exhaust and tuning. Because of the difficulties encountered initially, it is now required that a tube withstand at least fifty cycles of half-hour periods at the extreme temperatures of −40°C and 100°C without leaking.

The 1B50, Fig. 2·70, is made somewhat differently in that its body is fabricated out of three pieces of steel: a cavity block, and two cover plates. Since the diameter of the cover plates must be $2\frac{5}{8}$ in. to match the connector chokes, if the tube had been made of a solid piece of copper it would have been very heavy and expensive. Steel has the advantage that after heating it does not become dead soft as copper does, and therefore, it can be used in relatively thin sections. Its coefficient of thermal expansion is only 10×10^{-6}/°C as compared with 16×10^{-6}/°C for copper, which makes it easier to solder the windows in place. In fact, they are hard-soldered to the block in this tube and can withstand over 100 of the temperature cycles described. A steel cavity would have a very low Q_0. To overcome this, the cavity is copper-plated and then heated in a hydrogen atmosphere which causes the copper to flow and form a homogeneous surface over the steel. The gap of the 1B50, Fig. 2·71, is different from the gap of the other two tubes. In order to make a tube whose leakage power does not vary with tuning, the cones are made to overlap, so that the gap spacing remains constant as the tube is tuned. The use of an overlapping gap imposes severe requirements on the tuning mechanism. In order to make the tuning curve smooth, it is necessary to restrict the wobble of the movable cone to less than 0.0002 in.

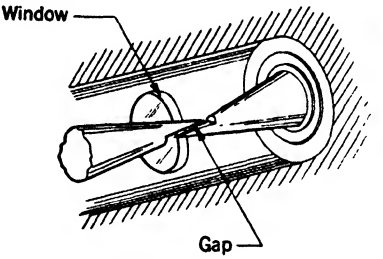

FIG. 2·71.—Overlapping gap of 1B50 TR tube.

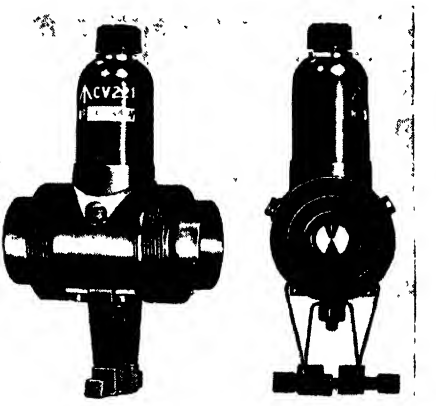

FIG. 2·72. CV221 (British) 3-cm integral-cavity TR tube.

Figure 2·72 shows a British 3-cm, integral-cavity TR tube, CV221. The body is copper and the windows are similar to those in the 1B24. Tuning is accomplished by squeezing the strut mechanism shown below the tube, and thus moving the lower cone up or down.

In Table 2·8 some of the more important electrical low-level characteristics are listed. These tubes all have equal input and output couplings and, if they are terminated by a matched receiver, the input voltage standing-wave ratio will be 1.2 to 1.3. They are designed to be mounted between waveguide choke connectors as shown in Fig. 2·73, and the body

TABLE 2·8.—LOW-LEVEL CHARACTERISTICS OF 1B26, 1B24, AND 1B50 TR-TUBES

Tube No.	Insertion loss (db)	Q_L	Minimum tuning range Mc/sec		Waveguide size, in.
			f max	f min	
1B26	1.4	220	24,580	23,420	$\frac{1}{2} \times \frac{1}{4} \times 0.040$ wall
1B24	1.2	300	9,600	8,500	$1 \times \frac{1}{2} \times 0.050$ wall
1B50	1.2		7,100	6,000	$1\frac{1}{2} \times \frac{3}{4} \times 0.064$ wall

diameter is large enough to allow the use of a pressurizing gasket as shown in the illustration.

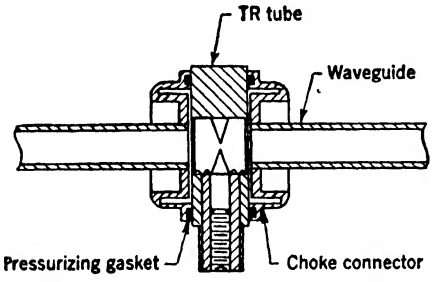

FIG. 2·73.—Integral-cavity TR tube mounted between waveguide choke connectors.

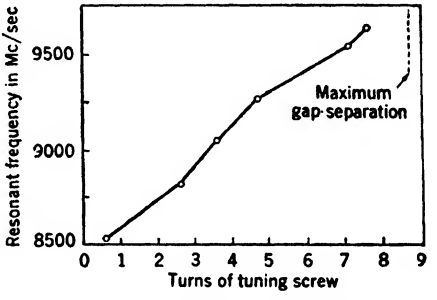

FIG. 2·74.—Tuning curve for 1B24 TR tube. (*Data are from the Sylvania Electric Products Co.*)

Table 2·9 gives the critical dimensions of the three tubes.

TABLE 2·9.—CRITICAL DIMENSIONS OF 1B26, 1B24, 1B50 TR TUBES

Dimension	1B26	1B24	1B50
Cavity diameter	0.250″	0.500″	0.725″
Cavity height	0.238″	0.454″	0.525″
Window diameter	0.148″	0.333″	0.494″
Cone tip diameter	0.002″	0.004″	
Cone separation	.....	.....	0.006″
Cone travel	0.009″	0.018″	0.070″
Cone angle	36°	36°	36°
Body diameter	1.015″	1.760″	2.625″

Figures 2·74 and 2·75 are tuning curves for the 1B24 and 1B26 TR tubes. The number of megacycles per second per turn is fairly high and, therefore, in order to ensure smooth tuning with little backlash, the

differential tuning screw must be spring-loaded as indicated in Fig. 2·68. The 1B50 has a similarly shaped tuning curve.

The shift of resonant frequency with temperature in a 1B24 TR tube is shown in Fig. 2·76, with a curve for an all-copper cavity superimposed, and lines which indicate the detuning that will cause ½ db and 1 db loss. The 1B24 and 1B26 tubes are of all-copper construction except for the tuning mechanism. By proper choice of materials for the shell and the

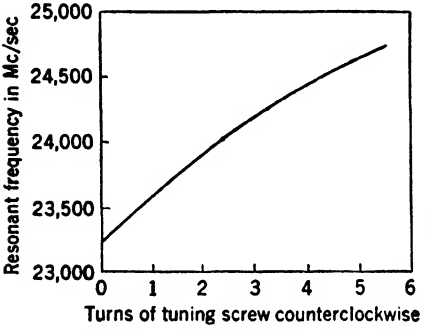

FIG. 2·75.—Average tuning curve for 1B26 TR tube. (*Data are from Westinghouse Electric Corporation.*)

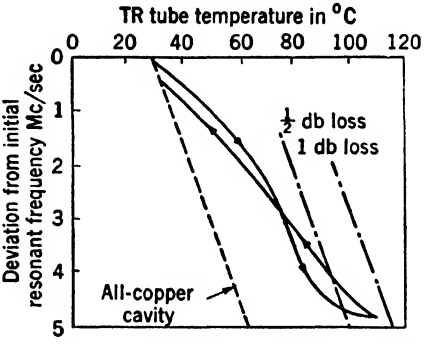

FIG. 2·76.—Typical temperature-tuning curve for a 1B24 TR tube. (*Data are from Westinghouse Electric Corporation.*) The initial tuning was at 9380 Mc/sec, and $Q_{L2} = 300$.

two screws, the combination can be made to move the cone at a rate nearly equal to that of an all-copper cavity. The 1B50 has a steel cavity with copper cones and diaphragm. Its over-all tuning changes at a rate of approximately −0.22 Mc/sec/°C. At 6500 Mc/sec an all-copper cavity changes at −0.10 Mc/sec/°C. With a *rise* of 80°C, the TR cavity will resonate at a frequency about 9.6 Mc/sec lower than the frequency of the copper cavity; and if $Q_{L2} = 250$, the signal loss will be increased by about 2 db.

CHAPTER 3

BANDPASS TR TUBES

By Wallace C. Caldwell

3·1. Introduction.—Early in the development of microwave radar it became evident that the presence of numerous tuning adjustments on the r-f components seriously handicapped maximum system efficiency. Although these controls presumably allowed the set to be tuned to its peak sensitivity, the complicated tune-up process that was necessary because of the interaction of the various controls usually resulted in a mistuning of the sets, with sensitivity down by 10 to 40 db. Early sets had the following adjustments: magnetron impedance tuner, TR phase shifter (to provide ATR action), TR tuning, two tuning adjustments on the crystal, four on the local oscillator, and an antenna tuner. By 1943 many of these controls had been eliminated by careful design of r-f components, so that their impedance was within about 10 per cent of line impedance in a 10 to 20 per cent frequency band. Eventually, a typical set had only the following r-f tuning controls: TR and ATR tuning, local-oscillator tuning, and local-oscillator coupling to the crystal. The advent of the thermally tuned local-oscillator and automatic-frequency-control circuits eliminated that manual adjustment, and the local-oscillator coupling could be set once for a given tube, and then ignored. This left only the TR and the ATR tuning adjustments. These elements with loaded Q's of 200 to 400 were still very sensitive to transmitter frequency, and it was not uncommon to find radar sets in the field with sensitivities 6 to 12 db down from optimum performance merely because of poor TR tuning.

The combination of the tunable-cavity magnetron, the band-pass TR tube, the low-Q ATR tube, and the thermally tuned local-oscillator tube made possible a "single-knob" tunable radar. The first and most obvious advantage of such a set is its operational simplicity. Second, the simple tuning adjustment allows selection of an operating frequency that will minimize interference from other radars and from enemy jamming. This frequency may be changed more or less continuously without interrupting regular operation, and intentional r-f jamming becomes almost impossible. The ability to adjust frequency during operation makes it possible to learn more about a particular target by observing its amplitude as a function of frequency. Echoes from targets

such as corner reflectors, cliffs, or battleships, have more or less characteristic frequency dependencies.

Thus the need or justification for a low-Q or bandpass TR tube is obvious. Historically, its development was the result of other requirements. In 1941, the development of a high-power 10-cm search set to operate at levels in excess of 500 kw was undertaken at the Radiation Laboratory. TR tubes were only in their infancy, and it was not believed that the soft Sutton tube (high-Q) could be used at such high powers. As a result, A. Longacre and his group developed the so-called "beetle" TR tube which was simply a low-Q resonant slit enclosed in a glass bubble, and designed to be clamped between two sections of 1½-in.-by-3-in. waveguide. These tubes had large leakage powers, but since they were required only to protect thermionic diode detectors, they were adequate. Two of these tubes were used in tandem; the first reduced the power incident on the second. These tubes were turned over to the General Electric Co. for further development and manufacture. M. D. Fiske of that company used several low-Q resonant irises to form a bandpass structure and began to work on this conception. Meanwhile, it was discovered that the 721A TR tube was able to protect crystals at powers in excess of 500 kw. Because of this, a last-minute change was made in the high-power systems just being produced by installing duplexers with 721A TR and ATR tubes, and with crystal mixers.

Thus, the original incentive for producing low-Q TR tubes, that is, high power, was removed; but interest in the bandpass features of the tube was aroused, and Fiske and his group continued their work under an OSRD development contract, sponsored by the Radiation Laboratory. The culmination of this work was the introduction of four TR tubes designed for use in the 3-cm and 10-cm bands, two pre-TR tubes, and nine low-Q ATR tubes for use in the 1.25-, 3-, and 10-cm bands. The TR and pre-TR tubes will be discussed in this chapter, and the ATR tubes will be discussed in Chap. 4.

The techniques that were used to develop a bandpass TR tube centered first around the fact that the reflections from small, identical, impedance discontinuities spaced $\lambda/4$ apart along a transmission line tend to cancel each other, and, secondly, around the design of a glass-covered resonant window whose frequency can be accurately controlled, and which is able to withstand the action of an intense r-f gas discharge along one face. In the bandpass TR tube, there are a number (2 or 3) of resonant slits (elements) spaced one-quarter guide wavelength along a piece of waveguide; the ends of the guide are closed off by glass-covered windows. The slits and windows are all tuned to the same resonant frequency. The loaded Q of the elements is usually of the order of 10, and that of the windows 2 to 5, as compared with 300 for a typical high-Q tube.

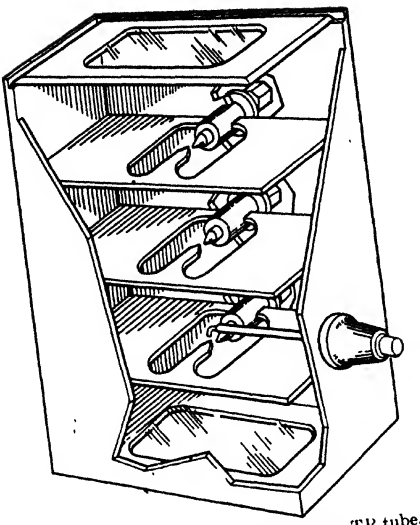

FIG. 3·1.—A three-gap bandpass TR tube.

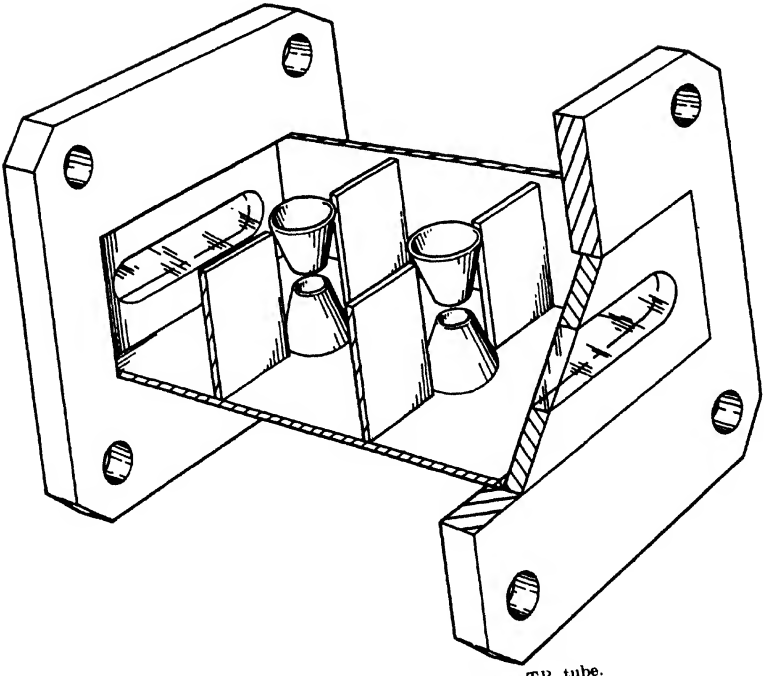

FIG. 3·2.—A two-gap bandpass TR tube.

The development of any desired bandpass characteristic is a comparatively simple task. It becomes difficult only when the leakage-power requirement imposed upon a TR tube has to be considered. Then, since minimum leakage power and maximum bandwidth are not obtained by the same design, compromises must be made in order to get the best over-all performance. This chapter will discuss the low-level design considerations, and the leakage power, or high-level characteristics, will be considered in Chap. 6.

At the beginning of this discussion, it is important to consider the physical form of a bandpass TR tube. Figure 3·1 shows a typical three-gap tube. A different shape of gap is used in the two-gap type shown in Fig. 3·2.

In the following sections the single-element circuit and then the multiple-element circuit will be presented. These will serve as an introduction to the experimental data and to the final discussion of achievements to date, and of problems still pending solution.

THEORETICAL CONSIDERATIONS

3·2. Resonant Elements.—Let us consider a thin diaphragm with a rectangular opening soldered into a waveguide as shown in Fig. 3·3*a*. The size of the opening may be chosen so that nearly all the energy of a

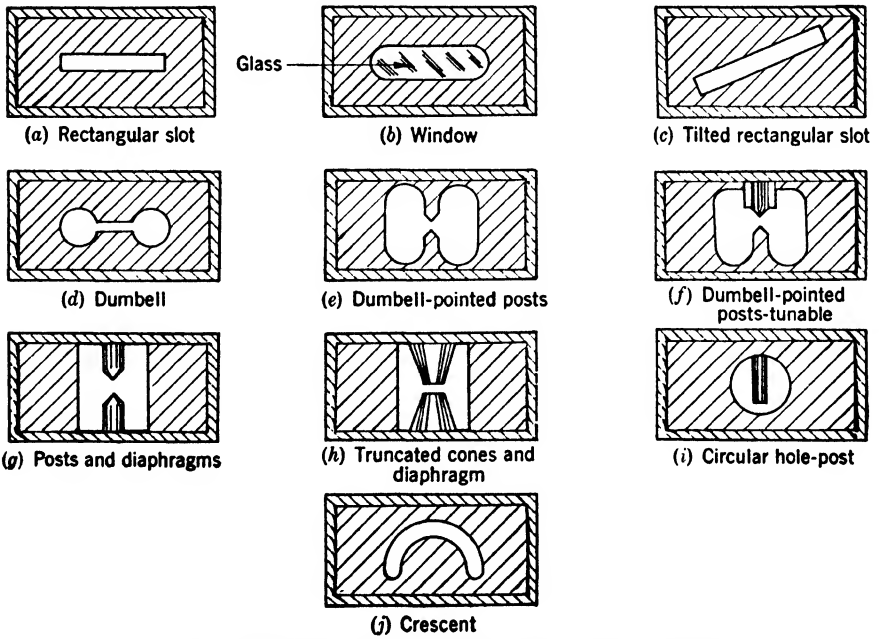

FIG. 3·3.—Miscellaneous resonant elements in rectangular guide.

given frequency incident on the diaphragm is transmitted through the diaphragm. Elements of a great variety of shapes may be made to resonate. The rectangular slot may be tilted with respect to the guide or it may be filled with dielectric. A resonant element of the dumbbell type may be made with a number of variations. In elements of some types, posts or cones are used which enable the resonant element to be tuned conveniently. A variety of elements are shown in Fig. 3·3.

To use the elements of Fig. 3·3 in complicated combinations, it is desirable to know the dependence of resonant frequency on the geometrical parameters of the elements, as well as to know the frequency dependence of transmission or reflection. Moreover, the energy lost in the element because of currents in the metal parts or displacement currents in the dielectric should be known. Unfortunately, even the simplest of the resonant elements—the rectangular slot—has not been analyzed theoretically to the extent of obtaining a numerical result. The problem may be attacked by finding experimentally the equivalent circuit of the resonant element. This equivalent circuit serves as the basis for calculations on the more complicated multiple-element circuit. An equivalent circuit will be assumed, its behavior analyzed, and the assumption verified by comparison with experimental data.

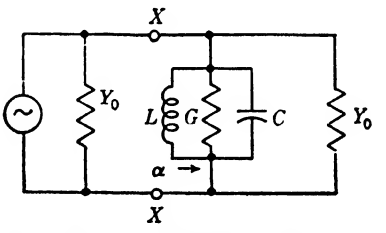

FIG. 3·4.—An equivalent circuit of a resonant element.

For analysis the resonant element may be regarded as a lumped inductance, capacitance, and conductance shunted across the line as shown in Fig. 3·4.

The susceptance B of the equivalent circuit of the resonant element may be defined by

$$B = \omega C - \frac{1}{\omega L}. \tag{1}$$

The frequency where $B = 0$ is the resonant angular frequency ω_0,

$$\omega_0^2 = \frac{1}{LC}. \tag{2}$$

The loaded Q_{L2} is defined (Sec. 2·2) by

$$Q_{L2} = \frac{\omega_0}{\omega_2 - \omega_1},$$

where ω_1 and ω_2 are the frequencies where the susceptance equals plus and minus the total conductance. They are given by

$$\omega_2 C - \frac{1}{\omega_2 L} = +(2Y_0 + G),$$
$$\omega_1 C - \frac{1}{\omega_1 L} = -(2Y_0 + G). \tag{3}$$

If the positive roots of Eqs. (3) are chosen,

$$Q_{L2} = \frac{\omega_0 C}{2Y_0 + G}. \tag{4}$$

Some investigators[1] have used a slightly different definition of Q_{L2}. They have defined

$$Q_{L2} = \frac{\omega_0}{\omega_2' - \omega_1'} \tag{5}$$

where ω_2' and ω_1' are the frequencies for which half the power is reflected. This definition is somewhat different from Eq. (4) if the conductance of the resonant element is not zero. Equation (3) gives the frequencies at which half of the power is transmitted by the resonant element, and these frequencies are not the same as ω_1' and ω_2'. To estimate the magnitude of inconsistency that might be expected, the power reflection at ω_2 will be computed. It is given by

$$B = 2Y_0 + G. \tag{6}$$

The admittance looking from left to right at X-X in the circuit of Fig. 3·4 is given, at ω_2, by

$$Y = Y_0 + G + j(2Y_0 + G). \tag{7}$$

The reflection coefficient is

$$\Gamma = -\frac{G + j(2Y_0 + G)}{2Y_0 + G + j(2Y_0 + G)}, \tag{8}$$

from which the fraction of the power reflected is

$$|\Gamma|^2 = \frac{1}{2} + \frac{G^2}{2(2Y_0 + G)^2}. \tag{9}$$

The resonant elements discussed in this chapter usually have a value of G less than $0.1Y_0$. This means a difference from half-power reflection of about 0.2 per cent. The effect of conductance in the resonant element, therefore, may be considered to be small, and either definition of Q_{L2} may be applied.

[1] See Ref. (4) in the bibliography at the end of the chapter. Hereafter superscript numbers refer to this bibliography.

The equation for the circuit of Fig. 3·4, relating the susceptance to frequency in terms of Q_{L2}, is

$$B = 2Q_{L2}(2Y_0 + G)\left(\frac{\omega - \omega_0}{\omega_0}\right).$$

Also, the power reflected has already been obtained

$$|\Gamma|^2 = \frac{G^2 + B^2}{(2Y_0 + G)^2 + B^2}. \qquad (9a)$$

It is often useful to have an expression for B in terms of r since it is r that is obtained by measurement. It is easily found that

$$B = \left[\frac{(Y_0^2 + Y_0G)(r-1)^2 - rG^2}{r}\right]^{1/2}, \qquad r \geqq 1. \qquad (10)$$

A measurement of r at the resonant frequency, that is, at the frequency for which $B = 0$, can be used to determine G,

$$G = Y_0(r - 1), \qquad r \geqq 1. \qquad (11)$$

In Fig. 3·5 are shown curves representing Eq. (9a) for $G/Y_0 = 0$ and $G/Y_0 = 0.3$. Such a large value of G is not typical for the resonant

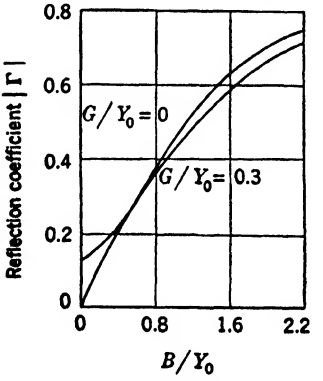

FIG. 3·5.—The absolute magnitude of the reflection coefficient as a function of susceptance of a single resonant circuit.

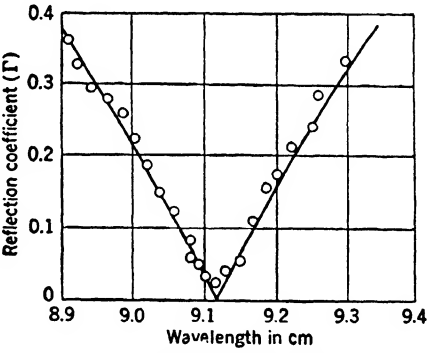

FIG. 3·6.—Comparison of experimental data with a theoretical resonant-circuit curve.

elements discussed in this chapter. The large value was chosen to give better portrayal of the curves.

In Fig. 3·6 the calculated reflection coefficient is plotted as a function of wavelength to compare with data taken on a resonant element. The calculations were made using the values of the resonant frequency and the Q_{L2} obtained from the experimental curve. The data for Q_{L2} were taken at $r = 2$ or $|\Gamma| = 0.33$; therefore the theoretical and experimental

curves should match at the resonant frequency, except for the fact that loss was neglected, and their width should be the same at $|\Gamma| = 0.33$. The fact that the experimental points lie closely on the theoretical curve indicates that, over the frequency range of the curve, the physical structure is well represented by the assumed circuit as far as reflections are concerned.

Throughout this discussion of the single resonant element, an equivalent circuit has been considered from the standpoint of the reflection characteristics of the element. To understand the gas-discharge properties of the element, it is important to know the electric field in the gap in terms of the voltage in the guide. For the simple circuit, if the capacitance were assumed to be concentrated in the gap, the voltage across the gap would be the same as across the waveguide. However, a rough measurement on a gap of the post type seems to indicate that the ratio of the voltage across the gap to the voltage across the guide is about

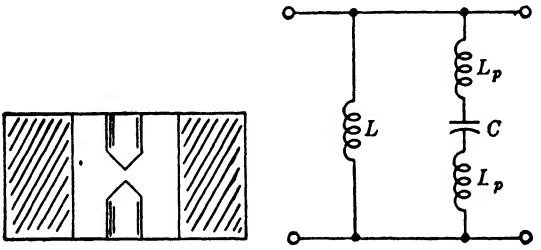

FIG. 3·7.—Equivalent circuit of resonant gap.

ten. This measurement was made by placing a platinized-glass resistor across the gap and measuring the standing-wave ratio at resonance. The resistance of the platinized-glass resistor at the microwave frequency was taken to be the d-c resistance. Furthermore, it is known from theory and from experiment that a post in the plane of the electric field in waveguide behaves as an inductance shunted across the line. In a resonant element of the post type, the inductance of the post would be expected to be in series with the capacitance of the gap. Both the rough experiment and the analysis of the resonant element in terms of simpler structures leads to an expectation of a stepup of gap voltage over guide voltage.

It is well to assume a very simple circuit to estimate the stepup in voltage. In Fig. 3·7 L_p is the inductance of each post, and L is the inductance associated with the magnetic-energy storage due to the narrowing of the guide. It is assumed that there is no mutual coupling between L and L_p. The discharge, or gas breakdown, takes place across the condenser C. The ratio between the voltage across the gap and the voltage across the guide may be calculated for two special cases. In the

fired condition the gap circuit may be represented as in Fig. 3·8*a* and for the unfired condition as in Fig. 3·8*b*.

The ratio $|E/e|$ for Fig. 3·8*a* is

$$\left|\frac{E}{e}\right| = \frac{Z_0 X}{\sqrt{Z_0^2(X + X_p)^2 + X_p^2 X^2}} \approx \frac{X}{X_p} \frac{Z_0}{\sqrt{Z_0^2 + X^2}}.$$

In the unfired case and where $X = \omega L_1$ and $X_p = 2\omega L_p$ at resonance, the ratio E/e for Fig. 3·8*b* may be written as

$$\left|\frac{E}{e}\right| = \frac{X}{X + X_p},$$

since $X_c = -(X + X_p)$, at resonance.

In the first case, it was assumed that the gap was broken down and that as a result, the gap voltage was held constant. In the second

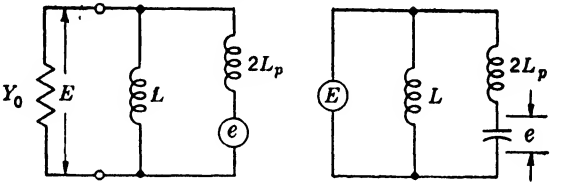

(*a*) (*b*)

FIG. 3·8.—Circuit of resonant gap for (*a*) fired condition; (*b*) unfired.

case, the gap is not fired and interest is in the gap voltage corresponding to a given fixed line voltage. The Q of the circuit of Fig. 3·8*b* is given by

$$Q = \frac{K}{X_c}\left(\frac{X + X_p}{X}\right)^2 = K\frac{X + X_p}{X^2}.$$

Let us now assume that the gap will ionize at some definite voltage $\bar{e}$, that this voltage is proportional to the gap spacing g, and that $X_c \propto g/a$, where a is the area of the end of the post. Then at resonance,

$$\bar{e} = kaX_c = ka(X + X_p),$$

and the critical line voltage will be

$$\bar{E} = \bar{e}\frac{X}{X + X_p} = kaX.$$

This equation indicates that for a fixed resonant frequency, the critical, or breakdown, voltage E is proportional to the area of the ends of the posts and the reactance X of the inductive iris. Examination of the equation for Q shows that if X is held constant, the loaded Q can be reduced by making X_p smaller without affecting $\bar{E}$. Since $\bar{E}$ is a measure of the spike energy, it should be possible, by proper shaping of the electrodes, to obtain a minimum value of Q for a given spike energy.

The assumptions and calculations made above are only the most elementary since they do not take into account mutual interaction between the fields of the inductive irises and the posts, nor do they consider the relative magnitude of the "stray" capacitance and the "lumped" capacitance of the gap. However, for a resonant iris of this type across a waveguide, the detailed solution of the boundary-value problem has never been carried out, and it is, therefore, necessary to approach the problem from the much simpler point of view used here..

3·3. Multiple Resonant Elements in Waveguides.—Several methods of analysis and representation have been used in the analysis of the problem of circuits containing more than one resonant element. As an introduction to this problem, a simplified method of calculating the power reflection and the insertion loss of the three-element circuit shown in Fig. 3·9 is presented here.

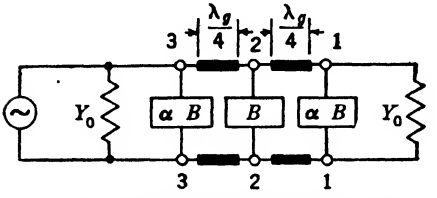

FIG. 3·9.—Three resonant elements separated by quarter wavelengths of line.

At the outset of the calculations, a line a quarter-wavelength long between the elements is assumed to be independent of frequency. Let the susceptance of the end elements be αB, and the susceptance of the center element be B. The following equations use normalized admittances, that is, $y = Y/Y_0$.

If y_1, y_2, and y_3 are regarded as the admittances looking from left to right at the appropriate terminals as shown in Fig. 3·9,

$$y_1 = 1 + j\alpha b, \tag{12}$$

$$y_2 = jb + \frac{1}{y_1} = jb + \frac{1}{1 + j\alpha b} = \frac{1 - \alpha b^2 + jb}{1 + j\alpha b}. \tag{13}$$

and

$$y_3 = j\alpha b + \frac{1}{y_2} = \frac{1 - \alpha b^2 + j(2\alpha b - \alpha^2 b^3)}{1 - \alpha b^2 + jb}. \tag{14}$$

By the use of

$$\Gamma = \frac{1 - y_3}{1 + y_3},$$

the reflection coefficient is then

$$\Gamma = \frac{j(b - 2\alpha b + \alpha^2 b^3)}{2 - 2\alpha b^2 + j(b + 2\alpha b - \alpha^2 b^3)}. \tag{15}$$

The reflected power becomes

$$|\Gamma|^2 = \frac{b^2(1 - 2\alpha + \alpha^2 b^2)^2}{4 + b^2(1 - 2\alpha + \alpha^2 b^2)^2}. \tag{16}$$

It is convenient to define power loss L as the reciprocal of the transmitted power expressed in decibels, thus

$$L = 10 \log_{10} \frac{\text{Input power}}{\text{Output power}}. \tag{17}$$

If there are no resistive losses in the circuit, the loss may be written in terms of the reflected power,

$$L = 10 \log_{10} \frac{1}{1 - |\Gamma|^2}. \tag{18}$$

For the case under consideration

$$L = 10 \log_{10} \left[1 + \frac{b^2}{4} (1 - 2\alpha + \alpha^2 b^2)^2 \right]. \tag{19}$$

If $\alpha = 1$,

$$L = 10 \log_{10} \left[1 + \frac{b^2}{4} (1 - b^2)^2 \right]. \tag{20}$$

If $\alpha = \frac{1}{2}$,

$$L = 10 \log_{10} \left(1 + \frac{b^6}{64} \right). \tag{21}$$

If the circuit is composed of more than two elements with quarter-wavelength separation between elements, zero loss occurs for values of b of the individual elements other than zero. Between zeros the loss may be significant; the greater the number of elements, the larger may be the loss. It should be observed that the zeros can be eliminated by proper choice of the susceptances for the various elements. For the circuit of Fig. 3·9 it can be seen from Eq. (19) that the loss has a single zero only when $\alpha = \frac{1}{2}$. The loss curve obtained for $\alpha = \frac{1}{2}$ is analogous to the loss curve for a critically coupled double-tuned circuit. For a number of particular circuits shown in Fig. 3·10, Table 3·1 presents the reflected power and the ratio of input power to output power as a function of b.

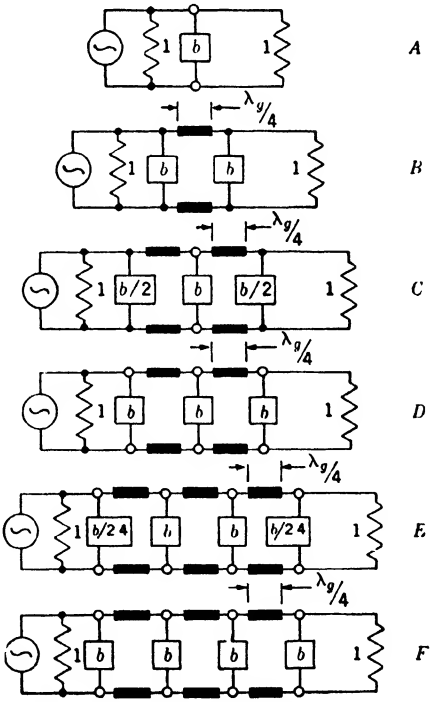

FIG. 3·10.—Multiple-element resonant circuits. The transmission characteristics are given in Table 3·1.

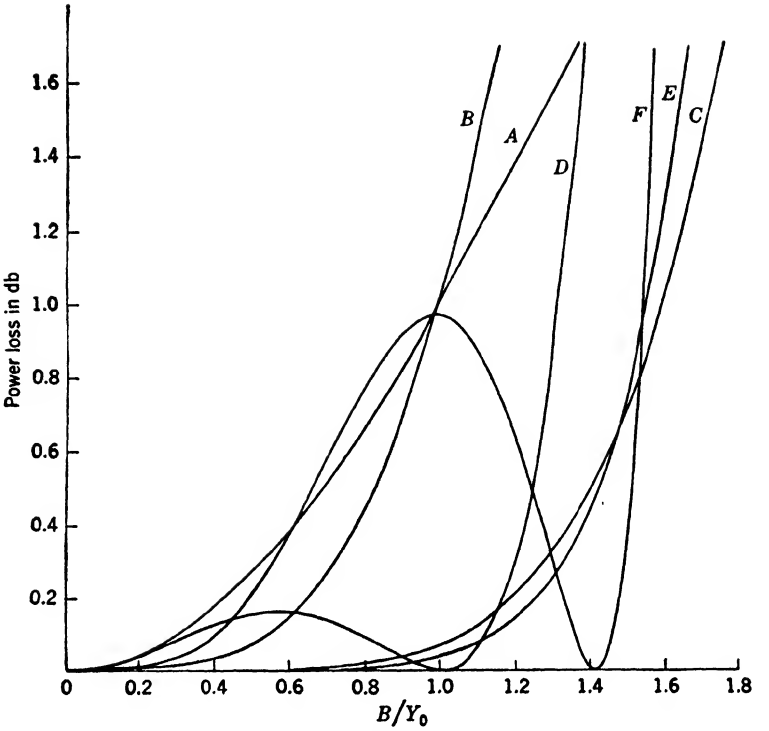

FIG. 3·11.—Bandpass characteristics according to the simple theory for the circuits of FIG. 3·10.

TABLE 3·1.—THE REFLECTED POWER AND THE RATIOS OF INPUT POWER TO OUTPUT POWER, EXPRESSED IN TERMS OF b FOR SEVERAL MULTIELEMENT CIRCUITS

Elements are separated by a quarter wavelength of line for the frequency corresponding to $b = 0$. The frequency dependence of the line length is neglected.

Circuit of Fig. 3·10	Reflected power	$\frac{\text{Input power}}{\text{Output power}}$
A	$\frac{b^2}{4 + b^2}$	$1 + \frac{b^2}{4}$
B	$\frac{b^4}{4 + b^4}$	$1 + \frac{b^4}{4}$
C	$\frac{b^6}{64 + b^6}$	$1 + \frac{b^6}{64}$
D	$\frac{b^2(b^2 - 1)^2}{4 + b^2(1 - b^2)^2}$	$1 + \frac{b^2}{4}(1 - b^2)^2$
E	$\frac{b^8}{136 + b^8}$	$1 + \frac{b^8}{136}$
F	$\frac{b^4(2 - b^2)^2}{4 + b^4(2 - b^2)^2}$	$1 + \frac{b^4}{4}(2 - b^2)^2$.

For the circuits of Table 3·1, Fig. 3·11 gives loss as a function of b. It is interesting to note that a condition can also be found for a four-element circuit which makes the loss characteristic a monotonically increasing function of b. For the four-element circuit the susceptance of the two end elements should be $1/(1 + \sqrt{2})$ times the susceptance of the central elements.

The importance of the magnitudes and the phases of both reflected and transmitted waves becomes clear in the discussion of microwave duplexers in Chap. 7 and in Vol. 16. The criterion of transmission band-

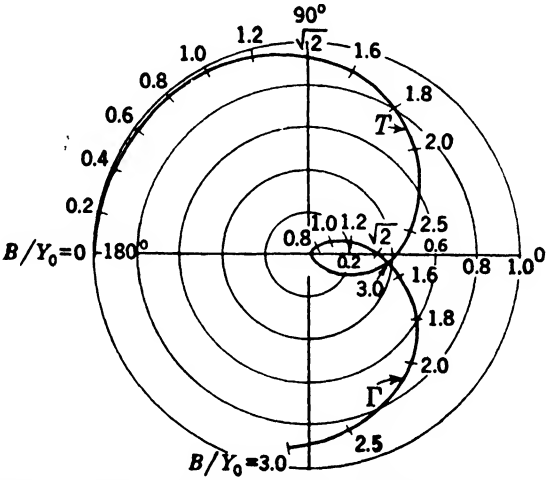

FIG. 3·12.—Reflection coefficient and transmission coefficient for circuit C of Table 3·1.

width of the TR tube may be considered to depend on the type of duplexer in which the tube is used.

From Eq. (15) and the expression for the transmission coefficient in voltage,

$$T = \frac{2}{1 + y_3}. \tag{22}$$

The reflection coefficient and the transmission coefficient can be presented as a polar plot on a Smith chart. These quantities are shown in Figs. 3·12 and 3·13 for two three-element circuits (C and D of Table 3·1). The susceptance is indicated along the curve. The phase of the reflection coefficient is measured at the element nearest the generator; the phase of the transmission coefficient is measured at the element nearest the load, with respect to the phase of the incident wave at the element nearest the generator.

The transmission coefficient is rotated through 180° corresponding to two quarter wavelengths of line at midband. In Fig. 3·12 only values

of the reflection and transmission coefficients for positive B were plotted since the curve is symmetrical about $B = 0$. It should be observed that for B/Y_0 between zero and 1.2, the angle of the reflection coefficient for the three-equal-element case varies between the limits $270° > \theta > 180°$ and $-30° < \theta < 0°$; for the unequal elements the range is $90° > \theta > 20°$. Although neither of the circuits possesses a

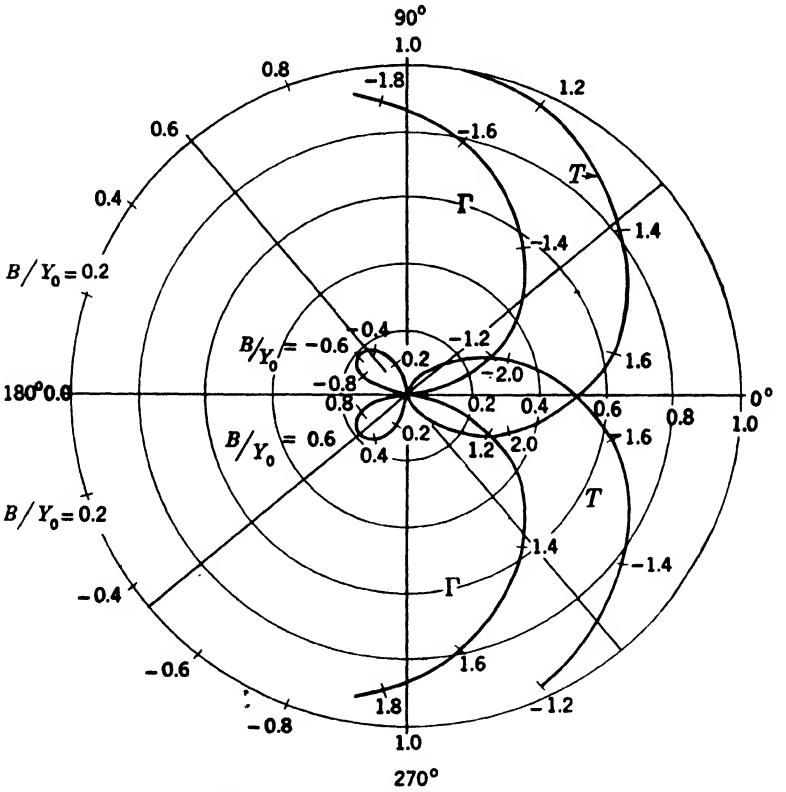

FIG. 3·13.—Reflection coefficient and transmission coefficient for circuit D of Table 3·1.

simple resonance behavior it seems more likely that, in the use of the TR tube in the duplexer, the unequal-element tube could be improved at the band edges by matching elements.

3·4. Wave Equilibrium Calculations.—By an equilibrium method of analysis, an expression can be obtained for the loss of a network composed of an arbitrary number of identical shunt elements equally spaced along a transmission line; and the frequency dependence of the spacing between elements need not be neglected. The presentation below was first used by Fiske and Warner[7] and later generalized by Marcus.[8]

In Fig. 3·14 are shown shunt elements with arbitrary spacings θ_p along a transmission line. To obtain either the reflection or the transmission from this complicated system, the multiple reflections could be considered, and the appropriate sum taken of the successive reflected and transmitted waves at the individual elements of the system. This becomes very complicated for more than two elements. A simpler method and the one adopted here relates the total traveling-wave amplitudes proceeding in each direction on each section of line in the equilibrium state to the amplitudes on the adjacent sections of line.

Let A_p and B_p represent the voltage amplitudes of waves traveling in the forward and backward directions at a reference position just after the pth element. Let t_p and r_p be the reflection and transmission coefficients for a wave advancing upon the pth element from the left, t'_p and

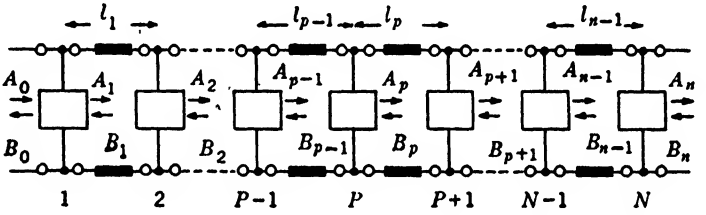

FIG. 3·14.—N lumped elements spaced at arbitrary intervals along a transmission line.

r'_p the coefficients for a wave advancing from the right. The electrical line length between the $(p-1)$th and the pth element is $\theta_{p-1} = 2\pi \dfrac{l_{p-1}}{\lambda_u}$ where l_{p-1} is the distance separating the elements. The total voltage wave advancing in the forward direction can be written

$$A_p = t_p A_{p-1} e^{-j\theta_{p-1}} + r'_p B_p, \tag{23}$$

if it is remembered that A_p, A_{p-1}, and B_p are all measured at the same instant of time; but the contribution to A_p from A_{p-1} was made earlier by a time interval corresponding to θ_{p-1}, hence the negative sign. For the wave in the negative direction,

$$B_{p-1} = r_p A_{p-1} e^{-2j\theta_{p-1}} + t'_p B_p e^{-j\theta_{p-1}}. \tag{24}$$

From Eqs. (23) and (24), B may be eliminated by solving Eq. (23), for B_{p+1}, substituting B_{p+1} into Eq. (23), solving Eq. (24) for B_p and then putting B_p back in Eq. (23). The result is

$$A_{p+1} + \left[\left(\frac{r_{p+1}r'_{p+1} - t_{p+1}t'_{p+1}}{t'_{p+1}}\right) e^{-j\theta_p} - \frac{r'_{p+1}}{r'_p t'_{p+1}} e^{j\theta_p}\right] A_p + \frac{r'_{p+1} t_p}{r'_p t'_{p+1}} e^{j(\theta_p - \theta_{p-1})} A_{p-1} = 0. \tag{25}$$

This equation may be simplified by assuming that the elements are all identical and are identically spaced. If $r_p = r$, $r'_p = r'$, $t_p = t'_p = t$, and $\theta_p = \theta$, are put into Eq. (25), it becomes

$$A_{p+1} + \left[\frac{(rr' - t^2)e^{-j\theta} - e^{j\theta}}{t}\right] A_p + A_{p-1} = 0. \tag{26}$$

For the n elements of Fig. 3·14, p runs from 1 to $n - 1$. To obtain the n ratios $A_1/A_0, \ldots, A_n/A_0$ requires one more equation. An additional equation is provided by the boundary condition that no wave is incident from the right, $B_n = 0$. From Eq. (23),

$$A_n = te^{-j\theta}A_{n-1}. \tag{27}$$

The general solution of Eq. (26) is given by

$$A_p = Me^{p\alpha} + Ne^{-p\alpha}, \tag{28}$$

provided that

$$\cosh \alpha = \frac{e^{j\theta} - (rr' - t^2)e^{-j\theta}}{2t}. \tag{29}$$

From Eq. (28)

$$A_0 = M + N,$$

and from Eqs. (27) and (28)

$$A_n = Me^{n\alpha} + Ne^{-n\alpha} = te^{-j\theta}[Me^{(n-1)\alpha} + Ne^{-(n-1)\alpha}]. \tag{30}$$

The transmission coefficient for the n elements, T_n, is defined by

$$T_n = \frac{A_n}{A_0}. \tag{31}$$

From Eq. (28)

$$T_n = \frac{\frac{M}{N}e^{n\alpha} + e^{-n\alpha}}{\frac{M}{N} + 1}. \tag{32}$$

If Eq. (30) is solved for M/N to substitute in Eq. (32)

$$T_n = \frac{te^{-j\theta}\sinh \alpha}{\sinh n\alpha - te^{-j\theta}\sinh (n-1)\alpha}, \tag{33}$$

or more conveniently

$$\frac{1}{T_n} = \cosh n\alpha + \frac{e^{\theta} + (rr' - t^2)e^{-j\theta}}{2t}\frac{\sinh n\alpha}{\sinh \alpha}. \tag{34}$$

In a similar manner the reflection coefficient $R_n = B_0/A_0$ is found to be

$$R_n = re^{-2j\theta}\left[\frac{\sinh n\alpha - \frac{t^2}{rr'}\cosh \alpha \sinh (n-1)\alpha}{\sinh n\alpha - te^{-j\theta}\sinh (n-1)\alpha}\right]. \tag{35}$$

If the transmission and the reflection coefficients of the individual elements are known, from Eqs. (33) and (35), the transmission and reflection from the network is known. It is convenient to write the equations in terms of circuit parameters. As yet, the elements have not actually been restricted to a shunt component; the elements may still be regarded as general T-sections. Since in this book, however, the general formulas will be applied only to shunt susceptances, Eqs. (34) and (35) are written in terms of shunt susceptance. For a symmetrical T-section $r = r'$. In terms of b, the reflection and transmission coefficients may be written

$$r = r' = -\frac{jb}{2 + jb}, \tag{36}$$

and

$$t = \frac{2}{2 + jb}. \tag{37}$$

Equations (35) and (36) become

$$\frac{1}{T_n} = \cosh n\alpha + j\left(\sin\theta + \frac{b}{2}\cos\theta\right)\frac{\sinh n\alpha}{\sinh\alpha}, \tag{38}$$

and

$$\frac{1}{R_n} = -\frac{2j}{b} - 1 + \frac{2j}{b}e^{j\theta}\frac{\sinh(n+1)\alpha}{\sinh n\alpha}, \tag{39}$$

where

$$\cos\alpha = \cos\theta - \frac{b}{2}\sin\theta. \tag{40}$$

If the line is terminated in its characteristic admittance, it is sufficient to know the absolute magnitude of the transmission

$$\left|\frac{1}{T_n}\right|^2 = 1 + \left(\frac{b}{2}\frac{\sinh n\alpha}{\sinh\alpha}\right)^2, \tag{41a}$$

or

$$\left|\frac{1}{T_n}\right|^2 = 1 + f_r^2. \tag{41b}$$

The information provided in Eqs. (41) makes it possible to obtain, for a given b and θ, either the loss, the reflected power, the transmitted power, or the voltage standing-wave ratio. It is convenient to prepare a chart as shown in Fig. 3·15 in which $2\theta/\pi$ is plotted against b for constant values of f. On this chart may be superimposed a curve relating the frequency dependence of susceptance of the individual element to θ. Points of intersection of this latter curve with the constant-f curves give data on voltage standing-wave ratio as a function of the susceptance of the individual element.

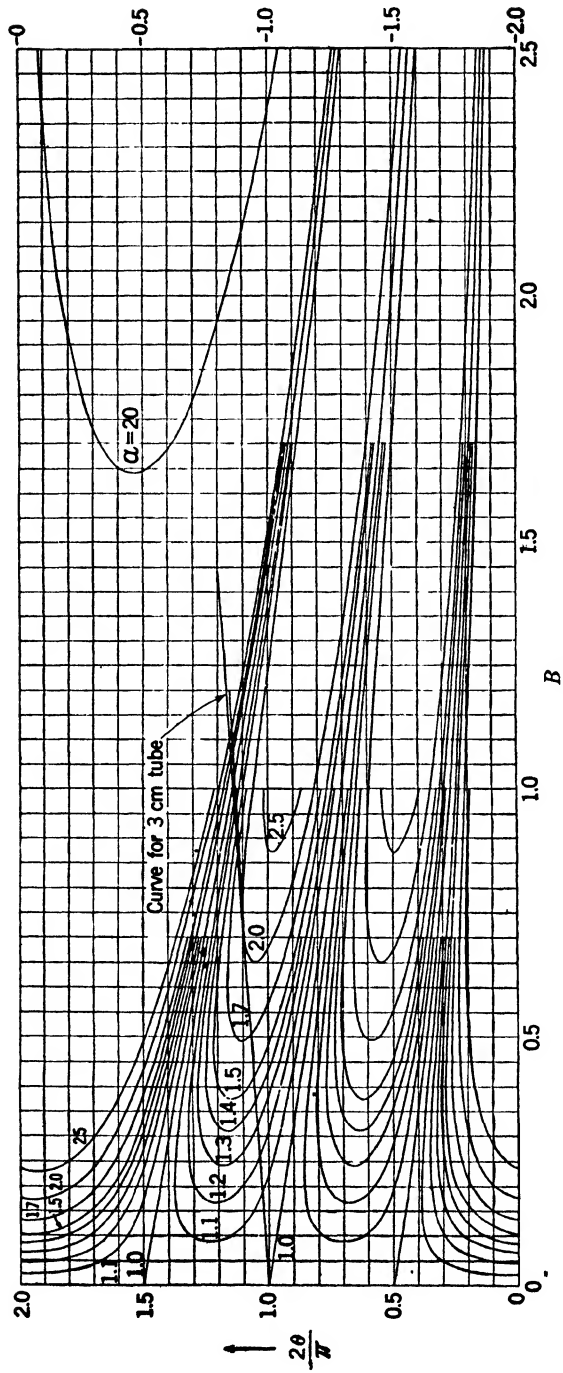

FIG. 3·15.—Marcus' chart for calculation of bandpass characteristics of four identical elements for arbitrary line frequency-sensitivity.

As an example of the use of the filter chart, consider four identical high-Q shunt elements usually spaced a quarter-wavelength apart. The term high-Q implies that the element separation remains essentially a quarter wavelength, or that $2\theta/\pi = 1$ over a wide range of b. Along the line $2\theta/\pi = 1$, as b increases from zero at midband, the standing-wave ratio increases to slightly over 2.5 and then decreases to unity for $b = 1.41$. As b increases from 1.41, the standing-wave ratio increases rapidly. If the frequency dependence of the spacing may be neglected, the transmission band will be symmetrical with respect to $b = 0$. The result of this procedure leads to the same result as that derived by the simple theory and shown by curve F in Fig. 3·11.

If the Q of the elements is so low that the electrical-line-length separation of the elements varies considerably over the transmission band, the frequency sensitivity of the element susceptance should be given as $b = f(2\theta/\pi)$. The bandpass characteristic can be traced out by following the $b = f(2\theta/\pi)$ curve just as, in the preceding case, the curve $2\theta/\pi = 1$ was followed. For negative b, to use the same chart, $2\theta/\pi$ has to run in the direction opposite to that for positive b. On the chart is superimposed a curve relating b to $2\theta/\pi$ for elements in standard 3-cm guide, whose Q_{L2} is four and whose resonant wavelength is 3.33 cm. Figure 3·16 shows the voltage standing-wave ratio as a function of b from data extracted from the chart. It is interesting to compare this curve with curve F of Fig. 3·11 which neglects the frequency dependence of the separation of the elements.

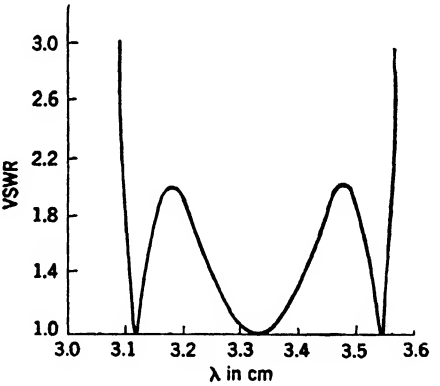

FIG. 3·16.—Four-equal-element bandpass characteristics extracted from Marcus' chart.

It should be pointed out that f is periodic in $2\theta/\pi$ with a period of 2. Therefore, if a susceptance curve runs off the top of the chart, it may be continued at the bottom. The value of $2\theta/\pi$ which yields the broadest transmission band is then near one. The reader should be interested in superimposing a family of susceptance curves on the chart with $2\theta/\pi$ at $b = 0$ as a parameter. From this family of curves and for the susceptance characteristic chosen, the optimum element separation for maximizing the bandwidth should be evident.

3·5. Matrix Method.—The use of the matrix notation leads to a fairly simple formula for loss. This method[2] may be applied satisfactorily to a multiple circuit of nonidentical elements, a difficult case to handle by the

equilibrium method. However, the general expressions for the loss of n elements, which are obtained by the equilibrium method, cannot be obtained easily by the matrix method.

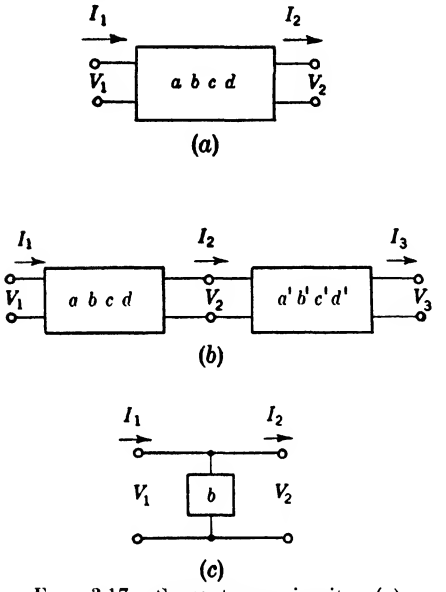

FIG. 3·17.—Susceptance circuits—(*a*) a four-terminal network; (*b*) two successive four-terminal networks; (*c*) a shunt susceptance.

If the four-terminal network of Fig. 3·17*a* is linear and passive, and if reciprocity applies, two linear equations relate any two of the quantities I_1, V_1, I_2, and V_2 to the other two. For example,

$$V_1 = aV_2 + bI_2, \qquad (41)$$
$$I_1 = cV_2 + dI_2.$$

In the matrix notation

$$\begin{pmatrix} V_1 \\ I_1 \end{pmatrix} = \begin{pmatrix} a & b \\ c & d \end{pmatrix} \begin{pmatrix} V_2 \\ I_2 \end{pmatrix}, \qquad (42)$$

where a, b, c, and d are constants defined by the electrical constants composing the network. The parameters must satisfy the following conditions:

1. For a lossless network the diagonal terms of the matrix are real and the off-diagonal terms are imaginary.
2. If reciprocity applies,
$$ad + bc = 1.$$
3. If the network is symmetrical,
$$a = d.$$

If there are two successive networks as in Fig. 3·17*b*, for the second network

$$\begin{pmatrix} V_2 \\ I_2 \end{pmatrix} = \begin{pmatrix} a' & b' \\ c' & d' \end{pmatrix} \begin{pmatrix} V_3 \\ I_3 \end{pmatrix}, \qquad (43)$$

and by substitution of Eq. (43) in Eq. (42), for the two networks

$$\begin{pmatrix} V_1 \\ I_1 \end{pmatrix} = \begin{pmatrix} a & b \\ c & d \end{pmatrix} \begin{pmatrix} a' & b' \\ c' & d' \end{pmatrix} \begin{pmatrix} V_3 \\ I_3 \end{pmatrix}. \qquad (44)$$

By multiplying the matrices of Eq. (44) and by using the first condition of the preceding paragraph, there is obtained for a lossless network

$$\begin{pmatrix} V_1 \\ I_1 \end{pmatrix} = \begin{pmatrix} A & jB \\ jC & D \end{pmatrix} \begin{pmatrix} V_3 \\ I_3 \end{pmatrix}, \qquad (45)$$

where V_1 and I_1 represent the input voltage and current to a sequence of networks, and V_3 and I_3 represent the output voltage and current.

In the present calculations, only shunt elements and lengths of line without loss are of interest. For the shunt element of Fig. 3·17*c*

$$\begin{aligned} V_1 &= V_2, \\ I_1 &= jbV_2 + I_2. \end{aligned} \tag{46}$$

The matrix representation of the shunt element is therefore

$$\begin{pmatrix} V_1 \\ I_1 \end{pmatrix} = \begin{pmatrix} 1 & 0 \\ jb & 1 \end{pmatrix} \begin{pmatrix} V_2 \\ I_2 \end{pmatrix}. \tag{47}$$

A line length of l may be represented by

$$\begin{pmatrix} V_1 \\ I_1 \end{pmatrix} = \begin{pmatrix} \cos\theta & jZ_0 \sin\theta \\ jY_0 \sin\theta & \cos\theta \end{pmatrix} \begin{pmatrix} V_2 \\ I_2 \end{pmatrix}, \tag{48}$$

where

$$\theta = \frac{2\pi l}{\lambda_g}.$$

Equation (48) may be verified by reducing it to the usual expression for the transformation of impedance through a length of line

$$Z_1 = \frac{Z_2 + jZ_0 \tan\theta}{jZ_2Y_0 \tan\theta + 1},$$

where $Z_1 = V_1/I_1$ and $Z_2 = V_2/I_2$.

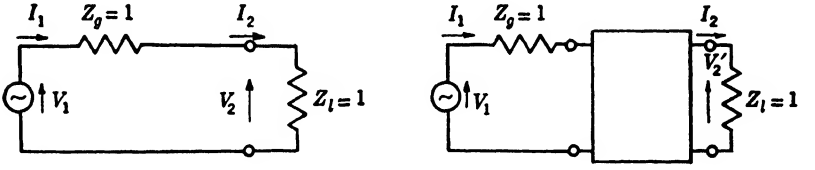

(*a*) (*b*)

FIG. 3·18.—Parameters for definition of insertion loss.

For the multiple-element network, it is desired to calculate the insertion loss. The insertion loss is the logarithm of the ratio of the power delivered to a load of unit relative impedance with the network removed from the line to the power delivered to the load with the network included. By reference to Fig. 3·18, it can be seen that the insertion loss is defined as

$$L = 10 \log_{10} \left|\frac{V_2}{V_2'}\right|^2. \tag{49}$$

From Fig. 3·18*a*,

$$\begin{pmatrix} V_1 \\ I_1 \end{pmatrix} = \begin{pmatrix} 1 & 1 \\ 0 & 1 \end{pmatrix} \begin{pmatrix} V_2 \\ I_2 \end{pmatrix}.$$

From Fig. 3·18*b*,

$$\begin{pmatrix} V_1 \\ I_1' \end{pmatrix} = \begin{pmatrix} 1 & 1 \\ 0 & 1 \end{pmatrix} \begin{pmatrix} A & jB \\ jC & D \end{pmatrix} \begin{pmatrix} V_2' \\ I_2' \end{pmatrix}.$$

With some manipulation

$$L = 10 \log_{10} [1 + \tfrac{1}{4}(B - C)^2]. \tag{50}$$

The method outlined will be applied to calculate the insertion loss due to a particular network including the frequency dependence of line length. The network of Fig. 3·19 will be considered and normalized admittances will be used. The middle element may be divided into two equal shunt elements. This permits transformation through the network by means of two identical matrices,

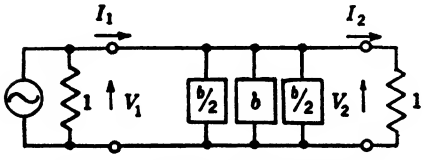

FIG. 3·19.—A three-element circuit.

$$\begin{pmatrix} V_1 \\ I_1 \end{pmatrix} = \mathsf{AA} \begin{pmatrix} V_2 \\ I_2 \end{pmatrix}, \tag{51}$$

where

$$\mathsf{A} = \begin{pmatrix} 1 & 0 \\ j\dfrac{b}{2} & 1 \end{pmatrix} \begin{pmatrix} \cos\theta & j\sin\theta \\ j\sin\theta & \cos\theta \end{pmatrix} \begin{pmatrix} 1 & 0 \\ j\dfrac{b}{2} & 1 \end{pmatrix}. \tag{52}$$

After the matrices of Eq. (52) are multiplied, it is relatively easy, by means of Eq.(50), to evaluate the insertion loss.

$$L = 10 \log_{10} \left\{ 1 + \left[\frac{b}{8} (b \sin\theta - 4\cos\theta)(b\sin\theta - 2\cos\theta) \right]^2 \right\}. \tag{53}$$

3·6. Numerical Results.—The results for transmission loss, obtained either by the equilibrium method or by the matrix method, should be presented in such a way that they can be compared easily with the experimental results. Experimentally, loss (standing-wave ratio, or reflection coefficient) is measured as a function of frequency or of free-space wavelength, whereas theoretically, loss is related implicitly, through the relation of susceptance and of phase separation between elements, to free-space wavelength. It is of interest to rewrite several of these implicit formulas for loss.

For three identical elements equally spaced,

$$L = 10 \log_{10} \left\{ 1 + \frac{b^2}{4} \left[4 \left(\frac{b}{2} \sin\theta - \cos\theta \right)^2 - 1 \right]^2 \right\}; \tag{54}$$

for three equally spaced elements of which the end elements have half the susceptance of the central element,

$$L = 10 \log_{10} \left\{ 1 + \left[\frac{b}{8} (b \sin \theta - 4 \cos \theta)(b \sin \theta - 2 \cos \theta) \right]^2 \right\}; \quad (55)$$

and for four identical elements equally spaced,

$$L = 10 \log_{10} \left\{ 1 + 4b^2 \left(\cos \theta - \frac{b}{2} \sin \theta \right)^2 \left[2 \left(\cos \theta - \frac{b}{2} \sin \theta \right)^2 - 1 \right]^2 \right\}. \quad (56)$$

In these expressions $\theta = 2\pi(l/\lambda_g)$ where l is the distance between the elements and λ_g is the guide wavelength. The guide wavelength is in turn a function of free-space wavelength and also of the dimensions of the waveguide. It is given by the relation

$$\lambda_g = \frac{\lambda}{\sqrt{1 - \left(\frac{\lambda}{\lambda_c}\right)^2}},$$

where λ_c is the cutoff wavelength of the guide. The experimental results, which hold well over the ± 6 per cent frequency range important in TR-tube studies, will be used for the susceptance. The experiments show that b is proportional to the difference in wavelength from the resonant wavelength.

Since some TR tubes are built with elements which have a loaded Q_{L2} of approximately four, several theoretical curves are presented for $Q_{L2} = 4.0$. Figure 3·20 shows two theoretical bandpass curves for three identical elements spaced one-quarter guide wavelength apart for a free-space wavelength of 3.33 cm. Curve B represents the result when the quarter-wavelength spacing is assumed to be independent of frequency. Curve A is a plot of Eq. (54) which takes into account the frequency dependence of the spacing between elements. The theory that assumes constant spacing predicts a broader transmission band and a higher loss in the pass band. The same general result may be observed in a comparison of the two theories applied

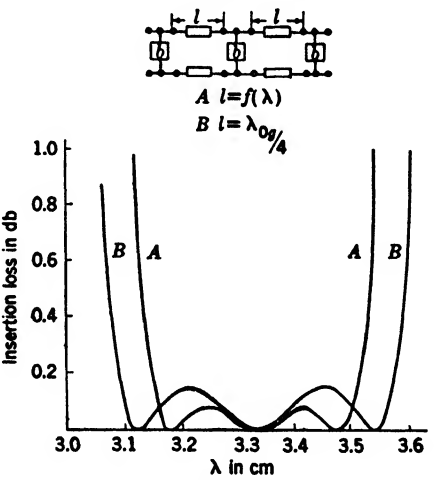

FIG. 3·20.—Comparison of two theories for three identical elements for which $Q_{L2} = 4.0$.

to a three-element circuit in which Q_{L2} of the end elements is half the value for the central element. This comparison is shown in Fig. 3·21. Note that the loss characteristic is very flat throughout the pass band.

Since θ depends on the guide wavelength, it can be expected that the percentage bandwidth will change if the center of the band is shifted and Q_{L2} of the elements kept the same. Waveguide of one size is used for three bands of particular interest centered about wavelengths of 8.475, 9.245, and 10.715 cm. In Fig. 3·22 the loss curves for three identical elements, $Q_{L2} = 4.0$, with quarter-wavelength (center of the band) spacings, are plotted as a function of λ/λ_0 to make the comparison

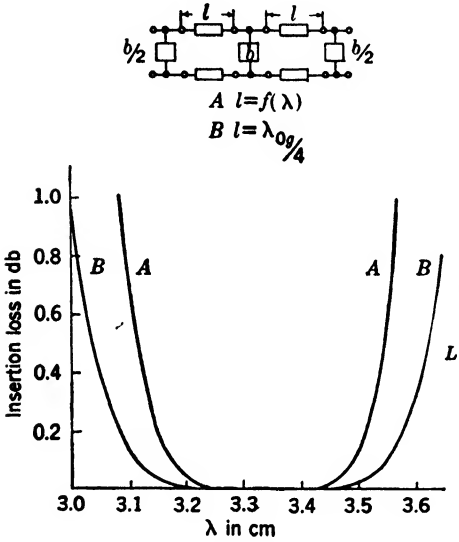

FIG. 3·21.—Comparison of two theories for three elements for which the middle element has $Q_{L2} = 4.0$.

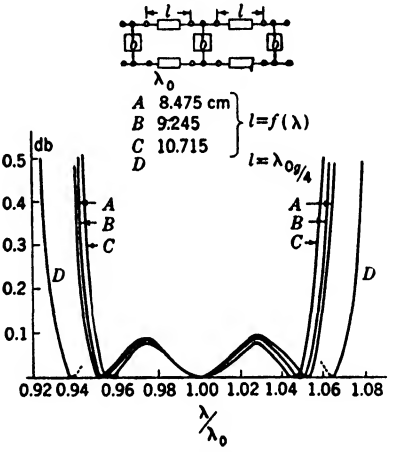

FIG. 3·22.—Effect of center band wavelength on insertion loss characteristic.

obvious. If the interval between the zeros of loss is used as a criterion of bandwidth, the percentage bandwidths are 10.0, 9.75, and 8.85 per cent respectively. The band becomes narrower and the loss in the pass band becomes less as the center wavelength approaches the cutoff wavelength for the guide. Curve *D* of Fig. 3·22 shows the pass band when the frequency sensitivity of the line lengths is neglected.

All the calculations presented in this chapter have been based on the assumption that the individual resonant circuit is lumped at a point along the transmission line. It is also assumed that the coupling between the resonant elements is negligible. At short wavelengths this assumption may not be valid. The comparison of theory with experimental data is made in Sec. 3·7.

EXPERIMENTAL RESULTS

3·7. Multiple-element Circuits.—Considerable data have been taken on loss or, more usually, voltage standing-wave ratio, as a function of wavelength for circuits with several elements. Qualitatively, the agreement between experiment and theory is good. No precision measurements have been taken because experimental research was concentrated upon the more formidable gas-discharge problem.

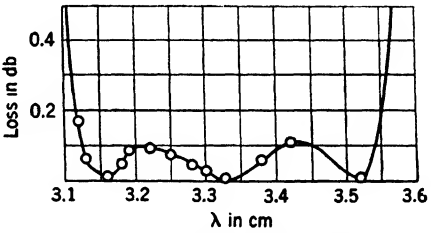

FIG. 3·23.—Experimental results on three-element bandpass. Q_{L2} of each element = 4.0.

One set of data is available for which the theoretical calculations have been presented. In the 3-cm region three identical elements, with equal spacings of a quarter guide wavelength, have $Q_{L2} = 4.0$. In Fig. 3·23 the loss in decibels is plotted as a function of wavelength to permit comparison with the theoretical curves of Fig. 3·20. One side of the band is not

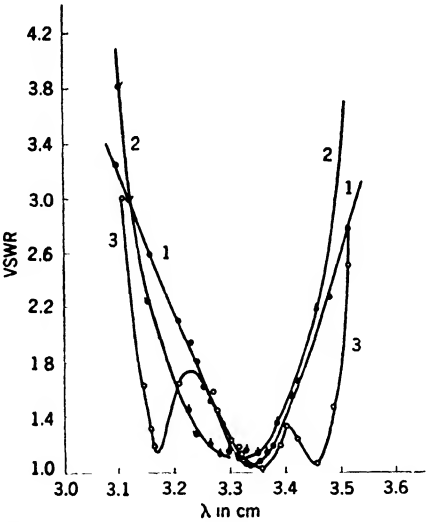

FIG. 3·24.—Experimental bandpass characteristic for one, two, and three elements. All elements essentially identical.

well defined because of lack of data; nevertheless it is fairly clear that the experimental result lies between the two theories. It would be expected that the experimental data would agree more closely with that theory which includes the effect of frequency dependence of line length.

The failure of the data to agree with this theory may be attributed either to coupling between the elements or to lack of precision in the measurements. It would be interesting to make more precise measurements in order to make a more reliable comparison with theory.

Another set of data[8] at 3-cm wavelength is shown in Fig. 3·24. The bandpass characteristics for one, two, and three elements were measured in terms of the voltage standing-wave ratios. These elements have a loaded Q_{L2} of 4.8 which is higher than the value for which theoretical calculations were made. Nevertheless, the three curves show clearly that the transmission bandwidth increases as the number of elements increases. For the three-element characteristic, three minima occur which correspond to the three zeros of loss in the theory of the three-element circuit. The three-element characteristic is not symmetrical because the elements are not all tuned accurately to the same frequency. For proper gas-discharge characteristics, the gap in the element has to be made small. A small gap implies that the ratio of the resonant-frequency shift to change in gap spacing is large; consequently, accuracy of tuning of the individual elements is one of the difficult problems in the manufacture of the bandpass TR tube.

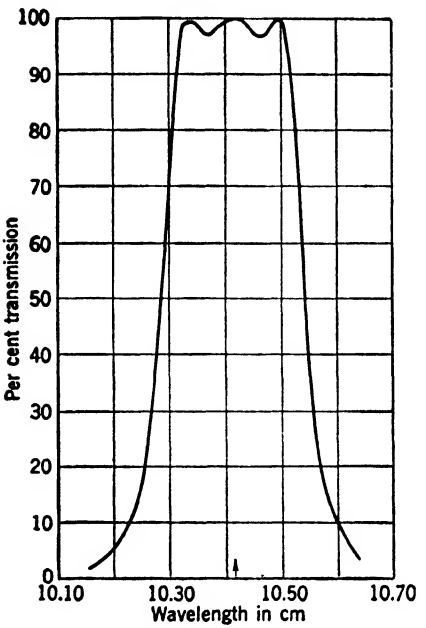

FIG. 3·25.—Three-element bandpass characteristic for elements with $Q_{L3} = 29$.

Another example of a three-element bandpass characteristic is shown in Fig. 3·25 for the 10-cm band and for elements with $Q_{L2} = 29$. For such large values of Q_{L2}, the bandpass width agrees closely with that predicted by the simple theory. Actually there is little departure from the simple theory for Q_{L2} above ten.

Figure 3·26 shows the effect of tuning each element of a two-element circuit to slightly different frequencies.[4] Curve A represents both elements tuned to $\lambda_0 = 9.692$ cm. For curve B one of the elements has been tuned to a different resonant wavelength, $\lambda = 9.592$ cm. When the two elements are tuned to the same frequency, the bandpass characteristic is centered about the resonant frequency; when they are tuned to different frequencies, the band center is at the mean of the frequencies.

For elements tuned to different frequencies, any gain in bandwidth is achieved at the expense of low loss within the band.

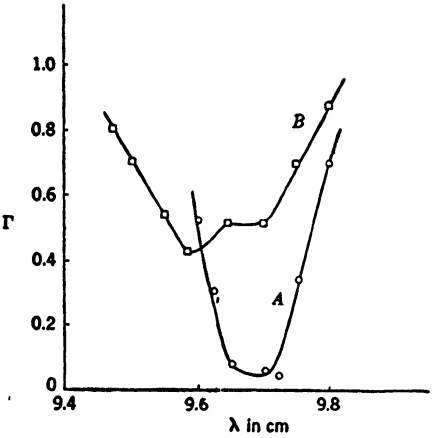

FIG. 3·26.—Effect of stagger-tuning two elements.

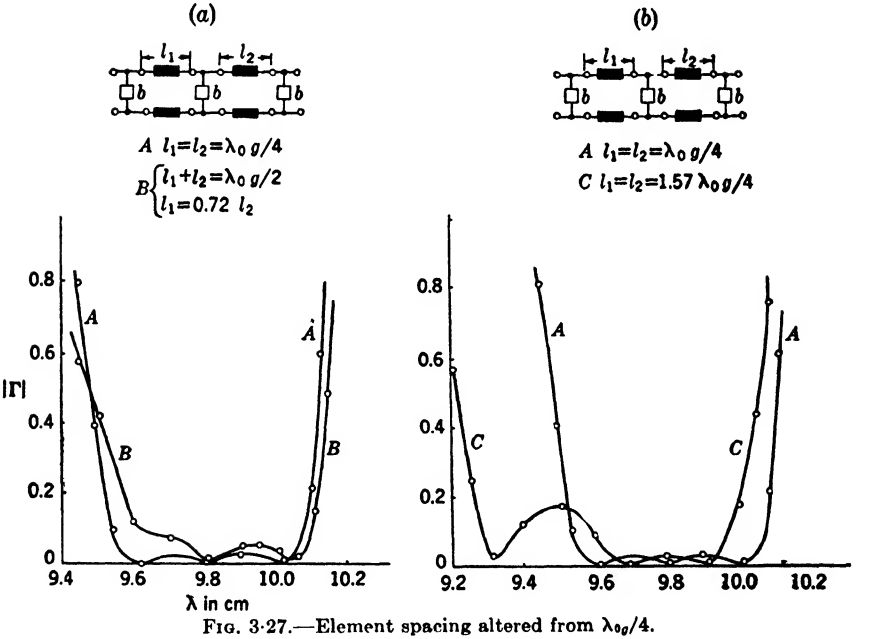

FIG. 3·27.—Element spacing altered from $\lambda_0 g/4$.

From Fig. 3·15 it has been seen that, in order to achieve maximum bandwidth for a circuit with four equal elements, it is best to space the elements about a quarter guide wavelength apart. This is also true for a three-element circuit. However, it is interesting to see the effect on

the bandpass characteristic as the spacing between elements is permitted to depart from a quarter guide wavelength. This effect is, in general, a destruction of the symmetry of the bandpass characteristic as shown by the curves[4] in Fig. 3·27. The elements in these circuits were tuned individually in a piece of waveguide and then removed to be incorporated in the multiple-element circuit. Another example[9] of the effect of altering the electrical spacing from a quarter wavelength is shown in Fig. 3·28. In both examples in Fig. 3·28 the elements of the circuit were tuned by the maximum-transmission method. Curve *A* was obtained when the tube was tuned to a center wavelength of 8.4 cm, for Curve *B* the tube was tuned at 8.54 cm. Figures 3·27, and 3·28 indicate that the bandwidth is increased by spacing the elements more than a quarter wavelength apart. For the increased spacing there is greater loss in the

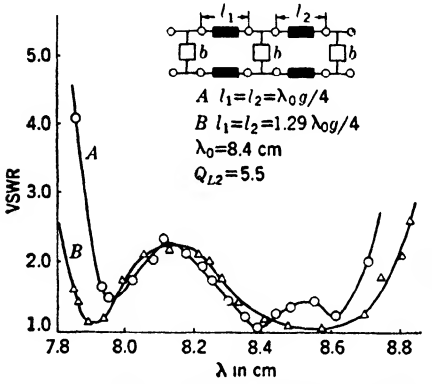

FIG. 3·28.—Element spacing altered from $\lambda_{0g}/4$ tuned by maximum transmission method.

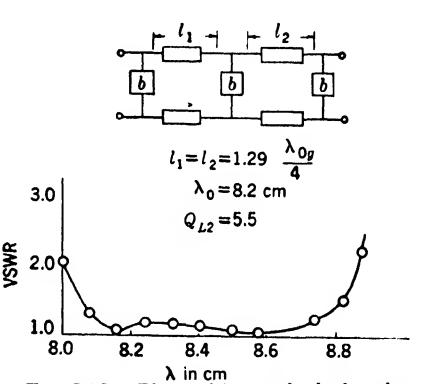

FIG. 3·29.—Phase-shift method of tuning.

transmission band. By a different tuning procedure, the phase-shift method, the bandpass characteristic can be made flat, Fig. 3·29. This is accomplished, perhaps, by compensating for the departure from quarter-wavelength spacing by a slight stagger-tuning. It should be observed that when the elements are tuned to give the flat bandpass characteristic, the bandwidth has been reduced. It seems likely that little can be gained by a combination of stagger-tuning and spacing of the elements; elements with quarter-wavelength spacing and identical tuning seem to yield the optimum bandwidth for elements all of which have the same Q_{L2}.

The four-element bandpass characteristic shown in Fig. 3·30 is interesting in that it confirms the theoretical result for a multiple-element circuit with the Q_{L2} of the end elements lower than that of the central elements. The central elements had a Q_{L2} of 4.5. Both the experimental

curve and curve D of Fig. 3·11 show a monotonic increase of loss with wavelength off the band center. The immediate supposition is that, if the Q_{L2} of the element is increased gradually, keeping the network symmetrical, a family of bandpass characteristics is obtained as curve D of Fig. 3·11 goes over into curve F. By accepting a somewhat increased loss within the pass band, it may be possible to extend the usual four-element band in this fashion.

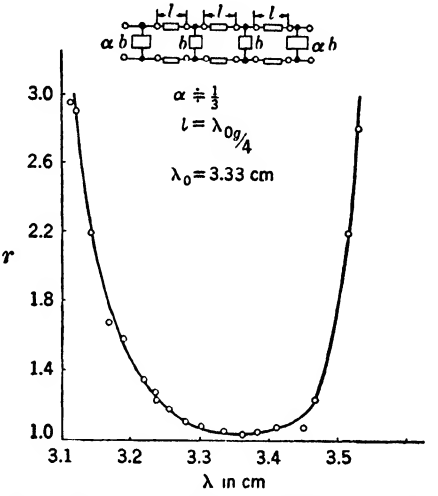

FIG. 3·30.—Four-element bandpass characteristic.

The theoretical calculations with which the experimental data have been compared all neglected the resistive losses in the resonant elements. If these losses were taken into account, the effect would be to increase the insertion loss slightly over the pass band. This is illustrated in Fig. 10·88 in Vol. 9 of this series.[2] The bandwidth over which the loss is less than a given small amount is reduced somewhat. The effects are, on the whole, rather small, and their neglect is justified for most cases.

3·8. Bandpass-TR-tube Design.—Throughout the preceding sections attention has been devoted solely to the consideration of multiple-resonant elements in waveguide and their effect on the transmission band. Now it is appropriate to mention briefly several additional factors which influence the design of a bandpass TR tube.

The most important factor is the fact that the TR tube must have such gas-discharge characteristics that the radar receiver is short-circuited promptly when the magnetron starts generating r-f power. In other words, the gas discharge in the gaps of the resonant elements must be formed so quickly that insufficient r-f power is transmitted to the receiver to burn out the mixer crystal. Crystal protection is the prime requisite of the TR tube. It will be seen in Chap. 5 that the gas discharge is initiated more quickly for a small gap spacing than for a large one, which implies that the resonant element has a high Q_{L2}. The gas-discharge phenomena dictate an upper limit to gap spacing and to a certain extent, a lower limit to Q_{L2}.

Since crystal protection demands a high Q_{L2}, and since an increase in bandwidth may be achieved only by reducing Q_{L2}, a compromise must be reached. To ensure that such a compromise approach an optimum,

considerable data have been accumulated on Q_{L2}, and on gap spacing of the resonant element as a function of its shape and size.

To build a tube which retains the appropriate gas at low pressure and which permits the transmission of r-f energy, a window is needed at each end of the tube. It is well to keep in mind the schematic diagram of the internal structure of the 3-cm band and the 10-cm band TR tubes which is shown in Figs. 3·2 and 3·1. The windows are made by sealing glass to a metal frame. If the proper dimensions are chosen, these windows can be made to resonate at a prescribed frequency.

Absorption loss has been neglected in the theory, and in the experimental results so far presented it has been negligible. In a TR tube which requires glass windows, however, the absorption loss may become quite important. In Sec. 3·10 it will be noted that the absorption loss and Q_{L2} (Q_{L2} of the window is considerably less than that of the resonant gaps) increase as the window is made narrower. Here arises another compromise with gas-discharge phenomena. Heating of the window and attenuation of the transmitted radar signal, due to the gas discharge, decreases as the window is made narrower.

In the next two sections detailed information will be presented on both the resonant gap and the resonant window. Such information must be obtained before it can be hoped to design a TR tube which approaches optimum bandwidth. After the data on the resonant gap and the resonant window have been investigated it will be possible to decide just how the results for experimental multiple elements can be applied in the design of a bandpass TR tube.

3·9. Resonant-gap Data.—As a result of a gradual metamorphosis, the resonant gap used[11,12] in the present designs of bandpass TR tubes has changed in shape from the rectangular resonant slot of Fig. 3·3*a* to the tunable-post forms of the resonant gap shown in Fig. 3·3*f*, *g*, *h*. To ensure rapid formation of a discharge in the gap, the gap spacing must be small. If the distance across the rectangular resonant slot in the direction of the electric field is made small, it is obvious that the capacitance will be large, which implies that Q_{L2} will be large. To retain a small gap spacing and at the same time reduce Q_{L2}, only a small section of the rectangular slot may be left small (preferably a central section where the electric field is highest) and the remainder of the slot broadened out, as in the dumbbell slot of Fig. 3·3*d*. Dimensions other than the gap spacing of the central section are used to adjust the inductance in the circuit to ensure that the element resonates at the proper frequency.

Historically, the next step was to make the central section of the dumbbell slot pointed as in Fig. 3·3*e*. For practical application to the TR tube, the gap spacing must be less than 0.010 in. This imposes such stringent tolerances on the gap spacing that the resonant structure can-

not be fabricated and tuned outside of the tube and then inserted in the tube with the expectation that it will remain tuned. This situation can be alleviated most conveniently by using a post fitted with a screw mechanism. Figure 3·3*f*, *g*, *h* shows structures used at present in TR tubes and in Fig. 3·3*i* is a resonant element of the type used in r-f filters.

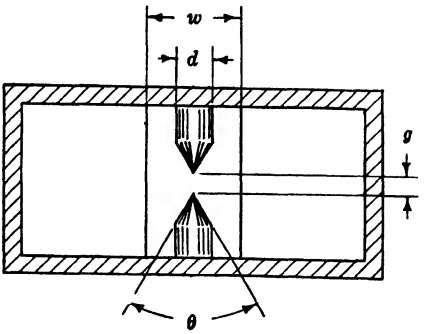

FIG. 3·31.—Single resonant element with posts.

In the 3-cm region the first detailed data were accumulated for a structure of the type shown in Fig. 3·31. In Fig. 3·32 are presented data[1] on gap spacing and Q_{L2} as a function of diaphragm opening with the post diameter and the angle of the conical point as parameters. In general, as the opening of the diaphragm w increases, the gap spacing g increases to maintain the circuit resonant at the same frequency. This means that with a decrease in capacitance in the gap, there is a corresponding increase in the opening of the diaphragm which represents an increase in inductance. This is in the right direction for qualitative agreement with the theory of the inductive diaphragm. As has been mentioned earlier in the text, in the present state of development of the theory, the shape of the resonant gap of Fig. 3·31 presents too difficult a problem for theoretical analysis. It

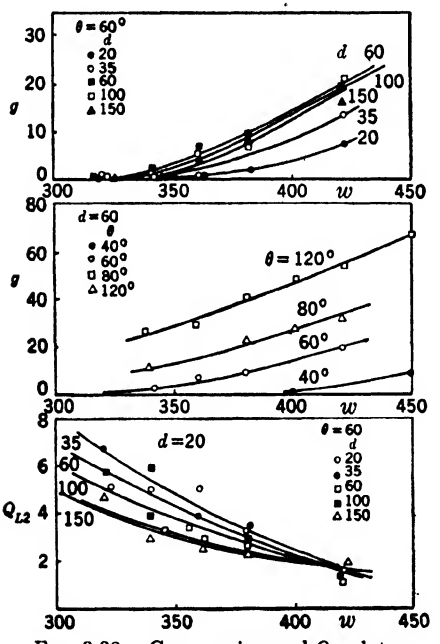

FIG. 3·32.—Gap-spacing and Q_{L2} data on the tunable-post gap of Fig. 3·31. All dimensions are in mils.

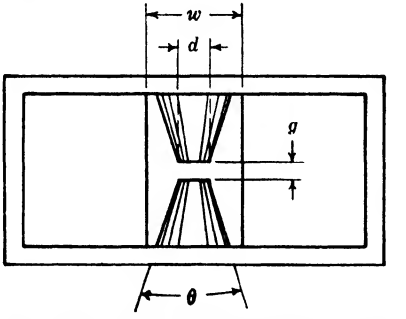

FIG. 3·33.—Single resonant element with truncated cones.

is also interesting to note that Q_{L2} decreases as the capacitance of the gap decreases which agrees qualitatively with Eq. (4). Since the variation of Q_{L2} with the angle of the conical point is less than the experimental error of measurement, such a set of curves does not appear in the figure.

Additional data[12] on the 3-cm band were obtained for a resonant gap of the truncated-cone type which is shown in Fig. 3·33. For this gap, Q_{L2} and the gap spacing are tabulated as a function of diaphragm opening, of cone angle, and of diameter of the apex of the truncated cone in Table 3·2. From Table 3·2 it is of interest to note that Q_{L2} is a minimum for an angle of about 35° and changes very slowly with θ on either side of 35°. The gap spacing seems to be relatively independent of angle over the range of angles presented in Table 3·2. Data on Q_{L2} and gap

TABLE 3·2.—TRUNCATED-CONE GAP RESONANT[12] AT $\lambda = 3.33$ CM

a. Dependence of Q_{L2} on diaphragm opening w, cone angle θ, and cone diameter d.

d mils	w mils	Cone angle θ						
		15°	30°	35°	40°	45°	50°	60°
15	258	6.6	4.9	4.4	4.5	4.4	4.1	5.0
	284	6.3		3.8	3.8	3.9	3.6	4.3
	320	4.6	3.2			3.1	2.8	3.3
	343	3.6	2.9	2.7	2.7	2.6	2.5	2.8
	398	2.8		2.1	2.0	1.9	1.9	2.2
	446	2.1		1.6	1.4	1.5		
	451		1.8		1.7		1.5	2.1
	467	2.1		1.5			1.3	1.7
	502		1.3		1.2		1.2	1.6
30	258	6.6	4 6	4.3		4.4	4.0	4.8
	284	6.3	4.1	4.0	3.7	3.6	3.7	4.2
	320	4.3		2.9	3.9	2.8	2.7	3.0
	343	3.8	2.9	2.1	2.6	2.6		
	398	2.9	2.2	2.1	2.1		2.0	2.1
	446	2.0		1.6	1.5			1.6
	451					1.6	1.5	1.9
	467	2.0	1.6	1.5	1.4	1.4	1.4	
	502	1.7			1.2		1.1	1.5
45	258	6.1	4.5	4.1	4.2	4.0	3.9	4.7
	284	5.3		3.7			3.5	4.7
	320	4.5	3.2	3.1	3.0	2.8	2.8	3.1
	343	3.5	2.8	2.4	2.5	2.5	2.2	2.5
	398	2.6	2.2	1.9	1.9	1.8		
	446	2.3	1.6	1.5	1.5	1.4	1.4	1.5
	451	2.0					1.5	1.6
	467						1.3	1.8
	502	1.5			1.2	1.4	1.2	

TABLE 3·2.—TRUNCATED-CONE GAP RESONANT[12] AT λ = 3.33 CM.—(*Continued*)

b. Dependence of gap spacing g on diaphragm opening w, cone angle θ, and cone diameter d.

d mils	w mils	Cone angle θ						
		15°	30°	35°	40°	45°	50°	60°
15	258	1.8	3.0	1.0	1.0	1.5	1.2	1.0
	284	2.4		2.5	3.0	3.0	3.0	3.8
	320	5.0	7.5			7.0	6	8.2
	343	6.4	9.0	8.0	7.0	10	9	8
	398	14		17.0	20	23	23	29
	446	26		26.5	36	40		
	451	25			37		43	52
	467	31	31	39.0			51	62
	502		55		64		74	
30	258	9	9.2	9		8.5	6	9
	284	13	13	12	13	12	12	14
	320	18		19	19	18	19	24
	343	22	22	24	23	25		
	398	36	39	41	40		41	56
	446	56		61	61			79
	451					65	63	79
	467	65	70	69	67	79	76	
	502	84						
45	258	20	20	19	15	17	15	15
	284	27		24			20	21
	320	34	34	34	33	33	31	33
	343	48	41	38	40	40	36	41
	398	62	63	60	60	66		
	446	84	85	87	86	92	84	
	451	84					86	
	467							
	502							

spacing have been extracted from the tables for a cone angle of 35° and plotted in Fig. 3·34. Since Q_{L2} is independent of the diameter of the apex of the truncated cone, only one curve relating Q_{L2} to w appears. Such a wide range of data results from the fact that the experiments were exploratory. Before the data were obtained, the appropriate dimensions for resonance had to be ascertained by trial and error. For application to the bandpass TR tube, the curves may be demonstrated for a specific case. Suppose mechanical considerations demanded that d be no less than 0.030 in., and the gas-discharge considerations demanded that g be no greater than 0.010 in. Then for the gap to resonate at 3·33 cm, w must be 0.266 in., and Q_{L2} will be 4.1.

All values of Q_{L2} at 3.33 cm were obtained by evaluating $d|\Gamma|/d\lambda$ near resonance from a plot of data on $|\Gamma|$ as a function of λ using Eq. (9·11) of Chap. 9. The conductance G of the resonant gap was so small that this method gave reliable results. The values of $|\Gamma|$ were obtained from standing-wave measurements using a calibrated crystal detector. Measurements of length were made on a traveling microscope to an accuracy of 0.0001 in. From the scattering of the experimental points, it can be seen that the data on Q_{L2} are consistent to within 10 per cent in the case of Fig. 3·32 and 3 per cent in the case of Fig. 3·34.

Direct coupling is another quantity whose importance becomes evident during the study of the gas-discharge problem. By direct coupling is meant the insertion loss of the element when it is highly detuned, that

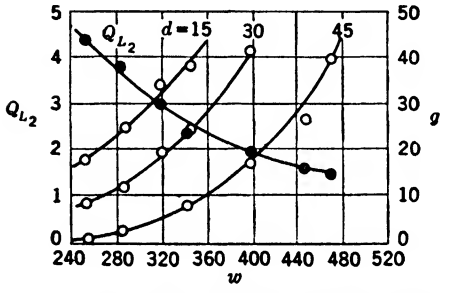

FIG. 3·34.—Gap-spacing and Q_{L2} data on the truncated cone gap of Fig. 3·33 for $\lambda = 3.33$ cm, $\theta = 35°$.

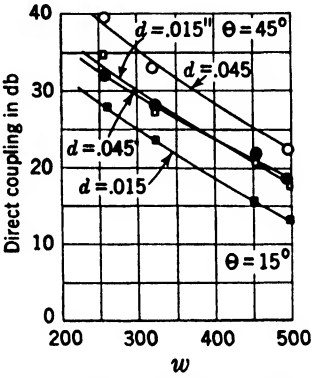

FIG. 3·35.—Direct coupling of truncated cone gap for $\lambda = 3.33$ cm.

is, when the gap is short-circuited by the discharge. From Fig. 3·35 it can be seen that for practical dimensions of the resonant gap, the direct coupling[1] may range from 25 to 35 db.

Not so broad a pass band is required for the 10-cm tubes as for the 3-cm tubes. This circumstance makes the compromise between linear and nonlinear operation of the tube so easy that manufacture of 10-cm tubes was commenced on the basis of very few measurements on the linear characteristics of the resonant gap. However, further measurements have since been made with the intention of improving the production design. Table 3·3 presents data on gap spacing, Q_{L2}, and direct coupling as functions of diaphragm opening, cone angle, and diameter of the apex of the truncated cone. Reference should be made to Fig. 3·33 for the meaning of the symbols. The results obtained at 10 cm are similar to the results obtained in the 3-cm band.

To scale by wavelength the dimensions of a gap, resonant at one frequency, to the appropriate dimensions for a gap resonant at another

TABLE 3·3.—TRUNCATED-CONE GAP RESONANT AT $\lambda = 10.4$ CM

Dependence of gap spacing, Q_{L_2}, and direct coupling on cone angle, cone diameter, and diaphragm opening.[12] All dimensions expressed in thousandths of an inch.

Gap spacing						Q_{L_2}			
d	w	Cone angle θ				Cone angle θ			
		25°	35°	45°	55°	25°	35°	45°	55°
0	795				0				4.3
	1010		0	0	28		3.5	2.96	2.8
	1200	2	12	38	157	2.4	2.4	2.04	1.90
	1400	70	155	233	364	1.75	1.65	1.39	1.40
20	795		1	3	7		4.2	4.6	4.2
	1010		15	22	36		3.3	2.9	2.8
	1200		60	128	183		2.2	2.3	2.0
29	795		8	5	9		5.0	4.6	4.3
	1010		27	38	65		3.2	2.9	2.7
	1200		94				2.2		
44	795		24	22	29		4.8	4.5	4.0
	1010		58	80	113		3.1	3.1	2.9

Direct coupling

d	w	Cone angle θ			
		25°	35°	45°	55°
0	795				28.5
	1010		19.0	23.9	24.1
	1200	9.2	15.4	18.6	21.2
	1400	12.8	8.3	15.2	17.9
20	795		26.5	28.3	28
	1010		22	21	25
	1200		19	20	21.4
29	795		27.7	27.2	30.0
	1010		22.6	23.6	25.1
	1200		18.8		
44	795		26.5	28.6	29.8
	1010		23.5	23.9	24.5

frequency can be done only very roughly. Even though the scaling is rough, it serves as a guide to give the range of dimensions to be investigated. It is possible to check the results of such scalings by using Tables 3·2 and 3·3.

3·10. Resonant-window Data.—Before the resonant glass window is considered, it is appropriate to turn attention to the rectangular resonant slot. The resonant window has the same shape as the rectangular slot except for the corners or ends which are rounded in order to avoid local stresses in the glass. For the rectangular resonant slot there is good experimental confirmation of theory.

This theory[14] proposes that the characteristic impedance of rectangular guide is

$$Z_0 = \sqrt{\frac{\mu}{\epsilon}} \frac{b}{a\sqrt{1 - \left(\frac{\lambda}{2a}\right)^2}}, \tag{57}$$

where μ is the permeability, ϵ the dielectric constant, and a and b are the wide and narrow dimensions of the guide. It can be seen that as either a or b is changed the other may be altered to retain the same value of Z_0. It is interesting to assume that two guides of different dimensions but the same characteristic impedance should yield no reflection at their junction. Equation (57) may be rewritten in the form

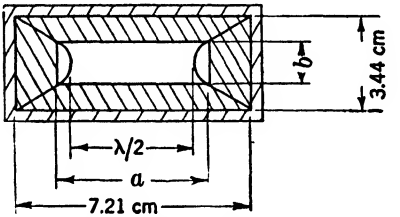

FIG. 3·36.—Junction of two guides; or a diaphragm with a rectangular slot in waveguide.

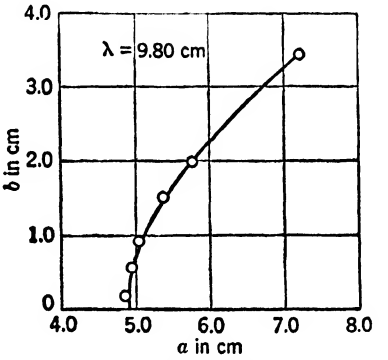

FIG. 3·37.—Rectangular slot in diaphragm. Comparison of theory and experiment.

$$b^2 = \frac{\epsilon}{\mu} Z_0^2 \left[a^2 - \left(\frac{\lambda}{2}\right)^2\right]. \tag{58}$$

Equation (58) represents a family of guides all of which have the same characteristic impedance, and all of whose corners lie on a hyperbola as shown in Fig. 3·36. The minimum width of the guide is just equal to half the free-space wavelength; $2a = \lambda$.

The diagram of Fig. 3·36 may represent not only the junction of two waveguides, but it may also represent a waveguide with a rectangular

aperture in a transverse diaphragm. Such a diaphragm may be regarded as a short length of guide joining the two guides on either side of the diaphragm. Normally the two guides that are connected will be of the same size, and for this case Fig. 3·37 presents a comparison of experimental data[8] with the constant-impedance theory. It may be observed that the agreement is good for large apertures, but for small apertures the length of the slot a must be about 1.5 per cent less than the length predicted by the theory.

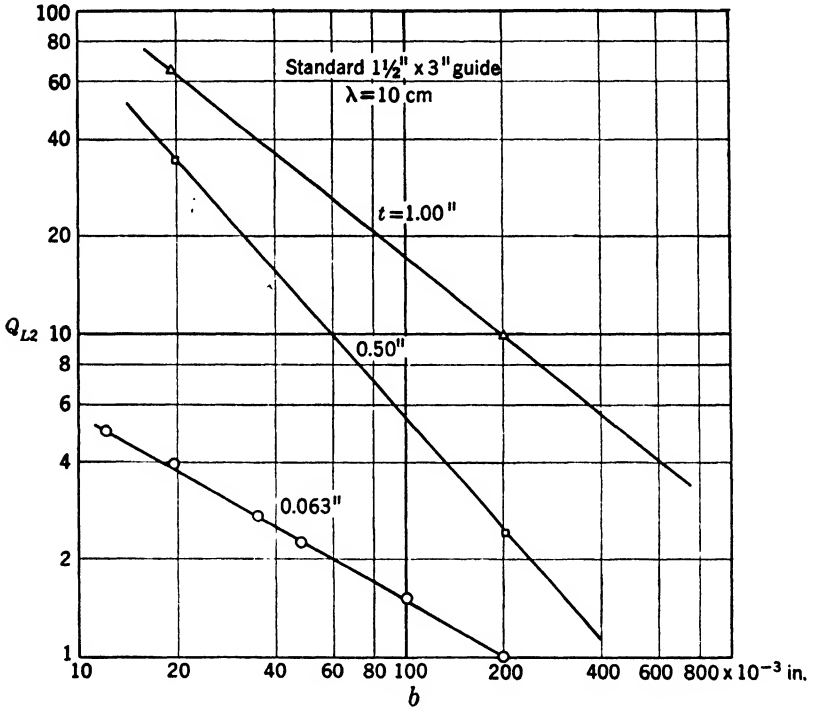

FIG. 3·38.—Q_{L2} of rectangular slot for three diaphragm thicknesses.

As the frequency of the electromagnetic wave is changed, the characteristic impedance of the short length of guide in the diaphragm aperture will change at a different rate from that of the connected guides. This means that on either side of a given frequency, a reflection will occur at the diaphragm. The frequency dependence of the reflection is important for practical applications. This has been measured for three thicknesses of diaphragm and has been expressed as Q_{L2} by evaluating $d|\Gamma|/d\lambda$ near the resonant wavelength, that is, the wavelength of minimum reflection. In Fig. 3·38 extensive data[8] on a thin diaphragm, 0.063 in. thick, show that a log-log plot of Q_{L2} as a function of b yields a straight line. Straight lines were therefore drawn through the very

sparse data on half-inch- and one-inch-thick diaphragms. Even though these data may not be so reliable, they are important in that they indicate a trend toward higher Q_{L_2} as the joining section of guide is made longer.

The general structure of the resonant window, a slotted metal frame filled with glass, is clearly shown in Fig. 3·39. It is difficult to obtain adequate data on window dimensions since to do so requires the preparation of glass-to-metal

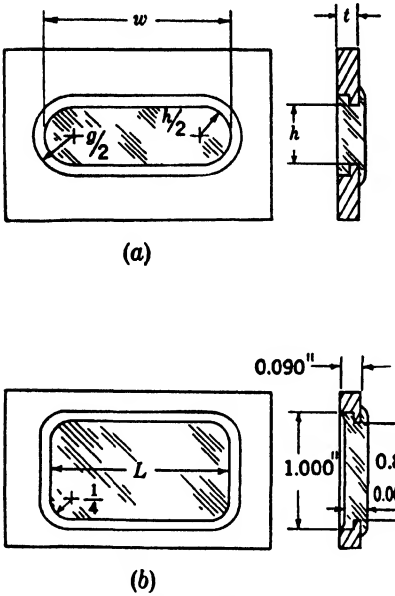

FIG. 3·39.—(*a*) Window dimensions for the 3-cm band; (*b*) window dimensions for the 10-cm band.

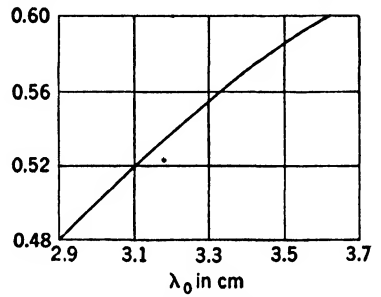

FIG. 3·40.—Resonant wavelengths for the 3-cm band window of Fig. 3·39*a*.

seals and careful grinding to the desired thickness. However, for a given window height h at 3 cm and at 10 cm, the length of the window as a function of resonant wavelength is presented[15] in Figs. 3·40 and 3·41. From Eq. (57) it may be observed that if the height of the slot remains constant, to maintain constant impedance

$$4a^2 - \lambda^2 = \text{constant}, \tag{59}$$

which gives for the rate of change of a with respect to λ

$$\frac{da}{d\lambda} = \frac{\lambda}{4a}. \tag{60}$$

Application of this equation to the 10-cm window which most closely resembles the rectangular slot yields

$$\frac{dL}{d\lambda} = \frac{\lambda}{4L} = 0.55, \tag{61}$$

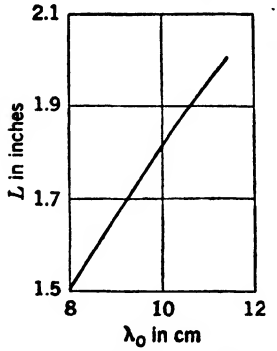

FIG. 3·41.—Resonant wavelengths in the 10-cm region for the window of Fig. 3·39*b*.

for $\lambda = 10.0$ cm and $L = 1.8$ in. Data taken from the curve of Fig. 3·41 give a slope equal to 0.37 which is considerably below the 0.55 obtained from the theory. The effect of the dielectric is immediately questioned. However, Eq. (57) seems to imply that given a length of slot, no matter what the dielectric and its resonant wavelength, the rate of change of length with respect to resonant wavelength should be independent of the dielectric.

Additional data[14] on windows for the 3-cm band are tabulated in Table 3·4. The variables are window height, thickness of glass, and

TABLE 3·4.—DATA ON WINDOWS RESONANT AT $\lambda = 3.33$ CM

						$d\lambda_{res}$ with respect to			One-way power loss	
h, mils	g, mils	t, mils	w, mils	glass	Q	dh, cm/mil	dt, cm/mil	dw, cm/mil	%	db
250	312	33.5	560	705	1.3	0.0037	0.039	0.0062	3.0	0.13
250	312	33.5	580	707	1.2	0.0030	0.043	0.0080	2.1	0.09
125	187	33.5	487	705	2.1	0.0062	0.055	0.0120	8.3	0.37
125	187	33.5	512	707	2.8	0.0047	0.042	0.0067	5.0	0.22
125	187	23.0	551	707	2.1	0.0075	0.065	0.0083	4.3	0.20
62.5	93.2	33.2	459	705	4.3	0.0020	0.130	0.0050	17.0	0.81
62.5	93.8	33.1	467	707	6.5	0.0063	0.037	0.0074	13.0	0.61
62.5	93.8	24.2	487	707	4.4	0.0070	0.051	0.0070	8.5	0.39

kind of glass for which the appropriate window length is presented, for resonance at $\lambda_0 = 3.33$ cm. Note that for $t = 0.0335$ in. and 705 glass, both Q_{L2} and the insertion loss increase as the window height is decreased. The value of Q_{L2} increases and the insertion loss decreases as the glass is changed from 705 to 707, which has a lower value of both real and imaginary parts of the dielectric constant. Furthermore, as the glass is made thinner both Q_{L2} and insertion loss decrease. The values of the dielectric constant for these two glasses are given in Table 2·5, Sec. 2.8.

It will be recalled that the narrow-band TR tubes have an insertion loss in the range from 1.0 to 1.5 db at midband. The bandpass tubes are intended to extend the band without appreciably increasing the insertion loss and, of course, it is desirable to decrease the loss. It is apparent then that with two windows in the bandpass TR tube, they should have a height greater than a sixteenth of an inch to avoid too large an insertion loss.

The three columns of data in Table 3·4 on rate of change of resonant wavelength with respect to window height, length, and thickness are useful in pointing out the mechanical tolerances imposed on the window. It is not yet known how closely the individual elements of a multiple-

element circuit must be tuned to the same frequency in order to attain the optimum bandpass. It will be recalled from Fig. 3·26 that stagger-tuning two elements by about 1 per cent resulted in a very poor bandpass characteristic. These elements had values of Q_{L2} low enough to obtain nearly 10 per cent bandwidth when tuned to the same frequency. If it is arbitrarily required that the individual elements must be tuned within 0.5 per cent of the center frequency of the band, the tolerances on the dimensions may be evaluated. For the use of the window in the fifth line from the top of Table 3·4 for which Q_{L2} is 2.1, a 0.5 per cent change in resonant frequency corresponds to a wavelength deviation of ± 0.017 cm and consequently to

$$\Delta h = \pm 0.0027 \quad \text{in.},$$
$$\Delta t = \pm 0.00026 \quad \text{in.},$$

or

$$\Delta w = \pm 0.0021 \quad \text{in.}$$

Equation (2·13) gives a value of susceptance tolerance of the window equal to ± 0.042, from which the voltage standing-wave ratio is found to be 1.05. In order to adhere to the 0.5 per cent tolerance on resonant frequency a VSWR of 1.05 at the center-band frequency must not be exceeded.

3·11. Present Band Coverage.—The microwave spectrum has been divided into bands according to the nominal range of frequencies of radar transmitters. The band designations and frequency or wavelength band limits are given in Table 3·5. In order to design a TR tube for a

TABLE 3·5.—NOMINAL TRANSMITTER-FREQUENCY BANDS

Band designation	Center wavelength, cm	Band limits	Percentage bandwidth of major bands, %
K	1.25		
X_S	3.23	3.13–3.33 cm	12
X_L	3.43	3.33–3.53 cm	
S_{W1}	8.285	3550–3700 Mc/sec	8.45
S_{W2}	8.640	3400–3550 Mc/sec	
S_{A1}	9.020	3250–3400 Mc/sec	9.23
S_{A2}	9.455	3100–3250 Mc/sec	
S_{B1}	9.840	3000–3100 Mc/sec	6.67
S_{B2}	10.170	2900–3000 Mc/sec	
S_{G1}	10.515	2800–2900 Mc/sec	7.14
S_{G2}	10.900	2700–2800 Mc/sec	

given band, it is more important to know the percentage bandwidth than to know the absolute bandwidth. The percentage bandwidth is

the ratio of the bandwidth in frequency to center frequency multiplied by 100. It is the percentage of frequency deviation from the resonant frequency which determines the susceptance of a resonant element and the deviation from one-quarter guide wavelength of the separations of the elements. The percentage bandwidths have been given for the major bands rather than for each subband since it has been found possible to design TR tubes that successfully cover the major bands.

No attempt has been made to build a bandpass TR tube of the multiple-element type for the 1-cm band. The scheme outlined in this chapter, however, is quite applicable and it would be interesting to build a 1-cm tube for comparison with data on 3-cm and 10-cm tubes, especially

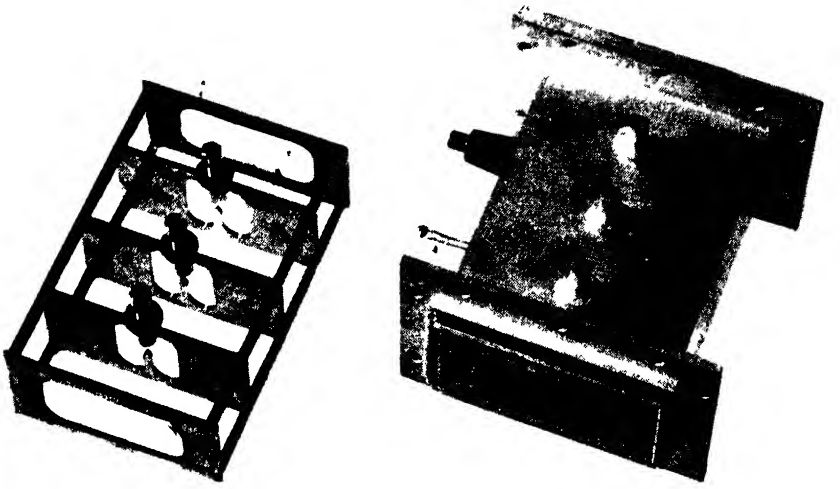

FIG. 3 42.—Photograph of 9 2-cm-band bandpass TR tube showing internal structure.

with regard to gas-discharge phenomena. The window would be more difficult to build but the gap should present no unusual problems. A somewhat different approach to a broadband 1-cm duplexer is described in Chap. 8.

It is difficult to arrive at the present design of the bandpass TR tubes from a logical consideration of the data and discussions of this chapter and of Chap. 6. The tubes were developed hurriedly and grew into their present forms as a result of a series of small changes and necessary compromises. Bandpass TR tubes have been designed for the 3-cm band and for several subdivisions of the 10-cm band. The manufacture of the 10-cm tubes was commenced before the design of the 3-cm tube was worked out. The three 10-cm tubes are consequently quite similar in design and also somewhat different from the 3-cm tube.

The 10-cm Tubes.—All the 10-cm tubes have the structure exemplified by the 9.2-cm bandpass TR tube shown in Fig. 3·42. The internal structure of the tube is shown with the gaps and windows held together by the same rectangular rods that fit into the corners of the tube body and serve as spacers for the gaps. Three gaps with Q_{L2} equal to about six were used in these tubes and the windows were designed with a very low Q_{L2}, about one. It was intended that the gaps with much higher Q_{L2} than the windows should govern the bandpass characteristic almost completely. In fact it is true that the bandpass characteristic of the three gaps is the same whether the windows are soldered in place or not.

TABLE 3·6.—GAP DIMENSIONS, WINDOW DIMENSIONS, AND ELEMENT SPACINGS FOR THREE TUBES FOR THE 10-CM BAND

Dimensions		Center wavelength RMA number		
Part and figure reference	Letter dimensions	8.463 cm 1B55	9.238 cm PS3S*	10.708 cm 1B58
Gap dimensions, refer to Fig. 3·44	a	0.125 in.	0 125 in.	0.125 in.
	d	0.313	0.313	0.375
	δ	0.182	0.182	0.130
	h	1.000	1.000	1.080
	r	0.171	0.187	0.250
	s	No. 10-32	No. 10-32	No. 8-32
	w	0.812	0.875	1.125
	θ	60°	60°	60°
	g	≈0.008	≈0.008	≈0.008
	Q_{L2}	5.5	7.0	5.5
Window dimensions, refer to Fig. 3·39	l	1.560 ± .004	1.665 ± .004	1.905 ± 004
	h	0.875	0.875	0 875
	t	0.060	0.060	0.060
	Q_{L2}	0 8	0.8	0.8
	glass	707	705	705
Element spacings, refer to Fig. 3·45	a	1.02	1.15	1.70
	d	1.34	1.15	1.63
	L	4.73	4.61	6.66
	$\lambda_{g/4}$	1.03	1.17	1.57

* Sperry Gyroscope Co. number.

The bandpass characteristic for each of the 10-cm tubes is shown in Fig. 3·43. These curves are quite similar to both the theoretical and experimental curves shown earlier in this chapter. It can be seen that the voltage standing-wave ratio for each of the tubes is less than 1.5 over the entire bandwidth to be covered. The 9.2-cm tube is not centered properly but this situation will probably be rectified by the

time this book is published. It should be noted that r equal to 1.5 corresponds to a loss in power of only 4 per cent or 0.2 db.

In Table 3·6 are given all the essential dimensions for three tubes for the 10-cm band. The gap dimensions may be interpreted by reference

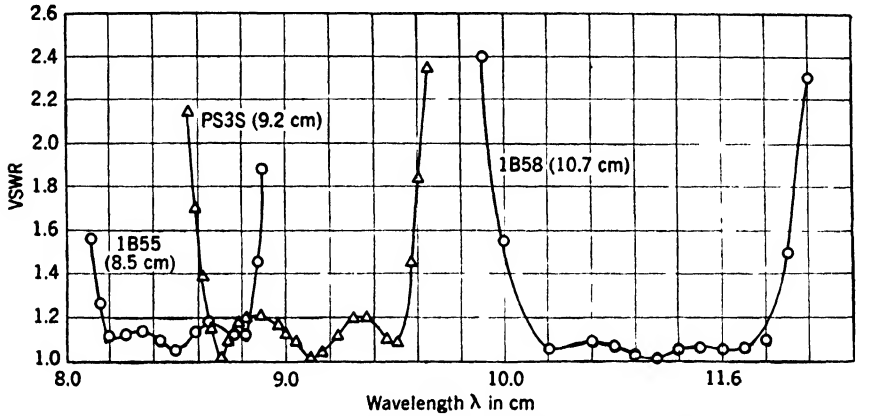

FIG. 3·43.—Bandpass characteristics for the 10-cm tubes.

to Fig. 3·44. These dimensions were the result of a relatively few experimental attempts to obtain a resonant gap with the appropriate gap spacing, Q_{L2}, and resonant frequency. There was no mapping of gap spacing or of Q_{L2} as functions of various dimensions for a given resonant frequency. The general trends shown in Figs. 3·32 and 3·34 and Table 3·3 are pertinent.

Table 3·6 and Fig. 3·39 provide the window dimensions for resonance at the center wavelength of each of the bands. These data may be compared with the curve of window length as a function of resonant wavelength in Fig. 3·41.

The element spacings as given in Table 3·6 with reference to Fig. 3·45 are all a quarter of a guide wavelength, $\lambda_g/4$, with the exception of those for the 8.5-cm tube.

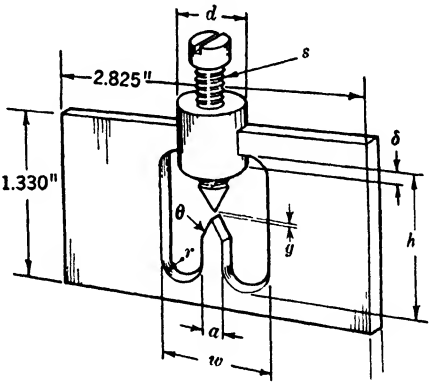

FIG. 3·44.—Gap dimensions of 10-cm TR tubes.

When the 8.5-cm tube was designed it was thought that increasing the spacing between elements would increase the bandwidth. When the elements are tuned to avoid any large bumps within the band, the bandwidth is quite comparable to the bandwidth with quarter-wavelength spacings. It is evident from this fact that the separation between

elements is not at all critical. This point was discussed earlier in the chapter and data on the 8.5-cm band were presented in Figs. 3·28 and 3·29.

Only the reflected loss is included in the bandpass characteristic. The absorption loss at midband is of the order of 0.5 to 0.8 db; of this

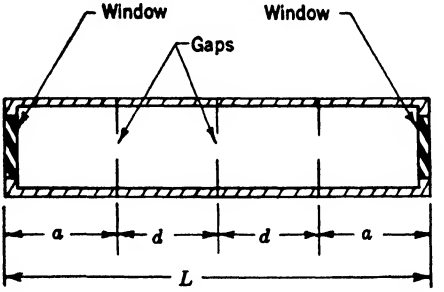

FIG. 3·45.—Spacing of elements of 10-cm TR tubes to accompany Table 3·6.

amount 0.05 to 0.1 db is caused by dielectric loss in each window, and the rest is resistive loss in the tube walls and the resonant gaps. Doubtless this loss will decrease a little as production methods are refined.

The 3-cm Tube.—It is of interest to mention that a few three-gap tubes were built for the 3-cm band according to a design that was essen-

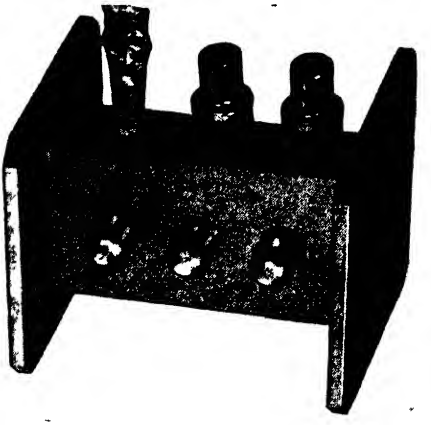

FIG. 3·46. A 3-cm band TR tube, three-gap bandpass.

tially the same as for the 10-cm tubes. A picture of one is shown in Fig. 3·46. By the time a few of the three-gap tubes were being built in pilot-plant production, a better understanding of the gas-discharge phenomena was being acquired. This better understanding prompted a design of a two-gap tube. Even a single-gap tube is nearly satisfactory. This will be made clear in Chap. 6. The two-gap tube, shown in Fig.

3·47, represents an improvement over the three-gap tube in that it is characterized by better gas-discharge and bandpass characteristics, and shorter length; it is easier to manufacture, and easier to tune.

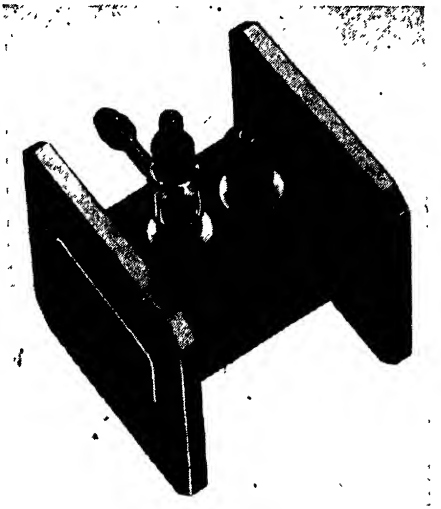

FIG. 3·47.—A 3-cm band TR tube, two-gap bandpass.

In Fig. 3·48 is shown a bandpass curve for the 3-cm TR tube. The pass band of the tube covers the entire 3-cm band which is 12 per cent wide. The 3-cm band is wider than any one of the 10-cm bands, and

TABLE 3·7.—GAP DIMENSIONS, WINDOW DIMENSIONS, AND ELEMENT SPACING FOR THE 3-CM TR TUBE (1B63)

Center wavelength	3.33 cm
Gap dimensions (refer to Fig. 3·33)	
w	0.275 in.
d	0.025
θ	60°
g	0.008
Q_{L2}	4.0
Window dimensions (refer to Fig. 3·39)	
l	0.551* (0.580†)
h	0.125 (0.250)
t	0.0230 (0.0335)
Q_{L2}	2.1 (1.2)
glass	707 (707)
Tube length L	1 555
Element spacings $a = d$	0.489
Quarter guide wavelength $\lambda_g/4$	0.478

* Window at high-power end of the tube.
† Window at mixer end of the tube.

considerably more care is required in the tube design to ensure crystal protection and complete band coverage simultaneously.

The tube dimensions are given in Table 3·7. It should be noted that Q_{L2} for the gaps is much lower than for the 10-cm tubes and that the gap spacing g is about the same.

Windows of two different sizes are used in the 3-cm tube. One is chosen with a high Q_{L2} so that the bandpass characteristic more nearly simulates the three-element case. Not so high a Q_{L2} as is desirable can be used because the insertion loss of the window becomes excessive. The high-Q_{L2} window is smaller and is used at the end of the tube which carries the high-current r-f discharge. The spacing between elements is the usual quarter wavelength.

The absorption loss at midband may be as low as 0.4 db for this tube if it is constructed carefully. A loss of 0.2 db in the high-Q_{L2} window,

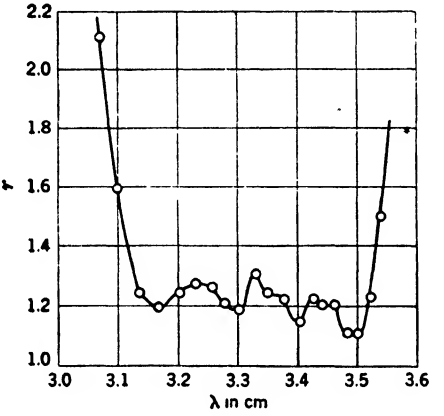

FIG. 3·48.—Bandpass characteristic for 3-cm band TR tube (1B63).

0.1 db in the low-Q_{L2} window, and 0.1 to 0.2 db in the resonant gaps and tube body add up to 0.4 to 0.5 db.

3·12. Suggestions for Further Improvements.—The linear problem of the bandpass TR tube resolves itself into two parts. The one part pertains to the problem of multiple-resonant circuits; the other part involves the study of the individual circuits. And this problem as a whole must be attacked with its limitation by the gas-discharge properties always in mind.

The multiple-resonant-circuit problem is the problem of finding the appropriate combination of elementary circuits which yields a maximum frequency range throughout which the insertion loss never exceeds some arbitrary value. The bandpass-TR-tube problem is related to the filter problem which has been considered in some detail by Fano and Lawson.[2] As the criterion of filter effectiveness, Fano has taken the ratio of the steepness of the sides of the insertion-loss characteristic to the maximum

loss within the pass band. A similar general analysis should be applied to the bandpass-TR-tube problem with the less restrictive criterion of bandwidth required of the TR tube. The bandpass TR tube is not intended to act as a filter and the steepness of the sides of the insertion-loss characteristic is not important.

It has been shown that the bandpass characteristic depends on the Q_{L2} of each element, the number of elements, the separation of the elements along the transmission line, and the resonant frequency of each element. It is desired to know the values of these four parameters which yield the maximum bandwidth consistent with the gas-discharge requirements. At present no method of analysis yields these parameters directly. Theoretically the problem has been approached by calculating the frequency dependence of insertion loss for various particular values of the four parameters. Experimentally the gross effects of each of the four parameters have been investigated. More detailed systematic measurements are needed in order to provide a complete understanding of the multiple-circuit portion of the bandpass-TR-tube problem.

To obtain more information on the bandpass characteristics of a multiple-element circuit, the experimenter should consider using the technique whereby a plot of transmitted power as a function of frequency is presented on an oscilloscope. This technique requires the use of an oscillator whose frequency can be swept over the range to be studied. The method can be made more sensitive to small values of insertion loss by using an r-f bridge in such a way that the power reflected from the circuit being studied is presented on the oscilloscope. It would be desirable to design the experiment so the parameters Q_{L2}, the separation of the elements, and the resonant frequency could be varied continuously. However, such a design might lead to insurmountable mechanical difficulties.

The second part of the linear problem—the study of the individual circuits—may be divided further into the consideration of the resonant gap and of the resonant window. Considerable data have been obtained in the 3-cm band on the resonant gap for shapes that have been thought proper for the optimum compromise between Q_{L2} and crystal protection. As will be seen in Chap. 6 the experimentation on crystal protection has not been extensive enough to predict the best shape of the resonant gap. Further research should be conducted on this problem using wavelengths near 3 cm at first, because a start has already been made there, and then later using other bands because the frequency dependence of the gas-discharge phenomena is not yet clearly understood. The remaining linear problem in regard to the absorption loss in the resonant gap is not important at present. The absorption loss due to two or three gaps is usually less than 0.1 to 0.2 db if the gaps are carefully soldered.

In the resonant window, absorption loss is important. It has been seen in Sec. 3·10 that the loss is 0.20 db or more in windows with Q_{L2} equal to 2.1 or greater. It is desirable to use narrower windows than are used at present without sacrificing on absorption loss and without increasing Q_{L2} too much. An improvement of the window in which the absorption loss is decreased demands new dielectric materials that have lower intrinsic losses. Two possible materials are quartz and mica; quartz because it has especially low loss, and mica because it can be cleaved so thin that its losses are unimportant. These possibilities will be discussed further in a later section devoted to the fabrication of bandpass TR tubes and tube parts.

BIBLIOGRAPHY FOR CHAPTER 3

1. H. A. LEITER: "A Microwave Bandpass Filter in Waveguide," RL Report 814, Nov. 16, 1945.
2. R. M. FANO and A. W. LAWSON: Chaps. 9 and 10, Vol. 9, Radiation Laboratory Series.
3. P. M. MARCUS: "The Interaction of Discontinuities on a Transmission Line," RL Report 930, Dec. 1, 1945.
4. M. D FISKE: "A Broadband TR Switch," GE Research Lab. Report, Oct. 18, 1943.
5. W. R. SMYTHE: *Static and Dynamic Electricity*, McGraw-Hill, New York, 1936, pp. 219, 366.
6. E. A. GUILLEMIN: *Communication Networks*, Vol. II, Wiley, New York, 1935.
7. M. D. FISKE and ANN D. WARNER: "Frequency Characteristics of Single and Multiple Lumped Circuits in Transmission Lines," GE Research Lab. Report, May 25, 1945.
8. M. D. FISKE: personal communication.
9. L. D. SMULLIN: "S-band Bandpass TR Tubes," RL Report 971, Dec. 1, 1945.
10. W. C. CALDWELL: "X-band Bandpass TR Tube," RL Report 970, Jan. 22, 1946.
11. M. D. FISKE and ANN D. WARNER: "Memorandum on Design Data for Resonant Apertures in the Broad Band XTR," GE Research Lab. Report, Aug. 6, 1945
12. C. Y. MENG: Radiation Laboratory Data.
13. J. C. SLATER: *Microwave Transmission*, McGraw-Hill, New York, 1943, pp. 183–185.
14. M. D. FISKE: "Resonant Windows for Vacuum Seals in Rectangular Waveguides," GE Research Lab. Report, Feb. 10, 1945.
15. R. N. HALL, "Resonant Slots and Waveguides Having Dumbbell-shaped Cross Section," GE Research Lab. Report, Feb. 18, 1943.

CHAPTER 4

CHARACTERISTICS OF ATR SWITCHES AT LOW POWER LEVELS

By Harold K. Farr

This chapter will be restricted to the distinctive aspects of the ATR switch, since much of the material already presented in connection with the TR switch applies directly to the ATR circuit. The discussion will be further restricted to the consideration of the ATR switch as an isolated circuit component; the dependence of duplexer performance on the ATR characteristics will be considered in Chap. 5.

4·1. Equivalent Circuits.—An ATR switch is a device which, placed in series with the transmitter line, has zero impedance at high level and infinite impedance at low level, and which, connected across the trans-

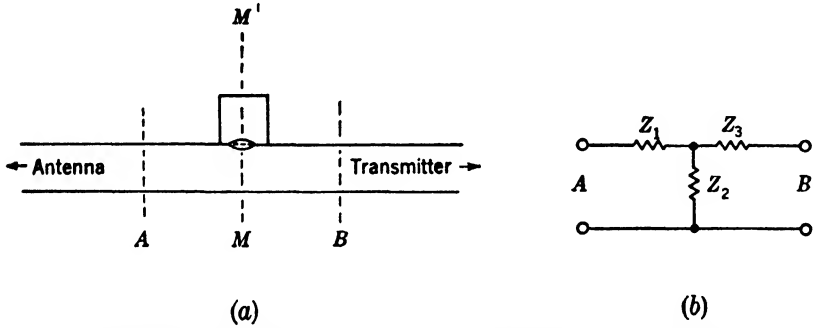

Fig. 4·1.—ATR switch at low level; (*a*) cavity and transmitter line in cross section; (*b*) equivalent circuit.

mission line, gives an infinite impedance at high level and a zero impedance at low level. Either the shunt or the series arrangement fulfills the requirements of an ATR switch. This switch is required to permit the flow of power from the transmitter toward the antenna, but to isolate the transmitter from the rest of the circuit during reception.

More accurately, a section of transmission line with an ATR switch mounted on one side as in Fig. 4·1*a* should be considered, at low level, as a four-terminal network. The ATR switch is then adequately described if its behavior is known in terms of measurements made at the two pairs of terminals, A and B. All the necessary electrical information is available if the impedance at A, for a known impedance at B, can be calculated. Such a circuit can be represented at one frequency as a T-network similar to that of Fig. 4·1*b*.

An ATR switch is usually symmetrical about some plane MM', and if the reference planes A and B are taken at an equal distance on either side, the equivalent T-network is also symmetrical, and $Z_1 = Z_3$. It is thus possible to describe an ATR switch in terms of two complex constants, Z_1 and Z_2. The values of these constants depend on the location of the reference planes A and B. These planes may be so chosen as to simplify the equivalent circuit. The end B is terminated in a matched load, and therefore, it is unnecessary to specify the exact location of the B plane; then the ATR cavity is tuned to resonance as indicated by a maximum standing-wave ratio measured at A. The reference plane A is located at that point closest to the cavity where the impedance is real. This point is usually very close to the center line MM'.

When the ATR cavity is mounted on the broad side of the waveguide it is said to form an E-plane junction with the waveguide, since the center lines of cavity and waveguide lie in the plane of the electric vector. For such a junction, the real impedance which appears at A is high compared with the characteristic transmission-line impedance. The ATR cavity itself usually presents a high impedance at the window at resonance, since at resonance the fields inside the cavity are highest, resulting in a high voltage across the window which is interpreted as a high impedance. The high cavity impedance may be verified by removing the cavity from its side-arm mounting and connecting it to the end of a waveguide for impedance measurement. Since the E-plane mounting leads to a high impedance opposite the ATR cavity, the cavity acts somewhat as though it were in series with the line at that point, and that junction is referred to as a "series junction." An ATR cavity which is coupled to a coaxial line by means of an iris in the outer conductor behaves in a similar manner.

The reference planes have been chosen in the manner indicated, and the values of the circuit constants of the equivalent T-network may now be found. A cavity mounted in the E-plane with the window flush with the waveguide wall will be considered first. For this case a careful determination of these quantities has been made with a low-Q ATR cavity of the 1B52 type for the 8-cm region. The cavity was tuned to resonance at one wavelength, and the circuit constants were determined for various wavelengths in this region without changing the tuning. It was found that in all cases the real part of Z_2 was about 300 times the line impedance, which meant that Z_2 could, within the limits of experimental error, be considered to be an open circuit; that is, the ATR cavity could be accurately represented as an impedance in series with the line at the reference point determined according to the above convention. In this case, therefore, the naive conception of the series circuit is vindi-

cated, a condition which is not at all an obvious consequence of the complicated fields existing at the junction.

The verification of the simple series representation of the E-plane mounting greatly simplifies the conception of the low-level ATR behavior. It permits the definition of $Z_1 + Z_3$ as the ATR impedance and, throughout this chapter and Chap. 7, Z will be used to designate this quantity. The value of Z and the position of the reference plane gives all the important information. Another important convention which will be used throughout this chapter and Chap. 7 follows. If any particular impedance has been defined by some subscript such as s, the real and imaginary components will be designated as R_s and X_s. Thus $Z_s = R_s + jX_s$. The corresponding admittance will be $Y_s = G_s + jB_s = 1/Z_s$. The reflection coefficient obtained by terminating a line of characteristic impedance Z_0 in the impedance Z_s will be $\Gamma_s = (Z_s - Z_0)/(Z_s + Z_0)$,

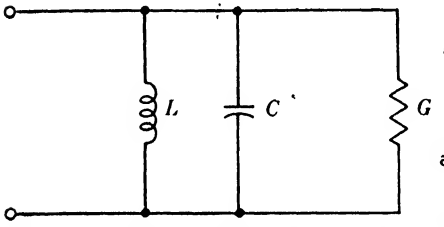

FIG. 4·2.—Equivalent circuit for an ATR cavity.

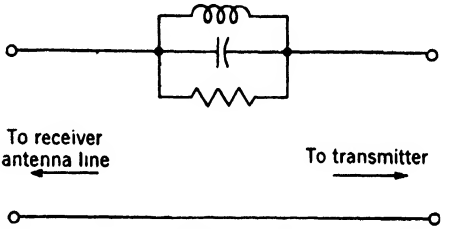

FIG. 4·3.—Equivalent circuit for series mount.

and the voltage standing-wave ratio (VSWR) set up by this termination will be $r_s = (1 + |\Gamma_s|)/(1 - |\Gamma_s|)$. Unless otherwise stated, it will be assumed that the impedances used have been normalized with respect to the characteristic line impedance so that $Z_0 = 1$.

If a matched load is connected at the reference point B, and the impedance is measured looking into A, Z is merely this impedance minus one. Determined as a function of frequency, Z is usually found to follow a rather simple law. If $1/Z = Y = G + jB$, it must follow from the choice of reference plane that $B = 0$ at resonance. It is also found that G is constant with frequency whereas B varies almost linearly over a frequency range of a few per cent near resonance. This behavior is characteristic of a simple shunt-resonant circuit like that of Fig. 4·2. On the basis of the theory of resonant cavities developed in Chap. 2, this is just the circuit that would be expected for high-Q cavities. Even with a cavity for which the frequency sensitivity is kept as low as possible (loaded Q of 5 or 10), the simple shunt-resonant circuit is a surprisingly good approximation. Hence, for an E-plane junction, the four-terminal network of Fig. 4·1 may usually be reduced to the circuit of Fig. 4·3.

The data on the equivalent circuit constants of the 1B52 tube, which have been mentioned, illustrate this behavior. For one tube, the conductance G, measured at seven different wavelengths over a wavelength band 6 per cent wide, remained between 0.016 and 0.019, or nearly constant within experimental error. The susceptance B for the same tube is plotted in Fig. 4·4 as a function of the percentage wavelength deviation $\Delta\lambda/\lambda_0$ from resonance. The deviation $\Delta\lambda$ is equal to $\lambda_1 - \lambda_0$ where λ_1 is the wavelength at which B is measured and λ_0 is the wavelength at resonance. The experimental points are indicated as circles and the solid line is the best straight line passing through the origin. It is clear that B is very nearly linear with wavelength.

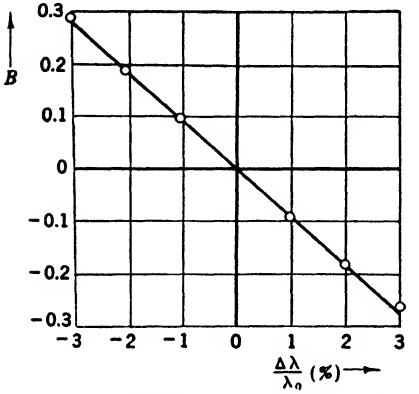

FIG. 4·4.—Susceptance of an ATR cavity.

Since B is linear, three parameters suffice to describe the ATR circuit once the reference plane or electrical center of the tube has been established. These quantities are the resonant wavelength λ_0, the cavity conductance G, and the loaded Q, Q_L. This last parameter may be thought of as a means of specifying the slope of the curve of Fig. 4·4 according to the expression

$$B = -2(1 + G)Q_L \frac{\Delta\lambda}{\lambda_0}. \quad (1)$$

From this definition it is seen that Q_L is also the Q of the circuit of Fig. 4·5, obtained by connecting the ATR circuit of Fig. 4·2 to a matched generator. In this circuit the total loading is $1 + G$ and the susceptance is given by Eq. (1) when $\Delta\lambda/\lambda_0$ is small.

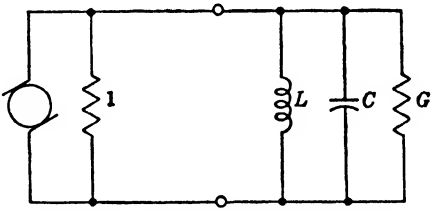

FIG. 4·5.—Loaded-Q of an ATR cavity.

For ATR measurements, the circuit of Fig. 4·2 is approximated if the cavity is mounted at the end of a transmission line and not on one side. Although the behavior for this mounting is well represented by the circuit of Fig. 4·5, the values of the parameters may differ from those for a side-mounted tube. It is usually more accurate, therefore, to make measurements with the tube mounted as it will be used in practice. For a series-mounted tube, measurements should be made using the circuit of Fig. 4·6*a*. The loaded Q of this circuit is different from that given by

Eq. (1) since the loading is now $(\frac{1}{2} + G)$. The original definition is retained, however, since it is desired to use Q_L as a parameter that characterizes the cavity rather than the circuit in which the cavity is used. With the circuit of Fig. 4·6*a*, therefore, Z_1 is measured; then B, the imaginary part of $Y = 1/(Z_1 - 1)$, is found; then Q_L is evaluated by means of Eq. (1). Even if this is done, it should not be assumed that the same value of Q_L, or for that matter of λ_0 or G, will be found when the cavity is mounted at the end of a waveguide as for the side mounting. For high-Q cavities the agreement between the different types of mounting may be fairly good, but in low-Q devices the field in the vicinity of the junction makes an important contribution to the cavity parameters which, therefore, depend on the type of junction.

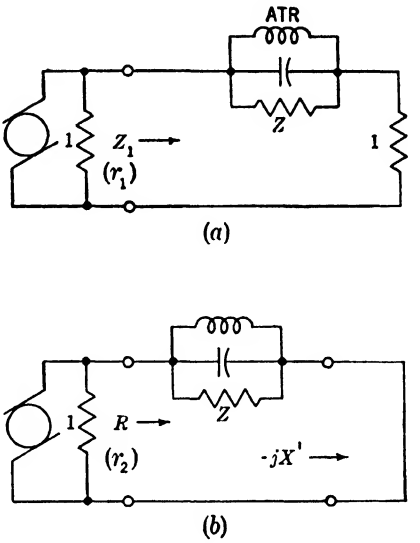

FIG. 4·6.—Circuits for parameter measurements.

It has been seen that an ATR cavity mounted on the wide side of the guide effectively places a high impedance in series with the transmission line at resonance. As has already been pointed out, however, a cavity is equally effective if it causes a short circuit across the line. If a cavity is mounted on the narrow side of the waveguide in the so-called H-plane and the real-impedance point is located at resonance as was done for the reference point A, this point will again be found close to the center line of the cavity, but its magnitude will be very small compared with the waveguide characteristic impedance. Since the cavity itself is known to have a high impedance, there must be a phase reversal between the H-plane-mounted cavity and the main waveguide. This is equivalent to connecting the cavity across the main line through a side arm

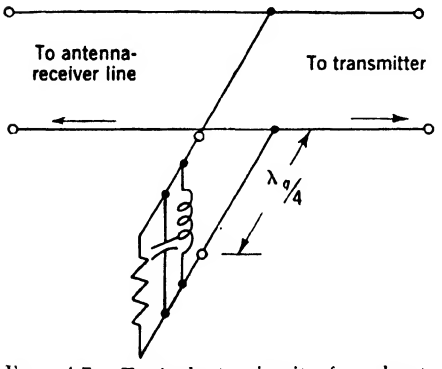

FIG. 4·7.—Equivalent circuit for shunt mount.

one-quarter wavelength long, as in Fig. 4·7. Because nearly all of the work on broadband ATR circuits has been done with the *E*-plane mount, the experimental verification of the circuit of Fig. 4·7 for the *H*-plane mount has not been as complete as that for the *E*-plane. Nevertheless, for the present, this representation will be assumed to be valid.

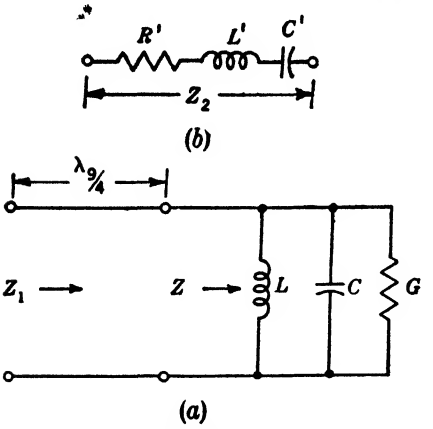

FIG. 4·8.—Equivalent circuits for a shunt-mounted cavity. (*a*) Shunt-resonant element with λ/4 line. (*b*) Series resonant element.

There is an alternative way of representing the shunt mount which establishes an interesting correspondence with the series mount. In Fig. 4·8*a* the impedance of the shunt-resonant circuit with a quarter-wavelength line is

$$Z_1 = \frac{1}{Z} = Y = G + j\left(C\omega - \frac{1}{L\omega}\right).$$

In Fig. 4·8*b* the impedance of the series-resonant circuit is

$$Z_2 = R' + j\left(L'\omega - \frac{1}{C'\omega}\right).$$

In order to have $Z_1 = Z_2$ it is necessary only that $R' = G$, $L' = C$, $C' = L$. If each circuit is connected to a matched generator, the loaded Q's will be the same, for the conductance loading on the shunt circuit is then $1 + G$ and $Q_L = C\omega/(1 + G)$. Similarly, the loaded Q of the series circuit is $L'\omega/(1 + R') = Q_L$. Furthermore,

$$\omega_0' = \frac{1}{\sqrt{L'C'}} = \frac{1}{\sqrt{LC}} = \omega_0,$$

and the three circuit parameters are therefore related by

$$R' = G, \qquad Q_L' = Q_L, \qquad \lambda_0' = \lambda_0.$$

Thus the *E*-plane mount can be represented as a shunt-resonant circuit in series with the line, while the *H*-plane corresponds to a series-resonant circuit in shunt with the line.

A very useful equivalence between the two types of mount is illustrated in Fig. 4·9. For the series mount, $Z_1 = Z + Z_l$ and for the shunt mount, Z_1 has the same value since

$$Z_1 = \frac{1}{Z_2} = Y_2 = Y' + Y_s = \frac{1}{Z'} + \frac{1}{Z_s} = Z + Z_l.$$

A series mount can evidently be made equivalent to a shunt mount by shifting the ATR circuit one-quarter wavelength along the line, provided the effective ATR impedance Z is the same in either case. If an actual

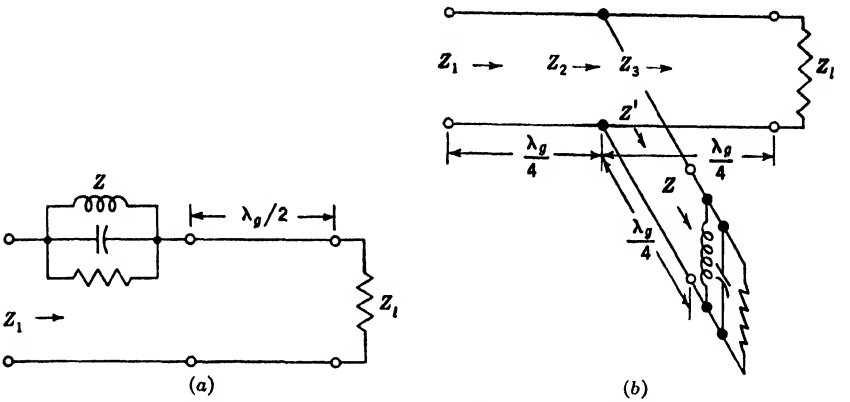

FIG. 4·9.—Equivalence of shunt and series mounting. (*a*) Series mount with λ/2 line. (*b*) Shunt mount with λ/4 line.

cavity were moved from the series position to a shunt position one-quarter wavelength down the line, the observed impedance Z_1 would change somewhat because of changes in tuning, in Q_L, and so forth.

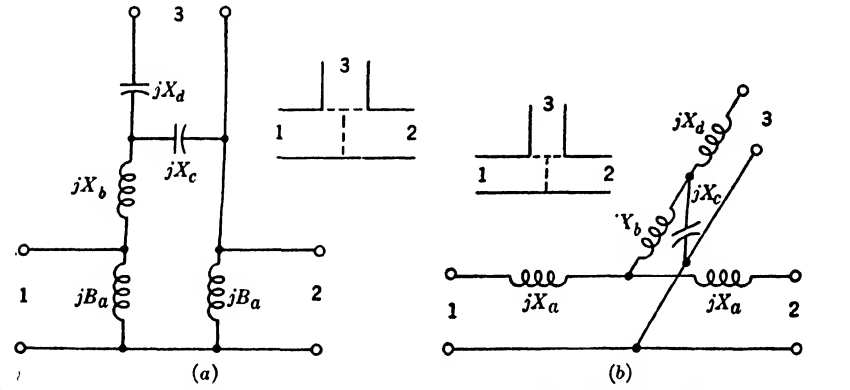

FIG. 4·10.—(*a*) Equivalent circuit of *E*-plane junction. (*b*) Equivalent circuit of *H*-plane junction.

However, the correct positions for locating series and shunt ATR cavities relative to the TR junction always differ by one-quarter wavelength plus the small correction due to the shift of the reference plane. Because of this equivalence, the parameters for the shunt-mounted cavity can be measured in the same manner as that described for the series case. For the shunt mount the impedance measured at the refer-

ence point A is Z_2, and its reciprocal Z_1 corresponds to the impedance measured at A with a series mount.

If a cavity is mounted on a side arm at a distance from the main transmission line, the cavity and the junction may be considered separately. It has been shown elsewhere that a simple waveguide junction of this kind in which the side arm makes an angle of 90° with the two arms of the main waveguide may be represented, at any given wavelength, by the circuits of Figs. 4·10*a* and *b* for *E*- and *H*-plane junctions respectively.[1] The terminals of the main waveguide are referred to the plane of symmetry and those of the side arm to the wall of the main waveguide as indicated by the broken lines in the sketch. Actually any measurements must be made in the waveguide one-half or one wavelength back from these positions because the fields are quite different in the region of the junction.

For a waveguide of internal dimensions 0.400 in. by 0.900 in., and for a free-space wavelength of 3.20 cm, the values of the circuit elements of Figs. 4·10*a* and *b* are given in Table 4·1. One of the elements B_a is given as a susceptance and the others as reactances X_a, X_b, ... The

TABLE 4·1.—EQUIVALENT CIRCUIT ELEMENTS FOR WAVEGUIDE T-JUNCTIONS

E-plane junction	*H*-plane junction
$B_a = -0.096$	$X_a = 0.17$
$X_b = 0.50$	$X_b = 0.19$
$X_c = -4.85$	$X_c = -1.04$
$X_d = -0.56$	$X_d = 1.00$

numbers represent values which have been normalized with respect to the line impedance. It should be remembered that such a representation is valid only at one frequency and that the behavior as a function of frequency is not necessarily given by such a simple circuit.

To find the complete circuit of the cavity on the side arm, it is necessary only to connect to terminals (3) a transmission line of the length of the side arm, terminated in Z, which is the impedance of the cavity as measured at the end of a straight waveguide. Neglecting the real part of Z, jX_s can be the impedance of the side arm and cavity as it is seen looking back at the cavity from terminals (3). The value of X_s should be adjusted to cause an open circuit in the line between terminals (1) and (2); that is,

$$\frac{1}{X_c} + \frac{1}{X_d + X_s} = 0 \tag{2}$$

for an *E*-plane junction.

The impedance seen at terminals (1), however, will not be infinite because of the admittance jB_a. Hence, in terms of the convention stated above for the reference plane, A will not appear at the center of

[1] RL Series, Vol. 10.

the junction to which the terminals (1) are referred, but will be displaced to the left an amount l where $B_a = \tan(2\pi l/\lambda_g)$. For the constants given in Table 4·1, $l = 0.027$ in. This shift of the electrical center from the geometrical center seems to be greater for a simple waveguide T-junction than for a flush-mounted cavity.

4·2. General Considerations of Design and Testing.—In this discussion of the design of an ATR switch, it will be necessary to make use of some of the results of Chap. 7, in regard to the dependence of duplexing losses on the ATR impedance. It is shown there that the loss depends on both the conductance G and the susceptance B of the cavity, so that the results obtained over a band of frequencies depend on all three parameters λ_0, Q_L, and G.

For a fixed-tuned cavity, λ_0 is usually set near the center of the band; and for a tunable cavity, it is set at the operating wavelength. As the losses almost inevitably increase with the susceptance, B is kept as small as possible. For a tunable cavity this is easy, but for a fixed-tuned cavity operating over a band of frequencies, it means that Q_L must be made as low as possible to reduce the losses at the edge of the band.

For a tunable cavity which is always operated at resonance, the maximum loss in decibels, according to Sec. 7·5, is $L = 20 \log_{10} \alpha$ where

$$\alpha = \frac{\text{input voltage}}{\text{output voltage}} = 1 + \frac{1}{2}G.$$

For such a cavity it is necessary, therefore, that G be as small as possible. For a fixed-tuned cavity, however, there is usually an optimum value of G which is somewhat vague since it depends partly on what sort of loss distribution is acceptable. The maximum possible loss, for a given ATR impedance, is usually determined by the real part, $R = G/(G^2 + B^2)$, according to $\alpha = 1 + (1/2R)$. If G is made either too small or too large, the maximum losses will be high. Setting G equal to the value of B at the band edge minimizes the maximum loss, but a considerably smaller value of G will usually be preferred because of the loss at other points.

The measurement of R is a rather convenient method of determining the cavity parameters. An adjustable short-circuiting plunger may be placed as shown in Fig. 4·6*b* and the impedance Z_1 of the combination observed; the plunger adds a variable reactance X' to the impedance of a series-mounted ATR switch so that $Z_1 = R + jX + jX'$. The resulting voltage standing-wave ratio is least when $X + X' = 0$ and is then equal to R. Hence, to evaluate R it is necessary only to read the standing-wave ratio when the plunger is adjusted to make it (SWR) a minimum. This is also true for a shunt-mounted cavity.

The resonant wavelength λ_0 is that wavelength at which R is greatest. Furthermore, $G = 1/R$ at this point. If G is known, B can be found

at any wavelength by measuring $R = G/(G^2 + B^2)$, whence

$$B = \pm \sqrt{G/R - G^2}.$$

If B is known as a function of frequency, Q_L can be found from Eq. (1).

It is important to notice that the measurement of R by the plunger method (Fig. 4·6*b*) is a much more sensitive method of determining small values of B and, hence, also λ_0 than that involving the use of a matched load (Fig. 4·6*a*). To understand this let r_1 and r_2 represent the voltage standing-wave ratios which must be measured in the two methods. At resonance the VSWR measured in the plunger experiment is $r_2 = R = 1/G$ while that measured with a matched load is $r_1 = 1 + 1/G$. Since G is usually quite small, r_1 and r_2 have about the same value at resonance. Farther from resonance, however, r_2 falls off much more rapidly than r_1, for the impedance measured in the latter case is $Z_1 = Z + 1$ and the reflection coefficient is

$$\Gamma_1 = \frac{Z_1 - 1}{Z_1 + 1} = \frac{1}{1 + \frac{2}{Z}},$$

$$\left|\frac{1}{\Gamma_1}\right| = |1 + 2Y| = \sqrt{(1 + 2G)^2 + 4B^2} = (1 + 2G)\sqrt{1 + 4\left(\frac{B}{1 + 2G}\right)^2}.$$

If only values of B and G which are small compared with one are considered, then

$$\left|\frac{1}{\Gamma_1}\right| \approx (1 + 2G)\left[1 + 2\left(\frac{B}{1 + 2G}\right)^2\right],$$

$$r_1 \approx \frac{\left|\frac{1}{\Gamma_1}\right| + 1}{\left|\frac{1}{\Gamma_1}\right| - 1} = \frac{1 + G + \left(\frac{B}{1 + 2G}\right)^2}{G + \left(\frac{B}{1 + 2G}\right)^2},$$

$$r_1 \approx \frac{1}{G + B^2},$$

$$r_2 = R = \frac{G}{G^2 + B^2}.$$

As B increases, r_2 begins to decrease appreciably as soon as B^2 becomes comparable with G^2. No appreciable change occurs in r_1 however, until B^2 compares with G. Hence the plunger method for determining resonance is more sensitive by a factor of $1/G$.

This comparison of r_1 and r_2 also shows that a measurement of the standing-wave ratio looking past an ATR cavity with a matched load beyond is a very insensitive check on its performance. The performance is indicated by R which gives the maximum loss and R can become quite small before r_1 drops appreciably.

If G is known and R is measured at the two ends of the band, a good check can be made on the performance of the ATR switch over the band. It will be seen from the results of Sec. 7·10 that setting a lower limit on R fixes the maximum loss, and setting an upper limit on G ensures that for most transmitter impedances the loss will be small compared with the maximum. This indicates that ATR cavities can be tested by measuring the SWR at the center of the band using a matched load and at the two ends using a short-circuiting plunger adjusted for minimum SWR. The use of the matched load to make the SWR as nearly independent of frequency as possible is the best method of measuring G. In this way it would probably be possible to test tubes by measurement at the nominal center frequency without the necessity of locating the resonant frequency. The plunger adjustment in the band-edge measurements would be aided by a directional coupler to measure the reflected power. It must be admitted that these tests, although sensitive, might be rather slow for production checking.

It is convenient to know that whatever design is used for cavity and junction, it is always possible to tune the cavity so as to get complete isolation between the two branches of the transmitter line provided only that the losses are small enough to be neglected. This is readily proved if it is assumed that the junction is a perfectly general network with three pairs of terminals, and that the ATR cavity can be adjusted to produce any desired reactance at one pair.

If the terminals are labeled (1), (2), (3), the currents and voltages at the various terminals are related by the equations

$$E_i = \sum^{3} z_{ij} I_j, \qquad (i = 1, 2, 3). \tag{2}$$

If an impedance z representing the ATR cavity is connected to the number (3) terminals, then $E_3 = -zI_3$ and the last of Eqs. (2) becomes

$$z_{31}I_1 + z_{32}I_2 + (z_{33} + z)I_3 = 0.$$

If this is used to eliminate I_3 from the first two of Eqs. (2)

$$E_1 = \left(z_{11} - \frac{z_{13}^2}{z + z_{33}}\right) I_1 + \left(z_{12} - \frac{z_{13}z_{23}}{z + z_{33}}\right) I_2,$$

$$E_2 = \left(z_{12} - \frac{z_{13}z_{23}}{z + z_{33}}\right) I_1 + \left(z_{22} - \frac{z_{23}^2}{z + z_{33}}\right) I_2.$$

The coefficients of I_1 and I_2 are the elements z'_{ij} of the impedance matrix of the 4-terminal network derived from the original 6-terminal network by connecting z to one pair of terminals. The condition that

there be no coupling between terminals (1) and (2) is $z'_{12} = 0$, that is,

$$z_{12} - \frac{z_{13}z_{23}}{z + z_{33}} = 0.$$

All the elements z_{ij} are purely imaginary since there is no loss in the network and there is, therefore, a solution z of this equation which is purely imaginary provided $z_{13} \neq 0$ and $z_{23} \neq 0$. The last two conditions merely state that there must be coupling between arms (1) and (3) and between arms (2) and (3). Granting this, there is a reactance which, when placed at (3), results in no coupling between (1) and (2).

The design of tunable ATR switches usually presents no particularly new problems compared with the corresponding TR switch. The same electrodes may be used and the cavity can be similar except for having one window instead of two. Where separate tubes and cavities are used, the same tube can usually be used for either a TR or an ATR switch although it is unnecessary to provide any keep-alive current for the ATR tube.

The coupling window is usually made larger in an ATR cavity since the high Q_L often used for TR cavities is undesirable. As the window opening is increased, it becomes necessary to move the electrodes closer to the main waveguide until finally the electrodes are in the plane of the waveguide wall. Further reduction of Q_L can be accomplished by increasing the electrode gap until, as in most low-Q tubes, the only electrodes are the edges of the window.

In any application of a fixed-tuned ATR cavity to a frequency band about one per cent wide or greater, the attainment of a sufficiently low Q_L becomes the paramount problem of the low-level design. The effectiveness of an ATR switch depends on the substitution at low level of a high impedance for the low impedance produced by the arc at high level. At microwave frequencies a high impedance can be obtained only by some sort of stub or cavity since a simple "open circuit" causes radiation. Any such cavity must store a certain amount of r-f energy which makes a contribution to the loaded Q. Further energy may be stored in the electrodes, the glass window, and the waveguide junction. The L and C of our equivalent circuit represent all this reactive energy lumped together.

The most obvious way to make an open circuit is by means of a waveguide one-quarter wavelength long, short-circuited at the far end. When such a "quarter-wavelength stub" is mounted on the side of a transmission line, it effectively isolates the two ends. Of course, the length of the stub, measured from the inside wall of the waveguide, is not exactly one-quarter wavelength because the junction is not an ideal series or shunt circuit. The stub length to give an open circuit can be found by

experiment, or it can be calculated if the circuit constants are known for the equivalent circuit of the junction.

If a window is sealed to the opening of the stub flush with the wall of the main waveguide and the resulting tube filled with gas at low pressure, the arc discharge across the window at high level gives continuity to the main waveguide. Most of the fixed-tuned tubes have been built in this manner.

If a glass window is added to a quarter-wavelength stub, the window can cause an appreciable change in the admittance. Compensation can be made for this by changing the length of the stub, or by proper design the window can be made "resonant" so as to add no susceptance to the stub. A resonant window is one which has been designed to give no reflections when placed across a waveguide. The design of such a window is the same as that for a broadband TR tube, and from the low-level point of view the important problem is to keep the susceptance as low as possible.

Since the change of ATR impedance with frequency is such a serious problem, an effort is made to effect an improvement by using more than one resonant element, as is done in the broad-band TR tube. It will be seen in Chap. 5 that good results can be obtained by using two or more resonant elements spaced along the transmitter line. As each of these requires a separate arc gap or window, it is preferable to use a network which is connected to the transmitter line at only a single junction. Nothing is gained, however, by adding additional reactive elements to a single junction, for Foster's reactance theorem states that the curve of susceptance versus frequency for any purely reactive physical network has a positive slope. It is, therefore, impossible to add any pure susceptance which will reduce the rate of change over the band.

Something might be accomplished by adding resonant elements with appreciable dissipation, but there may be some difficulty in introducing sufficient loss to obtain the necessary negative slope of the susceptance curve without at the same time increasing the cavity conductance unduly. Since no such network is known at present, it will be assumed that the problem is to minimize Q_L by keeping the frequency sensitivity of each element of the ATR circuit as small as possible.

4·3. Low-Q ATR Switches.—It was suggested in Sec. 4·2 that the various elements of an ATR circuit—the cavity, the window, and the junction—all contribute to Q_L. It is not possible to calculate all of these; but, by making some assumptions about the equivalent circuit and using experimental results, the relative importance of the different elements can be appreciated and it can be seen why such high values of Q_L are observed.

For a waveguide ATR switch made up of a quarter-wavelength stub

and a resonant window, the equivalent circuit can be derived by writing down the circuit for a T-junction and connecting to it the window and the stub. This involves the assumption that the three components can be treated as distinct even though some higher-mode interaction, at least between the window and the junction, might be expected.

For an E-plane junction the susceptance B_a of Fig. 4·10a is very small (Table 4·1), and its contribution to Q_L can be neglected. The stub reactance X_s, which is connected to terminals (3) at resonance, is given by Eq. (2) which becomes $X_s = -X_c - X_d = 5.41$. Since this is in series with X_d and is large compared with it, X_d will be neglected.

The junction susceptance will be called $B_j = -1/X_c$, the window susceptance B_w, and the stub susceptance $B_s = -1/X_s$. There is some question as to whether the window, which is also in series with arms (1) and (2), should be shown as connected across X_c plus X_b, or connected only to X_c. These two possibilities are shown in Fig. 4·11. They are equivalent, for by neglecting G in Eq. (1), Q_L can be defined as

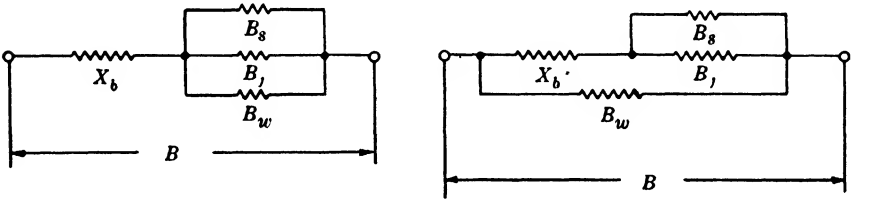

FIG. 4·11.—Circuit for calculating Q_L for a low-Q ATR switch from the parameters of a T-junction.

$$Q_L = -\frac{1}{2}\lambda_0\left(\frac{dB}{d\lambda}\right)_{\lambda_0} = -\frac{1}{2}B',$$

where B is the total susceptance in series between arms (1) and (2), and B' is the logarithmic derivative of B. Let $B_1 = B_s + B_j$, then in Fig. 4·11a

$$B = -\frac{1}{X_b - \dfrac{1}{B_1 + B_w}}.$$

If the derivative of this is taken and it is remembered that $B_1 + B_w = 0$ at resonance, $B' = B_1' + B_w'$. In Fig. 4·11b

$$B = B_w - \frac{1}{X_b - \dfrac{1}{B_1}}.$$

If the stub and window are each tuned to resonance separately, $B_1 = 0$, and again $B' = B'_1 + B'_w$. In either case

$$B' = B'_s + B'_j + B'_w$$

and the Q_L of the ATR switch is therefore independent of X_L and is the sum of the individual Q's of stub, junction, and window.

For the window Q the values of B'_w can be taken, measured with the window placed across a straight section of waveguide. The stub Q is easily calculated if the stub length l is known. For, if

$$\theta = \frac{2\pi l}{\lambda_g}, \tag{3}$$

then

$$B_s = -\cot\theta. \tag{4}$$

If the familiar waveguide equation,

$$\frac{1}{\lambda_g^2} = \frac{1}{\lambda^2} - \frac{1}{\lambda_c^2}, \tag{5}$$

is differentiated with respect to λ, there results

$$\frac{d\lambda_g}{d\lambda} = \left(\frac{\lambda_g}{\lambda}\right)^3, \tag{6}$$

since the cutoff wavelength λ_c is a constant which depends only on the size of the waveguide. Taking the logarithmic derivative,

$$\lambda'_g = \lambda\left(\frac{d\lambda_g}{d\lambda}\right) = \frac{\lambda_g^3}{\lambda^2};$$

therefore

$$B'_s = \theta' \csc^2\theta = -\theta\left(\frac{\lambda_g}{\lambda}\right)^2 \csc^2\theta,$$

or

$$Q_s = \frac{1}{2}\theta\left(\frac{\lambda_g}{\lambda}\right)^2 \csc^2\theta. \tag{7}$$

It is not so easy to calculate the junction Q since the frequency dependence of B_j is not known. For the susceptance B_i of a simple capacitive iris across a straight waveguide $B'_i = -(\lambda_g/\lambda)^2 B_i$. Since B_j should behave in approximately the same fashion, B'_j can be written as $B'_j = -a(\lambda_g/\lambda)^2 B_j$ where a is a factor which should be of the order of one. Since $B_j = -B_s$,

$$Q_j = -\frac{1}{2}B'_j = -\frac{a}{2}\left(\frac{\lambda_g}{\lambda}\right)^2 B_s,$$

and, by using Eq. (4)

$$Q_j = \frac{a}{2}\left(\frac{\lambda_g}{\lambda}\right)^2 \cot\theta. \tag{8}$$

By using experimental values for the other quantities, a can be calculated. Table 4·2 shows the results for measurements on the 1B52 type of switch mentioned previously. The observed values are λ_0, θ, Q_L, and Q_w. Equation (5) is used to calculate λ_g, and Q_s is calculated by Eq. (7). By setting $Q_j = Q_L - (Q_w + Q_s)$, Q_j is found, after which Eq.

TABLE 4·2.—THE DECOMPOSITION OF Q_L FOR AN ATR SWITCH

λ_0	$(\lambda_g/\lambda)^2$	θ	Q_L	Q_w	Q_s	Q_j	a
8.35	1.49	0.82	4.7	2.0	1.2	1.5	2.2
9.10	1.65	1.06	3.85	2.0	1.2	0.7	1.5
10.70	2.22	1.15	4.1	2.0	1.5	0.6	1.2

(8) suffices to determine a. The fact that a is somewhat greater than one can be explained if B_j is considered as the sum of two susceptances of opposite sign. These would give a greater variation with frequency than the simple element that was assumed. The data in Table 4·2 indicate that all three components make a significant contribution to Q_L although the window accounts for nearly half. The fact that the junction contributes to Q_L and that Q_L depends markedly on the type of junction was noted by Samuel, Crandell, and Clark of the Bell Telephone Laboratories.[1] Their measurements were made on a low-Q, fixed-tuned ATR tube for use at wavelengths between 3.13 and 3.53 cm. Since the electrodes were designed especially for better firing and lower arc loss, the Q_L was somewhat higher than that quoted in Table 4·2. Table 4·3 gives the values of Q_L for a tube of the same type mounted in different fashions. The total change in B over the wavelength band, which is the

TABLE 4·3.—Q_L FOR JUNCTIONS OF VARIOUS TYPES

End on	90° E-plane junction	90° H-plane junction	120° H-plane junction	Combined TR and ATR junction
4.5	6.3	11.1	8.1	9.4

average value of B' over the band rather than its value at the center, was used to determine Q_L. The 90° junction has the ATR cavity mounted on one side of a straight section of waveguide. In the 120° version the

[1] A. L. Samuel, C. F. Crandell, and J. E. Clark, "Broadband TR and Anti-TR tubes," NDRC, Div. 14, Report No. 402, September 30, 1944.

axes of the cavity and the two waveguide arms all make equal angles with one another. The combined TR-ATR junction consists of a 120° H-plane junction for the TR branch with the ATR cavity mounted on the axis of the junction as shown in Fig. 8·16 in Chap. 8. It is important to notice that the 90° E-plane T-junction has the lowest Q_L of any junction shown, although the value for the 120° E-plane junction might be interesting if known.

It has been customary to tune the window to the resonant frequency of the ATR switch on the assumption that this would give the lowest Q_L. If the window susceptance differs from zero at the frequency where resonance is desired, it is necessary for the cavity to introduce an opposite susceptance. Although the two susceptances have opposite signs, their derivatives always have the same sign, and this would be expected to increase Q_L.

Some data bearing on this question were taken in an effort to determine the feasibility of designing a switch to operate at wavelengths in the neighborhood of 8.45 cm with windows which were available only at resonant wavelengths of 9.1 cm or 10.7 cm. It was desired to compare these windows with one tuned to 8.45 cm, but the only one available for the experiment was tuned to 8.3 cm. Table 4·4 gives the values of Q_L for each window with the ATR switch tuned to resonance at 8.45 cm in each case by adjusting the stub length to cancel the window susceptance. Unfortunately, no data were taken for windows tuned to shorter wavelengths, but those available confirm the assumption that Q_L is least when the window is tuned to the resonance point of the ATR switch.

TABLE 4·4.—Q_L OF AN ATR SWITCH TUNED TO 8.45 CM FOR VARIOUS WINDOWS

Resonant wavelength of window (cm)	Over-all Q_L
8.3	5.85
9.1	6.5
10.7	6.76

4·4. ATR Switches in Use.—In reviewing the ATR switches that have been in actual use, it is natural to divide them into two groups—the tunable and the fixed tuned. These same groups could also be called high-Q and low-Q respectively since there have been no high-Q fixed-tuned circuits or low-Q tunable circuits. The cavity of the high-Q switch is separate from the electrode tube. The tube is the same as that used in the corresponding TR switch, and the cavity is similar to the TR cavity except for having but one window. The low-Q tube comprises cavity and electrodes in one unit. It has a window of the same type as the fixed-tuned TR tube but does not use the extra gaps.

The tunable cavities have been used at 3-cm and longer wavelengths but not at 1.25 cm. The reasons for this are partly historical since the

fixed-tuned cavities and 1.25-cm systems were both developed more recently. Systems developed since the fixed-tuned cavities became available have used them almost exclusively.

Few data are available on the use of ATR switches in coaxial circuits although such use is quite feasible. One switch described in Chap. 8, although identical in design with a coaxial ATR switch, is different in function.

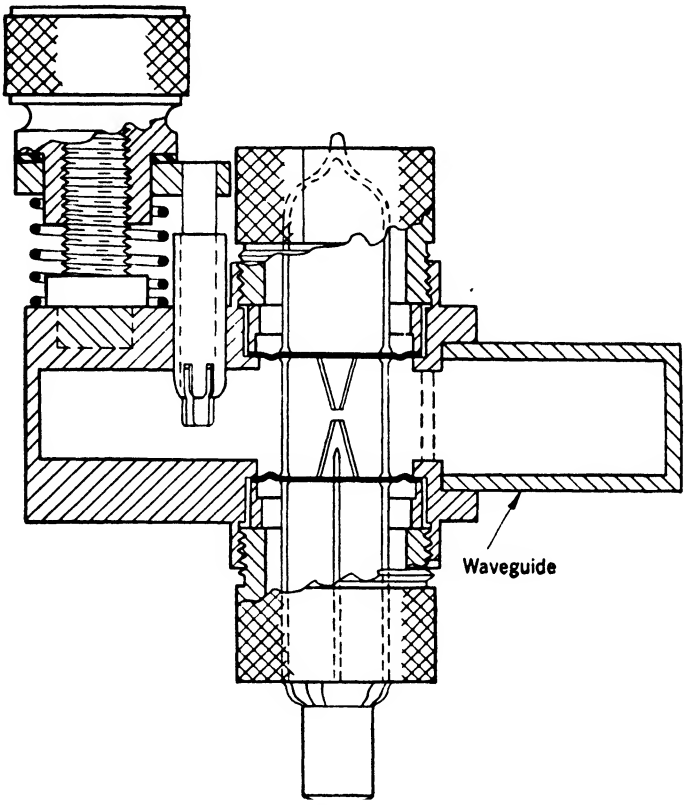

FIG. 4·12.—Cross section of the 3-cm wide-range ATR switch.

In the 10-cm region the 721A and 1B27 tubes have been used in tunable ATR circuits for waveguide as have the 724A and B tubes at 3 cm. An experimental tube for 3 cm was built by the Westinghouse Manufacturing Company to tune over a wider range than that available with the usual cavities for 724 tubes. It was similar to the 1B24 TR tube but had a larger input window and no output window. Another tube corresponding to the 1B26 was built by the same company for 1.25 cm. Neither of these tubes was put into production because of the advent of the fixed-tuned tubes. It should be noticed that TR tubes, such as

the 1B24 and 1B26, should not be used as ATR tubes without increasing the size of the input window. The high Q_L of these tubes leads to a high value of the conductance. An ATR tube made by short-circuiting the output window of a 1B24 tube, for example, would have $G = 0.3$ which could result in a loss as high as 1.2 db. For the similar ATR tube with the larger window mentioned above, $G = 0.055$ which would keep the loss below 0.23 db.

A 3-cm ATR cavity which was designed for tuning over a band 12 per cent wide is of some interest here as almost the only tunable circuit that is much different from those discussed in Chap. 2. Such cavities were developed at Radiation Laboratory and at Bell Telephone Laboratories at about the same time. Previous cavities using the 724 tubes were tuned by inductive screws in the magnetic plane which permitted a frequency range of about 2 per cent. A tuning screw is usually much more effective

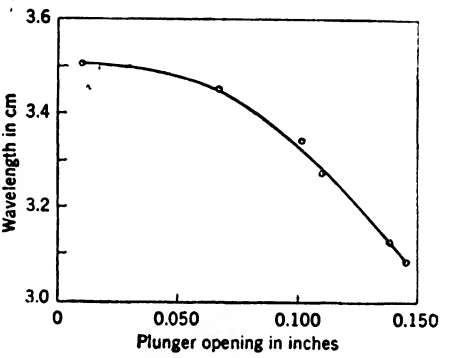

FIG. 4·13.—Tuning curve of the 3-cm wide-range cavity.

if used as a capacitive element. In an ordinary cavity using tubes of the 724 type, however, most of the capacitance is in the electrodes which are fixed. In the present device a second resonant circuit is formed by extending the cavity in the direction of the magnetic plane and adding a capacitive plunger as shown in the sketch of the Radiation Laboratory design in Fig. 4·12. Since both circuits are in the same cavity, they are tightly coupled and only one resonant mode is observed within the tuning range of 3.10 to 3.50 cm. The curve of Fig. 4·13 shows the resonant wavelength as a function of the distance between the end of the plunger and the bottom of the cavity. The cavity is mounted with shunt coupling to waveguide of 0.400 in. by 0.900 in. ID with the window opened to the full height of the guide and width of the cavity. This gives $G = 0.10$ at 3.5-cm wavelength and $G = 0.05$ at 3.1-cm wavelength. Figure 4·14 is an exterior view of the Radiation Laboratory model.

The fixed-tuned cavities which have so far been put into manufacture consist of a quarter wavelength of waveguide with a short circuit at

TABLE 4·5.—CHARACTERISTICS OF FIXED-TUNED ATR TUBES

JAN tube designation	Band designation	Nominal resonant wavelength, cm	Transmitter band	Specified upper limit			Measured values		Inside waveguide dimensions, in.	Manufacturer
				High level VSWR	Q_L	G	Q_L	G		
1B36	K	1.25		1.10	7.5	0.10	6.0	0.055	0.170 × 0.420	GE, Sylvania
1B35	X_S	3.23	3.13–3.33 cm	1.10	6.5	0.10	5.0	0.035	0.400 × 0.900	GE, Sylvania
1B37	X_L	3.43	3.33–3.53 cm	1.10	6.5	0.10	5.0	0.035	0.400 × 0.900	GE, Sylvania
1B52	S_{W1}	8.285	3700–3550 Mc/sec	1.20	5.5	0.05			1 340 × 2.840	Sylvania
1B53	S_{W2}	8.640	3550–3400 Mc/sec	1.20	5.5	0.05	4.0	0.015	1.340 × 2.840	Sylvania
1B57	S_{A1}	9.020	3400–3250 Mc/sec	1.20	5.5	0.05	4.0	0.015	1.340 × 2.840	Sperry
	S_{A2}	9.455	3250–3100 Mc/sec							
	S_{S1}	9.840	3100–3000 Mc/sec							
	S_{S2}	10.170	3000–2900 Mc/sec							
1B56	S_{G1}	10.515	2900–2800 Mc/sec	1.15	5.5	0.05	4.0	0.015	1.340 × 2.840	Sperry
1B44	S_{G2}	10.900	2800–2700 Mc/sec	1.15	5.5	0.05			1.340 × 2.840	Sperry

one end and a resonant window at the other end. The 3-cm and 1-cm tubes include a gas reservoir made by extending the waveguide beyond the short-circuiting plate. The latter has a small hole which allows the gas to circulate but does not affect the electrical properties.

An outline of the characteristics of these tubes is given in Table 4·5. The transmitter band denotes the range of frequencies covered by the corresponding transmitting tubes. No definite bands can be assigned to the ATR tubes since the usable band depends on the amount of loss that can be tolerated and the number of ATR tubes used. The measured values of G and Q_L refer to representative values of measurements made at Radiation Laboratory and at Evans Signal Laboratory. The specified upper limit of a quantity denotes the present JAN specification for the 3-cm and 1-cm tubes and that proposed for the 10-cm tubes. The waveguide dimensions refer to the transmission line on which the tube is mounted. In all these tubes, except the 1B36, the cavity is made of a section of rectangular waveguide of the same size. For ease of manufacture and mounting the 1B36 cavity is made from cylindrical tubing

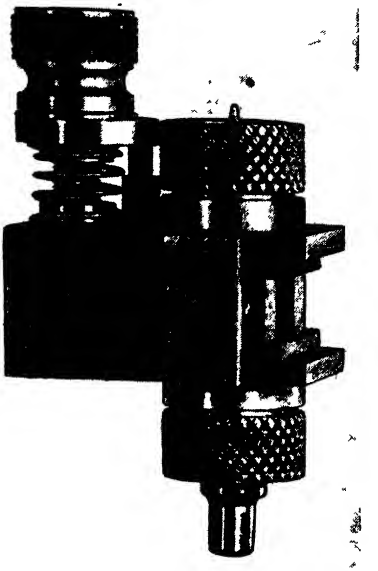

FIG. 4.14.—The 3-cm wide-range ATR switch

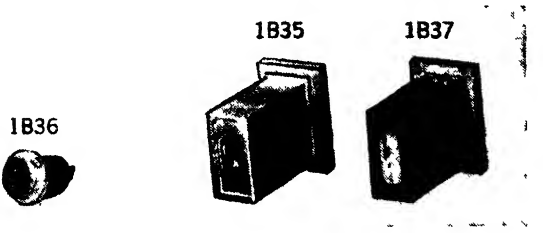

FIG. 4.15.—Fixed-tuned ATR tubes

Figures 4·15 and 4·16 are photographs of some of these tubes. They are all designed for mounting on the broad side of rectangular waveguide (series circuit) with the window flush with the waveguide wall. Those made at General Electric and Sperry are held at the correct resonant frequency by careful control of the window and cavity dimensions.

Sylvania makes use of a tuning adjustment which is set at the factory. On the 1B36 tube this consists of a tuning screw in the back of the cavity

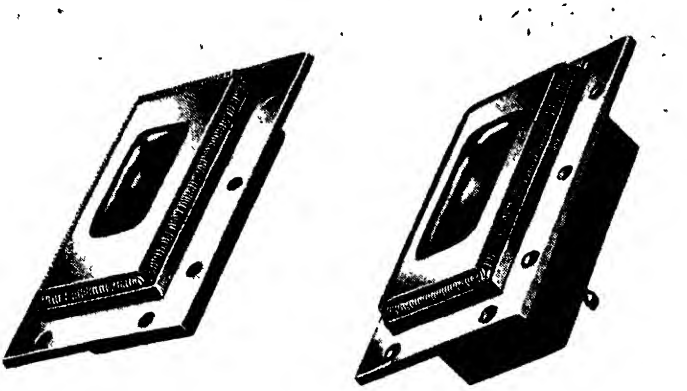

FIG. 4·16.—Fixed-tuned ATR tubes.

which is accessible through the evacuating tubulation before the latter is sealed off. The 3-cm and 10-cm tubes have a deformable diaphragm in the back of the cavity which can be adjusted by means of a strut that passes out through the tubulation as shown in Fig. 4·17. The strut is removed before the tubulation is sealed off.[1]

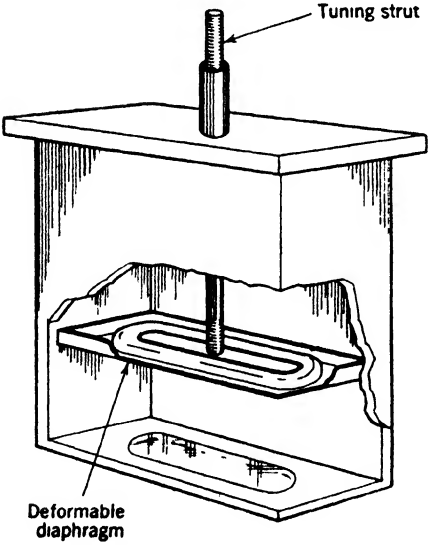

FIG. 4·17.—Sylvania method of presetting ATR tubes.

Fixed-tuned tubes of the various types are distinguished largely by their sizes and methods of mounting. The mounting is an important problem since the tube must be easily replaced and yet must make good electrical connection with the waveguide wall all around the opening. For broadband applications, the flush mounting, the proximity of the TR tube, and possibly, also, of an additional ATR tube leave insufficient space for a choke coupling of the type used to connect two waveguides. Hence, all these tubes rely on actual contact.

[1] Sylvania Electric Products, Publication No. IEB-8, "Report on OSRD Tube Development Sub-contract on RL Purchase Order DIC 182032."

In the 1B36 tube this contact is made by means of a beveled edge as shown in Fig. 4·18. Because of the circular outline, the bevel can be machined accurately, making the contact uniform all around the tube. Care must be taken to ensure that the beveled seat for the tube is not too large in diameter. If the diameter is too large, the face of the tube pro-

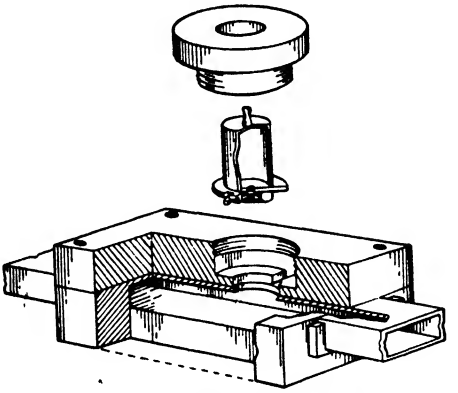

FIG. 4·18.—1B36 tube and mount.

trudes into the interior of the waveguide, as shown in Fig. 4·19, and the susceptance of the combination is altered. The change in susceptance ΔB is proportional to the insertion d, and

$$\Delta B = 0.013d$$

if d is measured in thousandths of an inch.

The 10-cm tubes have a fine coiled spring around the periphery which is compressed between the edges of the tube and waveguide. For systems using a pressurized transmission line, a flat rubber gasket under the flange makes the assembly airtight.

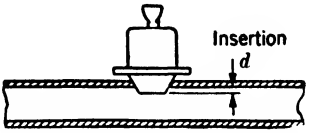

FIG. 4·19.—Effect of too large a seat for 1B36 tube.

The 3-cm ATR tubes were too small to use the coiled-spring contacts, and the circular mounting of the type used with the 1B36 tube was too bulky for certain 3-cm-band applications. A flat flange permitted sufficiently accurate machining to ensure good contact but did not provide a contact which was flush with the inside surface of the waveguide wall. The flange was, therefore, set back one wavelength from the main waveguide wall as shown in Fig. 4·20 and a little space was left between the tube and mount on all four sides of the tube. This space formed a small waveguide which, being one wavelength long, transformed the short circuit at the flange to one at the main waveguide wall and thus provided the necessary continuity between the ATR tube and the main waveguide. A flat nickel gasket a few thousandths of

an inch thick was provided with each tube to improve the contact at the flange. In principle the little waveguide could have been one-half wavelength instead of one wavelength long. However, a higher-mode resonance, which appeared only when the shorter length was used, gave rise to some reflections on high-level operation, and for this reason the half-wave length mount was ruled out.

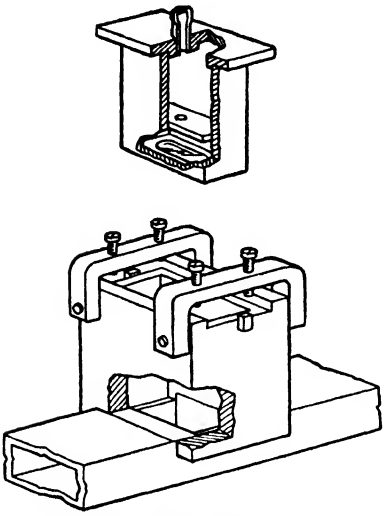

FIG. 4·20.—1B35 tube and mount.

The length of the little waveguide was made slightly greater for the 1B37 tube than for the 1B35 tube in order to keep the high-level reflections as small as possible. To accomplish this the 1B35 tubes were designed with a plane flange and the mount was made just one wavelength long at the center of the 3.23-cm band. The 1B37 tubes were then built with a small groove around the inside edge of the flange. The width of the groove is the same as that of the little waveguide, and its depth is such that it extends the waveguide sufficiently to make it just one wavelength long at the center of the 3.43-cm band. In this way the same mount may be used for either tube.[1]

An interesting 3-cm ATR tube, illustrated in Fig. 4·21 was developed but not put into production.[2] It made use of a pair of sharp-pointed, closely spaced electrodes placed a short distance behind the window to reduce the arc loss. This permits high-level operation at considerably lower powers than is possible with the other low-Q tubes but seems to result in a slightly higher Q_L. For this tube, $Q_L = 6.3$, whereas for the 1B35 and 1B37 tubes, $Q_L = 5.0$.

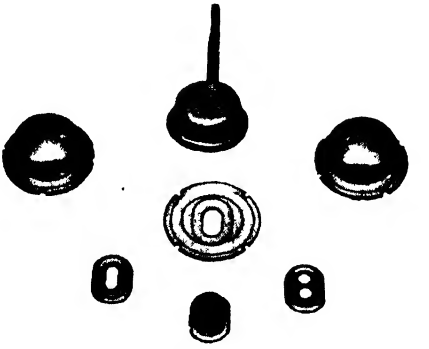

FIG. 4·21.—BTL design of fixed-tuned 3-cm ATR tube.

[1] W. C. Caldwell and H. K. Farr, "Mounting for 1B35 and 1B37 Fixed-tuned ATR," RL Report No. 53, Aug. 12, 1944.

[2] Samuel, Crandell, Clark, *op. cit.*, Sec. 4·3.

CHAPTER 5

MICROWAVE GAS DISCHARGES

By Louis D. Smullin

5·1. Introduction.—In the preceding chapters the discussion was centered on the linear properties of TR and ATR tubes. With the exception of the treatment of direct-coupling attenuation, and the standing-wave ratios produced in the main line by the fired TR tube, the discussion was limited to the operation of these tubes at power levels less than that required to initiate a discharge in the tube. In this chapter some of the characteristics of the high-frequency gas discharges of the type occurring in TR and ATR tubes will be discussed.

To understand nonlinear phenomena is always difficult, and gas-discharge phenomena are especially noted for their complexity. Although a complete theoretical understanding of the quantitative relations has not been achieved, the processes are well known, and a vast body of literature exists describing d-c and low-frequency gas discharges. The domain of high- and ultrahigh-frequency discharges has received comparatively little attention. It is only in recent years that sufficiently intense power sources and accurate measuring equipment have become available which permit quantitative experiments to be made at these high frequencies. Before 1941 little or no data on gas discharges at frequencies higher than 300 Mc/sec were available. Since that time, however, because of the rapid development of microwave radar, most of the studies of ultrahigh-frequency gas discharges have been in the 3000- 10,000- and 24,000-Mc/sec bands.

Because the goal of the work in the years from 1941 to 1945 was the development of better TR tubes or new TR tubes to be used in new equipments, and because so little time was available, only recently has a systematic study of the discharge itself apart from the TR tube begun. However, the properties of the fired TR tube that were measured were those that directly affect its quality. These quantities are

1. Leakage power.
2. Arc power.
3. Recovery time.
4. Power range.
5. Life.

The leakage power includes all the r-f power incident on the receiver during the transmitting period. It may be subdivided into the following components: spike, arc leakage power, direct-coupled power, and harmonic power. The last two are really linear properties of the fired TR cavity, and have been discussed in Chap. 2. The *spike leakage energy* is the energy transmitted to the receiver during the time interval between the beginning of the transmitter pulse and the establishment of the r-f steady-state discharge. During this interval the voltage across the gap builds up to several times the sustaining voltage of the discharge. The total time involved is usually less than 10^{-8} seconds, and the energy is of the order of 0.1 erg or less.

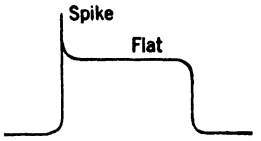

FIG. 5·1.—Envelope of TR-tube leakage power.

The arc leakage power is the power incident on the receiver caused by the voltage drop across the discharge. As is true for many low-frequency and d-c discharges, the voltage drop across the r-f discharge in the usual operating range is very nearly independent of the current which it carries. The envelope of the leakage power from a typical TR tube is shown in Fig. 5·1. The "flat" is the sum of the arc leakage power, direct-coupled power, and harmonic power.

The spike energy and flat leakage power of a TR tube are the quantities which determine whether or not it is possible to protect the receiver from damage by the transmitter power. In all modern microwave radars superheterodyne receivers are used with silicon, or germanium, first-detector crystals. To achieve good sensitivity it is necessary to use a rather delicate contact between the tungsten "cat whisker" and the silicon crystal. As a result, it is possible to damage the contact with impulses (duration 10^{-8} sec) of 0.2 to 0.5 erg energy, or with steady-state leakage powers of the order of 1 watt. To ensure adequate factors of safety, most TR tubes are designed to have a spike leakage energy of less than 0.1 erg, and an arc leakage power of less than 100 mw.

The power dissipated in the discharge is called the *arc power*. This power is important, first, because it must be furnished by the transmitter, and thus represents a loss, and second, because it is a source of heat that warms up the TR tube, and in extreme cases may cause it to crack or break. Heat which results from arc loss is of particular importance in low-Q ATR tubes, pre-TR, and bandpass TR tubes. Finally, the intensity of the discharge affects the rate at which the gas content of the tube is changed.

In order for a radar set to detect echoes from near-by targets, the attenuation through the cavity must decrease rapidly from its value of 60 to 70 db during the transmitting period to its "cold" value of about 1 db. This means that the gap must be rapidly deionized. Deioniza-

tion cannot take place instantly, but it can be made to proceed at a rate fast enough to bring the attenuation down below 3 db in less than 10 μsec. The time for the attenuation to fall to some specified value, such as 3 or 6 db, is called the recovery time. In extreme cases, if the recovery time is too large, the ability of the radar set to detect small, near-by objects will be limited; or targets detected at long range will be lost when they move in to a shorter range lying within the recovery period.

The range of powers over which a TR or an ATR tube will operate may be defined in several ways. It may be defined in terms of the ability to protect the receiver; in terms of the effect upon the transmitter; or, finally, it may be in terms of the possibility of damaging the tube itself. To ensure satisfactory crystal protection, the power incident on the crystal must be limited to a safe value for any incident power greater than zero and less than the maximum rating of the tube. This is necessary to ensure protection against stray radiation from nearby radar sets, where the power incident upon the TR tube may be many decibels below the transmitter power level, but is still large enough to damage a crystal unless it is suitably clipped or attenuated. Similarly, the power reflected from large nearby targets may be large enough to burn out crystals unless it is suitably attenuated. If the leakage power is limited to about 0.5 watt for incident powers between 0 and 20 watts, the protection is considered satisfactory, even though a limit of less than 0.1 watt is required for normal operation. This larger leakage power is permissible only because it is never applied to the crystal for any considerable length of time. At a repetition rate of 400 pulses per second, a pulse leakage power of 50 mw will cause no change in crystal characteristics over periods of 1000 hours or longer. Pulse leakage powers of 200 to 300 mw will cause deterioration of about 1 db in signal-to-noise ratio of the crystal for every hundred hours of operation.

The minimum power level at which the arc loss becomes small enough to be neglected is considerably higher than the minimum firing power of the tube. In a multigap tube the input window may break down at a power level of the order of several hundred watts. Until it does break down the short circuit in the TR tube is one-quarter guide wavelength from the correct position to ensure proper transmitter action. The breakdown power of the window is the quantity that determines the minimum transmitter power at which a low-Q tube may be used.

The maximum power at which a tube may be used is specified in terms of crystal protection and possible damage of the tube. The spike energy and arc leakage power are remarkably independent of line power, but direct-coupled leakage power imposes a definite limit to the use of high-Q TR tubes. In some high-Q tubes a secondary glow discharge is formed at high power levels across the input window or inside the glass

cylinder adjacent to it. This secondary discharge greatly reduces direct-coupled power, but the heat generated often damages the tube. No direct-coupled power is passed by pre-TR and bandpass TR tubes and they protect crystals at all powers available at present, with no evidence that they cannot be used at still higher pulse powers. However, these tubes have an upper *average power* limit determined by the heating of the input window. Thus, at low duty ratios, extremely high peak powers may be safely used (10 Mw or more). If the duty ratio is increased the maximum allowable transmitter pulse power is correspondingly decreased.

The life of a TR or an ATR tube, if physical breakage from mishandling and the results of exposure to excessive power are ignored, is limited by the rate at which the gas content of the tube is changed by the r-f discharge or the d-c discharge of the keep-alive electrode. Depending upon the type of tube under consideration, the end of the useful life produced by a change in gas content will be indicated by an excessive increase either in recovery time or in leakage power. A tube to be really useful should have an operational life of at least 500 to 1000 hours. Most TR tubes just meet this requirement. Recent low-Q ATR tubes have lives in excess of 2000 hours, while some TR tubes have indicated lives of more than 1000 hours.

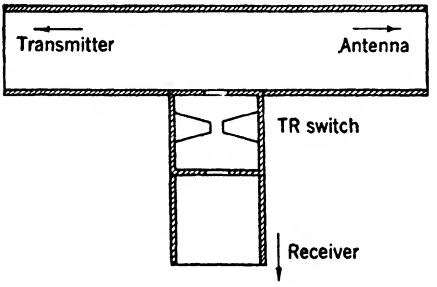

FIG. 5·2.—A TR tube mounted between the main transmission line and the receiver.

Before presenting detailed experimental data and theoretical interpretations of the data, a brief phenomenological description of the fired TR tube will be made. In most respects the TR and the ATR tubes behave alike, and therefore unless specifically noted to the contrary "TR" will include tubes of both types. Figure 5·2 shows a TR tube mounted in a conventional manner between the main transmission line and the receiver. The tube is on a T-junction, often one-half guide wavelength from the main transmission line. When the TR cavity is detuned by the discharge across the gap, the high input susceptance is reflected as a short circuit in the wall of the main guide, and power flows from the transmitter to the antenna without reflection. If the transmitter pulse has a flat top, the envelope of the leakage power will be as shown in Fig. 5·1. In most high-Q TR tubes, the arc leakage power is constant during the pulse to within a few per cent and is usually independent of the transmitter power over ranges of the order of 10^3 or more. In the 721A TR tube this is true for transmitter pulse power levels from 100 to

10^6 watts. It is independent of the cold resonant frequency of the TR cavity over very wide limits.

In a given tube the spike energy has been found to be remarkably constant for a wide range of variables. Within the experimental accuracy, $\pm$ 1 db, the spike energy is constant over as wide a range as is the arc leakage power. It is also independent of the relative tuning of the TR cavity and the transmitter over a range of at least 6 ω_0/Q_{L2} (six half-widths of the resonant circuit). It is not known how the shape of the leading edge of the transmitter pulse affects the spike energy. Until 1945 when oscillographs with very fast sweeps and high resolving power were developed, there was no method of correlating changes in spike energy with changes in the transmitter pulse shape. From measurements of the frequency spectrum of the energy in the spike, the duration of the spike has been estimated to be between 2 and 6 $\times$ 10^{-9} sec for most high-Q TR tubes.

The energy in the spike may be reduced considerably if electrons from an external source are present in the r-f gap at the beginning of the pulse. The source of these electrons is the keep-alive discharge. The keep-alive discharge is a d-c discharge maintained between the keep-alive electrode and some portion of the tube, so located as to have a minimum effect upon the r-f fields in the cavity. The spike energy is inversely proportional to n_0, the number of electrons in the gap at the beginning of the transmitter pulse. It is not possible to increase n_0 indefinitely, however, because of the effect upon the low-level properties of the cavity. The electrons in the gap have an equivalent admittance that is proportional to their density. In practice it is usual to limit n_0 to a value such that the electronic admittance causes less than 0.1 db loss of received signal. By using a pulsed keep-alive discharge, "prepulsing," just before the transmitter pulse, a large value of n_0 may be used and the spike energy may be reduced to very low levels. During most of the receiving period the discharge will be out, and the keep-alive will have no effect upon the low-level insertion loss of the cavity.

When the transmitter is turned off, the excitation is removed and there is no further ionization of the gas in the r-f gap. The electrons and ions already present in the gap do not, however, disappear or recombine instantly. If the filling of the tube is a gas with a closed electron system such as H_2, N_2, A, Ne, or He, the only process which can be used for the removal of electrons is diffusion. This is an extremely slow process, and the recovery time is hundreds of microseconds for such fillings. If, however, a gas with a large electron-capture cross section is used, the removal of electrons will be greatly accelerated and recovery times of the order of a few microseconds may be obtained. Such gases are O_2, H_2O, the halogens, SO_2, and NO.

The gas fillings most commonly used in TR tubes are H_2 and H_2O or A and H_2O at about equal partial pressures and at a total pressure of 10 to 30 mm Hg. Operated on pulsed power alone, at a duty ratio of about $\frac{1}{1000}$, and with no keep-alive discharge, high-Q TR tubes may be run for several thousand hours with little or no effect upon their characteristics. If a d-c keep-alive discharge is maintained, however, then the tube life may be shortened to as little as 250 hours. Two distinct processes operate to cause this short life. The slower, and therefore less important, process is the gradual reduction of the gas pressure by sputtering. The other process is the reduction and change in gas content by chemical action. The water, under the action of the discharge, is dissociated according to $H_2O \rightarrow H^+ + OH^-$. The OH^- radical reacts with the copper walls of the tube to form cuprous oxide, and free hydrogen is released. In this way the partial pressure of H_2O is rapidly reduced, while that of H_2 is actually increased. The result of this process is, first, an increase in recovery time caused by the removal of H_2O; and second, an increase in leakage power as the total gas pressure is reduced by sputtering.

The rate of gas cleanup, and therefore the tube life, is largely determined by the current flowing in the keep-alive discharge. In fact, the life varies inversely with the keep-alive current to a good approximation. Usual operating currents are from 100 to 200 μa. Lower currents would be desirable but although satisfactory levels of spike energy may be held with currents as low as 50 μa such low-current discharges are likely to be unstable. If the discharge is unstable and extinguishes occasionally, very large levels of spike energy may reach the receiver while the discharge is out.

The discharge in high-Q TR tubes takes place between the ends of the cones and is usually of a pale blue color. The *peak* light intensity is moderately high, but at a duty ratio of $\frac{1}{1000}$, the average light flux is low. If the transmitter pulse power is too high for the particular tube used, a secondary discharge may take place across the glass adjacent to the input coupling. In the pre-TR tube, low-Q ATR tube, and bandpass TR tubes, the main discharge takes place across the inside of the input window, and completely covers it with a smooth glow. The internal gaps in a bandpass TR tube break down in a manner similar to the breakdown in a high-Q tube.

In the following sections of this chapter, the material will be presented in the following sequence: (1) A brief view of the more important characteristics of the high-frequency discharge and a comparison with d-c discharges. (2) A detailed discussion of leakage power with a presentation of pertinent data and theoretical interpretations where possible. (3) Recovery-time data and theory. (4) Keep-alive and gas-cleanup problems.

5·2. High-frequency Gas Discharges.—The high-frequency gas discharge is different in many ways from the low-frequency or direct-current discharge. (1) First, its superficial character or structure is different. The high-frequency glow discharge presents a smooth appearance and no particular structure is apparent. This is in contrast with the d-c glow discharge with its various bands or bright and dark spaces. The appearance of the high-frequency discharge is most like that of the positive column in the d-c glow discharge. It will be shown later that this resemblance is more than superficial. (2) The electrodes in the r-f discharge play a very minor role as compared with the major role which they often play in the low-frequency discharges. An extreme example of this is the high-frequency electrodeless discharge, in which the electrodes are completely insulated from the discharge. (3) In low-frequency discharges, both positive and negative ions, as well as electrons, acquire appreciable energy from the applied field, and take part in the ionizing process. At high frequencies, only the electrons acquire any appreciable energy, and all electron production is by energetic electrons. At low frequencies, ions acquire enough energy to cause heating of the electrodes and to produce sputtering. At high frequencies, this process is of little consequence except in discharges of very high power. (4) The electron density of the high-frequency discharge may reach very high levels before the glow discharge is transformed into an arc. Electron densities have been estimated to be as high as 10^{15} per cm^3, and current densities have been estimated to be of the order of 15 amp/cm^2.

Before considering the much more complicated problem of the actual gas discharge, let us consider two fairly simple problems. First, consider the motion of a charged particle of mass m and charge e in a vacuum under the influence of an electric field $E \sin \omega t$,

$$\begin{aligned} m\frac{d^2x}{dt^2} &= eE \sin \omega t, \\ v = \frac{dx}{dt} &= \frac{eE}{\omega m}(1 - \cos \omega t) + v_0, \\ x &= \left(\frac{eE}{\omega m} + v_0\right)t - \frac{eE}{\omega^2 m}\sin \omega t, \end{aligned} \tag{1}$$

where x is the direction of the applied field, and v_0 is the initial velocity of the particle. The particle has a continuous x-directed motion upon which is superimposed an oscillating motion in time phase with the electric field. The energy of the particle is

$$W = \frac{1}{2}mv^2 = \frac{1}{2}m\left[\left(\frac{eE}{\omega m}\right)^2(1 - \cos \omega t)^2 + 2\frac{eEv_0}{\omega m}(1 - \cos \omega t) + v_0^2\right]. \tag{2}$$

If the initial velocity is small compared with that derived from the field,

the energy acquired by the particle is inversely proportional to its mass and to the square of the frequency.

K. K. Darrow has suggested a simple but illuminating method of accounting for the effect of collisions upon the motion of an electron in a field.[1] This method, although admittedly crude, gives an insight into the general mechanisms involved. It is assumed that the gas molecules are so massive compared with the electron that they are stationary, and also that their density is great enough to make the collisions of the electron with the molecules act as a net frictional force opposing the motion of the electron. Using g for the "coefficient of friction,"

$$m\frac{d^2x}{dt^2} + g\frac{dx}{dt} = eE\sin\omega t$$

$$v = \frac{dx}{dt} = \frac{eE}{m\left(\omega^2 + \frac{g^2}{m^2}\right)}\left(\frac{g}{m}\sin\omega t - \omega\cos\omega t\right) + \left[\frac{eE\omega}{m\left(\omega^2 + \frac{g^2}{m^2}\right)} + v_0\right]e^{-\frac{g}{m}t}. \quad (3)$$

As before, there is an oscillatory and a drift velocity. The latter, however, is exponentially damped by the "frictional" force, and is small compared with the oscillatory speed.

Since $ne\ (dx/dt)$ is the current density across a given plane, where n is the number of charged particles per cubic centimeter, Eq. (3) also represents current flow. *In-phase* and *out-of-phase* or *quadrature* components of current relative to the applied voltage are recognized. The *in-phase* component varies inversely with frequency and has its maximum value at $\omega = 0$. The *quadrature* component has a maximum value at $\omega^2 = g^2/m^2$, and is zero at $\omega = 0$ and ∞. Increasing g by increasing the gas pressure reduces the quadrature relative to the in-phase components of the current.

A "conductivity" and "dielectric constant" of such a cloud of charged particles may be defined. From Eq. (3), the in-phase current is

$$\frac{ne^2g}{\omega^2m^2 + g^2}E\sin\omega t = \sigma E\sin\omega t. \quad (4)$$

Similarly, the *total* quadrature current across the gap, including displacement current, is

$$\frac{1}{4\pi}\left(\epsilon_0 - 4\pi\frac{ne^2m\omega}{\omega^2m^2 + g^2}\right)E\cos\omega t = \frac{\epsilon}{4\pi}\cos\omega t, \quad (5)$$

[1] K. K. Darrow, *Bell Syst. Techn. J.*, 576 (October 1932).

which gives the familiar result that the dielectric constant of a space-charge region is less than that of vacuum.

This highly simplified theory indicates the following important facts:

1. The in-phase current carried by the electrons decreases with increasing frequency.
2. At very high frequencies, the quadrature component exceeds the in-phase component.
3. The relatively heavy positive and negative ions, $m_i \geqq 1847m_e$, get very little energy directly from the electric field.

It has been stated that the r-f discharge strongly resembles the d-c positive column. Some of the salient features of the positive column are listed[1] here:

1. No net charge—equal numbers of positive and negative charges.
2. Low gas temperature, about 100°C.
3. Low ion temperature; high electron temperature.
4. Voltage gradient less for monatomic than for diatomic gases.

The r-f discharge has no net charge, since the entire ionization takes place within the discharge itself, and the drift velocity of the charged particles is very small. The instantaneous gas temperature of the r-f discharge has never been measured. However, under pulsed, high-current operation, the window of a low-Q ATR tube may attain a steady temperature in excess of 100°C with a transmitter duty ratio of $\frac{1}{1000}$. Thus, the maximum gas temperature must be much higher than 100°C. Since the r-f discharge current is measured in amperes or tens of amperes, whereas the d-c glow discharge current is usually measured in milli-amperes, the difference in temperature is not surprising. The ion temperature in the r-f discharge is low compared with that of the electrons since the ions, because of their large mass, get little energy from the field but get all their energy by collisions with electrons. The total voltage drop across the r-f discharge is less for monatomic than for diatomic gases. The order of the various gases may be seen in the comparison in Table 5.1. The first row of the table is taken from Cobine[2] and gives the

TABLE 5·1.—COMPARISON OF VOLTAGE DROP ACROSS R-F DISCHARGE IN VARIOUS GASES

	Air	O_2	H_2	N_2	He	Ne	A
E_c/p (positive column)	17	14	8.5	4.3	2.3	0.45	0.22
Arc voltage (r-f discharge)		3.3	2.9	3.1	1.4	1.2	0.65

[1] Cobine, *Gaseous Conductors*, McGraw-Hill, New York, 1941, p. 233.
[2] Cobine, *op. cit.*, Chap. VIII.

electrical gradient along the column divided by the gas pressure for a given shape of discharge tube and at currents of 0.1 to 0.2 amp. The second row is derived from measurements of the arc leakage power of a 1B27 TR tube at a pressure of 10 mm Hg, and the numbers are in arbitrary units. It is felt that the exact ratios between the values for the various gases have no significance because the shapes of the discharge tubes and the discharge currents are so different in the d-c and r-f cases. Nevertheless, the orders in the two cases are about the same.

Spectrographic observations were made of the r-f discharge, and no particular features were noted that distinguished it from the low-fre-

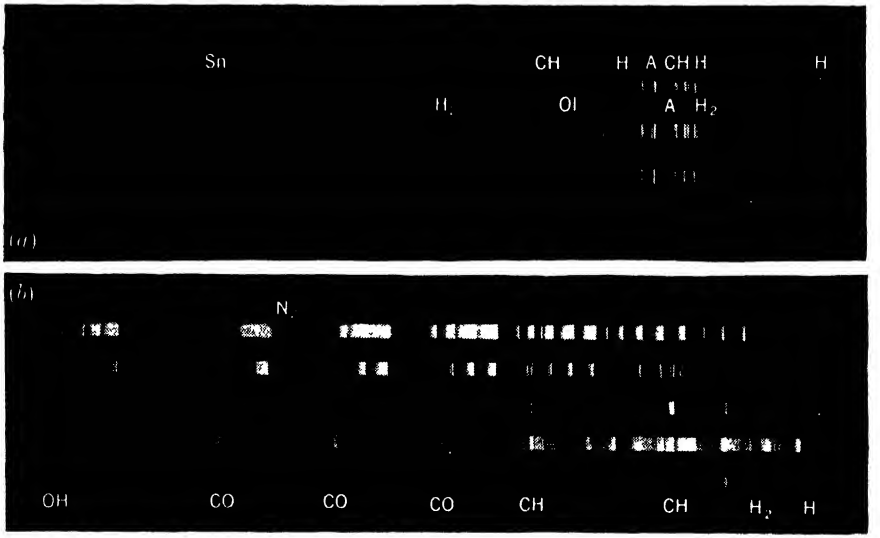

FIG. 5·3.—Spectograms of r-f discharge in several 1B38 pre-TR tubes.

quency discharge. Figure 5·3 is a reproduction of a few typical spectrograms of the light from 10-cm, argon-filled, pre-TR tubes.[1] No accurate measurements of the efficiency with which light is produced by the r-f discharge have been made. The light from a 10-cm pre-TR tube was measured with a General Electric photographic exposure-meter. With a line power of 5×10^5 watts and a duty ratio of $\frac{1}{2000}$, the indicated average surface brightness was 2.5×10^{-3} lumen/cm^2. This instrument has a barrier-layer photovoltaic cell with a nonlinear characteristic and therefore the maximum brightness was probably much greater than the calculated value of 5 lumen/cm^2.

In a self-sustaining discharge, the rates of production and destruction, or removal of ions, are equal. Deionization in a low-frequency discharge may take place by two processes only: recombination, and diffusion.

[1] These were made by R. McNally, Jr., of the Spectroscopy Laboratory of M.I.T.

Recombination of a positive ion and an electron is a relatively improbable process,[1] and can usually be neglected in comparison with the loss of charge by diffusion to the walls or electrodes. Since most of the negative charge in the d-c discharge is carried by free electrons, the more probable recombination of positive ions and negative ions can also be neglected. In the r-f discharge, the entire alternating current is carried by the free electrons. This means that capture of electrons by neutral atoms or molecules to form negative ions effectively "deionizes" the gap in the sense that its current-carrying capacity is reduced. Thus, in the d-c positive column, ionization must take place at a rate equal to the deionization by diffusion whereas in the r-f discharge it must equal the combined rates of diffusion and electron capture.

The processes involved in the transition to a self-sustaining discharge are markedly different in the low- and in the high-frequency regions. In both cases, the initial ionization must result from some outside source, for example, cosmic rays or photoelectric emission from the cathode. The electrons produced in this way are accelerated by the applied field until they in turn can make ionizing collisions, and thus release more electrons. It is here that the differences become important. In the d-c discharge there is a fairly rapid drift of the electrons in the direction of the field. They eventually reach the anode where they are lost to the discharge. If only ionization by energetic electrons is considered, the number of electrons between the anode and cathode is

$$n = n_0 \epsilon^{\alpha x} \tag{6}$$

where n_0 is the number of electrons produced at the cathode by an external source, x is the distance measured from the cathode, and α is the number of ionizing collisions made by an electron per centimeter of path in the direction of the field. Clearly, the anode current is directly proportional to n_0 and will be zero when n_0 is zero. Thus, a self-sustaining discharge cannot be achieved at low frequencies if ionization depends entirely upon electrons. Recognizing this, J. S. Townsend proposed a second method of ionization, ionization by positive ions.[2] This resulted in the equation,

$$n = n_0 \frac{(\alpha - \beta)\epsilon^{(\alpha-\beta)x}}{\alpha - \beta\epsilon^{(\alpha-\beta)x}}, \tag{7}$$

in which β represents the number of ionizing collisions made by a positive ion per centimeter of path in the direction of the cathode. If the denominator of Eq. (7) can be made equal to zero, n will increase without limit,

[1] Loeb, *Fundamental Processes of Electrical Discharges in Gases*, Wiley, New York, 1939, Chap. 2.

[2] For a more complete discussion of cumulative ionization in d-c discharges, see Loeb, *op. cit.*, Chaps. 9 and 10.

and thus become independent of n_0. Although considerable doubt now exists as to the actual physical process described by Townsend's second coefficient β, it is agreed that some secondary ionizing process is necessary to produce cumulative ionization in a d-c field. Derivations based on the assumption that the secondary process consists of release of photoelectrons from the cathode by light generated in the discharge have the same form as Eq. (7).[1]

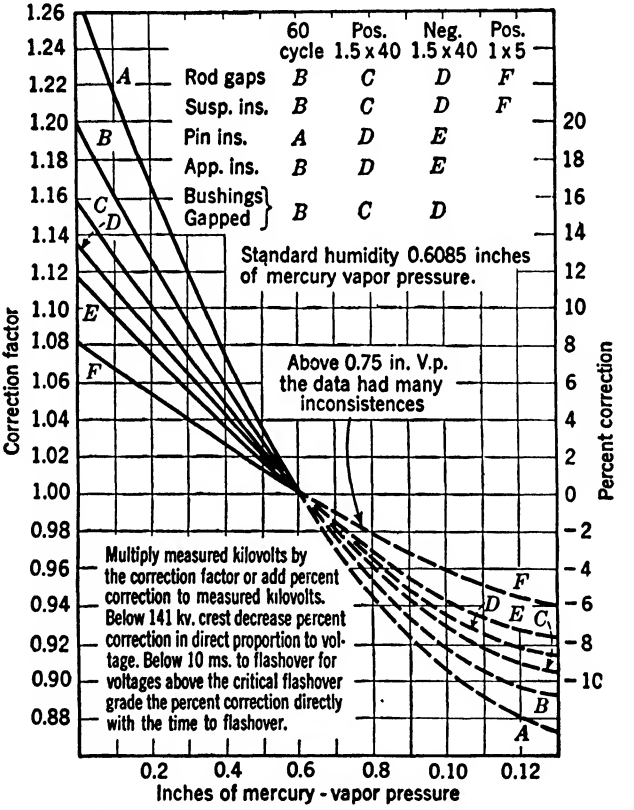

FIG. 5·4.—Effect of water vapor pressure on breakdown potential (from Cobine, *Gaseous Conductors*, McGraw-Hill, 1939.)

In the high-frequency discharge, the drift velocity of the electrons is much less than in the d-c case. If the extreme case where the drift velocity is zero is considered then, except for those electrons that are within one mean free path of the electrodes, there will be no loss of electrons from the discharge and each electron can make a limitless number of ionizing collisions. Once the process is started, the initial electron source may be removed without affecting the final current. At the

[1] Loeb, *loc. cit.*

extreme frequencies of 3000 to 10,000 Mc/sec the existence of a secondary ionizing mechanism of the type postulated by Townsend, ionization by positive ions, seems highly improbable; however, the production of photoelectrons at the electrodes or in the gas by light from the discharge cannot be ruled out until measurements of the ionization process have been made in detail.

The presence of a gas such as H_2O, which has a comparatively high probability of capturing a free electron to form a negative ion (high electron-capture cross section), effectively increases the breadkown voltage of a gap. Capture of electrons effectively removes them from the discharge since the probability of ionization by negative ions is very small, and energies of the order of 3 to 4 volts are needed to detach an electron from a negative ion. Figure 5·4 illustrates the effect of water-vapor pressure on the breakdown voltage of rod gaps, suspension insulators, pin and apparatus insulators, and bushings.[1]

A similar result would be expected in high-frequency discharges. So far, at least, in the pressure region of 5 to 30 mm Hg, the observed effect of H_2O on spike energy, which is proportional to the breakdown voltage, does not permit such a generalization.

5·3. Leakage Power and Crystal Burnout.—The most difficult requirement placed upon the TR tube is that the leakage power be limited to a value low enough to ensure the protection of the silicon crystal used as the first detector of the receiver. At frequencies below 1000 Mc/sec the conversion of the received signal to a lower, intermediate frequency may be performed in diode or triode vacuum tubes with excellent signal-to-noise characteristics. Such tubes are rugged and are not easily damaged by pulsed leakage power of the order of tens of watts. In the microwave region, however, transit-time effects make the construction of good thermionic tubes very difficult because of the delicate and minute spacings between electrodes which are necessary in order to obtain good performance. Diode converters have been built for use at 10 cm; but their performance (signal-to-noise ratio) has always been poorer than that of a silicon crystal by about 6 db.

Silicon crystals have been brought to their present state of excellence by improving the purity, the etching, and the polishing of the silicon, and also by better control of the location and shape of the tungsten "cat whisker."[2] Typical performance characteristics of crystals for the 10-cm, 3-cm, and 1.25-cm bands are given in Table 5·2.

This excellent performance is the result of the extremely small contact area between the tungsten and the silicon, which is of the order of

[1] Joint Committee on Insulation Research, EEI-NEMA, "Recommendations for High-voltage Testing." *Trans. Amer. Inst. Elect. Engrs.*, 59, 598 (1940).

[2] See Vol. 5 of this series, *Crystal Rectifiers*.

TABLE 5·2.—TYPICAL CRYSTAL PERFORMANCE FIGURES

Type	Band, cm	Conversion loss, db	Noise* factor
1N21B	10	5.5	1.3
1N23B	3.3	6	1.5
1N26	1.25	7	1.5

* The noise factor expresses the noise power as a multiple of the noise produced at room temperature by an ideal resistor of a resistance equal to that of the crystal.

3×10^{-8} in.^{2} Most of the ohmic resistance of the crystal is in the volume immediately adjacent to the contact and, consequently, despite the high melting point of tungsten, the power density is so great that only a few watts are required to fuse the tungsten point and to destroy the rectifying contact.

There are two important ways in which the leakage power can change or impair the performance of a crystal. One is characterized by a slow, continuous degradation of the signal-to-noise ratio of the crystal at leakage powers of the order of 200 mw. The rate of deterioration depends only upon the total time of application of the power. Thus, at a duty ratio of $\frac{1}{1000}$, the crystal changes by about 1 db per hundred hours with 200 mw applied. If the same power is applied as continuous wave power, the crystal changes 1000 times as fast. Damage of this type is not the result of heat, and is probably associated with the total charge transported across the rectifying layer.

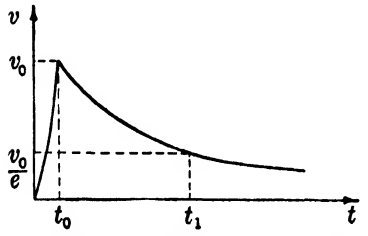

FIG. 5·5.—Waveform of test voltage applied to silicon crystals in simulated spike burnout tests.

The other type of crystal failure is thermal "burnout" in which local heating permanently changes the contact between the cat whisker and crystal. Thermal burnout may be divided into two general types according to the manner in which the power is applied. In one, the power is applied for a time long compared with the thermal time constant of the crystal contact. The final temperature is directly proportional to the *power* dissipated at the contact. In the other, the power is applied for a time short compared with the thermal time constant, and the temperature of the contact is proportional to the *total energy* dissipated at the contact, that is, the heating is ballistic.

Theoretical studies and the experiments on crystal detectors indicate that the shortest thermal time constant of any consequence is of the order of 10^{-8} sec. Crystals are required to withstand a d-c pulse of the type

illustrated in Fig. 5·5 and still have satisfactory signal-to-noise characteristics. The decay time constant t_1 is 5×10^{-9} sec, and $t_0 \ll t_1$. This pulse is obtained by suddenly discharging a capacitor through the crystal. The total energy dissipated in the crystal in these tests varies from 0.1 erg in the 1N26 to 2 ergs in the 1N21B. At energies roughly twice these test levels, a large fraction of the crystals are damaged.

When the study of crystal burnout was first begun only "steady state" burnout by the application of long pulses (1 μsec) was considered. Early crystals (1943) were impaired by powers of 0.5 to 1 watt. With improvement in the crystals this power has been increased, and modern crystals will withstand 3 to 10 watts without serious damage. It soon became apparent that most TR tubes had flat leakage powers of the order of 100 mw or less, so that steady-state burnout was really no problem. The energy in the spike of the average TR tube, however, was much closer to the danger level. For this reason, it was decided to specify crystal burnout properties n terms of ballistic heating as just described.

In Sec. 5·1, it was pointed out that the envelope of the TR leakage power could be divided into two parts, the spike and the flat, as shown in Fig. 5·1. This picture can be seen if the leakage power is rectified and passed through an amplifier of 5- to 10-Mc/sec bandwidth before being displayed on a cathode-ray-tube screen. It has been determined by experiment that the duration of the spike is usually less than 10^{-8} sec and, for high-Q TR tubes, is from 3 to 6×10^{-9} sec. The energy in the spike is about 0.05 erg for most high-Q tubes. Bandpass tubes usually exhibit a spike energy two or three times as great.

The arc leakage power lies between 10 and 50 mw for practically all microwave TR tubes, and therefore this in itself can hardly damage a crystal. The flat leakage power, however, is the sum of the arc, harmonic, and direct-coupled leakage powers, and care must be taken to ensure that harmonic and direct-coupled leakage powers do not reach dangerous levels.

5·4. The Spike.—On the basis of the introductory description, the spike can be defined as follows: the spike energy is that energy transmitted to the receiver during the time interval between the beginning of the transmitter pulse and the formation of the steady-state discharge across the gap of the TR tube. Figure 5·6 shows, on an expanded scale, the presumed envelope of the leakage power through the TR tube near the start of the transmitter pulse.

Until recently, the exact shape of the spike had never been observed directly. Conventional video-frequency amplifiers and cathode-ray oscillographs are incapable of resolving transients whose duration is 10^{-8} sec or less. As a result, the analysis presented in the following

sections was developed by inference or deduction from the observable properties of the spike: total energy and spectrum. In April, 1946, C. W. Zabel succeeded in obtaining an oscillogram of the spike energy leaking through a 1B38 pre-TR tube. This was done in the Insulation Laboratory of the Massachusetts Institute of Technology on the high-speed oscillograph developed by Lee.[1] The results of these measurements are entirely consistent with previously developed theoretical analysis.

Step by step, the processes in the spike are as follows. At the very beginning of the transmitter pulse, there is an initial number of electrons n_0 in the gap of the TR tube. As the transmitter voltage increases, the voltage across the TR gap also increases, but at a slower rate because of the comparatively high Q of the TR cavity. In bandpass TR tubes, the voltage buildup follows that of the transmitter with no appreciable time lag. This will be discussed in greater detail in a later section. The electrons are accelerated by the voltage across the gap until they attain sufficient energy to produce further ionization. The electron density in the gap then increases very rapidly and begins to short-circuit the gap and to reduce the power transmitted through the TR cavity to the receiver. The rate of ionization continues to increase as the power increases until an equilibrium is reached with the incident power. The leakage power in the equilibrium condition is called the *arc leakage power*, P_a.

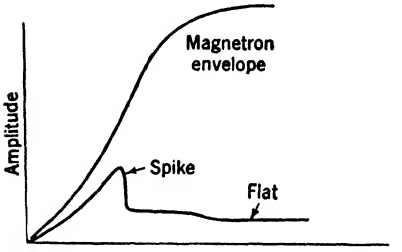

FIG. 5·6.—Presumed shape of spike leakage envelope relative to magnetron buildup.

The detailed structure of the spike cannot be observed easily, but two significant measurements can be made which characterize it. These are measurements of the total energy in the spike, and measurements of its frequency spectrum. The spike energy W_s can be measured in several different ways (see Chap. 9). From a measurement of the total leakage energy for two different transmitter-pulse widths, assuming that W_s and P_a are independent of the pulse width, W_s can be computed. Alternatively, the fact may be used that the attenuation through the TR cavity, during the steady-state discharge, is of the order of 60 db and is only a few db during the spike. This allows the arc leakage power to be canceled with a small amount of power obtained from the main transmitter line through an attenuator, without altering the spike envelope.

[1] Gordon M. Lee, "A Three-beam Oscillograph for Recording at Frequencies up to 10,000 Megacycles," *Proc. Inst. Radio Engrs.*, N.Y., 34, 121*a* (March 1946).

Under this condition the spike energy may be measured directly. The two methods, if used under the proper conditions, give equivalent results, and good TR tubes have spike energies of the order of 0.05 erg per pulse.

The measurement of the duration of the spike is much less certain than the measurement of the energy. The only direct experimental method is to measure the frequency spectrum of the spike when the flat leakage power is canceled as just described. Such measurements are restricted to the *amplitudes* of the various frequency components. Since phase measurements are impossible with present techniques, the shape of the spike cannot be reconstructed by the inverse Fourier transformation. However, on the assumption that the spike is rectangular, and by the use of the relation between pulse width τ_s and the frequency interval Δf between the first two minima in the spectrum,

$$\tau_s = \frac{2}{\Delta f},$$

the duration has been estimated to be about 5×10^{-9} sec in a typical high-Q TR tube.

The spike energy is of primary interest because of the problem of crystal burnout. Most of the measurements quoted in the following sections will relate to it, whereas measurements of spike duration will receive rather scant attention. A simplified theory of the spike will be presented first and then the dependence of spike energy upon the following parameters will be discussed:

1. Gas content.
2. Initial number of electrons, n_0.
3. Gap shape.
4. Tuning of TR cavity.
5. Transmitter power level.
6. Transmitter-pulse shape.
7. External circuit.

The variation of spike energy with the gas content of the TR tube is a straightforward measurement and has received more attention than the other measurements. No absolute measurements of the effect of n_0 upon W_s have been made because of the difficulty of measuring n_0. Qualitative results, however, have been obtained. Gap shape has been investigated only by varying the gap length of a given tube and by noting the variation in W_s. The effects of tuning and transmitter power level have been measured, and coherent results obtained. No data are available on the effect of the transmitter-pulse shape. Some data exist on the effect of the impedance and Q of the external load upon W_s.

5·5. Linear Theory of the Spike.—There is, at present, nothing that can be dignified by the title of "theory of the spike." It is known that at the start of the transmitter pulse there are a few electrons in the gap. These are accelerated by the high-frequency field until their energy is sufficient to cause ionization and produce more electrons. The number of electrons increases exponentially with time until the electronic r-f admittance across the gap becomes very large and the discharge passes into the steady-state or flat condition. It is not possible yet to calculate the rate at which the ionization process takes place even for simple gases like helium, and for gases having many excitation levels at energies below the ionizing potential such calculations are even farther from realization.

Even with these limitations, it is possible to make some pertinent calculations on the basis of a much simplified model. The justification for the use of the simple model lies in the fact that the calculations based on it give results that agree with experiment. This simple model of the

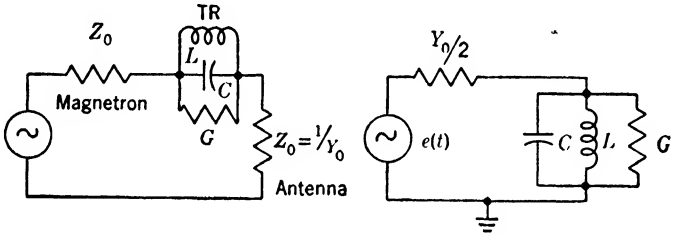

FIG. 5·7.—Lumped-constant circuit of TR cavity loaded with magnetron oscillator and antenna.

spike assumes that the electronic admittance across the gap of the TR tube is negligible until a critical voltage is reached, at which time the gap ionizes instantly and completely. The linear transient response of the TR cavity to the transmitter pulse is calculated up to the time t_s at which time the gap breaks down. It is assumed that the spike energy is the energy calculated in this manner.

A further sophistication of the theory includes the effect of electronic loading on the transient response. The rate of ionization is calculated but it is assumed that inelastic collisions that do not ionize can be neglected. This calculation involves a knowledge of the velocity distribution functions of the electrons and the probability of ionization corresponding to different electron energies. T. Holstein of the Westinghouse Research Laboratories has studied this problem in considerable detail, but no results are yet available.

In this section the behavior of the simplified linear model described above will be presented. The electrical circuit of the r-f section of a radar set including the transmitter, TR tube and receiver, and the antenna, may be represented by the equivalent lumped-constant circuit

of Fig. 5·7. The TR cavity is assumed to be connected in series with the transmitter line, and the generator and antenna are matched to the characteristic admittance Y_0 of the main line, while the receiver has a conductance G. The differential equation for the voltage V across the resonant TR circuit is then

$$V_g(t)\frac{Y_0}{2} = V\left(\frac{Y_0}{2} + G\right) + C\frac{dV}{dt} + \frac{1}{L}\int V\,dt. \tag{8}$$

If the generator voltage $V_g(t)$ is known, it is possible to solve for V and finally get an expression for the energy dissipated in the receiver load G for any assumed time interval between $t = 0$, the start of the transmitter pulse, and τ, the beginning of the discharge. The first problem, then, is to choose the proper function for $V_g(t)$.

First, it is necessary to consider only self-excited oscillators such as the magnetron, since master-oscillator–power-amplifier combinations are not yet available in the microwave region. It is known that the oscillations in a self-excited thermionic oscillator build up from zero in the following manner. As the anode voltage is increased, current begins to flow. At low voltages the gain around the positive-feedback loop is not sufficient to make the oscillator have a negative dynamic conductance equal in magnitude to the total conductance loading the tube, and there are no self-sustained oscillations. There is, however, noise power delivered to the load. As the voltage and gain of the tube increase, the negative conductance increases until finally self-sustained oscillations begin.

In the magnetron, while the voltage is still below the cutoff level, the rotating space charge has two effects. First, it acts as a noise generator; and second, the noise voltages induced in the resonant cavities couple back to the space charge, like positive feedback, and tend to bunch it. At the critical voltage, the coupling between the space charge and the resonant cavities of the magnetron becomes so tight that oscillatory energy may be delivered to an external load with enough voltage left over to keep the space charge properly bunched, and thus maintain stable oscillations in the circuit.

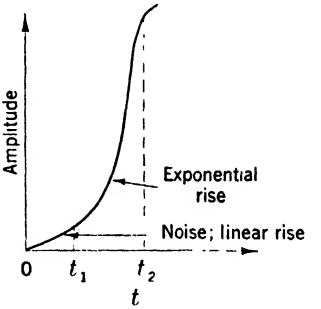

FIG. 5·8.—Envelope of build-up of oscillations in a pulsed magnetron.

The output power of the magnetron is shown in Fig. 5·8. In the interval $0 < t < t_1$, the tube has an increasing, positive value of Q and is driven by a constant-current noise source. The *output noise* does not have the usual wide noise spectrum, but has the frequency characteristics

determined by the effective Q of the tube. The noise output power increases linearly with time. At time t_1 the negative electronic conductance becomes greater in absolute magnitude than the total dissipative conductance. The Q of the tube becomes *negative*, and the amplitude of oscillation increases exponentially with time until it reaches a limit imposed by the external power supply, cathode emission, and space charge.

For purposes of analysis of the spike, it will be assumed that the magnetron has a constant, high, positive value of Q during the noise buildup. The noise source is the space charge and is assumed to have a very high impedance. It may be considered as a constant-current source whose strength increases linearly with time. The output power of the magnetron during this period, and under these assumptions, consists of a narrow spectrum of noise, narrow compared with the TR-cavity bandwidth, about a center frequency ω, and with amplitude increasing linearly from zero. Because the Q of the magnetron is so high in the interval $0 < t < t_1$, the output power is essentially a continuous wave in terms of the comparatively low-Q TR cavity. During this noise-buildup period

$$V_g(t) = \frac{V_0}{t_1} t \sin \omega t \qquad 0 < t < t_1. \tag{9}$$

For $t > t_1$, the output increases exponentially and

$$V_g(t) = V_0 e^{\alpha(t-t_1)} \sin \omega t. \tag{10}$$

Let us consider the response of the TR cavity to these two functions. Measurements on 10-cm magnetrons indicate that the maximum noise power is of the order of 20 watts when the magnetic field is 1300 gauss, and the r-f pulse power is about 50 kw. A typical value is $V_0 = \sqrt{20/Y_0}$, where Y_0 is the characteristic admittance of the transmission line coupled to the magnetron. The time t_1 depends upon the steepness of the applied d-c pulse, and is about 10^{-8} sec.

To get the response of the cavity to this linear rise, Eq. (8) is rewritten

$$\frac{V_0 Y_0}{2t_1} t \sin \omega t = V\left(\frac{Y_0}{2} + G\right) + C\frac{dV}{dt} + \frac{1}{L}\int V dt, \qquad 0 < t < t_1. \tag{11}$$

This equation is conveniently solved by the method of the Laplace transformation.[1] The transformation of the differential equation into an algebraic equation gives

$$\frac{V_0 Y_0}{2t_1} - \frac{\omega s}{(s^2 + \omega^2)^2} = V(s)\left[s^2 + \frac{\frac{Y_0}{2} + G}{C} s + \frac{1}{LC}\right]\frac{C}{s}, \tag{12}$$

[1] Gardner and Barnes, *Transients in Linear Systems*, Vol. I, Wiley, New York, 1942.

where $V(s)$ is the $\mathfrak{L}$-transform of V, and s is the Laplace operator. The solution for $V(s)$ is

$$V(s) = \frac{V_0 Y_0\, \omega}{2t_1 C} \frac{s^2}{(s^2 + \omega^2)^2\,(s + \beta + j\omega)\,(s + \beta - j\omega)}, \tag{13}$$

where $1/LC = \omega^2$, $\beta = (Y_0/2 + G)/2C = \omega/2Q_{L2}$ and $\omega \gg \beta$. If the inverse, or $\mathfrak{L}^{-1}$, transformation is made

$$V = \frac{V_0 Y_0}{4t_1 C\beta}\left\{\left[t - \frac{1}{\beta}(1 - e^{-\beta t})\right]\sin \omega t + \left[\frac{t}{2} - \frac{1}{\beta}(1 - e^{-\frac{\beta}{t}})\right]\cos \omega t\right\}. \tag{14}$$

Usual values of Q_L for a TR cavity are between 300 and 400; therefore $\beta \approx 10^7$ sec^{-1}. With $\omega = 2 \times 10^{10}$ sec^{-1}, β may be neglected by comparison, and Eq. (14) becomes

$$V \approx \frac{V_0 Y_0}{4t_1 C\beta}\left[t - \frac{1}{\beta}(1 - e^{-\beta t})\right]\sin \omega t. \tag{15}$$

If $e^{-\beta t}$ is expanded in powers of βt,

$$V \approx \frac{V_0 Y_0}{8t_1 C}\, t^2 \sin \omega t. \tag{16}$$

The power dissipated in the conductance G is

$$P = |V|^2 G = \frac{V_0^2 Y_0^2 G}{64 t_1^2 C^2}\, t^4 \sin^2 \omega t, \tag{17}$$

and the energy dissipated in the time τ is

$$W = \int_0^t P\, dt = \frac{V_0^2 Y_0^2 G}{64 t_1^2 C^2}\int_0^\tau t^4 \sin^2 \omega t\, dt,$$

or

$$W \approx \frac{V_0^2 Y_0^2 G}{640 C^2 t_1^2}\tau^5 \qquad 10^{-9} < \tau < 10^{-8} \text{ sec}. \tag{18}$$

If it is assumed that the gap breaks down instantaneously at the time τ, then Eq. (18) gives the spike energy W_s dissipated in the conductance G. Experimentally, it is known that W_s is independent of transmitter power over a range of at least 1000 to 1. For Eq. (18) to be correct W must be independent of V_0. If it is assumed that the gap breaks down at a critical voltage V', then, from Eq. (16),

$$\tau' = \sqrt{\frac{8Ct_1 V'}{Y_0 V_0}}. \tag{19}$$

If Eq. (19) is substituted into Eq. (18),

$$W = \frac{1}{5}\sqrt{\frac{2Ct_1}{Y_0 V_0}}\, V'^{5/2}. \tag{20}$$

Thus, W is not independent of V_0 and does not satisfy the experimental results, unless V' is also a function of V_0 as defined by Eq. (20). Moreover, if numbers are put into Eq. (18), then for $V_0 = \sqrt{20/Y_0}$, $t_1 = 10^{-8}$ sec, $Q = 300$, $\tau = 5 \times 10^{-9}$ sec, and $Y_0 = G$, the computed energy is too low by a factor of more than 1000.

Thus, it has been demonstrated that the value of W_s calculated on the assumption of an instantaneous breakdown of the gap at a critical voltage V' is much too low if available estimates of the rate of noise buildup are used and the computations are confined to the linearly rising portion of the magnetron-starting characteristic. Further investigation shows that W_s is not independent of the cavity tuning. That is, for $1/LC \neq \omega^2$, the energy delivered to G varies with the value of LC. Let us now investigate the energy dissipated in G during the exponentially rising voltage output period, $t_1 < t < t_2$.

To simplify notation, let us shift the time scale so that t_1 is zero time. Then $V_g(t) = V_0 e^{\alpha t}$. Since the energy contributed by the linear rise is so small, it will be neglected here, and it will be assumed that at $t = 0$, $V_g(t)$ is suddenly applied to the network. If the solution for V is found in the same way as before, the $\mathcal{L}$-transform equation is

$$V(s) = \frac{V_0 \omega Y_0}{2C} \frac{s}{(s - \alpha + j\omega)(s - \alpha - j\omega)(s + \beta + j\omega)(s + \beta - j\omega)}. \tag{21}$$

Finally, if $\omega \gg \beta, \alpha$

$$V \approx \frac{V_0 Y_0}{4C(\alpha + \beta)} (e^{\alpha t} - e^{-\beta t}) \sin \omega t. \tag{22}$$

The energy dissipated in G is

$$W \approx \frac{V_0^2 Y_0^2 G}{32C^2(\alpha + \beta)^2} \left[\frac{1}{2\alpha} (e^{2\alpha\tau} - 1) - \frac{2}{\alpha - \beta} (e^{(\alpha-\beta)t} - 1) - \frac{1}{2\beta} (e^{-2\beta\tau} - 1) \right]. \tag{23}$$

The quantities Y_0, β, C, and G are defined as before. The time constant of the magnetron is $\alpha = \omega/2Q_m$, where the buildup Q has a typical value of $Q_m = -25$. In the 10-cm band $\alpha = 4 \times 10^8$ sec^{-1}. Since the values of τ are between 5×10^{-9} and 10^{-8} sec, Eq. (23) cannot be expanded into a short series of one or two terms as was done for Eq. (15). A graphical solution of Eq. (22) and Eq. (23) shows that for $\tau > 2 \times 10^{-9}$ sec, the energy is independent of V_0 over a wide range Furthermore, if $V_0 = \sqrt{20/Y_0}$, $G = Y_0$, $\alpha = 4 \times 10^8$, $\beta = 2.5 \times 10^7$, $C = 3 \times 10^{-8} Y_0$, and $\tau = 9 \times 10^{-9}$ sec, then it is found from Eq. (23) that $W = 0.07$ erg, which is in good agreement with experiment.

Since this simple theory agrees with experiment when the magnetron and TR cavity are tuned to the same frequency, $\omega^2 = 1/LC$, it is inter-

esting to see what happens when the two are tuned differently, and

$$\frac{1}{LC} = (\omega + \Delta\omega)^2.$$

If this relationship is substituted into the initial differential equation, then the £-transformed equation is

$$V(s) = \frac{V_0 \omega Y_0}{2C} \times$$

$$\frac{s}{(s - \alpha + j\omega)(s - \alpha - j\omega)[s + \beta + j(\omega + \Delta\omega)][s + \beta - j(\omega + \Delta\omega)]}. \quad (24)$$

The inverse transformation of this equation gives

$$V \approx \frac{V_0 Y_0}{4C[\Delta\omega^2 + (\alpha + \beta)^2]} \{[\Delta\omega \cos \omega t + (\alpha + \beta) \sin \omega t]e^{\alpha t} - [\Delta\omega \cos (\omega + \Delta\omega)t + (\alpha + \beta) \sin (\omega + \Delta\omega)t]e^{-\beta t}\} \quad (25)$$

where ω is large compared with α, β, and $\Delta\omega$. This expression may be rewritten as

$$V = \frac{V_0 Y_0}{4C\sqrt{(\Delta\omega)^2 + (\alpha + \beta)^2}} [(e^{\alpha t} - e^{-\beta t} \cos \Delta\omega t) \sin (\omega t + \phi) - e^{-\beta t} \cos (\omega t + \phi) \sin \Delta\omega t], \quad (26)$$

where $\phi = \tan^{-1}[(\alpha + \beta)/\Delta\omega]$. The absolute value is

$$|V| = \frac{V_0 Y_0}{4C\sqrt{(\Delta\omega)^2 + (\alpha + \beta)^2}} \sqrt{e^{2\alpha t} - 2e^{(\alpha-\beta)t} + 1}. \quad (27)$$

This equation is similar in form to Eq. (22) and for t greater than 5 or 6×10^{-9} sec, a change of $\Delta\omega$ has the same effect as changing V_0, and therefore has no effect upon the spike energy. This agrees with experiment which has shown that W_s is independent of $\Delta\omega$ over a range of at least

$$0 < \left|\frac{\Delta\omega}{\omega}\right| < \frac{6}{Q_L}.$$

Thus, an extremely simple empirical theory of the spike has been formulated. Its claim to validity rests upon the fact that if typical data for magnetron starting, TR-cavity Q, and spike duration are used, the calculated value of spike energy W_s agrees with experiment and also upon the fact that it predicts the *independence* of W_s upon V_0 and $\Delta\omega$, which is consistent with experiment. The two assumptions involved concern the starting of the magnetron and the instantaneous breakdown of the gap.

5·6. Nonlinear Theory of the Spike.—If a cloud of electrons in a gas subject to an accelerating field is considered, the rate of increase of electrons may be written as

$$\frac{dn}{dt} = np\frac{S}{L}, \tag{28}$$

where n is the electron density, S is the average electron speed, L the mean free path, and p is the probability of ionization per collision. This may be written

$$\frac{1}{n}\frac{dn}{dt} = f(V), \tag{29}$$

where V is the voltage across the gap. It will be shown in Sec. 5·13 that the r-f admittance of a cloud of electrons is proportional to n, and therefore,

$$\frac{1}{g_e}\frac{dg_e}{dt} = \phi(V), \tag{30}$$

where the electronic admittance is assumed to be a pure conductance g_e. The equivalent circuit is shown schematically in Fig. 5·9*a*. The solution of the nonlinear differential equation of this circuit for V is a tedious task. Numerical solutions have been carried out by T. Holstein of the Westinghouse Research Laboratory but reports of this work have not yet been published.

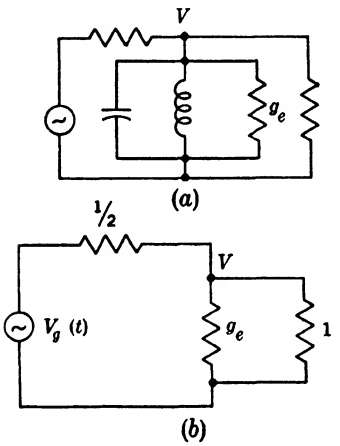

FIG. 5·9.— Circuit for analysis of spike energy.

First, let us consider the circuit of Fig. 5·9*b*. This circuit represents a nonresonant (or very-low-Q) TR tube such as a pre-TR or bandpass tube. In this circuit the voltage across the gap is given by

$$V = \frac{\frac{1}{2}}{\frac{3}{2} + g_e} V_g(t). \tag{31}$$

For simplicity, let it be assumed that $\phi(V)$ in Eq. (30) is a linear function kV. That is, the probability of ionization increases linearly with the applied voltage. Now, if Eqs. (30) and (31) are combined,

$$kV = \frac{1}{g_e}\frac{dg_e}{dt} = \frac{k}{3 + 2g_e} V_g(t). \tag{32}$$

Integration of Eq. (32) gives

$$(g_e - g_0) + \frac{3}{2}\ln\frac{g_e}{g_0} = \frac{k}{2}\int_0^t V_g(t)\,dt, \tag{33}$$

where g_0 is the electronic conductance corresponding to n_0, the initial electron density in the gap, furnished by the keep-alive discharge. Since the circuit is assumed to be nonresonant, the periodic generator voltage $V_g(t)$ may be replaced by its envelope $V_0(\epsilon^{\alpha t} - 1)$, where V_0 and α are the quantities defined in Sec. 5·5. The numerical solutions of these equations are presented in Fig. 5·10, where all the constants have been normalized. These results indicate that the spike energy is relatively insensitive to n_0 (or g_0), in view of the fact that a range of 100/1 in g_0 is represented by the extreme curves. The area under the *squares* of

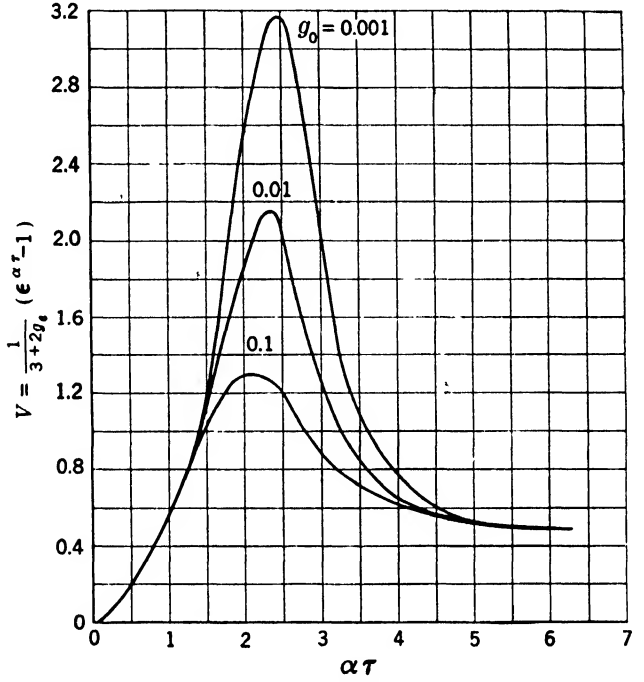

FIG. 5·10.—Calculated spike transient of low-Q TR tube.

these curves is proportional to the energy delivered to the load. For the three values of g_0 assumed, the energies lie in the ratio 1, 1.4, and 2.6 for $g_0 = 0.1$, 0.01 and 0.001 respectively.

Similar results have been obtained by Holstein for the high-Q case. It is interesting to note that this theory predicts the existence of a "pseudo-flat." This is the flat portion after the initial spike transient; it is at a considerably higher level than the arc leakage power of the steady-state discharge. The pseudo-flat lasts until the transmitter power has reached its peak and leveled off, at which time the steady-state discharge is established. Until recently it was impossible to prove or to disprove the existence of the pseudo-flat. Figure 5·11 is a retouched

oscillogram of the leakage power through a 1B38 pre-TR tube. This oscillogram was taken by C. W. Zabel of the Radiation Laboratory on

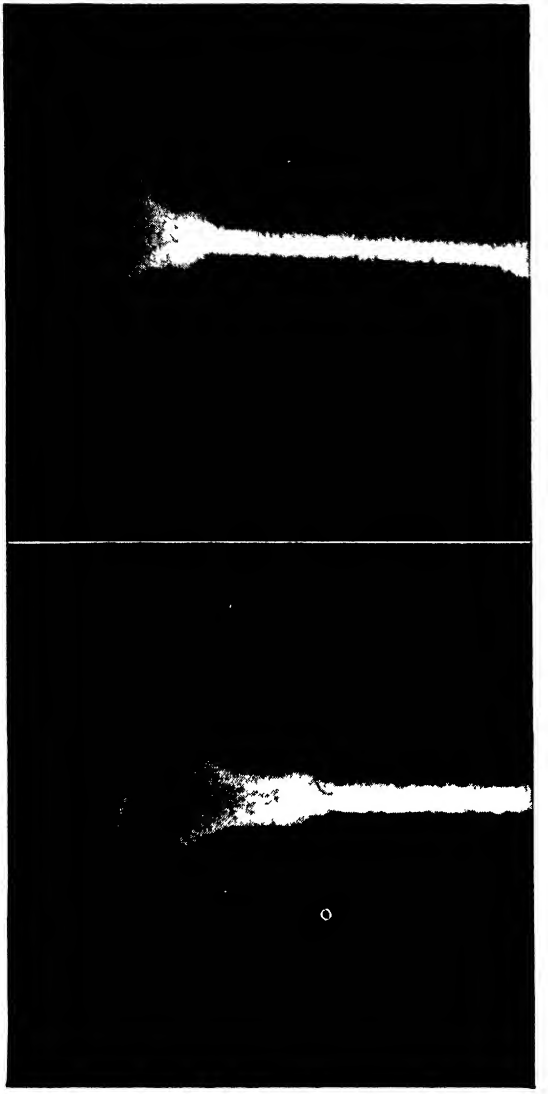

FIG. 5·11.—Oscillogram of spike from 1B38 pre-TR tube.

the high-speed oscillograph at the Massachusetts Institute of Technology Insulation Laboratory. The picture shows quite clearly the spike, pseudo-flat, and the transition to the true flat. The deflection sensitivity

of this oscillograph is very low and therefore it is impossible, unfortunately, to record the breakdown transient in a high-Q TR tube, where the spike leakage energy is about 10^{-4} that in the 1B38 pre-TR tube.

The calculated curves of Fig. 5·10 show a comparatively slow drop in voltage after the peak of the spike. This is in strong contrast with the assumption made in Sec. 5·5 that the breakdown is instantaneous. This same contrast is furnished by the oscillogram shown in Fig. 5·11 where the breakdown time is as long as the buildup time or longer. The numerical calculations for the high-Q circuit made by Holstein show the relatively short breakdown time assumed in Sec. 5·5 Thus, there appears to be a difference between the spikes in low- and high-Q TR tubes. This is probably best explained if, in Eq. (22), it is noted that the voltage V is independent of the load conductance G in the time interval under consideration. This is equivalent to saying that the surge admittance of the cavity is very large compared with Y_0. Since g_0 is about $0.01Y_0$, g_e/g_0 must reach very much larger values than are required in the nonresonant TR tube in order to produce a given reduction in voltage. Since n, or g_e, grows exponentially, when the voltage is reduced by electronic loading, it falls very rapidly, and gives a sharp breakdown characteristic.

One of the larger voids in the understanding of TR phenomena concerns the relationship between spike leakage energy and the Q of the TR cavity. Quantitative experiments to determine this relationship have been few, and the results are conflicting. It is known, however, that although W_s is relatively independent of the input coupling (Q_{in}), it is a strong function of the output coupling (Q_{out}). These relationships hold for a given TR tube in the region $100 < Q_{L2} < 400$.

The jump from high-Q TR tubes to bandpass tubes, however, where $Q_{L2} \approx 5$ is difficult to understand, since W_s in the bandpass tubes is about 0.1 erg as compared with 0.03 erg in the high-Q tubes. Moreover, where 0.1 to 0.3 erg of spike leakage energy from a high-Q tube damages many crystals, the same total energy from a bandpass tube, if allowed to fall upon a crystal for hundreds of hours, does not damage it. The difference is believed to result from the difference in shape of the spike in the two tubes. In a high-Q tube, the energy is confined to a time interval short compared with the thermal time constant of the crystal. In the bandpass tube, the slower breakdown, it is believed, causes the spike energy to be distributed over a longer time interval. If this time is longer than the crystal time constant, then burnout is caused by a combination of ballistic heating and steady-state heating. Estimated time constants are of the order of 10^{-8} sec, whereas the duration of the spike is about 5×10^{-9} sec for the high-Q tubes, and 10^{-8} sec for the bandpass tubes. Thus, the bandpass tube is just in the borderline

region, and the explanation given above is at least plausible. Further experiments and continued study of these phenomena should not prove too difficult and should yield interesting results.

5·7. Effect of n_0 upon Spike Leakage Energy.—The curves of Fig. 5·10 indicate the dependence of W_s upon n_0, the number of electrons initially in the TR-tube gap. It has been observed from experiment that the spike leakage energy varies inversely with n_0; however, no quantitative data which give the exact relationship exist.

The nature of the TR tube is responsible for this gap in the basic understanding of the breakdown. The initial, or priming, electrons are furnished by the d-c keep-alive discharge. The density n_0 of these electrons can be controlled by varying the discharge current, or by changing the position of the discharge relative to the gap, but neither of these parameters bears a simple relation to n_0. Furthermore, in normal engineering practice, it is usual so to arrange the keep-alive electrode that with a normal current ($\approx$ 100 μa) the keep-alive interaction, the reduction in low-level transmission due to g_0, is about .1 per cent. The rest of the tube—gas, shape, and coupling—is then adjusted to make the spike leakage energy low enough for safety. Thus, the desired results are measured directly rather than by means of the rather academic quantity n_0.

However, it would be of value to have experimental results of the effect of n_0 on W_s. In principle, at least, n_0 can be measured directly by means of d-c probes in the gap. In cell TR tubes, it is possible to measure the current collected on the cone across the gap from the keep-alive, when it is at a small positive potential. Thus, a calibration of n_0 against keep-alive current can be obtained, and can then be used to interpret a curve of W_s as a function of keep-alive current.

The interaction of n_0 upon the low-level transmission may be measured. A cloud of electrons in a gas may be represented (see Sec. 5·13) by an admittance $Y_0 = g_0 + jb_0$ referred to the input terminals of the TR cavity, the cavity losses may be represented by g_c', and the generator and load conductances by unity. The relative transmission of power to the load in such a circuit is

$$T_e = \frac{1}{\left(1 + \frac{g_c'}{2} + \frac{g_0}{2}\right)^2 + \left(\frac{b_0}{2}\right)^2}. \tag{34}$$

Measurements on a special tube indicate that the electronic admittance is mainly real ($g_0 > b_0$).[1] Then, if b_0 is neglected, the solution for g_0 is

[1] Ting-Sui Kê and L. D. Smullin, "A Low Power X-Band R-f Gas Switch," RL Report No. 841, Oct. 19, 1945.

$$g_0 = \frac{1}{\sqrt{T_e}} - \frac{1}{\sqrt{T}}, \tag{35}$$

where

$$T = \left(1 + \frac{g_c'}{2}\right)^{-2}.$$

Since $g_0 \propto n_0$,

$$n_0 \propto g_0 = \frac{1}{\sqrt{T}}\left(\frac{1-a}{a}\right), \tag{36}$$

where $a = \sqrt{T_e/T}$. Thus, Eq. (36) is a means of determining the relative values of n_0 in a given TR tube for various conditions of the keep-alive circuit.

Figure 5·12 shows the spike leakage energy through a 724A TR tube, operated without a keep-alive discharge, as a function of transmitter repetition rate. In this experiment the electrons in the gap at the start of a pulse were those left over from the previous r-f discharge. Thus the higher the repetition rate (shorter time between pulses), the greater is n_0, and the smaller is W_s. An experiment of this type, coupled with the recovery-time analysis discussed in Sec. 5·13, might give some interesting quantitative results regarding n_0.

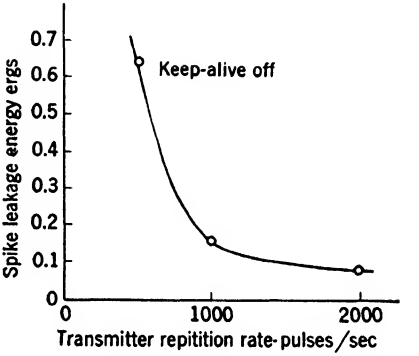

FIG. 5·12.—Effect of transmitter repetition rate on spike leakage energy for a 724A tube at a line power of 20 kw.

5·8. Effect of Gas Filling upon Spike Energy.—In the preceding sections an attempt was made to present a more or less rational explanation of the gross aspects of the spike, and of the process of breakdown. No attempt, however, was made to explain the detailed process of ionization. This involves accurate knowledge of the excitation and ionization levels and cross sections of the particular gas under consideration, and a means of calculating the actual electron energy distribution function at every instant during the breakdown process. This has not yet been done and is certainly beyond the scope of this book.

From the engineering point of view, however, what is desired is a knowledge of the effect of pressure and of the particular gas or mixture of gases upon W_s. These data have been obtained from measurements upon particular TR tubes. Because the work at the time was urgent, emphasis was always placed upon the development of a particular tube. As a result, complete sets of measurements on a particular tube, using different gases and pressures, are almost nonexistent. No attempt has

been made to correlate the optimum pressure (minimum W_s) with gap spacing and frequency. It is doubtful whether the data now available would be amenable to such analysis.

The variation of W_s with the kind of gas used seems to be consistent for tubes of different types and of different frequency bands. The TR tubes have been filled with mixtures of either H_2 and H_2O or A and H_2O. The water vapor is used to ensure short recovery time, while the hydrogen or argon is used to ensure adequate crystal protection at sub-zero temperatures and also to increase tube life.

Figure 5·13 is a plot of the spike leakage energy W_s through a 1B27 TR tube operating at 9.1 cm with $Q_{L2} = 300$. The data were obtained

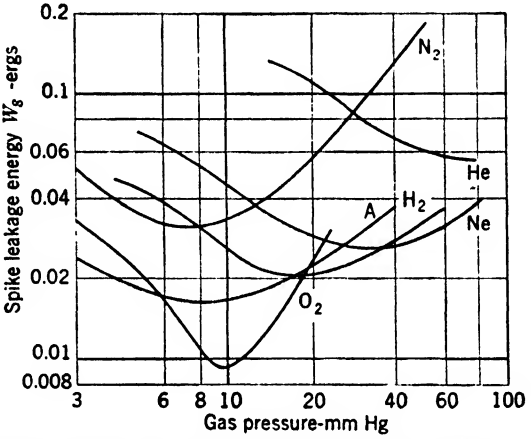

FIG. 5·13.—Spike leakage energy W_s through a 1B27 TR tube for various gases.

by measuring the leakage power through the TR tube at two pulse widths and assuming that the arc leakage power was flat and independent of pulse length. No attempt was made to view the leakage pulse on an oscilloscope during these experiments. These precautionary statements are made principally because of the curve for O_2. The other gases behaved as expected; but the very low spike energy obtained with oxygen was somewhat startling. Because these particular tests were made at the end of 1945, there has been no opportunity to check them. It might be concluded that monatomic gases would ionize more easily than diatomic gases, since diatomic gases can absorb electron energy in molecular vibration thus reducing the probability and the rate of ionization. The curves of Fig. 5·13 do not support this conclusion. On the other hand, Fig. 5·14 represents data taken on a 1B26 TR tube at 1.25 cm in which the minimum spike energy for argon is about one-eighth that for hydrogen. In this case W_s was measured by canceling the flat leakage power with power through a linear attenuator which did not pass through

the TR tube. Measurements on the 3-cm bandpass TR tube[1] give the same relative spike leakage energies for the noble gases, argon, neon, and helium as those shown in Fig. 5·13.

Many measurements of spike leakage energy which are not presented here had to be omitted because of the questionable purity of the gases used. The effect of impurities is apparently most serious in the case of the noble gases.[2] Ordinary TR tubes do not easily lend themselves to

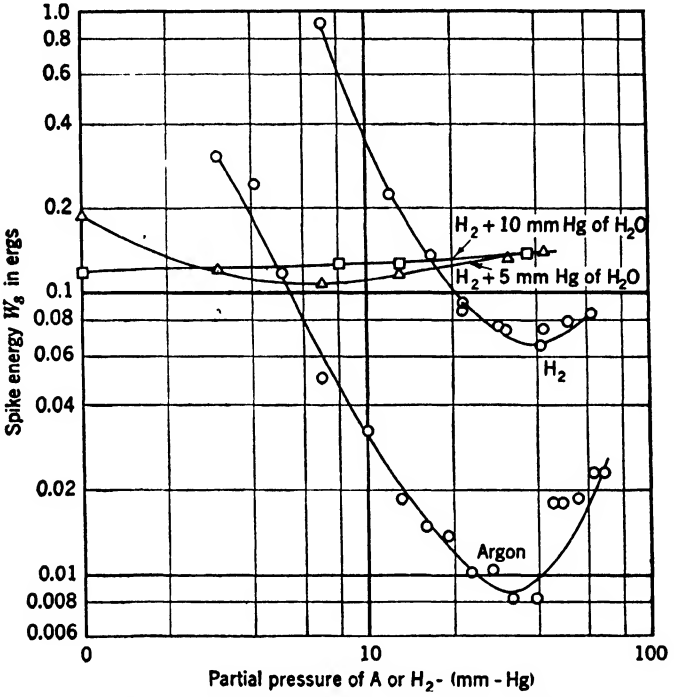

FIG. 5·14.—Spike-pressure characteristic for a 1B26 TR tube at 1.25 cm.

high-temperature outgassing because of soft-soldered joints, or comparatively weak copper-glass butt seals. Thus, these data must be treated as representative of leakage energies that can be expected from commerical tubes rather than as an indication of the intrinsic properties of the particular pure gas.

Figures 5·14 and 5·15 show the effect of the addition of water vapor to an H_2-filled TR tube upon W_s. In both the 1.25-cm and the 10-cm tubes, the use of H_2O makes the spike energy surprisingly independent

[1] M. D. Fiske, "Final Technical Report on OSRD Contract OEMsr-1306," GE Research Laboratory, Nov. 7, 1945.

[2] Loeb, "Fundamental Processes of Electrical Discharges in Gases," Wiley, New York, 1939, Chap. 2.

of the partial pressure of H_2 or H_2O. Thus, the choice of the proper gas filling must be dictated by considerations other than spike leakage energy. These factors, arc power, recovery time, and life, will be discussed in succeeding sections.

Although Fig. 5·14 indicates that the use of pure argon results in exceptionally low values of W_s, this is of little importance in a TR tube designed for radar use because of the extremely long recovery time of such

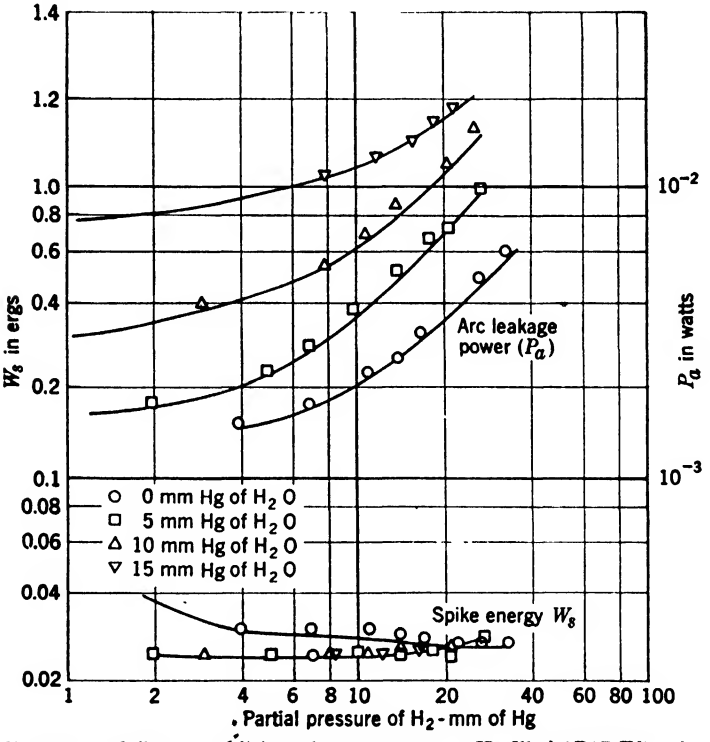

FIG. 5·15.—Effect of addition of water vapor to H_2-filled 1B27 TR tube.

a tube. The addition of sufficient water vapor to ensure short recovery time and reasonably long tube life, makes the A and H_2O spike energy about the same as that for the H_2 and H_2O mixture.

Effect of Gap Length upon W_s.—In the TR tube, spike leakage energy increases with increasing gap length, if other factors (except tuning) remain constant. Figure 5·16 shows the characteristics of the 1B24 (3-cm) and 1B27(10-cm) TR tubes; W_s is plotted against revolutions of the tuning screw, which produce a linear motion of the cone. These data were obtained with the exciting power coming from a fixed-frequency magnetron and, therefore, the TR cavity was detuned from the magnetron by about ± 6 per cent at the extremes of the tuning range. Other

tests in which the magnetron frequency was varied over a comparable range while the TR cavity was kept tuned to a constant frequency showed variations of W_s of 1 db or less. The curves of Fig. 5·16 obviously obey different laws. How much of this results from differences in frequency and how much from electrode shape is not known.

Some indications of a minimum spacing, below which W_s starts to rise again, have been found. This occurs in the 1B27 at a spacing of about 0.005 in. No quantitative data of this part of the curve exist, and no data exist for other frequencies. Accurate measurements of this minimum as a function of frequency and pressure should prove valuable in affording a clearer insight into the fundamental processes. It is believed that this minimum has the same significance as that of the Paschen curve for low frequencies. When the gap becomes short enough, a large fraction of the electrons in the gap may be lost to the electrodes before they can contribute to the further ionization of the gas.

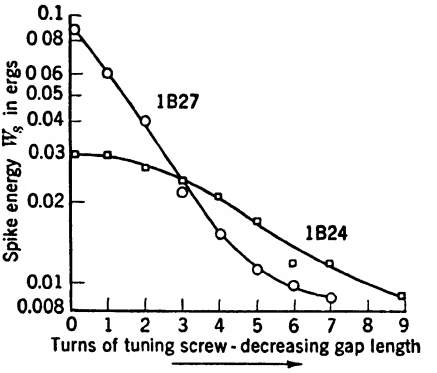

FIG. 5·16.—Variation of spike leakage energy with gap length in 1B27 and 1B24 TR tubes.

5·9. Arc Leakage Power.—The arc leakage power is the power dissipated in the receiver load and results from the steady-state voltage drop across the high-frequency discharge in the TR tube. In the normal pressure and current range encountered in TR tubes, the voltage drop across the discharge is very nearly independent of the current carried by it, and for most cases the discharge can be treated as a zero-impedance, constant-voltage source.

Some of the similarities between the high-frequency discharge and the positive column of the d-c discharge have been indicated earlier in this chapter. In this and the following sections, the self-sustaining r-f discharge in TR tubes will be discussed, in which the quantities of interest are the *arc leakage power* and the *arc loss*, the power dissipated in the discharge. Some of the independent variables that affect the discharge are:

1. Gas content.
2. Transmitter power level.
3. External circuit (cavity couplings, etc.).
4. Gap shape.

The only quantities which can be measured conveniently are the arc

leakage power, arc loss, and the transformed discharge impedance. No measurements have been made of the electron density or of temperature in the discharge, although estimates of the former have been made. It should be possible to measure the electron temperature by means of probes similar to those used in the study of d-c discharges.[1]

Before presenting the experimental data, or discussing some of the theoretical aspects of this problem, let us see how the measured leakage power varies with the design of the TR cavity. Figure 5·17*a* is a schematic diagram of a TR tube connected in series with a transmission line which is energized by a matched generator and terminated in a matched load. The TR cavity is loaded by an arbitrary, real conductance $G/Y_0 = g$. The equivalent lumped-constant circuit is shown in Fig. 5·17*b*, where the reference plane has been chosen at the center of the

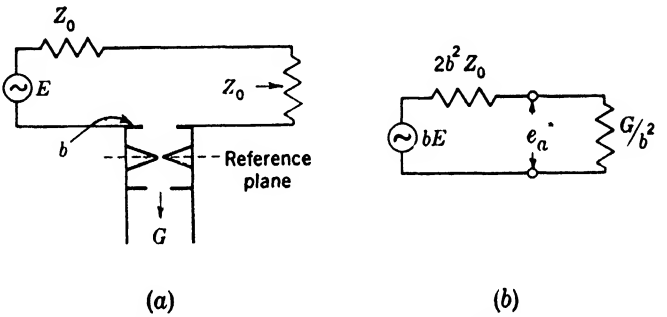

FIG. 5·17.—Equivalent circuit for arc leakage power.

TR tube. The equivalent generator seen at the center of the TR tube is obtained by the use of Thévenin's theorem. The internal impedance is $2b^2Z_0$ and the open-circuit voltage is bE, where $B/Y_0 = b$ is the susceptance of the TR-cavity coupling irises. If $b = 10$, then the generator impedance seen from the gap is $200Z_0$. If a line power of 1-kw peaks, and a 50-ohm coaxial transmission line are assumed, then $E = 1400$ volts rms, and the transformed generator voltage $bE = 14{,}000$ volts. Measurements made on the 721A TR tube indicate that the voltage drop across the discharge, e_a, is about 100 volts[2] when an H_2-H_2O gas filling is used, and is 200 to 300 volts in the argon-filled 10-cm pre-TR tubes. This large ratio between e_a and bE allows the discharge to be treated as if it were energized from a *constant-current source.* The magnitude of the discharge current depends upon the transmitter power, upon the amplitude and phase of standing waves in the main transmission line, and upon the coupling to the TR cavity.

[1] Cobine, *Gaseous Conductors*, McGraw-Hill, New York, 1941, Chap. 6.

[2] Bethe, Marshak, Schwinger, "Theoretical Results on the TR-Box," NDRC Report D1-116, Jan. 20, 1943.

It is an experimental fact that within the accuracy of the experiments, the arc leakage power of a TR tube into a given load is independent of transmitter power over a range of several thousand to one. This means that the arc voltage remains constant while the current is varied by a factor of fifty or more, and allows the discharge to be treated as if it had a zero dynamic impedance and constant voltage drop.

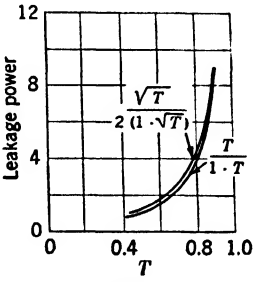

FIG. 5·18.—Variation of arc leakage power with transmission through the TR switch.

The power delivered by a constant-voltage generator to a load is $P = E^2g$, where g is the conductance of the load. The load susceptance has no effect upon the total power absorbed by the load. Measurements of arc leakage power as a function of load admittance give contours of constant power which fall upon lines of constant conductance on transmission-line charts, and which show little or no dependence on the susceptance. The receiver conductance seen by the discharge is g/b_2^2, and therefore, the leakage power is

$$P_a = e_a^2 \frac{g}{b_2^2}. \tag{37}$$

The external Q of the output circuit is

$$Q_{\text{out}} = K \frac{b_2^2}{g},$$

and therefore

$$P_a \approx \frac{e_a^2}{Q_{\text{out}}}. \tag{38}$$

For convenience in calculating, this simple relationship may be expressed in terms of some other parameters.[1]

1. For a cavity coupled for matched input conductance,

$$1 - b_1^2 g_c = \left(\frac{b_1}{b_2}\right)^2 g,$$

$$P_a = e_a^2 g_c \frac{T}{1-T}. \tag{39}$$

2. For equal input and output coupling ($1/b_1^2 = g/b_2^2$),

$$P_a = \frac{e_a^2 g_c}{2} \frac{\sqrt{T}}{1-\sqrt{T}}, \tag{40}$$

where T is the signal transmission ratio, the ratio of transmitted power to the available power, and g_c is the cavity conductance. Figure 5·18 is a

[1] Samuel, McCrea, and Mumford, "The Gas Discharge TR Switch," BTL MM-42-140-26, April 17, 1942.

plot of P_a for these two cases as a function of T. Note that P_a is directly proportional to the cavity conductance g_c, and therefore, for a given insertion loss, the arc leakage power varies inversely with the unloaded Q of the cavity.

The power dissipated in the discharge may be calculated in a similar manner.[1] The current in the discharge is

$$i_a = \frac{\sqrt{P_l Y_0}}{b}, \tag{41}$$

and the power is

$$P_g = i_a e_a = e_a \frac{\sqrt{P_l Y_0}}{b}. \tag{42}$$

As before, the power dissipated in the gap may be rewritten for two special cases.

1. Matched input coupling,

$$P_g = e_a \sqrt{\frac{P_l g_c}{T - 1}} = \sqrt{\frac{P_l P_a}{T}} \tag{43}$$

2. Equal couplings,

$$P_g = \sqrt{P_l P_a}. \tag{44}$$

Thus, the dissipated power is proportional to the geometric mean of the line power P_l, and of the arc leakage power P_a.

These relations indicate that in order to describe the leakage power of a TR tube, either the output coupling, or the cavity transmission, shunt conductance, and ratio of input to output coupling corresponding to any given value of P_a, must be specified.

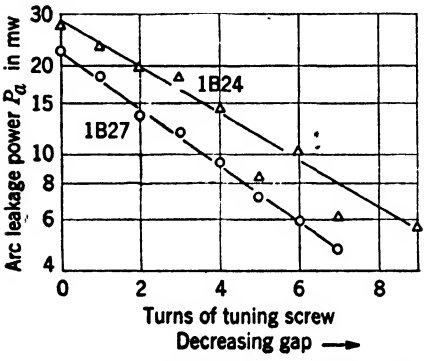

FIG. 5·19.—Variation of arc leakage power with gap length.

Detuning the TR cavity from the transmitter frequency by means of tuning plugs in the TR cavity (or detuning the transmitter) has practically no effect upon the arc leakage power. Once the gap has broken down, the conductance of the discharge is very large compared with the susceptance introduced by the detuning of the cavity. Detuning the TR cavity by varying the gap spacing has a marked effect upon P_a. Figure 5·19 shows the variation of P_a with gap spacing (adjust-

[1] *Ibid.*

ment of the tuning screw) in the 1B24 and 1B27 TR tubes. These data were taken at the same time as those of Fig. 5·16 on the respective tubes. These curves have the form $P_a = Ce^{kl}$, where C and k are constants and l is the gap length. On a linear plot of P_a, the data might be fitted by a square-law curve, $P_a = Al^2$, where A is a constant. A simple picture of the discharge postulates a constant *gradient*, the voltage drop varies linearly with spacing, and the leakage power therefore varies with the square of the spacing. As an engineering approximation, it is probably safe to assume that the arc leakage power is proportional to the square of the gap length.

5·10. Dependence of Arc Leakage Power upon Transmitting Power.—The arc voltage e_a is independent of the discharge current in radar equipments operating under normal conditions. At line powers just above the minimum breakdown level, the discharge exhibits a decided negative characteristic. Figure 5·20 illustrates the linear variation of leakage

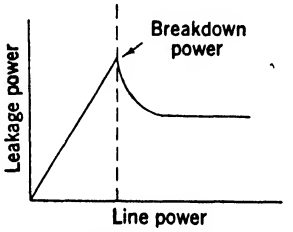

FIG. 5·20.—Leakage power at very low levels as a function of line power.

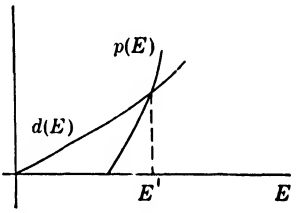

FIG. 5·21.—Production and destruction of electrons as a function of field strength.

power with line power up to the point of breakdown, beyond which it falls off with increasing power and finally reaches a constant level. A theory to explain this behavior has been advanced by Margenau.[1]

Let us consider the following differential equation, which is simply a statement of equilibrium,

$$\frac{dn}{dt} = p(E)n - d(E)n = 0, \tag{45}$$

where n is the number of electrons per cubic centimeter in the discharge, and $p(E)$ and $d(E)$ are the voltage-dependent rates of production and destruction (diffusion) of electrons. This equation has only one equilibrium voltage E_1' at which $p(E) = d(E)$, Fig. 5·21. The number of electrons n does not affect the result, and consequently, if this equation described an r-f discharge, its voltage would be a constant, independent of current density. However, a correct theory should predict the experimental curve of Fig. 5·20.

[1] H. Margenau, "Theory of Alternating Current Discharges in Gases," RL Report No. 967, Jan. 10, 1946.

Equation (45) may be modified by adding to it a constant term c. Then, at equilibrium,

$$\frac{dn}{dt} = [p(E) - d(E)]n - c = 0, \tag{46}$$

and

$$n = \frac{c}{p(E) - d(E)}. \tag{47}$$

Figure 5·22 is a plot of Eq. (47). The left portion $n(E)$ is negative and has no physical significance; however, the right portion, if replotted with the axis suitably rotated, gives a curve of the same form as Fig. 5·20.

This constant c is physically significant for it implies a mechanism for the destruction of electrons at a rate independent of n. It can be shown that the capture of electrons by neutral atoms or molecules to form negative ions obeys such a law. Some gases such as the noble gases, hydrogen, and nitrogen, have zero electron-capture cross section; others, however, like oxygen, the halogens, and water vapor, have comparatively large electron-capture cross sections. Let us consider a TR tube which has an atmosphere, part of which has a finite electron-capture cross section. The analysis will use the following symbols:

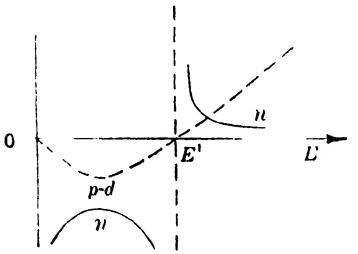

FIG. 5·22.—Stability conditions for a steady-state discharge.

n = electron density.
Y = number of neutral captors.
Y' = number of negative ions.
$M = Y + Y'$.
Q = collision cross section of electrons and gas molecules.
h_{cap} = probability of electron capture per collision.
h_{rel} = probability of electron release per collision.
v = electron velocity.
$C = Qvh_{cap}$ = probability of electron capture per sec.
$R = Qvh_{rel}$ = probability of electron release per sec.

Then,

$$\frac{dY'}{dt} = Cn(M - Y') - RnY'. \tag{48}$$

Since only the steady-state discharge is considered, n may be assumed constant. Then by solving for Y', the following equation is obtained,

$$Y' = \frac{CM}{R + C}[1 - e^{-(R+C)nt}]. \tag{49}$$

In the discharge, the electron temperature is high, probably about 10 electron volts, and the probability of release is much greater than that of capture, $R \gg C$. Then at $t = \infty$,

$$Y' = \frac{C}{R} M = \frac{h_{cap}}{h_{rel}} M. \tag{50}$$

Thus for a given concentration M of captor molecules, the number of negative ions formed is a function only of the ratio of the probability of electron capture to that of release when the electron energy is high. There will be a continual diffusion of Y' out of the discharge to the walls or to the electrodes. This rate will be independent of n and independent of E. Therefore, once steady-state conditions have been reached, electrons will be captured at a rate just rapid enough to make up for the number of negative ions lost by diffusion, and thus a physical process corresponding to the constant c of Eq. (46) results.

If this theory is correct, it would be expected that a TR tube filled with gas such as argon would not have a negative slope in the leakage-power characteristic, whereas a tube containing H_2O would be expected to have a large negative slope. Before determining whether this conclusion is justified by experimental data, the actual measurements involved should be considered. The measurable quantities are arc leakage power, which is proportional to e_a^2, input admittance of the fired cavity, incident power, and power dissipated in the discharge. The easiest combination to measure is incident power as a function of arc leakage power, as in Fig. 5·20. Although this curve contains all of the information which is needed from the viewpoint of practical duplexer design, it really tells very little about the discharge itself. This is because the abscissa, or line power, is an unknown function of the actual discharge current.

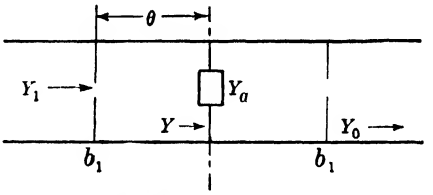

FIG. 5·23.—Diagram to illustrate admittance relations in a cavity.

Consider the circuit of Fig. 5·23. The cavity is loaded at its center by the discharge admittance Y_a. With $Y_a = 0$, the cavity is presumed to be resonant and the admittance at the center is $Y_a + (Y_0/b_1^2) = Y$. The input admittance is

$$\frac{Y_1}{Y_0} = jb_1 + \frac{Y - jb_1}{1 - jYb_1}. \tag{51}$$

If this equation is separated into its real and its imaginary parts, and if $b_1^2 \gg 1$ is assumed,

$$\frac{Y_1}{Y_0} = \frac{gb_1^2}{(1 + bb_1)^2 + g^2b_1^2} + j\left[b_1 + \frac{(b^2 - bb_1 + g^2 - 1)b_1}{(1 + bb_1)^2 + g^2b_1^2}\right]. \tag{52}$$

Examination of Eq. (52) indicates that when g_a and b_a are of the order of magnitude $1/b_1^2$, the input susceptance will be a strong function of Y_a. As the arc admittance increases, however, the input admittance approaches a limit,

$$\lim_{Y_a \to \infty} Y_1 = \frac{1}{g_a} + jb_1, \tag{53}$$

and it becomes difficult to make accurate measurements of the imaginary

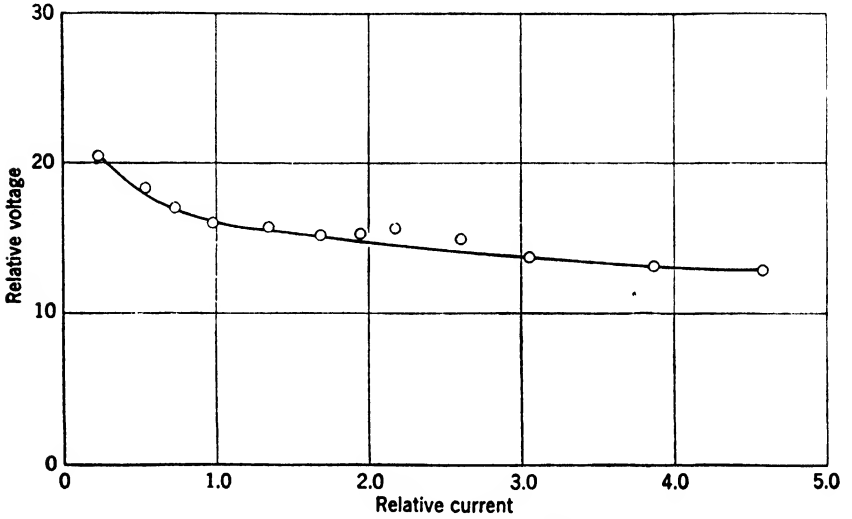

FIG. 5·24.—Relative r-f current and voltage of discharge at low levels.

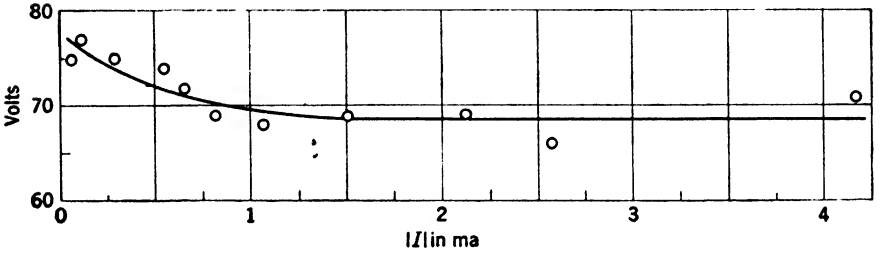

FIG. 5·25.—Magnitude of r-f current vs. voltage in helium.

component of Y_a, although the conductance will be directly proportional to the input standing-wave ratio.

$$r_1 = \frac{1 + |\Gamma|}{1 - |\Gamma|} \approx \frac{2b_1 + 1 + \dfrac{1}{g_a^2}}{\dfrac{2}{g_a}} \approx g_a b_1. \tag{54}$$

Thus a measurement of the *level* and the *standing-wave ratio* are sufficient to give numbers *proportional* to the voltage and current in the discharge.

If the shape of the cavity is accurately known, the *absolute* voltage and current in the discharge can be computed.

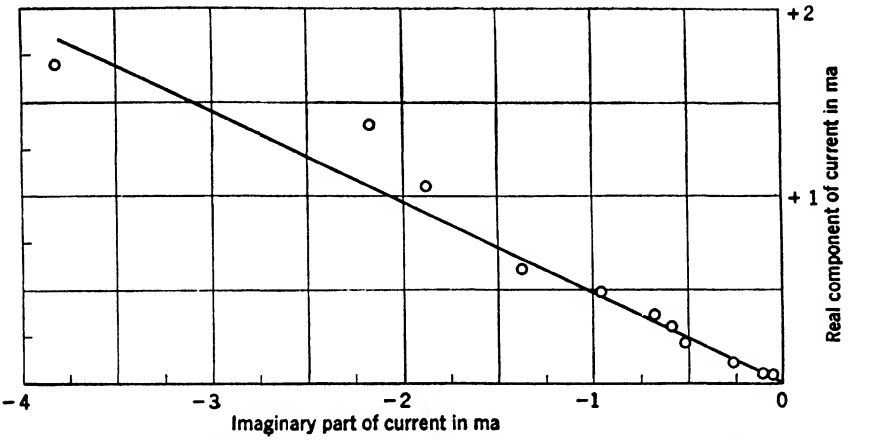

FIG. 5·26.—Real vs. imaginary parts of r-f current in helium discharge.

Figure 5·24 is a curve of the relative current vs. voltage in the discharge of a 1B24 TR tube filled with 15 mm Hg each of H_2 and H_2O. Figure 5·25 is a similar curve[1] measured in a special cavity filled with helium at 3.2 mm pressure and $\lambda = 9.8$ cm. By standing-wave measurements it was possible to find the phase angle of the current with respect to the voltage. Figure 5·26 shows the real part of the current plotted against the imaginary part.

Figure 5·27 is a similar plot for a number of different gas fillings in a 1B24 TR tube. The two figures do not necessarily agree since they were taken with different tubes, tuned to different frequencies.

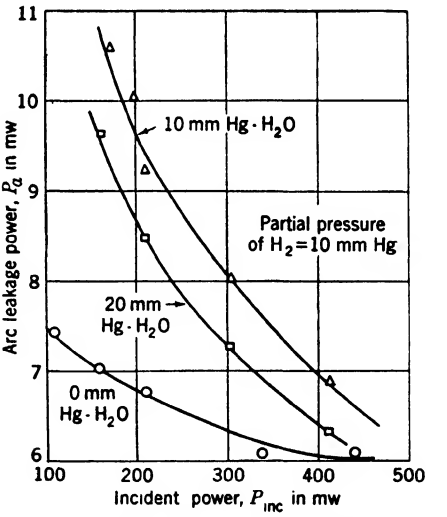

FIG. 5·27.—Leakage power as a function of incident power in a 1B24 tube with various fillings.

5·11. Effect of Gas Filling upon P_a.—As in the case of the spike, it is difficult to predict theoretically not only how gases will differ in arc leakage power, but also how they will vary with pressure. It has been seen, however, that the

[1] M. A. Herlin and S. C. Brown, *Bull. Amer. Phys. Soc.* **21**, 28 (1946).

order of the voltage drop for various gases in the r-f discharge is the same as that for the positive column in the d-c discharge.

The characteristics of a gas which affect the r-f voltage drop can be listed. First to be considered, referring to Eq. (45), are the rates of production and destruction of electrons as functions of gap voltage. Destruction can be limited to diffusion, since the recombination of an electron and a positive ion is an extremely improbable event. The diffusion is of the so-called ambipolar type which takes place at about twice the rate of diffusion of gas molecules. Thus, it would be expected that the lighter gases would diffuse more rapidly, and the sustaining voltage would be increased. The rate of production of electrons, or of ioniza-

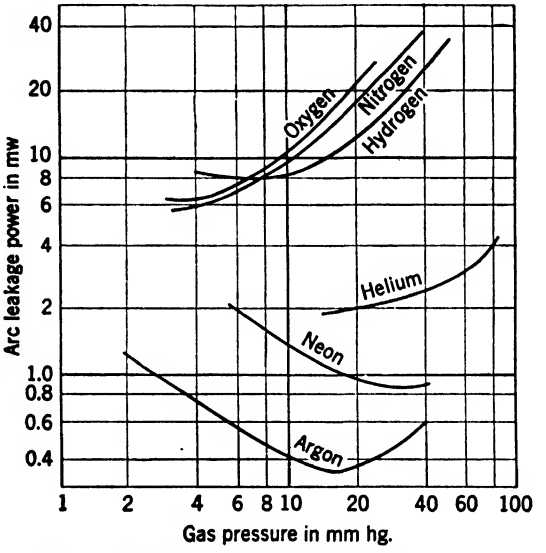

FIG. 5·28.—Arc leakage power from a 1B27 TR tube as a function of pressure.

tion, is determined in part by the ionization potential, the number of excitation levels below the ionization level, and the number of molecular resonances which can absorb electron energy without resulting in further ionization of the gas.

Figure 5·28 is a plot of the arc leakage power in a 1B27 TR tube as a function of the pressure of the various gases tested. These curves were obtained from the same experiment as those of Fig. 5·13, and the same comments apply. The noble gases lie well below the other gases. In these curves, the minimum value of P_a for argon is about 0.05 that for hydrogen. Other investigators report even lower values for argon. Extreme purity apparently results in the lowest values of P_a for argon. No reliable data exist for those mixtures of noble gases which give a very low breakdown voltage in d-c discharges.

Margenau, in a theoretical study of the r-f discharge,[1] has proposed a similarity principle for such discharges. On the assumption that the sources of ionization remain in play over the range considered, he derives an expression for the minimum of the voltage-pressure curve for a given gas, which states that at the minimum,

$$\left.\begin{aligned}\frac{\omega}{p} &= a\\ \frac{E}{p} &= b\end{aligned}\right\} \tag{55}$$

where a and b are constants, p is the gas pressure, and ω and E are the angular frequency and amplitude of the impressed field. This states that the pressure for minimum voltage drop, and the actual value of the minimum drop, are proportional to ω. Figure 5·29 illustrates this relationship. This theory has not been checked with data taken with a single tube of fixed shape. The experiment is not difficult, and it should prove valuable in extending the understanding of the r-f discharge.

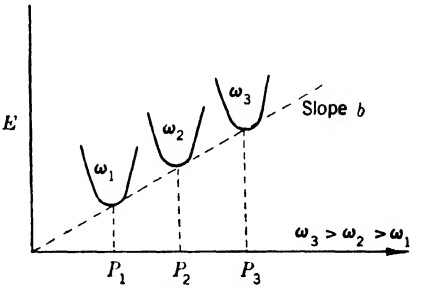

FIG. 5·29.—Diagram to illustrate similarity principle for r-f discharges.

5·12. The Recovery Period.—The recovery period is the time after the transmitter power has fallen to zero. During this time the gap in the TR tube deionizes, and the attenuation through the TR tube drops from the value of 60 or 70 db during the transmitting period to 1 or 2 db. In Sec. 5·2 a crude formulation of the admittance of a space-charge region was presented. If the electrons are in a vacuum they lose no energy by collision with heavy atoms, and the current represented by their motion is in quadrature with the applied field, and therefore the space-charge region appears as a pure admittance with a dielectric constant less than unity. If the electrons are not in a vacuum and therefore make collisions with atoms or molecules, some of the oscillatory energy the electrons obtain from the applied field is changed into thermal energy by the collisions, and cannot be returned to the external circuit. There is therefore a net input power to the discharge, and the gap admittance has a real component.

The electron energy in the r-f discharge is comparatively high, and it is much greater than that of the gas. Because of their random motion

[1] H. Margenau, "Theory of Alternating Current Discharges in Gases," RL Report No. 967, Jan. 10, 1946.

there is a constant diffusion of electrons out of the gap. The rate of this process is retarded by the positive ions in the discharge which exert a field opposing the rapid outward motion of the electrons. The net drift of electrons and positive ions is referred to as ambipolar diffusion, and takes place at a rate corresponding to twice the mobility of the ions. When the excitation is removed, the electron temperature is quickly reduced, by collisions, to the temperature of the gas. It reaches a value of twice the gas temperature in about 1 μsec. It will be shown that the diffusion process is much too slow to be relied upon for the recovery of TR tubes.

To make the recovery time sufficiently short, it is necessary to remove electrons by some other means. Electron recombination by means of a three-body collision has little probability, and therefore cannot cause a sufficiently rapid recovery. Capture of electrons by neutral atoms or molecules has a comparatively high probability. The use of a gas such as H_2O with a large electron-capture cross section gives tubes with a recovery time of only a few microseconds.

In the following sections the theory of the recovery period will be presented first. This will be followed by a discussion of the properties of various gases and a presentation of experimental data.

5·13. Theory of the Recovery Period.—The following analysis is due to Margenau.[1] In Sec. 5·12, three possible mechanisms for reducing the electron density in the discharge were mentioned: diffusion, recombination, and capture. These will be examined in this order.

Diffusion.—In order to calculate the rate of diffusion, it is necessary to know the electron and ion temperatures. During the discharge the electron temperature is very high, many thousand degrees. In the recovery period this energy is reduced by collisions with gas molecules. The rate at which this reduction takes place may be determined as follows. Let v be the average electron velocity, L the mean free path, T the electron temperature, and T_0 the gas temperature. Then the mean loss of energy by the electron per collision is

$$\Delta E = \frac{4m}{M} k(T - T_0). \tag{56}$$

The rate at which the mean energy decreases is

$$-\frac{d}{dt}\left(\frac{3}{2}kT\right) = k(T - T_0)\left(\frac{3kT}{m}\right)^{1/2}\frac{4m}{ML}. \tag{57}$$

[1] H. Margenau, "Theoretical Interpretation of the Recovery Time of TR Boxes," RL Report No. 929, Jan. 9, 1946.

The solution of this is

$$\frac{\sqrt{T} - \sqrt{T_0}}{\sqrt{T} + \sqrt{T_0}} = \frac{\sqrt{T_1} - \sqrt{T_0}}{\sqrt{T_1} + \sqrt{T_0}} e^{-g\sqrt{T_0}t} \tag{58}$$

where the subscripts 1 and 0 refer to initial and final conditions, and

$$g = \frac{8}{ML}\left(\frac{km}{3}\right)^{1/2}.$$

The time required for the average speed to drop to α times its final value is given by

$$t_a = -\frac{1}{g\sqrt{T_0}} \ln \frac{\alpha + 1}{\alpha - 1} \tag{59}$$

where $T_1 \gg T_0$.

For argon at a pressure of 10 mm Hg and $\alpha = 2$, the relaxation period is about 1.5 μsec. Thus, for times longer than 5 or 10 μsec, the electrons may be considered to be at the gas temperature T_0.

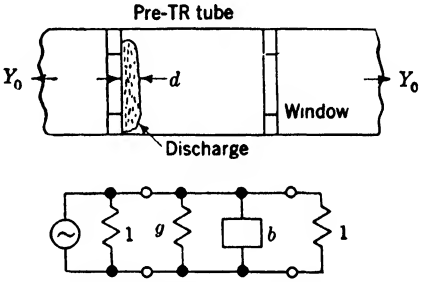

FIG. 5·30.—Discharge in pre-TR tube and equivalent circuit.

The calculation of the rate of diffusion of electrons out of the gap of a high-Q TR tube involves some very difficult computations, and has not been carried out. However, as a pertinent example, let us consider the recovery of a pre-TR tube, where the discharge is assumed to be in the form of a thin slab of thickness d adjacent to, and covering, the low-Q input window, Fig. 5·30.

The diffusion equation is

$$\nabla^2 n - \frac{1}{D}\frac{\partial n}{\partial t} = 0, \tag{60}$$

where n is the electron density and D is the mobility or coefficient of diffusion. For the shape under consideration, if the electron density n_0 is uniform at the end of the transmitter pulse,

$$n = n_0 \left\{ \phi\left(\frac{x}{2\sqrt{Dt}}\right) - \frac{1}{2}\left[\phi\left(\frac{d+x}{2\sqrt{Dt}}\right) - \phi\left(\frac{d-x}{2\sqrt{Dt}}\right)\right]\right\}, \tag{61}$$

where

$$\phi(u) = \frac{2}{\sqrt{\pi}} \int_0^u e^{-x^2}\, dx.$$

In Eq. (61) the assumption is made that the diffusion takes place only to the input window, and that since d is small, the loss of electrons from

the edges of the discharge is negligible. The diffusion coefficient D is not that predicted by kinetic theory for a cloud of electrons. The diffusion that takes place is called ambipolar.[1] It takes place at a reduced rate because the massive, slow-moving positive ions act as a brake on the electrons. Thus, as soon as a few electrons have left the discharge, a positive space charge is set up that inhibits the loss of any more electrons until an equal number of positive ions have diffused out of the discharge. The net rate is about twice that of the gas molecules alone. In the 1B38 pre-TR tube filled with 10 mm Hg of argon, the ambipolar diffusion coefficient is about 5 cm²/sec, and if the thickness of the discharge d is 1 mm, the recovery time would be several thousand microseconds. Since it is necessary to have recovery times of the order of 1 to 10 μsec, diffusion alone can contribute very little.

A calculation of the effect of the recombination of electrons and positive ions on recovery time indicates that about 1 sec would be required to deionize the gap sufficiently. Since diffusion and recombination as mechanisms for obtaining short recovery times have been discussed, let us next consider the capture of electrons by neutral atoms.

In the calculation of the effect of capture upon arc leakage power (Sec. 5·10), the electron density n was considered constant. In the recovery period there is no production of electrons and the *constant term is the total negative charge*,

$$N = \text{const} = n + Y'.$$

As before,

$$M = \text{const} = Y + Y_0'.$$

The rate of change of electron density is

$$\frac{dn}{dt} = vQ\,\{(h_{cap} + h_{rel})n^2 + [Mh_{cap} - N(h_{cap} + h_{rel})]\,n\}. \tag{62}$$

In the recovery period, after the first microsecond, the electron energy is low and $h_{rel} \approx 0$. During the first few microseconds, the electrons are losing energy rapidly and neither h_{cap} nor h_{rel} are constants, and the solution of Eq. (62) becomes extremely difficult. Later, however,

$$\frac{dn}{dt} = -vQh_{cap}\,(M - N)n \approx -vQh_{cap}Mn, \tag{63}$$

where the initial number of neutral atoms $Y_0 \approx M \gg n_0$.

This is an expression for the rate of change of electron density. Let us now see how this causes the attenuation through the TR tube to vary with time. The transmission through an attenuating medium between

[1] Cobine, *Gaseous Conductors*, McGraw-Hill, New York, 1941.

two uniform, nondissipative media may be written[1] as

$$\frac{E_o}{E_i} = \frac{\cos \gamma_1 d + j \sin \gamma_1 d}{\cos \gamma_2 d - \frac{j}{2}\left(\frac{Z_1}{Z_2} + \frac{Z_2}{Z_1}\right) \sin \gamma_2 d}, \tag{64}$$

where E_o and E_i are the output and input fields: γ_1 and γ_2 are the propagation constants in the nonlossy and lossy media, respectively; Z_1 and Z_2 are the respective characteristic impedances; and d is the thickness of the attenuating medium, Fig. 5·31. The characteristic impedance of a waveguide is

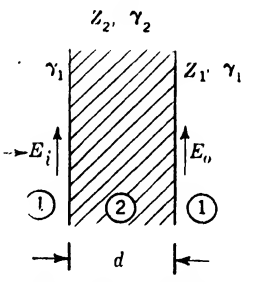

FIG. 5·31.—Terminology for transmission through attenuating medium.

$$Z = \frac{E_x}{H_y} = \frac{\mu j \omega}{\gamma}, \tag{65}$$

$$\gamma^2 = -\left(\frac{2\pi}{\lambda}\right)^2 + \left(\frac{\pi}{a}\right)^2 + \sigma, \tag{66}$$

where $E_x = E_o e^{j\gamma d}$, a is the wide dimension of the guide, and σ is the conductivity of the medium. If γd is assumed small, Eqs. (65) and (66) are substituted into Eq. (64), and $\sigma = \sigma_r + j\sigma_i$, then

$$\frac{E_o}{E_i} = \frac{1 - j\gamma_1 d}{\left(1 + \frac{1}{2}\sqrt{\frac{\mu}{\epsilon}}\frac{\lambda g}{\lambda}\sigma_r d\right) + j\left(\frac{1}{2}\sqrt{\frac{\mu}{\epsilon}}\frac{\lambda g}{\lambda}\sigma_i d - \gamma_1 d\right)}. \tag{67}$$

Finally, if $\sigma \gg Y_1 = \sqrt{\epsilon/\mu}\ \lambda/\lambda_g$, and $\gamma_2 d \ll 1$,

$$\left(\frac{E_o}{E_i}\right) = \frac{1}{\left(1 + \frac{1}{2}\frac{\sigma_r d}{Y_1}\right)^2 + \left(\frac{\sigma_i d}{2Y_1}\right)^2}. \tag{68}$$

This equation is of the same form as the expression for the attenuation due to a lumped-constant shunt admittance replacing the discharge, see Fig. 5·30, where the transmission is $[(1 + g/2)^2 + (b/2)^2]^{-1}$, and g and b are the normalized components of the discharge admittance.

Conductivity of the Ionized Gas.—Margenau[2] has shown that if the electron mean free path, and the frequency and the amplitude of the impressed high-frequency voltage are adjusted so that the electrons make relatively few collisions per cycle, and the electron energy is below the ionizing level, then the distribution of electron velocities will be Maxwel-

[1] J. A. Stratton, *Electromagnetic Theory*, McGraw-Hill, New York, 1941, p. 511.

[2] H. Margenau, "Dispersion of High Frequency Radio Waves in Ionized Gases," RL Report No. 836, Oct. 26, 1945.

lian. At the operating pressures encountered in TR tubes (10 to 30 mm Hg) these conditions are satisfied in the recovery period where the impressed voltage (received signal) is relatively weak. Under these conditions the conductivity of the gas is

$$\sigma = \frac{4}{3}\frac{e^2Ln}{(2\pi mkT)^{1/2}}\,[K_2(x_1) - jx_1^{1/2}K_{3/2}(x_1)], \tag{69}$$

where e, m, and n are the electron charge, mass, and density; L is the electron mean free path; k is the Boltzmann constant; T is the absolute temperature; $x_1 = m(\omega L)^2/2kT$; and the functions K_2 and $K_{3/2}$ are[1]

$$\begin{aligned} K_2(x_1) &= 1 - x_1 - x_1^2 e^{x_1} E_i(-x_1) \\ K_{3/2}(x_1) &= (\tfrac{1}{2} - x_1)\pi^{1/2} + \pi x_1^{3/2}\, e^{x_1}\,[1 - \mathrm{Erf}\,(\sqrt{x_1})]. \end{aligned} \tag{70}$$

In TR tubes with $\omega \approx 2 \times 10^{10}$ and $L \approx 0.005$ cm, $x_1 \geqq 100$ and the following limiting forms may be used,

$$\left.\begin{aligned} \lim_{x_1 \to \infty} K_2(x_1) &= \frac{2}{x_1} \\ \lim_{x_1 \to \infty} K_{3/2}(x_1) &= \frac{3\pi^{1/2}}{4x_1} \end{aligned}\right\}. \tag{71}$$

If these limiting forms are substituted in Eq. (69),

$$\sigma = \sigma_r + j\sigma_i = n\left[\frac{16}{3}\frac{e^2}{m\omega^2 L}\left(\frac{kT}{2\pi m}\right)^{1/2} + j\frac{e^2}{m\omega}\right]. \tag{72}$$

At a frequency of 2800 Mc/sec and a gas pressure of 5 mm Hg the numerical results are

$$\begin{aligned} \sigma_r &= 1.9 \times 10^{-13} n, \\ \sigma_i &= 1.6 \times 10^{-12} n. \end{aligned} \qquad \text{(mks units)}$$

The imaginary term of Eq. (72) will be recognized as the result which would be obtained for electrons in a vacuum. This term varies inversely with frequency, and is independent of pressure. The real component of σ, however, has a maximum value when the mean free time between collisions is about equal to the period of the impressed r-f voltage, $t = 2\pi/\omega$. Specifically, the maximum occurs for a value of

$$x_1 = 2.1 = \frac{m\omega L^2}{2kT}.$$

For a given set of conditions, frequency and pressure, the density of electrons n that will result in a certain value of attenuation may be calcu-

[1] The exponential integral $E_i(-x_1)$ and the error function $\mathrm{Erf}(\sqrt{x_1})$ are defined in Jahnke and Emde, *Table of Functions*, Stechert, New York, 1938.

lated, if the shape is known and is amenable to computation. In the present example of the pre-TR tube, with the discharge confined to a thin slab of thickness d, Eqs. (68) and (72) can be used to make this conversion. By this method, measured recovery-time curves have been converted to n-vs.-time curves, and from a knowledge of the partial pressures of the gases present, electron-capture cross sections may be computed.

The attenuation varies with the square of the shunt admittance; therefore, for the gas discharge, it varies with n^2.

5·14. Electron-capture Properties of Various Gases.—The mechanism by which electrons are captured by atoms or molecules is not simple, nor is it unique.[1,2,3] The electronegative character of the gas is one of the more important factors which influence capture. The kinetic energy of the electrons is important. Depending upon the particular gas under consideration, the probability of capture may either increase or decrease with increasing electron energy. As in most discharge phenomena, impurities play a role that is not very well understood.

In the recovery period of a TR tube, interest is primarily in fairly weak signals of the order of 10^{-6} to 10^{-12} watt intensity. The electric fields produced by such signals across the gap of a typical high-Q TR tube, will be smaller than the breakdown potential by a factor lying in the range between 10 and 10,000. Consequently, it is assumed that the energy imparted to the electrons by the received signal is negligible compared with their thermal energy. This thermal energy will be a function of the gas temperature and the time that has elapsed since the end of the transmitter pulse.

The electron affinity of an atom may be described in terms of the work done on an electron by the field between it and the atom. Atomic oxygen and the halogens have electron affinities of 3 or more electron volts. Hydrogen, on the other hand, has a value of 0.76 ev, and the noble gases have negative values which indicate that they form unstable ions. A more useful way, for our purposes, of comparing gases is in terms of their electron attachment coefficient δ, where δ is the average number of collisions an electron must make with the atoms of the gas before it is captured. In Table 5·3, there are tabulated for several gases values of δ, of N, the number of electron collisions with gas molecules per second at one atmosphere and room temperature, and of $t_a = \delta/N$, the average time required for an electron to be captured.[4]

The capture of electrons by molecular gases may take place by a

[1] Loeb, *op. cit.*, Chap. 6.

[2] Massey, *Negative Ions*, Cambridge Tracts, MacMillan, New York, 1938.

[3] Cobine, *op. cit.*, Chap. 4.

[4] K. T. Compton and I. Langmuir, *Rev. Mod. Phys.* **2**, 193 (1930).

TABLE 5·3.—ELECTRON ATTACHMENT COEFFICIENT, COLLISIONS PER SECOND, AND TIME FOR CAPTURE FOR VARIOUS GASES

Gas	δ	N	$t_a = \delta/N$
Noble gases, N_2, and H_2	∞		
CO	1.6×10^8	2.22×10^{11}	0.72×10^{-3} sec
NH_3	9.9×10^7	2.95×10^{11}	3.35×10^{-4}
N_2O	6.1×10^5	3.36×10^{11}	1.82×10^{-6}
Air	2.0×10^5	3.17×10^{11}	0.63×10^{-6}
O_2	4.0×10^4	2.06×10^{11}	1.94×10^{-7}
H_2O	4.0×10^4	2.83×10^{11}	1.41×10^{-7}
Cl_2	2.1×10^3	4.5×10^{11}	0.467×10^{-8}

number of different processes. On the basis of a series of measurements made by Bradbury,[1] and Bradbury and Tatel,[2] Loeb[3] has postulated a number of different reactions which are presented in Table 5·4.

TABLE 5·4.—MINIMUM ELECTRON ENERGY AND MECHANISM OF ELECTRON CAPTURE IN VARIOUS GASES

Gas	Ground state	Neg. ions of gas formed	Min. electron energy for attachment	Reaction
Cl_2, Br_2, I_2	$^1\Sigma$	No	0	$Cl_2 + e \rightarrow Cl^- + Cl + (4.1 - 1.5)$ ev
HCl, HBr, HI	$^1\Sigma$	No	0.4 ev in HCl	$HCl + e + (4.5 - 4.1)$ ev $\rightarrow H + Cl^-$
NH_3	..	No	3 ev	$NH_3 + e + 3$ ev $\rightarrow NH^- + H_2$
N_2O	$^1\Sigma$	No	1.7 ev	$N_2O + e + 1.7$ ev $\rightarrow O^- + N_2$
CO_2	$^1\Sigma$	No		
H_2S	.	No	3.7 ev	$H_2S + e + 3.7$ ev $\rightarrow HS^- + H$
O_2	$^3\Sigma$	Yes	0	$O_2 + e \rightarrow O_2^-$
O	$^3P_2$	Yes	0	$O + e \rightarrow O^-$
SO_2	.	Yes	0	$SO_2 + e \rightarrow SO_2^-$
NO	$^3\Pi$	Yes	0	$2NO \rightarrow (NO)_2 + e \rightarrow NO^- + NO$
H_2O	..	No	0	$2(H_2O) + e \rightarrow 2(H_2O)^-$
H_2O	..	No	5.4 ev	$H_2O + e + 5.4$ ev $\rightarrow HO^- + H$

Gases such as O_2 and SO_2 form negative molecular ions directly by the capture of electrons. Molecular ions are formed by NO; but the probability of electron capture is dependent upon pressure and it is

[1] Bradbury, *J. Chem. Phys.*, **2**, 827 (1934); **2**, 840 (1934).

[2] Bradbury and Tatel, *J. Chem. Phys.*, **2**, 835 (1934).

[3] Loeb, "Fundamental Processes of Electrical Discharges in Gases," Wiley, New York, 1939, Chap. 2.

assumed that a complex, $(NO)_2$, must be formed. This complex is then assumed to capture an electron and form NO^-, the excess energy of the

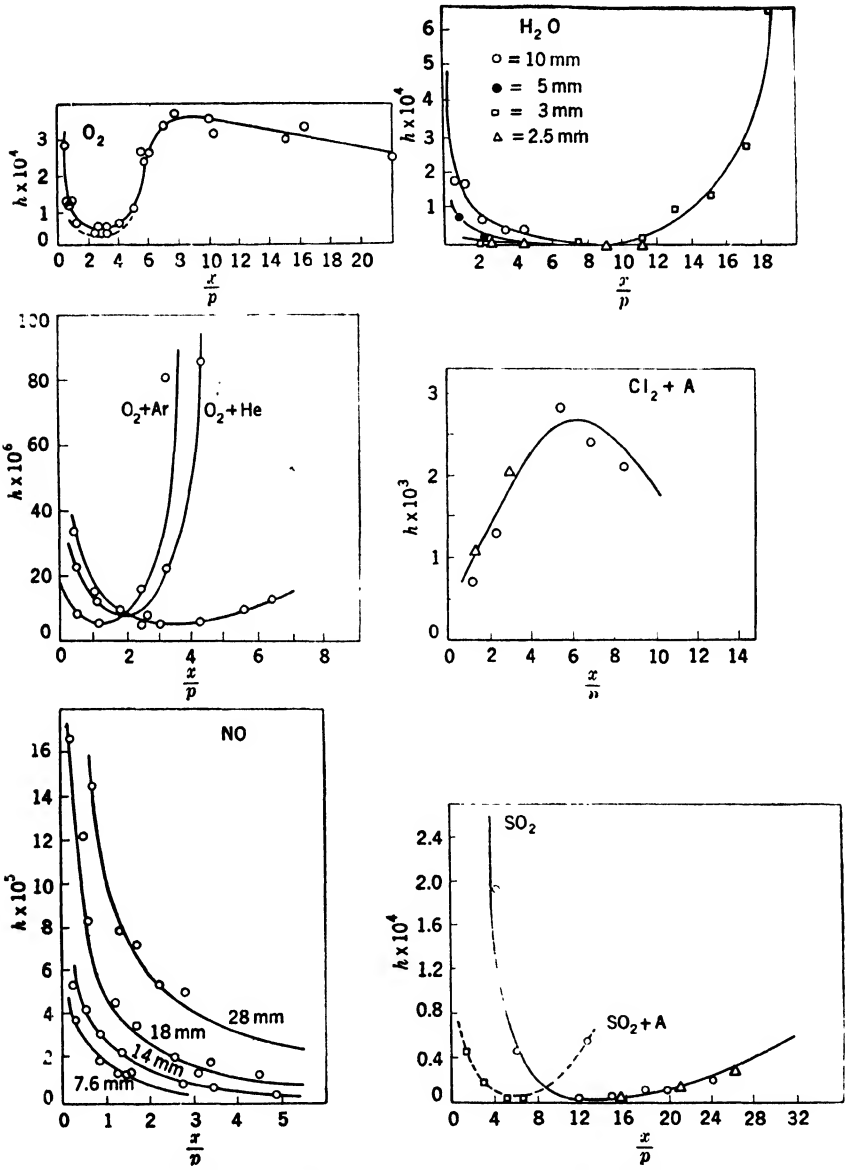

FIG. 5·32.—Probabilities of electron capture for various gases.

electron being carried away by the neutral NO. Alone, H_2O should not capture electrons, since it has a closed electron system. With sufficient

energy, $\geqq 5.4$ ev, an electron will dissociate the water into HO^- and H. However, it is true that water has a large electron-capture cross section for the slow-moving electrons. Bradbury and Tatel report that the probability of capture of slow electrons in H_2O is strongly pressure-dependent. At a pressure of 2.5 mm Hg of H_2O no capture of slow electrons was observed. At higher pressures, the probability of capture rose rapidly. This was taken as evidence that a complex, $2(H_2O)$, was formed, which could then be ionized directly. Figure 5·32 gives the probability of electron capture h as a function of the parameter x/p for various gases, as measured by Bradbury and Tatel. In this case x is the voltage gradient, and p the pressure in mm Hg. Figure 5·32*a* shows the values of h for O_2. As x/p increases from very low values, h drops rapidly. At $x/p \approx 5$, the curve rises sharply. At this point the electron energy is about 1.6 ev, corresponding to a metastable excitation level in O_2. Electrons which make these inelastic collisions have their energy reduced to a level at which the probability of capture is again high. Figure 5·32*b* shows the effect of mixing argon, helium, or nitrogen, with O_2, in equal volumes.

Figure 5·32*c* shows the pressure dependence of electron capture in NO which has been discussed. Figure 5·32*d* shows the probability of capture in a mixture of argon with Cl_2. The gas Cl_2 is a *chemically inert* gas which has a closed electronic system, and therefore Cl_2^- ions cannot be formed. Instead, it is believed that the ionizing process is the one indicated in Table 5·4. Figure 5·32*e* is for electron capture in SO_2, and SO_2 plus A.

Figure 5·32*f* shows the pressure dependence of electron capture in H_2O. This is explained by assuming the formation of nuclei of condensation, which then makes these complexes capable of capturing low-velocity electrons. Impurities such as CO_2 or O_2 are presumed to aid this effect, whereas A or N_2 do not. In the next section (Sec. 5·15) the available data on recovery time in TR tubes will be examined to see what can be learned about effective probabilities of electron capture.

5·15. Recovery-time Data.—The recovery characteristic of a TR tube is a curve in which attenuation through the tube as a function of the time after the transmitter pulse is plotted. The attenuation plotted is the difference in decibels between the instantaneous value and the attenuation through the "cold" or unfired tube. Time is measured from the *end* of the transmitter pulse.

Figure 5·33 shows typical recovery curves of a 1B27 TR tube[1] measured at several different levels of transmitter power. The tube is filled with a mixture of 10 mm Hg, each, of H_2 and H_2O. Figure 5·34 shows

[1] Smullin and Leiter, "The 1B27 TR Tube," RL Report No. 594, Oct. 4, 1944.

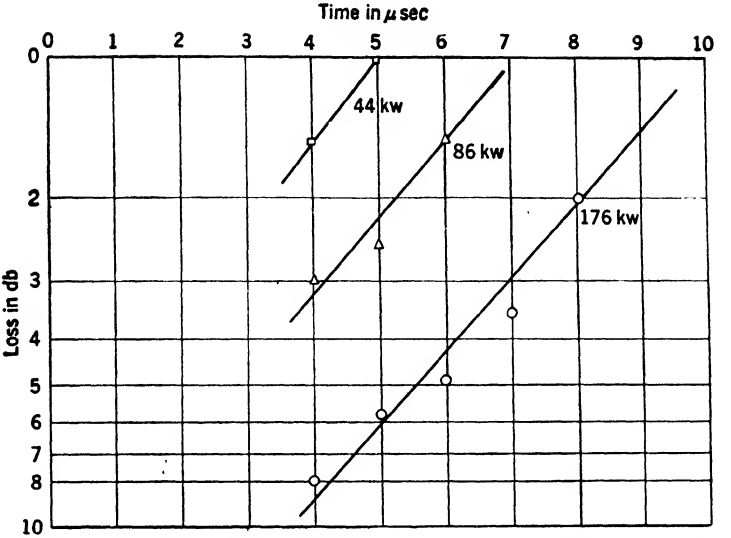

FIG. 5·33.—Recovery curves of 1B27 TR tube for three incident power levels.

the effect of the water-vapor content upon the recovery time of a 1B27 TR tube, when the partial pressure of H_2 is held constant.

Recovery curves for 3-cm and 1-cm TR tubes are similar in shape to those shown here; but the time scale is considerably shorter. No quantitative explanation of this difference has been proposed. It is thought, however, to be the result of the smaller volume of the discharge in the high-frequency tubes, which allows diffusion to play a relatively more important role. M. D. Fiske has proposed a "sweeping" type of diffusion. In this, right at the end of the transmitter pulse, some of the high-energy electrons near the electrodes actually reach the electrodes and are lost. This produces a positive space charge near the electrodes which attracts electrons from the center of the discharge. Some of these electrons go right through to the electrodes, and are lost, and so on. No quantitative analysis of this mechanism has been made; but it seems a plausible process, since the effect should be larger for the smaller tubes.

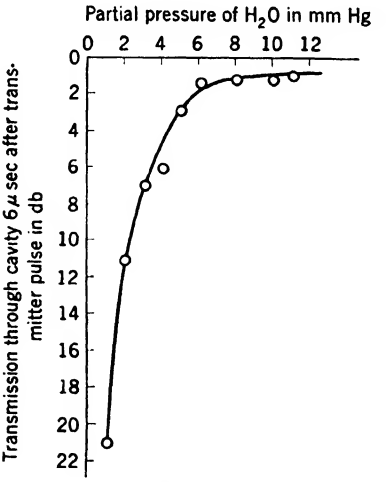

FIG. 5·34.—Recovery characteristics of 1B27 TR tube as a function of pressure of water vapor. The transmitter power was 100 kw, and the partial pressure of H_2 was 10 mm Hg.

The life of most TR tubes is limited by the rate at which the water vapor is cleaned up, or decomposed, thus increasing the recovery time. Because of the relatively short life of pre-TR tubes operating at high

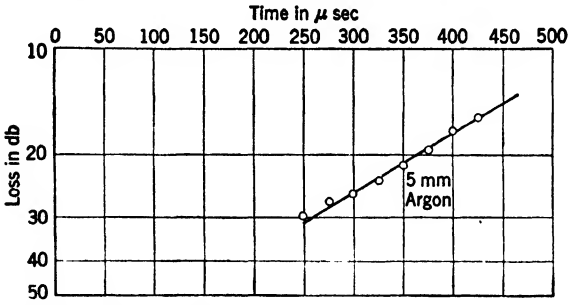

FIG. 5·35.—Recovery characteristic of well-baked 1B38 tube filled with pure argon.

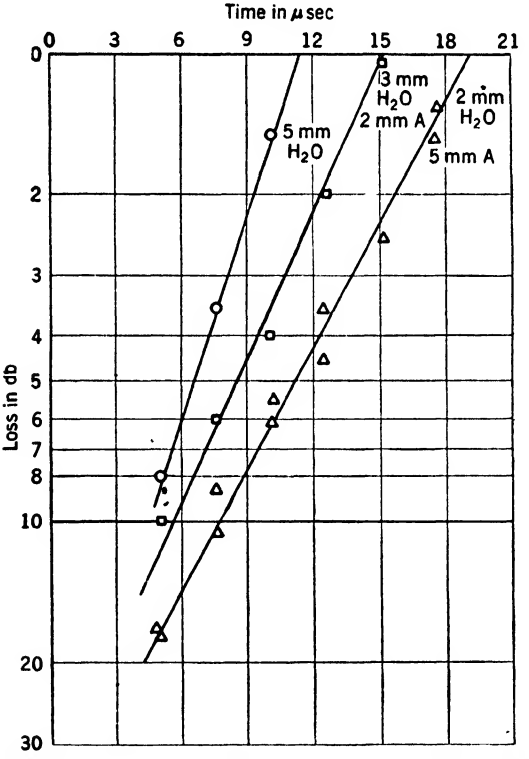

FIG. 5·36.—Recovery of mixtures of argon and water vapor.

line powers, a study of various gases was undertaken to determine whether a substitute for H_2O might be found. The measurements were all made in 1B38 pre-TR tubes at a line power of about 700 kw. The gases used

in these measurements were the purest obtainable commercially, and the tubes were carefully cleaned and pumped before filling.[1] The following curves are taken from these experiments.

Figure 5·35 is the recovery characteristic of a carefully cleaned and baked tube filled with commercial "spectroscopically pure" argon; this tube has an extremely long recovery time. Figure 5·36 shows the recovery

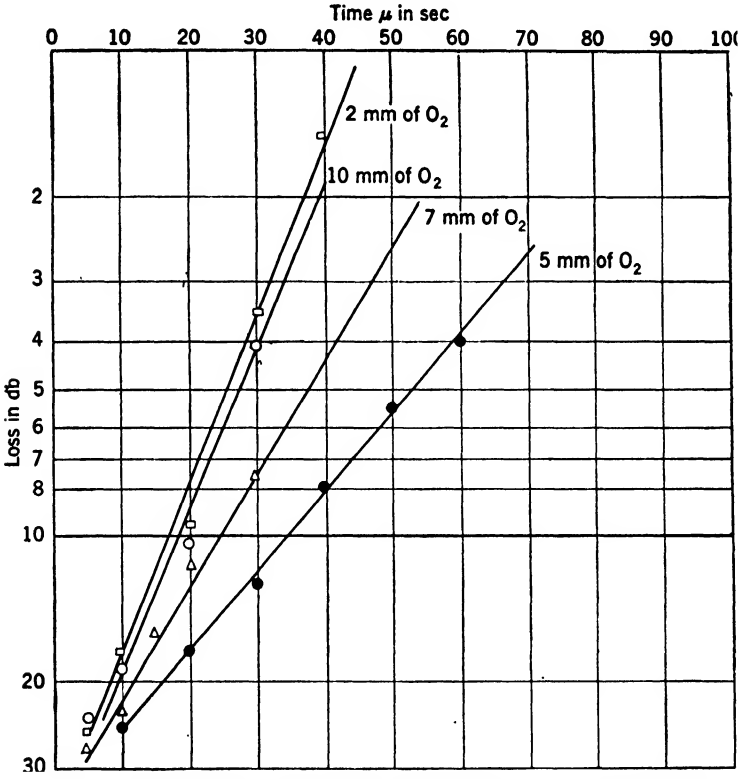

FIG. 5·37.—Recovery characteristic of oxygen at various pressures.

time for various mixtures of H_2O and A.; Fig. 5·37 is for various pressures of pure O_2; Figs. 5·38 and 5·39 are for mixtures of argon and chlorine, and argon and pentene. Other gases tested, but not shown here, were H_2S, CH_4, C_2H_2, C_2H_4, benzene, iodoform, and methyliodide. All of these exhibited short recovery times. The purity of the organic gases was more or less uncertain, since the chemical reactions involved usually produce a number of different gases besides the interesting gas.

The importance of a high degree of purity is best illustrated by the experience with CO. Commercial 1B38 tubes are filled with 10 mm Hg

[1] F. L. McMillan, I. H. Dearnley, C. H. Pearsall, "Recovery Time Measurements in Bandpass TR's for Various Gases," RL Report No. 895, Dec. 18, 1945.

of commercial argon. The tube itself is assembled with soft solder, and therefore it cannot be outgassed by baking. As a result, even though no water is put into the tube, the recovery time of most of the tubes is short. Spectroscopic measurements made on a large number of these tubes showed, among the other things, that CO was almost invariably present in tubes having a short recovery time. Although it has been reported to have zero electron-capture probability,[1] it was decided to test a CO-A mixture. Independent measurements by Fiske at the General Electric Research Laboratories and McMillan at Radiation Laboratory showed very short recovery times for such mixtures. Subsequent tests, however, with pure CO, prepared chemically in the vacuum system, showed that CO really had no effect upon the recovery time, and the initial results must have been caused by some other gas present as an impurity.

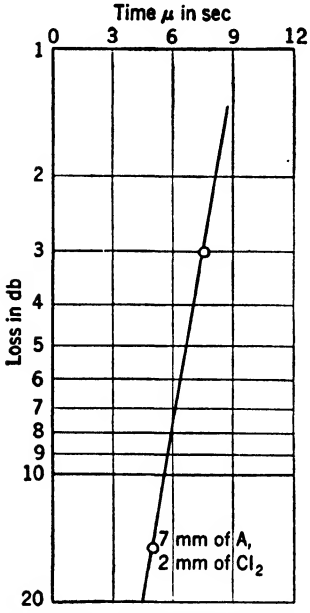

FIG. 5·38.—Recovery of argon-chlorine mixture.

Let us now consider some of these curves in detail. The variation in recovery time with line power, illustrated in Fig. 5·33, shows the expected phenomenon of longer recovery times for higher powers. This, of course, can be interpreted as corresponding to larger values of n_a, the electron density in the discharge, since the rate of capture of electrons $dn/n\,dt$ is constant, regardless of line power.

Figure 5·34 shows clearly that the rate of capture of electrons is dependent upon the amount of water present, and that H_2 has a small, perhaps zero, electron-capture cross section.

Figure 5·35 shows the expected long recovery time for pure argon. If the data are recalculated to give a curve of n vs. t, it can be shown[2] that the function $-td(\ln N)/dt$ is about 3, where $N = nd$, d being the thickness of the discharge. If only diffusion is operative, this quantity cannot have a value greater than $\frac{1}{2}$. Thus, the recovery time is shorter than expected. Under the conditions of this particular experiment, no impurities were present at a pressure greater than 0.01 per cent of that of the argon. If the impurity had a capture efficiency equal to that of H_2O,

[1] Loeb, "Fundamental Processes of Electrical Discharges in Gases," Wiley, New York, 1939, Chap. 2.

[2] H. Margenau, "Theoretical Interpretation of the Recovery Time of TR Boxes," RL Report No. 929, Jan. 9, 1946.

it would have had to be present at a pressure of 0.18 mm Hg, which is out of the question. There are thus two possibilities—the presence of an extremely efficient electron-capture agent, or the formation of some unknown ion, as A_2^-. Negative argon ions seem more likely; the analogous ion He_2^- is known to exist.

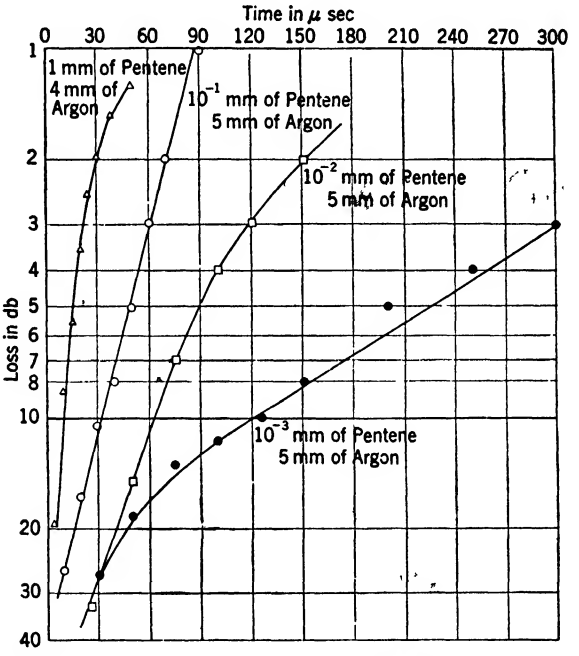

FIG. 5·39.—Recovery of mixtures of argon and pentene.

The data of Fig. 5·36 may be used to determine the capture cross section of H_2O, by replotting in terms of ln n and t, and using Eq. (63) which may be rewritten

$$h_{cap} = -\frac{1}{vQM}\frac{d}{dt}(\ln n). \tag{73}$$

If these calculations are made with $Q = 15 \times 10^{-16}$ cm^2, v corresponding to 300° K as $(3kT)^{1/2}/m = 1 \cdot 2 \times 10^7$ cm/sec, then the values for h_{cap} are

1.0×10^{-4}	from the 2 mm curve.
0.93×10^{-4}	from the 3 mm curve.
0.94×10^{-4}	from the 5 mm curve.

These capture probabilities are for thermal velocities, which have not been obtained by any other means. They agree in order of magnitude

with the results of Bradbury and Tatel,[1] who list values as high as 4×10^{-4} at somewhat greater energies. The important difference lies in the fact that no pressure dependence is indicated by these results. This might be interpreted as meaning that single H_2O molecules can capture thermal electrons. On the basis of present knowledge, this seems improbable, and further study is required.

Figure 5·37 shows an interesting anomaly, which is that the recovery time is not a monotonic function of the oxygen pressure. Margenau[2] has explained this on the basis of the fact that both O_2 and O are present

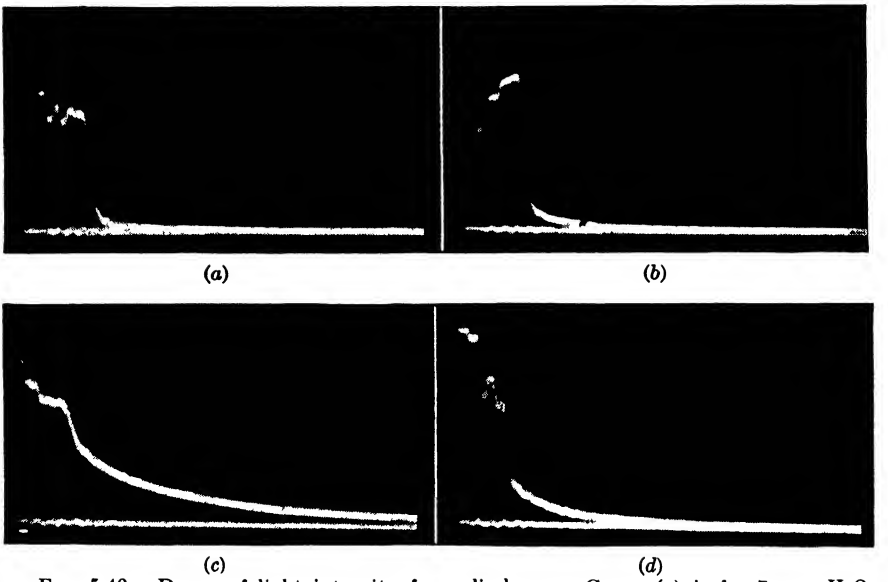

(*a*) (*b*)

(*c*) (*d*)

FIG. 5·40.—Decay of light intensity from discharge. Curve (*a*) is for 7 mm H_2O; curve (*b*) is for 10 mm argon and 1.5 mm H_2O; curve (*c*) is for 20 mm Hg of lamp argon (0.5% N_2); curve (*d*) is for 20 mm of dry tank N_2.

in the discharge. The data can then be interpreted as an indication of different electron affinities for the molecule and for the atom. If it is assumed that most of the oxygen is in atomic form at the end of the discharge, then the atoms recombine into O_2 by way of a three-body collision, and the rate will be proportional to the square of the pressure. Thus, O will last longer at low pressures. According to the data, then, above 5 mm pressure O_2 is the more active capture agent; and below 5 mm O is the more active. On this interpretation, 2 mm pressure, which corresponds to 4 mm of atomic oxygen, is as effective as 10 mm of O_2. The numerical results based on this argument are $h_{cap} \approx 3.2 \times 10^{-4}$ for O, and $h_{cap} \approx 1.5 \times 10^{-4}$ for O_2.

[1] Bradbury and Tatel, *J. Chem. Phys.*, **2**, 835 (1934).

[2] Margenau, *loc. cit.*

Figure 5·39 shows the transition from conditions in which there are enough captors to eliminate all electrons to those in which there are not enough. The corresponding ln n-vs.-t curves show straight terminal slopes for pressures of 1 mm Hg and 0.1 mm Hg of pentane, but definitely curved characteristics for the 10^{-2} and 10^{-3} mm Hg pressures. The latter two are probably tending towards a diffusion as opposed to a capture characteristic. If the transition is assumed to lie between 0.1 and 0.01 mm Hg partial pressure, this indicates that the initial electron density in the discharge is between 3.5×10^{14} and 3.5×10^{15} per cm^3. This value is in agreement with estimates obtained by extrapolating the curves of ln n to zero time.

In one attempt, which was unsuccessful, to devise a simple production recovery-time test, measurements were made of the decay of light intensity with time after the transmitter pulse. Figure 5·40 shows the decay of light intensity from the discharge after the excitation, transmitter power, is removed. These characteristics were obtained by measuring the light of a 1B38 pre-TR tube with a photomultiplier tube connected to a video amplifier and cathode-ray oscillograph. The tubes filled with argon and with nitrogen exhibit long recovery times, while in those containing H_2O, the light is very quickly quenched. No particular study has been made of this phenomenon, but it is believed that the "afterglow" is caused by the presence of metastable atoms which may have fairly long lives.

5·16. Effect of Keep-alive Discharge on Recovery Time.—In Sec. 5·7 it was shown that in order to make the spike energy small, and to make the variations in energy from pulse to pulse low, it is necessary to introduce electrons into the gap from an external source. This source is a d-c glow discharge so located that the desired n_0 electrons are furnished to the gap by diffusion, Fig. 5·41. If the keep-alive electrode is negative with respect to the TR tube, electrons are accelerated toward the gap. If the keep-alive is positive, however, electrons move away from the gap. Under these conditions, the spike energy is many times larger than when the keep-alive is negative, and it is usually impossible to protect crystals. For the moment the leakage-power considerations will be neglected and the effect of keep-alive polarity on recovery time will be discussed.

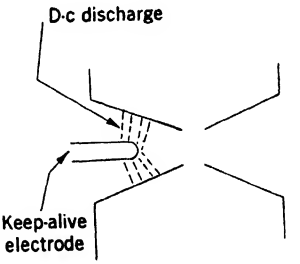

FIG. 5·41.—Keep-alive electrode within the cones of TR tube.

The recovery characteristics of an argon-filled 721A TR tube for positive and negative keep-alive polarities are illustrated in Fig. 5·42. The effect of the positive keep-alive is marked. The difference between

the two curves can be explained if the structure of the discharge is considered, see Fig. 5·43. With the keep-alive positive, there will be a positive column extending toward the TR tube gap, as shown. Since most of the voltage drop in the d-c discharge occurs near the cathode, this will have the effect of producing a new "virtual anode" at the cathode end of the positive column. As a result, the penetration of the d-c field into the gap is enhanced. The difference in position between the virtual anode and the keep-alive electrode may be estimated from the fact that the length of the cathode fall with a copper cathode is 0.3 to 0.8 mm at a pressure of 10 mm Hg.[1] The distance of the keep-alive electrode from the cone is about 5 mm. Thus the virtual anode is about 0.15 as far from the gap as is the keep-alive, with the resulting increase of the d-c field in the gap. The direction of the field serves to sweep electrons out of the gap, and thus overcomes the retarding force of the positive ions.

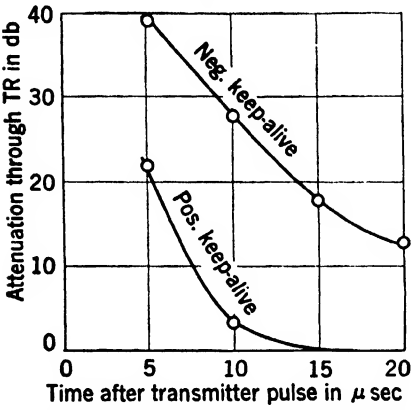

FIG. 5·42.—Recovery of a 721A TR tube filled with 10 mm Hg argon, at 50 kw pulse power with positive and negative keep-alive discharge.

This phenomenon has been known for some time, and suggestions have been made for the use of an argon-filled TR tube that would have very low leakage power with a negative keep-alive, and could be made to have a short recovery time by making the keep-alive positive just after the transmitter pulse. The keep-alive polarity would vary with time somewhat as shown in Fig. 5·44. This type of operation is entirely feasible, and was, in fact, used by the British in one radar installation. It has the advantage of longer tube life, since there is no chemically active

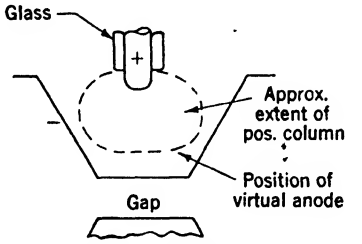

FIG. 5·43.—Extent of positive column and virtual anode in keep-alive discharge.

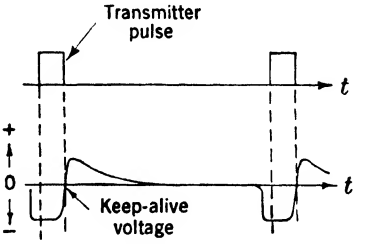

FIG. 5·44.—Pulsed keep-alive voltage.

[1] Cobine, *Gaseous Conductors*, McGraw-Hill, New York, 1941, pp. 215–218.

gas such as H_2O to react with the metal part of the tube. This, it will be shown later, is the most serious factor limiting tube life in conventional TR tubes. The disadvantage of a tube of this type is that the circuit necessary to produce the alternately negative and positive keep-alive is more complicated than the simple high-voltage rectifier needed for conventional tubes. Although the actual complication is not excessive, designers have usually avoided it on the basis that failure or partial failure of this circuit would result in crystal burnout and failure of the entire radar set. This is certainly a moot question and should, in the author's opinion, receive further study.

The application of d-c sweeping fields to aid recovery time has not been extended to bandpass TR tubes, where the recovery time of the tube is limited by that of the low-Q input window. To sweep the electrons away from the window would require a grid-like electrode across the waveguide and just behind the window. The construction of the tube would be seriously complicated by the addition of such a structure.

5·17. The Keep-alive.—The keep-alive circuit is of equal importance with the gas filling and the shape of a TR tube in determining the spike leakage energy. The keep-alive discharge is generally a low-current, d-c glow maintained between the keep-alive electrode and some portion of the TR tube, and is so located that the resultant density of electrons in the r-f gap is sufficient to keep the spike leakage energy W_s to a safe level. Since the keep-alive is an auxiliary device which is concerned only with the high-level operation of the tube, it must be designed to have little or no effect upon the low-level performance of the TR tube. This means, first of all, that the keep-alive electrode must either be shielded from the r-f field in the cavity or, if it is within the cavity proper, it must be so disposed that r-f currents flowing along it will be minimized. Similarly, the glow discharge must not cause any appreciable decrease in low-level transmission through the cavity, either because of its own conductance or because of the conductance caused by the electrons it furnishes to the gap. This last requirement must of necessity be a compromise with the need for having n_0 large enough to give adequate leakage-power protection. To ensure minimum interference with the reception of weak signals, r-f noise coupled directly to the first detector, or lower-frequency noise coupled to the i-f amplifier from the discharge, must be small.

It was pointed out in Sec. 5·16 that the keep-alive polarity must be negative if electrons are to be furnished to the r-f gap. In the discussion which follows, a negative keep-alive polarity will always be assumed unless otherwise stated.

In practical TR tubes it has been possible to maintain sufficiently low values of W_s with a keep-alive discharge that causes a change of low-level

transmission of less than one per cent. The reflection and dissipation losses caused by r-f currents flowing in the keep-alive electrode are nearly zero in one type to be described, and of the order of 1 per cent in another type. The glow discharge produces r-f noise so low that it makes the measured values unreliable because of experimental errors; however, it

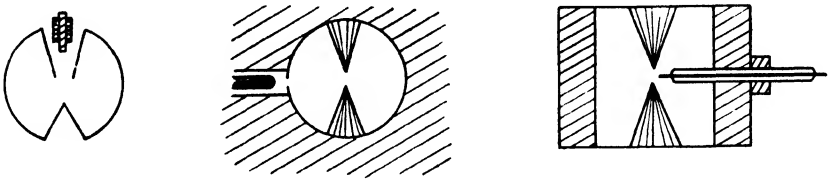

FIG. 5 45.—Types of keep-alive electrodes.

certainly causes less than 0.1 db change in signal-to-noise ratio of the receiver. Under certain circumstances, i-f noise can be appreciable; but it is not difficult to keep it out of the receiver circuits.

A classification of keep-alive electrodes based upon shape or construction recognizes three major types. These are the coaxial electrode, Fig. 5·45*a*, and two modifications of the side-arm type, Fig. 5·45*b* and *c*

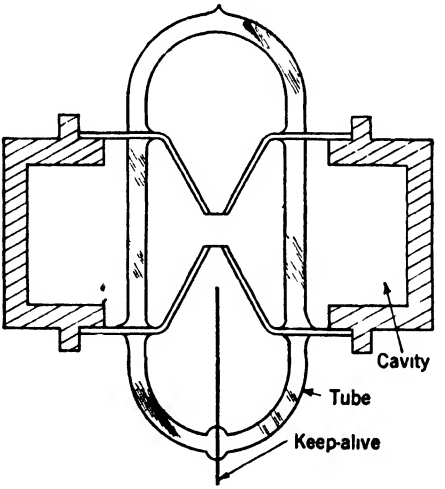

FIG. 5·46.—Keep-alive electrode in tube inserted in cavity.

Historically, the coaxial keep-alive electrode is the oldest. As shown in the sketch, it is mounted within one of the hollow electrodes or cones forming the r-f spark gap. A d-c discharge is maintained between the keep-alive electrode and the inside of the cone. This type of electrode is particularly suitable for use in the cell-type TR tube. For this tube it

is desired to have construction that is axially symmetric in order to be able to clamp the tube into a split annular cavity, Fig. 5·46. The keep-alive electrode and discharges are both completely shielded from the r-f field within the TR cavity, and thus have no effect upon low-level transmission. The position of the electrode within the cone, however, must be maintained within rather close limits since the electron density in the gap is a sensitive function of the distance of the keep-alive electrode from the gap; and therefore, the low-level loss or "keep-alive interaction" caused by n_0 changes rapidly with position.

Keep-alive electrodes of the types shown in Fig. 5·45*a* and *b* are used in integral-cavity TR tubes. The 1B24 tube uses a coaxial keep-alive, while the 1B26 and 1B50 use the side-arm type. In bandpass TR tubes, electrodes similar to those of Fig. 5·45*a* and *c* have been used. The side-arm electrode in *c* actually extends into the r-f field within the tube; however, since it is perpendicular to the electric field no longitudinal currents are induced on it. Since the electrode radius is small, the capacitance introduced by it is small, and the resulting reflections are negligible.

In common with many other technical problems, the design of a keep-alive system involves a number of compromises. To reduce the spike leakage energy to a safe level, the number of electrons n_0 in the gap should be large. However, n_0 must not be so large that the low-level transmission is seriously affected. A further restriction on the keep-alive arises from the fact that the d-c discharge changes the gas content of the tube either by chemical decomposition of the gas, or by sputtering whereby gas molecules are driven into the walls and captured. This process takes place at a rate that increases with the current carried by the discharge. Therefore, to obtain maximum tube life, the keep-alive discharge should be run at a current level as low as possible, consistent with safe values of W_s. This limit is set by two restrictions. A limit is determined by the current level at which, for a given electrode shape, n_0 becomes too small. Before this limit is reached, however, the discharge may become unstable or break into a relaxation oscillation. With the discharge intermittent, there is a finite probability that it will be out just before and during a transmitter pulse. When this happens n_0 will be small and the spike leakage energy will be very large, and crystal burnout may result.

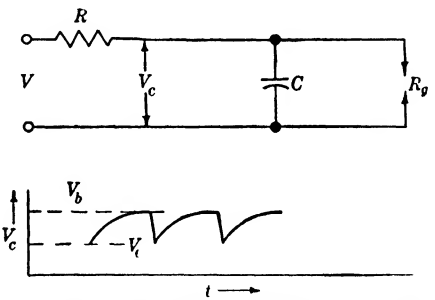

FIG. 5·47.—Relaxation oscillations of a gas discharge.

The relaxation oscillation encountered here is similar to a gas-filled-tube sawtooth oscillator, Fig. 5·47. If the resistance R_g of the discharge is small compared with the resistance of the power supply, and the voltage V is greater than the breakdown voltage of the gap V_b, then oscillations of the type shown will take place. The capacitor voltage V_c will rise at a rate determined by the time constant RC, until the breakdown voltage V_b is reached. At this point the gap will break down and discharge the capacitor until the extinction voltage V_e is reached. The discharge will go out, the voltage will build up as before, and the cycle will be repeated periodically. It is entirely feasible to make a circuit that oscillates with a period considerably in excess of one second. The maximum frequency of oscillation attainable is limited by the deionization time of the gap and may be of the order of several hundred kilocycles per second.

In the keep-alive discharge, such oscillation must either be entirely suppressed, or be made to have such a high frequency that even though the discharge is periodically extinguished, the density of electrons in the r-f gap will experience only small fluctuations. If the discharge current is to be maintained within a relatively narrow fixed range, then the frequency of oscillations cannot be seriously affected by a change of the power-supply voltage V, since the series resistance R, and hence the charging time constant, must be changed to maintain the given current despite the change in V. If the characteristics of the gap are assumed fixed, then the only way to increase the frequency is to reduce C. The capacitance of interest here includes all lumped and stray capacitances to ground, from the keep-alive electrode to the first large current-limiting resistor. By placing this resistance right at the TR tube, the total capacitance becomes just that of the keep-alive electrode, and is of the order of 1 $\mu\mu$f. If R is 4 megohms, a typical value, the oscillation frequency will be of the order of 200 kc/sec. If there are several inches of *unshielded* wire between the resistance and the tube, the frequency will be reduced by a factor of five, approximately, and if *shielded* wire is used, the reduction in frequency will be much greater.

Let us examine in greater detail the factors affecting the oscillation. If $R_g \ll R$, at the instant of breakdown nearly all of the discharge current will flow from the capacitor C. In Fig. 5·48 when V_c reaches V_b the gap breaks down and the operating point moves out to some point such as A on the V-I curve of the discharge. As the charge on C is drained off, the operating point moves away from A to the left until it reaches the constant-voltage portion of the curve beginning at B. If the equilibrium voltage $v = VR_g/(R_g + R) < V_B$, the discharge will go out at this point and v_c, since there is no current drain, will now procede to build up towards V_b again. If, however, $v = VR_g/(R_g + R) > V_B$ there

will be a stable operating point, and a continuous discharge will be maintained. Thus, increasing V or decreasing R is in the right direction to stop oscillations. Similarly, redesigning the electrode or changing the gas filling of the TR tube may change the gap resistance R_g either up or down.

To change the gas content in order to get stable operation of the keep-alive discharge is usually not possible since the gas filling must be chosen for minimum leakage power, shortest recovery time, and longest life, and it is too much to expect to find a single gas filling that will satisfy all of these conditions plus the additional one of avoiding keep-alive oscillations. Fortunately, the shape can be so modified as to eliminate oscillations almost entirely.

In the normal glow discharge the voltage drop between electrodes is nearly independent of the current, and the current density at the cathode

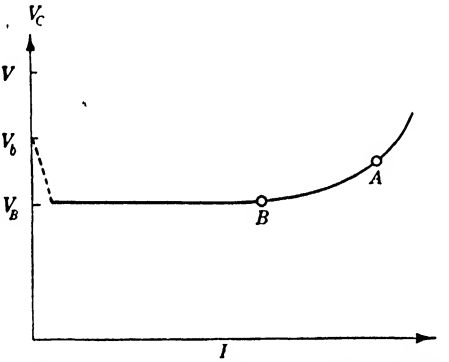

FIG. 5·48.—Volt-ampere curve of d-c glow discharge.

is also independent of the total current. This characteristic results because the glow is able to cover more and more of the cathode area as the current is increased.[1] Once the entire cathode area has been covered, a further increase of current is accompanied by an increase in voltage drop, and the discharge characteristic takes on a positive dynamic resistance. Therefore, by restricting the cathode area, the current at which the V-I slope becomes positive may be reduced, and thus, the current at which oscillation occurs may be decreased.

Early TR tubes such as the 721A and 724A, had simple tungsten keep-alive electrodes. Some time after these tubes had been produced and were being used, keep-alive relaxation oscillations were "discovered." The critical current above which oscillations ceased, was of the order of 200 to 400 μa. By reducing stray capacitance to a minimum by placing the limiting resistor directly at the TR tube, it was usually possible either to eliminate the oscillations or to make their frequency very high for

[1] Cobine, *Gaseous Conductors*, McGraw-Hill, New York, 1941, Chap. 4.

normal keep-alive currents. The spike leakage energy with an oscillating keep-alive discharge is illustrated in Fig. 5·49*a* whereas Fig. 5·49*b* is for a nonoscillating discharge. The individual lines represent the spike energy in successive pulses. These variations were first measured and correlated with keep-alive oscillations in a study of the 724A and 1B24 TR tubes.[1] Depending upon the repetition rate and transmitter power, the spike energy during the "off period" of the keep-alive discharge may be 10 to 25 db greater than the normal level.

Coated keep-alive electrodes are now used almost exclusively. They are made by covering the electrode with a glass or ceramic sleeve down to the end, which is exposed by grinding off the insulation. Although the oscillation-free region extends to currents as low as 30 μa, operating currents are usually maintained between 100 and 200 μa. There are two reasons for this. The voltage drop across the discharge is about 400 volts, and therefore, the d-c resistance is about 4 megohms at a current of 100 μa and about 20 megohms at a current of 20 μa. For military service, it is difficult to maintain a leakage resistance large compared with 20 megohms, and the low-current discharge may actually be extinguished by surface leakage on the TR tube.

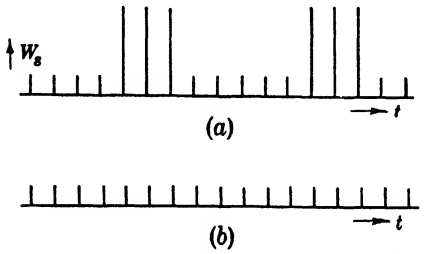

FIG. 5·49.—Time variations in spike leakage energy; (*a*) oscillating and (*b*) nonoscillating keep-alive discharge.

Figure 5·50 illustrates typical keep-alive voltampere curves for "coated" and "uncoated" electrodes. The uncoated electrode of the 721A tube shows a positive slope at currents above 200 μa. A coated electrode with an exposed area of about 10^{-3} in.^{2} has a positive slope down to currents of 50 μa or less. The 1B24 has a coated electrode, and the *V-I* curve has a positive slope down to 50 μa. The dotted lines which indicate regions with negative slope, are the result of d-c measurements made while the discharge was oscillating. As a result, the readings are averages and have no particular significance.

Another reason for choosing the higher current is that in order to maintain a given n_0 in the r-f gap, the keep-alive electrode must be placed closer to the gap for the low-current discharge than for the high-current discharge. The mechanical difficulties involved are rather severe as can be seen from a consideration of the actual dimensions involved. The accurate location of the keep-alive electrode within the hollow cone of a TR tube such as the 1B24 or 724A is a moderately difficult task. The

[1] J. B. Wiesner and F. L. McMillan, Jr., "Preignition Transmission through TR Tubes," RL Report No. 254, July 3, 1943.

only support for the electrode is at the metal-to-glass seal where it goes through the glass envelope of the tube. This point may be as much as two inches from the end of the electrode from which the discharge takes place. Since it is usually impossible to locate the end of the electrode by any jigs or spacers, it is difficult to locate the end within ±0.010 in. of

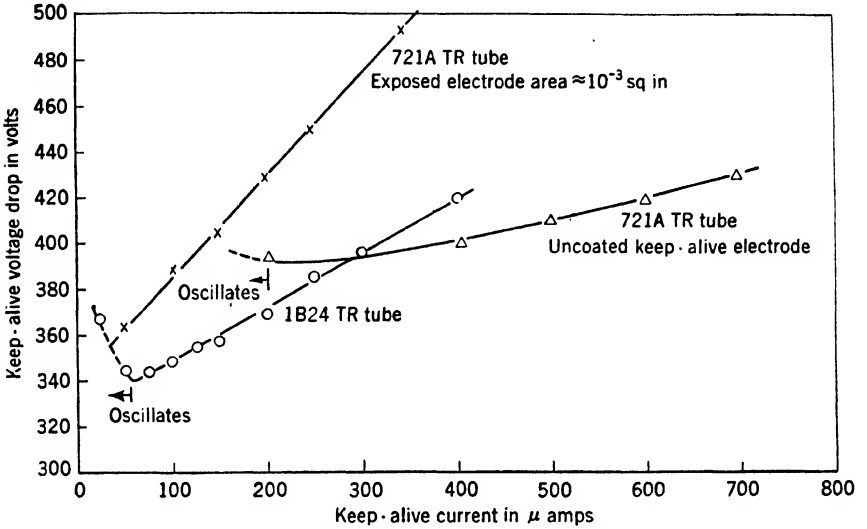

FIG. 5·50.—Volt-ampere characteristics of keep-alive discharges.

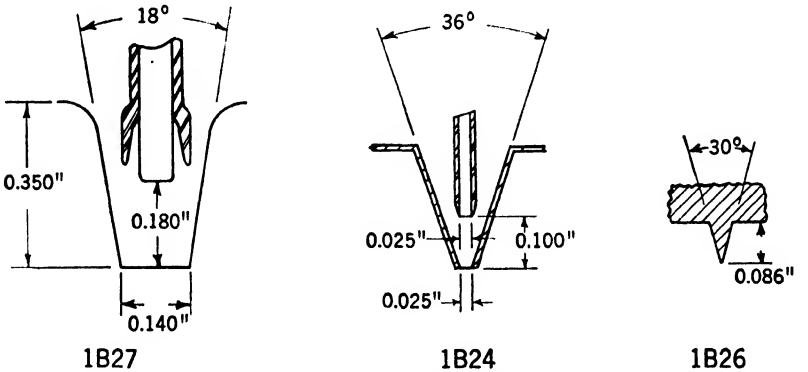

FIG. 5·51.—Details of cones and keep-alive electrodes of some TR tubes.

the nominal position inside the cone. In the 1B27, the diameter of the cone at the end of the keep-alive electrode is about $\frac{3}{16}$ in. In the 1B24, however, the corresponding diameter is only 0.055 in. Figure 5·51 shows the position of the keep-alive electrode within the cones of the 1B24 and 1B27 TR tubes. It would be almost impossible to make a 1.25-cm TR tube with this type of construction.

Since n_0 must be held within the limits imposed by low-level transmission on the one hand and low spike leakage energy on the other hand, let us consider what effect the location of the electrode has upon n_0. The discharge is shown more or less schematically in Fig. 5·52. The electrons, under the influence of the d-c field, drift in the direction of the cone. The number of electrons that pass through the hole in the cone into the r-f gap is a function of the hole diameter, the distance of the electrode from the hole, the average temperature of the electrons, the electron mean free path, and the discharge current.

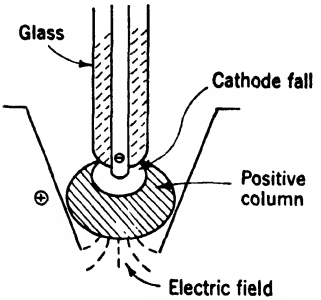

FIG. 5·52.—Structure of keep-alive discharge.

In the usual pressure range for TR tubes, 10 to 30 mm Hg, the electron mean free path is of the order of 10^{-4} in. An electron makes a great many collisions per second, and the influence of the field is mainly to increase the random velocity or temperature of the electrons, in addition to causing a relatively slow drift in the direction of the field. If it is assumed that the positive column ends at some surface, such as that shown in Fig. 5·52, the diffusion of the electrons out of it may be found, in principle, by solving the diffusion equation. The electron density n is subject to the boundary conditions that $n = 0$ at the walls of the cone, and $n = f(r,z)$ at the edge of the discharge, r = radial and z = axial dimensions. While this cannot be solved formally, it can be realized intuitively that, if the discharge ends at a distance from the gap larger than the diameter of the cone, the number of electrons reaching the gap will vary by a factor of about 30 for every increase of this distance by one diameter.[1] Thus, if the cone is large, the permissible *absolute* error in location of the keep-alive electrode for a given tolerance in n_0 is larger than that for a small cone by about the ratio of the cone diameters.

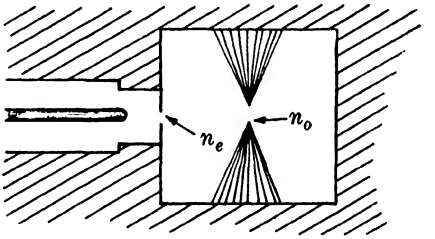

FIG. 5·53.—Side-arm keep-alive electrode.

It is evident, on the basis of these considerations, that it would be very difficult to make a coaxial keep-alive electrode for a 1.25-cm tube because of the small size of the cones in such a tube. To avoid these difficulties, the structure illustrated in Fig. 5·45*b* was evolved. In this

[1] This number is arrived at by analogy with the attenuation of electromagnetic waves in waveguides beyond cutoff.

construction, the electrode is placed in a fairly large hole at the side of the cavity, and the exit hole through which electrons diffuse is $\frac{1}{16}$ in. in diameter. In this design, the number of electrons entering the cavity, n_e, must be much larger than the number finally reaching the gap, n_0. Because the electric field is so weak in the outer regions of the cavity, this large value of n_e has very little effect upon low-level transmission, Fig. 5·53.

The electrons spread out from the exit post according to the diffusion equation, subject to the boundary conditions $n = 0$ at all metal surfaces. Because the gap is partially shielded by the cones, and because of the distance from the wall to the gap,

$$\frac{n_0}{n_e} \ll 1.$$

Besides the advantage of greater ease of construction in small tubes, the side-arm electrode has the further advantage of allowing greater freedom in the design of the r-f gap. The design of the 1B26 TR tube required sharp points on the cones in order to bring the leakage power down to a usable level. This would have been impossible on the cone surrounding a coaxial keep-alive. Similarly, in the 1B50 tube, the use of a side-arm keep-alive made possible a design with the points of the cones overlapping, Fig. 5·54. This tube has nearly constant leakage power over the entire tuning range because the gap *length* remains unchanged as one cone moves axially relative to the other.

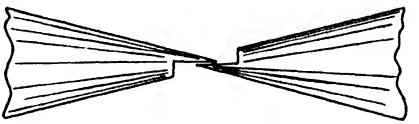

FIG. 5·54.—Overlapping gap of 1B50 TR tube.

The coaxial keep-alive electrode and the side-arm electrode, Fig. 5·45*a* and *c* have found equal use in bandpass TR tubes. The reasons for choosing one or the other of these electrodes are still not clear. The side-arm electrode must be accurately aligned perpendicular to the electric field in order to avoid excessive low-level losses. On the other hand, the coaxial electrode must be carefully aligned within the cone to prevent short circuits. Neither of these difficulties is insuperable, and sufficiently close tolerances can be maintained with proper jigging of the assembly.

Historically, the side-arm electrode was the first to be used in bandpass tubes. A discharge is maintained between it and the ends of the electrodes or cones forming the r-f gap. The resonant elements of the bandpass tube have low Q's, $Q_{L2} \approx 4$ as compared with 300 for a high-Q tube. As a result, the transformation ratio is low, and n_0 can be much larger than in a high-Q tube for the same low-level interaction. This is fortunate, since it takes a large n_0 to reduce spike leakage energy to a

safe value. A 200-μa discharge directly to the ends of the cones produces about 0.05 db change in low-level transmission. Because the cones are the anode of the discharge, n_0 is practically independent of the distance of the keep-alive electrode from the r-f gap, at a constant current level.

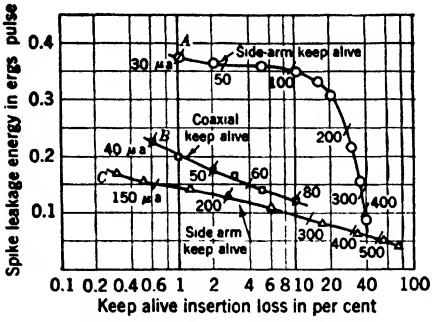

FIG. 5·55.—Efficiency of keep-alive discharges.

In the many 10-cm bandpass tubes tested, including those used for experimental purposes and those produced commercially, there is no record of serious keep-alive interaction for this style of electrode with discharge currents of less than 250 μa.

In bandpass tubes it has been observed that the coaxial keep-alive has as much as 8 db of interaction when pushed too far forward. Thus, it apparently can produce a larger value of n_0 than can the side-arm electrode. Tests made on a 3-cm bandpass tube indicate less spike leakage energy for a given interaction for the coaxial than for the side-arm electrode, Fig. 5·55. Just why this is so is not immediately obvious, since interaction is apparently a measure of n_0, unless the electrons from the side-arm electrode are loading the fringing field of the gap rather than the central portion where breakdown takes place. Comparison, in the 1B55 bandpass tube for 8.5 cm, of the coaxial and side-arm electrodes indicated little difference between the two.

5·18. Keep-alive Characteristics.—Since the gas filling of a TR tube is determined by the leakage power and the recovery characteristics, the characteristics of the d-c discharge are more or less determined by the r-f discharge characteristics. Figure 5·56 shows the dependence of the keep-alive voltage drop upon the gas filling of a 1B24 TR tube. The characteristics of other high-Q TR tubes are not very different from these.

In Sec. 5·7 it was pointed out that no direct measurements had been made of the electron density n_0 produced in the r-f gap by the keep-alive discharge. This is a serious lack in the understanding of spike phenomena. From the point of view of TR-tube design, however, it is sufficient to measure spike energy and keep-alive interaction. Thus, an experimental approach to the design of a tube would be, first, to choose an r-f circuit which has the desired Q or bandpass characteristics, and which has a short r-f gap. Then, under high-power test, the gas pressure would be varied, and W_s and P_a measured. For each gas pressure, the keep-alive current should be brought to a level that results in about 0.01 db of interaction. If the current required to obtain this is too high or too

low, the position of the keep-alive electrode should be readjusted. Such a procedure would allow truly optimum leakage power characteristics to

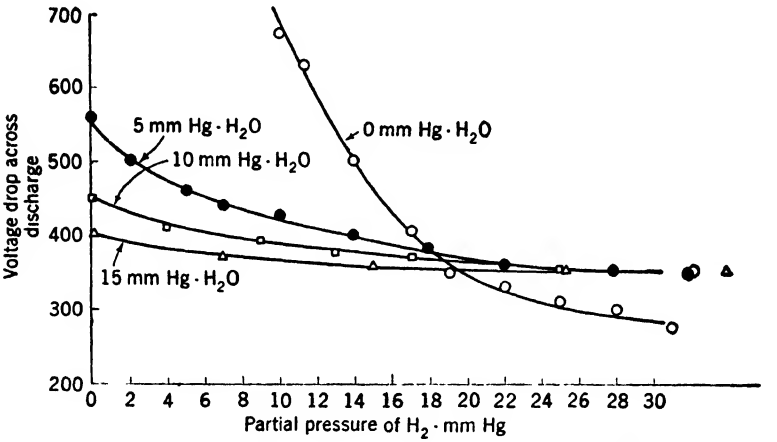

FIG. 5·56.—Keep-alive pressure-voltage characteristic of 1B24 TR tube. The discharge current varies from 100 to 150 μa.

be obtained, but it requires an adjustable keep-alive electrode. Although this procedure has not been followed in the past, it appears that the use of such an electrode would result in an appreciable economy in development time and in the number of experimental tubes required. It would, furthermore, establish tolerances upon electrode location. In the past, such information has usually been obtained by making a number of different tubes with varying electrode locations, and measuring W_s and interaction.

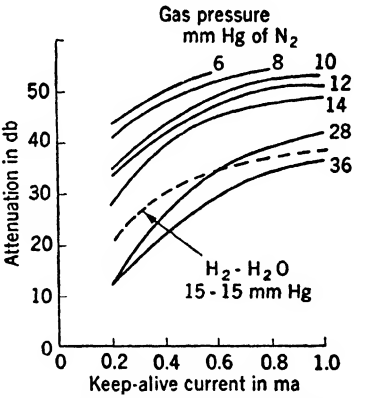

FIG. 5·57.—Low-level signal attenuation caused by keep-alive discharge in modified 1B24 TR tube.

The interaction, or low-level insertion loss, can be pushed to extreme limits by moving the coaxial electrode of a 1B24, or similar tube, closer to the r-f gap, by enlarging the hole in the end of the cone, and by changing the gas content of the tube. In fact, d-c-controlled r-f switches have been made out of 1B24 and 1B27 TR tubes. In these, a keep-alive current of 300 μa produces an r-f attentuation of about 40 db.[1] In a 1B24,

[1] Ting-Sui Kê and L. D. Smullin, "A Low Power X-Band R-f Gas Switch," RL Report No. 841, Oct. 19, 1945; T. S. Kê, "Note on a Low Power S-band Gas Switch," RL Report No. 979, Dec. 10, 1945.

filled with 15 mm Hg each of H_2 and H_2O, an attentuation of about 25 db could be obtained with currents of about 1 ma if the keep-alive electrode were in the position to give greatest interaction. If the gas content is changed to N_2, attentuations of 40 db are obtained. Figure 5·57 shows the variation in attentuation with keep-alive current for various gas fillings. It should be noted that high interaction is obtained only with *negative* keep-alive polarities.

5·19. Keep-alive Discharge and Tube Life.—Under the action of the d-c glow discharge, there is a continual modification of the gas content of the tube. This change is the result of two different mechanisms: sputtering, and chemical reaction.

Sputtering is a process in which the cathode is heated by positive-ion bombardment to the point where particles are boiled out of the cathode and finally condense on the anode or on the tube walls. These particles may collide with gas molecules and carry these molecules with them to the tube walls, where the gas is trapped. Thus, the rate at which metal is sputtered from the cathode is a measure of the rate at which the gas pressure will be reduced in a given tube. Table 5·5 gives the normal cathode fall[1] in H_2 and A, for a number of metals, and the rate of sputtering for the same metals in H_2 with a cathode fall of 850 volts.

TABLE 5·5.—NORMAL CATHODE FALL IN A AND H_2, AND SPUTTERING RATE IN H_2 (CATHODE FALL = 850 V) FOR VARIOUS METALS

Metal	Normal cathode fall		Sputtering rate in H_2, μgr/a. sec
	A	H_2	
Al	100v	170v	8
Ag	130	216	205
Au	130	247	130
Cu	130	214	84
Fe	165	250	19
Mg	119	153	2.5
Ni	131	211	18
Pt	131	276	
Sn	124	226	55
W			16

The only metals that have been used for the keep-alive electrode are tungsten and Kovar. Examination of the table indicates that, in regard to sputtering, aluminum might have made an excellent keep-alive electrode. It cannot, of course, be sealed to glass, and would have to be welded to a suitable glass-sealing metal such as tungsten or Kovar. To prevent oscillations, the electrode must be covered with an insulating

[1] Cobine, *Gaseous Conductors*, McGraw-Hill, New York, 1941, Chap. 8.

material. Tungsten or Kovar electrodes are simply glassed right down to the end. If aluminum were used, it could be covered with a suitable insulating cement such as Insalute cement. To the author's knowledge, no tests have been made with aluminum keep-alive electrodes; but the considerations presented here might warrant such tests.

Tungsten is a very unfortunate choice as a keep-alive electrode for TR tubes containing water vapor. Many years ago lamp manufacturers discovered the so-called "tungsten water cycle" and learned that they could get long life from their tungsten filaments only if water vapor were carefully kept out of the lamps. This phenomenon involves the formation of an unstable tungsten oxide and the release of atomic hydrogen in the discharge. The oxide diffuses through the tube, and condenses on the walls. In time, however, the oxide is reduced and the oxygen and hydrogen recombine to form water vapor. Thus, although the water serves as a carrier to transport tungsten away from the cathode or filament, it is not consumed. The amount of tungsten carried away in this manner is not large enough to destroy the keep-alive electrode in any reasonable length of time. It is sufficient, however, to form filaments or "hairs" and, in a small tube such as the 1B24 or 1B26, these may actually bridge the gap between cathode and anode and short-circuit the discharge. Exactly what determines the rate of this process is not known; but short circuits have developed after operating times of only 10 to 100 hours at a discharge current of 100 μa. The effect is most serious, and was first noticed, in TR tubes with insulated keep-alive electrodes. Because of this, Kovar is used in the tubes with glassed keep-alive electrodes, the 1B24, 1B26, 1B27, and the various bandpass tubes.

5·20. Keep-alive Circuits and Power Supplies.—The large majority of all radar sets have used simple, d-c keep-alive discharges. These are energized either from a negative voltage already available or from a simple auxiliary half-wave rectifier, suitably filtered. The voltage available must be 750 to 1000 volts negative, on open circuit, and the current is limited to 100 to 200 μa.

In a few cases, a device known as prepulsing is used. In this device a pulse of current of the order of a milliampere is passed through the discharge a few tenths of a microsecond before the transmitter pulse, and is made to overlap it. This pulsed discharge may be used alone or in conjunction with a low-current d-c discharge. In this way, a large value of n_0 can be produced in the gap and the spike energy greatly reduced. The fact that the interaction may also be large is unimportant, since it occurs only for a few tenths of a microsecond at the very end of the receiving period.

Let us first consider the external circuit of the d-c discharge. The dynamic resistance, or slope of the keep-alive discharge characteristic is

small compared with the static resistance obtained by taking the quotient of the operating voltage and current (see Fig. 5·50). In the first approximation, it may be assumed that the dynamic resistance is zero; that is, the discharge is a constant-voltage device. If the voltage drop is V_a, the current is I, the open circuit voltage of the source is V_0, and the series limiting resistance is R,

$$I = \frac{V_0 - V_a}{R} = \frac{\Delta V}{R}$$

$$\frac{1}{I}\frac{dI}{d\Delta V} = \frac{1}{\Delta V}. \tag{74}$$

Thus, if either V_0 or V_a is subject to fluctuations caused by power-line variations or differences in individual TR tubes, the percentage of current change for a given voltage change will be inversely proportional to $V_0 - V_a$. It therefore appears desirable to make ΔV large by increasing V_0, and to maintain the proper current by a corresponding increase of R.

Most high-Q TR tubes with H_2 and H_2O fillings have a keep-alive voltage drop $V_a \approx 400$ volts, and the operating current I is between 100 and 200 μa. However, because of manufacturing tolerances, V_a is allowed to vary between 350 and 475 volts in new tubes, and during the life of the tube it may increase by 50 to 100 volts. If the design point is at $V_a = 400$ volts and $I = 100$ μa, with $V_0 = 700$ volts, I will fall to 67 μa if V_a should rise up to 500 volts. If $V_0 = 1000$ volts, I will fall to 83 μa for a similar increase in V_a. This might be carried to the extent of making V_0 very large, and thus reduce still further the variation in I with changes in V_a. At the operating conditions assumed above, if $V_0 = 1000$, $R = 6$ megohms. Since the voltage required to fire the gap initially is about 600 volts, it would require a surface leakage of 8 or 9 megohms to reduce the voltage at the tube to a point where it would never fire. Under military operating conditions, the accumulation of dirt, moisture, or salt on insulating surfaces might easily result in leakage resistances as low as 10 or 20 megohms. On this basis 1000 volts is usually considered the maximum safe value for V_0. In large, fixed, land installations, where the equipment is indoors, higher values of V_0 may of course be used.

5·21. Prepulsed Keep-alive Circuits.—It has been indicated that the d-c discharge changes the gas content of the tube, and thus affects the tube life. In fact, in high-Q TR tubes, the tube life is almost independent of the r-f discharge, and is inversely proportional to the current in the keep-alive discharge. It thus appears desirable to reduce the average keep-alive current to as low a level as possible. One way of doing this is to turn off the discharge between pulses, and to turn it on only in time to get the required value of n_0 in the gap when the transmitter pulse starts. Depending upon the repetition rate, the average current would

be reduced by a factor of about 1000 if the instantaneous value of the current were kept constant, and therefore the tube life would be increased by a very large factor.

If the instantaneous current is made 10 or 20 times the normal d-c value, the average current will still be 50 to 100 times less, the increase in tube life will still be substantial, but n_0 will be increased and the spike energy decreased. If this double effect, longer life and lower W_s, is to be utilized, a knowledge of W_s as a function of keep-alive current is necessary. Unfortunately, no detailed information of this kind exists. From 50 to 200 or 300 μa, the spike leakage energy is nearly constant in most high-Q TR tubes. Apparently n_0 remains constant in this range. This may indicate that the discharge extends back, *away* from the r-f gap, with increasing current in this range. With currents of the order of 1 to 5 ma, W_s is 7 to 10 db lower than at normal operating currents in high-Q tubes with coaxial keep-alives.

This reduction in W_s is substantial, but prepulsing has found little application. There is one immediate objection to a prepulsed discharge in which no continuous discharge is maintained, that is, it is incapable of protecting against high-power pulses from nearby radars operating in the same frequency band, because the prepulse is synchronized to its own transmitter, but not to nearby transmitters. In military or naval operations, a large number of radars may be operating in a restricted area. Once an aircraft is aloft, unless a group of planes are flying in tight formation, there is little probability of crystal burnout by a nearby radar. On the ground, however, with planes lined up close together, mutual burnout can be a serious problem.

Because of the danger of random pulses causing burnout, the TR tube must be capable of protecting crystals continuously with a low-current d-c discharge. If the TR tube can already protect crystals with a d-c discharge, it seems that little is to be gained by reducing W_s another 10 db by means of a prepulse superimposed on the d-c discharge. Only by extensive life tests on a large number of TR tubes and crystals can it be shown whether or not any appreciable improvement in crystal protection can be obtained by reducing W_s.

All TR tubes now in use afford good crystal protection with a d-c keep-alive and, although occasional "unexplained" burnouts do occur, the same tube will again protect crystals for several hundred hours more. If these burnouts are caused by rare bursts of large spike leakage energy, they might be eliminated by the use of prepulsing which not only reduces the average value of W_s, but also reduces the variation in energy between individual spikes.

It is worth while to examine some of the circuits used to produce a prepulse. The two important variables to be considered are the relative

timing of the prepulse and the transmitter pulse, and the magnitude of the prepulse current. Measurements made on a 724A TR tube using a prepulse of $\frac{1}{10}$-μsec duration superimposed upon a 100-μa d-c discharge gave the results shown in Fig. 5·58. If the prepulse starts *after* the transmitter pulse, it has no effect on W_s. When it leads the transmitter by about 0.1 μsec, as in this experiment, W_s is 8 db down from its d-c value. As the lead is increased beyond 0.1 μsec, the number of electrons furnished to the r-f gap by the discharge becomes smaller, and W_s approaches the d-c level. The increase in W_s to values 12 db greater than normal when the prepulse leads by 5 to 7 μsec, was caused by a positive overshoot on the prepulse, which turned off the d-c discharge and reduced n_0 momentarily.

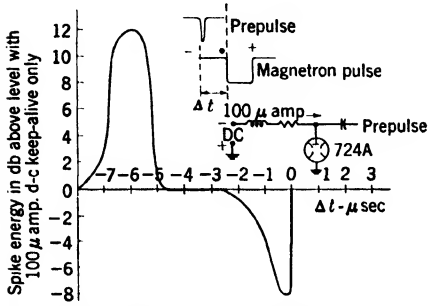

FIG. 5·58.—Effect of prepulse timing on spike energy of a 724A TR tube.

A prepulse must be added to a d-c circuit in such a way that the pulsing circuit has little or no effect upon the d-c discharge. Normally, to prevent relaxation oscillations, a resistor of $\frac{1}{2}$ to 4 megohms is put right at the keep-alive cap on the TR tube. To produce a prepulse current of several milliamperes with a reasonable voltage, there must be little or no limiting resistance between the source and the tube. Thus, if the prepulse circuit is connected between the d-c limiting resistor and the electrode, the stray capacitance of the prepulse circuit must not be large enough to allow relaxation oscillations to take place. Figure 5·59 indicates such a connection with a 10-$\mu\mu$f capacitor used to isolate the two circuits.

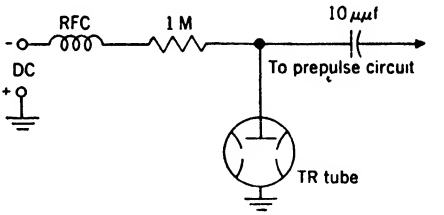

FIG. 5·59.—Circuit for prepulsing TR tube.

The prepulse voltage may be obtained in a number of ways. It may, of course, be generated by a blocking oscillator or similar circuit properly timed with respect to the transmitter. This is possible only if the transmitter is triggered from some external source that can also be used to trigger the prepulser. If a "self-synchronous" transmitter modulator is used, such as a rotary or series spark-gap modulator, there is an uncertainty in the time between successive pulses of perhaps 50 μsec. Since all trigger voltages in such a set are derived from the transmitter pulse, there is no way of triggering a prepulser so that it will *lead* the transmitter

by a fraction of a microsecond. In such cases, and even in the case of synchronous transmitters, it is desirable to use some voltage within the modulator that leads the voltage on the transmitter tube (magnetron) by the proper amount. The primary winding of the stepup pulse transformer that drives the magnetron is a convenient source of such a voltage. It is possible, by taking advantage of the finite rise time of the modulator pulse $\approx \frac{1}{10}$ μsec, and the magnitude of the pulse (several thousand volts on the primary), to produce a high-current pulse in the TR keep-alive circuit that leads the r-f output power of the magnetron by about $\frac{1}{20}$ μsec.

Figure 5·60 illustrates a convenient way of obtaining the necessary prepulse voltage from the pulse transformer by means of a high-voltage capacitor made from a length of high-voltage pulse cable. The pick-off

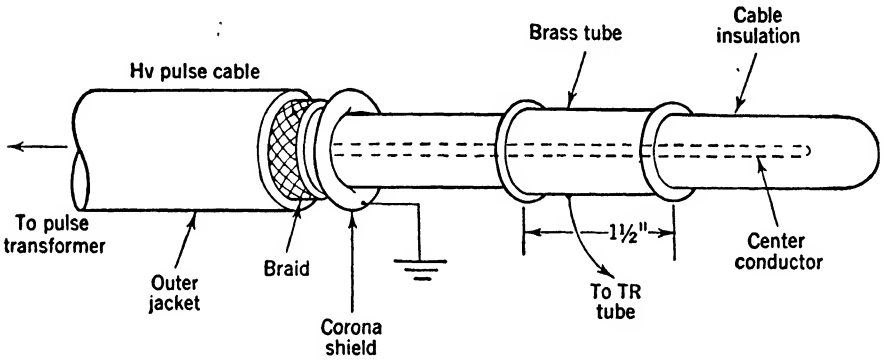

FIG. 5·60.—Voltage divider for prepulsing TR tube.

tube has a capacitance of about 5 μμf to the high-voltage lead. Thus the total *charge* that can flow in the prepulse circuit is $q = CV$ where V is the maximum value of the pulse voltage. In a typical high-power set, $V = 10$ kv, $C = 5$ μμf, $q = 5 \times 10^{-8}$ coulomb. If the rise time is 0.1 μsec, the average current is $\frac{1}{2}$ amp (averaged over 0.1 μsec), and the average d-c current is 25 μa. It is important to keep all the time constants of such a circuit as small as possible, since there is probably less than 0.05 μsec that can be wasted in charging the various circuit components.

Another method of reducing the spike leakage energy has been suggested many times. This method is to insulate one of the electrodes forming the r-f gap through a suitable r-f choke, and to strike a d-c discharge directly across the gap just before and during the transmitter pulse. Such a scheme has been tested on the 1B27 TR tube, and more recently on the 3-cm bandpass tube. The results in both cases were surprising in that the spike energy *increased* by about 7 db when a d-c

current of 900 μa was caused to flow across the gap. The explanation of this phenomenon is not yet known.

Another interesting proposal is to use a radio-frequency (about 5 Mc/sec) high-voltage supply for the keep-alive. This would be used where space or weight did not permit the use of a transformer, rectifier, and filter for 60 or 400 cps. A single oscillator tube operated from a low-voltage supply, and a resonant transformer can furnish enough voltage and current for a TR tube keep-alive discharge. Only rudimentary tests have been made of such a system with the alternating current applied directly to the keep-alive electrode. The measured spike leakage energy was not appreciably different from that of a d-c keep-alive discharge. No attention was paid to the problem of shielding this high radio-frequency voltage and the development of simple, low-capacitance, high-voltage shielding may be very difficult, unless the oscillator and the TR tube are housed within a common shield. This proposal merits further consideration.

5·22. Radioactive Priming.—To initiate a d-c discharge, it is necessary to have a number of free electrons in the gap between the electrodes, or the voltage must be raised to a level high enough to cause field emission from the cathode. Normally there are free electrons present in a gas volume. These are released photoelectrically or by high-energy cosmic- or γ-ray particles. A TR tube, however, is usually enclosed in a light-tight metal container and is surrounded by fairly massive pieces of metal, therefore the probability of ionization by external radiation is very small. Experimental tubes that have been idle for several days become so completely inactivated that several minutes may elapse between the application of the keep-alive voltage and the striking of the discharge. The length of time is determined by the probability of an ionizing ray of sufficient energy passing through the tube.

The TR tube will not, in general, protect crystals if the keep-alive discharge is off; and, in particular, the very first pulse of leakage energy when the transmitter is turned on will be extremely large. Thus, rapid and reliable firing of the keep-alive under all circumstances must be ensured. This can be accomplished by producing a small amount of ionization within the tube by means of a radioactive substance. Two materials have been used for this purpose: radium bromide and an artificially radioactive cobalt chloride. The radium bromide produces α-, β-, and γ-rays, whereas the cobalt chloride is only β- and γ-ray active and has a half-life of 5 years. Although this life is short compared with that of 1690 years for radium, it is ample for most purposes. The cobalt chloride has the important advantage of being completely nontoxic and it is easy to make in comparatively large quantities. During the war, it was produced by the cyclotron group of the Massachusetts Institute

of Technology. There seems to be little excuse to use the highly toxic radium salts since the artificially radioactive cobalt chloride is easily available.

In practice, the cobalt chloride is used in a water solution and diluted to a concentration that has an equivalent radioactivity of 0.1 μg of radium per drop. A drop of the solution is put on the cone adjacent to the keep-alive electrode before sealing off the tube. During the sealing-off and evacuating process, the water is evaporated. This amount of radioactivity is sufficient to guarantee the starting of the tube within less than 5 sec after the application of the voltage.

5·23. Tube Life and Gas Cleanup.—The life of a TR tube is determined by the rate at which the gas content changes. This rate is determined by the action of the r-f or the d-c discharge. With continued operation either the leakage power becomes too large or the recovery time becomes too long. Occasionally, a tube may be found in which the discharge has deposited a thin layer of metal upon a glass surface and thereby has decreased the low-level transmission. However, this phenomenon is so rare as to be considered a freak.

There is no quantitative information on the rate at which the r-f discharge changes the gas content of the tube. It is known that a high-Q tube operated without a keep-alive discharge may be run for several thousand hours without seriously changing either its leakage power or its recovery-time characteristics. The same tube will have a life of only 500 to 1000 hours with a d-c keep-alive discharge current of 100 μa even if there is no r-f discharge. The usual keep-alive voltage drop is about 400 volts and the power dissipated is about 40 mw. The power dissipated in the r-f discharge is equal to the geometric mean of the transmitter and the arc leakage power. Typical values for these are 100 kw and 40 mw, respectively, and therefore the pulse power dissipated in the discharge is about 60 watts. If a duty ratio of 1 to 1000 is assumed, the average power dissipated in 60 mw. Thus, the average powers dissipated in the r-f and d-c discharges are roughly equal, and the difference in the rate of gas cleanup must be attributed to some other factor.

The process that takes place most rapidly in TR tubes is the cleanup of the water vapor. This apparently takes place by chemical action, since the copper cone that serves as the anode for the keep-alive discharge becomes oxidized, and the partial pressure of hydrogen increases[1] as that of the H_2O decreases.

The process involved is probably the following one. Under the action of the discharge, OH ions are produced. In the d-c discharge of the keep-alive, these ions drift across to the anode. They are highly

[1] W. G. Guldner, "The Change in Composition of the Gas Present in a 721A Type Tube as a Result of Operation," BTL MM-43-120-98, Sept. 22, 1943.

active, and therefore, they react with the copper, forming copper oxide and releasing atomic hydrogen. In the r-f discharge the massive ions are unaffected by the electric field and their motion is completely random; the number reaching the electrodes will be roughly proportional to the solid angle subtended by the electrodes. It is probably this difference in the motion of the ions that makes the d-c discharge so much more effective than the r-f discharge for destroying the water vapor.

The r-f discharge across the low-Q input window of the pre-TR, low-Q ATR, or bandpass TR tubes is much more intense than in the high-Q tubes. When the transmitter power is 10^6 watts, the pulse power dissipated in a 10-cm pre-TR tube (1B38) is about 7 kw. Furthermore, the exposed electrode area, the area of the tube walls, is much greater than in the high-Q tubes. In these tubes, the r-f discharge plays the major role in the decomposition of the water vapor.

An example of the comparative activity of the d-c and the r-f discharges is furnished by a conventional duplexer in which the same TR cell is used for both the TR and the ATR switches: a 721A tube, for instance. In the TR tube a keep-alive discharge is maintained and, as a result, after about three hundred hours the tube will have to be replaced, because the recovery time will have become too long. In the ATR tube, on the other hand, no d-c discharge is maintained, and although the r-f power dissipated in the discharge is about 50 per cent greater than that in the TR tube, the recovery time remains unchanged even after 1000 to 2000 hours of operation.

An obvious way to increase the life of a TR tube is to increase the volume of gas contained in it, since the life of a tube is proportional to its volume of gas. In a cell TR tube, the volume is limited rather severely by the desired tuning range and by the cavities into which it must fit. Integral-cavity TR tubes, however, may have protuberances on them since there is no external cavity into which the tube must be clamped. Table 5·6 lists some of the more common high-Q TR tubes and gives the volumes of their envelopes.

TABLE 5·6.—VOLUMES OF VARIOUS HIGH-Q TR TUBES

Tube	Type	Volume, cm³
724A/B	3-cm cell	1.5
1B27	10-cm cell	5.3
1B26	1.25-cm integral cavity	18
1B24	3-cm integral cavity	19
721A/B	10-cm cell	25

It is to be noted that the 1B27, which has to a large extent replaced the 721A in new equipments, has only about one-fifth the volume of the

721A. This reduction in volume resulted from the desire to make the tube tune down to 8.0 cm or less, whereas the 721A would go only as low as 8.7 cm; it also resulted from the fact that the tuning mechanism occupies one end of the tube and is at atmospheric pressure, which reduces the effective volume to two-thirds that of a fixed-tuned tube of the same size. This reduction in volume was realized when the tube was first introduced, but the advantages of smooth, single-knob tuning, and the wide range of frequencies that could be covered with various cavities made it seem worth while to examine the possibility of artificially increasing the tube life. A similar problem had been faced in the case of the 1B24 and 1B26 TR tubes. In these tubes the cavity proper is very small, 1 cc or less; however, the use of an external reservoir increased the gas volume to about 25 cc, and resulted in excellent tube life. Such a solution was not possible for the 1B27 tube.

5·24. Chemical Reservoirs.—The life of the 721A tube was barely long enough to make it a usable tube, for, after approximately 300 hours of operation, the recovery time became excessive. The 1B27 tube, with only one-fifth the volume, would be completely useless if its life were correspondingly reduced. R. Levine suggested that a chemical water reservoir in the form of a hygroscopic salt be incorporated into the 1B27 tube. In this way a large quantity of water could be stored in a few milligrams of salt and the effective volume of the tube would be greatly increased. An investigation of pertinent data was made to determine if there were any salts with suitable characteristics. The most important characteristic to be considered was the variation of vapor pressure with temperature. Military conditions require tubes to withstand temperatures of −55°C to 100°C, and to give satisfactory operation within a range of −10°C to 100°C. Therefore, a hygroscopic salt, in order to be useful, must have a maximum vapor pressure of 20 to 30 mm Hg at 100°C to prevent the leakage power from increasing to the point where crystal burnout is likely to occur. On the other hand, the vapor pressure at −10°C must be of the order of a few millimeters to keep the recovery time reasonably short (see Fig. 5·34).

Data on various salts indicated that above 40°C, the increase in vapor pressure was so rapid as to make most of the salts useless.[1,2] Figure 5·61 is a typical curve of H_2O vapor pressure plotted against temperature. Nickel and cobalt perchlorates have satisfactorily flat pressure characteristics, but their explosive nature would probably decrease rather than increase the life of the tube.

[1] *International Critical Tables*, McGraw-Hill, 1933.

[2] R. Levine, F. L. McMillan, "Chemical Methods for Maintaining the Partial Pressure of Water in TR Tubes," RL Report No. 593, July 13, 1944.

Water can be obtained by an equilibrium reaction with H_2O as an end product, for example

$$TlOH \rightleftarrows Tl_2O + H_2O.$$

Here too, however, the rate of evolution of H_2O is too great at temperatures above 60°C.

Finally, adsorbents and absorbents were considered. In the first group are activated alumina and silica gel. Figure 5·62 gives the pressure-temperature characteristics for these substances. The silica gel was 14 to 20 mesh, and was dried in a vacuum at 100°C before being charged by exposure to an atmosphere of 23 mm Hg of H_2O at 90°C. This charge gave a water-vapor content for the silica gel of 2.6 per cent by weight. The activated alumina was 8 to 14 mesh, and after having been dried at 100°C was charged in an atmosphere of 18 mm Hg of H_2O at 98°C; the water-vapor content of the alumina was 1.33 per cent by weight.

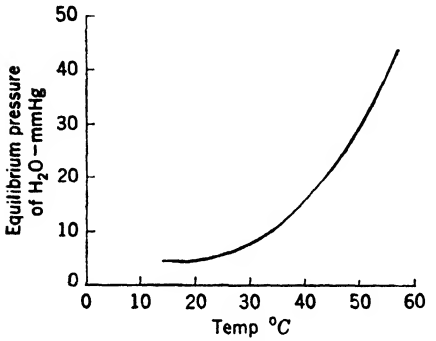

FIG. 5·61.—Vapor pressure as a function of temperature for a typical hydrate: $NiCl_2 \cdot 4H_2O = NiCl_2 \cdot 2H_2O + 2H_2O$.

Although far from perfect, both of these substances showed enough promise to warrant life tests in TR tubes. The 1B27 TR tubes were used with 0.5 g of silica gel. If the gel was charged with 22 mm Hg of

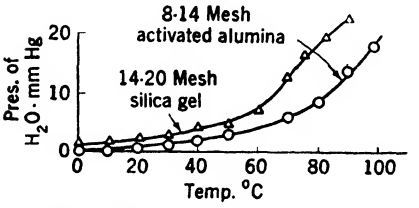

FIG. 5·62.—Vapor pressure of alumina and silica gel.

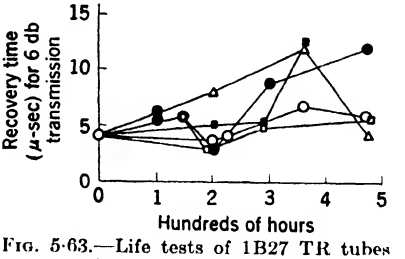

FIG. 5·63.—Life tests of 1B27 TR tubes using silica-gel reservoirs.

H_2O at a temperature above 90°C, at room temperature the recovery time was poor. On the other hand, charging with the same pressure at 75°C caused excessive leakage power at 100°C. Tubes which were charged to 22 mm Hg of H_2O at 85°C protected crystals at 100°C and showed good recovery time at 5°C.

Figure 5·63 shows the time after the transmitter pulse which is required for the low-level transmission through the TR tube to climb to

within 6 db of its cold value, for five tubes. These tubes were operated at 500-kw pulse power with a duty ratio of 1 to 2500 and with a keep-alive current of 150 μa. During the last 200 hours of these tests, the tubes were maintained at a temperature of 100°C. Although the recovery time and the leakage power were satisfactory for the duration of the tests, it was found that the unloaded Q of the TR tubes and the cavity had fallen from 2500 or 3000 to 1400 or 1900, and the copper cones had become covered with a reddish copper oxide. Those tubes charged initially with the most water showed the largest change in Q_0.

At various times, a number of other chemicals and other methods of storing water were proposed. Silver oxide is an unstable compound that maintains an equilibrium pressure with O_2; and this oxygen could be used as the electron-capture agent. Copper sulphate with one molecule of H_2O, is a very stable compound that gives off its water very slowly; (no quantitative data for copper sulphate are available). M. D. Fiske suggested and later used asbestos as an absorbent; it is similar to silica gel but has a flatter vapor-pressure curve. Some evidence exists that zinc chloride, which is sometimes present in TR tubes as a solder flux, may give off Cl_2 slowly. If zinc chloride were used in a tube with brass walls, such as a 10-cm bandpass TR tube, an equilibrium would be reached as the released chlorine reacted with the tube walls to form $ZnCl_2$ again. With the exception of the asbestos, these chemicals have been the subject of speculation, but have not been used in definitive experiments.

5·25. Inert Coatings.—The chemical reservoirs of H_2O, in addition to their unsatisfactory pressure-temperature curves, are undesirable because the continual evolution of H_2O results in the formation of a thick copper oxide on the tube electrodes. This results in a lower Q_0, and the H_2 pressure is continually increased.

The preferred method of improving the life of the tube is to maintain the H_2O pressure constant by preventing a reaction with the electrodes. This was treated in a report by Guldner[1] of the Bell Telephone Laboratories, and was applied to the 1B27 tube by H. J. McCarthy of the Sylvania Electric Products Co. The early tubes that were tried had a layer of black copper oxide (CuO) on the cones of the tube. The oxide was made with a commercial alkaline solution "Ebonol." These tubes operated well except that, after about one hundred hours of operation, the recovery time *decreased* and the leakage power *increased*, thus indicating an increase of the partial pressure of H_2O. Simultaneously, the black oxide was reduced in patches to a red cuprous oxide, Cu_2O.

The other tubes were made with a coating of Cu_2O inside the cone where the keep-alive electrode is located. These tubes showed a sub-

[1] W. G. Guldner, "The Change in Composition of the Gas Present in a 721A Type Tube as a Result of Operation," BTL MM-43-120-98, Sept. 22, 1943.

stantially increased life, as long as 700 hours with good recovery-time and leakage-power characteristics. Figure 5·64 shows the recovery time, keep-alive voltage drop, and total leakage power as a function of operating time for a typical 1B27 tube with a Cu_2O coating.

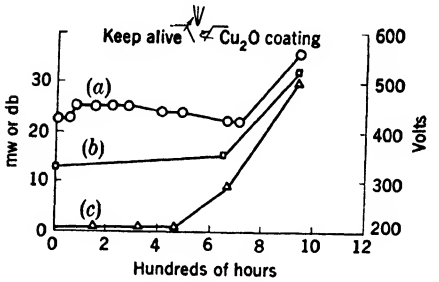

FIG. 5·64.—Life test of 1B27 TR tube; (*a*) keep-alive voltage drop; (*b*) total leakage power, mw, 1 μsec pulses; (*c*) loss in signal, db, 6 μsec after transmission pulse.

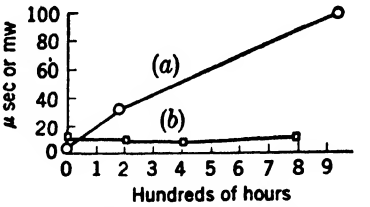

FIG. 5·65.—Life test of 721A TR tube with untreated cones; (*a*) recovery time in μsec for −6db transmission; (*b*) total leakage power in mw.

Figure 5·65 is a plot of recovery time and leakage power for an unoxidized 721A TR tube. Figure 5·66 is a similar plot for a 721B tube which is the successor to the 721A, and which has oxidized cones.

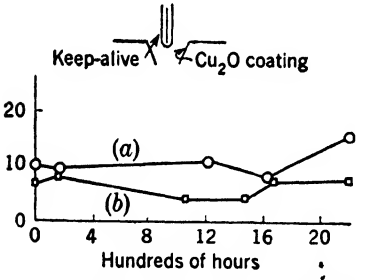

FIG. 5·66.—Life test of 721B TR tube; (*a*) total leakage power in mw; (*b*) recovery times in μsec.

A peculiar feature of these tubes is the fact that the leakage power and recovery time are constant up to the end of life, but then suddenly increase rapidly. In the unoxidized tubes, the recovery time increases continually from the time the tube is first turned on. A similar phenomenon has been observed in Geiger-Mueller counter tubes with oxidized anodes in which, at the end of life, there is a rapid transition from normal operation with good quenching to complete failure to quench.

Since the development of the Cu_2O coating, it has been found that gold-plating the copper cones is almost as effective as the Cu_2O in preventing cleanup of the water vapor. Other dense, inert coatings such as monel metal should also prove effective. Although the cuprous-oxide and gold-plate techniques have multiplied the lives of the 1B27, 721B, and the 3-cm bandpass TR tube many times, they have not done so for the 3-cm cell TR tube, the 724B. The life of this tube has a maximum value of 250 to 300 hr. Then, no matter how the cones are treated, the leakage power becomes excessive. No explanation exists for this

difference; it may result from the cleanup of the gas by sputtering. A better understanding of this problem could be obtained if life tests were run with a manometer sealed to the tube so that the partial pressure of H_2 and H_2O could be continually checked. The two pressures may be obtained by observing the total pressure and then freezing the H_2O to get the H_2 pressure.

The life characteristics of the 1.25-cm and 3-cm high-Q TR tubes are quite different from those of the 10-cm tubes. In the 10-cm tube, the recovery time is usually the limiting factor. In the higher-frequency tubes, diffusion plays a much stronger role in the recovery process than it plays in the larger 10-cm tube, and consequently the recovery time is less sensitive to the amount of water vapor in the tube. The 1B24 3-cm tube has a volume only 0.8 that of the 721A tube; but its useful life is almost six times as great, although no attempt is made to inhibit the H_2O cleanup by inert coatings. Figures 5·67 and 5·68 are curves of leakage power and keep-alive voltage drop during the lives of typical 1B24 and 1B26 TR tubes. The recovery time after 2000 hours of operation is only 5 to 10 μsec for $T = -6$db at a transmitter-power level of 40 kw.

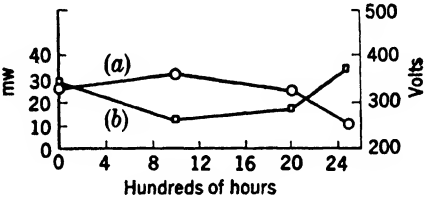

FIG. 5·67.—Life test of 1B24 TR tube; (*a*) keep-alive voltage drop; (*b*) total leakage power in mw for ½-μsec pulse.

5·26. Bandpass and Pre-TR Tubes.—It is the intense r-f discharge across the low-Q input window that plays the dominant role in changing the gas content of the bandpass and the pre-TR tubes; the keep-alive discharge has almost no effect. The volumes of these tubes are very large: the 1B38 pre-TR tube has a cubic content of 110 cc and the 1B58 bandpass TR tube has a volume of about 400 cc, whereas the 721B has a volume of only 25 cc. Despite this large volume, the recovery time of a 1B38 pre-TR tube *may* become excessively long in 200 to 500 hours of operation at 1-Mw pulse power with a duty ratio of 1/2500.

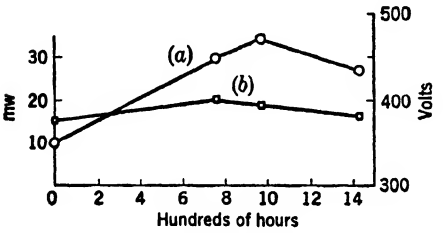

FIG. 5·68.—Life test of 1B26 TR tube; (*a*) keep-alive voltage drop; (*b*) total leakage power in mw for ½-μsec pulse.

It is important to note the qualifying verb "*may*" in the above statement. If the 1B38 pre-TR tube is filled initially with argon and H_2O, the recovery time of this tube will almost invariably become too long in

the 200 to 300 hours. Fortunately, production tubes, which were nominally filled with argon alone, could be operated with good recovery time as long as those containing argon and H_2O and very often longer. In fact, such "argon filled" tubes often showed a shorter recovery time after some time of operation. This, of course, is assumed to indicate the evolution of gas from the tube walls. Measurements[1] on commercial 1B38 tubes indicated for one of the tubes tested an increase in pressure

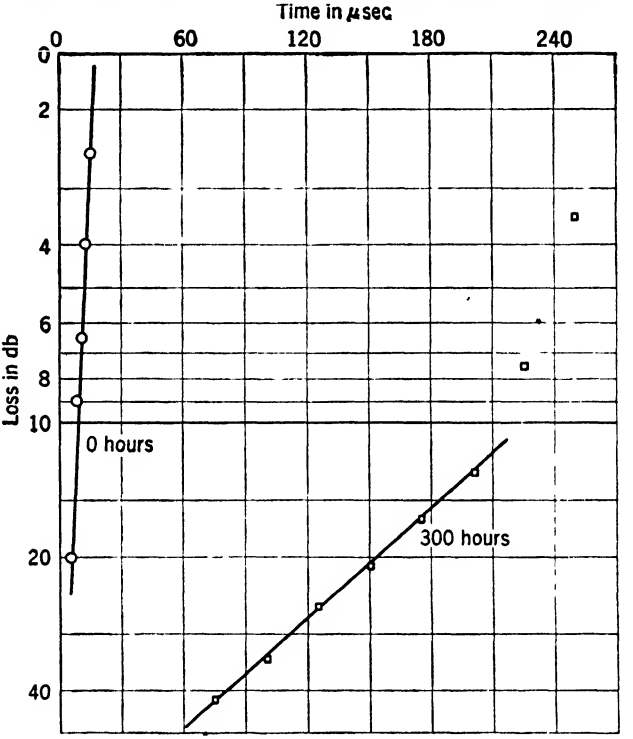

FIG. 5·69.—Recovery-time curve of 1B38 pre-TR tube filled with 5 mm argon and 2 mm H_2O.

of 15 per cent after one hour of operation; for another tube, an increase of 38 per cent after 1000 hours was measured. It is not surprising that the recovery time remained fairly short in these tubes. What is surprising is that, when H_2O is added to argon, the life is definitely limited to a few hundred hours. Figures 5·69 and 5·70 are typical curves for a 1B38 tube filled with 5 mm Hg of argon and 2 mm Hg of H_2O, and for a production tube filled with 10 mm Hg of argon.

Bandpass tubes have received comparatively few conclusive life tests. A 3-cm tube, which had been gold-plated, ran for more than 500 hours at 30-kw pulse power, with little or no change in performance. The

[1] F. L. McMillan, C. H. Pearsall, I. H. Dearnley, *loc. cit.*, Sec. 5·15.

10-cm bandpass tubes, which had no treatment of the brass walls, and with initial fillings of 5 and 3 mm Hg, respectively, of A and H_2O, ran for several hundred hours with no change of recovery time. However, the results are still inconclusive and further study of these tubes is needed. One serious consideration is whether a hard-soldered 10-cm

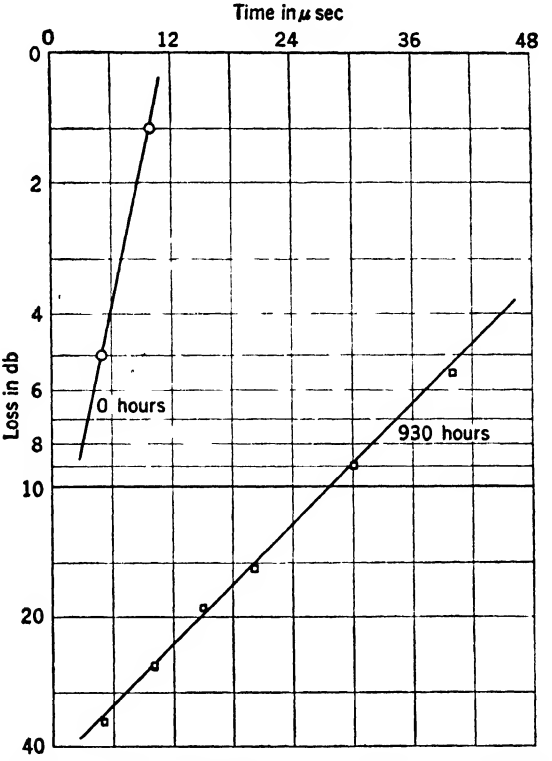

FIG. 5·70.—Example of change of recovery time with life of a 1B38 tube filled with 10 mm argon.

tube with its walls fairly well outgassed would have a shorter life than the present tube. Although the present "dirty" tubes apparently have long lives, this is an insecure basis for generalization so long as the quality and the quantity of the "dirt" are not known and are not controllable.

CHAPTER 6

THE TR AND ATR TUBES AT HIGH POWER

By L. D. Smullin and W. C. Caldwell

6·1. Introduction.—This chapter will present, in addition to a summary of the high-power characteristics of the various high-Q TR tubes, a detailed discussion of bandpass and pre-TR tubes, and of low-Q ATR tubes at high power.

The high-Q tubes to be discussed are the types 721B, 724B, 1B24, 1B26, and the 1B27. These tubes are all designed to protect the most sensitive crystals now in use and to protect them at any power level from zero up to a maximum determined by direct-coupled power, by harmonic leakage power, or by the establishment of secondary discharges which might shorten the life of the tube.

The establishment of production tests and specifications that ensured uniform tube quality was a difficult task since the tests had to be designed for use by relatively unskilled personnel, and with only the simplest possible equipment. As a result, recovery-time characteristics are specified only as a type approval test under the joint Army-Navy (JAN) specifications, whereas leakage power is a production test on most TR tubes. In some of the earlier specifications, considerable effort was made to devise "equivalent tests" that would measure certain intrinsic qualities of the tube but at the same time would not require the use of pulse and other complicated techniques. More recently, however, the tendency has been to make the production test measure the actual quantities of interest when the tube is in use, and to measure these quantities under similar conditions of use. The various tests and specifications currently used will be listed.

In the second part of the chapter, the characteristics of bandpass TR tubes, pre-TR tubes, and low-Q ATR tubes will be discussed. These tubes are characterized, in general, by the fact that their minimum operating power level is considerably in excess of that for high-Q tubes, that they can be used at considerably higher peak powers, and that their direct-coupling attenuation is practically infinite for both the carrier and the harmonic frequencies of the transmitter. This last feature was shared by only one high-Q tube, a tube developed by J. Lawson and B. Cork at the Radiation Laboratory. Because it was developed at about the same time as the bandpass and the pre-TR tubes, it was never put into production.

The last part of the chapter will present a brief discussion of manufacturing techniques and mechanical design techniques for both high-Q and low-Q tubes.

6·2. High-power Characteristics of High-Q TR Tubes.—Table 6·1 lists the various high-Q tubes and their characteristics. These characteristics are total leakage power (flat plus spike leakage for some given pulse length), arc leakage power, spike leakage energy, recovery time, keep-alive voltage drop, and gas content. The "starred" items are specified quantities.

The 721B tube, as can be observed from the table, does not have a pulsed-leakage-power specification. Instead, a measurement of the c-w leakage power is made and is converted into a quantity P_0 (or P_j). This quantity is the reactive power stored in the cavity, and is proportional to the square of the arc voltage.[1,2] Two readings are taken, one at room

TABLE 6·1.—HIGH-LEVEL CHARACTERISTICS OF VARIOUS HIGH-Q TR TUBES

Tube	Wavelength in cm	††P_a in mw	††W_s in ergs	Total leakage power† P_T in mw	P_j in va	$\Delta P_j/P_j$	Recovery time‡	Keep-alive voltage drop at 100 μa	Gas filling mm Hg	
									H_2	H_2O
721B	10	30 to 40	0.04	.....	*7 to 30	*0.5 to 0.7	*3 db at 7 μ sec	350	10	10
724B	3	20	0.05	*40 max	.....	.....	3 db at 4 μ sec	400	10	7
1B24	3	10	0.02	*30 max	.....	.....	*3 db at 4 μ sec	*325 to 450	15	15
1B26	1.25	15	0.05	*25 max	.....	.....	*3 db at 4 μ sec	*325 to 480	10	10
1B27	10	15	0.03	*25 max	.....	.....	*3 db at 5 μ sec	*370 to 480	15	10
1B50	4	.	....	18 avg	.	....	.....	300 to 425	20	20

* See paragraph 1, Sec. 6·2.

†† The 721A and 1B27 were measured with $Q_0 = 2500$, $L = -1.5$ db, matched input.

† Pulse length 0.5 μsec for all tubes except for the 1B50 where it is 0.35 μsec.

‡ The transmitter-power level is 50KW for the 721B and 1B27, 10KW for the 1B24, and 8KW for the 1B26.

temperature, and one with the water vapor frozen out at dry-ice temperature. The value P_j at room temperature, and also the change $\Delta P_j/P_j$ when the water is condensed, are specified. Together, these values give a reasonably accurate indication of the relative proportions of H_2 and H_2O in a tube of a given type, tested under known conditions. This test suffers from the fact that P_j is a sensitive function of the

[1] Samuel, McCrea, and Mumford, "Gas Discharge TR Switch," BTL MM-42-140-26, April 27, 1942.

[2] Sinclair, Garoff, Gilbarg, "Measurements of Gas Fillings in 721A TR Tubes," CESL Report No. T-18, Sept. 11, 1943.

incident power level if it is less than about 0.5 to 1 watt (see Fig. 5·23); furthermore it gives no indication of keep-alive effectiveness, and consequently no indication of spike leakage energy.[1]

The other tubes have a specified *total* leakage power at some definite line pulse power and pulse length. At the time these specifications were written, because of the complicated apparatus and techniques involved, it was not deemed advisable to attempt to measure spike leakage energy and arc leakage power separately. For some time the method for measuring total leakage power at two different pulse lengths and then computing W_s and P_a on the assumption that P_a is constant had been known, but had never been applied (Chap. 9).[2]

An attempt was made to determine the quality of the 1B27 tube, the gas content, and the keep-alive effectiveness, by measuring the total leakage power with the keep-alive on and with it off.[3] Although the specification has remained in force, the conclusion must be drawn that this test was not too successful, and that only the test with the keep-alive on had any significance. The test indicated, however, that no drastic change in production technique occurred from day to day. The specifications for the 724B, 1B24, and 1B26 tubes require only a measurement of total leakage power with the keep-alive on.

In the tunable tubes, with the exception of the 1B50 tube, the leakage power is a function of gap spacing. No particular gap length in inches is specified, but it is required that the tubes be tuned to a specified frequency in order that the leakage power measured will be truly indicative of the operating performance.

The maximum power at which these tubes may be operated is difficult to define exactly. The 1B24 tube was initially rated (unofficially) at a power near 100kw, at which level a secondary discharge is established just back of the input window. When high-power 3-cm magnetrons (200kw) became available, the 1B24 tube was tested at the higher power level. In initial tests, tubes available at the Radiation Laboratory failed after 10 to 100 hours. In all the tests the leakage power increased markedly, and in most tubes the insertion loss increased. Later, in tests on tubes of more recent manufacture and with care taken to keep solder flux and excess solder out of the cavity, tubes were run for 500 hours.

[1] Although this test gave a good correlation with leakage power and recovery time in the 721A tube, the correlation changed completely when the oxide coating was added to make the 721B. This was observed at Evans Signal Laboratory in 1945, but no explanation of it was advanced up to the end of the war.

[2] This method was apparently developed independently at the Radiation Laboratory and at the Bell Telephone Laboratories.

J. W. Clark, "The Gas Discharge Switch; VIII. A Method of Analyzing Leakage Power Data," BTL MM-43-140-50, Oct. 11, 1943.

[3] Smullin and Leiter, "The 1B27 TR Tube," RL Report No. 594, Oct. 4, 1944.

These tubes gave no indication of serious deterioration, although a fairly intense discharge was maintained across the input window. Whether or not such performance is characteristic of all production tubes was never definitely established.

The 721B and the 1B27 tubes are used successfully at power levels of the order of 1 Mw so long as the harmonic content of the transmitter is low. At power levels greater than 1 Mw there is, in the small-diameter cavities, a tendency for a discharge to strike across the glass cylinder adjacent to the input coupling. It is believed that this discharge appreciably shortens the tube life.

Some magnetrons, when operated at high power levels, show a tendency to spark occasionally and also to jump into an inefficient electronic mode that is very rich in harmonic content. A magnetron which operated in this way was first noticed when a 10-cm duplexer using 1B27 TR and ATR tubes was tested with the 4J44 series of magnetrons at powers near 1 Mw. When a hard-tube modulator was used, the 1B27 tube protected crystals for long periods at a line power of 1 Mw. When a spark-gap modulator was used, however, crystals were burned out almost instantly. A long series of experiments by L. D. Smullin and A. W. Lawson finally established the fact that these burnouts were coincident with the sparking of the magnetron, and that during these periods excessive leakage power did not occur at the nominal wavelength of 10.7 cm, but was present at the second, third, and fourth harmonics of a 9-cm mode. That this was another magnetron mode that could be excited under certain conditions of the r-f loading and exciting circuits was shown later by Clogston and Rieke. A number of attempts to put harmonic filters into the TR cavity were made, but none of the filters gave enough attenuation over a sufficiently large frequency range. It was estimated that a minimum of 30 db of additional attenuation at all harmonic frequencies was needed to ensure crystal protection. This particular problem was finally solved by the use of a pre-TR tube[1] ahead of the 1B27 TR tube. The pre-TR tube will be discussed further in the sections on low-Q and bandpass TR tubes.

Tube life was still a rather indefinite quantity even as late as the end of the war. Although laboratory life tests on dozens of 1B24 and 1B26 tubes indicated a usable life of 2000 hours or more, the life of the 1B24 tube in the field seemed to be only a few hundred hours. Comparatively few tubes were returned for examination but those few tubes indicated that about 40 to 50 per cent of the tubes marked "bad" were bad tubes originally, and most of those had air leaks at cracked windows or solder joints. As a result of this experience with the 1B24 tubes, all

[1] L. D. Smullin, "The 1B38 Pre-TR," RL Report No. 641, Dec. 5, 1944.

TR tubes were required to pass a type approval temperature-cycle test of half-hour exposures to −55°C, to room temperature, and to 100°C. These tests had to be repeated fifty times without failure.

Results obtained with 721A tubes were the opposite of those obtained with the 1B24 tubes. Laboratory tests had shown that recovery time became unduly long after a life of about 300 to 400 hours, although crystal protection was good for more than 1000 hours. It was very difficult to persuade service personnel to replace the tubes frequently enough.

The 721B tube has a life of 1000 hours or more, and the 1B27 tube operates for about 700 hours. The 724B has a life of approximately 250 hours, at the expiration of which it will no longer protect crystals.

6·3. High-level Characteristics of Bandpass and Pre-TR Tubes and Low-Q ATR Tubes.—Breakdown and recovery are fundamental processes of both the high-Q and the low-Q or bandpass tubes. These phenomena are, in general, more complicated in the bandpass tubes since as many as three or four different discharges must be considered, whereas in the high-Q tubes only one discharge need be considered. The intensity of the various discharges in a bandpass tube varies by orders of magnitude, and some probably last for only a fraction of the period of the transmitter pulse.

The loaded Q's of the resonant elements in bandpass tubes are lower than those of conventional high-Q tubes by factors of 50, approximately. As a result, the voltage buildup across the gaps follows the magnetron rise with almost no time delay and consequently the entire spike-transient analysis becomes quite different from that of the high-Q tube The fact that several gaps fire in sequence within a time interval of about 10^{-8} sec probably makes the "fine structure" of the spike of a bandpass tube very complicated indeed.

One of the most striking features of the low-Q tubes, as they exist today, is the discharge which covers the input window. At very low power levels, the discharge is just a filament across the center of the window. As the power is increased, the discharge spreads until it covers the entire window with a smooth glow. The power dissipated in the discharge is very large. An argon-filled 10-cm tube such as the 1B38 pre-TR tube may have a pulse dissipation of 5 to 7 kw, as compared with 5 to 10 watts for an argon-filled high-Q tube, or 50 to 60 watts for high-Q tubes filled with an H_2-H_2O mixture.

The arc leakage power of a typical bandpass tube is 30 mw or less, and spike leakage energy is about 0.1 erg. Corresponding values for high-Q tubes are 20 to 30 mw and 0.03 erg. It is well known that both P_a and W_s increase rapidly as the loaded Q (Q_{L2}) in high-Q tubes decreases. In fact, the 1B24 or 1B27 tubes no longer protect crystals if Q_{L2} is made

less than about 200. How crystal protection is obtained with the low-Q elements in bandpass tubes has not been completely determined.

It is found that the spike leakage energy varies inversely with Q_{L2} (more specifically the output Q, Q_{out}) when n_0 is kept constant, but that it does not vary in this way when the equivalent conductance, or keep-alive interaction, is kept constant. Practically all measurements of W_s vs. Q_{out} have been made with constant keep-alive current and location (constant n_0). These experiments, therefore, cannot be used to give a curve for high values of Q_{L2} that could be extrapolated to meet the observed values of W_s for very low Q_{L2}. Rough calculations similar to those indicated in Sec. 5·6 show that for a constant value of interaction, W_s changes very slowly with Q_{out}.

The arc leakage power of a 721A TR tube filled with an H_2-H_2O mixture is about 40 mw, for $Q_{L2} = 300$ and an insertion loss of 1.5 db. This corresponds to a voltage across the discharge of 100 volts rms.[1] The same tube filled with argon might have a voltage drop of approximately 30 volts. Conversely, a typical bandpass tube filled with argon has a flat leakage power of 1 mw or less, which corresponds to a gap voltage of about 3.5 volts, if the element transformation ratio is taken as 5. A mixture of A-H_2O gives $P_a \approx 20$ mw and a gap voltage of about 15 volts. These numbers become roughly comparable if a correction is made for the gap length, which is about 0.030 in. in the high-Q tube, and 0.008 in. in the bandpass tube. However, the necessity to explain a self-sustaining discharge which has a total voltage drop less than the ionization potential of the gas remains. This effect has also been observed in electrodeless discharges at lower frequencies and has been reported in the literature by various authors.

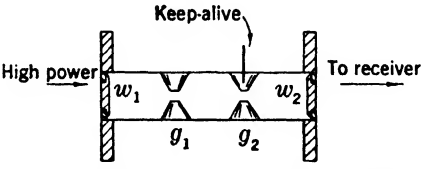

FIG. 6·1.—Cross section of a 3-cm bandpass TR tube, 1B63.

In addition to arc leakage power, high-Q tubes have direct-coupled and harmonic leakage powers, and either one may be larger than the arc leakage power. Bandpass tubes and pre-TR tubes have practically infinite direct-coupling attenuation because of the discharge that covers the input windows. Harmonics also are very highly attenuated.

Figure 6·1 is a cross section of a 3-cm bandpass tube (1B63) with two resonant gaps and two low-Q resonant windows. The keep-alive electrode is at the gap closest to the receiver. Although no direct experimental determinations have been made of the breakdown sequence, it is believed to be as follows. In the interval $t_0 < t < t_1$, Fig. 6·2, the

[1] H. A. Bethe, R. E. Marshak, and J. Schwinger "Theoretical Results on the TR Box," NDRC Report No. 14-116, *loc. cit.*, Cornell Univ., Jan. 20, 1943.

voltage builds up across the gaps and is in phase with the transmitter voltage. At about t_1 the electronic conductance of the second gap g_2, which has the keep-alive electrode, begins to increase rapidly, as described in Sec. 5·6. During the interval $t_1 < t < t_2$, the impedance across this gap is very low, and the standing wave which results doubles the voltage at the first gap g_1. This gap depends for its initial ionization n_0 upon carry-over from the previous discharge and possibly upon photoelectrons released by the light from the discharge in the second gap. Although n_0 is very small, the doubled voltage which results from the breakdown of the second gap probably breaks down the first gap almost instantly. This, in turn, causes the voltage to double at the input window w_1, and this, too, finally breaks down.

The direct-coupling attenuation through a fired gap is about 30 db. Thus, the power incident upon the second gap g_2 is the sum of the arc leakage power of g_1 and the window leakage power attenuated by 30 db. This power is probably 20 to 50 mw which is not sufficient to maintain the discharge at g_2. The electronic loading at g_2, however, does not disappear instantly; therefore while the gap is recovering, the leakage power, incident upon the receiver, varies from about 0.001 of the leakage power through g_1 up to the full leakage power through g_1. This is illustrated in curve A of Fig. 6·2. Curves similar to B and C are observed when the amount of H_2O in the tube is reduced, with a consequent increase in the recovery time. In 10-cm tubes, the flat leakage power is usually too small to be seen on an oscilloscope. Although tests have not been made, it is believed that with a 5-μsec transmitter pulse the leakage power envelope of a 10-cm tube would be similar to that of the 3-cm tube and that the arc leakage power would become appreciable. In the 3-cm tube the characteristics illustrated in Fig. 6·2 can be observed with 0.5-μsec transmitter pulses.

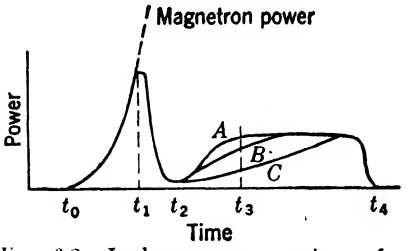

FIG. 6·2.—Leakage power envelope of a 3-cm bandpass TR tube.

6·4. Spike Leakage Energy.—In bandpass tubes as in high-Q TR tubes, the margin between crystal protection and burnout is much narrower for the spike leakage energy than for the flat leakage power. As a result, most experimental effort was directed towards the reduction of W_s, and the flat leakage power received more or less perfunctory attention.

The experimental work can be classified in three main divisions: gap design, gas content, and keep-alive design. The first division, gap design, involved the problem of developing resonant elements which had

the smallest product of $Q_{L2} \cdot W_s$. For these experiments, it was tacitly assumed (and this assumption was later partially verified) that a gap design which gave optimum performance for one gas was equally good for all other gases. This simplified the experimental technique, for after the gap design was chosen, it was necessary only to determine the gas filling of the tube for the longest life, the shortest recovery time, and the least leakage power.

In Sec. 6·3 it was seen that the flat leakage power was far from constant during the pulse. Because of this, it was difficult to separate the spike transient from the arc leakage power by the usual techniques of cancellation or pulse-length increment (see Chap. 9). The use of pure argon, however, resulted in a very small arc leakage power, and the spike leakage energy constituted more than 95 per cent of the total energy in the leakage pulse. Thus, since there is uncertainty concerning only a small percentage of the power, it can be assumed that the total energy is equal to the spike energy.

Window Leakage.—The design of the input window has been based primarily upon low-level considerations of Q_{L2} and upon dissipative loss. The leakage past a typical window is of the order of hundreds of ergs compared with the tenths of an erg that is actually incident upon the receiver. Figure 6·3 shows the total leakage energy through various low-Q resonant windows for various pressures of argon. Curve A is the leakage energy through a 1B38 pre-TR tube, in which both windows have $Q_{L2} \approx 1$ and a height of 0.875 in. The measurements were made with a transmitter-pulse power of 50 kw at 10.7 cm but check measurements made at 1000 kw agreed with these data within the experimental error of about ± 1 db. The arc leakage power was about 50 watts at a pressure of 10 mm Hg of argon, and thus constituted about one-third the total energy for a 1-μsec pulse.

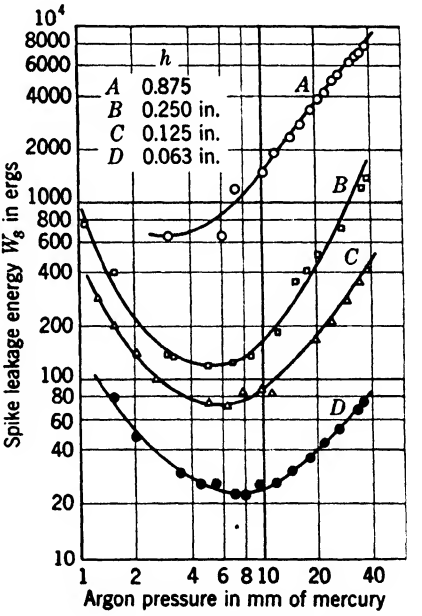

FIG. 6·3.—Leakage-energy characteristics of various low-Q glass windows. A is for a 10-cm window, and B, C, and D are for 3-cm windows.

Curves B, C, and D of Fig. 6·3 give the total leakage energy for three different windows measured at a wavelength of 3.2 cm. Their heights

were 0.250 in., 0.125 in., and 0.063 in., respectively, and Q_{L2} was 1.1, 2.1, and 6. There is not the 4-to-1 ratio between successive curves that would be expected if the breakdown voltage were a linear function of the window height. One test at 8.5 cm did give a fourfold change in total leakage power when a window with one-half the height of the standard one was used. At the present writing it is not clear whether this represents poor experimental technique or whether it results from the fact that breakdown along a dielectric surface is a highly complicated, and little understood phenomenon.

The curves illustrate pressure dependence of the usual type with fairly well-defined minima. For the 10-cm tube at least, in which the arc leakage energy is about 30 per cent of the total leakage energy, the minimum has little theoretical importance. This minimum is the result obtained by adding the curves (automatically) of W_s and P_a which have different shapes and different minima.

The data presented in these curves were obtained with the leakage energy of the window dissipated in a matched receiver load. In actual use, as in the input window to a bandpass tube, the voltage buildup across the window follows the magnetron very closely until the breakdown of the resonant gap one-quarter guide wavelength away from it causes the voltage to double. This must undoubtedly change the spike transient, and it probably reduces the spike leakage energy incident upon the next gap. The extent of this reduction in energy is not known, and is probably of little practical importance. A cathode-ray oscillogram of the spike transient in a 1B38 pre-TR tube was shown in Fig. 5·11 and a discussion of this transient is found in Sec. 5·6.

Careful consideration of Fig. 6·3 emphasizes the fact that at a wavelength of 1.25 cm or less, the total leakage through such a low-Q window would be about 1 to 2 ergs. Furthermore, if thin mica is used instead of glass, the height of the window may be reduced by a factor of almost two and thus the total leakage through a window would be well below 1 erg.[1] This, together with the fact that 1.25-cm crystals (1N26) can withstand about 0.3 erg of spike energy, should make it possible to design a very simple bandpass TR tube for this wavelength.

The pre-TR tube is used in conjunction with a high-Q TR tube in order to minimize both harmonic and direct-coupled leakage power. To ensure proper operation, the transmission line between the two-tubes is adjusted so that the detuned high-Q cavity produces a voltage maximum at the input window of the pre-TR tube. Since the pre-TR tube is one-quarter guide wavelength long, the connecting line is made one-half guide wavelength long. It has already been seen in Chap. 5 that the

[1] Some unpublished results of experiments by C. W. Zabel at the Radiation Laboratory confirm this.

input admittance to a TR cavity during the entire spike transient is very large compared with Y_0; therefore, the pre-TR tube is working into an open circuit during the entire transmitter pulse, and the leakage energy is presumably smaller than when it is terminated in a matched load.

6·5. Spike Leakage Energy. Gap Design.—Early experiments on bandpass TR tubes were concerned primarily with the development of a tube that would work. The pressure of war made it necessary in this experimentation to use many intuitive deductions and extrapolations based upon insufficient data. Only after a usable tube had been produced was it possible to make a systematic study of the influence of various parameters on leakage energy characteristics. This systematic investigation[1] began in 1944 and ended at the close of the war in 1945.

The leakage power through a complete bandpass tube is a complicated function and results from the superposition of several different discharges. From a narrow pragmatic point of view only the total leakage energy is important, and in fact most leakage-power data were taken with complete tubes. There can be no doubt, however, that a complete understanding of what happens within a single gap would implement the design of a better tube than any now in existence.

Figure 6·4 shows the leakage energy from 3-gap, 3-cm bandpass TR tubes which have different gap designs, as a function of argon pressure. The arc leakage power is negligibly small, and therefore the total energy is nearly equal to the spike leakage energy. All gaps are of the type illustrated in Fig. 3·31 and all the curves exhibit the familiar shape of leakage-power curves with rather pronounced minima.

Figure 6·5 is a plot of the square root of the leakage power ($W_s^{1/2}$) against gap spacing at an argon pressure of 10 mm Hg and is based upon data taken from Fig. 6·4. With the exception of the smallest gap spacing, the points define a straight line passing through the origin. This is to be expected if the voltage transformation ratio is constant for the various gaps, and if the gradient increases linearly as g^{-1}.

The point for the shortest gap (0.0047 in.) lies above the straight line defined by the other three points and the origin. It may be possible to clarify further this behavior by a consideration of the electrons lost to the electrodes. In general the electrons in an r-f discharge suffer almost no net displacement in the direction of the field, and therefore very few are lost to the electrodes. There is a small region adjacent to the electrodes, which is of the order of one mean free path long, through which electrons may be accelerated and thus reach the electrodes. With

[1] Most of the leakage power data, particularly on 3-cm tubes, were obtained at the GE Research Laboratories by the group under M. D. Fiske. W. C. Caldwell of the Radiation Laboratory worked with this group for almost a year on the development of the 3-cm tube.

mean free paths of the order of 0.001 in., the two regions adjacent to the electrodes occupy a large part of the total gap of 0.0047 in., but for larger gaps they are less important. The loss of electrons by this mechanism requires a higher rate of electron production and, therefore, higher gap voltages and higher spike leakage energy. This phenomenon is very similar to that which causes the minimum of the Paschen curve for d-c breakdown. Similar effects were observed by Posin in a study of r-f breakdown in waveguides at atmospheric pressure.[1]

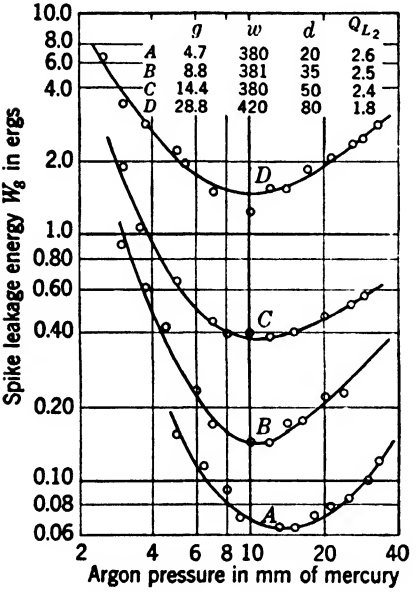

FIG. 6·4.—Spike leakage energy through 3-cm bandpass TR tubes for various gap spacings.

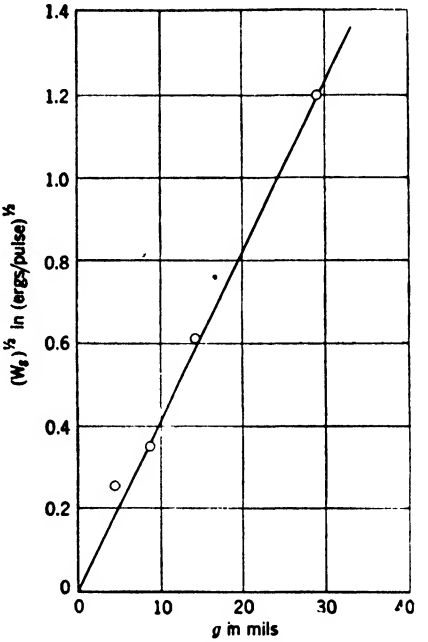

FIG. 6·5.—The square root of the spike leakage energy of Fig. 6·4 plotted against gap spacing for a pressure of 10 mm Hg of argon.

The influence of the particular shape of the ends of the electrodes upon spike leakage energy has been for some time the subject of controversy. It remains an open question. It is argued that if pointed electrodes are used, the gap length required to tune a given resonant element will be less because of the smaller capacitance between the ends. Since $W_s^{1/2}$ decreases almost linearly with gap spacing, the smallest gap should give the smallest values of leakage energy. But there is also evidence to support the contention that the *effective volume* of a gap has a strong

[1] D. Q. Posin, I. Mansur, H. Clarke, "Experiments in Microwave Breakdown," RL Report No. 731, Nov. 28, 1945.

influence upon the spike. That is, for equal gap lengths, the gap with the largest volume should break down at the lowest voltage since the probability of finding an electron within the region of high field is greatest. No definite comparison of these two arguments has been made although some indirect experimental evidence exists in support of each point of view. The 3-cm tube (1B63) uses truncated cones, and the 10-cm tubes (1B55, 1B58, and the 9.1-cm tube) have pointed electrodes; but it is not possible to determine from their performance which gap is better. A direct comparison of the two gaps made at the same wavelength and with the same measuring equipment would be a straightforward experiment, and would be well worth while.

The analysis presented in Sec. 3·3 indicates that the spike energy of a low-Q resonant gap should vary directly with the susceptance of the inductive iris, and inversely with the area of the electrodes which form the gap. If the validity of this relationship could be established it might eliminate fruitless experimentation with odd gap shapes in the effort to combine minimum Q_{L2} with minimum leakage energy.

6·6. Direct-coupled Spike Leakage Energy.—In Chap. 3 it was seen that the direct-coupling attenuation through a typical resonant gap is 25 to 30 db. The spike leakage energy past an input window is about 1000 ergs in 10-cm tubes, and about 100 ergs in 3-cm tubes. Thus, it is evident that the energy leaking past the first gap can not be less than about 1 erg and 0.1 erg respectively, for the two tubes, even if the gap is completely short-circuited.

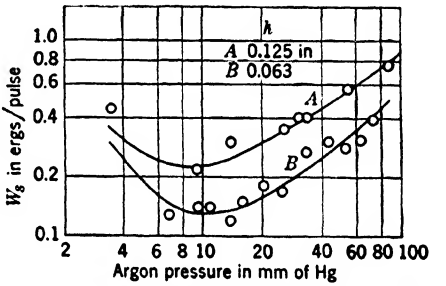

FIG. 6·6.—Spike leakage energy through single gap 3-cm bandpass TR tubes with different input-window heights.

Figure 6·6 shows the spike leakage energy through one-gap bandpass tubes with input windows of different sizes. Curve A is for a tube with an input window $\frac{1}{8}$ in. high, and curve B is for a tube with a $\frac{1}{16}$-in. window. The gap used in each tube had the following dimensions: $\theta = 45°$, $d = 0.030$ in., $w = 0.250$ in. (Fig. 3·33) and it had a direct-coupling attenuation of 35 db. By referring to Fig. 6·3, it can be seen that at a pressure of 10 mm Hg of argon, the window spike leakage energy is 90 ergs for the $\frac{1}{8}$-in. window and 25 ergs for the $\frac{1}{16}$-in. window, respectively. Thus, if the gaps are short-circuited during the entire pulse, leakage energies of about 0.3 and 0.08 erg through the two tubes can be expected. The observed values were 0.24 and 0.13 erg. Although the curves of Figs. 6·3 and 6·6 were taken at different times and none of

the tubes were baked out before filling, there is nevertheless good agreement between the measured and the predicted results.

At this point the question that most naturally occurs to the tube designer is whether it is possible to measure separately the leakage power characteristics of a window and of a resonant gap, and to predict for a tube with one or more gaps the resultant leakage characteristics. At present this is not possible. Although fairly complete data on window leakage have been compiled very little accurate information exists regarding the leakage characteristics of a single resonant gap. M. D. Fiske has measured the leakage characteristics on 3-cm gaps, and L. D. Smullin and C. Y. Meng made similar measurements on 10-cm gaps. The experiments were mainly exploratory and have not been published.

One of the most serious difficulties encountered in the early experiments for the comparison of the leakage energy of various gaps was the fact that the tubes were not clean. This difficulty did not occur with glass tubes such as the 721A since the tubes had to be clean in order to form the copper-glass seals. The bandpass tubes, however, are, except for the windows, of all-metal construction, and all parts are assembled by soldering. Unless great precautions are taken, the leakage characteristics of a soft-soldered tube will be seriously affected by many impurities in its gas content. Hard-soldered tubes are easy to keep clean but it is difficult to modify them after they are assembled. It is, therefore, often desirable to use soft-soldered experimental tubes, but it is necessary to clean the tubes thoroughly after soldering.

A great deal of information can be obtained from a resonant gap that can be adjusted without breaking the vacuum seal. The gap length may be varied by bringing one of the electrodes out through an r-f choke and a flexible bellows, or the gap point may be driven in and out by a screw mounted in a tapered, lapped joint sealed with vacuum-pump oil. The inductive irises, also, may be moved in and out through flexible, vacuum-tight bellows. All of these adjustable elements were made, but there was no opportunity to make complete measurements of their characteristics.

6·7. Arc Leakage Power.—In 3-cm bandpass tubes, as in high-Q tubes, the arc leakage power is much greater for diatomic than for monatomic gases. In 3-cm bandpass tubes the flat power is negligibly small when pure argon is used. Figure 6·7 however, gives typical results[1] for three diatomic gases used in a 3-cm tube; the gases used were hydrogen, oxygen, and nitrogen. The powers shown here for these gases are many times greater than the powers for argon or helium. It has been seen in Fig. 5·28, that a ratio of 20 or 30 to 1 may be expected in the arc leakage powers for argon and hydrogen in high-Q tubes. Here, however, the

[1] M. D. Fiske, "Final Report on OSRD Contract OEMsr 1306," GE, Schenectady, Nov. 7, 1945.

ratio seems to be much larger. It may be possible to explain this by means of the recovery-time phenomenon postulated in Sec. 6·3.

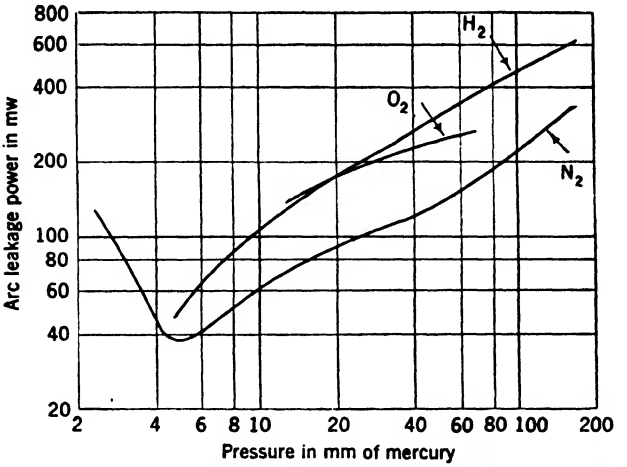

FIG. 6·7.—Arc leakage power through a 3-cm bandpass TR tube for various diatomic gases.

In a practical tube, however, in order to shorten the recovery time to a usable value it is necessary to employ water vapor. The use of water vapor results in a substantial increase in arc leakage power over that for argon alone. Figure 6·8 shows the spike leakage energy W_s, and arc leakage power P_a through a 3-gap tube (the same tube used for curve A of Fig. 6·4) as a function of argon pressure, with a partial pressure of 4.5 mm Hg of H_2O. It can be observed that the spike leakage energy is only slightly higher than for pure argon, Fig. 6·4 curve A, and that the minimum value of W_s occurs at about the same *total pressure* in both cases.

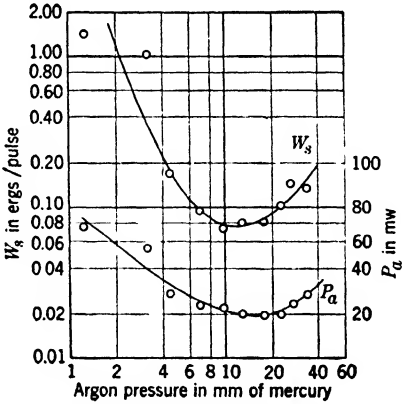

FIG. 6·8.—Spike leakage energy and arc leakage power through a 3-cm bandpass TR tube with a partial pressure of H_2O of 4.5 mm Hg.

Because, in general, it has been possible to maintain P_a below an approximate value of about 30 mw, there has been little incentive to study the problem in greater detail.

Figure 6·9 gives W_s and P_a as functions of *total gas pressure* for various mixtures of argon and H_2O in a 1B55 (8.5-cm) tube.

6·8. Effect of Gas-filling upon High-power Characteristics.—Because of the comparatively intense discharge at the input windows of bandpass

TR tubes, pre-TR tubes, and low-Q ATR tubes, it is necessary to choose a gas filling that will not only minimize the power dissipated in this dis-

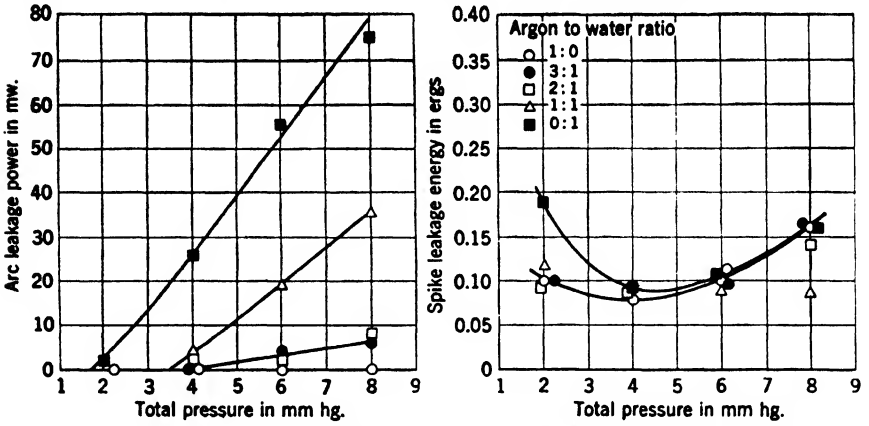

FIG. 6·9.—Spike and arc leakage through an 8.5-cm bandpass TR tube for various mixtures of argon and H_2O.

charge, in order to avoid cracking the window, but will also increase the general tube life.

Figure 6·10 shows the arc loss in the discharge across the window of a 10.7-cm tube, operating in series with a line carrying 50 kw of pulse power. The curve for argon is obviously much lower than for any of the other gases. Primarily on the basis of these tests, argon was chosen as the major component of the gas filling of all tubes in this general category.

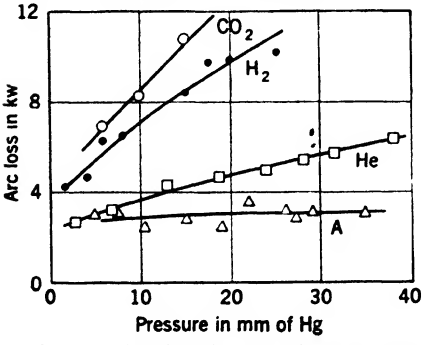

FIG. 6·10.—Arc loss in the discharge across a 10-cm low-Q window (h = 0.875″) for various gases at a line power of 50 kw.

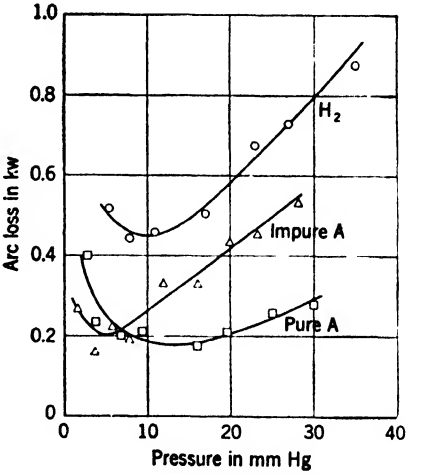

FIG. 6·11.—Arc loss in the discharge across a 1B35 tube window at λ = 3.2 cm and 3-kw line power.

Figure 6·11 is a similar curve for the arc loss in the window of a 1B35 (3.2-cm) low-Q ATR tube measured at a line power of 3kw. Figure 6·12

shows W_s for various noble gases in a 3-cm bandpass tube. For this tube also, argon is clearly the best of the gases tested. No tests have been made with xenon or krypton, or mixtures of these gases with argon. Some mixtures of this kind have very low d-c breakdown voltages.

Because a short recovery time is required for this tube, the use of a gas such as water vapor which has a high electron-capture cross section is demanded. Up to the present, H_2O is the only gas used for this purpose, although there are other gases which may be more stable and which may have equal or greater capture-cross sections, as has been indicated in Chap. 5.

Measurements on high-Q TR tubes indicate (Fig. 5·13) that the spike leakage energy through a hydrogen-filled tube is not much greater than that through an argon-filled tube. Some rather old measurements indi-

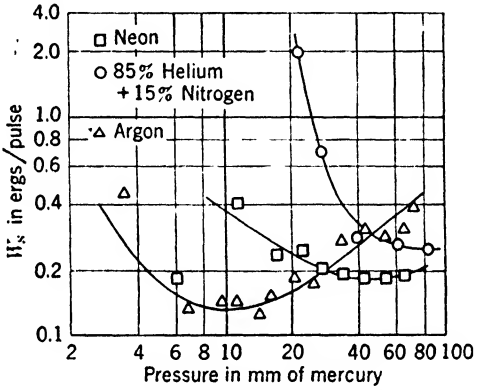

FIG. 6·12.—Spike leakage energy through a 3-cm bandpass TR tube as a function of gas content.

cate that in bandpass tubes W_s is about five times greater for H_2 than for A. No explanation for this difference in the behavior of the two tubes has been advanced.

It is much simpler to choose the gas filling for pre-TR and low-Q ATR tubes than for bandpass tubes. There are three conditions that must be met: (1) low firing power, (2) low arc loss, and (3) short recovery time. The filling generally adopted for all these tubes in the 1.25-, 3-, and 10-cm bands is about 10 mm Hg of argon. If these tubes were to be carefully made and carefully cleaned, their recovery time would be much too long. Most tubes, however, contain enough impurities to ensure fast recovery of the tubes for hundreds or even for thousands of hours. It has already been pointed out in Sec. 5·26 that the argon-H_2O-filled pre-TR tubes had shorter tube lives than did "commercially dirty" tubes.

The arc loss in argon-filled pre-TR and ATR tubes is so low that no tubes have ever failed because of cracked windows, even at the very

highest transmitter-power levels. The addition of H_2O greatly increases the arc loss, and care must be taken to keep the window cool enough to prevent cracking.

Table 6·2 illustrates the effect of water vapor and of window dimensions upon the arc loss in 3-cm low-Q tubes. If it is assumed that the

TABLE 6·2.—ARC LOSS IN DISCHARGES ACROSS 3-CM LOW-Q WINDOWS

Window height	Gas content, mm Hg		Transmitter pulse power	Arc loss
	A	H_2O		
0.250 in.	15	4	70 kw	0.35 db
0.125	15	4	70	0.19
0.250	15	4	150	0.27
0.125	15	4	150	0.09
0.250	10	0	70	< 0.09

voltage drop across the discharge remains constant, then the loss P_L should vary with the square root of the transmitter power P_T. If the loss ratio at any given power level is known, the ratio at any other power level may be found as follows: If $P_L \approx \sqrt{P_T}$, then

$$\frac{P'_L}{P_L} = \sqrt{\frac{P'_T}{P_T}},$$

and

$$\frac{P'_L + P'_T}{P'_T} = 1 + \frac{P'_L}{P'_T} = 1 + \frac{P_L}{P_T}\sqrt{\frac{P_T}{P'_T}},$$

which is the loss ratio and is expressed in decibels in the table. The experimental loss ratios for the two line powers given in the table obey this relationship very closely.

The 0.125-in. window is the one in actual use in the 3-cm bandpass TR tube. At 150 kw the pulse power dissipated in the arc (P_L) is 3 kw. If the duty ratio is $\frac{1}{1000}$, this indicates an average power dissipation of 3 watts at the input window. In a typical installation, this dissipation results in a temperature rise of the window of more than 50°C. Similar tests made on 10-cm pre-TR tubes which operated at 2 Mw line power, with a duty ratio of $\frac{1}{2000}$, indicated window temperatures in excess of 100°C with an ambient temperature of 25°C.

Although dire results were predicted for the addition of several millimeters of mercury of water vapor to the argon filling of 10-cm bandpass tubes, no tube failures due to window cracks at high transmitter powers resulted.

6·9. Effect of Line Power upon Leakage Characteristics.—It has already been seen that the power lost in the window discharge varies as the square root of the line power. Tests on pre-TR tubes indicate essentially constant values of W_s and P_a from about 5 kw to more than 1000 kw of line power. Below the minimum firing power (about 5 kw), the leakage power becomes approximately half the line power, and the tube offers no protection. Similarly, below a certain power level a TR tube will not fire, and about half of the incident line power goes to the receiver. It is an accepted necessity that a TR tube must protect its receiver at any level of line power below the maximum rating of the tube. For a bandpass TR tube, this means that at least one of the gaps must fire at a power level low enough to ensure crystal protection, even though the window does not fire at powers below 1 kw.

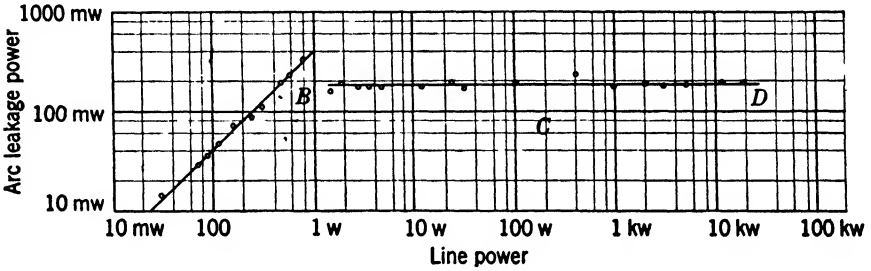

FIG. 6·13.—Arc leakage power through a 2-gap 3-cm bandpass TR tube as a function of line power.

Figure 6·13[1] shows the arc leakage power through a 2-gap 3-cm tube as a function of line power. The tube was filled with a mixture of 5 mm Hg of H_2 and 10 mm Hg of A. This, however, is not a standard gas filling, and the arc leakage power is almost 10 times that from a standard filling. Up to a line power of approximately 1 watt, the leakage power increases linearly. At higher power levels the gaps break down, after which P_a remains constant for all higher power levels.

Fig. 6·14[2] shows the variation of spike leakage energy with line power, in an argon-filled 3-cm 2-gap tube. The negative slope of the curves, just beyond the point of maximum energy, may be explained, according to Fiske, by the nature of the experiment. The line power was adjusted in these experiments by passing the power from a 30-kw magnetron through a power divider or attenuator. Thus, when the line power was about 0.1 watt, the gap broke down near the top of the pulse rather than at the foot of the exponentially rising front. As a result the voltage buildup was approximately linear. It was seen in Chap. 5 that a

[1] M. D. Fiske, H. N. Wallace, and A. D. Warner, "Final Technical Report on Contract OEMsr-1306, Nov. 7, 1945.

[2] Fiske, *op. cit.*

linear voltage rise on the magnetron pulse results in a spike leakage energy that varies inversely as the square root of the transmitter pulse power. The dashed lines represent such a square-root variation.

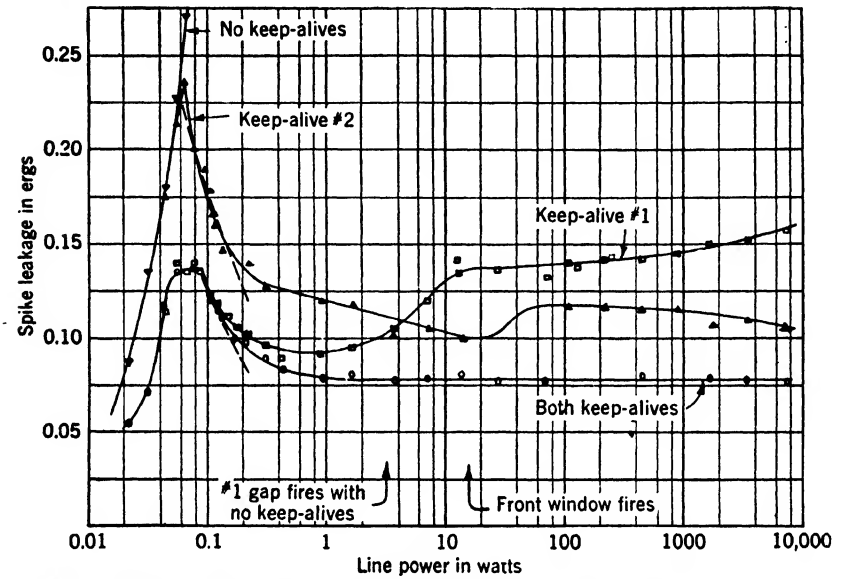

FIG. 6·14.—Spike leakage energy through a 2-gap 3-cm bandpass TR tube as a function of line power. Tube is filled with pure argon. (Gap No. 1 is closer to the input window.)

Measurements on 3-cm tubes at power levels up to 250 kw, and on 10-cm tubes at power levels up to 1000 kw, have shown no increase in leakage power over that at 10 to 50 kw. It is felt that the maximum transmitter powers now in use may be doubled with no increase in the leakage power of the TR tubes.

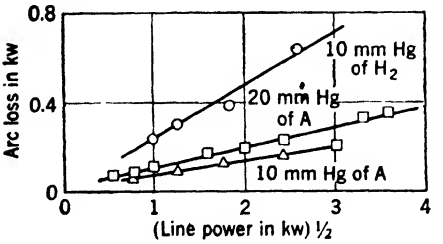

FIG. 6·15.—Arc loss in the discharge of a 1B35 ATR tube window as a function of line power for various gases.

The minimum transmitter power at which these tubes may be used is determined by the firing of the input window. Detailed specifications will be given later; but nominal minimum values are about 1 kw, 5 kw, and 10 kw at 1.25 cm, 3 cm, and 10 cm, respectively.

Figure 6·15 shows the variations in window arc loss in a 1B35 ATR tube as a function of the square root of the line power for various gas fillings. The experimental points lie very closely upon straight lines, and thus indicate the correctness of the assumption that the discharge

voltage is essentially constant and that the arc loss is directly proportional to the current in the main line.

6·10. Keep-alive Electrodes.—The problem of the keep-alive has already been discussed in general terms in Chap. 5. In this section some of the more detailed considerations applicable to bandpass tubes will be presented. Figure 6·16 illustrates the side-arm and coaxial electrodes

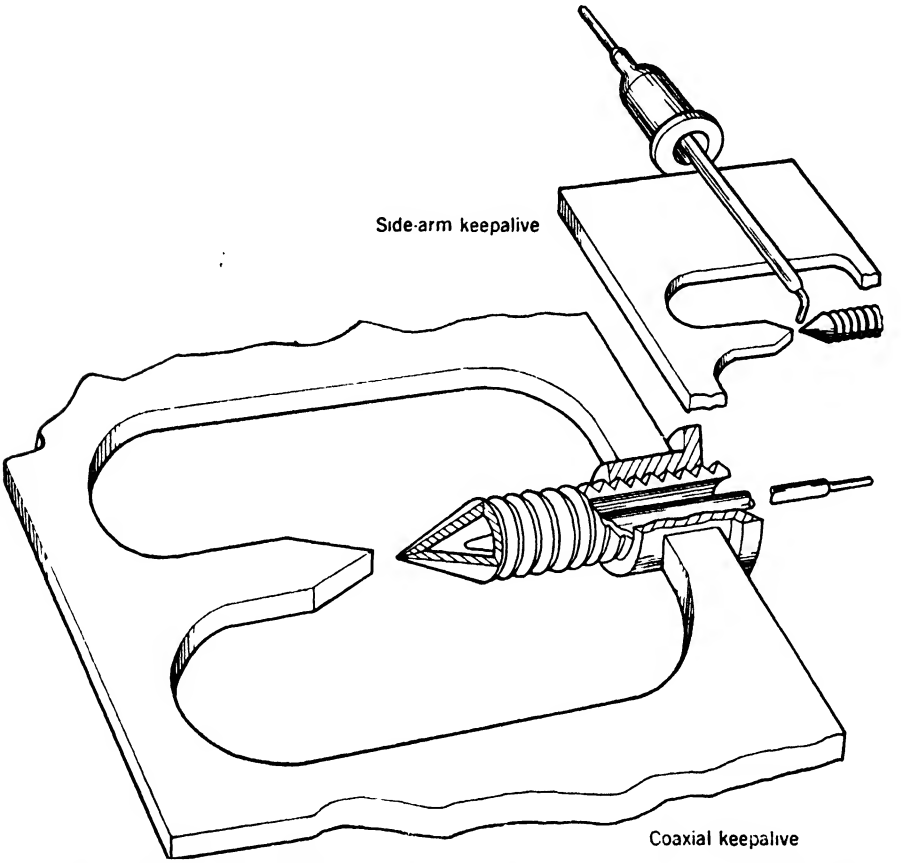

FIG. 6·16.—Side-arm and coaxial keep-alive electrodes used in 10-cm bandpass TR tubes.

used in the 10.7-cm and 8.5-cm (1B58 and 1B55) TR tubes. Figure 6·17 illustrates the coaxial electrode used by the General Electric Co. in one variation of the 3-cm tube. The 3-cm tube made by the Sylvania Electric Products Co. utilizes a coaxial electrode very similar to that used in the 1B24 TR tube.

The end of the side-arm keep-alive electrode used in 10-cm tubes is bent towards the gap as shown and it ends about $\frac{1}{32}$ in. from the axis of the gap. The low-level signal loss (interaction) due to the d-c discharge

is almost completely independent of the positioning of an electrode of this type. The coaxial electrodes differ in this respect, and the low-level signal loss increases rapidly as the electrode tip approaches the gap. At a discharge current of 100 μa, the interaction can be as high as 5 db for a

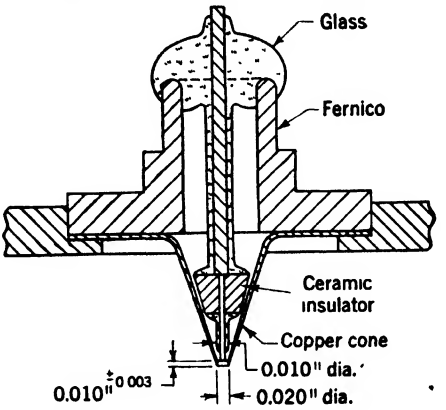

FIG. 6·17.—Coaxial keep-alive electrode for the GE 3-cm bandpass TR tube.

coaxial electrode while it can hardly exceed 0.1 db with a side-arm electrode.

Figure 5·55, curves *A* and *B*, shows the spike leakage energy through a 3-cm tube that has truncated-cone elements. Both a coaxial and a side-arm electrode are mounted at the same gap. The coaxial electrode appears to be by far the more efficient of the two. The numbers along the curve represent the keep-alive current. Curve *C*, however, is for a side-arm electrode in a tube using conical-post resonant elements. Although it is dangerous to compare this curve with the first two curves directly, it is obvious that the last structure at least approximates the efficiency of a coaxial electrode in a truncated-cone gap. No clear explanation for this difference has been advanced. A reasonable explanation is based on the fact that all of the electrons from the coaxial electrode are furnished to the gap, whereas many of the electrons from the side-arm type reach the conical electrodes by paths that are not in the region of the highest r-f electric field. Thus, in the truncated-cone gaps, it is difficult to send electrons into the r-f gap from a side-arm electrode. If pointed,

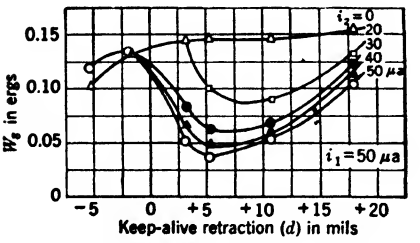

FIG. 6·18.—Spike leakage energy vs. distance of coaxial keep-alive electrode from the end of the cone in a 3-cm bandpass TR tube.

conical electrodes are used, a greater n_0 can be produced in the gap with the side-arm electrode than in the truncated-cone gap, since the post diameter is much smaller and the performance begins to approach that of the coaxial electrode.

Figures 6·18, 6·19 and 6·20 represent the results of another interesting experiment by Fiske. A coaxial keep-alive electrode was mounted in a bellows arrangement at the second gap so that its axial position could be varied from 0.020 in. away from the gap to 0.010 in. into the r-f gap. The keep-alive electrode was in its normal position at gap No. 1 and was maintained at a current of 50 μa. Figure 6·18 shows the variation of W_s for different keep-alive currents as a function of electrode position. The distances back from the gap are plotted as positive. Figure 6·19 shows the corresponding values of low-level loss (interaction). If Fig. 6·19 is replotted by a reciprocal transformation

$$S = \frac{0.021}{L},$$

where L is the fractional transmission loss given in Fig. 6·19, then Fig. 6·20 is derived. The similarity between this figure and Fig. 6·18 is striking, and it provides fairly convincing proof that both phenomena are governed by the electron density in the gap.

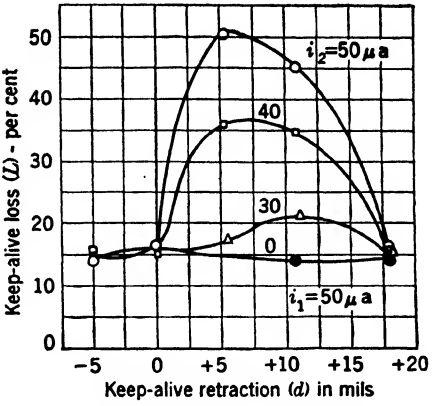

FIG. 6·19.—Low-level keep-alive interaction vs. coaxial keep-alive position for the same tube as in Fig. 6·18.

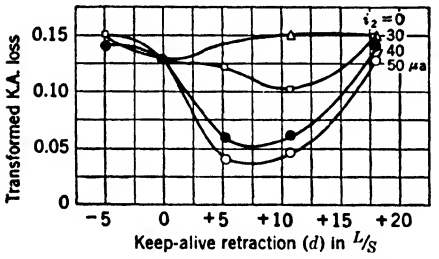

FIG. 6·20.—Data of Fig. 6·19 transformed to resemble spike energy curves of Fig. 6·18.

6·11. High-power Characteristics.—The high-power characteristics of a TR tube that can be specified are as follows: leakage power—flat and spike; arc loss; recovery time; minimum firing power; minimum and maximum operating powers; keep-alive voltage drop, keep-alive current and keep-alive interaction; gas filling; and life.

The tubes now in use may be divided into low-Q ATR tubes, pre-TR tubes, and bandpass TR tubes.

Table 6·3 gives the pertinent characteristics of the various ATR tubes. The gas filling is 10 mm Hg. of argon in all cases.

TABLE 6·3.—HIGH-POWER CHARACTERISTICS OF LOW-Q ATR TUBES

Tube No.	Min. firing power, kw	Arc loss db	Power level at which arc loss is measured, kw	Min. operating power, kw
1B35	4	0.7	4	5
1B37	4	0 7	4	5
1B36	1	0 5	1	2
1B44	10*	0 3	50	20
1B52	10*	0 3	50	20
1B53	10*	0 3	50	20
1B56	10*	0 3	50	20
1B57	10*	0 3	50	20

* Approximate.

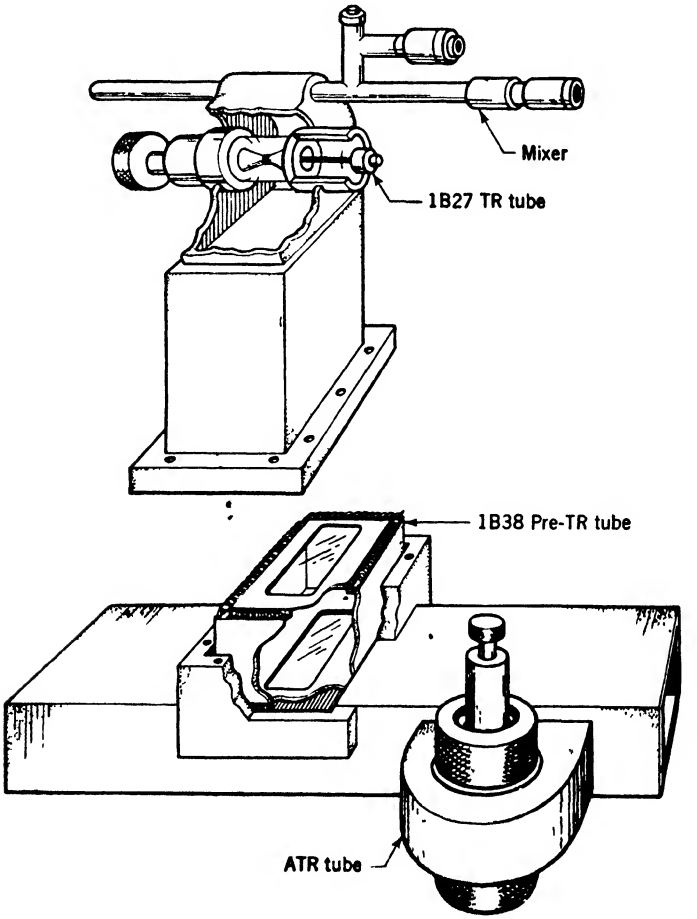

FIG. 6·21.—10-cm duplexer using 1B38 pre-TR tube.

The 1B35 and 1B37 3-cm tubes, and the 1B36 1.25-cm tubes are required to fire within 5 sec after the power is applied at the minimum firing power level indicated in the table. After they have fired, the arc loss of the tubes must be less than the value indicated. It was planned originally to require the various tubes in the 10-cm band to undergo similar tests. The apparatus for these tests was so bulky, however, that a much simpler test was devised in which the firing voltage of a 7 Mc/sec electrodeless discharge was correlated with the actual operating characteristics of the tubes (see Chap. 9).

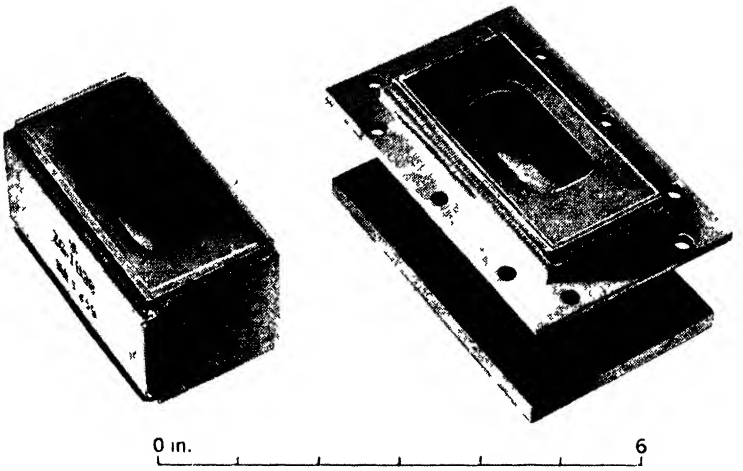

FIG. 6·22.—1B38 and 1B54 pre-TR tubes for use at 10.7 cm and 8.5 cm respectively. The 1B38 tube has contact springs at both ends.

At present, no upper limit to the power level at which the tube can be operated has been reached. Tube life is indeed an unknown quantity, for little is known about the recovery time of ATR tubes. Tubes have been run for thousands of hours at high power levels without breaking and without increasing the arc loss; however, for these long periods of operation, no recovery-time measurements were made. If the experimental results with the 1B38 pre-TR tubes are applied to these tubes, it can be concluded that tubes assembled with soft solder should average good recovery-time life, approximately 1000 hours. Tubes assembled by hard soldering, however, for example, the Sylvania 1B36, 1B35 and 1B37 tubes and the 1B52 and 1B53 tubes are probably "too clean" and the recovery time is without doubt long even when the tubes are new.

The pre-TR tubes that were put into production were the 1B38 at 10.7 cm and the 1B54 at 8.5 cm. Figure 6·21 shows a typical duplexer employing a 1B38 pre-TR tube in conjunction with a high-Q tube.

Figure 6·22 is a photograph of the 1B38 and 1B54 tubes. The 1B38 tube has contact springs at both ends, whereas the 1B54 tube has a contact spring at the high-power end, and a flange connection at the receiver end.

Table 6·4 gives data pertinent to the operation of pre-TR tubes. The recovery time of these tubes has already been discussed in Chap. 5.

The 1B38 tube is required to pass a leakage-energy test in order, primarily, to determine whether the initial gas filling is correct and also to ensure that air has not leaked into the tube. The 1B54 tube which was developed later was required to pass only the 7-Mc/sec discharge test. Very few tests have been made on the 1B54 tube since it is very similar to the 1B38 tube and therefore it is assumed that all the important characteristics are alike.

TABLE 6·4.—CHARACTERISTICS OF 1B38 (10.7 CM) AND 1B54 (8.5 CM) PRE-TR TUBES

Characteristic	Value
Gas filling	10 mm Hg of argon
Total leakage energy	1500 ergs
Arc loss	0.3 db
Power for arc-loss measurement	50 kw
Minimum operating power	20 kw

Since the low-Q windows used in all 10-cm tubes in this group (TR, ATR, or pre-TR tubes) have the same height and the gas fillings are the same, minimum operating power levels are the same. No upper limit for the operating power level has yet been reached.

Table 6·5 gives pertinent high-level data on the various bandpass TR tubes.

TABLE 6·5.—HIGH-LEVEL CHARACTERISTICS OF BANDPASS TR TUBES

Tube No.	Band, cm	No. of gaps	Keep-alive electrode	Gas filling, mm Hg		W_s, erg	P_s, mw	Recovery time to 6 db	Power for recovery-time measurement
				A	H_2O				
1B63	3	2	Coaxial	15	4	0.1	30	< 2 μsec	40 kw
1B55	8.5	3	Coaxial	4	2	0.1	5	10	700
	9.1	3	Side-arm	6	0	0.1	< 1	< 100	50
1B58	10.7	3	Side-arm	4	2	0.1	5	10	700

The three tubes in the 10-cm band are of the 3-gap type and have low-Q input and output windows, whereas the 1B63 3-cm tube has a high-Q input window and has two resonant gaps. At the end of the war, work had just begun on the design of a 2-gap 10-cm tube using a high-Q input window. The advantages of this tube would have been: a shorter tube (about 1½ in. shorter in the 10.7-cm tube), and a longer tube life. It was believed that the use of a high-Q input window, about half the

height, or less, of the present windows, would reduce the arc loss by a factor of about four, and the cleanup of H_2O would be correspondingly retarded. Unfortunately, only preliminary low-level tests had been made before all developmental work was stopped.

The 9.1-cm tube[1] is filled with argon alone. This tube was designed for use in radar beacons and was to be operated at about 50 kw of line power. A recovery time of approximately 100 μsec was tolerable; but tube life had to be thousands of hours in order to meet the rigid requirements of aircraft beacon systems. The tubes were assembled by soft-soldering and the impurities introduced into the tube were sufficient to keep the recovery time below 20 μsec during several thousand hours of operation. Under normal operating conditions, the beacon transmitter is on only while it is being interrogated by an airplane. The duty ratio which results is very low. At a busy airport, the ratio of "on" to "off" time averaged over several hundred hours is certainly less than $\frac{1}{100}$. Thus, the r-f discharge plays a negligible part in the gas cleanup process; and the 100-μa keep-alive discharge operating on the 260 cc of gas should give a tube life of at least 5000 hours if an extrapolation may be made from the 1B27 or 721B tubes (Sec. 5·23).

The 1B55 and the 1B58 tubes were designed for high-power radar sets to be operated at line powers of 500 to 1000 kw, and duty ratios of at most $\frac{1}{1000}$. Preliminary tests on three or four hand-made, soft-soldered tubes of each type showed continued crystal protection and good recovery time after 500 hours at 1000 kw, and a duty ratio of $\frac{1}{2000}$. For what length of time it is possible for clean, hard-soldered tubes to give good recovery time is not known. This time can probably be extrapolated from tests on the 1B38 pre-TR tube which has one-fourth the volume of these tubes, and appears to have a life of 100 to 200 hours when filled with an A-H_2O mixture.

The 3-cm tube has a volume of about 7 cc, or about $\frac{1}{35}$ the volume of the 1B58 tube. On the other hand, the window height is about one-seventh that of the 10-cm tube. Therefore, if a square-law variation of arc loss with window height is assumed, the arc loss will be less by a factor of 40 or 50, approximately, for equivalent line powers in the 3-cm tube. Thus, at equal line powers, tube life should be about the same for the two tubes. At present, 3-cm magnetrons with an output power of 300 kw are available, while 1000-kw tubes are in use at 10 cm. Developmental magnetrons that have twice the powers have been tested. On this basis, the 3-cm tube might be expected to have about three times the life of the 10-cm tubes, *if the tubes are clean and hard-soldered,* and are filled with argon and water vapor.

[1] L. D. Smullin, "S-Band Bandpass TR Tubes," RL Report No. 971, Jan. 23, 1946.

Actual life tests have been too few in number to allow any definite conclusions to be drawn. Some tubes operated at 30 kw for more than 500 hours. A few gold-plated tubes (this plating prevents oxidation) have run several hundred hours at 180 kw with little change in recovery time.

Although considerable thought was given to the use of water reservoirs in these tubes (Chap. 5), any idea of their use was abandoned because of the danger of excessive H_2O pressures at temperatures near 100°C, and also because the continual dissociation of the H_2O results in an increase of partial pressure of H_2 in the tube. This results in excessive arc loss and leakage power. Fiske has proposed the use of a palladium window in the tube in order to "drain" out the hydrogen. The possibility of using other gases than H_2O and the merits of inert coatings have already been discussed in Chap. 5. All possibilities of gold-plating to increase tube life have not yet been fully realized. In large tubes such as the 1B58 it is probably necessary to plate only the region around the input window.

6·12. Present and Future Status of Low-Q and Bandpass Tubes and ATR Tubes.—There does not seem to be any immediate prospect of improving in any way the low-level performance of these tubes, for it is not possible to lower, to any marked degree, the loaded Q. A substantial reduction in arc loss and minimum firing power would make it possible to use these tubes in low-power ($<$1kw) beacon installations. This reduction might be obtained either by an extension of the tube designed by Samuel (Chap. 4) or by the use of narrower windows—a possibility if mica is used instead of glass. The methods of mounting that involve current-carrying contacts need further investigation. There is at present no information available on how these contacts withstand the rigors of extreme variations in climatic conditions, although they operate with no difficulty under normal indoor conditions.

Pre-TR Tubes.—These tubes were introduced as a stopgap and were designed to protect crystals from certain high-power magnetrons. It was felt that their usefulness would end when bandpass tubes of corresponding frequency coverage became available. These tubes are now available, and there is little point in the further development or use of pre-TR tubes.

Bandpass TR Tubes.—These tubes in their present state of development have bandpass characteristics of about 10 to 12 per cent and protect crystals at high power levels for periods of more than 1000 hours. Recovery-time life is still an unresolved problem, although, in various ways, it is possible to improve the recovery-time life of these tubes. These methods for improvement include the use of inert coatings or platings inside the tube; the discovery of a captor gas less chemically active than

H_2O; the development of water reservoirs plus a suitable means of getting rid of H_2; and the reduction of the intensity of the window discharge. Of these, the first and the last will in all probability give positive results. Gold plating has already been tried with some success. Chromium plating, if used judiciously near the input window, may be equally good. Because of the poor r-f loss characteristics of chromium plating, it can not be put on resonant elements, but can be used only on the walls adjacent to the input window. No experiments have been made with preoxidized surfaces similar to those used in the 1B27.

The intensity of the window discharge may be reduced by decreasing the window height. The use of the same thickness of dielectric results in an increase of loaded Q and in an increase of r-f loss in the dielectric. In 10-cm bandpass TR tubes, it is possible to use a window with two or three times the Q of the present windows; this reduces the arc loss by a large factor and probably increases the tube life about 5 times. The r-f loss in the windows would probably be less than 0.1 db if 707 glass were used. In 3-cm tubes, the present windows, $\frac{1}{8}$ in. high, are probably the best that can be made with glass. The loss increases rapidly with any further decrease in height. The present thickness is 0.023 in. The use of thinner glass reduces the loss, but glass windows 0.010 in. thick are very fragile.

The r-f loss of quartz is considerably less than that of 707 glass. Therefore, with quartz it would be possible to make a smaller window than can be made with the glass and to do so without incurring excessive losses. The Q would be increased, of course, if the thickness were not reduced. Since the present 3-cm windows already have a Q_{L2} of 2, it is not possible to proceed indefinitely in this direction. Even if the higher Q can be accepted, the problem of sealing the quartz to metal still remains. Almost the only practical method available is to metalize the edge of a quartz or a "Vicor" (Corning 709 glass, about 90 per cent quartz) window and then to soft-solder it to an Invar frame. A much more promising solution of this problem may be found in the use of mica instead of glass. The technique for making vacuum-tight mica windows was applied by Malter[1] in the construction of a magnetron coupling window. M. D. Fiske used this technique to make TR-tube windows. A window resonant at 3.33 cm, $\frac{1}{8}$ in. high, and covered with mica 0.004 in. thick, had a Q_{L2} of 0.3, and no measurable loss. It thus appears that, by the use of mica, a window $\frac{1}{16}$ in. high or even less could be made.

Although this appears to be a very attractive solution a number of problems involved with this design remain. The mica sheet is sealed to a nickel-steel frame with a special low-melting point (550°C) glass. This

[1] L. Malter, R. L. Jepson, L. R. Bloom, "Mica Windows for Waveguide Output Magnetrons," NDRC Div. 14, Report 366, Dec. 5, 1944.

makes it impossible to hard-solder the frame to the tube by ordinary techniques.[1] Because the mica is sealed to the steel at the edges only, it should be on the outside of the frame in order to relieve the seals from the extra strain of atmospheric pressure. This, however, requires that the entire inside of the frame be coated with glass to prevent sputtering by the discharge. A window of this type has not yet been made, but at least it seems possible to use this as a method of construction. The higher-Q (about 2) window would be useful in TR tubes, whereas the lower-Q (about 0.3) window would be useful in ATR tubes.

Table 6·6 is a summary of the various parameters involved in TR-tube design and the interrelation of these parameters with the various

TABLE 6·6—DESIGN VARIABLES FOR BROADBAND TR TUBES

	Band-width	Spike leak-age energy	Flat leak-age power	K-a loss	Arc loss	Re-covery time	Life	Max. and min. power	Inser-tion loss
No. elements.....	x	x							
Q_{L_2} of elements...	x	x	x						
Gap.....		x	x						
Kind of gas.....		x	x	x	x	x	x	x	
Gas pressure.....		x	x	x	x	x	x	x	
K-a current and position.....		x		x			x		
Peak power.....					x	x	x		
Average power...					x		x		
Window size.....	x				x		x	x	x
Window dielectric.					x				x

performance characteristics of the tube. Thus the number of elements affects the bandwidth and the spike leakage energy but does not affect the other properties. Further improvement of these tubes, in addition to the improvements just discussed, will most likely consist of an increase in the bandwidth with no definite increase in the leakage power. A 10-cm 3-gap tube whose pass band extended from 9.4 cm to 11.1 cm was tested at the Radiation Laboratory. Its spike leakage energy was high, about 0.8 erg, but, because no careful study of keep-alive location and gas filling has been made, it has not yet been established that such a tube cannot be altered to protect crystals. The experiments did indicate however that with careful design, a low-Q gap with low spike leakage energy could be made.

[1] Extensive research has been done in the development of low-melting-point hard solders, and a suitable solder may already exist.

6·13. Construction Techniques—Metal-to-glass Seals.—The metal-to-glass seals used in microwave TR tubes may be classified under three main headings: (1) wire feed-through seals, (2) balanced copper-to-glass seals, and (3) Kovar or Fernico window seals. The first type, the feed-through seal, is used mainly for keep-alive electrodes. Such seals are of fairly simple construction and will not be described here.

The balanced seal is extremely useful in that it allows a butt joint to be made between a glass cylinder and a copper disk as in the 1B27 TR tube. In this seal, advantage is taken of the fact that glass is stronger in shear than it is in tension. If a disk of copper were sealed directly to one glass cylinder, when the cylinder cooled the copper would expand radially more rapidly than the glass. The resulting bending of the copper disk pulls it away from the glass and breaks the seal. If now, however, the disk is sealed between two glass cylinders, it can no longer pull away from either one and the differential expansion of the two materials results in a radial force which exerts essentially pure shear upon the glass. Such seals will withstand temperatures varying from several hundred degrees centigrade down to $-50°C$ or less.

There are two important methods for making balanced seals: the "borated" and the "beaded" seal techniques. These have been used extensively in TR tubes of the cell type. The borated seal is prepared as follows:

1. The copper flanges are thoroughly cleaned, etched, and then washed in water and alcohol.
2. The copper is oxidized in a gas flame and is then allowed to cool.
3. The flanges are dipped into a solution of sodium tetraborate, $Na_2B_4O_7$, 1.5 gr to 100 cc of H_2O.
4. After drying, the flanges are heated by a gas flame or an induction coil to form cuprous oxide of a deep red color.
5. The flanges and glass cylinders are then stacked in the assembly, jigged and heated by r-f induction to make the seals. This is done in an atmosphere of CO_2 to prevent excessive oxidation.
6. After annealing, the entire tube is cleaned with acid to remove the oxide.
7. If an inert coating is desired (Sec. 5·25), the section to be left oxidized is coated with a lacquer before the acid cleaning, after which the lacquer is dissolved in alcohol.

The beaded seal is considerably stronger than the borated seal, although it is slightly more difficult to make. It is used almost exclusively now in all cell TR tubes. The seal is made by sealing thin glass rings to each side of the oxidized copper disk in a direct copper-glass seal. A hydrogen flame is used to make this seal. The glass cylinders are then

sealed to the beads in a hydrogen flame. After annealing, the tube is cleaned as above.

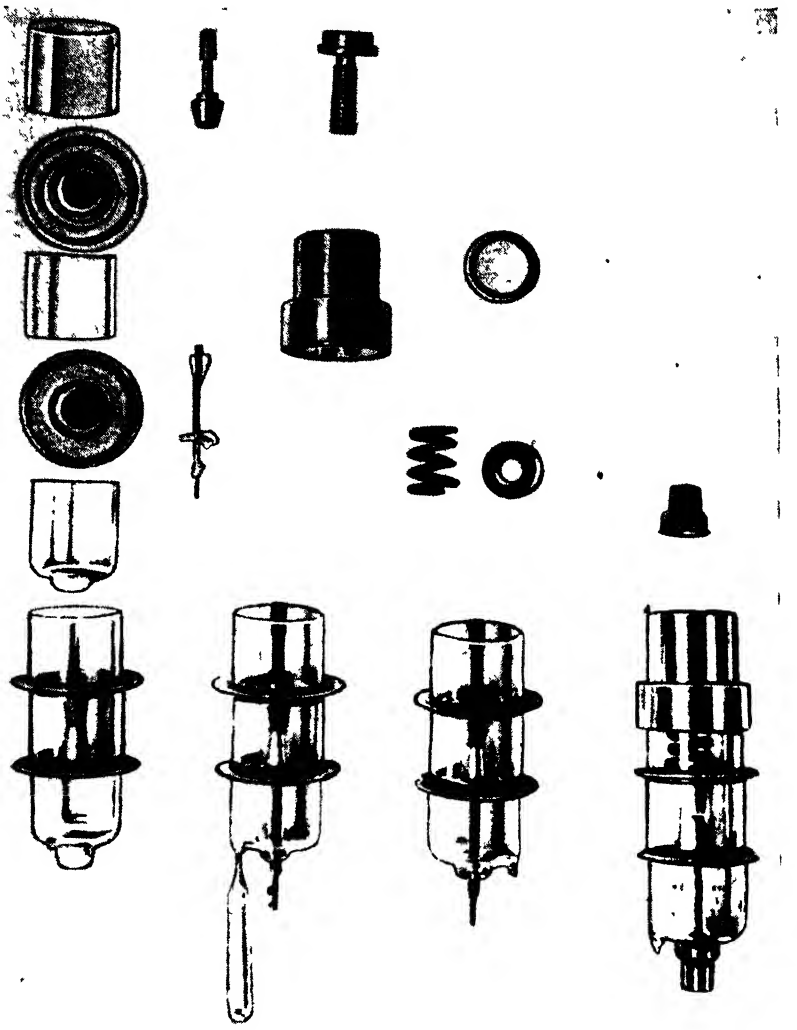

FIG. 6 23.—The various stages in the construction of the 1B27 TR tube. This tube is an excellent example of the use of the balanced copper-glass seal. (*Courtesy Sylvania Electric Products Co.*)

In addition to being mechanically stronger, the beaded seal overcomes the main defect of the borated seal in that it cannot be spoiled by long exposure to warm, moist air. Borated seals can be dissolved in boiling water, of course, and there was some evidence that prolonged exposure to moist air in the tropics also weakened them. Figure 6·23 shows the

parts and stages of manufacture of a 1B27 tube, a good example of the use of copper-glass seals.

The third group of seals involves the use of glass-sealing alloys with suitable coefficients of expansion. The balanced copper-glass seals can be made with any glass, but Corning 707 glass is commonly used because of its low loss factor. Kovar[1] is designed to match 706 (705AO) glass, which has an expansion coefficient of 5×10^{-6} per °C; but successful seals have been made to 707 glass which has a coefficient of 3.1×10^{-6} per °C. Flat windows sealed in Kovar frames are used in the 1B24, 1B26, and in the 1B50 integral-cavity TR tubes, and in all the low-Q ATR, pre-TR, and bandpass TR tubes.

The general process of making these windows is as follows:

1. The Kovar frame is heated in air by an induction coil to oxidize it. The proper depth of oxidation is important and must be recognized by the proper shade of grey.
2. The glass blank is then placed on the frame and the combination is heated in a CO_2 atmosphere until the seal is made.

For low-Q windows in ATR and other tubes it is necessary to add a further refinement. The intensity of the window discharge is so great that if the window consists simply of a piece of glass in a Kovar frame, the discharge cleans up the gas very rapidly by what seems to be a sputtering action. To prevent this, M. D. Fiske[2] coated the inside surface of the Kovar frame with glass. This coating is now used in all tubes of this kind. The glass coating may be applied in one of two ways. Fiske's method consists of spraying the oxidized metal with a suspension of powdered glass in alcohol. The edges must first be masked so that the frame can subsequently be soldered into the tube. The frame is then heated in air to a temperature of 950°C for 10 minutes. The next step is to place the frame on a graphite block, set the glass window in place, and then cover it with another graphite block. The assembly is again heated to 950°C for 15 minutes.

A much simpler method for 3-cm low-Q windows was devised by McCarthy of the Sylvania Co. It consists simply of placing on the oxidized frame a glass block that is bigger than the opening. It is then induction heated in a CO_2 atmosphere. The most intense heat is generated around the periphery of the frame and this causes the glass at first to run out towards the edges of the frame and then finally to soften at the center. When this softening occurs, a lavite paddle is used to press

[1] "Kovar" is used here as a generic term to include both Kovar and Fernico.

[2] M. D. Fiske, "Resonant Windows for Vacuum Seals in Rectangular Waveguides," GE Report, Feb. 10, 1945.

it into place. Although this method is satisfactory for small windows, it is apparently impractical for 10-cm windows.

Although 707 glass has a lower coefficient of expansion than Kovar, very excellent flat windows have been made with it. Under a polarized-light strain analyzer, a good window made with 706 glass shows almost no signs of strain. Windows made of 707 glass, however, show marked strain lines that indicate that the glass is under compression at room temperature. Although there are no definitive experiments, it is reasonable to suppose that the 707 windows are stronger since the glass can never be under tension. The most that can be said is that windows of both types, when they are well made, meet all possible service requirements.

6·14. Soldering of Windows into Cavities.—In Sec. 2·12 it has been seen that in order successfully to solder the Kovar window frame into the copper block of the 1B24 and 1B26 TR tubes, the frames must have wrinkles (Fig. 2·69) that allow the outer edges to move in and out with the copper block without cracking the window. The linear coefficient of copper is about 16×10^{-6} per degree C, or approximately 3 times that of Kovar.

The actual soldering process consists of heating the tube body by means of a large electric heater, such as a soldering iron, or a hot plate. This is done with the pretinned window frame in place. When the desired temperature is reached, additional solder in the form of a fine wire is applied to the edge of the frame.

On the 1B50 tube which has a steel body, it is possible to hard-solder the window into place. This makes a much stronger seal, and it eliminates the possibility of soft-solder flux getting into the tube cavity.

The low-Q windows in pre-TR and similar tubes are soldered into the ends of rectangular waveguides. In the original tubes made by Fiske, pure tin solder was used. The window was dropped into a seat formed by cutting the guide wall to half its thickness. Because of the rectangular shape of the window and because of the relative stiffness of the Kovar frame, it is very important to make the heating uniform in order to prevent cracking of the glass. Since the solder must be fed in by hand while the tube is hot, gas heating is impossible, and electrical heating only can be used.

The technique of soft-soldering the flat frames into the waveguide recesses was never really perfected from a production standpoint except in the smaller tubes such as the 1B35 and 1B36 tubes. The first definite variation from this technique was made by Sylvania in the 1B35 and the 1B36 tubes. The 1B36 tube was of all-steel construction, except for the frame, and was completely assembled with hard solder. The 1B35 body was brass waveguide but the Sylvania engineers succeeded in hard-

soldering the window directly to the end of the waveguide, in a butt joint.

Engineers both of Sperry and Sylvania designed 10-cm ATR tubes and bandpass TR tubes that were completely assembled with hard solder. None of these tubes reached the production stage.

In the Sylvania 1B52 and 1B53 ATR tubes, the 1B54 pre-TR tubes, and the 1B55 bandpass TR tubes, the brass waveguide was replaced by steel tubing, and the flat Kovar frame was replaced by a rectangular cup or dish, whose cross section matched that of the waveguide.[1] The two were butted together and the steel mounting flange was slipped over the outside. This three-piece combination was then soft-soldered together. This construction is apparently much stronger than the construction just described. One indication of this is the fact that few 10-cm tubes with flat window frames and brass bodies can withstand more than 20 temperature cycles from −40°C to 100°C without failing, whereas tubes made with this new type of construction have withstood several hundred such cycles.

6·15. Tuning Techniques.—The 721B and 724B tubes, since they are fixed-tuned tubes, must be pretuned in standard cavities to standard frequencies. This is accomplished by pushing one of the cones in or out by means of a special tool pushed in through the pumping tubulation.

The 1B24, 1B26, 1B27, and 1B50 tubes are tunable tubes. The tuning is accomplished by pushing one of the cones in or out with a differential-screw mechanism. The complete range is covered in a motion of 0.030 in. or less. In the 1B24 tube for instance, a motion of approximately 0.015 in. results in a change of tuning of 1200 Mc/sec. With $Q_{L2} \approx 300$, the half-power bandwidth of the tube is about 30 Mc/sec. Thus, a motion of 0.0001 in. of the cone results in a detuning of about 8 Mc/sec, and in an increase of insertion loss of about 1 db. Although the differential screw provides a convenient method for producing such small increments of motion, unless very accurate, and also very expensive, threads are used, it is necessary to use spring loading to eliminate backlash. This is shown in Fig. 2·68. The diaphragm through which the motion is transmitted to the cone exerts an axial force upon the screw, but as the diaphragm passes through its neutral position the force becomes zero and then changes sign; consequently, there is a region in which it is very difficult to tune accurately. Spring loading can be used to overcome this difficulty.

The tuning of bandpass TR tubes is the final operation before evacuation and sealing. The 10-cm gaps are of the form shown in Fig. 6·16 with one of the posts arranged to screw in or out. After the gaps are

[1] Sylvania Electric Products, Inc., "Report on OSRD Tube Development Subcontract on Radiation Laboratory Purchase Order D1C-182032," Feb. 5, 1946.

tuned, the posts must be locked and sealed. This was done originally by soft-soldering the screw to the outside of the guide; however, unless the screws were very tight there was danger of moving the screw. L. Sorg of Sperry Gyroscope Co. suggested simply locking the post with a lock nut, but at the same time surrounding it by a little cylinder, hard-soldered to the outside of the guide, on which a lid may be soldered after the final tuneup.

The 3-cm bandpass tube uses cones similar to the hollow cones in the 1B24 tube. The movable cone is sealed at the apex and is pushed in and out from the outside by means of a screw that is soldered after being adjusted.

The low-Q ATR tubes may be tuned in two ways. One method is to make the cavity accurately to dimension and to grind the windows accurately to the proper thickness, with the result that when the tube is finally assembled it is automatically tuned correctly. This was the technique used by the General Electric engineers in the construction of the 1B35, 1B37, 1B36, and the 1B38 tubes.[1] It was possible in this way to make most of the ATR tubes tune to within ± 0.5 per cent of their nominal frequency.

The engineers at Sylvania, however, chose to allow more tolerance in window tuning by eliminating the grinding operation, and by tuning the final tube after assembly, as described in Chap. 4. This method was accepted as completely satisfactory until some time after the end of the war, when it was observed that the variation in the thickness of the glass resulted in a much larger error than was desirable in the position of the effective short circuit of the fired tube. It thus appears that unless closer control of glass thickness can be maintained in the sealing process, it will be necessary to grind the windows to definite thicknesses in order to maintain the necessary tolerance in arc position.

6·16. Mounting Devices.—The methods for mounting the various low-Q ATR tubes have already been described in Chap. 4. The coiled-spring contact used on the various 10-cm ATR tubes is also used for all the 10-cm TR and pre-TR tubes. The springs are beryllium-copper, wound of No. 26 (0.0159 in.) wire to 0.125 in. outside diameter, 40 turns to the inch. If the springs are properly mounted, and the seats in the duplexer are accurately machined, excellent contact is assured. It is felt, however, that a softer contact material is preferable, and some thought has been given to the use of a woven-metal gasket about $\frac{1}{8}$ in. square, made of Monel ribbon. Although such gaskets make excellent contact, no satisfactory method of securing them to the tubes has been developed.

[1] T. P. Curtiss, F. E. Dickey, G. H. Floyd, W. T. Posey, "Final Technical Report on OSRD Contract OEMsr-1306," Tube Division Section, Nov. 1945.

The 3-cm bandpass TR tube has standard waveguide flanges on either end for coupling to waveguide choke connectors. These flanges are in the planes of the windows. Because of their size, the flanges are very stiff and can exert severe radial stresses upon the windows. Early experimental tubes had brass flanges. The life of these tubes at high power levels was relatively short, and almost all failures resulted from cracked windows. The use of Kovar flanges relieved the extra temperature strains and almost no more failures of this kind occurred. The present 1B63, tube, which is made by Sylvania, uses steel flanges and hard-soldered window frames. Although the expansion of steel is twice that of Kovar, these tubes withstand about 50 temperature cycles with a temperature range of $-40°$ to 100°C.

CHAPTER 7

THE PRINCIPLES OF BRANCHED DUPLEXING CIRCUITS

By Harold K. Farr

The gas-filled switches commonly used in duplexers have been discussed; the circuits used to connect these switches to other components and to each other will now be examined. To a large extent duplexing circuits have been built around the fundamental structure of a three-way transmission-line junction or T-junction with the arms leading to antenna, receiver, and transmitter and with a suitable switch in the receiver arm and possibly also in the transmitter arm. This chapter will be concerned with duplexers of this type which will be referred to as *branched circuits* to distinguish them from the so-called *balanced circuits* to be discussed in Chap. 8.

It will be assumed that the reader is familiar with the transmission-line impedance charts of the two types representing the complex impedance plane and the complex reflection-coefficient plane respectively. The notation used in Chap. 4 will also be employed here. This means that the identification of any impedance Z_s by a subscript s at once defines all other related quantities according to the equations

$$Z_s = R_s + jX_s = \frac{1}{Y_s} = \frac{1}{G_s + jB_s},$$

$$\Gamma_s = \frac{Z_S - Z_0}{Z_s + Z_0}, \qquad r_s = \frac{1 + |\Gamma_s|}{1 - |\Gamma_s|}.$$

7·1. The Junction Circuit.—Since the salient feature of a branched duplexer is the three-way junction, the properties of this circuit will be discussed. Let us consider first a perfectly general lossless linear network with three pairs of terminals designated as (1), (2), and (3) for antenna, transmitter, and receiver.

During transmission the line leading to the receiver is short-circuited at some point by the TR tube as in Fig. 7·1. This places a pure reactance at the terminals (3) which can be made any value desired by adjusting the distance l from the junction to the short-circuit. The first requirement for the junction is that there be some value of l which will give perfect transmission from (2) to (1).

On reception it is necessary that there be a pure reactance at the terminals (2), and it is required of the junction that perfect transmission take place from (1) to (3) for some value of this reactance. In practice

the impedance at the terminals (2) may not always be a pure reactance, because of the wrong transmitter impedance or an inadequate ATR circuit, but, for the present, it will be considered purely imaginary. In the transmission case the impedance due to the TR switch is actually very close to a pure reactance.

The requirement for transmission is fulfilled for any sort of lossless three-way junction provided only that it is symmetrical about the receiver arm. If the receiver arm is short-circuited such a device becomes a nondissipative symmetrical four-terminal network. Such a circuit always has a characteristic impedance R which is either purely real or purely imaginary. If R is connected across the output pair of terminals, the impedance seen at the input pair will also be R. It might be expected that, by adjusting the position of the short circuit on the receiver arm, R could be made equal to Z_0, the characteristic impedance of the transmission line.

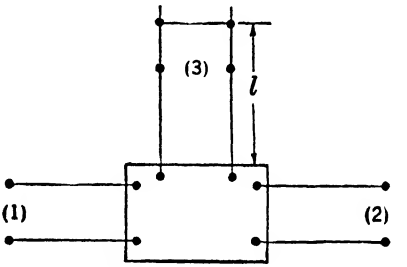

FIG. 7·1.—Representation of a waveguide junction.

To prove this the three equations are written

$$E_i = \sum_{j=1}^{3} z_{ij} I_j \qquad (i = 1, 2, 3), \tag{1}$$

expressing the voltage at any pair of terminals in terms of the current at each of the three pairs of terminals. Because $z_{ij} = z_{ji}$ and because of the symmetry of terminals (1) and (2), the impedance matrix can be written as

$$(z_{ij}) = \mathsf{Z} = \begin{pmatrix} A & B & D \\ B & A & D \\ D & D & C \end{pmatrix}.$$

A generator will be connected to terminals (1), a matched load of impedance unity to terminals (2), and an arbitrary reactance $z = jx$ to terminals (3). The condition that the input impedance be unity is then imposed. This gives the three equations

$$E_1 = I_1, \qquad E_2 = -I_2, \qquad E_3 = -zI_3,$$

which allows the elimination of the E_i's from Eqs. (1) with the result

$$\left.\begin{aligned} (A-1)I_1 + BI_2 + DI_3 &= 0 \\ BI_1 + (A+1)I_2 + DI_3 &= 0 \\ DI_1 + DI_2 + (C+z)I_3 &= 0 \end{aligned}\right\}. \tag{2}$$

Since there must obviously be coupling between any two arms, $B \neq 0$ and $D \neq 0$. It is therefore impossible for any row or column of coefficients to vanish. Hence the necessary and sufficient condition that the equations have a solution $I_1 \neq 0$ is that their determinant vanish. Since there is no loss, the elements of (z_{ij}) are all imaginary, and $A = ja$, $B = jb$, $\cdots$ where a, b $\cdots$ are real. The condition for solution is then

$$\begin{vmatrix} (a+j) & b & d \\ b & (a-j) & d \\ d & d & (c+x) \end{vmatrix} = 0.$$

If the determinant is expanded, the imaginary terms cancel out, permitting a real solution for x of the form

$$(c+x)(a^2 - b^2 + 1) + 2d^2(b-a) = 0.$$

In case $a^2 - b^2 + 1 = 0$, it is merely necessary to open-circuit terminals (3) for then $I_3 = 0$ and the condition that the first two of Eqs. (1) have a solution is

$$\begin{vmatrix} (a+j) & b \\ b & (a-j) \end{vmatrix} = a^2 - b^2 + 1 = 0.$$

This shows that there is always a reactance x which makes the system of Eqs. (2) consistent under the assumption that the input and output impedances are unity; that is, there is a reactance that matches the junction.

For mechanical reasons it is quite natural to construct a junction by adding a side arm for the receiver to a straight section of the transmission line which runs from transmitter to antenna. In such a "T-junction" the symmetry conditions for transmission are satisfied automatically and the junction may be matched for reception by some device, such as an inductive iris, in the receiver arm. After this device has been added, the distance from the junction to the TR switch can be adjusted to match the junction for transmission. Most T-junctions have rather small reception loss even without the addition of a matching device. In some cases this may permit the mounting of the TR switch at the closest position which gives good transmission since it is unnecessary to leave room for matching. This close position usually has the window of the TR cavity approximately flush with the wall of the waveguide or outer conductor of the coaxial line since the window presents a short circuit when the switch is fired.

The requirements for reflected power are ordinarily much more stringent during transmission than during reception, because the impedance presented at the transmitter has a very marked influence on the

transmitter efficiency and stability. In view of the contributions made to the reflected power by the other r-f components, a voltage standing-wave ratio above 1.10 during transmission may sometimes be considered excessive for a TR junction and 1.05 may be a desirable figure. In contrast to this, a VSWR of 1.10 would cause a reception loss of only 0.010 db, a value which would hardly be considered serious. This makes clear the advantage of mounting the TR cavity so that the window is flush with the surface of a straight section of transmission line. The symmetry makes possible a good match for the transmitted signal and the match can be maintained over a wide frequency band because of the proximity of window and transmission line.

An obvious extension of the symmetry principle leads to a junction in which *any* two arms are symmetrical with respect to the third. The junction is then matched for either transmission or reception if the arm not in use is short-circuited at the proper point. This eliminates the need for any matching device and, consequently, finds application in wideband systems. Since the three arms are at angles of 120° with one another, this Y-junction lacks the mechanical simplicity of the T-junction, with arms at angles of 90° or 180°. The principle of three-way symmetry has not had much application to coaxial duplexers, but has been used in waveguide circuits.

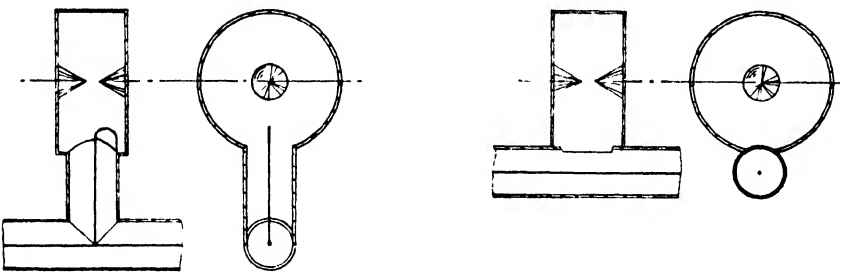

(*a*) (*b*)

FIG. 7·2.—Cavity coupling to a coaxial line; (*a*) loop-coupled cavity; (*b*) iris-coupled cavity.

7·2. Coaxial Junctions.—Coaxial duplexers have been used principally at wavelengths of 8 cm or longer. At shorter wavelengths, waveguide circuits are usually simpler. A coaxial line can be coupled to a TR or to an ATR cavity by a loop connected between inner and outer conductors, or by an iris. With an iris, no direct connection is made to the inner conductor, but an opening in the outer conductor establishes

coupling between the field in the cavity and that in the coaxial line. The iris coupling, which has mechanical advantages, may not be feasible where rather tight coupling is desired or where small-diameter lines are used. These two types of coupling are illustrated schematically in Fig. 7·2. When the cavity fires, a short circuit appears across the loop, and since the loop is connected across the side arm which is in shunt with the main transmitter line, the loop must be placed at a point effectively a quarter wavelength from the main line. This type of coupling is referred to as a shunt circuit. In the iris-coupled coaxial junction, the iris is sometimes considered as being in series with the outer conductor. When the switch is fired in this case, the short circuit which appears at the iris gives continuity to the coaxial line.

R. V. Pound of the Radiation Laboratory has developed a coaxial T-junction, based on the principle of his broadband T-stub, for $\frac{7}{8}$-in.-diameter, 46.4-ohm line for a loop-coupled TR cavity. This is a quarter-wavelength stub used as a mechanical support for the center conductor of a coaxial line as shown in Fig. 7·3. According to the symmetry principle just discussed, the length of the stub may be adjusted to secure a good match; and since the stub is in shunt with the line, this length is about one-quarter wavelength. If it is set for a good match at the center of a frequency band, however, there will be some mismatch at frequencies toward the edges of the band. To compensate for this, a transformer consisting of a sleeve one-half wavelength long is added to the center conductor of the main line as shown.

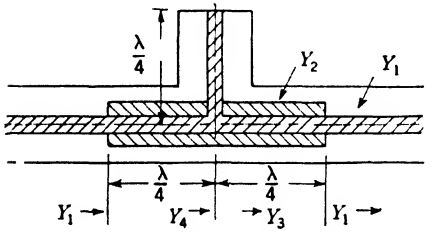

FIG. 7·3.—Broadband T-stub.

To understand the action of the half-wavelength transformer, let Y_1 and Y_2 be the characteristic admittances of the main coaxial line and of the section with the transformer respectively. Therefore $Y_2 > Y_1$ since the characteristic admittance of a coaxial transmission line is given by

$$\frac{1}{Y} = 60 \ln \left(\frac{\text{radius of outer conductor}}{\text{radius of inner conductor}} \right).$$

If the right-hand end of the line of Fig. 7·3 is terminated in a matched load, then the admittance looking toward the right at various points moving from the right-hand end toward the left can be determined. Figure 7·4*a* shows the locus of this admittance in the complex plane determined at the center frequency of the band. The admittance is Y_1 until the transformer is reached. It then moves around a circle

centered near Y_2 and, since the stub has no effect at this frequency, returns to Y_1 at the other end of the transformer.

At the low-frequency edge of the band the effective electrical lengths l/λ of both the stub and the transformer are reduced. Hence, in moving from the right-hand end to the center of the transformer, the admittance point travels less than halfway around the circle to the point Y_3 of Fig. 7·4*b*. To get Y_4, the admittance jB_s of the stub must be added to Y_3. Since the stub is now shorter than one-quarter wavelength, its admittance is inductive, and B_s is negative. This makes it possible to

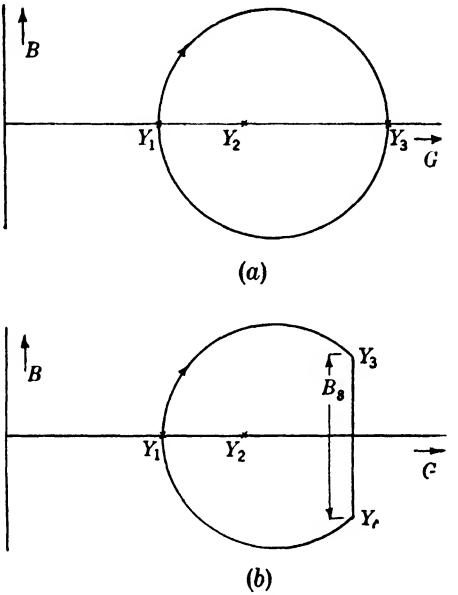

FIG. 7·4.—Admittance diagram for a broadband T-stub; (*a*) at center frequency; (*b*) at low-frequency edge of the band.

adjust the diameter of the transformer to give a value of Y_2/Y_1 such that $B_3 = -B_s/2$. The complex conjugate of Y_3 is then Y_4, and the admittance at the left end of the transformer will again be Y_1. A similar condition will be realized at the other end of the band so that the T-stub is perfectly matched at three frequencies. In this way it has been possible to design a single T-stub which can be used anywhere in the wavelength region from 9.0 to 11.1 cm (9.2-cm, 10.0-cm, 10.7-cm bands) with a VSWR less than 1.08.

Figure 7·5 illustrates a duplexer T-junction which uses this broadbanding technique. At high power level the situation is similar to that for the simple T-stub. However, in addition to the quarter-wavelength stub, which is retained for mechanical support, the TR arm acts as a three-quarter-wavelength stub since there is insufficient space to mount

the cavity at the one-quarter-wavelength position. This means that the total stub susceptance at the band edge is four times that for a simple T-stub and that the diameter of the half-wavelength transformer on the main line must be much greater.

At low power level the distance from the junction to the transmitter must first be adjusted so that the admittance of the transmitter arm is zero. It is then necessary to add another quarter-wavelength transformer A to the TR arm to match that portion of the half-wavelength transformer in the antenna arm. Without such a transformer a matched TR cavity and receiver would result in a VSWR, as seen from the antenna, of $(Y_2/Y_1)^2$. The presence of the transformer A, however, increases the rate of change with frequency of the susceptance of the TR arm at high power level. This makes it necessary to increase the diameter of the half-wavelength transformer and hence of A. But this, in turn necessitates a still larger half-wavelength transformer and a still larger transformer A. The process converges slowly to a diameter giving a good match for both high level and low level.

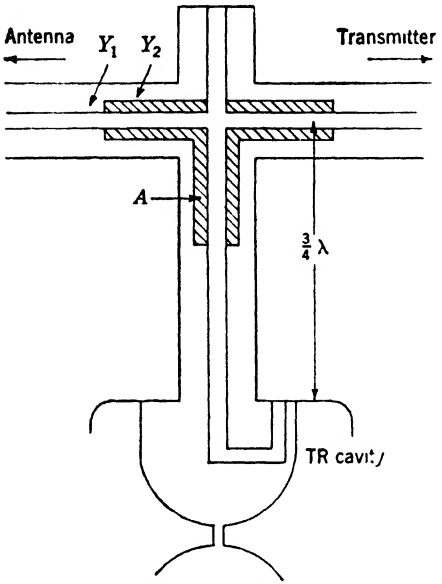

FIG. 7·5.—Coaxial T-junction with broadband transformer.

For a transformer of 0.555-in. diameter, the high-level VSWR remains below 1.25 from 8.5 to 12.2 cm wavelength. Since such a large transformer reduces the power that can be transmitted without breakdown, and since a narrower band permits a smaller transformer, it was decided to use a separate design for each of the 9.2-cm, 10.0-cm, and 10.7-cm bands in the wavelength region from 9.0 to 11.1 cm. A diameter of 0.486 in. was satisfactory for the reduced bands, giving a VSWR below 1.20 over the band from 10.4 to 11.1 cm, for example.

It is possible to eliminate the transformer A by changing the coupling of the input loop of the TR cavity. If the admittance of the TR switch as seen at the junction is Y_{TR}, then in order that this result in a match (admittance Y_1) as seen from the antenna arm, it is necessary that $Y_1/Y_{TR} = Y_2$ because of the quarter-wavelength transformer in the antenna arm. To satisfy this, Y_{TR} must be larger than Y_1 and since the junction is three quarters of a wavelength from the TR cavity,

the admittance at the loop must be less than Y_1. This means that the loop should be made larger in order to increase the coupling. This was done and some improvement resulted although difficulty was encountered in making the loop large enough because of the small space available in the cavity. If the loop could be adjusted to match the T-junction without the transformer A, the half-wavelength transformer could be made considerably smaller for a given bandwidth.

It will be noticed that at high level the T-junction is matched over the band while at low level it is matched only at the band center. This is because of the necessity for much better matching at high level. Although it is not so important to match the T-junction at more than one frequency for the low-level operation, it is usually necessary to employ some matching procedure to match at one wavelength, and to prevent the signal losses from becoming too high.

It is possible to use a design similar to that of Fig. 7·5, but with the transmitter connected to the side arm and the antenna and TR switch connected to the main arms. In this case moderate reflections may be tolerated for power transmitted between the two main arms (low-level condition) but the best possible match should be sought for transmission "around the corner" from the side arm to one of the main arms (high-level condition). This is the reverse of the requirement for the junction with the TR cavity on the side arm.

7·3. Waveguide Junctions.—Waveguide duplexers at microwave frequencies are of necessity built with iris coupling, since there is no center conductor to connect to a loop. The iris may be coupled either to the end of a side arm or to the main transmitter line. Rectangular waveguide in the fundamental TE_{10}-mode is the usual type and coupling may be made either to the broad or to the narrow side of the waveguide. A waveguide junction in which a side arm attaches to the broad side of another waveguide is called an E-plane junction since all three arms lie in the plane of the electric vector. Similarly, connection to the narrow side is called an H-plane junction in reference to the magnetic plane.

It was pointed out in Chap. 4 in connection with the ATR switch that an E-plane junction has some of the characteristics of a simple series branching circuit and that the H-plane junction displays shunt properties. Since this turns out to be a very convenient concept for duplexer design, it will be examined more closely at this time. A qualitative understanding can be gained by a consideration of the fields and currents in a waveguide. In the TE_{10}-mode the currents in the central portions of the two broad sides flow longitudinally in opposite directions, and the electric field extends across the intervening space from one of the broad sides to the other. These two central strips thus resemble the two halves of a simple transmission-line pair. In terms of these strips the

series and shunt characteristics of the two junctions of Fig. 7·6 appear quite plausible.

It can be observed that the side arm of the shunt junction meets the wall of the main waveguide at a certain distance from the central strip. If the side arm is short-circuited in the plane of the main waveguide wall, energy will travel down that waveguide without interruption. For that reason the distance from the central strip out to the side arm is thought of as being one-quarter wavelength in the shunt junction. No such phase shift is assumed in the series junction.

To justify this equivalent-circuit concept, it is necessary to refer to the experimental data. Here the results depend on the wavelength and the dimensions of the waveguide. Furthermore, a cavity attached to the side arm one-half wavelength from the main waveguide may give results which differ from those for a cavity mounted flush with the wall. The simple waveguide circuit with all terminations kept at a distance from the junction has been studied theoretically and experimentally. The results are embodied in the equivalent circuits of Figs. 4·10*a* and *b* which were considered in Chap. 4. At first glance these circuits do not seem to resemble a simple series or shunt junction but they do approximate them in certain respects. The network for the *E*-plane junction would be a simple series branch if B_a, X_b, X_d were zero and X_c infinite. It is seen from Table 4·1, Chap. 4, that B_a is small, X_c is large, and X_b and X_d would almost cancel if X_c were large enough to be neglected. This junction, therefore, closely resembles the simple series branch.

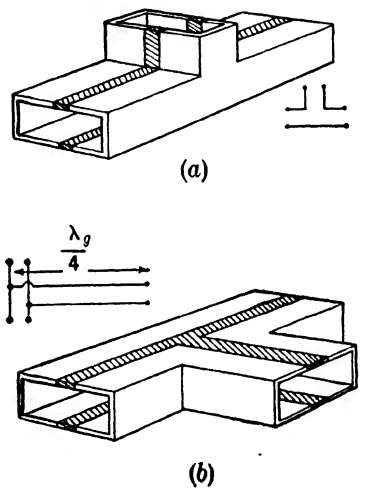

FIG. 7·6.—Waveguide as a transmission-line pair; (*a*) series junction, *E*-plane; (*b*) shunt junction, *H*-plane.

The *H*-plane junction is not so simple, for, although X_a and X_b are small, X_c and X_d are far from negligible. These last two quantities are nearly equal and opposite. This means that a short circuit placed at terminals (3) results in almost complete cancellation, and leaves only a very high impedance across the main line in agreement with the idealized circuit of Fig. 7·6. The simple shunt representation would also require that an open circuit at terminals (3) result in a short circuit across the line, whereas it actually shunts the line with a reactance of about one. Of course, there is a point on the side arm where an open circuit would

result in a short circuit across the main line but it is about five eighths of a wavelength from the main waveguide rather than one-half wavelength.

If such a junction were used in a duplexer, this departure from ideal behavior might not be noticed. At high level the short circuit at the window of the TR or ATR cavity would be placed at the waveguide wall since for this case the junction resembles an ideal shunt circuit. At low level it would be necessary to add a matching transformer to the junction if it were to be used as a TR mount. As an ATR junction, however, it would be necessary only to tune the ATR cavity until its reactance resonated with the junction. In Sec. 7·10 it will be shown that the difference between the actual TR junction and a simple series or shunt branch can nevertheless be important in broadband applications.

The equivalent circuits of Figs. 4·10*a* and *b* can be used to calculate the minimum standing-wave ratio that can be obtained looking into arm (1) with a matched load on arm (3) and an adjustable short circuit on arm (2), but with no additional matching devices. According to the symmetry principle the match between arms (1) and (2) (straight through) can be made perfect but the match "looking around the corner," as in the ordinary case for reception, will depend on the particular junction.

If an impedance unity is connected across terminals (3) of the series junction, the admittance seen looking out toward arm (3) from the terminals of jX_c is

$$Y_1 = \frac{1}{jX_c} + \frac{1}{1 + jX_d}.$$

If the values in Table 4·1 are used,

$$R_1 = \frac{X_c^2}{1 + (X_c + X_d)^2} = 0.78.$$

The short circuit in arm (2) can be adjusted to produce any desired reactance in series with Z_1. If $Z_1' = R_1 + jX'$ where X' may have any value, the admittance seen looking into arm (1) is $Y_2 = Y_1' + jB_a$. The locus of Z_1' on a Smith chart is simply the resistance contour $R_1 = 0.78$. If this circle is rotated 180° to give Y_1' and then displaced an amount $B_a = -0.096$, the resulting locus is Y_2. The point on the locus which approaches closest to the origin gives the minimum attainable standing-wave ratio.

The value of this quantity in voltage is $r = 1.3$ for a series junction and $r = 1.7$ for a shunt junction when the constants in Table 4·1 are used. Apparently the series T-junction is superior although the reflec-

tion loss from a shunt junction would be only 0.30 db even with no matching iris.

Although the right-angle T-junction can be matched with an iris so that the transmission is the same as for a symmetrical 120° type, the behavior over a band of frequencies will be inferior to that of the symmetrical junction. A set of data relative to this question is reproduced in Fig. 7·7 from a report by D. H. Ring of the Bell Telephone Laboratories.[1] Measurements were made, on a number of different junctions, of the variation with wavelength of the standing-wave ratio seen looking into one arm with an adjustable short-circuiting plunger in a second arm and a matched load terminating the third. The plunger was adjusted to give the minimum possible standing-wave ratio at the center wavelength of 3.33 cm and kept at the same position for all the other wavelengths. This corresponds to the use of the junction in a duplexer where a single position must be chosen for the ATR cavity for operation over a band of frequencies. Right-angle T-junctions and 120° Y-junctions were tested in waveguides of two sizes—0.400 in. by 0.900 in. ID and 0.500 in. by 1.125 in. ID. The 90° junctions were tested "looking around the corner" from one of the main arms to the side arm. No matching devices were used. If the standing-wave ratios are converted to voltage, the values for series and shunt are 1.2 and 1.6 for the 0.400 in. by 0.900 in. T-junctions at 3.33 cm. These agree approximately with the values of 1.3 and 1.7 previously calculated on the basis of the constants for 3.2 cm.

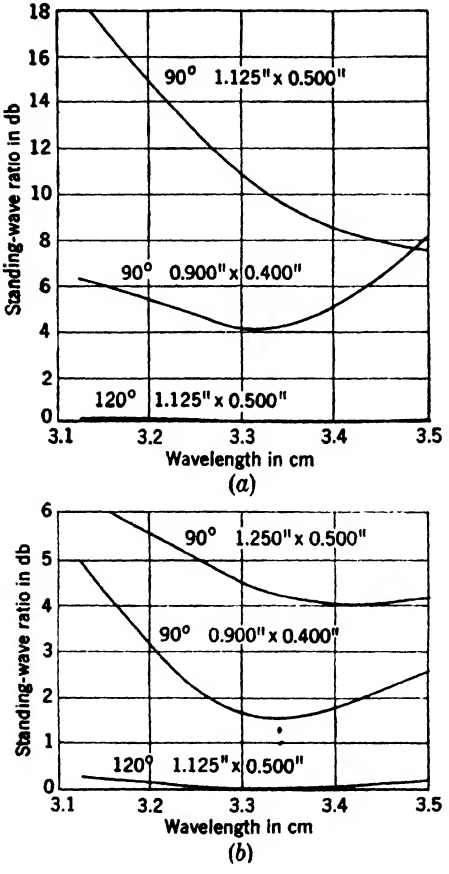

FIG. 7·7.—Standing-wave-ratio curves for T-junctions of various types; (*a*) *H*-plane junctions; (*b*) *E*-plane junctions.

[1] D. H. Ring, "Progress Report on a Broad Band TR-RT Switch," BTL MM-43-160-189, Oct. 9, 1943.

It will be seen that the 120° junction is much superior to the 90° junction because, even if the latter were matched at the center wavelength, it would give high reflections at other wavelengths. Of the two 120° junctions, the *H*-plane type is superior, whereas better results with 90° junctions are obtained if the *E*-plane branching is used. Furthermore, the small waveguide is better than the large. It is concluded that for narrow-band work the 90° junction can be used by matching at one wavelength; otherwise the 120° design is better.

The high-level standing-wave ratio can be made good with either the T- or the Y-junctions. For work over a band of frequencies, however, a cavity (either TR or ATR) mounted one-half wavelength from the junction on a side arm can lead to objectionable standing waves at the band edges because of changes in electrical length of the side arm. In such a case the voltage standing-wave ratio can be readily calculated at a wavelength differing by $\Delta\lambda$ from the wavelength at which the junction is matched if the simple series representation of the junction is assumed. The reactance of the side arm is $X_1 = \tan \beta$, where $\beta = 2\pi l/\lambda_g$ is the electrical length in radians from the junction to the window. Since $\beta = n\pi + \Delta\beta$ where $\Delta\beta$ is small,

$$X_1 \approx \Delta\beta \approx \frac{d\beta}{d\lambda}\Delta\lambda = -\frac{\beta}{\lambda_g}\frac{d\lambda_g}{d\lambda}\Delta\lambda = -\beta\left(\frac{\lambda_g}{\lambda}\right)^2\frac{\Delta\lambda}{\lambda}$$

because of Eq. (4·6). If a matched load is assumed for the antenna, the impedance seen by the transmitter is $Z_2 = 1 + jX_1$, and the corresponding reflection coefficient is

$$\Gamma_2 = \frac{Z_2 - 1}{Z_2 + 1} = \frac{jX_1}{2 + jX_1}.$$

Since X_1 is small, $|\Gamma_2| \approx |X_1/2|$ and the voltage standing-wave ratio is

$$r = \frac{1 + |\Gamma_2|}{1 - |\Gamma_2|} \approx 1 + |X_1| = 1 + \beta\left(\frac{\lambda_g}{\lambda}\right)^2\left|\frac{\Delta\lambda}{\lambda}\right|.$$

The shunt junction gives the same result. For $l = \lambda_g/2$, $\beta = \pi$, and for a 2 per cent bandwidth $\Delta\lambda/\lambda = 0.01$, and a representative value of $(\lambda_g/\lambda)^2$ is 2. These values give $r = 1.06$.

In practical applications of the 120° junctions it is advantageous for mechanical reasons to preserve the outward form of the 90° junction. This can be achieved by making additional 30° bends in the transmitter and the antenna arms quite close to the junction. A so-called "vestigial" 120° junction, in which the 120° sections are considerably abbreviated, is illustrated in Fig. 7·8 as designed for branching in the *H*-plane. In place of the receiver arm there is a choke coupling for

mounting a 1B24 TR tube close to the junction. On the outside corner of each 30° bend, a reflecting plate is added at an angle of 15° to either section of waveguide and placed so as to match the bend. For transmission between the two parallel arms, the voltage standing-wave ratio remains below 1.05 over a band of wavelengths from 3.13 to 3.53 cm. For testing transmission between the side arm and one of the parallel arms, a short-circuiting plunger was placed one-half wavelength back from the closest correct position, to simulate an ATR cavity, which must be at a distance from the junction because of lack of space. With fixed plunger position the variation of the standing-wave ratio with frequency was then found to be about the same as that to be expected from an ideal shunt junction with a three-quarter-wavelength stub.

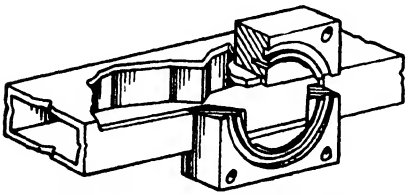

FIG. 7·8.—Vestigial 120° junction.

It will be noticed that the 120° junction provides more room for attaching the TR cavity than is provided by a 90° side arm. In the latter arrangement, there may be some difficulty in mounting the cavity so that it is flush with the waveguide wall, and easily removable for maintenance. Fortunately, it is found possible in some cases to obtain a rather good match between transmitter and antenna with the window of the TR cavity placed a small distance back from the inside wall of the waveguide on a 90° side arm.

When a TR or ATR tube is mounted with the window flush with the waveguide wall, the constants in Table 4·1 no longer apply. It was seen in Chap. 4 that for at least one such ATR switch, the simple series representation held accurately. The simple circuit seems to apply as well in such cases as for the isolated junction. This does not mean that a cavity mounted out on a side arm will show exactly the same behavior as when flush with the waveguide, but a proper readjustment of the circuit constants will still allow an approximate shunt or series representation.

In the next few sections it will be assumed, for simplicity, that the T-junction can be represented as a simple shunt or series circuit. In Sec. 7·10 a more accurate representation will be discussed and a comparison will be made between an actual junction and the ideal circuit.

7·4. Duplexing Loss without an ATR Tube.—In radar operation the losses suffered by either the transmitted or the received signal are of interest. The simple dissipative losses in waveguide are common to both of these signals but, except for the cavity losses, they make an insignificant contribution to the duplexing losses.

On transmission, the only important loss is the so-called arc loss due to the power dissipated in the arcs of the TR and ATR tubes. This is also small, ordinarily, and the importance of the effect results not so much from the power dissipated as from the dependence of transmitter efficiency on the reflected power. As the subject of arc loss is discussed in connection with TR and ATR switches it need not be considered at this time.

On reception, the duplexing loss can be conveniently divided into two parts: the TR loss, caused by dissipation in or reflection from the TR switch, and the "branching loss," due to improper impedance of the transmitter branch. The TR loss is adequately covered in the chapter on the low-level operation of the TR tube and branching loss will be discussed in the next few sections of this chapter.

A duplex radar system may be operated satisfactorily without an ATR switch if the transmitter, as seen from the antenna, presents the correct impedance at the TR junction. The received signal will then be conducted from antenna to receiver without any appreciable loss attributable to the transmitter.

This situation is indicated in Fig. 7·9, which represents TR junctions of the series and shunt type. For the purposes of this section, it will be assumed that the receiver is matched, as seen from the TR cavity, and that the cavity introduces no mismatch and may be neglected in low-level considerations. It will also be assumed that the junction can be represented as a simple series or shunt branching circuit.

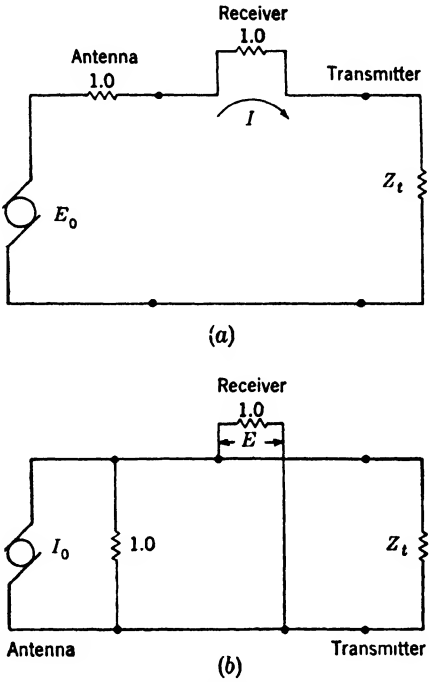

FIG. 7·9.—Duplexing circuits at low level; (*a*) with series TR switch; (*b*) with shunt TR switch.

If Z_t represents the transmitter impedance seen at the TR junction, then for perfect reception it is necessary that $Z_t = 0$ for the series TR junction or $Z_t = \infty$ for a shunt junction. The impedance Z_c, presented by a transmitter at its output terminals when not operating, is referred to as the *cold impedance* of the transmitter. Where there is no ATR switch, Z_t is simply the impedance Z_c transformed down the line from

the transmitter to the TR junction. If Z_c is purely reactive, that is, if the cold transmitter reflects completely, the phase shift between transmitter and TR junction can be adjusted to make $Z_t = 0$ or ∞ as necessary. For some transmitters Z_c has an appreciable real component which will dissipate some of the received signal unless an ATR switch is used; many others, however, are satisfactory in this respect. If the phase of Z_c is sufficiently constant from one tube to another, it may be possible to choose the length of the line connecting transmitter and TR tube so that Z_t will always have the correct phase. This is the most desirable arrangement when no ATR switch is used. Unfortunately differences between tubes lead to errors in Z_t, and changes in wavelength produce changes in the phase shift between transmitter and TR junction. This phase shift is given by the so-called "electrical length" $\theta = 2\pi(l/\lambda_g)$ of the connecting transmission line where l is its physical length. By making the distance l between transmitter and TR junction as small as possible, the variation in θ due to changes in wavelength can be kept to a minimum.

If the phase of Z_c varies too widely among transmitters, a phase control, called a "line stretcher," may be inserted between transmitter and TR junction. Since the impedance depends cyclically on θ with period π, the line stretcher must have a range $\theta = \pi$ or $l = \frac{1}{2}\lambda_g$. One device, called a "trombone," which has been used in coaxial lines, employs a sliding U-shaped section of line. In rectangular waveguide the wavelength depends on the inside width a of the waveguide according to the expression

$$\lambda_g = \frac{\lambda}{\sqrt{1 - \left(\frac{\lambda}{2a}\right)^2}},$$

and θ can be changed by varying a. If a slot is cut for a sufficient distance along the center of each of the wide sides of the waveguide, a can be changed by squeezing the two halves together. This "squeeze section" eliminates the need for any sliding contacts but requires a long section of waveguide, particularly at long wavelengths. A more compact waveguide line stretcher consists of a section of dielectric material which is supported by thin rods extending across the waveguide normal to the electric field. Phase may be varied by moving the dielectric from one side of the waveguide where the field is weak toward the strong field in the center.

If the antenna system is not perfectly matched, the variation in line length effected by the line stretcher causes a change in the impedance seen by the transmitter. This may result in changes in transmitter power and frequency. If this is objectionable, it can be prevented by

using two line stretchers, one on each side of the duplexer ganged together to cancel each other.

To determine the loss in the received signal when the impedance Z_t of the transmitter branch does not have the correct value, the case of a series TR junction may be considered. As can be seen by reference to Fig. 7·9, the power delivered to the receiver is

$$P = |I|^2 = \frac{|E_0|^2}{|2 + Z_t|^2} = \frac{|E_0|^2}{4|1 + \frac{1}{2}Z_t|^2}. \tag{3}$$

To match the receiver to the antenna, Z_t must be zero. This gives

$$P_0 = \frac{|E_0|^2}{4}. \tag{4}$$

If α is the *branching-loss factor* in voltage, then the loss factor in power is

$$\alpha^2 = \frac{P_0}{P} = \left|1 + \frac{1}{2}Z_t\right|^2. \tag{5}$$

Hence, for the series TR junction,

$$\alpha = |1 + \tfrac{1}{2}Z_t|. \tag{6}$$

The loss in decibels is $L = 20 \log_{10} \alpha$.

For the shunt junction

$$\alpha = |1 + \tfrac{1}{2}Y_t|, \tag{7}$$

where

$$Y_t = \frac{1}{Z_t}.$$

Equations (6) and (7) show that a *series TR junction is equivalent to a shunt junction if one is shifted one-quarter wavelength along the transmitter line with respect to the other.* A similar theorem for the ATR switch was discussed in Sec. 4·1.

It is frequently convenient to represent graphically the relation between α and Y_t. As an example, α will be determined for various settings of the line stretcher with a shunt TR junction, and a transmitter which, when off, has a voltage standing-wave ratio of $r_c = 3.0$. In Fig. 7·10 Y_t is mapped on the complex plane with G_t and B_t as coordinates. The locus of all values of Y_t obtained by varying the line stretcher is the

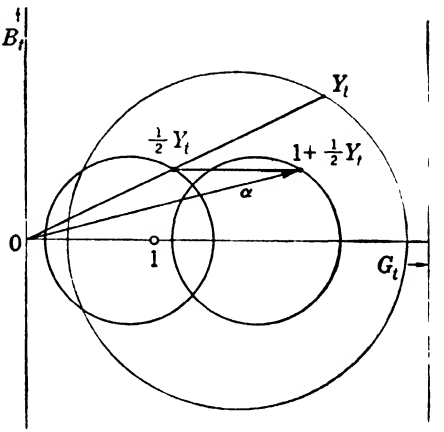

FIG. 7·10.—Duplexing branching-loss diagram.

familiar admittance circle of constant standing-wave ratio. This type of transmission-line chart, in which the rectangular coordinates G and B (or R and X) are used, will be called a cartesian chart to distinguish it from the reflection-coefficient Smith chart in which the admittance or impedance components are plotted in curvilinear coordinates.

The loci of $Y' = \frac{1}{2}Y_t$ and $Y'' = 1 + \frac{1}{2}Y_t$ are also circles. In fact, in the theory of functions of a complex variable it is shown that any transformation from Y to Y' of the form

$$Y' = \frac{aY + b}{cY + d}, \tag{8}$$

where a, b, c, and d are constants, maps a circle into a circle. It is known as a linear fractional transformation or as a "circular transformation." Because of this property it is a simple matter to construct Y'' and then to determine α according to Eq. (7) as the length of the vector $1 + \frac{1}{2}Y_t$.

It appears that the loss is a minimum where the left side of the circle intersects the real axis. At this point $Y_t = 1/r_c$, so that the minimum loss is

$$\alpha_n = 1 + \frac{1}{2r_c}. \tag{9}$$

This represents the lowest loss obtainable with a line stretcher. The worst transmitter is one for which $r_c = 1$ since this makes α_n a maximum. In such a case the loss L is $20 \log_{10} (\frac{3}{2}) = 3.5$ db.

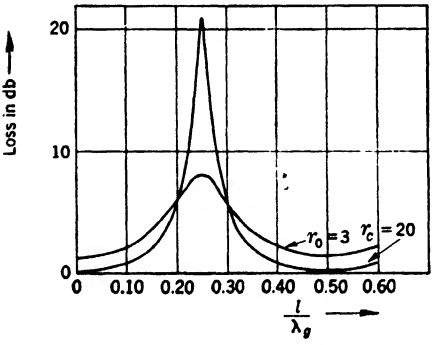

FIG. 7·11.—Loss vs. transmitter phase with no ATR switch.

When the phase changes introduced by the line stretcher are considered, it is often convenient for numerical work to use the quantity $\theta/2\pi = l/\lambda_g$ which expresses the line length in units of a wavelength rather than to use θ which is expressed in radians. The value of l/λ_g corresponding to each Y_t can be read from a conventional transmission-line chart and associated with the corresponding α by projecting from Y_t to $\frac{1}{2}Y_t$, to $1 + \frac{1}{2}Y_t$, and then measuring off α. The two curves of Fig. 7·11 give the results for transmitters having $r_c = 3$ and 20 respectively. They are periodic in l/λ_g of period 0.50.

Because of the equivalence of series and shunt junctions the curves of Fig. 7·11 would be the same for a series TR junction except that the abscissae are shifted a quarter wavelength. In this section and in Sec.

7·5 the discussion will refer to the shunt TR junction unless the series junction is specifically mentioned. In most cases the results will be immediately applicable to the series case through the use of the equivalence principle.

The broad region of low losses in Fig. 7·11 indicates the possibility of using a simplified form of line stretcher which has only two positions, differing by one-quarter wavelength. Since the loss curve has a cycle of one-half wavelength, one could always operate in that half of the phase range where the losses are smaller. The curve for $r_c = 20$ in Fig. 7·11 remains below 1.30 db over the interval of length 0.25 which extends from 0 to 0.125, and from 0.375 to 0.500. Many transmitting tubes have cold impedances which are almost purely reactive. For these $Y_t = jB_t = j \cot \theta$, and from Eq. (7)

$$\alpha^2 = |1 + \tfrac{1}{2}j \cot \theta|^2 = 1 + \tfrac{1}{4} \cot^2 \theta.$$

The maximum loss over the minimum half of the phase range is realized for $\theta = \pi/4$, which gives $\alpha^2 = \frac{5}{4}$, or a loss of 0.97 db.

7·5. Duplexing Loss with an ATR Switch.—In the examination of the branching loss when an ATR switch is used, there are four different fundamental duplexer circuits to be considered. They represent different combinations of series and shunt TR and ATR junctions. Any combination of the two kinds may be used if the distance between the junctions is properly chosen. These distances, as given in Table 7·1, are based on equivalent-circuit concepts and are, therefore, only nominal. The actual distances for best efficiency are slightly different and must be determined experimentally.

TABLE 7·1.—BASIC DUPLEXER CIRCUITS

TR junction	ATR junction	TR to ATR distance (nominal)
Shunt	Series	$\frac{1}{2}\lambda_g$
Shunt	Shunt	$\frac{1}{4}\lambda_g$
Series	Series	$\frac{1}{4}\lambda_g$
Series	Shunt	$\frac{1}{2}\lambda_g$

The equivalent circuit for the shunt-TR, series-ATR duplexer is shown in Fig. 7·12. Since the receiver is in parallel with the transmitter-antenna line, the ATR switch should cause the transmitter to appear as a high impedance at the TR junction in order that the antenna be matched to the receiver. Since the series ATR switch itself appears as a high impedance, it would be correct to insert it in the line right next to the TR junction. At microwave frequencies this is usually impossible, and the

ATR switch is placed at the equivalent position one-half waveguide wavelength away.

As was pointed out in Chap. 4 a shunt ATR switch is equivalent to a series-connected one if moved down the line a quarter wavelength. If the shunt ATR switch is used with the same shunt TR junction, the distance between the two becomes one-quarter wavelength. Similar considerations give the correct distance in the other two cases.

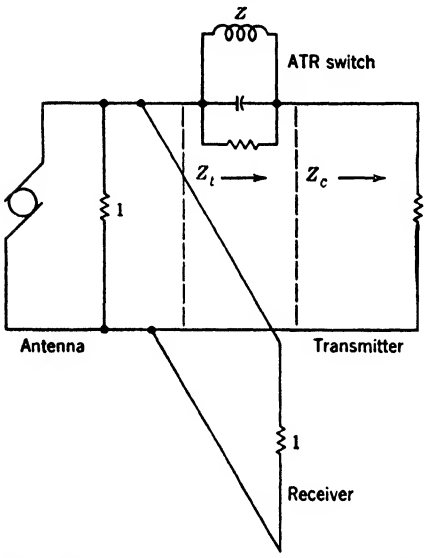

FIG. 7·12.—Duplexer circuit with shunt TR and series ATR switches.

Because of the equivalence of the two types of ATR switch and the equality of the branching losses with the two types of TR junction, as shown in Eqs. (6) and (7), a detailed analysis will be made only of the shunt-TR, series-ATR circuit.. The results will then apply with very little change to the other types of duplexer. In the first circuit to be considered, the ATR switch will be located correctly, that is, effectively next to the TR junction. The normalized ATR impedance will be designated by Z and the transmitter impedance, $Z_c = R_c + jX_c$, referred to the ATR junction. Then the impedance seen at the TR junction looking toward the transmitter is $Z_t = Z + Z_c$, and the branching-loss factor from Eq. (7) is

$$\therefore \alpha = \left| 1 + \frac{1}{2} \frac{1}{Z + Z_c} \right|.$$

For the ATR circuit tuned to resonance, $X = 0$ and

$$\alpha = \left| 1 + \frac{1}{2} \frac{1}{R + Z_c} \right|. \tag{10}$$

Before considering the branching loss under normal conditions, some mention should be made of the influence of the ATR tube on the recovery time of a duplexer. It was seen in Chap. 5 that the presence of ions in the TR gap may seriously attenuate signals which immediately follow the transmitted pulse. Under certain conditions the ATR tube may have a similar effect. If the transmitter impedance Z_c were zero and if the TR tube were already recovered, the loss would be given according

to Eq. (10) by the factor

$$\alpha = 1 + \tfrac{1}{2}G,$$

where G during recovery is determined by the conduction in the gap. When Z_c differs from zero, the added impedance in series with R decreases the loss so that this expression gives the upper limit of the loss. The same expression would be found if the ATR but not the TR tube had recovered and if G were the conductance of the TR tube. In that case, however, the expression would hold for any value of Z_c. Since G increases with Q, the usual TR tube would tend to recover more slowly than a low-Q ATR tube which has large gaps of low conductance.

In considering Eq. (10) it is convenient to make use of the so-called "Smith chart" type of transmission-line representation, which maps the complex reflection coefficient Γ rather than the impedance Z. This quantity, which is given by

$$\Gamma = \frac{Z - 1}{Z + 1}, \tag{11}$$

is limited to the interior of the unit circle, $|\Gamma| = 1$. By associating with each point Γ the corresponding Z, contours of constant R and X can be constructed, which form a system of curvilinear coordinates for Z.

If the point R representing the resonant ATR impedance is plotted on a Smith chart, the area corresponding to all possible values of $Z_t = R + Z_c$, when Z_c is allowed to take any physically realizable value, is found to be a circle like the small circle on the right side of Fig. 7·13 which was drawn for $R = 5$. A glance at a conventional Smith chart shows that Z_t is limited to the interior of this circle because R_c cannot be negative. In diagrams such as Fig. 7·13 the impedance coordinates will be omitted, except for the real axis which will be drawn horizontal and will increase from left to right. The $(R + Z_c)$-circle intersects the real axis at $Z_t = R$ and ∞.

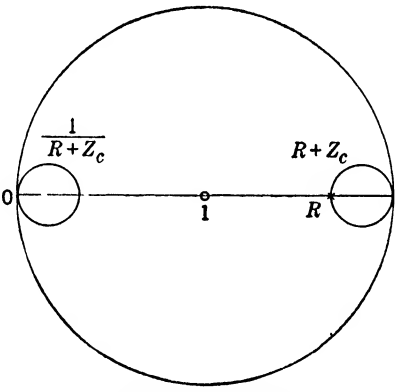

FIG. 7·13.—Smith-chart plot for duplexer with ATR cavity at resonance.

On a Smith chart the reciprocal of an impedance Z is represented by a point diametrically opposite to Z. Thus the locus of $1/(R + Z_c)$ is the circle on the left which crosses the real axis at 0 and $1/R$.

It is now convenient to transform to cartesian coordinates. In so doing, it is useful to remember that the transformation from a Smith

chart to a cartesian chart always maps a circle into a circle. This is because the transformation, given by

$$Z = \frac{1 + \Gamma}{1 - \Gamma} \tag{12}$$

has the form of Eq. (8). Of course this is also true for the reverse transformation of Eq. (11).

Thus the locus of $1/(R + Z_c)$ in cartesian coordinates is a circle intersecting the real axis at 0 and $1/R$ as in Fig. 7·14. Likewise the locus

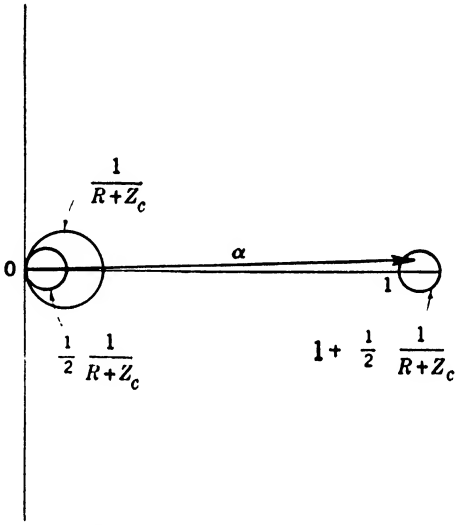

FIG. 7·14.—Loss diagram for a duplexer with ATR switch at resonance.

of $1 + \frac{1}{2}[1/(R + Z_c)]$ is a circle which crosses the axis at 1 and at $1/2R$. Since the vector whose magnitude is α must fall within this circle, α must have a value between 1 and $1 + 1/2R$. That is, for an ATR switch tuned to resonance the maximum branching loss is given by the factor

$$\alpha_z = 1 + \tfrac{1}{2}G, \tag{13}$$

where G is the cavity conductance. If $G = 0.05$, which is a reasonable value, the maximum α is 1.025, which means a loss of 0.21 db. With an ATR cavity of $G = 0.05$, tuned to resonance and located the proper distance from the TR junction, the branching loss must be between 0 and 0.21 db, no matter what the transmitter impedance.

For the impedance transformations associated with a loss calculation, the Smith chart is frequently more convenient than the cartesian chart. It would therefore be helpful to be able to determine α directly from a Smith-chart plot of Y_t, without the necessity for transforming to cartesian coordinates. To facilitate this, contours of constant loss, which will show

the loss corresponding to each value of Z_t, can be plotted on the Smith chart.

These contours can be determined by plotting loci of constant α in cartesian coordinates of $1 + \frac{1}{2}Y_t$ and then transforming them back to the Smith chart for Z_t. In the first case, they are merely circles concentric with the origin and of radius α as shown in Fig. 7·15 which indicates the loss in decibels for each contour. It is necessary to transform only the points of intersection with the real axis since the contours on the Smith chart must be circles with centers on the real axis. One intersection is at

$$1 + \tfrac{1}{2}Y_t = \alpha,$$

or

$$Y_t = 2(\alpha - 1). \qquad (14)$$

On the Smith chart for Z_t, this point is at

$$\Gamma_1 = \frac{1 - Y_t}{1 + Y_t}. \qquad (15)$$

If Eq. (14) is substituted into Eq. (15), then

$$\Gamma_1 = -\frac{2\alpha - 3}{2\alpha - 1}. \qquad (16)$$

Likewise the left-hand intersection is at $1 + \frac{1}{2}Y_t = -\alpha$, which gives

$$\Gamma_2 = -\frac{2\alpha + 3}{2\alpha + 1}.$$

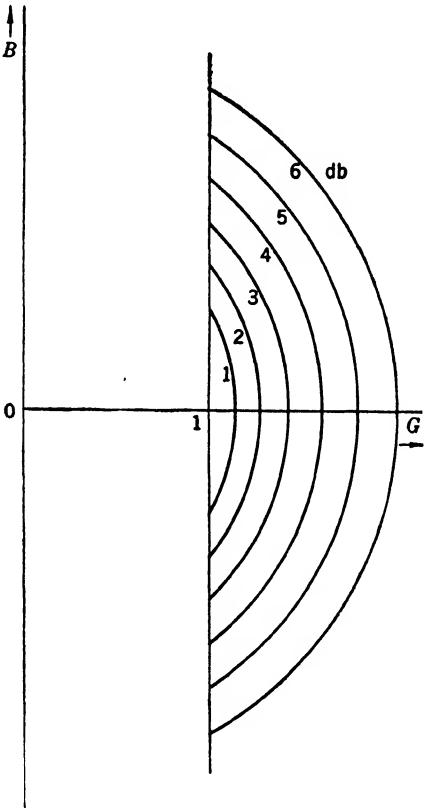

FIG. 7·15.—Loss contours on cartesian chart for $1 + \frac{1}{2}Y_t$.

The center of the circle is at

$$\Gamma_0 = \frac{1}{2}(\Gamma_2 + \Gamma_1) = -\frac{4\alpha^2 - 3}{4\alpha^2 - 1}, \qquad (17)$$

and the radius is

$$\rho = \frac{1}{2}(\Gamma_1 - \Gamma_2) = \frac{4\alpha}{4\alpha^2 - 1}. \qquad (18)$$

In plotting Γ, distances are measured from the center of the Smith chart, on a scale such that the outside circle has radius unity. The resulting contours are shown in Fig. 7·16. It is convenient to draw this diagram

on transparent paper so that it may be laid over a Z_t-plot. In fact, after such a contour diagram has been constructed, the cartesian plot for branching-loss calculations will rarely be used.

This same contour chart which was derived for a shunt TR junction may be used for a series junction except that, for a series junction, it will have to be applied to a Smith-chart plot of Y_t rather than of Z_t.

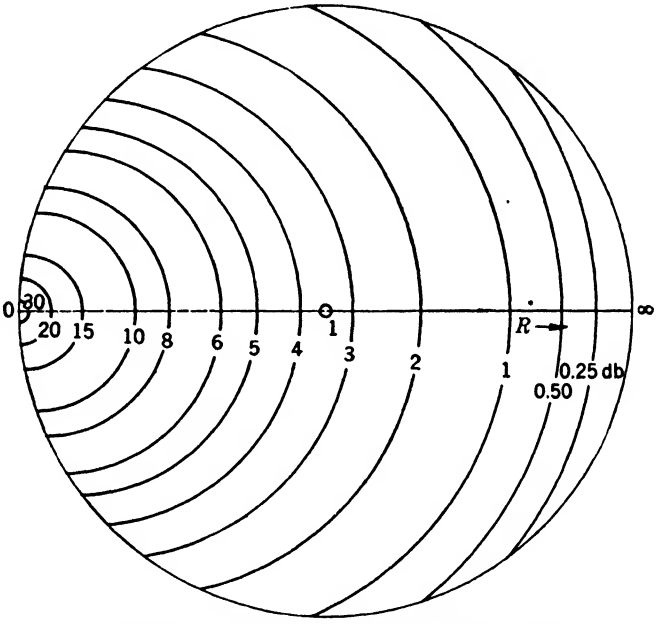

FIG. 7·16.—Loss contours on Smith chart for Z_t.

7·6. Tuning of the ATR Switch.—The loss-contour diagram can be used to study the effect of ATR-switch tuning. Since the admittance of the ATR switch consists of a constant conductance plus a variable susceptance, its locus on a Smith chart will be a circular arc, like the one labeled Y in Fig. 7·17. The similar arc on the opposite side of the diagram gives the impedance Z. If a particular point Z on this arc is chosen and Z_c is allowed to assume any value whatever, it will be found that the point, $Z_t = Z + Z_c$, will fall somewhere within the circle that passes through Z and ∞ and has its center on the real axis. If the loss contours, taken from Fig. 7·16, are drawn, the range of branching losses to be expected is found.

For the particular value of Y chosen here, $(0.05 - j0.16)$, it is seen that the loss can vary from 0 to more than 2 db, for different transmitter impedances. Comparison of this result with those just obtained for an ATR switch at resonance shows that an amount of detuning sufficient

to give a susceptance of only 0.16 will raise the branching loss from a maximum of 0.21 db, to more than 2 db.

Susceptances as large as this can easily appear. If, for example, the values $G = 0.05$, $B = 0.16$ and $Q_L = 4.0$ are substituted in Eq. (4·1),

$$\delta = \frac{\Delta\lambda}{\lambda_0} = \frac{B}{2(1+G)Q_L} = 0.02.$$

Thus, a deviation of 2 per cent from the resonant frequency will permit a loss of 2 db. Since it is not easy to obtain loaded Q's much lower than

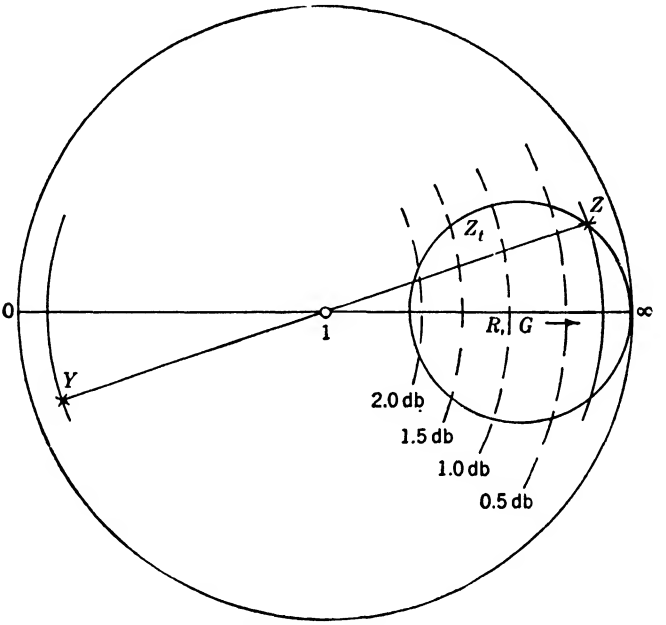

FIG. 7·17.—Loss diagram for ATR switch off resonance.

4, it is apparent why it is difficult to get good ATR-switch action over broad bands.

The tuning effect can be readily visualized from Fig. 7·17 since the effect of detuning is to move Y and Z away from the real axis. This, in turn, expands the Z_t circle toward the left, where it intersects the contours of higher loss.

More specifically, if a transmitter with a cold voltage standing-wave ratio of $r_c = 20$ is selected, a possible value of Z_c would be $0.6 + j3.0$, the impedance seen at a distance of $\theta/2\pi = 0.45$ from an impedance of 20. This value of Z_c and the previous ATR conductance of $G = 0.05$ will be used in constructing the locus of $Z_t = Z + Z_c$ when B is varied, in order to find the loss as a function of B (that is, of ATR-switch tuning).

Since the locus of Z is a circle, it follows that Z_t will also be a circle;

for the Z-locus may be transformed to rectangular coordinates, the constant Z_c added, and the resulting Z_t-locus transformed back to the Smith chart. Since each of these operations is of the form of Eq. (8), the result is a circle.

A formal expression for transforming the center and radius of a circle when a constant is added can presumably be obtained. This transformation, however, which is so elementary in cartesian coordinates, proves to be rather awkward on the Smith chart. The following procedure, though less elegant, is practical. The value of Z for some point on the

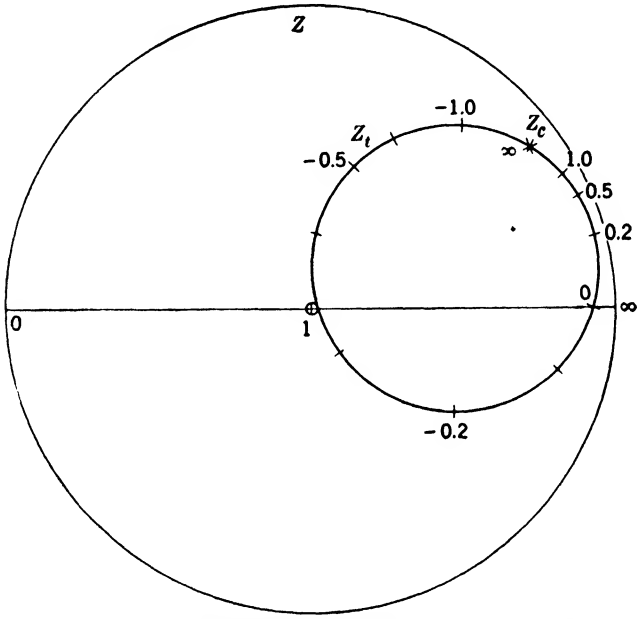

FIG. 7·18.—Diagram for determination of tuning curve.

Z-circle is read from the Smith chart, the constant Z_c added, and the resulting Z_t plotted again on the Smith chart. When three different Z_t points are plotted in this way, a circle passing through all of them can be constructed, and this is the Z_t-locus. More than three points are usually plotted, in order to provide a check, and also because the first three points might all lie on a small arc which would not provide the necessary accuracy. After the Z_t-points have been plotted, the circle can be found by trial and error rather than by the use of a formal construction. The result is shown in Fig. 7·18.

A value of Z_t can be associated with each value of the tuning parameter B. By means of the Smith chart, values of B are marked off on the Y-circle. These points are then rotated 180° to give the Z-plot. At each of these points, the imaginary component of Z is read, the imagi-

nary component of Z_c added (-3.0 in this case), and the intersection of the resulting reactance line with the Z_t-circle found. (In some cases it may be more accurate to use resistance instead of reactance.) In Fig. 7·18 values of B are marked off in tenths on the Z_t circle. It is now a simple matter to read off the loss for each point by using the contour diagram of Fig. 7·16. The result is the curve labeled $\theta/2\pi = 0.45$, in Fig. 7·19. The other curves are plotted for the same ATR switch and transmitter but for different phases, $\theta/2\pi = l/\lambda_g$, l being the distance

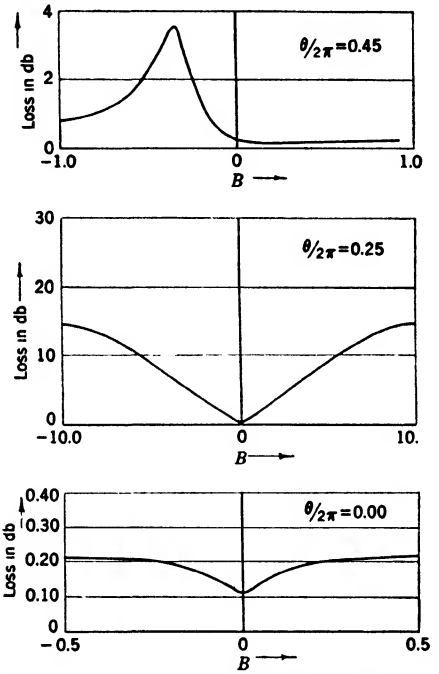

FIG. 7·19.—Tuning curves for ATR switch, $G = 0.05$, $r_c = 20$.

from the ATR switch, toward the transmitter, to the point where the transmitter impedance is 20. The curve for $\theta/2\pi = 0.25$ ($Z_c = 0.05$) is found in the same way as the first one. For $\theta/2\pi = 0$ ($Z_c = 20.0$), the variation is so small that the graphical method is inconvenient. This is a simple case and it can be calculated directly. In fact, since $G = 1/Z_c$ in this case,

$$\alpha^2 = 1 + \frac{2 + \left(\frac{B}{G}\right)^2}{4 + \left(\frac{B}{G}\right)^2} G$$

is obtained by neglecting small quantities in Eq. (7).

The difference in scale of the curves of Fig. 7·19 should be noted. For $\theta/2\pi = 0$, the loss is always small, whether or not the ATR switch is tuned to resonance, whereas for $\theta/2\pi = 0.25$, the loss is small at resonance but increases rapidly off resonance. For $\theta/2\pi = 0.45$, the loss is small at most tuning positions but becomes appreciable over a small range off resonance. In this region the reactances in Z and Z_c tend to cancel, corresponding to a sort of resonance between ATR switch and transmitter. This type of curve is rather general; the other two symmetrical curves represent special cases (Z_c is real).

It is evident that an ATR switch may be tuned without causing any appreciable increase in signal, or the signal may be strong for nearly all settings of the tuner and fall off sharply over a small range. This behavior is sometimes cited to show that the ATR switch is unnecessary. This, of course, is true for that particular transmitter, but if good operation is expected when the transmitter has some widely different impedance, the ATR switch, or some equivalent device, must be used.

7·7. Distance between TR and ATR Switches.—It has been assumed up to this point that the ATR switch has been located on the transmitter line at the correct distance from the TR junction: effectively $(n/2)\lambda_g$ or $\left(\frac{n}{2} + \frac{1}{4}\right)\lambda_g$ away, depending on the circuit used. Actually, the electrical distance changes with frequency, and it is necessary to determine how this affects the branching loss.

To determine this, $Z + Z_c$ is calculated as before Then Z_t, instead of being set equal to $Z + Z_c$, is obtained by transforming $Z + Z_c$ down the line an amount equal to the error in θ. As before, the contour diagram can be applied to find the loss. Since the transformation for line length is simply a rotation on the Smith chart, this can be accomplished by rotating the contour diagram with respect to the $(Z + Z_c)$-plot.

For the ATR switch at resonance, $Z + Z_c$ will be a point near the right-hand end of the real axis in Fig. 7·16. If the distance between the switches is varied, the situation is the same as that discussed in Sec. 7·4 where, with no ATR switch, the distance between the TR switch and the transmitter was varied. Hence, in Fig. 7·11 the portion of the $(r_c = 20)$-curve, in the region of $l = 0$ or 0.50, is similar to a loss-vs.-frequency plot for a tunable ATR switch.

If such an ATR switch is mounted on a waveguide transmitter line a certain distance from the TR junction, and the system is used over a certain frequency band, it may be desirable to know the branching loss at the band edge. As the distance between the TR and the ATR switches is usually chosen so that it is correct at the center of the band, the error in this distance, when the frequency has changed to the edge of the band, must be determined.

The electrical length is

$$\theta = \frac{2\pi l}{\lambda_g}. \tag{19}$$

It is necessary to find the correction $\Delta\theta = \theta_1 - \theta$, where θ_1 is the length at the edge of the band, and θ is that at the center. Since the changes are small

$$\theta_1 = \theta + \theta'\Delta\lambda + \tfrac{1}{2}\theta''(\Delta\lambda)^2,$$

where the primes indicate differentiation with respect to λ, and $\Delta\lambda$ is the change in wavelength from band center to edge. This may be written

$$\Delta\theta = \theta'\Delta\lambda + \tfrac{1}{2}\theta''(\Delta\lambda)^2. \tag{20}$$

If the second term is neglected, the fractional error introduced in $\Delta\theta$ is

$$\beta = \frac{\frac{1}{2}\theta''(\Delta\lambda)^2}{\Delta\theta},$$

and if $\Delta\theta$ is replaced by $\theta'\Delta\lambda$ this is approximately

$$\beta = \frac{1}{2}\frac{\theta''}{\theta'}\Delta\lambda. \tag{21}$$

To find β,

$$\theta' = -\frac{2\pi l}{\lambda_g^2}\lambda_g',$$

or, by using Eq. (4·6)

$$\theta' = -\frac{2\pi l\lambda_g}{\lambda^3}, \tag{22}$$

$$\theta'' = -2\pi l\left(\frac{\lambda_g'}{\lambda^3} - \frac{3\lambda_g}{\lambda^4}\right) = -2\pi l\frac{\lambda_g}{\lambda^4}\left[\left(\frac{\lambda_g}{\lambda}\right)^2 - 3\right],$$

and

$$\beta = \frac{1}{2}\left[\left(\frac{\lambda_g}{\lambda}\right)^2 - 3\right]\frac{\Delta\lambda}{\lambda}.$$

By the introduction of the cutoff wavelength λ_c,

$$\beta = \frac{1}{2}\left[\frac{1}{1 - \left(\frac{\lambda}{\lambda_c}\right)^2} - 3\right]\frac{\Delta\lambda}{\lambda}.$$

A waveguide of inside width 0.900 in. is commonly used for a band centered at $\lambda = 3.33$ cm. For that case $\lambda_c = 2 \times 0.900$ in. $= 4.56$ cm., $\lambda/\lambda_c = 0.730$ and $\beta = -0.43\frac{\Delta\lambda}{\lambda}$. This value of β is a representative one for waveguide, since the value chosen for λ/λ_c is usually near the one given above.

For coaxial line, however,

$$\beta = -\frac{\Delta\lambda}{\lambda},$$

which represents a somewhat larger error. It is interesting that $\beta = 0$ when $\lambda/\lambda_c = \sqrt{\frac{2}{3}} = 0.816$, a figure close to the 0.730 used above.

For a 12 per cent band, $\Delta\lambda/\lambda = 0.06$ giving $\beta = 0.026$ for the waveguide constants chosen. Since this is small enough to be neglected, the

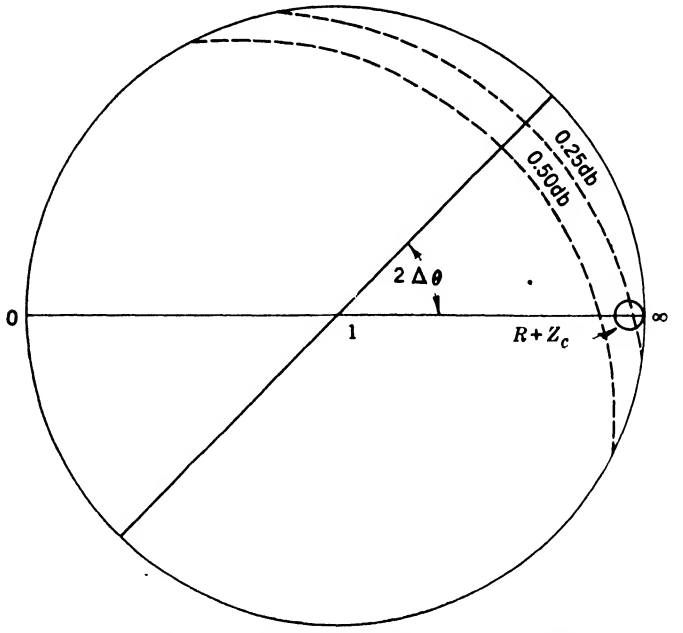

FIG. 7·20.—Loss diagram with line-length correction.

second term in Eq. (20) may be dropped, and with the aid of Eqs. (19) and (22), Eq. (20) becomes

$$\Delta\theta = -\theta\left(\frac{\lambda_g}{\lambda}\right)^2\frac{\Delta\lambda}{\lambda} = -\frac{\theta}{\left(\frac{\lambda}{\lambda_c}\right)^2}\frac{\Delta\lambda}{\lambda}. \tag{23}$$

Again, by the use of $\lambda/\lambda_c = 0.730$,

$$\Delta\theta = -2.14\theta\frac{\Delta\lambda}{\lambda}. \tag{24}$$

As an illustration, if the distance between the TR and ATR switches is $\frac{1}{2}\lambda_g$, and the bandwidth is 12 per cent, then $\theta = \pi$, and $\Delta\lambda/\lambda = -0.06$, so that $\Delta\theta = 0.402$.

To find the branching loss, $R + Z_c$ is plotted as shown in Fig. 7·13. Then the contour diagram of Fig. 7·16 is applied, but with the axis rotated

by an angle $2\Delta\theta$ radians with respect to that of the $(R + Z_c)$-plot. (Angles measured on the Smith chart are 2θ.) As shown in Fig. 7·20, the loss, for all values of Z_c, remains less than 0.4 db.

When it is essential to keep the error in electrical length to a minimum, there is some small advantage in choosing l so that there is equal error at each end of the band, rather than setting $l = (n/4)\lambda_g$ at the center of the band. To do this, let θ_1 and θ_2 be the phase lengths at the two ends of the band, and let θ_3 be the correct value $(n\pi/2)$. If $\theta_1 - \theta_3$ is set equal to $\theta_3 - \theta_2$, then $\theta_3 = (\theta_1 + \theta_2)/2$ is given which means that

$$\frac{1}{\lambda_{g_3}} = \frac{1}{2}\left(\frac{1}{\lambda_{g_1}} + \frac{1}{\lambda_{g_2}}\right). \tag{25}$$

That is, the waveguide wavelengths λ_{g_1} and λ_{g_2} are calculated at each end of the band, λ_{g_3} is determined from Eq. (25) and l is set equal to $\theta_3\lambda_{g_3}$.

Actually, l is usually determined experimentally. If the measurement is to be made at only one wavelength, it should be made at that which corresponds to λ_{g_3}. It is more accurate, however, to make the measurements at each end of the band, and find the two values l_1 and l_2. Then, for equal error, the actual value of l must satisfy the condition

$$\frac{l}{\lambda_{g_1}} - \frac{l_1}{\lambda_{g_1}} = \frac{l_2}{\lambda_{g_2}} - \frac{l}{\lambda_{g_2}},$$

or

$$l = \frac{l_1\lambda_{g_2} + l_2\lambda_{g_1}}{\lambda_{g_2} + \lambda_{g_1}}.$$

Ordinarily this method offers so little improvement over the previous method that it is impractical.

It should be observed that the distance between the TR and the ATR junctions is important, but that if the TR switch and the receiver are matched and the ATR switch is tunable, the distance from the TR switch to its junction and the distance from the ATR switch to its junction are unimportant so far as the received signal is concerned. For the TR switch, this is true because a matched load always looks the same at any distance. For the ATR switch, it is obviously true if the ATR switch is a pure susceptance. In this case, any change in the distance from the ATR switch to its junction merely changes the susceptance presented at the junction, and this can be corrected by tuning the ATR switch.

If, to be more correct, it is assumed that the ATR admittance consists of a constant conductance plus a variable susceptance, then the admittance locus Y is that shown in Fig. 7·17. Any change in the distance from the ATR switch to its junction rotates this locus about the

origin. Since G is small, this locus is very nearly concentric with the origin. Hence the rotation produces only a small change in G and the change in B can be corrected by tuning.

7·8. Branching Loss for Fixed-tuned ATR Circuits.—A fixed-tuned ATR switch of a certain Q_L, tuned to a certain wavelength, may be used in a duplexer in which the distance between TR and ATR junctions is adjusted to be correct at some particular wavelength. Ordinarily both of these wavelengths will be near the center of the band and for the present it will be assumed that they are equal to the center wavelength, λ_0. The branching loss which may then be expected at some particular wavelength—for example, at one end of the band—may be calculated. A general approach to this problem is the determination of the loss for each value of the transmitter cold impedance, Z_c. A representation of this solution due to A. L. Samuel[1] consists of a contour diagram transformed from that of Fig. 7·16 back to the Smith chart for Z_c. To accomplish this transformation it is necessary to know the correction $\Delta\theta$ for the distance between the TR and ATR junctions and the ATR impedance Z.

For illustration, the line length when $\lambda = \lambda_0$ will be assumed to be $\theta = \pi$. The loss will be calculated at a wavelength which differs from λ_0 by an amount such that $\Delta\lambda/\lambda_0 = 0.015$. With the same value of λ/λ_c as was used in the previous section, $\Delta\theta$ is given by Eq. (24) so that $\Delta(l/\lambda_g) = \Delta\theta/2\pi = -0.016$.

If $Q_L = 8.0$ and $G = 0.05$, then

$$B = -2(1 + G)Q_L \frac{\Delta\lambda}{\lambda_0} = -0.25.$$

Hence, $Y = 0.05 - j0.25$ and $Z = 0.75 + j3.8$. Now loss contours are plotted on the Smith chart for $Z_c + Z$ by rotating the Z_t diagram of Fig. 7·16 by an amount $-\Delta(l/\lambda_g) = 0.016$. To transform any contour to the Z_c chart a circle is constructed through three or four points plotted by subtracting Z from the values on the $(Z + Z_c)$-plot. The result is shown in Fig. 7·21.

When such a construction is made it is helpful to know that the centers of the circles fall on a straight line. This follows from the fact that the circles on the original cartesian diagram for $1 + \frac{1}{2}Y_t$ of Fig. 7·15 are concentric and that a bilinear transformation always changes concentric circles into coaxial circles. Successive bilinear transformations leave them coaxial since any number of such transformations are equivalent to a single one.

Since the high-loss contours are all crowded into a small region, it could be said that a high loss is rather improbable. This, of course,

[1] Samuel, *op. cit.*

assumes that all values of the transmitter reflection coefficient Γ_c are equally probable. The probability of the loss exceeding a stated value at a given wavelength can be calculated assuming random phase of Γ_c or it may be determined for a stated wavelength band assuming that phase and wavelength are random.[1] The probability of high losses is usually rather low. In some applications, unfortunately, any probability greater than zero may be unacceptable.

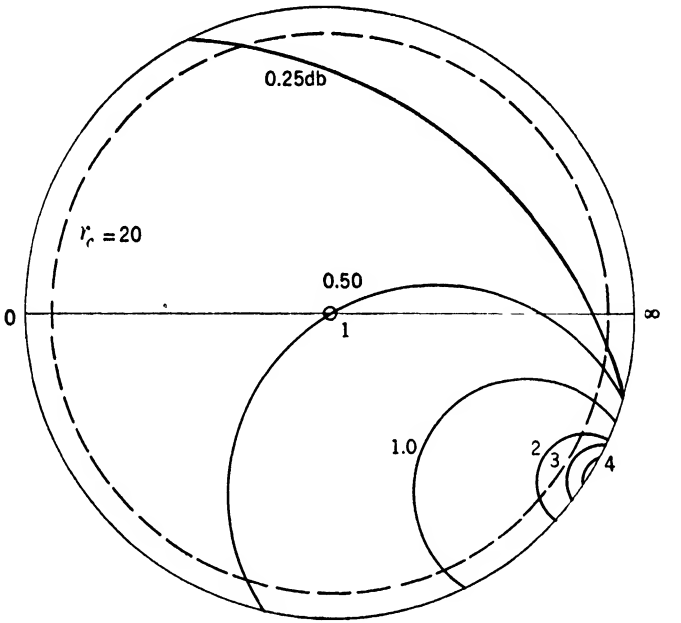

FIG. 7·21.—Loss contours for Z_c.

There is usually an upper limit to r_c and it is clear from Fig. 7·21 that the maximum value of the loss decreases with the maximum value of r_c, for the loci of constant r_c are circles concentric with the origin whose radii decrease with r_c.

Although the setting of an upper limit to r_c reduces the maximum possible loss, this upper limit may be so high, for some transmitters, as to be of little help. Thus, measurements made on one type of 10-cm magnetron used as a radar transmitter gave values of r_c^2 around 30 db and with some tubes it was as high as 50 db. On the other hand, values for one type of 3-cm band tube were near 20 db with a maximum of about 26 db ($r_c = 20$).

The circle for $r_c = 20$, shown in Fig. 7·21 as a broken line, corresponds to a maximum branching loss of 2.5 db rather than the 4.5 db which

[1] H. K. Farr, "Characteristics of Fixed Tuned X Band Anti-TR," RL Report No 53-May 13, 1944.

would be attained if there were no restriction on r_c. After the construction of the contour diagram, it is a simple matter to plot loss as a function of transmitter phase, for the maximum expected r_c, by reading off the loss values versus angle around the r_c circle. This gives an indication of the probability of encountering a certain loss when a transmitter of that r_c is used. Two of these curves with $r_c = 20$ and ∞, respectively, are shown in Fig. 7·22. The phase is measured from the point of minimum impedance so that the phase $l/\lambda_g = 0$ corresponds to $Z_c = 0$ or 0.05. The two curves are almost identical over most of the phase range, differing only in the region of the maximum.

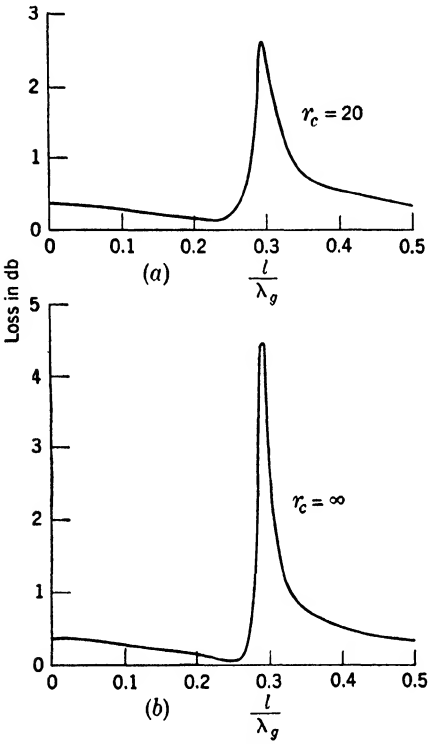

FIG. 7·22.—Branching loss vs. transmitter phase with ATR cavity off resonance.

The strong dependence of loss on magnetron phase indicates the desirability of some control over this phase. Of course, when r_c is high there is no necessity for an ATR switch if the phase can be given the proper value; this is just what is accomplished by the line stretcher mentioned in Sec. 7·4. Nevertheless, the possibility of choosing the best fixed line length between transmitter and ATR tube should not be neglected completely. In cases where there is enough variation in Z_c from one transmitting tube to another to make an ATR switch necessary, it may still be possible to choose the line length so that the transmitter impedance "helps" the ATR switch.

It should be noticed, however, that the optimum distance from the TR junction to the transmitter will differ by about a quarter of a wavelength, depending on whether or not an ATR switch is used. With a shunt TR switch, for example, the transmitter should present a high impedance at a point one-half wavelength from the TR junction when no ATR switch is used. A series ATR switch is likewise placed at this point to produce a high impedance. The combination of a high ATR reactance and a high transmitter reactance of opposite sign at the same point results, however, in resonance with high branching loss. This is

seen from the curves of Fig. 7·22, which exhibit maximum loss at a phase near $l/\lambda_g = 0.25$ which corresponds to large Z_c. This point diverges from 0.25 as the frequency moves toward the band edge.

A quantity of practical importance is the maximum possible loss of a duplexer when the transmitter may have any impedance whatever. A closer examination of the factors affecting this maximum loss should, therefore, be made. For simplicity the distance between TR and ATR junctions will be assumed correct. Examination of Fig. 7·17 then shows that the maximum loss is realized at the point $Z_t = Z + Z_c = R$ where the left edge of the Z_t-circle intersects the real axis. The corresponding transmitter impedance $Z_c = jX_c = -jX$ is purely reactive and just cancels the ATR reactance at that point. The corresponding loss factor is

$$\alpha_x = 1 + \frac{1}{2}\frac{1}{R} = 1 + \frac{1}{2}\frac{G^2 + B^2}{G}. \tag{26}$$

When G is small compared with B, this is approximately

$$\alpha_x = 1 + \frac{1}{2}\frac{B^2}{G}, \tag{27}$$

which shows that the ATR conductance G has an important influence on the maximum loss. When G is small, the maximum loss decreases as G increases.

If a limitation is placed on the transmitter standing-wave ratio so that the cold impedance is not purely reactive, it will be found that the dissipation in the transmitter also tends to lower the maximum branching loss. In limiting the standing-wave ratio, an upper limit is placed on $|\Gamma_c|$. This means that Z_t is confined to a circular area smaller than that in Fig. 7·17 but still centered on the real axis. As before, the maximum loss is attained for real Z_t with $X = -X_c$ and

$$\alpha_x = 1 + \frac{1}{2}Y_t = 1 + \frac{1}{2}\frac{1}{R + R_c}. \tag{28}$$

Now

$$Z = \frac{1}{G + jB} = \frac{G}{G^2 + B^2} - j\frac{B}{G^2 + B^2}$$

If G is small enough, G^2 may be neglected compared with B^2, so that

$$X = -\frac{1}{B}, \qquad R = \frac{G}{B^2}. \tag{29}$$

On the other hand,

$$Z_c = \frac{r_c + j\tan\phi}{1 + jr_c\tan\phi},$$

where $\phi = 2\pi\,(l/\lambda_g)$ is the angular distance from the ATR junction to the point where the transmitter impedance is r_c. The rationalization of Z_c gives

$$R_c = \frac{r_c(1 + \tan^2 \phi)}{1 + r_c^2 \tan^2 \phi}, \tag{30}$$

$$X_c = \frac{(1 - r_c^2) \tan \phi}{1 + r_c^2 \tan^2 \phi}. \tag{31}$$

Now $\tan \phi$ can be eliminated between these two expressions. However, to keep the algebra from becoming unwieldy some approximations will be made. It will be assumed that r_c is large compared with one, and that R_c in Eq. (28) is of such a magnitude as to make some contribution to α but not so large as to cause inordinate losses. A value of $R + R_c = 1$ gives a loss of 3.5 db; therefore R_c is assumed to be of the order of magnitude of unity. This is not incompatible with our assumption regarding the magnitude of r_c since R_c may have any value between $1/r_c$ and r_c. To find the order of $\tan \phi$ under these assumptions, R_c is set equal to one, and Eq. (30) is solved for $\tan \phi$, which gives $\tan^2 \phi = 1/r_c$. It is therefore possible to neglect $\tan^2 \phi$ in comparison with 1 and write

$$R_c = \frac{r_c}{1 + r_c^2 \tan^2 \phi}. \tag{32}$$

If Eq. (31) is divided by this expression, then

$$\frac{X_c}{R_c} = \frac{1 - r_c^2}{r_c} \tan \phi \approx -r_c \tan \phi.$$

The substitution of this into Eq. (32) gives

$$R_c = \frac{r_c}{1 + \left(\dfrac{X_c}{R_c}\right)^2}. \tag{33}$$

Again, the use of the assumption that $R_c \approx 1$ means that $1 + (X_c/R_c)^2$ is of the order of r_c and can be replaced therefore by $(X_c/R_c)^2$ in Eq. (33). The solution for R_c is then

$$R_c = \frac{X_c^2}{r_c} = \frac{X^2}{r_c} = \frac{1}{B^2 r_c}.$$

At this point a conductance $G_1 = 1/r_c$ may be introduced. This is the admittance seen one-quarter wavelength away from the window or loop of the transmitter cavity (not to be confused with G_c seen at the ATR junction). The substitution of $R_c = G_1/B^2$ and Eq. (29) into Eq. (28) gives

$$\alpha_x = 1 + \frac{1}{2}\frac{B^2}{G_1 + G_c}. \tag{34}$$

This is an approximate expression for the maximum loss factor when the transmitter voltage standing-wave ratio remains less than $1/G_1$. Evidently the ATR and transmitter conductances, G and G_1, have a similar effect on the maximum loss over this interesting range. It is clear that if r_c is to be very large (G_1 small) then the conductance G of the ATR switch should not be too small.

If there is a possibility that G_1 will be so small as to be of little help in limiting the maximum loss, G can be adjusted to make α_x as small as possible for some particular frequency, for example, at the edge of the band. This is done by changing the cavity losses. This optimum value of G is $|B|$ as can be found by setting the first derivative of α_x equal to zero in Eq. (26) and noting that the second derivative B^2/G^3 is positive. The minimum value of α_x at the band edge is then $\alpha_x = 1 + G$ and at the band center $\alpha_x' = 1 + \frac{1}{2}G$.

The ATR switch used as an example in this section has $B = -0.25$. If $G = 0.25$ is taken, a loss is given at the band edge of 2 db ($\alpha_x = 1.25$) and a loss, at the band center, of 1 db. On the other hand, the old value of $G = 0.05$ if used in Eq. (26) gives a maximum loss of 4.4 db at the band edge and 0.2 db at the band center. That is, the maximum loss at the band edge is reduced from 4.4 to 2 db at the expense of an increase from 0.2 to 1 db at the band center.

For a better understanding of the relative merits of different values of G, transmitter phases other than those leading to the maximum loss must be considered. A curve of loss vs. transmitter phase can be plotted by transforming loss contours to the Z_c-plane as was done to obtain the curves in Fig. 7·22. Since only what happens for $r_c = \infty$ however, is important, it is unnecessary to make such an elaborate diagram.

The locus of $Z + Z_c$ for $r_c = \infty$ may be constructed and the standard contour diagram of Fig. 7·16 applied to determine the losses. This locus is a circle through R and ∞ with its center on the real axis. Points may be marked off on this circle corresponding to various values of the transmitter phase l/λ_g by reading off the value of X_c corresponding to each phase, adding X and locating the intersection of the reactance contour $X + X_c$ with the $(Z + Z_c)$-circle. The resulting Fig. 7·23 which is drawn for $Y = 0.05 - j0.25$ is seen to be similar to Fig. 7·18 for the ATR-tuning curve. In the first figure it is the transmitter impedance and in the second the ATR impedance, that is varied.

The application of the loss-contour diagram gives the loss vs. transmitter phase. Figure 7·24*a* shows the curves drawn for the edge of the band ($B = 0.25$); the dashed curve is for $G = 0.05$, and the solid curve for $G = 0.25$. The latter value, $G = 0.25$, makes the maximum loss at this frequency as small as possible. Figure 7·24*b* gives the same data

at the center of the band, again for the two values of $G = 0.05$ and $G = 0.25$. Figure 7·25 is a plot of the maximum loss, as B is varied, for the same two values of G.

It is clear that as far as the maximum loss is concerned, there is a considerable improvement in using the larger G. The smaller G gives much lower loss values, however, for most points not at the maximum. The choice of the optimum G depends on the relative importance attached to maximum loss and to the loss under other conditions. The fixed-

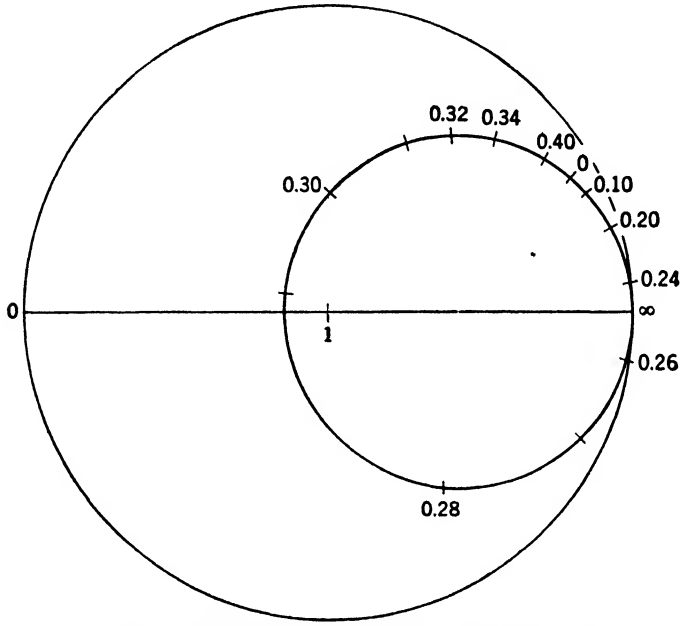

FIG. 7·23.—Diagram of Z_t for variable transmitter phase.

tuned ATR switches in use at present have low values of G which characterize copper cavities.

Instead of determining the maximum possible loss at each wavelength as was done for the curve of Fig. 7·25, it might be asked how the actual loss would vary as the frequency of a tunable transmitter was changed. To answer this question, A. L. Samuel[1] assumed that the cold impedance remains constant as seen at the output window or iris of the transmitting tube. Because of the change in electrical length of the line between the transmitter and the ATR tube, the phase of the cold impedance Z_c as seen at the ATR junction will increase steadily as the wavelength decreases. The point at which the loss is read on a curve

[1] Samuel, *op. cit.*

like that of Fig. 7·22 will move to the right. At the same time the curve itself will change because of the change in ATR impedance, and the peak

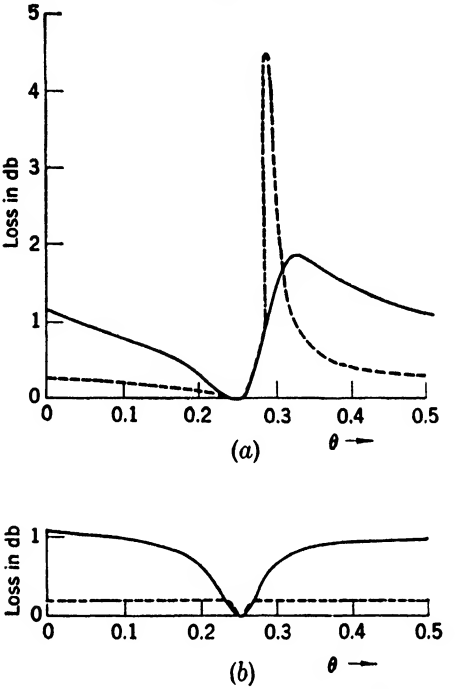

FIG. 7·24.—Loss vs. transmitter phase, (*a*) at band edge, (*b*) at band center. In the solid curves G is chosen to minimize the maximum loss at the edge of the band; $G = 0.05$ in the dashed curves.

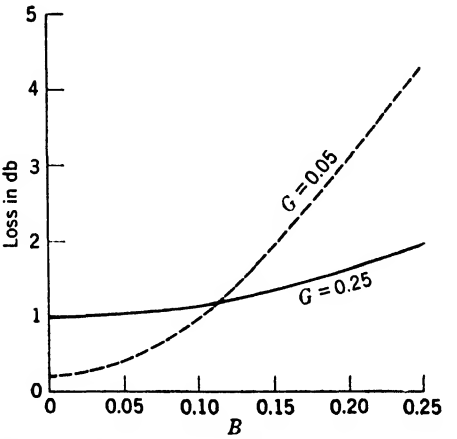

FIG. 7·25.—Maximum loss vs. ATR susceptance from band center to the edge of the band.

will increase and move toward the right. For a low-Q ATR cavity and a transmitter line of moderate length, the phase of Z_c will move faster and

may even cross the loss peak several times in the band. The resulting curve of branching loss against wavelength will resemble that of Fig. 7·26. Where there are several peaks the Q of the transmitter line would be large compared with that of the ATR cavity and the number of peaks in a wavelength range $\Delta\lambda$ would be given approximately by

$$-2\frac{d}{d\lambda}\left(\frac{l}{\lambda_g}\right)\Delta\lambda = 2\frac{l}{\lambda_g}\left(\frac{\lambda_g}{\lambda}\right)^2\frac{\Delta\lambda}{\lambda},$$

where l is the distance from the ATR junction to the transmitter. The peaks of the curve, of course, fall on the maximum loss curve of the type shown in Fig. 7·25.

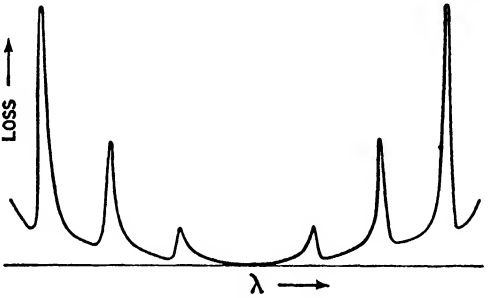

FIG. 7·26.—Branching loss for a tunable transmitter.

7·9. Duplexing Loss under Conditions of Receiver Mismatch.—In previous sections the loss in received signal between the antenna line and the TR tube has been considered, under the assumption that the TR tube and mixer were correctly matched. This simplification, which allows the branching loss to be calculated more easily, is justified in that it permits an insight into such factors as ATR and transmitter impedances and the intercomponent line lengths. Nevertheless, the more general case of a mixer and a TR tube which present some arbitrary admittance at the junction should be analyzed.

For this purpose it will be convenient to lump together the mixer, the TR tube, and any other components beyond the input window of the TR tube, and refer to them as the receiver. Since part of the loss in signal between the antenna line and the TR tube or receiver is caused by reflection from the receiver, the definition of branching loss must now be made more explicit. For an arbitrary receiver admittance, the branching loss will refer to the actual signal loss minus the loss with an ideal ATR circuit. The total loss in received signal is simply the sum of the branching loss and the conventionally defined TR loss.

Figure 7·27 represents a duplexer with a transmitter branch of admittance Y_t and a shunt TR junction. The admittance of the receiver as

seen at the input window of the TR tube is represented by Y_r. This point is effectively one-quarter wavelength from the junction so that the admittance seen at the junction is $1/Y_r = Z_r$. If the antenna acts as a matched generator, it can be represented by a current source of internal conductance unity. Then the total admittance across the generator is $1 + Z_r + Y_t$, and the generator voltage is $V = I/(1 + Z_r + Y_t)$ where I is the generator current. The conductance presented by the receiver at the junction is R_r, the real part of $1/Y_r$, and the power delivered to the receiver is

$$P = |V|^2 R_r = \frac{|I|^2 R_r}{|1 + Z_r + Y_t|^2}. \quad (35)$$

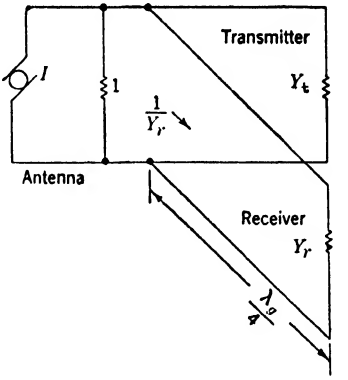

FIG. 7·27.- Circuit for determination of branching loss with receiver mismatched.

The power delivered to a matched load is $P_0 = \frac{1}{4}|I|^2$ and the total loss factor β is given by

$$\beta^2 = \frac{P_0}{P} = \frac{1}{4R_r}|1 + Z_r + Y_t|^2. \quad (36)$$

If Y_t is set equal to 0 the value β' is given for an ideal ATR circuit. The branching loss is then

$$\alpha = \frac{\beta}{\beta'} = \left|1 + \frac{Y_t}{1 + Z_r}\right|.$$

If the reflection coefficient Γ_r given by $Z_r = \frac{1 + \Gamma_r}{1 - \Gamma_r}$, is used then

$$\alpha = |1 + \tfrac{1}{2}(1 - \Gamma_r)Y_t|. \quad (37)$$

Equation (37) applies to a shunt TR junction. The corresponding expression for the series junction is $\alpha = |1 + \frac{1}{2}(1 - \Gamma_r)Z_t|$, where Γ_r still refers to the input window of the TR tube.

If the quantity

$$Y_t' = (1 - \Gamma_r)Y_t \quad (38)$$

is introduced, Eq. (37) has the same form as Eq. (7), which gives the branching loss for an ideal receiver. Hence if Eq. (38) is written as

$$Z_t' = \frac{1}{1 - \Gamma_r} Z_t, \quad (39)$$

the branching loss for an unmatched receiver can be determined by plotting Z_t' on the Smith chart, and using the same loss-contour diagram of Fig. 7·16 as was used for a matched receiver.

The construction of the Z_t' plot from the Z_t plot is easy when Γ_r is known. Since Γ_r is constant at any one frequency, the transformation of Eq. (39) is seen to be circular, since it has the form of Eq. (8). Hence, if Z_t is a circle, it is only necessary to calculate three or four points to find the Z_t' locus.

As an illustration it is assumed that the receiver has a reflection coefficient of $\Gamma_r = re^{j\phi}$ where $r = 0.50$ and $\phi = -45°$. As in Sec. 7·8

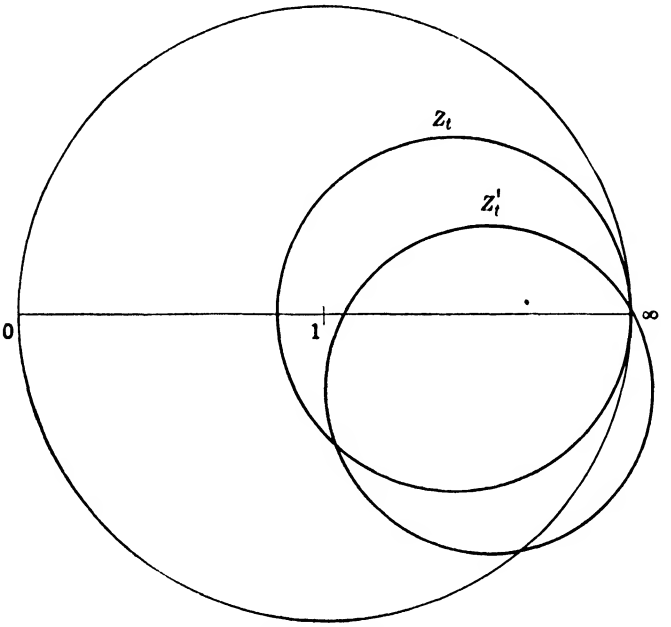

FIG. 7·28.—Branching-loss diagram showing effect of receiver mismatch.

an ATR circuit is assumed for which $Y = 0.05 - j0.25$, and a transmitter for which $r_c = \infty$. Hence

$$\frac{1}{1 - \Gamma_r} = 1.19 - j0.64.$$

The line-length correction is neglected so that $Z_t = Z + Z_c$.

Figure 7·28 is a Smith-chart plot of Z_t and Z_t' for this case. Comparison of the two loci, with the aid of the contour diagram of Fig. 7·16, shows the effect of the receiver mismatch on the branching loss. It will be noticed that the Z_t' locus is partly outside the area of the usual Smith chart. This region outside the unit circle $|\Gamma_t| = 1$, corresponds to negative values of R_t'. Since Z_t' is not an actual impedance but merely a symbol for the quantity $Z_t/(1 - \Gamma_r)$, it is not surprising that its real part should be negative. In order to read losses in this region, the contours of Fig. 7·16 must be extended beyond the unit circle. It will

be found that in order to cover all the Γ_t-plane it is necessary to use values of α smaller than unity, corresponding to negative values of the loss in decibels. A negative branching loss merely means that the actual ATR circuit results in less total duplexing loss than the ideal ATR circuit for which $Z_t = \infty$. Naturally this is possible only when there is some reflection loss from the receiver. In the illustration the branching loss actually falls to -0.2 db at one point.

If the steps taken in constructing the original loss-contour diagram are followed, it will be seen that the process can be extended, without

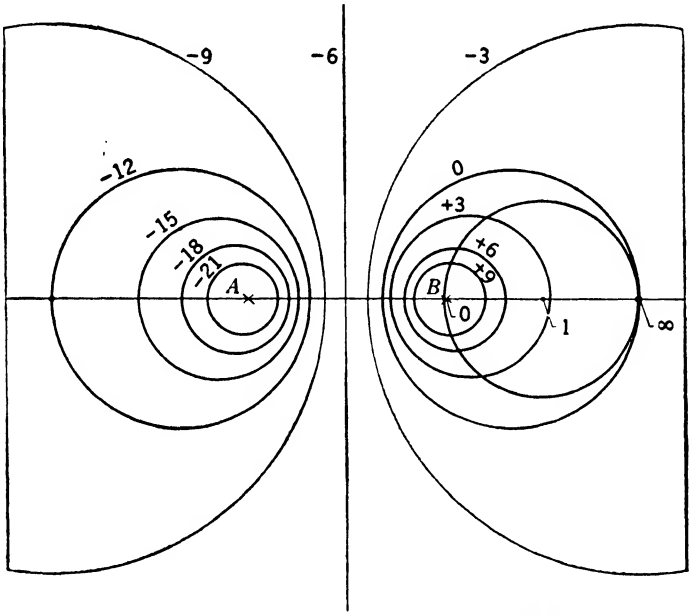

FIG. 7·29.—Smith-chart loss-contour diagram for Z_t, generalized to include negative values.

any changes, to the more general case of $|\Gamma_t'| > 1$ and $\alpha < 1$. The diagram has been redrawn in Fig. 7·29 to show the general form of the contours for all values of loss. On the scale used here, the area comprising the conventional Smith chart lies inside the small circle on the right-hand side with the real intercepts $(0, \infty)$. The numbers on the contours give the branching loss in decibels. Much of the area shown outside this circle would rarely correspond to any practical duplexer. For any physical value of Γ_r and Y_t, however, Γ_t' may have any value in the whole complex plane except on the real axis to the left of -1.

To understand the geometry of Fig. 7·29, α can be eliminated between Eqs. (17) and (18) which give the radius and center (ρ and Γ_0) of a circle of constant α. This results in $\rho^2 = (1 + \Gamma_0)(3 + \Gamma_0)$. If a new origin

2 units to the left of the origin for Γ is chosen, and x_0 is the distance from the new origin to the center of the circle, then $\Gamma_0 = x_0 - 2$ and

$$\rho^2 = x_0^2 - 1. \tag{40}$$

This shows that two circles whose centers are equidistant from the new origin have the same radius and the imaginary axis is a line of symmetry. Let α and α' be the loss factors corresponding to two such circles, and L and L' the corresponding values in decibels. Then if Eq. (17) is solved for α

$$4\alpha^2 = \frac{3 + \Gamma_0}{1 + \Gamma_0},$$

or

$$4\alpha^2 = \frac{x_0 + 1}{x_0 - 1}.$$

The negative of x_0 must give α'; therefore

$$4\alpha'^2 = \frac{x_0 - 1}{x_0 + 1} = \frac{1}{4\alpha^2}.$$

That is, $L' = -(12 + L)$, so that once the circles on one side of the axis of symmetry are computed, those on the other side can be found immediately. When $L' = L$, $L = -6$ db—the contour value for the axis of symmetry.

If x_1 and x_2 are the intercepts of a circle on the real axis, then $x_1x_2 = (x_0 - \rho)(x_0 + \rho) = x_0^2 - \rho^2 = 1$, because of Eq. (40). The real intercepts are reciprocal, which is just the property of the circles of constant standing-wave ratio on an impedance chart in cartesian coordinates. The loss-contour family on the Smith chart for Z_t is seen to be the same as the family of "impedance circles" in cartesian coordinates, or as the double family used in bipolar coordinates.

Since the impedance coordinates on the conventional Smith chart do not extend outside the unit circle, these must be constructed when negative values of R_t are encountered. The reactance circles are found by extending those already present, and the resistance circles can be found from their real intercepts at $(R - 1)/(R + 1)$ and $+1$.

For an evaluation of the seriousness of the receiver mismatch, a comparison of Eq. (37), written as $\alpha = |1 + \frac{1}{2}Y_t - \frac{1}{2}\Gamma_r Y_t|$, with Eq. (7) shows that the contribution of the receiver mismatch to the branching loss results from the term $-\frac{1}{2}\Gamma_r Y_t$. It was found in Sec. 7·8 that when the transmitter phase was varied the maximum loss occurred at the point where Y_t was real, provided the TR-to-ATR distance was correct. Hence the correction term $-\frac{1}{2}\Gamma_r Y_t$ will be of most interest when Y_t is real. For real Y_t and a fixed value of $|\Gamma_r|$, the branching loss is highest

if the phase of the receiver mismatch is such that Γ_r is real and negative. Likewise, a positive real Γ_r will minimize the branching loss.

As an illustration, a value of $Y_t = 1$ results in a loss of 3.5 db if the receiver is matched. If, however, $Y_r = 1.5$, and $Y_t = 1$, then $\Gamma_r = -0.20$, $Y_t' = 1.20$, and the loss is 4.1 db. Thus, the receiver mismatch causes an increase of 0.6 db in the branching loss whereas the reflection loss for this value of Γ_r is only $-20 \log (1 - \Gamma_r^2) = 0.18$ db. If Y_t is taken equal to 0.05, the branching losses for $Y_r = 1.0$ and 1.5 are 0.214 and 0.256 db, respectively, representing an increase of only 0.042 db because of receiver mismatch. Thus, the receiver mismatch may in some cases be more important to the branching loss than to the reflection loss.

Figure 7·30 is a diagram, in cartesian coordinates, of Y_t and Y_t', which shows how the branching loss varies if the magnitude of Γ_r is

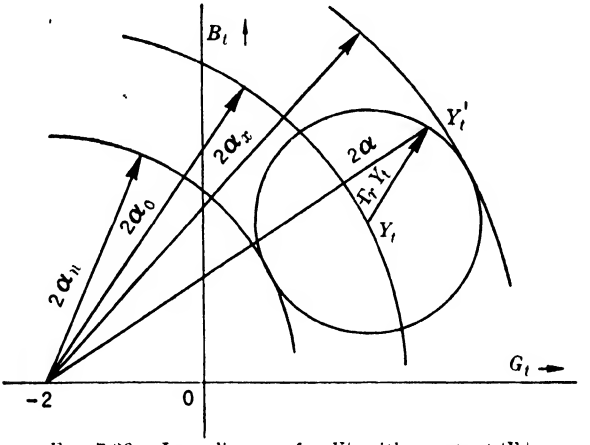

FIG. 7·30. -Loss diagram for Y_t with constant $|\Gamma_r|$.

held constant while the phase changes. If Eq. (7) is written as $|2 + Y_t| = 2\alpha$ it is clear that the loss contours are circles of radius 2α centered at (-2).

Since $Y_t' - Y_t = -\Gamma_r Y_t$, Y_t' must fall somewhere on a circle of radius $|\Gamma_r Y_t|$ about Y_t as a center. Where Γ_r is real and positive, $-\Gamma_r Y_t$ is directed toward the origin so that this phase of Γ_r still tends to reduce the branching loss, even though Y_t is not real.

In Chap. 3 phase data were reproduced for the reflection coefficients of certain fixed-tuned TR tubes which would enable the determination of their contribution to the branching loss. In many cases, however, the phase of the reflection coefficient may not be known, although its magnitude, or an upper limit of the magnitude, may be known. Hence, it is useful to know the maximum change in the branching loss that could be caused by a Γ_r, of a certain magnitude but unknown phase.

Figure 7·30 shows that

$$\alpha_n = \alpha_0 - \tfrac{1}{2}|\Gamma_r Y_t| \leqq \alpha \leqq \alpha_0 + \tfrac{1}{2}|\Gamma_r Y_t| = \alpha_x,$$

where $\alpha_0 = |1 + \frac{1}{2}Y_t|$ is the branching loss for a matched receiver. Since

$$\frac{\alpha}{\alpha_0} \leqq 1 + \frac{\frac{1}{2}|\Gamma_r Y_t|}{|1 + \frac{1}{2}Y_t|},$$

the upper limit, in decibels, of the amount by which the actual branching loss for a receiver of reflection coefficient $|\Gamma_r|$ can exceed that for a matched receiver is

$$20 \log_{10}\left(1 + \left|\frac{\Gamma_r}{1 + 2Z_t}\right|\right).$$

An important example of receiver mismatch is that encountered in tuning a TR cavity. With an ideal duplexer the TR cavity is tuned to resonance for maximum signal. Since this is not generally true for an arbitrary ATR circuit, the question arises as to how much improvement in signal could be expected by tuning the TR switch for maximum signal instead of for resonance.

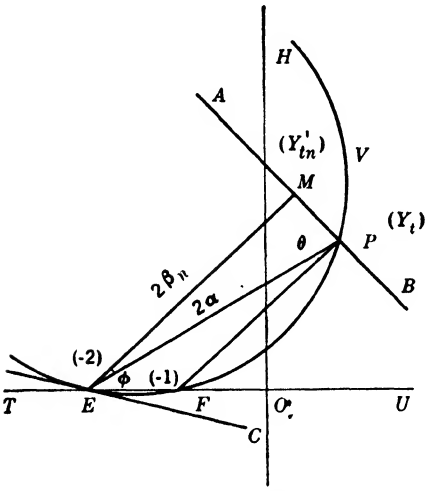

FIG. 7·31.—Gain contour for tunable TR tube in the Y_t-plane.

In this case the over-all loss factor β rather than the branching loss is the quantity of interest. The substitution of $R_r = G_r/|Y_r|^2$ in Eq. (36) results in

$$\beta^2 = \frac{1}{4G_r}|1 + Y_r(1 + Y_t)|^2.$$

If the TR cavity is matched through at resonance, then off resonance $Y_r = 1 + jB_r$ where B_r can be varied by tuning. Since $G_r = 1$, $\beta = |1 + \frac{1}{2}[Y_t + jB_r(1 + Y_t)]|$, and if Y'_t is set equal to

$$Y_t + jB_r(1 + Y_t),$$

$\beta = |1 + \frac{1}{2}Y'_t|$ so that the ordinary contour diagram for Y'_t is again applicable. Of course, this is not the same Y'_t as was used for computing the branching loss.

This is illustrated in Fig. 7·31 where point P represents Y_t in cartesian coordinates, and TU and HO the real and imaginary axes, respectively.

The vector $jB_r(1 + Y_t)$ will be at right angles to $(1 + Y_t)$ so that Y'_t will fall somewhere on the line AB, which passes through P and is perpendicular to the line from P to (-1). As in Fig. 7·30, the contours of constant loss are circles concentric about the point (-2). Hence, the value of Y'_t which results in the least loss will be represented by that point Y'_{tn} on line AB which is closest to (-2). This point, at the foot of the perpendicular from (-2), is labeled M.

The gain in signal voltage obtained by tuning the TR cavity from the matched condition to that for maximum signal is the ratio α/β_n, where α is the loss factor corresponding to Y_t, and β_n that for Y'_{tn}. Since $\phi = \theta$, the gain is

$$\frac{\alpha}{\beta_n} = \sec \theta, \tag{41}$$

and the gain contours are also θ-contours.

Since the locus of a point P which subtends a constant angle θ at two fixed points E and F is a circle through E and F, the θ-contours are circles through E and F, similar to the one shown. This family of circles can be transformed to the Γ_t-plane by transforming the points E and F according to the equation

$$\Gamma_t = (1 - Y_t)/(1 + Y_t).$$

The resulting points are -3 and ∞, which means that the contours are a family of straight lines through -3. In the Y_t-plane a contour makes the angle CEF with the real axis, and this angle is equal to θ, as can be seen by moving P around the contour into coincidence with E. Since the transformation is conformal, the contours make an angle θ with the real axis in the Γ_t-plane as well. This makes it possible to draw the gain-contour diagram for a Smith chart, at once, by the use of Eq. (41). The construction is indicated in Fig. 7·32, which is drawn for the Γ_t-plane. The circle centered at the origin is the boundary of the ordinary Smith chart, and the line through (-3), making an angle θ with the real axis, is a gain contour. For the maximum gain, $\sin \theta = \frac{1}{3}$, that is, the maximum improvement to be expected from the use of a tunable TR cavity to correct the branching loss, is $20 \log_{10} \sec \sin^{-1} \frac{1}{3} = 0.51$ db.

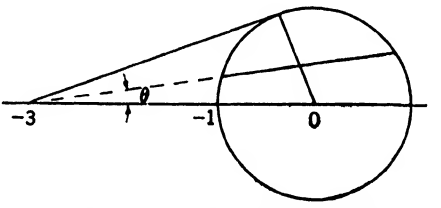

FIG. 7·32.—Gain-contour construction in the Γ_t-plane.

Figure 7·33 shows the contours in more detail. Comparison with Fig. 7·16 shows that the improvement is very small for any ordinary duplexer, especially at the maximum loss which occurs near the real axis.

As usual, the results of this section, which were obtained on the basis

of the shunt TR junction, can be applied at once to the series TR junction. The equation corresponding to Eq. (36) for the over-all loss factor is then

$$\beta^2 = \frac{1}{4R_r}|1 + Z_r + Z_t|^2,$$

which differs only in the replacement of Y_t by Z_t, so that exactly the same operations are performed in the Z_t plane for the series TR circuit as were carried out for the shunt TR junction in the Y_t-plane.

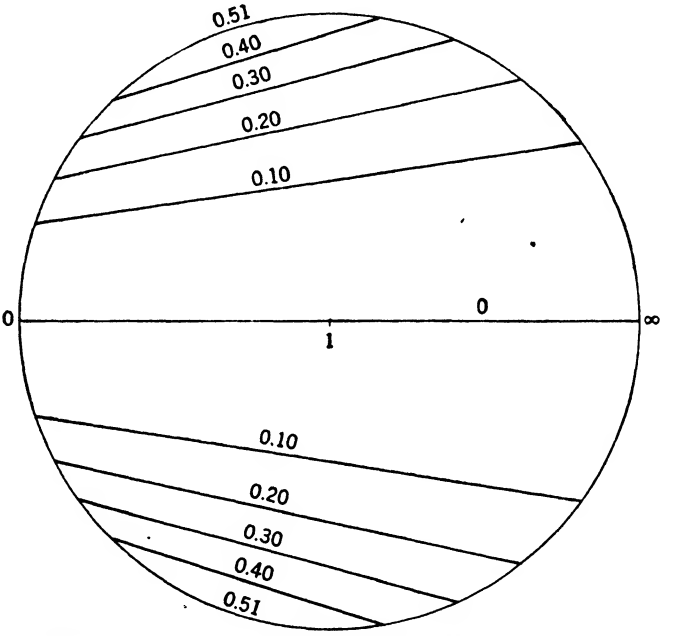

FIG. 7·33.—Gain contours for tunable TR tubes on a Smith chart.

7·10. Duplexers with Multiple ATR Circuits.—In an ATR circuit of the type which has been considered, it is evident from Fig. 7·17 or from Eqs. (26) or (34) that the maximum branching loss increases rapidly with the ATR susceptance B. For a given wavelength band, B at the edge of the band is determined essentially by the loaded Q of the ATR cavity. Because it is difficult to design a simple ATR cavity with a sufficiently low loaded Q, circuits with more than one resonant element are often used in an attempt to widen the effective wavelength range of the ATR switch.

In Chap. 4 it was pointed out that the improvement of a two-terminal device by the addition of circuit elements connected across the terminals appears to be precluded by the reactance theorem. This means that there is available a two-terminal device whose change in susceptance

over the band has been made as low as possible, and some improvement can be obtained only by using several elements connected into the transmitter line in such a way as to minimize $\alpha = |1 + \frac{1}{2}Y_t|$.

Since two elements of admittance Y give an admittance $\frac{1}{2}Y$ when connected in series, the use of two tubes reduces the susceptance to half its value. If n tubes are used in series, the susceptance is reduced to one nth of its value. The same effect can be gained by spacing tubes one-half waveguide wavelength apart along the transmitter line provided that the effect of line-length variation can be neglected.

The use of two tubes, spaced one-quarter waveguide wavelength apart, also effects a marked improvement over the use of a single tube. This is to be expected because, as previously explained, the high branching losses appear when the transmitter reactance cancels the large reactance of the ATR tube, whereas the effect of adding a second tube one-quarter wavelength closer to the transmitter is to present a low impedance at the first tube.

The question naturally arises as to whether any spacing other than zero or one-quarter wavelength would give good results. It is not necessary at present to consider spacings of one-half wavelength or more, since they are equivalent to the shorter ones but with a greater correction for variation due to frequency changes. Actually the only satisfactory spacings for broadband work are zero or one-quarter wavelength, or their equivalent, because only these spacings will result in equal losses at the two ends of the band. Any other spacing gives a lower loss at one end of the band and a higher loss at the other, provided that the cavities are tuned to the center of the band.

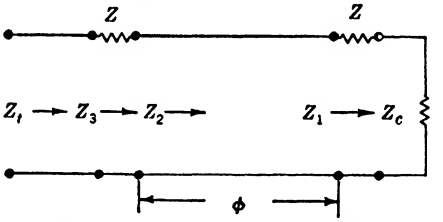

FIG. 7·34.—Equivalent circuit for two series-coupled ATR tubes.

An analysis will be made of the variation in branching loss for two ATR tubes as the phase distance $\phi = 2\pi l/\lambda_g$ between the two junctions is changed. In Fig. 7·34, Z_c is the transmitter impedance as seen at the first ATR junction and Z is the impedance of either ATR tube since the two are assumed for the present to be identical. Also $Z_1 = Z + Z_c$; Z_2 is Z_1 transformed down the line a distance ϕ to the next ATR junction; $Z_3 = Z + Z_2$ and Z_t is Z_3 transformed back to the TR junction. It is assumed that $Z_t = Z_3$ since the effect of an error in the TR-ATR distance can be readily determined by a rotation of the loss-contour diagram.

Figure 7·35 gives the Smith-chart representation of these impedances for a particular value of Z, at a particular frequency. As in some previous

illustrations $G = 0.05$. Since the ATR cavity is assumed to be detuned to $B = -0.33$ on the low-frequency side of resonance, $Z = 0.45 + j2.96$. If Z_c is allowed to take any value, Z_1 is confined to the interior of the circle, marked T in Fig. 7·35*a*, which passes through Z and ∞. This is the same circle that previously represented Z_t for a single ATR cavity

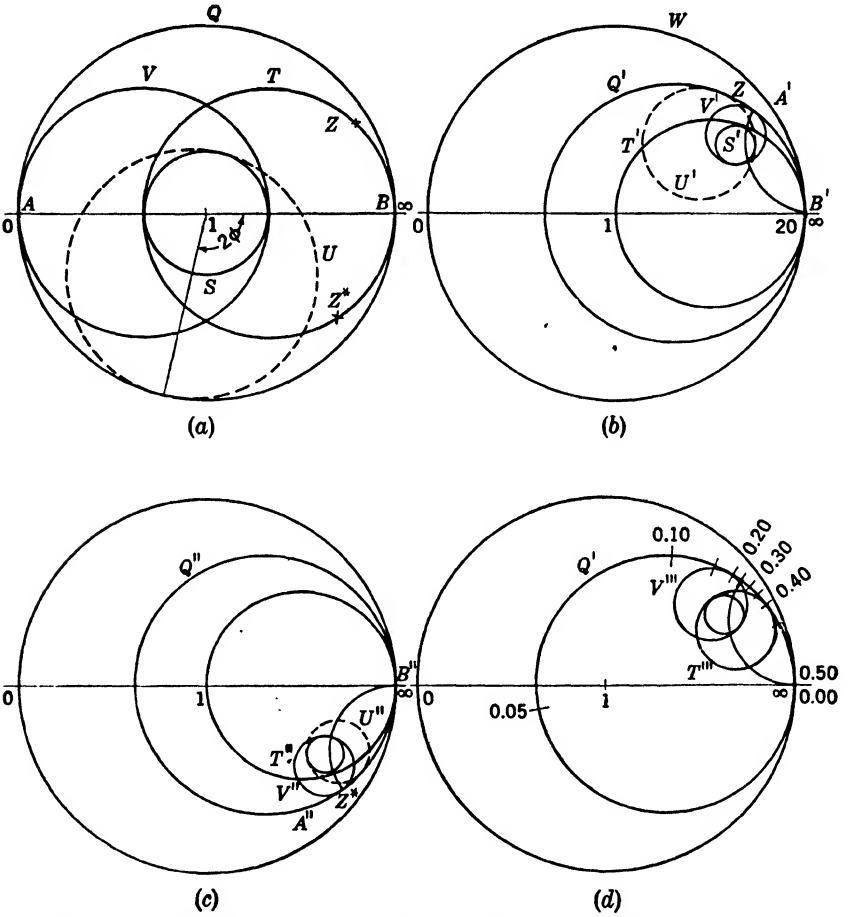

FIG. 7·35.— Loss diagrams for ATR tubes; (*a*) Smith chart for Z_2; (*b*) Z_2 at low frequencies; (*c*) Z_2 at high frequencies; (*d*) Z_2 with decrease in ϕ.

with no line-length errors. To obtain Z_2 the Z_1 circle is rotated about the origin by an amount $2\phi = 4\pi l/\lambda_g$ radians to some position such as that of the circle U. The circles T and V represent Z_2 for $\phi = 0$ and $\pi/2$ respectively; S is merely a fixed circle which is always tangent to U as ϕ is varied. The boundary circle Q of the Smith chart has the same property.

The addition of the constant Z transforms this complete Z_2-diagram to the Z_3-diagram of Fig. 7·35*b*. When this is done the line AB of zero reactance becomes the arc $A'B'$ of reactance X which connects Z and ∞. The circle Q representing zero resistance goes over into Q' representing the resistance R. Since Q, S, T, and V are orthogonal to the line AB, the transformed circles Q', S', T', and V' are orthogonal to $A'B'$. Since the circles T, U, and V are tangent to Q and S, they will remain tangent after transformation. Since $Z + \infty = \infty$, Q', and T' must pass through ∞ and must be tangent to the unit circle W.

When the circles Q' and S' have been drawn, it is easy to follow the behavior of the circle U', which represents the range of impedance Z_3 for some arbitrary line length ϕ. As ϕ increases, U' moves around in a clockwise direction, always remaining tangent to the two fixed circles Q' and S' and assuming the positions T'' and V' when $\phi = 0$ and $\pi/2$. If it is assumed that the nearer ATR tube is 0 or $\frac{1}{2}\lambda_g$ distant from the TR junction and that the junction is of the shunt type as usual, then $Z_t = Z_3$ and the ordinary loss-contour diagram Fig. 7·16 gives the range of loss for any position of the circle U'. The circle Q' is identical with the circle T', which represents Z_t for a single ATR tube since both pass through Z and ∞. Hence, comparison of U' and Q' indicates the relative improvement of two ATR tubes over a single tube.

Figure 7·35*b* represents conditions at the lower end of a frequency band with the ATR cavities resonant near the center. As the frequency is increased from the lower end of the band toward the upper end Z moves down toward the point 20 on the real axis and reaches it at resonance. The circle Q', with all the circles inside, collapses into the small circle through 20 and ∞. At still higher frequencies Z moves down below the real axis and at the upper end of the band the conditions of Fig. 7·35*c* are realized.

If the resonant frequencies of the ATR cavities are adjusted for the same detuning at each end of the band, as would be done for minimum loss, Z will be the same at each end except for a change in sign of the reactance and the values at the low and high ends can be designated by Z and Z^*. In Fig. 7·35*a* the circle T is the same at both ends of the band. For the moment the change in ϕ across the band will be neglected and this means that all of Fig. 7·35*a* will be identical at the two ends of the band. In Figs. 7·35*b* and *c* representing the two ends of the band, $A''B''$ is the image of $A'B'$ in the real axis since Z^* is the image of Z. Since the circles Q, S, T, and V are symmetrical with respect to the axis AB, Q'' will be the image of Q', S'' of S', and so forth. In particular T'' will cover the same range of losses as T', and V'' as V'.

On the other hand the circle U, which in general is not symmetrical relative to AB, will transform to circles U' and U'' which are not images.

The relative positions of U' and U'' may be visualized by noting that U' is tangent to Q at a point on Q between B and A when moving clockwise from B to A. This property must hold for the transformed circles. It follows then that any spacing other than zero and one-quarter guide wavelength will, in general, give unequal losses at the two ends of the band, and will give a greater maximum loss at one end of the band than that realized by one of the two spacings 0 or $\frac{1}{4}\lambda_g$.[1]

The effect of the variation in ϕ between the two ends of the band will be considered next. Suppose that ϕ is set at either $\pi/2$ or π ($l = \frac{1}{4}\lambda_g$ or $\frac{1}{2}\lambda_g$) at the band center and that ϕ is sufficiently linear to have the error the same at each end. The change in ϕ merely causes each of the circles which were at T' and V' to take up one of the positions of the variable circle U'. On the low-frequency side ϕ, which is measured clockwise on a Smith chart, becomes smaller and the circles are shifted counterclockwise with respect to T' and V' (that is, the point of tangency with Q' is shifted in that sense).

In Fig. 7·35*d*, V''' and T''' have been shifted by an amount

$$\frac{\Delta\phi}{2\pi} = \Delta\left(\frac{l}{\lambda_g}\right) = 0.05 \text{ and } 0.10,$$

relative to V' and T' respectively. This corresponds to the fact that a spacing of one-half wavelength results in twice the shift expected from a one-quarter-wavelength spacing. On the high-frequency end the shift is equal and opposite so that circles representing the two ends of the band on a Z_2-chart will be images in the real axis AB. Hence the Z_3-diagrams are also images and the argument about the optimum spacing is the same as before.

It is concluded that even where there is appreciable phase shift across the band in the distance between ATR junctions, the best results are obtained by the use of spacing either one-quarter guide wavelength or one-half guide wavelength at the center of the band. A similar symmetry consideration applies to changes in the distance between the TR

[1] To prove this, the locus is constructed of the point on U' which gives maximum loss as ϕ is varied. The point on this locus where the loss is a maximum or a minimum (for ϕ) is a point where an envelope of the circles U' is tangent to a loss contour. There must be at least four such points: a maximum and minimum of this locus, and a maximum and minimum of the similar locus of the point on U' which gives a minimum loss. There are just two envelopes, the circles Q' and S', and each of these is tangent to a loss contour at only two points making just four in all or one each of the extremum points enumerated.

The two loci of the maximum point at the two ends of the band are images. If $L(\phi)$ is the loss at one end, $L'(\phi)$ that at the other end, L_1 and L_2 the values for $\phi = 0$ and $\pi/2$, then $L(\phi)$ and $L'(\phi)$ traverse the same values in opposite directions and are equal at $\phi = 0$ and $\pi/2$. From the fact that L has only one maximum and one minimum and is never constant it follows that either L or L' is greater than one of L_1 and L_2 at all times except when $\phi = 0$ or $\pi/2$.

and adjacent ATR junctions so that this spacing should also be set at the equivalent one-half guide wavelength at the band center (for shunt TR and series ATR circuits). Furthermore the conclusion for the inter-ATR spacing still holds when the TR-ATR spacing changes with frequency.

Comparison of b and d of Fig. 7·35 shows that the frequency dependence of ϕ causes V''' to be shifted somewhat to the left relative to V', with a corresponding increase in the maximum loss, while T''' has contracted relative to T' with a considerable decrease in the maximum loss (actually a drop from 3.5 to 1.3 db in this particular case). Thus, the quarter-wavelength spacing is considerably better than the half-wavelength spacing when the frequency sensitivity of the spacing is negligible. But when the phase shift becomes appreciable it tends to increase the maximum loss in the quarter-wavelength case and to decrease it for the half-wavelength separation until the latter is actually superior.

Of course, if the phase shift goes far enough the loss for the half-wavelength spacing will increase. Examination of the tangent point of a Z_3-circle on Q', which has been marked off in Fig. 7·35d for values of spacing 0.10 apart, shows, however, that the points tend to bunch around 0.25 where the loss is small. Hence a fairly small decrease in ϕ brings the T' circle into this region where it remains until ϕ has dropped to a very low value. Although quarter-wavelength and half-wavelength spacing are good for a narrow and a broad band respectively, zero spacing is not to be recommended.

A clearer view of the branching-loss variation is obtained from the curves of Fig. 7·36 which plot the branching loss as a function of transmitter phase θ with a transmitter of $r_c = \infty$ for various separations ϕ of the two ATR junctions.[1] The same value of Z was taken as that used

[1] To compute these curves the tangent circles S' and Q' are constructed. The point of tangency of the circle U' is marked off on Q' for each value of ϕ by transforming it from the Q-circle. The Z_3-circle U' for any ϕ can then be drawn at once. For each such circle, however, it is necessary to mark off points corresponding to various values of the transmitter phase θ. This can be done by starting with a Z_1-diagram like the Z_t-diagram of Fig. 7·23 and then transforming individually the point corresponding to each value of θ. To avoid repeating this procedure for every ϕ, loci of constant θ can be drawn on the Z_3-diagram, making it possible to determine θ, for each point on the Z_3-circle, from the locus intersecting at that point.

In the construction of these loci it is noticed that as ϕ varies, the θ-points on the U-circle of Fig. 7·35a trace out concentric circles about the origin. Hence, the transformation of these loci to the Z_3-plane yields a family of circles with centers lying on a straight line. The line of centers is determined by the point $Z_3 = Z + 1$, which is the transformation of the center of the concentric family, and by the center of Q' which is a member of the family. By adding R to the intersection R_2 of any θ-circle with the AB-axis, the intersection R_3 with the arc $A'B'$ is found. With two such intersections and the center line it is easy to construct any θ-circle. The usual loss-contour diagram can then be applied to any Z_3-circle to find the loss for each value of θ.

for the diagrams of Fig. 7·35. The TR-ATR distance was assumed to be zero. A moderate change in this distance tends to raise the general loss level without greatly changing the form of the curves.

It is evident that the best conditions obtain with $\phi/2\pi = l/\lambda_g = 0.40$. A moderate decrease in spacing from one-half wavelength is quite

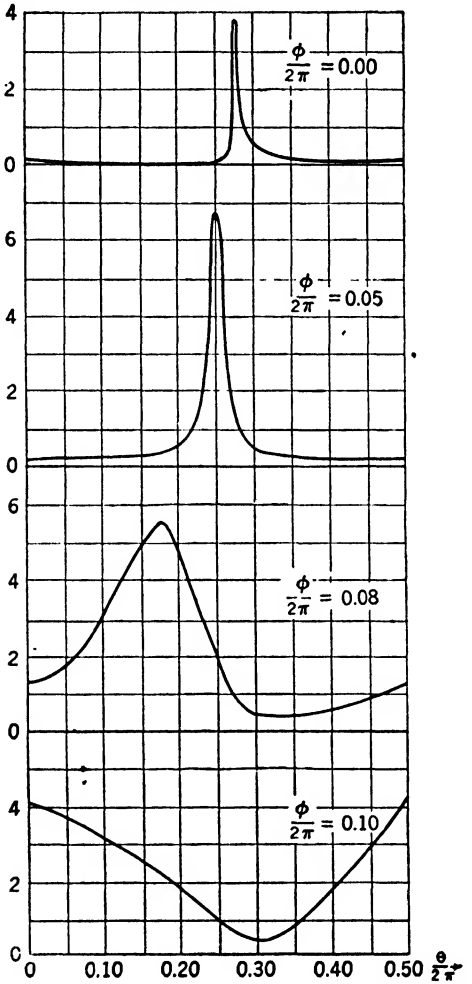

FIG. 7·36.—Loss vs. transmitter phase for

beneficial whereas a small increase in the separation causes the losses to rise and spread out over a large part of the phase range. If the same values of ϕ are read at the other end of the band (the high-frequency side) a set of curves similar, but in reverse order, results.

It appears desirable to use half-wavelength spacing at the center of the band and arrange to have ϕ change with frequency so as to have an

optimum value at the band edge. In this particular example a shift in $\phi/2\pi$ of 0.10 between the center and either end of the band would result in the best loss curve ($\phi/2\pi = 0.40$ in Fig. 7·36) at each end. If, in Eq. (24), θ is set equal to π and $\Delta\theta/2\pi = -0.10$, then $\Delta\lambda/\lambda = 0.094$. Hence with half-wavelength spacing and the waveguide constants assumed in

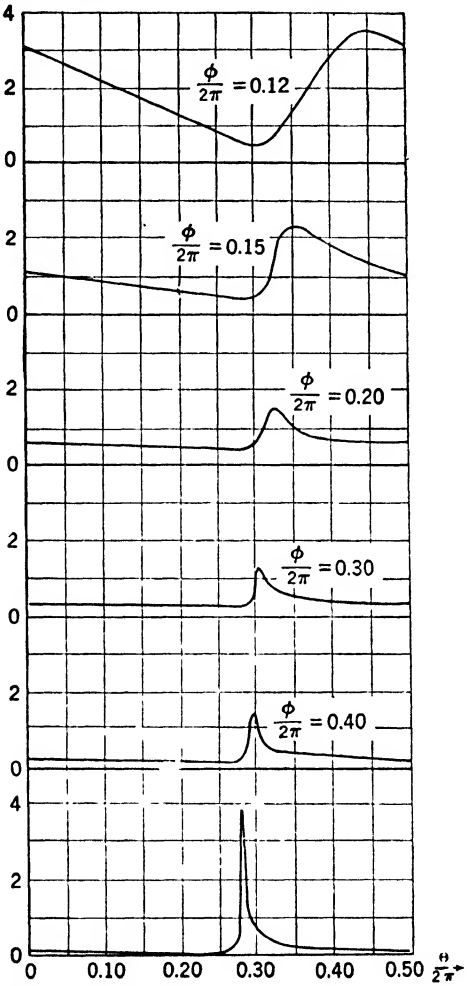

two ATR circuits with various spacings.

Eq. (24), a 19 per cent band would be required to produce the optimum phase shift. With the more commonly used bandwidths of five or ten per cent an ATR spacing of one or two wavelengths is indicated. The necessary phase shift might also be obtained with a shorter spacing by reducing the waveguide width so as to make λ_c smaller.

The curve for $\phi/2\pi = 0.10$ is of particular interest. If Z is trans-

formed down the line a distance of $\phi/2\pi = 0.10$ the result will be very close to the conjugate of Z. This condition, which arises when the complex conjugate of Z is equal to the value of Z_2 obtained with $Z_c = 0$, will be referred to as a "mutual" resonance between the two ATR tubes. This condition usually exists at the normal resonant frequency. When it happens at a frequency far enough from the center frequency, however, the losses usually become high over much of the phase range of Z_c.

In order to understand this, reference is again made to Fig. 7·23 which corresponds to a Z_1-plot in the present case and which shows most of the Z_c phase points crowded together in the neighborhood of the point Z where $\theta = 0$. This is because $X_c = \tan\theta$ and half the range of θ corresponds to values of $X \leqq 1$. Since the X_1-contours of the Smith chart are close in the vicinity of Z, this range of X_c is only a short interval on the chart. On the Z_3-chart also, the phase points tend to congregate about $\theta = 0$. It would be expected, then, that if this point were in a region where the losses were high, they would be so for much of the range of θ. When mutual resonance occurs the ($\theta = 0$)-point ($Z_c = 0$) gives $Z_3 = 2R$. If this frequency differs very greatly from the center frequency, R is small, the losses are large, and the result is a curve like that for $\phi/2\pi = 0.10$.

Fortunately this behavior occurs only over a small range of ϕ. This can be explained by applying the same sort of reasoning to ϕ as was just used for θ. If values of ϕ are marked off on the ($\theta = 0$)-locus in the Z_2 Smith chart, the point $\phi/2\pi = 0.10$ occurs at a large value of X_2 while the point at $X_2 = 0$ is $\phi/2\pi = 0.30$. When this locus is transformed to the Z_3-diagram, the ϕ-points bunch around $\phi/2\pi = 0.30$ and are rather widely spaced at $\phi/2\pi = 0.10$. Since the former value of ϕ gives a loss curve with a sharp peak, that type of curve will be realized for most values of ϕ and the curve with the broad maximum will be met only when $\phi/2\pi$ is close to 0.10.

This mutual resonance will appear if the ATR separation differs even slightly from $\frac{1}{2}\lambda_g$. It is then quite close to the individual resonance point and does not cause high losses. Its presence is readily detected, however, if the standing-wave ratio is measured as a function of frequency looking toward Z_3, with Z_c a matched load. When ϕ is correct a simple resonance curve with a single maximum is obtained. If the error $\Delta\phi$ is appreciable, however, the resulting curve will have a dip at the mutual resonance point, which provides a sensitive means of determining the error Δl in the cavity separation l.

The point of the dip is given approximately by $B = -\frac{1}{2}\Delta'\phi$ where $\Delta'\phi$ is the error in ϕ at that frequency ($\Delta\phi$ corresponds to the individual resonance frequency). This is seen by finding the admittance Y_2 of the first cavity as seen at the second,

$$Y_2 = \frac{Y + j \tan \Delta'\phi}{1 + jY \tan \Delta'\phi} = \frac{G + j(B + \tan \Delta'\phi)}{1 - B \tan \Delta'\phi + jG \tan \Delta'\phi}.$$

If G, B, and $\Delta'\phi$ are all small, $Y_2 \approx G + j(B + \Delta'\phi)$. When $\Delta'\phi = -2B$, $Y_2 \approx G - jB$ and $X = -X_2$; the condition for mutual resonance is therefore satisfied.

If the separation $\Delta\lambda$ of the mutual and individual resonances is known, the error Δl can be found. For $\Delta'\phi$ can be thought of as the sum of the error $\Delta\phi$ at the individual resonance point plus the error $\Delta''\phi$ due to the change in frequency from that point to the mutual resonance point. That is, $\Delta\phi = \Delta'\phi - \Delta''\phi$, and

$$\Delta'\phi = -2B \approx 4Q_L \frac{\Delta\lambda}{\lambda},$$

while

$$\Delta''\phi = \Delta\left(2\pi \frac{l}{\lambda_g}\right) = -\frac{2\pi l}{\lambda_g^2} \frac{d\lambda_g}{d\lambda} \Delta\lambda = -\frac{2\pi l}{\lambda_g} \left(\frac{\lambda_g}{\lambda}\right)^2 \frac{\Delta\lambda}{\lambda}.$$

Since $\Delta l = \Delta\phi\lambda_g/2\pi$,

$$\frac{\Delta l}{l} = \left[\frac{2}{\pi} \frac{\lambda_g}{l} Q_L + \left(\frac{\lambda_g}{\lambda}\right)^2\right] \frac{\Delta\lambda}{\lambda}. \tag{42}$$

When l is too long, the dip in the standing-wave-ratio curve will be on the long-wavelength side of the individual resonance point. When two cavities are properly spaced, but not tuned to exactly the same frequency, a mutual resonance will appear at a point halfway between the two individual resonance points where $B_1 = -B_2$. The standing-wave-ratio curve will also show a dip in this case. To determine whether these errors are serious, it is necessary, at least in theory, to find the maximum loss in the usual way as Z_c is varied. However, the loss corresponding to $Z_c = 0$ would probably be fairly representative in this case, and this is found by using $Z_3 = 2R = 2G/(G^2 + B^2)$.

7·11. Double Tuning for Wideband ATR Circuits.—In any attempt to design wideband ATR circuits, it is important to consider the possibility of "staggered" tuning which involves tuning one of the pair of ATR cavities to resonance near each end of the band. With half-wavelength spacing, the loss would be negligible at each of the two resonant frequencies, assuming no error in the ATR spacings. Since under these conditions the two ATR cavities are in series, either one will insert the proper high impedance at resonance. When changes in the ATR separation due to frequency dependence are considered, the loss is the same at the resonant frequency of the first ATR cavity (the one nearest the TR junction), and is slightly higher at the other resonant frequency.

At the center frequency, however, the mutual resonance appears and the loss curve has a very broad maximum. As this occurs at the center

of the band it is not possible to make use of the favorable shift in ϕ which appears at the ends of the band. This type of circuit does not appear to offer any advantages for broadband applications, although it is satisfactory where it is desired to operate at only two distinct frequencies, for example, for combined radar and beacon reception.

Staggered tuning with quarter-wavelength spacing between ATR cavities does merit consideration. The losses are low at each of the two ATR resonant frequencies, but no mutual resonance appears at the center frequency. If one cavity is tuned to each end of the band, the maximum loss at the center frequency is the same as if the two cavities were tuned to the center frequency and the loss determined at one end of the band assuming no error in ϕ. This is true because the Z_1-circles are identical for a given value of Z and for the conjugate of Z. With the two cavities tuned to frequencies somewhat inside the two ends of the band, the overall maximum loss is considerably below that for synchronous tuning.

With double tuning the difference in susceptance of the two cavities is a constant approximately independent of frequency. If this difference is made too large with quarter-wavelength spacing, a mutual resonance will appear at the band edge. As the susceptance difference is increased, the resonance point moves in toward the center of the band. It appears, therefore, that the results for double tuning with quarter-wavelength spacing would be good for moderate bandwidths but would deteriorate rapidly for very wide bands.

There is some practical disadvantage in using cavities tuned to different frequencies. In low-Q circuits it is necessary to make the tube and cavity integral and fixed-tuned and this means the use of two tube types if two resonant frequencies are desired.

The analysis of the double ATR circuit indicates two possibilities. (1) For very wideband operation, both cavities are tuned to the center frequency and spaced $(n/2)\lambda_g$ apart. The frequency sensitivity of the waveguide between the two cavities is adjusted to give optimum electrical length at the band edge. (2) For moderate bandwidth the cavities are spaced one-quarter wavelength apart and stagger-tuned. The resonant frequencies are adjusted to give the lowest loss over the band.

7·12. ATR Circuits with More than Two Switches.—Where a circuit using two ATR cavities fails to cover the frequency band properly the use of additional cavities may reduce the branching loss still further. If, for instance, one has n identical cavities with half-wavelength spacing and impedance Z, the resultant impedance, assuming all distances are correct, is $Z_t = nZ + Z_c$ and the maximum loss is obtained by setting $Z_t = nR$. By the addition of more tubes this loss could be made as small as desired if the correct spacing over the band could be maintained.

The situation is not quite so simple when the variation in the phase

length of the spacing is taken into account. Figure 7·37 shows plots of Z_t for different numbers of ATR tubes. By the extension of the notation of Fig. 7·34, Z_1, Z_3, Z_5 . . . represent the values of Z_t for 1, 2, 3, . . . ATR cavities. As usual each circle is drawn to represent the range of Z_n when Z_c is allowed any value. For each tube Z was taken to be $0.20 + j2.00$, which represented a cavity with a conductance of $G = 0.05$ detuned far enough to permit a maximum branching loss of about 11 db when used alone. The successive cavities are spaced a distance

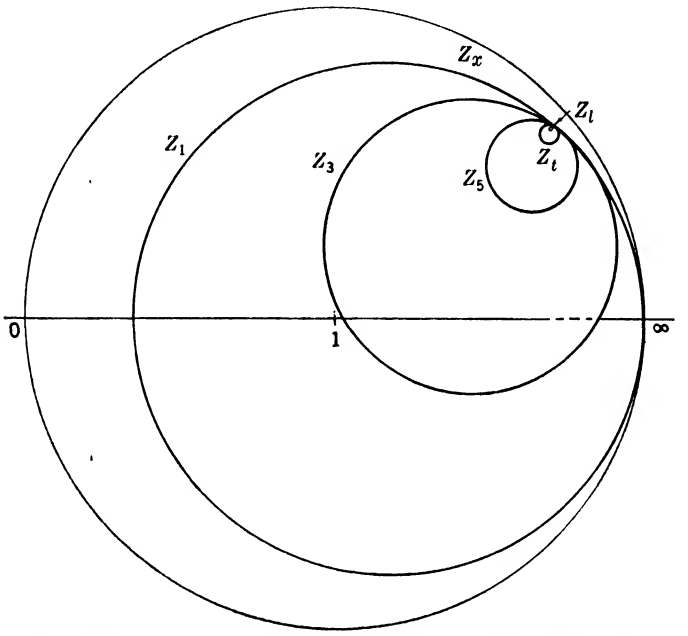

FIG. 7·37.—Impedance plots for successively added ATR cavities.

$l/\lambda_g = 0.40$ apart which makes allowance for a drop from half-wavelength spacing at the band center.

The construction was made in the usual manner by rotating one circle a distance of 0.40 and then adding Z to a few points to get the next circle. If the correct TR distance is assumed, the maximum loss for 1, 2, 3 . . . tubes is 11 db, 3.5 db, 1.00 db, 0.40 db, 0.30 db, 0.27 db, 0.27 db . . . .

The impedances Z_1, Z_3, Z_5 . . . approach a limiting value Z_l which may be found easily if the tubes and spacings are all identical. It is merely the iterative or characteristic impedance of the structure. The structure can be divided into identical symmetrical elements by bisecting each ATR cavity. Then each element is a transmission line of length $\phi = 2\pi l/\lambda_g$ in series with $\frac{1}{2}Z$ at each end. The characteristic impedance

is then $\sqrt{Z_{oo}Z_{sc}}$, where Z_{oo} and Z_{sc} are the open-circuit and short-circuit impedances of the element. The impedance of an open-end transmission line is $-j \cot \phi$ so that $Z_{oo} = \frac{1}{2}Z - j \cot \phi$. When one end of the element is short-circuited the line is terminated by $\frac{1}{2}Z$. By the use of the standard transmission-line formula, the impedance Z_{sc} is

$$Z_{sc} = \frac{1}{2}Z + \frac{\frac{1}{2}Z + j \tan \phi}{1 + j\frac{1}{2}Z \tan \phi}.$$

Since the impedance seen from just in front of the first ATR cavity is of interest

$$Z_l = \frac{1}{2}Z + \sqrt{Z_{oo}Z_{sc}} = \frac{1}{2}Z + \sqrt{1 + \frac{Z^2}{4} - jZ \cot \phi}.$$

This shows that Z_l can become infinite only when $\phi = n\pi$. Hence half-wavelength spacing is to be preferred. Contrary to the situation for only two tubes, the departure from one-half wavelength over the band should be kept as small as possible.

For quarter-wavelength spacing Z_l reduces to $\frac{1}{2}Z + \sqrt{1 + \frac{Z^2}{4}}$ which is the expression for the continued fraction

$$Z + \cfrac{1}{Z + \cfrac{1}{Z + \quad \ddots}}$$

obtained by adding the elements in one at a time.

If two structures of identical elements which have quarter-wavelength and half-wavelength spacings, respectively, at the center of a band are compared, it appears that the loss at the ends of the band is less for the half-wavelength separation. Unlike the case of only two ATR tubes, this is true whether or not ϕ changes with frequency. It has already been seen that this is true when ϕ is constant.

Figure 7·37 illustrates the half-wavelength case at the low-frequency end of the band where the spacing has dropped to 0.40 wavelength. It is seen that Z_l has moved around from Z in the direction of lower losse. A consideration of the successive points Z_n on the Smith chart will show that this is normal, whereas in the quarter-wavelength case Z_l tends to shift in the opposite direction.

The principles of double tuning can also be carried over to more than one pair of ATR tubes. Thus with an even number of ATR cavities

uniformly spaced every other cavity could be tuned to one frequency near one end of the band and the remainder to another frequency near the other end. If enough cavities are used to approximate the limiting impedance then, unlike the situation for only two tubes, the half-wavelength spacing with double tuning compares favorably with the quarter-wavelength spacing.

It will be remembered that the half-wavelength spacing with double tuning was unsatisfactory for two tubes because the curve of loss vs. transmitter phase had a very broad maximum at the center of the band. With additional pairs this will still be true but it will be of no importance, for the maximum can be made as small as desired. The impedance of two tubes at the transmitter phase which gives maximum loss at the center of the band is $Z + Z^* = 2R$. For n pairs it is $2nR$, and this increases rapidly with n, causing the loss to approach zero and giving $Z_l = \infty$. Near the ends of the band the loss will also be low since one of the first two tubes will be resonant.

For quarter-wavelength spacing with double tuning the maximum loss at the band center cannot be made to approach zero since Z_l will be complex. Near the band ends it will also be inferior to half-wavelength spacing because of the effect just discussed for synchronous tuning.

These results on the branching loss for duplexers which use a sufficient number of ATR cavities to approach the limiting impedance indicate that the half-wavelength spacing is satisfactory for both synchronous and double tuning and that the departure from one-half wavelength should be made as small as possible over the band.

The discussion of multiple ATR circuits on the basis of the limiting impedance Z_l appears a little academic since, in practice, n can never approach infinity. However, the actual impedance usually approaches Z_l rather rapidly, and the limiting conditions may afford a simple although approximate picture of the behavior of a small number of elements. For any specific case the actual loss can be determined graphically.

A rather severe limitation is placed on the number of tubes by the arc loss. Since this is appreciable for low-Q tubes, the loss at high level increases with any attempt to decrease the loss at low level by adding more tubes. In addition, the problem of minimizing the reflection at high level becomes more serious as elements are added. This reflection is usually important from the point of view of efficient transmitter operation and would be smallest with quarter-wavelength spacing where cancellation would occur.

Finally, the variation with frequency of the TR-to-ATR distance may introduce an appreciable loss even with $Z_l = \infty$. There does not appear to be any way to cancel this effect at both ends of the band by

means of special ATR circuits. However, an error in this distance which causes considerable loss with poor ATR circuits may be inappreciable when the circuits are efficient.

7·13. Branching Loss with the Available ATR Tubes.—As a matter of practical interest, curves are reproduced in Figs. 7·38, 7·39 and 7·40 which show the maximum branching loss to be expected from duplexers using ATR tubes with the measured values of G and Q_L given in Table 4·4 of Chap. 4. The curves for the 3-cm band were calculated assuming a wavelength band centered at 3.33 cm and waveguide of inside width 0.900 in. The curves for the 10-cm band assumed a center wavelength of 10.7 cm and waveguide 2.840 in. wide. The TR tube and receiver were assumed to be matched. The loss value read from a curve is the maximum loss that could occur for any transmitter impedance at a wavelength differing by $\Delta\lambda$ from the center of the band. It is also the maximum loss anywhere over a correctly centered band of width $2\Delta\lambda$.

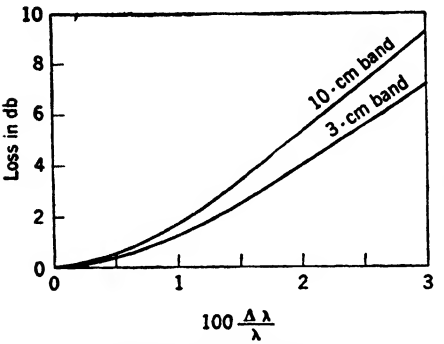

FIG. 7·38.—Maximum branching loss for a duplexer with one ATR tube.

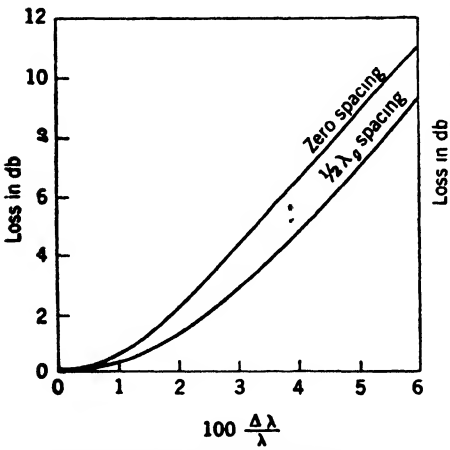

FIG. 7·39.—Maximum branching loss for a 3-cm-band duplexer with two ATR tubes.

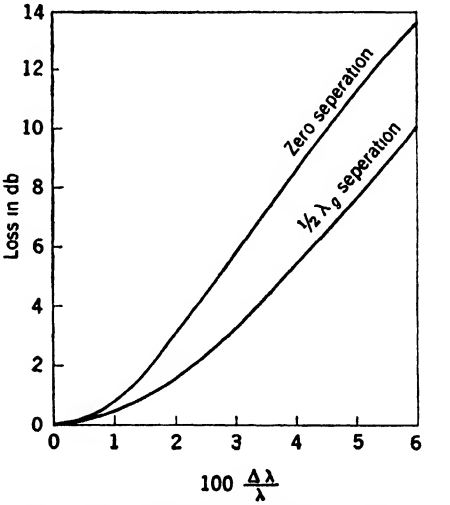

FIG. 7·40.—Maximum branching loss for a 10-cm-band duplexer with two ATR tubes.

The variation with wavelength of the electrical distance between TR and ATR junctions was neglected in calculating the curves of Fig. 7·38

for a single ATR tube. The effect is small and separations of both one-half wavelength and one wavelength have been used in different duplexers. For this simple case the maximum loss in decibels at any wavelength is found from Eq. (26) to be

$$L = 20 \log_{10} \left[1 + \frac{1}{2} G + \frac{2Q_L^2}{G} \left(\frac{\Delta\lambda}{\lambda} \right)^2 \right].$$

The fact that the losses are lower in the 3-cm than in the 10-cm band is caused by the higher G of the 3-cm-band tube which more than makes up for its higher Q.

The curves labeled "$\frac{1}{2}\lambda_g$ spacing" in Figs. 7·39, 7·40 are applicable to a duplexer with two ATR cavities separated by one-half wavelength, the nearer one being also one-half wavelength from the TR junction. In the curves marked "zero spacing" no correction was made for the variation in electrical length of these two distances. It is seen that the improvement afforded by the phase shift in the ATR spacing more than offsets the added loss due to the phase shift of the TR-to-ATR distance.

The use of two ATR tubes apparently provides a band about twice as wide as that for one tube. Actually the improvement might be made greater. The half-wavelength ATR spacing represents that generally used at present, but it probably does not give the optimum frequency dependence of this important electrical length.

7·14. Branching Loss for a General T-junction.—Up to this point the discussion has been based on the simplest series- or shunt-branching circuit representation of the T-junction. An actual waveguide T-junction used for connecting receiver, transmitter, and antenna lines is in general more complicated than this, and can be represented only by the three-terminal-pair network of Fig. 7·1. In principle, six complex quantities can be determined by experiment, for example, the elements of the impedance matrix, which will completely characterize the T-junction at one frequency. If the transmitter, receiver, and antenna impedances, Z_t, Z_R, and Z_B, are known the total loss in received signal at the junction can be found.

If arm (1) goes to the antenna, arm (2) to the transmitter, and arm (3) to the receiver, and if E_0 is the antenna generator voltage,

$$\begin{aligned} E_1 &= E_0 - I_1 Z_B = Z_{11} I_1 + Z_{12} I_2 + Z_{13} I_3, \\ E_2 &= -I_2 Z_t = Z_{21} I_1 + Z_{22} I_2 + Z_{23} I_3, \\ E_3 &= -I_3 Z_R = Z_{31} I_1 + Z_{32} I_2 + Z_{33} I_3. \end{aligned}$$

To find the loss it is merely necessary to solve the system of equations for I_3,

$$\left.\begin{aligned} (Z_{11} + Z_B) I_1 + Z_{12} I_2 + Z_{13} I_3 &= E_0, \\ Z_{21} I_1 + (Z_{22} + Z_t) I_2 + Z_{23} I_3 &= 0, \\ Z_{31} I_1 + Z_{32} I_2 + (Z_{33} + Z_R) I_3 &= 0. \end{aligned}\right\} \tag{43}$$

For a properly matched system, $I_3 = \frac{1}{2}E_0$, and the loss in any other case is $20 \log_{10} \left|\frac{E_0}{2I_3}\right|$.

It is not possible to say much about the loss for a general T-junction. However, for the dependence on Z_t, the loss contours on the Smith chart will still be the familiar bipolar family of circles. This is evident since Z_t occurs in only one term of the Eqs. (43), and the solution can be written in the form

$$I_3 = \frac{a + bZ_t}{c + dZ_t} E_0.$$

The loss factor is then

$$\beta = \left|\frac{E_0}{2I_3}\right| = \frac{1}{2}\left|\frac{c + dZ_t}{a + bZ_t}\right|. \tag{44}$$

If

$$Z_1 = \frac{c + dZ_t}{a + bZ_t},$$

the loss contours in the Z_1-plane will be the concentric family of circles $2\beta = |Z_1|$. Since the transformation of Eq. (44) is circular, the contours in the Z_t- or Γ_t-plane will be a bipolar family.

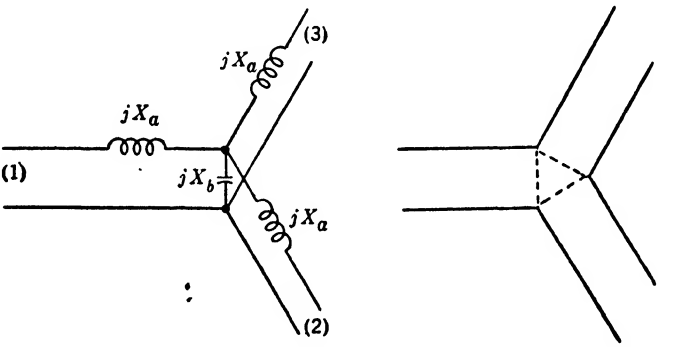

FIG. 7·41.—The equivalent circuit of a 120° Y-junction in the H-plane.

As an illustration, the contour diagram for an H-plane (shunt) waveguide T-junction of the symmetrical 120° type will be constructed with the use of the circuit constants for waveguide 0.400 in. by 0.900 in. ID at a wavelength of 3.20 cm in free space and it will be assumed that the antenna and receiver are matched. The equivalent circuit for the junction is shown in Fig. 7·41 with the reference planes given by the broken lines in the sketch to the right. The values of the constants are

$$X_a = 1.46, \qquad X_b = -0.65,$$

normalized with respect to the waveguide impedance.

To facilitate comparison with the ideal shunt junction, Z_t will be referred to a point on the transmitter arm where an open circuit would be placed to produce a match between the other two arms. This will ensure that, at least for large enough values of Z_t, the behavior of the ideal and the actual junction will be about the same. Since the reference point for Z_t will be at a certain distance from the terminals (2) of the equivalent circuit, Z_1 will be called the transmitter impedance referred to those terminals. The diagram for Z_1 will then be constructed from which that for Z_t may be obtained by a simple rotation.

Let Z_2 equal the total impedance across the terminals of jX_b looking out arm (2) which will be considered the transmitter arm.

$$Z_2 = \frac{Z_b(Z_a + Z_1)}{Z_a + Z_b + Z_1},$$

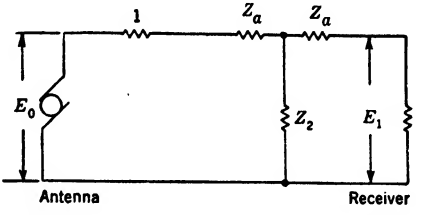

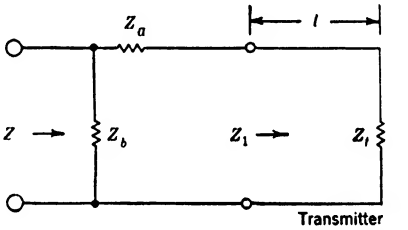

FIG. 7·42.—Duplexer circuit using the Y-junction of Fig. 7·41.

and the loss between arms (1) and (2) can be found by using the circuit of Fig. 7·42. In fact,

$$\frac{E_1}{E_0} = \frac{Z_2}{(1 + Z_a)(1 + Z_a + 2Z_2)}.$$

When the junction is matched, $E_1 = \frac{1}{2}E_0$; for other cases the branching loss is given by the factor

$$\beta = \frac{1}{2}\left|\frac{E_0}{E_1}\right| = |1 + Z_a| \cdot \left|1 + \frac{1}{2}(1 + Z_a)Y_2\right|.$$

If

$$Y_3 = (1 + Z_a)Y_2 = \frac{(Z_a + Z_b + Z_1)(1 + Z_a)}{Z_b(Z_1 + Z_a)}, \tag{45}$$

and

$$m = |1 + Z_a| = \sqrt{1 + X_a^2} = 1.77,$$

then

$$\beta = m|1 + \tfrac{1}{2}Y_3|, \tag{46}$$

which is just m times the usual loss factor for a simple shunt junction with transmitter admittance Y_3. If Eq. (45) is solved for Z_1,

$$Z_1 = \frac{1}{\dfrac{Y_3}{1+Z_a} - Y_b} - Z_a. \tag{47}$$

It is now possible to begin with the standard loss diagram drawn for Y_3, multiply the value of each contour by m, and then transform the whole family from the Y_3-plane to the Z_1-plane by means of Eq. (47). From there it can be transformed to the Γ_1-plane (Smith chart) by the usual Eq. (11). The diagram may be rotated to bring the zero-loss

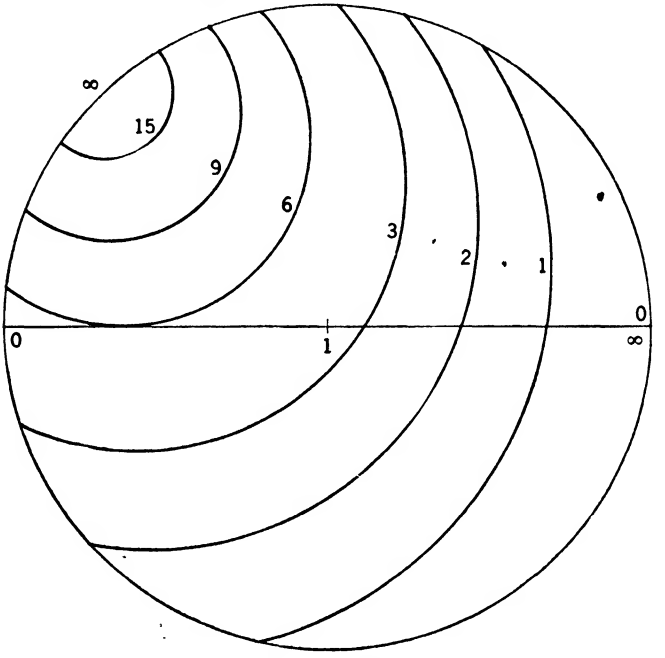

FIG. 7·43.—Loss diagram for the junction of Fig. 7·41 plotted on Smith chart for Z_t.

point around to the infinite-impedance point and the result is shown in Fig. 7·43, the loss-contour diagram on the Smith chart for Z_t.

In making the transformation of Eq. (47) between Z_1 and Y_3 or between Γ_1 and Y_3, the work can be simplified by making use of certain properties of general circular transformations. Since a bipolar family of circles is completely determined by its two foci, it is necessary only to transform these two points. The foci are the points A and B of Fig. 7·29 about which the circles converge for extreme values of the parameter. The family given by Eq. (46) is the concentric system of circles of Fig. 7·15 with the foci -2 and ∞.

Comparison of Figs. 7·43 and 7·16 shows the difference between a particular waveguide T-junction and an ideal shunt-branching circuit.

The most important aspect is the shift of the infinite-loss point around closer to the zero-loss point with consequent increase in loss in the upper half of the Smith chart. In previous sections, ATR circuits have been considered which resulted in values of Z_t such that positive and negative reactances are equally probable. Because of the lack of symmetry of Fig. 7·43, it might be well to adopt an ATR circuit which would favor the negative reactances where the losses are smaller. This could be done by tuning the ATR cavity to a slightly lower frequency or, instead of choosing the TR-to-ATR distance so as to give zero loss with the ATR switch at resonance, it could be made slightly longer. In any case, the amount of correction would depend on the expected range of the Z_t values and on the particular junction used, since the contour diagram would presumably be different for each junction.

The question arises as to what can be done to an actual junction to make it look like a simple shunt (or series) circuit. This circuit is considered ideal because of its symmetrical loss characteristics. It is not difficult to prove that nothing is accomplished by inserting any sort of transformer in any one arm of the junction. Such a transformer would have to be matched to the line, and it would, therefore, change nothing in either the receiver or antenna arms which are assumed to be connected to a matched load and matched generator. It can be shown that in the transmitter arm it would only change the line length, for a four-terminal network can be matched to the line only if it is symmetrical, and it then acts merely as a length of transmission line.

The only changes that will benefit the junction must involve all three arms, since no unmatched device can be inserted in only one or two arms. It would appear that the T-junction would be considerably improved if it were possible to adjust the relative positions of maximum and minimum loss on the Smith chart so that they occurred diametrically opposite, that is, one-quarter wavelength apart as in the ideal shunt circuit rather than in the distorted positions of Fig. 7·43.

If this is accomplished, the question arises as to whether any further improvement can be realized; that is, could the junction be manipulated to squeeze the loss contours over to the left side of the Smith chart so that the losses would be low in the operating region. The answer to this question is no.

If a short circuit is placed in arm (3) and the transmission between arms (1) and (2) is measured, the two adjacent positions of the short circuit which result in zero and in complete transmission may be located. A lossless T-junction with 120° symmetry is identical with a simple shunt junction if these two positions are one-quarter wavelength apart. Its properties are, therefore, completely determined and no further improvement is possible. The reason can be pictured quite simply.

In the impedance matrix all the diagonal terms are equal, and all the nondiagonal terms are equal because of symmetry. There are, thus, only two independent terms and as they are both imaginary, two real constants suffice to describe the junction. Now if l is the distance between the two positions of the short circuit which give zero or complete transmission, l is a function of these two constants and specifying $l = \frac{1}{4}\lambda_g$ places a condition on them which allows one to be eliminated. The remaining constant depends on the position of the reference point for measuring impedance. By proper choice of the reference point this constant may be made equal to that of a simple shunt circuit.

This indicates the possibility of making a waveguide T-junction accurately equivalent to a simple shunt circuit by varying some one dimension which does not destroy the symmetry. The electrical measurement involves only an elementary experiment with a plunger. To the author's knowledge this experiment has not been attempted.

It can be shown in the same way that *any* lossless junction is equivalent to a shunt junction if it is possible to match between any two arms by a short circuit in the third, and if the two short-circuit positions for zero and complete transmission are one-quarter wavelength apart. The general network with three pairs of terminals has a three-row impedance matrix with nine elements. Since the nondiagonal elements are equal in pairs, there are six independent constants. The requirement of matching places two conditions, and the choice of reference planes, three more. The property of one-quarter-wavelength shift for cutoff makes a total of six conditions which fixes all the constants.

It will be noticed that no distinction is made between shunt and series junctions, as they are equivalent if the reference planes are not specified. In fact, the scattering matrices for simple shunt and series branching circuits are

Series

$$\begin{pmatrix} \frac{1}{3} & \frac{2}{3} & \frac{2}{3} \\ \frac{2}{3} & \frac{1}{3} & -\frac{2}{3} \\ \frac{2}{3} & -\frac{2}{3} & \frac{1}{3} \end{pmatrix}$$

Shunt

$$\begin{pmatrix} -\frac{1}{3} & \frac{2}{3} & \frac{2}{3} \\ \frac{2}{3} & -\frac{1}{3} & \frac{2}{3} \\ \frac{2}{3} & \frac{2}{3} & -\frac{1}{3} \end{pmatrix}$$

If each reference plane for the series junction is shifted one-quarter wavelength, the sign of every matrix element will be reversed, and then all the nondiagonal elements can be made positive by reversing the terminals on arm (1). The result is identical with the matrix for the shunt junction.

CHAPTER 8

PRACTICAL BRANCHED DUPLEXERS AND BALANCED DUPLEXERS

By Harold K. Farr and Carroll W. Zabel

The first part of this chapter is devoted to a review of examples of branched duplexers which have been used and to some of the observed results of this use. These examples are divided into two classes—coaxial-line duplexers and waveguide duplexers. The coaxial-line duplexers have been used at 10 cm and at longer wavelengths; waveguide duplexers have been used in high-power installations at 10 cm and at all power levels at shorter wavelengths. Few coaxial duplexers have used ATR switches whereas most waveguide duplexers have included them. In the second part of the chapter, balanced duplexers are described.

BRANCHED DUPLEXERS

By Harold K. Farr

8·1. The Electrical Design of a Duplexer.—In selecting a switch it is necessary to choose between the fixed-tuned and the tunable types. Systems developed since the fixed-tuned tubes became available have used these tubes almost exclusively. It is important to keep the number of different adjustments in a radar system as low as possible. This not only facilitates maintenance and tuneup but reduces the possibility of incorrect adjustments. To attain this objective, it may be necessary to make some concessions in performance.

It has been seen that the limitations in fixed-tuned ATR tubes may lead to some loss. However, the usual tunable ATR cavity which has a much higher Q may also cause losses due to temperature detuning or transmitter-frequency drift. Furthermore, the reception of signals at more than one frequency, which occurs when beacon reception is combined with radar, may be extremely inefficient. There seems to be no deterioration in performance using fixed-tuned TR tubes since the reception loss usually compares favorably with the corresponding tunable tubes. If a narrow r-f filter happens to be desirable, as for image rejection, then, of course, a tunable TR tube may be preferred.

The mechanical simplicity of the fixed-tuned ATR tubes makes them cheaper than the corresponding tunable circuits. However, when

length of life is taken into account, the cost of the fixed-tuned TR tubes will be comparable with the tunable ones.

After the switches have been selected, the junction for the TR switch is the next consideration. A junction with 120° symmetry has the best electrical properties, but for narrow-band applications other kinds which offer mechanical advantages may be used. If a 120° junction is chosen and if the lowest possible reception loss is desired over a wide band of frequencies, the necessary alteration should be made to ensure that the junction is equivalent to an ideal shunt or series circuit as explained in Sec. 7·1. It would probably be impractical to attempt this with any junction other than the 120° junction.

If the complete 120° symmetry is not used, there should, if possible, be symmetry of the transmitter and antenna arms with respect to the other arm since the proper transmitter match is most important. If the two arms used for reception (or transmission) lack symmetry with respect to the third, they should be checked for reflection loss with a plunger in the third arm.

The ATR junction has been discussed in Chap. 4. At low power level the only important aspect is its effect on the Q. At high power level the problem is the same for both TR and ATR junctions. The distance from the window to the waveguide wall must be adjusted to give a good match for transmitter power. In principle, this is done at high power level so that the switch will be broken down. In practice, it is much simpler to make such measurements at low power level, and to simulate the conditions of high power level by short-circuiting the electrodes or detuning sufficiently. For low-Q tubes with large windows, it is necessary to cover the inside of the window with Wood's metal or with some other conductive coating.

It is more accurate in one respect to make this sort of standing-wave-ratio test at low power level. Because of the finite firing time of the arc, the standing wave measured at high power will be an average of that before and after firing although the standing-wave ratio of interest is that measured after firing. If the detecting element reads average power, the "apparent" standing-wave ratio in power at high power level is

$$r^2 = \frac{W_x}{W_n},$$

where W is the total energy per pulse received by the probe, and W_x and W_n are its maximum and minimum values as the probe is moved in the slot. If it is assumed, for example, that the line is matched when the tube is fired,

$$r^2 = \frac{T_1P_{1x} + T_2P_2}{T_1P_{1n} + T_2P_2},$$

where T_1 and T_2 are the lengths of the portions of the pulse before and after firing, P_{1x} and P_{1n} are the maximum and minimum powers in the standing wave before firing, and P_2 is the power after firing. If it is assumed that the junction reflects completely before firing, $P_{1n} = 0$ and $P_{1x} = (V_{1x})^2 = (2V_2)^2 = 4P_2$ where V_{1x} and V_2 are the voltages corresponding to the powers P_{1x} and P_2, if unity impedance is assumed. Finally,

$$r^2 = 1 + 4\frac{T_1}{T_2}.$$

If, for instance, the firing time is one tenth of the remainder of the pulse, then $r^2 = 1.4$, whereas the actual standing-wave ratio after firing is 1.0. This effect is not ordinarily noticeable for long pulses but may be so for pulse lengths of 0.1 μsec or less.

If the junction is to be used over a band of frequencies greater than 1 or 2 per cent, it will probably be necessary to mount the cavity with the window flush with the wall of the transmitter line although, for narrow bands, it can be set back one-half wavelength.

High-Q cavities are often iris-coupled to the narrow side of a waveguide simply by cutting a small hole in the waveguide wall. At high power level the hole usually appears as a capacitive susceptance of small magnitude. This can be canceled by adding a small transverse strip of metal on the opposite side, as for the inductive matching iris, or the mismatch may be small enough to be neglected. If TR and ATR cavities which have the same mismatch are mounted one-quarter wavelength apart, the susceptances will cancel almost completely. Unfortunately the ATR cavity usually has a much larger window than any high-Q TR cavity. A voltage standing-wave ratio of 1.15 has been observed for such a combination.

The window of a low-Q cavity is distinct from the waveguide wall and may, therefore, be moved in until the high-level match is achieved. Specifications for the voltage standing-wave ratio of fixed-tuned tubes are given in Table 4·4 of Chap. 4. Some of the 10-cm-band tubes could doubtless be improved by changes in the mount.

Where a pre-TR switch is used, the TR cavity must be mounted with the input window an odd number of quarter wavelengths from the input window of the pre-TR tube. In the 10-cm duplexers this distance is usually three quarters of a wavelength. This arrangement places the input window of the pre-TR tube at a point of maximum voltage when the TR tube is fired.

The distance between TR and ATR junctions must be adjusted for best signal reception. For simple iris coupling to the main waveguide, this distance is often very close to the nominal one-quarter or one-half

wavelength. Therefore, it may be assumed that it is this distance and the complete duplexer merely checked as mentioned below. For the simple types of waveguide junctions where the equivalent-circuit constants are known, the correction to the nominal spacing can be calculated without recourse to experiment but such calculations are valid only when the cavity and other components are kept at a distance from the junction of at least a quarter wavelength.

The experimental determination of the correct spacing is made in two steps: a measurement on the ATR switch alone, and one on the TR junction alone. With the ATR switch tuned to resonance, the position of the minimum point of the standing-wave pattern is found relative to the ATR junction. Then by means of an adjustable short-circuiting plunger in the transmitter arm, that position of the minimum point relative to the TR junction which gives the best match for received signal is determined. As explained in Sec. 7·7, this determination of the TR-to-ATR distance is best done at a frequency corresponding to the waveguide wavelength given by Eq. (7·25). This is near, but not necessarily at, the center of the band.

The measurement of the position of the standing-wave pattern relative to the ATR junction is the determination of the distance of plane *A* of Fig. 4·1 from the center of the junction. This correction is small and may be negligible. To make this test, it is necessary to add a tuning adjustment to the cavity, if none is present, and to check for resonance by measuring R with a plunger as described in Sec. 4·2. A small error in cavity tuning would invalidate the phase measurement. To help eliminate phase errors which arise if the ATR window is not properly centered, the measurement should be repeated after the cavity has been removed from the mount, turned 180°, and replaced. The two readings can then be averaged.

After the TR and the ATR circuits have been combined, the TR-to-ATR distance should be checked again by measuring the voltage standing-wave ratio looking in from the antenna end. Because of the difficulty of making accurate phase measurements in these tests, the distance may be found to be in error at this point. To correct it, the plunger position which gives the same impedance at the antenna arm as that given by the ATR switch is determined. A measurement of the change in plunger position from this point to the point of best match gives the error in the TR-to-ATR distance.

If more than one ATR switch is used, the separation between cavities must be determined at the same frequency used for the TR-to-ATR distance. The data are given by the measurement already made on the ATR switch. By using these data, the correct separation is the nominal distance plus twice the correction given by the distance of the reference

plane from the center of the tube, the correction being counted once for each of the two tubes. For a series mount the correct separation may be slightly greater than the nominal one-quarter or one-half wavelength, as indicated by an inductive susceptance B_a in Fig. 4·10*a*. For a shunt mount, the correction has the opposite sign.

When the two ATR switches have been combined with half-wavelength spacing, their separation may be checked by the mutual-resonance method of Sec. 7·10. The error in spacing is then given by Eq. (7·42). This sensitive check is not applicable to quarter-wavelength spacing, but for that spacing the separation is probably less critical. When making this test, it is important to have both cavities tuned exactly to resonance at the frequency for which the spacing is to be one-half wavelength. Each cavity can be tuned separately by using the plunger method if the other cavity is replaced by a short-circuited dummy.

In actual operation it is best for a fixed-tuned cavity to be set at a frequency which will give equal susceptance at the two ends of the band. As this may not be exactly the same as the frequency at which the line lengths are adjusted, there may be a slight mutual resonance at some frequency if two ATR cavities are used. As this effect will, very probably, be small, it is better to tolerate it in order to have the minimum loss at band edge.

8·2. Mechanical Design Problems.—A mechanical problem of considerable importance is that of the method to be used for attaching the TR and the ATR switches to the main waveguide or other components. This problem was considered in Chap. 4 in connection with the ATR switch, and some of the methods discussed there have been applied to TR circuits. One of the most convenient methods is that of the choke-flange coupling used for making ordinary waveguide connections. The 1B26 TR tube at 1.25 cm, and the 1B24 and the fixed-tuned TR tube at 3 cm, connect to a standard choke coupling with the window in the plane of the flange to permit mounting flush with the waveguide wall. The choke-flange connectors used at 3 cm on the cavities for the 724 tubes were mounted about one-quarter wavelength from the windows which were placed one-half wavelength from the main waveguide.

There is some difficulty in building a waveguide junction with a flush choke coupling. Because of interference between the choke and the waveguide, it is virtually impossible to do this in a series junction. In a shunt junction it can be accomplished by eliminating the part of the choke occupied by the waveguide and leaving two arc-shaped openings on either side of the waveguide.

The 1B24 TR tube at 3 cm has been mounted on a simple 90° T-junction using split chokes in this manner. Fortunately, because of the

peculiar fields at the junction, it was possible to obtain a good high-level match with the input flange of the tube mounted 0.040 in. back from the inside wall of the waveguide, a circumstance which greatly facilitated the construction of the mount.

A duplexer designed at the Bell Telephone Laboratories made use of a 1B24 TR tube and an ATR tube of similar construction, both mounted on simple 120° *H*-plane junctions using split chokes.[1] In this way the main waveguide made a 60° bend at each junction but in opposite directions and, consequently, the antenna and the transmitter arms were parallel. The same choke construction was applied to the vestigial 120° junction of Fig. 7·8.

At low power level the split chokes are satisfactory since the match is not critical. At high power level, because of the distorted fields in the junction, a good contact may be required between the flanges of the tube and the mount on the 120° junction. The 90° junction seems less critical in this respect, but breakdown across the choke gap will occur at powers where the 120° junction is satisfactory.

The high-Q cavities used at 10 cm are often attached permanently to the main waveguide since the tubes may be replaced without removing the cavities. Similarly, an iris-coupled mixer may be permanently attached to such a TR cavity. Most of the fixed-tuned 10-cm tubes use the coiled-spring contact described in Chap. 4. In loop-coupled circuits the input and output loops often plug into a keyed hole.

In many systems which must operate at high altitudes or which handle high power, the r-f lines are filled with gas (usually air) under pressure. For such a pressurized system special precautions are necessary in order to make all joints airtight. Pressurizing a duplexer usually means sealing off the cavities from the main waveguide. Of course, only the components that carry the transmitter power need be pressurized. This eliminates not only the output circuit of the TR switch, but even the interior of the cavity since the cavity is only weakly coupled to the main line during transmission. Naturally the part of the cavity that contains the special gas for the r-f discharge must be sealed off from the atmosphere.

One way to pressurize a cavity is to enclose it completely and to provide special pressurized fittings for the output terminal, the keep-alive connection, and the tuning controls. Figure 8·1 shows an example of this technique as applied to the 721A cavity used on $\frac{7}{8}$-in. coaxial line. The removable parts of the cover are sealed with rubber gaskets. The 3-cm ATR tubes, 1B35 and 1B37, must be mounted in a special holder, Fig. 4·20, which encloses the tube except for one end. These

[1] A. B. Crawford, "X Band Duplex Circuit for 1B24 Type TR and ATR Tubes," BTL Report No. MM-44-160-92, Apr. 22, 1944.

tubes have been pressurized by adding an outer flange on the holder to take a cover that goes over the exposed end of the tube and by a rubber gasket that seals the cover.

Tubes that have a glass window sealed in the iris of the cavity may be pressurized by sealing the cavity to the waveguide with a rubber gasket. The cavity window is then part of the pressurized system. At 3 cm the fixed-tuned TR tube and the tunable 1B24 tube are made to fit the standard UG-40/U waveguide connector which is provided with a groove for a rubber gasket. At 10 cm the fixed-tuned TR and ATR

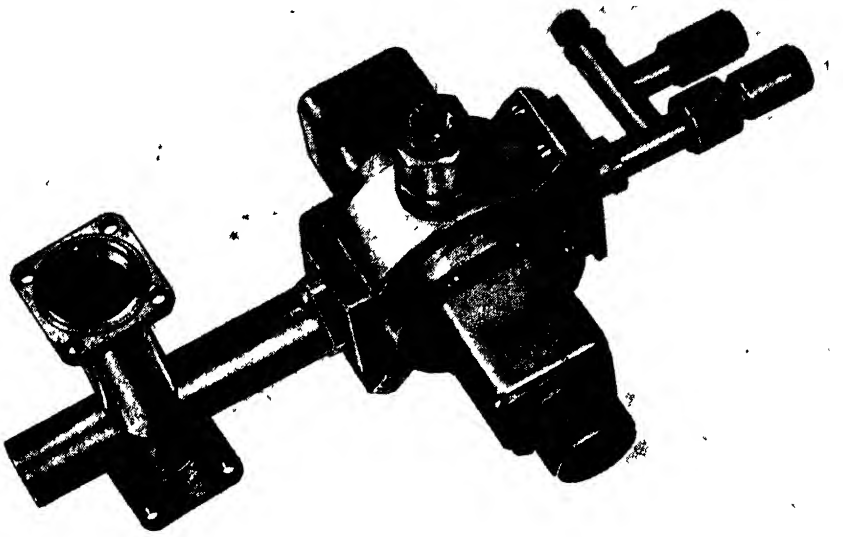

FIG. 8 1.—Pressurized coaxial duplexer

tubes have a flat flange which compresses a flat rubber gasket. The 1B38 pre-TR tube carries no flange but is mounted in a housing which has a joint with a flat flange and gasket. Since the pre-TR tube itself is not sealed to the housing, the output waveguide and TR cavity must still be pressurized.

Cavities that are iris-coupled to waveguide or to coaxial line have been sealed by cementing polyglas across the input window. In 10-cm waveguide duplexers a sheet about $\frac{1}{32}$ in. thick is sealed to the inside surface of the waveguide by means of Pliobond cement.

A problem analogous to pressurization is that of the elimination of the r-f leakage. Where high transmitter powers are used, r-f energy which radiates from joints in the transmission line may cause serious interference with other circuits, particularly the automatic-frequency-control circuit whose functioning is most critical during transmission.

Of course, any method of connecting microwave transmission lines involves efficient chokes or uniform contact to ensure a match. Even when this is done, however, there may be appreciable leakage which necessitates additional shielding. Where pressurization is not required, metal gaskets may be used in the grooves intended for rubber pressurizing gaskets. These gaskets have been made by compressing thin shavings of monel metal in a mold of the same shape as the gasket.

8.3. Duplexers in Coaxial Line.—*Coaxial duplexers based on the broadband T-junction described in Sec. 7.1 have been widely used for 10-cm-band radar systems in $\frac{7}{8}$-in. diameter line. Figure 8.2 shows such a duplexer with a 721A TR tube. The antenna connection is at the upper*

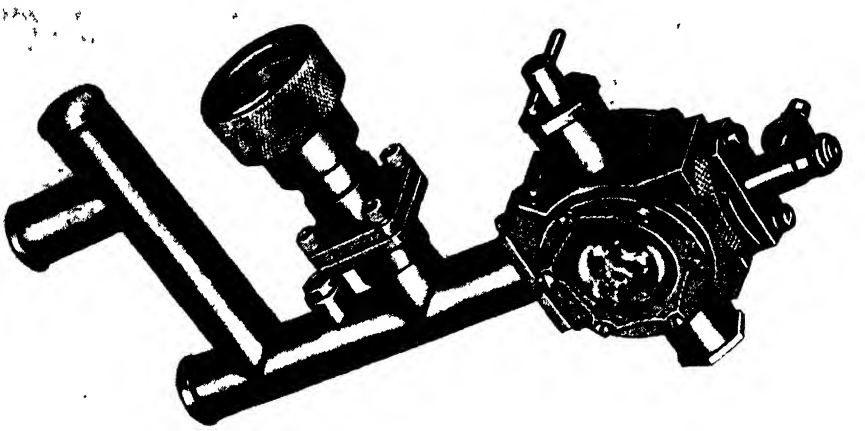

FIG. 8.2 —A 10-cm band loop-coupled coaxial duplexer for $\frac{7}{8}$-in. line.

left, and the magnetron transmitting tube is connected directly to the side arm in the upper center. The distance from the junction to the magnetron cavity is kept as small as possible to minimize the variation in the cold impedance seen at the junction. Figure 8.1 is a pressurized duplexer for $\frac{7}{8}$-in. line. The loop-coupled mixer appears at the top of the picture.

The effect of cold impedance on received signal for a duplexer of this type was studied by R. V. Pound and Rose Berger for 10.7-cm magnetrons.[1] They found that the cold impedance of these tubes was sufficiently uniform to permit setting a manufacturing specification limiting the standing-wave ratio to values greater than 20 db and the phase variation to ± 5 mm beyond that which is due to wavelength changes. The maximum signal loss from improper cold impedance to be expected

[1] R. V. Pound and Rose Berger, "Preplumbing of Tees for G-Band," RL Report 238, Nov. 3, 1942.

anywhere within the 7 per cent band was then 0.8 db, of which 0.4 db was caused by the finite standing-wave ratio of the magnetron.

Figure 8·3 illustrates a duplexer in $\frac{7}{8}$-in. coaxial line using iris-coupled cavities and 721A tubes. A circuit of this type was designed at Radiation

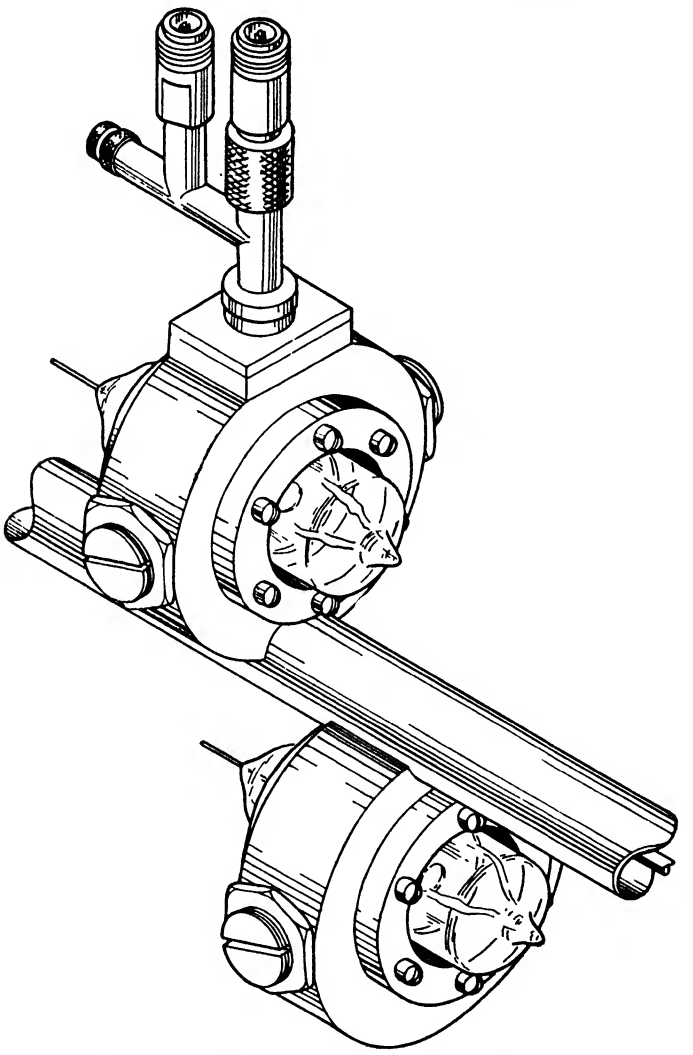

FIG. 8·3.—Coaxial duplexer with iris-coupled cavities.

Laboratory and represents one of the few coaxial applications of an ATR switch. An iris-coupled TR cavity at 10 cm was also designed at the Bell Telephone Laboratories.[1]

[1] J. P. Schafer, "SCR-545 Standard Loop Output TR Boxes," BTL MM-43-160-28 March 18, 1943.

Figure 8·4 shows a small low-powered assembly of r-f transmitting and receiving components for a 10-cm system using tubes of the lighthouse type for transmitter and local oscillator. The TR cavity with a 1B27 tube is seen near the center of the picture and the type N antenna fitting projects upward at the right center. Just to the left of this, the

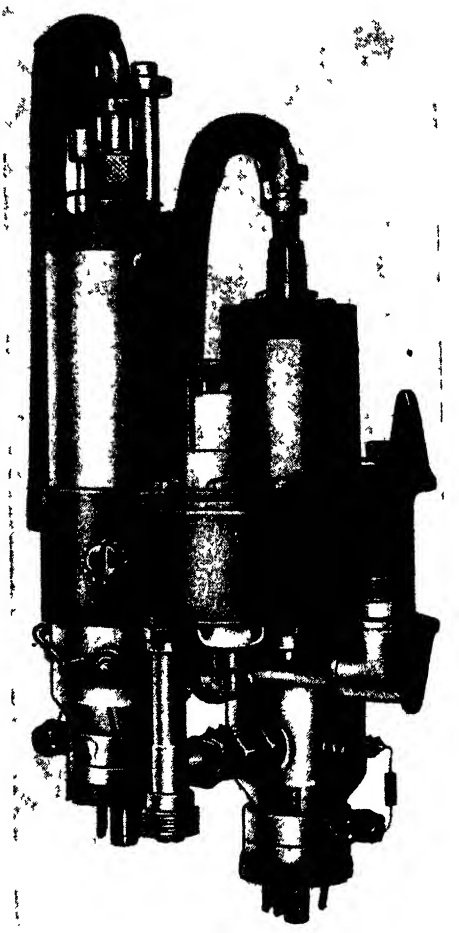

FIG. 8 4.—Lighthouse-tube assembly of transmitting and receiving components.

side arm of the T-junction leads up to the input loop at the right side of the bottom of the TR cavity.

The control of the transmitter cold impedance presented a special problem in this system since the transmitter cavity was coupled to the line by means of an adjustable probe. To get maximum power from the transmitter it was necessary to compensate for the variation among tubes

and cavities by an adjustment of this kind. This adjustment, however, had a marked effect on the cold impedance, and it was usually necessary to decouple the probe to a point at which the transmitted power was somewhat below the maximum in order to get a satisfactory match for the received signal.

At a later stage of development a study was made of the dependence of the transmitted power and the phase of the cold impedance on the depth and diameter of the probe for a number of transmitter tubes and wavelengths.[1] A junction distance and a probe design which would minimize the over-all loss of transmitted and received signal were chosen. It was concluded that the elimination of the probe adjustment by this design would permit a loss totaling not more than a few decibels for the usual tubes and cavities.

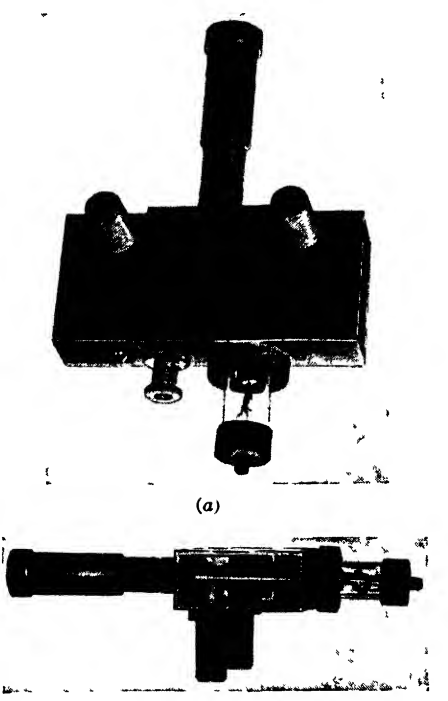

(*a*)

(*b*)

FIG. 8·5.—Duplexer for 1050 Mc/sec.

8·4. A Double-tuned Duplexer. The duplexer of Fig. 8·5 was designed for 1050 Mc/sec and differs rather radically from those used at shorter wavelengths. This device, which was developed at Naval Research Laboratory, provides for coupling the transmitter, antenna, mixer, and local oscillator directly to the TR cavity.[2] For comparison, Fig. 8·6 is a schematic representation of a more conventional radar system. The transformers represent coupling loops or irises in the cavities of transmitter, TR switch, and local oscillator. At high power level the TR cavity introduces a short circuit in loop L_2 so that the transmitter is connected directly to the antenna. If the transmitter cavity is sufficiently detuned when the electron beam is turned off, a short circuit is introduced across loop L_1 at low power level, and the antenna is coupled directly to the TR cavity. Since the received signal differs from the resonant frequency of the local oscillator by the intermediate frequency

[1] R. E. Taylor, "TR Distance and Fixed Probe Possibilities for the LHTR Unit," RL Report No. 52-12/27/44.

[2] M. Clark, "The Double Tuned R. F. System: The TR Box," NRL Report CRG-56, Dec. 19, 1944.

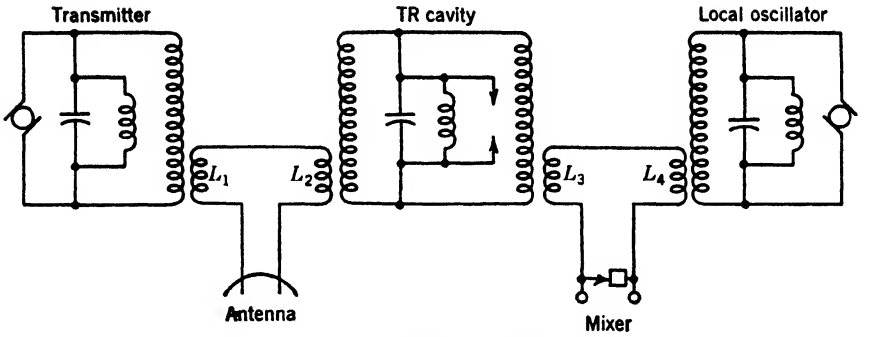

FIG. 8·6.—Radar r-f system.

of the receiver, the loop L_4 appears as a short circuit to the signal which is matched into the mixer. Likewise L_3 is a short circuit for the local-oscillator power which also goes into the mixer.

In the present duplexer the transmitter and TR cavities were placed close together so that loops L_1 and L_2 could be replaced by a single loop coupled to both cavities. Similarly L_3 and L_4 were reduced to one loop. In Fig. 8·5*a* the type N coaxial fitting at the right is the antenna connection, and that at the left is the mixer lead. The TR cavity consists of the central portion of the large section of rectangular tubing which forms the body of the duplexer, and the open ends of the tubing are the transmitter and the local-oscillator connections. The cavities of these oscillators are attached directly to the duplexer with the transmitter on the right and the local oscillator on the left. Figure 8·5*b* is a view looking in from the transmitter end at the antenna coupling loop.

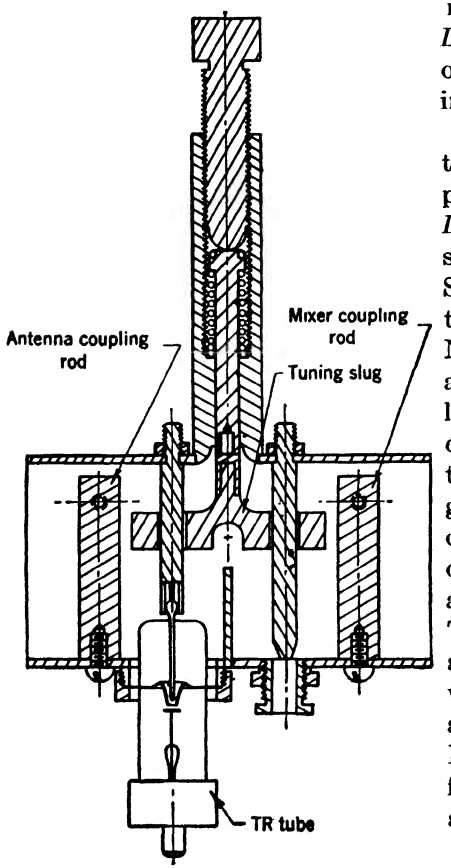

FIG. 8·7.—Cross section of the duplexer for 1050 Mc/sec.

The TR cavity is actually a double-tuned circuit with a pass band about 2.5 per cent wide at 3 db. The partition shown in Fig. 8·7 extending part way across the center

of the duplexer divides it into two cavities with a common iris. There is a post down the center of each cavity and a small gap between the post and the cavity wall. The cavity voltage is developed across this gap which, on the transmitter side, is formed by the electrodes of the TR tube.

Two tuning rings which move along the two center posts of the cavities can bring any frequency from 950 to 1150 Mc/sec within the pass band. These rings are made of silver-plated ceramic material supported by a ceramic bridge. The tuning is linear with the displacement of the tuning slugs and requires about $\frac{3}{4}$-in. travel to cover the band of 200 Mc/sec. The two cavities must have the same characteristics to obtain the proper bandwidth. This is accomplished by means of an adjustment on the gap in the right-hand cavity to match variations in TR tubes.

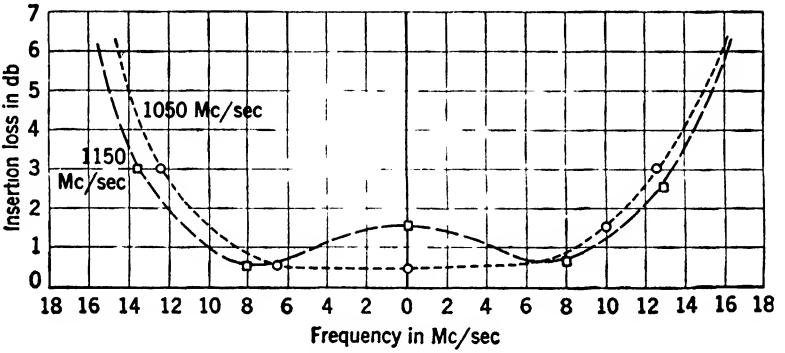

FIG. 8 8.—Bandpass characteristics of the double-tuned TR circuit.

Figure 8·8 shows plots of the transmission characteristics of the TR circuit with the center of the pass band set at 1050 and 1150 Mc/sec. The curve for 950 Mc/sec is similar to that for 1150 Mc/sec.

The attenuation through the TR cavity of the third harmonic of the transmitter frequency was so slight (about 1 db) that a special third-harmonic filter was added between the TR cavity and the mixer to prevent crystal burnout.[1]

8·5. Waveguide Duplexers.—Figure 8·9 shows a waveguide duplexer for the wavelength range 8.1 to 8.8 cm with shunt-coupled TR and ATR cavities for the tunable 1B27 tube. Since the cavities are placed only one-quarter wavelength apart, space limitations make it necessary to mount them on opposite sides of the waveguide. The two coaxial fittings projecting toward the camera are the connections on the mixer which is iris-coupled to the TR cavity. The large solenoid operates the crystal gate which protects the crystal when the keep-alive current

[1] R. Novick, "The Double Tuned R-F System: The Mixer," NRL Report CRG-57 Dec. 23, 1944.

is turned off. The left end of the waveguide goes, of course, to the antenna, and the right end goes to the transmitter.

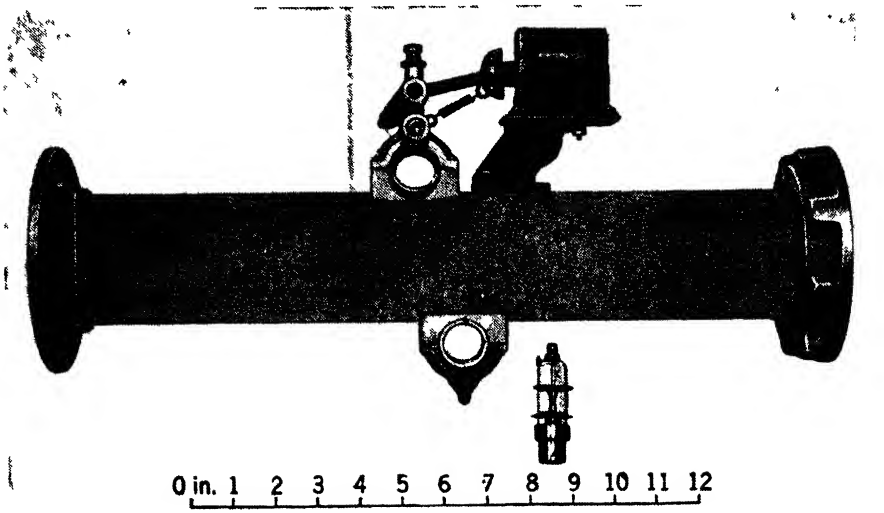

FIG. 8·9.—Duplexer with tunable 1B27 tubes for 8 5 cm.

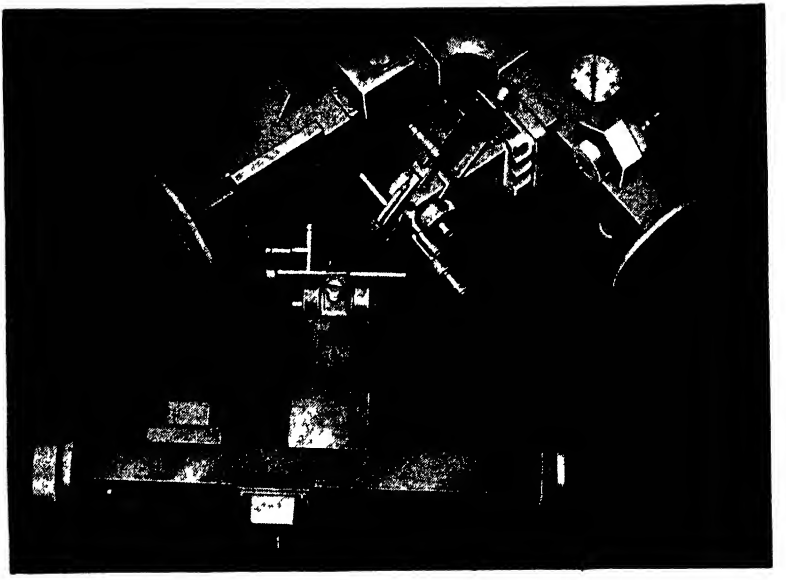

FIG. 8·10.—Duplexers for 10.7 cm.

The upper duplexer of Fig. 8·10 is used in the band from 10.3 to 11.1 cm with a series-coupled pre-TR switch and tunable 1B27 TR and ATR tubes, the latter shunt-coupled. The TR and ATR junctions are one-

half wavelength apart. The iris-coupled mixer is mounted on the TR cavity and the crystal-gate solenoid to the right of the cavity. The short waveguide at the top, which makes an acute angle to the transmission line, is a directional coupler for checking system performance. The system is pressurized with polyglas at the windows of the TR and the ATR cavities and with a rubber gasket at the flange on the pre-TR housing.

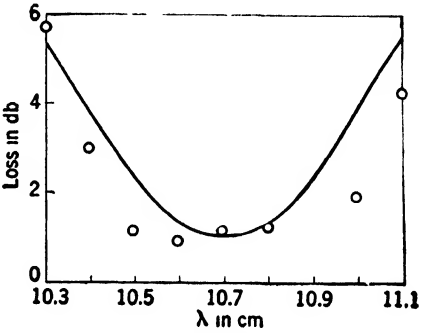

FIG 8 11 —Maximum reception loss for a 10 7-cm band duplexer. The points are experimental values, and the curve is the calculated branching loss.

The lower duplexer of Fig 8·10, which is also designed for the 10.7-cm band, has the same TR and pre-TR circuit but uses two fixed-tuned series-coupled ATR tubes separated by one-half wavelength. The pre-TR tube is one-quarter wavelength from the first ATR tube. Figure 8 11 shows the results of some measurements of the loss in received signal in a duplexer of this kind. The transmitter was replaced by

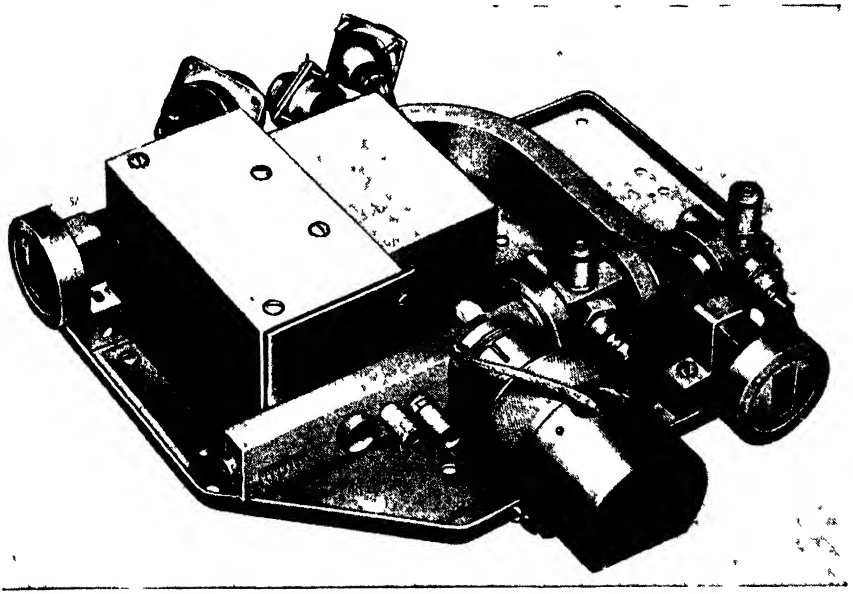

FIG 8 12 —A 3-cm duplexer for 724B tubes with tunable mixer

a short-circuiting plunger which was adjusted at each wavelength to give minimum power at the receiver. The accompanying curve is the calculated maximum total loss at each wavelength. This was determined

by assuming a 1-db loss for the TR circuit plus the maximum possible branching loss by using the measured values of G and Q_L given in Table 4·4 for the 10.7-cm band ATR tube. The actual values of G and Q_L for the tubes used were not available and may have been somewhat different judging by the low values for the experimental losses. The asymmetrical

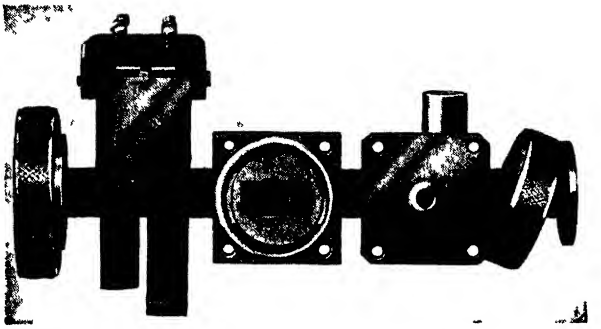

FIG. 8 13 —A 3-cm duplexer for fixed ATR and tunable TR tubes

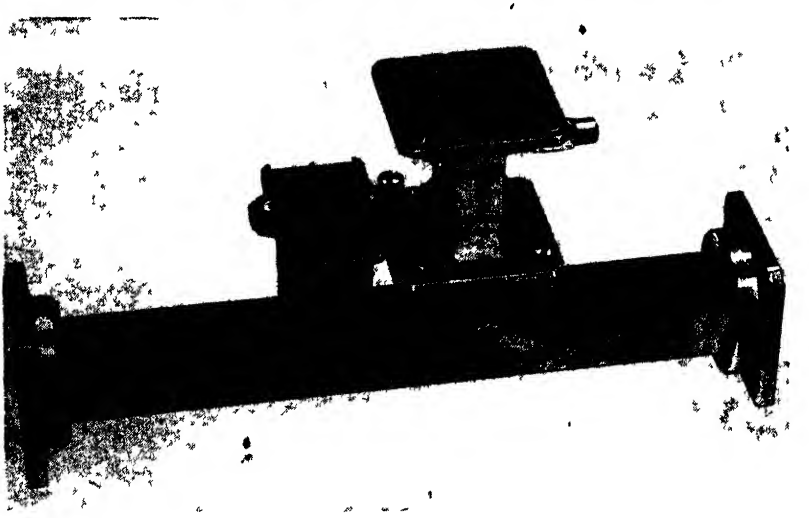

FIG 8 14 —Narrow-band fixed-tuned duplexer for 3 cm

distribution of the experimental points is probably caused by some error in the separation of the ATR cavities or in their tuning.

Figure 8·12 is an early 3-cm duplexer and mixer assembly. The tunable cavities with 724B tubes are mounted one-half wavelength from the main waveguide on series T-junctions one-quarter wavelength apart. They are connected to the waveguide through choke-flange couplings with knurled nuts and aligning pins. The mixer is tuned by the plunger and tuning screws.

A more recent 3-cm duplexer is shown in Fig. 8·13. The rectangular

box on the left is the mount for the fixed-tuned 1B35 ATR tube. The tunable 1B24 TR tube is attached to the flange mounted at the center of the waveguide to form a shunt junction of the vestigial 120°-Y type shown in Fig. 7·8. The large-diameter groove in this flange holds a pressed metal gasket which prevents r-f leakage. The flange to the right of this one connects to a small attenuating waveguide which is used to couple out one or two milliwatts of the transmitter power to operate the automatic-frequency-control circuits for the receiver. The small cylinder

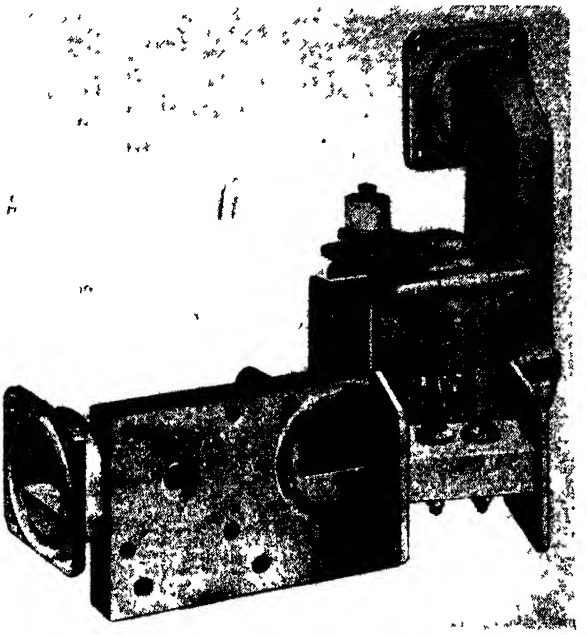

FIG. 8·15.—Wideband fixed-tuned duplexer for 3-cm.

above the flange is the connection to a directional coupler. For mechanical simplicity the separation between TR and ATR junctions is made one wavelength rather than one-half wavelength. This is permissible since the duplexer is designed to be used over a band only 2.6 per cent wide.

The duplexer of Fig. 8·14 is designed for the same band and has the same ATR circuit but uses a fixed-tuned TR tube shown mounted one-half wavelength from the main waveguide on a series T-junction matched with an inductive iris in the TR arm. The external appearance of the ATR mount is slightly different from the preceding model, but it has the same interior and fits the same tube.

The duplexer of Fig. 8·15 uses the same tubes as the preceding duplexer but can be operated over the much broader band of 12 per cent from 3.13 to 3.53 cm. This is made possible by mounting the TR tube flush with

the main waveguide wall on a vestigial 120° Y-junction and using two ATR tubes one-half wavelength apart with the first tube one-half wavelength from the TR junction. For the lower half of the band from 3.13 to 3.33 cm, 1B35 ATR tubes are used, and for the upper half from 3.33 to 3.53 cm, 1B37 tubes are used.

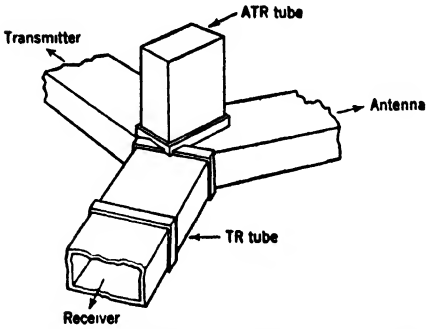

FIG. 8·16.—Duplexer with TR and ATR tubes at the same junction.

The duplexer shown in Fig. 8·16 is an attempt to place the ATR tube close to the TR junction to avoid the adverse effects of the variation with wavelength of the distance between TR and ATR tubes.[1] The advantage of this construction seems to be partly offset by the increased Q_L of the ATR cavity as shown in Table 4·3 of Chap. 4.

Figure 8·17 is a view of a duplexer for 1.25-cm wavelength with the 1B26 tunable TR tube in front. The waveguide connection just to the

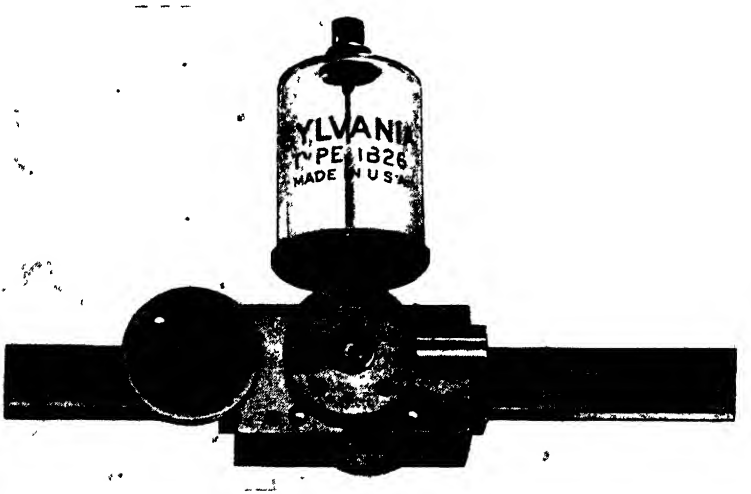

FIG. 8·17.—A 1.25-cm duplexer.

left of the TR tube carries the r-f power for automatic frequency control. Another view of the same duplexer in Fig. 8·18 shows the mixer attached just above the duplexer. The two coaxial fittings of the BN type are the i-f leads from the two crystals, the left one for automatic

[1] Samuel, Crandall, and Clark, "Final Report on Broad-Band TR and ATR Tubes," NDRC-14-402, Sept. 30, 1944.

frequency control and the right one for the radar signal. The 1B36 fixed-tuned ATR tube plugs into the lower part of the duplexer where it is secured by the large knurled nut. The TR and the ATR tubes are both series-mounted and spaced one-quarter wavelength apart.

8·6. Two-channel Duplexers.—In certain systems it may be desirable to receive simultaneously two signals, for example, radar and beacon, on two separate receivers tuned to different frequencies. A convenient method of isolating the two channels is the use of two high-Q cavities, one for each channel.

The assembly shown in Fig. 8·19 uses two tunable TR cavities with a single pre-TR switch.[1] Since in this instance the signals differed in

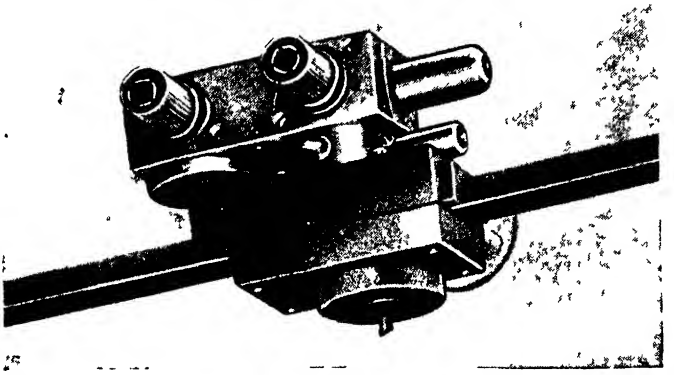

FIG. 8·18. A 1·25-cm duplexer and mixer

frequency by about 6 per cent, the window of the radar TR cavity appeared as a short circuit to the beacon signal and vice versa. The additional TR cavity, therefore, introduced no complication in matching the line to the receiver at either frequency. A tunable ATR switch was used at the radar frequency but none was used for the beacon signal. The branching loss of the beacon signal was minimized by a favorable transmitter cold impedance.

The necessity for sharing the pre-TR tube should be noticed. Since the window of a TR cavity mounted behind a pre-TR tube is three quarters of a wavelength from the main waveguide, it presents a high impedance at the main waveguide wall when tuned off resonance. If each TR cavity were mounted with its own pre-TR tube at a different point on the transmitter line, the one nearer the antenna would interrupt the signal destined for the further one.

[1] L. D. Smullin, "Modification of CPS-6 Duplexer to Allow Simultaneous Beacon and Radar Reception," RL Report No. 53-4/16/46.

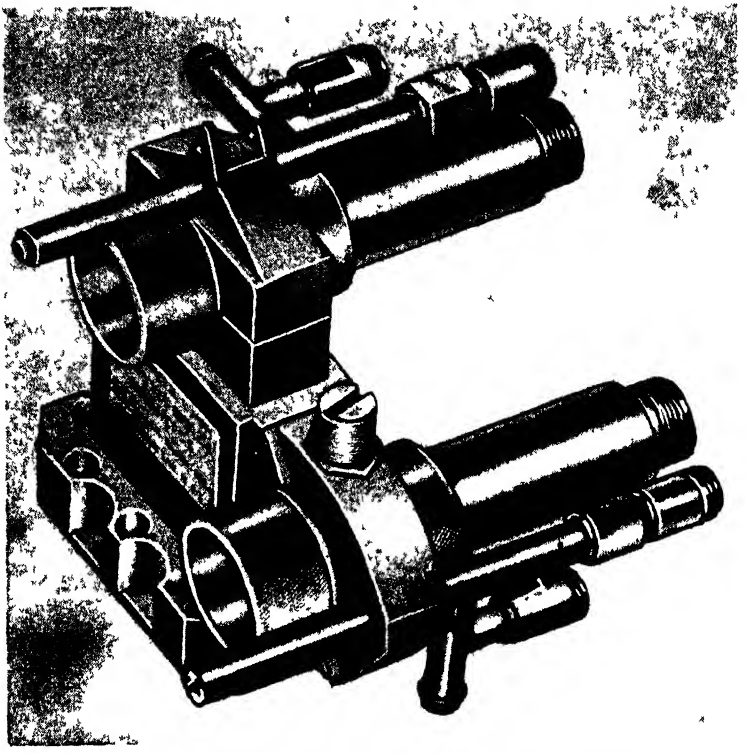

FIG 8 19 —Two-channel duplexer for 10 cm with a pre-TR tube

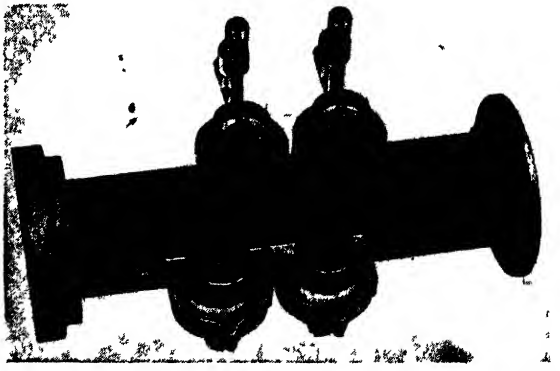

FIG. 8·20.—Duplexer for two channels using two ATR tubes.

Figure 8·20 illustrates another form of two-channel duplexer. It comprises an ATR switch for each channel, and since no pre-TR tube is necessary, two TR cavities are mounted directly on the main waveguide.

8·7. An Attenuator Switch.—In some radar systems the transmitted power is attenuated at times in order to confuse enemy listening stations. This attenuation, which might be as high as 20 or 30 db, would normally be introduced between transmitter and duplexer where it would not affect the received signal. In some sets, however, it has proved more convenient to install the attenuator between duplexer and antenna and to add an ATR switching device to allow attenuation only during transmission.

Since it may be necessary for the attenuator to absorb virtually all of the transmitter power, it is preferable to divert this unused power into another line which can be terminated in a special load capable of high power dissipation. The power entering the transmitter arm of Fig. 8·21 divides at the junction between the antenna arm and the arm leading to a dissipative load. If the extensions of the plungers in the two stub arms differ by one-quarter wavelength and if the two output arms are matched, the impedance seen from the transmitter arm will be a match. By moving the plungers synchronously, the transmitter power may be divided between antenna and load in any desired ratio. The switch, which is fired during transmission, has no effect on the plunger action.

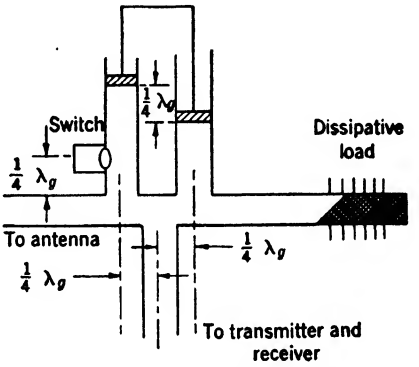

FIG. 8·21.—Attenuator switch.

The least power will reach the antenna arm when the plunger in the left-hand stub arm inserts a high impedance in the line. At that time the received signal would also be largely reflected if there were no switch. The switch, however, ensures a low impedance for every plunger position, and the signal encounters no mismatch except at the junction. When all the transmitted power is being delivered to the antenna, the received signal suffers no loss at the junction. When maximum transmitter power is being diverted to the load, the right-hand stub arm presents a low impedance. The received signal at the junction is then presented with a match in both the receiver and in the load arms. The power divides equally between the two arms and, including reflections from the terminating impedance $Z_T = 2$, the total signal loss is 3.5 db.

By an examination of the transmission ratio

$$\frac{P}{P_0} = \frac{1 + X_s^2}{2\frac{1}{4} + X_s^2}$$

expressed in terms of the reactance X_s of the right-hand stub, it may be confirmed that the received signal loss always lies between 0 and 3.5 db. If it is necessary, this loss can be obviated by a second switch on the right-hand stub.

BALANCED DUPLEXERS

BY CARROLL W. ZABEL

It becomes difficult to use the branched-duplexer technique when a very flexible, broadband duplexing unit is desired, or when a c-w power source is used instead of a pulsed power source. For these uses the development of a variety of magic T's has made possible a new technique.

8·8. Properties of a Magic T. The general properties of a magic T are most easily described by considering the symmetrical combination of an E-plane T and an H-plane T (Fig. 8·22). This device is completely symmetric about a plane which bisects the E-plane and the H-plane T's. If generators and loads are placed on the various arms in such a way that the symmetry of the device is not disturbed, then the electric field in the waveguide must be either even or odd about the symmetry plane, or it must be a linear combination of the even and odd fields. The symmetry of an electric field at a distance x from this symmetry plane is described by the equations

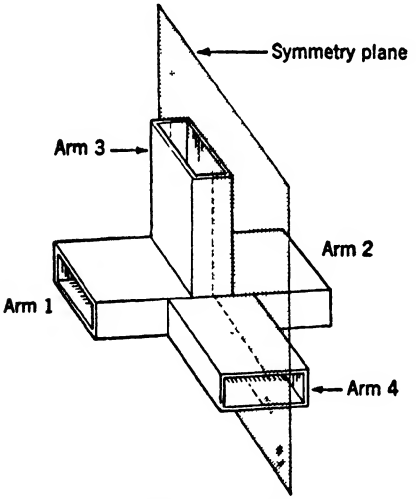

FIG. 8·22.—A magic T.

$$E(x) = E(-x),$$

if the field is even, or

$$E(x) = -E(-x)$$

if the field is odd. Let us consider, for example, a generator on arm (4) and matched loads on the other three arms. The symmetry has not been disturbed. Since the electric field in arm (4) is even about the symmetry plane, the electric field must be distributed with an even symmetry throughout the entire structure. Thus at any instant of time

the phase of a wave in arm (1) at a distance d from the symmetry plane must have the same phase as a wave in arm (2) at the same distance d from the symmetry plane. Arm (3), however, will not propagate a mode which is even about the symmetry plane, and therefore no power will be coupled into this arm. In general there will be a reflected wave in arm (4), but this can be eliminated by introducing a matching device which is symmetrical about the symmetry plane. The device usually employed is a post placed in the bottom of guide (1)–(2) projecting up into arm (3). With this device in place, one-half the generator power will couple to arm (1) and one-half to arm (2).

Next consider a generator on arm (3) with matched loads on the remaining three arms. Here again the symmetry is preserved but now, since the field in arm (3) is odd about the symmetry plane, the electric field in the entire structure must be odd about the symmetry plane. No power will be coupled into arm (4) because the only mode that arm (4) will propagate has an even distribution of the electric field about the symmetry plane. However, the phase, at any instant of time, of the wave in arm (1) at a distance d from the symmetry plane will be out of phase with a wave in arm (2) at the same distance d from the symmetry plane. Any reflected wave in arm (3) may be eliminated by introducing a matching device symmetrically about the symmetry plane; this is usually an inductive iris. Here again all the generator power divides equally between arm (1) and arm (2).

The result of placing two coherent generators on the device may now be considered: one on arm (3), the other on arm (4), and matched loads on arms (1) and (2). Under these conditions, also, the symmetry is not disturbed. Since arm (3) is independent of arm (4) the amplitudes and the phases of the two waves may be varied independently. In particular, the amplitudes may be adjusted until they are equal, and the phases adjusted until the wave coupled from arm (3) to arm (1) is in phase with the wave coupled from arm (4) to arm (1). This adjustment makes the waves in arm (2) just out of phase, and hence no power will be coupled to arm (2). Thus, with due regard to phase and amplitude, power incident at arm (3) and arm (4) couples only to arm (1). By reversing the direction of time, therefore, power incident in arm (1) couples only to arm (3) and arm (4), and not to arm (2). The amplitudes of the waves in arm (3) and arm (4) are equal and there is a particular phase relationship between the two waves. The above argument may be repeated, but this time the phases of the waves in arms (3) and (4) are adjusted

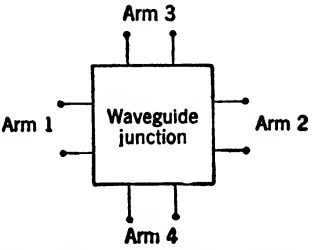

FIG. 8·23.—A lossless passive four-terminal-pair network.

exist a three-terminal-pair, linear, lossless network that will satisfy the requirements of a linear duplexer.

Let us now ask if there exists a linear, lossless, four-terminal-pair network which may be used. It is desired that S_{12} be zero, and that $|S_{13}|^2|S_{23}|^2$ be a maximum. Each termination may be removed and replaced with a lumped impedance and a matched termination without destroying any of its properties. That is, S_{12} will still be zero and $|S_{13}|^2|S_{23}|^2$ will still be the maximum. Now, however, S_{11} and S_{22} must be zero. If this were not true the generator could be mismatched and S_{13} increased without changing S_{23}. But $|S_{13}|^2|S_{23}|^2$ is already a maximum, therefore S_{11} must be zero. Similarly S_{22} must be zero. Now the scattering matrix is

$$\mathsf{S} = \begin{pmatrix} 0 & 0 & S_{13} & S_{14} \\ 0 & 0 & S_{23} & S_{24} \\ S_{13} & S_{23} & S_{33} & S_{34} \\ S_{14} & S_{24} & S_{34} & S_{44} \end{pmatrix}.$$

Since $\mathsf{SS}^* = \mathsf{I}$,

$$\begin{aligned} |S_{13}|^2 + |S_{14}|^2 &= 1, \\ |S_{23}|^2 + |S_{24}|^2 &= 1, \qquad (1) \\ |S_{13}|^2 + |S_{23}|^2 + |S_{33}|^2 + |S_{34}|^2 &= 1, \\ |S_{14}|^2 + |S_{24}|^2 + |S_{34}|^2 + |S_{44}|^2 &= 1. \qquad (2) \end{aligned}$$

If the first two equations are added,

$$|S_{13}|^2 + |S_{14}|^2 + |S_{24}|^2 + |S_{23}|^2 = 2.$$

From the second two equations

$$|S_{13}|^2 + |S_{23}|^2 + |S_{14}|^2 + |S_{24}|^2 + |S_{33}|^2 + |S_{44}|^2 + 2|S_{34}|^2 = 2.$$

Thus

$$|S_{33}|^2 + |S_{44}|^2 + 2|S_{34}|^2 = 0,$$

and, since each term must be positive, each term must vanish. From Eqs. (2), this means that

$$\begin{aligned} |S_{13}|^2 + |S_{23}|^2 &= 1, \\ |S_{14}|^2 + |S_{24}|^2 &= 1. \qquad (3) \end{aligned}$$

If these equations are substituted in Eq. (1),

$$|S_{13}| = |S_{24}|,$$

and

$$|S_{14}| = |S_{23}|.$$

If the first of Eqs. (3) is squared

$$|S_{13}|^2|S_{23}|^2 = \tfrac{1}{2}(1 - |S_{13}|^4 - |S_{23}|^4).$$

If $|S_{13}|^2|S_{23}|^2$ is a maximum, the derivative with respect to S_{23} must be zero, or

$$2|S_{23}|^3 - 1 + \frac{|S_{23}|}{(1 - |S_{23}|^2)^{1/2}} = 0,$$

and

$$|S_{23}|^2 = \tfrac{1}{2}.$$

If this result is substituted in Eqs. (1) and (3)

$$|S_{23}| = |S_{13}| = |S_{14}| = |S_{24}| = \frac{1}{\sqrt{2}}.$$

This device is, however, the magic T. Therefore it has been proved that the best possible four-terminal-pair, lossless, linear network for use as a linear duplexer is the magic T. Furthermore, the maximum value of $|S_{13}|^2|S_{23}|^2$ is $\frac{1}{4}$. The maximum amount of useful power is thus 6 db below the generator power, and the minimum amount of loss in such a device is 6 db.

8·10. Nonlinear Balanced Duplexer.—If it is possible to add nonlinear elements to a duplexer, much better use of the magic T may be made. Let us consider, first, the possibilities when a pulsed magnetron is used as the power source, and TR gas switches are used as the nonlinear elements. It will be assumed that the waveguide type of magic T discussed in Sec. 8·8 is used.

Consider first an arrangement of two magic T's as indicated in Fig. 8·26. Power incident in arm (4) will divide between arms (1) and (2) in an even fashion: at a given distance from arm (4), the voltage in arm (1) will be in phase with the voltage in arm (2). If the upper path to the second T has the same electrical length as the lower path, the two waves will arrive in arms (1′) and (2′) in phase. These two waves will thus couple only to arm (4′). Similarly, power incident in arm (3) will arrive in arms (1′) and (2′) out of phase, and thus couple only to arm (3′).

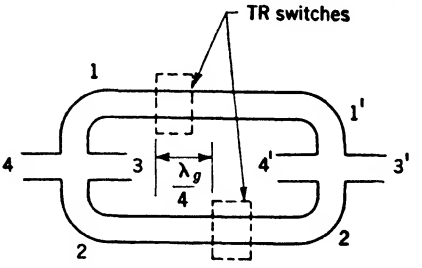

FIG. 8·26.—A balanced magic-T duplexer.

If a pulsed transmitter is placed on arm (4) and a TR switch is inserted in the upper path at a distance d from the first magic T, the TR switch will fire, reflecting most of the power back to arm (1). The leakage power will be incident in arm (1′). A second TR switch, identical with the first, may be placed in the lower path in various positions. If it is placed at the distance $d + \lambda_g/4$ from the first magic T, then the total path of

the power from the T to the lower TR switch and back to the T will be a half-wavelength longer than the similar path to the upper TR switch. The reflected wave in arm (1) will then be 180° out of phase with the reflected wave in arm (2). Now the transmitter power will couple only to arm (3), and the transmitter will see a matched load. The leakage power from the lower TR switch will arrive in arm (2′) in phase with the leakage power in arm (1′) from the upper TR switch, and, therefore, the leakage power will all couple to arm (4′). A low-power signal arriving in arm (3) will not fire the TR switches and, therefore, will couple only to arm (3′).

Several observations may be made about the operation of such a duplexer. First, the antenna is completely disconnected from the transmitter when the TR tubes are not firing. Regardless of its impedance, there will be no loss of signal to the transmitter. Since no ATR tubes are required, it might be possible to make a device matched over a broader frequency band than is possible by the branched-duplexer technique.

Second, all the leakage power will be dissipated in the matched load in arm (4′) while no leakage power is coupled to the receiver on arm (3′). In order for this to be true, both the relative phase and the amplitudes of the waves in arms (1′) and (2′) must be identical. Thus, not only must the electrical length of the transmission lines or waveguides in the upper path be the same as in the lower path, but the phase shift in the two TR switches must be the same. In order for the device to be used over a band of frequencies, the Q of the two TR switches must be identical. Since the amplitudes of the two waves must be equal, the amplitudes of the leakage powers from the two TR switches must be the same throughout the entire magnetron pulse. This is difficult to accomplish. The gas discharges in the two TR tubes must start at the same time and in the same manner. In practice some leakage power enters arm (3′) to the receiver. The leakage power from each TR tube must be low enough to protect the receiver. The amount of decoupling of the leakage power to the receiver must not be relied upon too heavily.

The bandwidth of this device is controlled by the impedance seen by the transmitter and by the Q of the TR switch. The Q of the TR switch determines the bandwidth in exactly the same manner as it determines the bandwidth for the branched duplexers. The standing-wave ratio seen by the magnetron is determined by the difference in path to the upper and to the lower TR switch. When the difference is exactly one-quarter guide wavelength, there is no reflected wave. As the wavelength is changed, the difference in path length is altered and a reflected wave is produced. Moreover, the magic T itself has a finite band over which it is well matched.

8·11. Ring-circuit Duplexer.—There are several balanced duplexers that operate on the general principles discussed in Sec. 8·10, but which differ physically. The power-handling capacity as well as the maximum bandwidth varies considerably. They also differ in the type of magic T used. The balanced duplexer that uses a combination of E-plane and H-plane T's is limited to power levels of less than 150 kw, at 3 cm, for arcing occurs at about that power level around the matching post. It has a bandwidth of about 12 per cent.

A magic T described as a ring circuit has been particularly successful for making a good balanced duplexer. A ring circuit consists of a loop or ring, Fig. 8·27, of waveguide to which four waveguides are joined to form four E-plane T's. The electric vector is parallel to the plane of the paper. The mean circumference of the loop is one and one-half guide wavelengths. The distance between arms (1) and (3), (3) and (2), and (2) and (4) is a quarter of a guide wavelength along the mean circumference. The characteristic impedance of the loop is $1/\sqrt{2}$ times that of the four arms.

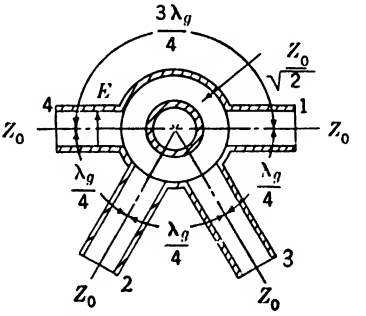

FIG. 8·27.—Diagram of a ring-circuit magic T.

If the E-plane T is considered to be a pure series junction with no junction effects, the properties of the ring circuit may be obtained by the same general method used in Sec. 8·8. The ring circuit is symmetrical about a plane between arms (2) and (3). As before, fields that are even and odd about the symmetry plane are considered. These two solutions may be combined to give a general solution. First, if the electric field is odd about the symmetry plane, the electric field must be zero at the plane of symmetry. A sheet of metal may be placed along the symmetry plane without disturbing the fields.

Only one half of the ring circuit is now considered. The impedance matrix of this device is obtained in the ordinary way from the linear equations of a two-terminal-pair network,

$$V_1 = Z_{11}I_1 + Z_{13}I_3,$$
$$V_3 = Z_{12}I_1 + Z_{33}I_3.$$

The impedance seen at the reference plane of arm (1), when there is no current at arm (3), is Z_{11}. In the lower section there is, then, the impedance of a short circuit, transformed one-eighth wavelength around the loop, plus the impedance of an open circuit on arm (3), and the sum transformed one-fourth wavelength to arm (1). This results in zero impedance from the lower section at arm (1). From the upper section

there is the impedance of a short circuit transformed three-eighths wavelength or $-j/\sqrt{2}$. Thus

$$Z_{11} = \frac{-j}{\sqrt{2}}.$$

Similarly, the other matrix elements are found with the result

$$\mathsf{Z}_{\text{odd}} = j \begin{pmatrix} -\frac{1}{\sqrt{2}} & +\frac{1}{\sqrt{2}} \\ +\frac{1}{\sqrt{2}} & +\frac{1}{\sqrt{2}} \end{pmatrix}.$$

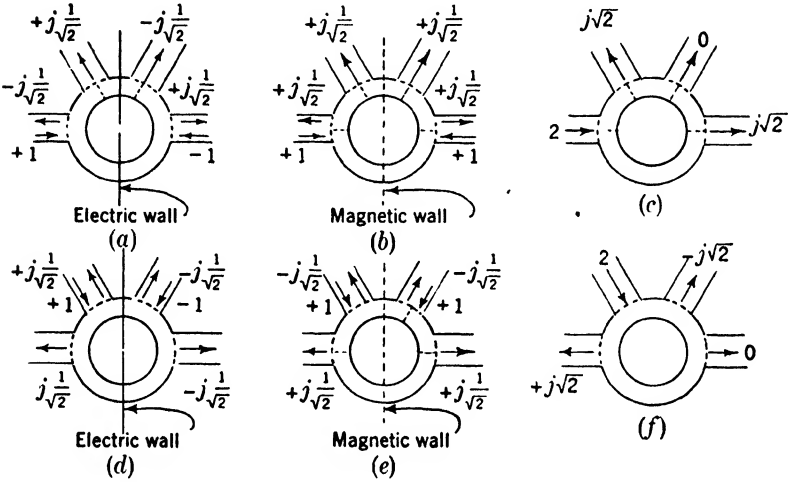

FIG. 8·28.—Diagram to illustrate the calculation of the scattering matrix of a ring-circuit magic T.

For the even case the sheet of metal must be replaced with a magnetic wall which maintains an open circuit at the symmetry plane. In this case

$$\mathsf{Z}_{\text{even}} = j \begin{pmatrix} +\frac{1}{\sqrt{2}} & +\frac{1}{\sqrt{2}} \\ +\frac{1}{\sqrt{2}} & -\frac{1}{\sqrt{2}} \end{pmatrix}.$$

In both cases the result of squaring the matrix is just $-\mathsf{I}$.

$$\mathsf{Z}^2_{\text{odd}} = -\mathsf{I},$$
$$\mathsf{Z}^2_{\text{even}} = -\mathsf{I}.$$

The scattering matrix S is

$$\mathsf{S} = (\mathsf{Z} - \mathsf{I})(\mathsf{Z} + \mathsf{I})^{-1}, \tag{4}$$

or

$$\mathsf{S} = (\mathsf{Z}^2 - 2\mathsf{Z} + \mathsf{I})(\mathsf{Z}^2 - \mathsf{I})^{-1}.$$

If $Z^2 = -1$, then

$$S = Z.$$

Hence, in the even case $Z_{11} = S_{11} = +j/\sqrt{2}$, and this is the reflection coefficient in arm (1). The complex wave coupled to arm (3) is $Z_{13} = S_{13} = j/\sqrt{2}$. The scattered waves in each arm for the two cases

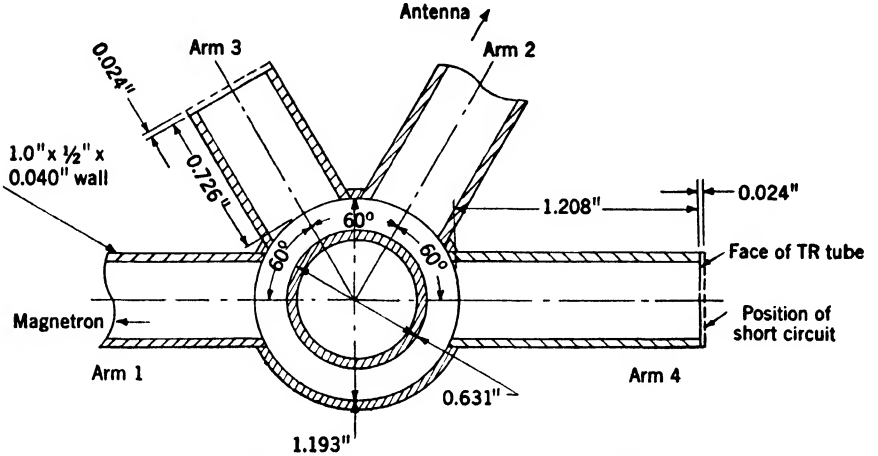

FIG. 8·29.—Dimensions for a ring circuit at 3.33 cm.

are known, as indicated in Fig. 8·28*a* and *b*. The even and odd solutions may be added in any way. For example, the two solutions shown in Fig. 8·28*a* and *b* may be added with the result, Fig. 8·28*c*, that a wave of amplitude 2 is incident in arm (1) which couples a wave of amplitude $\sqrt{2}$ to arms (3) and (4). No wave is coupled to arm (2) nor is there a reflected wave in arm (1). By symmetry, it is seen that an amplitude of 2 incident in arm (4) will couple a wave of amplitude $\sqrt{2}$ to arms (1) and (2) with no reflected wave or coupled wave to arm (3). From the same impedance matrix, the result of a wave incident in arms (3) or (2) can be found (Fig. 8·28*d*, *e*, and *f*). The power incident in any arm divides equally between the two adjacent arms with no coupling to the opposite arm and no reflected power. Thus, the ring circuit is a magic T.

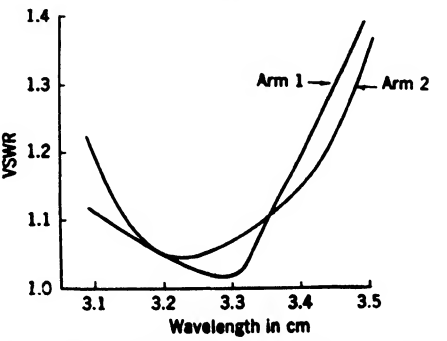

FIG. 8·30.—Standing-wave ratio of ring-circuit magic T.

It is obvious that the ring circuit is somewhat frequency-sensitive since its operation depends upon correct line lengths. The voltage

standing-wave ratio at arm (1) and arm (2), with matched loads on the remaining arms, plotted against wavelength is shown in Fig. 8·30 for a ring circuit constructed according to Fig. 8·29. Figure 8·31 is a plot

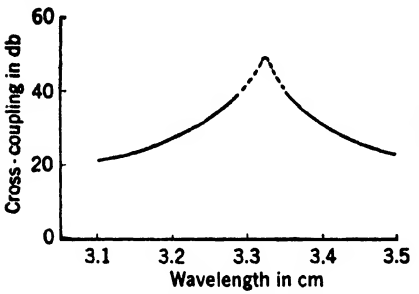

FIG. 8·31.—Cross coupling between arms (1) and (2).

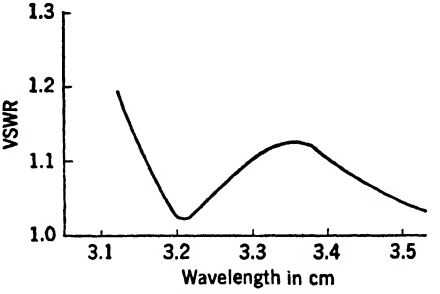

FIG. 8·32.—Standing-wave ratio presented to the magnetron by ring-circuit duplexer.

of the ratio, expressed in decibels, of power incident in arm (1) to power coupled to arm (2).

A nonlinear balanced duplexer may be construoted with ring circuits. As before, care must be taken in placing the TR switches if the maximum

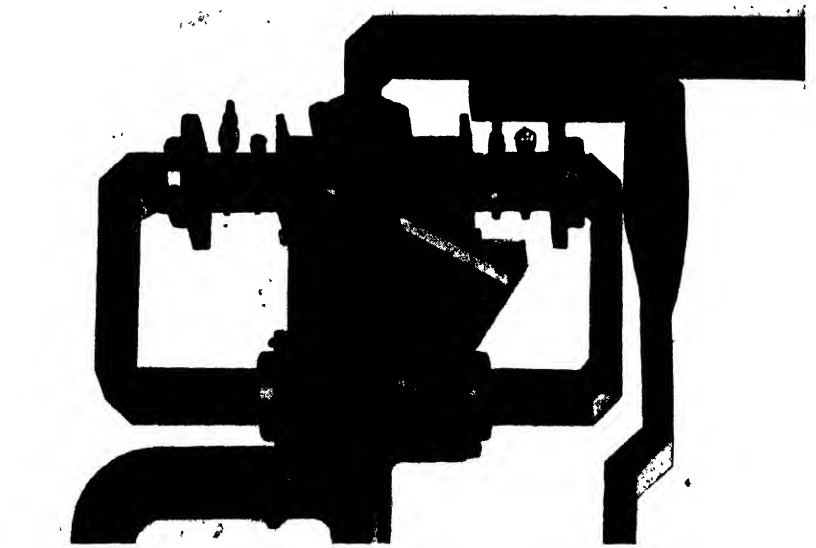

FIG. 8·33.—Ring-circuit duplexer milled from aluminum. The top half has been removed to show the details. The two halves are split along the center of the wide side of the waveguide.

bandwidth is desired. As the frequency is changed, the standing-wave ratio presented to the transmitter will change, not only from a change in the characteristics of the ring circuit, but also from a change in the electrical positions of the TR switches. In the ring-circuit duplexer,

these two effects are nearly equal. If the TR switches are placed at the correct distance from the ring circuit, the effects can be made to cancel each other. On the drawing of the ring-circuit balanced duplexer shown in Fig. 8·29 the positions of the TR tubes are indicated. The TR switches are the broadband type 1B63. Figure 8·33 is a photograph of a ring-circuit balanced duplexer milled from aluminum. The voltage standing-wave ratio presented to the transmitter as a function of wavelength is plotted in Fig. 8·32. The duplexer can be used up to peak power levels of 350 kw at 1-μsec pulse length and a pulse recurrence frequency of 500 per sec if the corners inside the E-plane T's are slightly rounded.

8·12. Practical Magic T's.—In the discussion of the magic T which consists of a combination of E-plane and H-plane T's, Fig. 8·22, the procedure that was followed in the matching of the junction was inherently important in deriving the magic-T properties. To obtain the desired result, it is necessary to match the two arms that lie in the symmetry plane. It is clear, however, that had the arms which are on each side of the symmetry plane been matched, there would have been no reason to expect that the resulting construction would be a magic T. The coupling between opposite arms would not have been zero, and the two arms in the plane of symmetry would not have been matched. In the first case, four independent adjustments are made, the amplitude and the phase of a reflection coefficient in each of the two arms in the plane of symmetry. In the second case, only two adjustments are made, since the resulting device must remain symmetrical. For this type of symmetry, four independent parameters in the two arms are necessary. These arms are in the plane of symmetry.

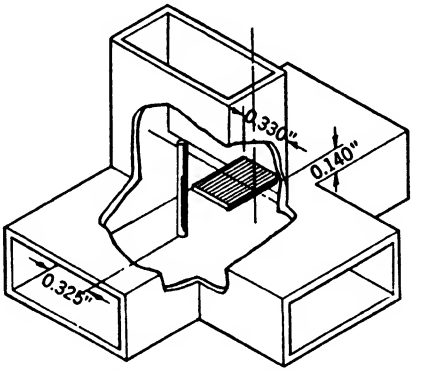

FIG. 8·34.—Position of post and iris for matching a magic T in ½-in. by 1-in. waveguide.

These four adjustments may be made in a variety of ways all of which depend upon the shape of the device and the desired bandwidth and power-handling capacity. As seen by Fig. 8·34 the H-plane arm is matched by adjusting the length and the position of a cylindrical post placed inside the junction while the E-plane arm is matched by the size and position of an assymmetrical inductive iris. The post is 0.125 in. in diameter and 0.650 in. high. The iris is 0.032 in. thick. This method of matching results in a magic T that is less frequency-sensitive than a

magic T in which both arms are matched by using lumped constants such as capacitive or inductive irises. The 10-cm-band magic T is similarly matched, as shown in Fig. 8·35. The post is 0.375 in. in diameter and is 1.750 in. high. The iris is 0.032 in. thick. The 1.25-cm-band magic T has the post replaced with a metal fin, Fig. 8·36. The irises are 0.020 in.

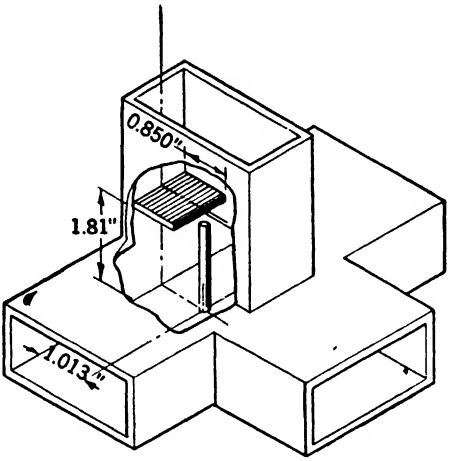

FIG. 8·35.—Position of post and iris for matching a magic T in 1½-in. by 3-in. waveguide.

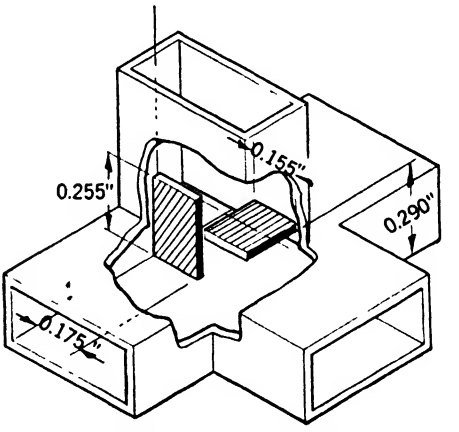

FIG. 8·36.—Position of post and iris for matching a magic T in ¾-in. by ½-in. waveguide.

thick. The frequency sensitivities of the three magic T's are shown in Figs. 8·37, 8·38, 8·39. The curves show the standing-wave ratio vs. wavelength in each arm for magic T's before and after the matching devices are added.

It is seen that the standing-wave ratios for the unmatched magic T are high. By changing the dimensions of the various arms, these standing-wave ratios may be lowered considerably and the final match

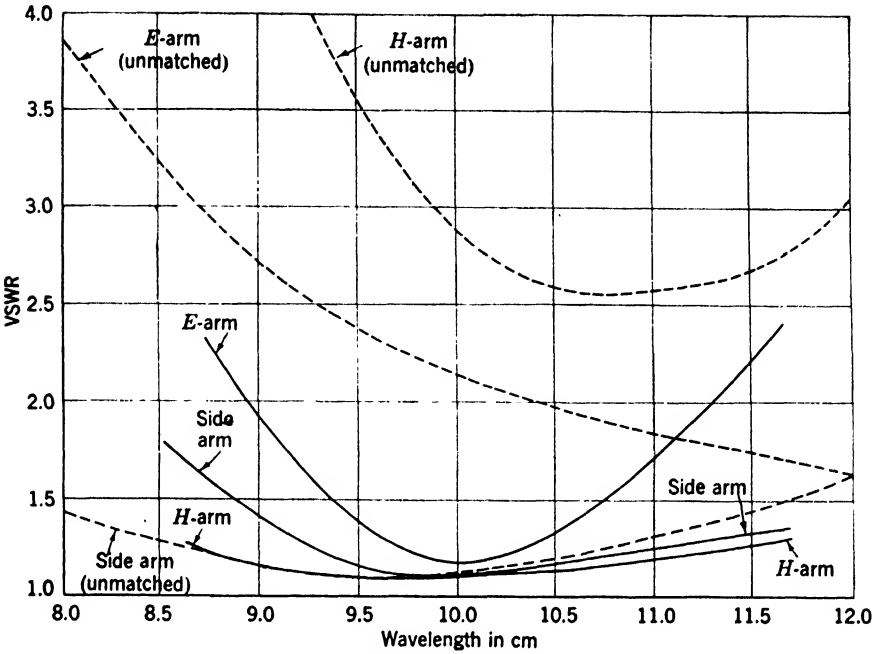

FIG. 8·37.—Effects of a post and iris for matching a magic T in 1½-in. by 3-in. waveguide.

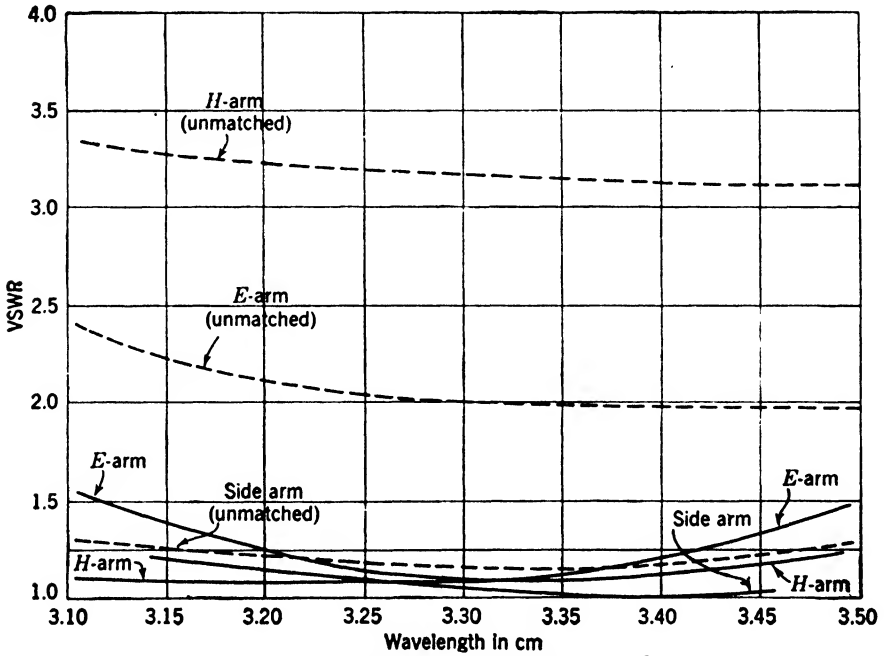

FIG. 8·38.—Effects of a post and iris for matching a magic T in ½-in. by 1-in. waveguide.

more easily attained. Such a magic T has been constructed[1] at the Telecommunications Research Establishment in England. If the *E*-plane arm is considered to be a pure series connection with no junction effects, a match in this arm could be attained by making the characteristic impedance of the symmetrical arms one half the characteristic impedance of the *E*-plane T. Quarter-wavelength transformers or a tapered guide may then be used to return to a guide of standard size. It is convenient then, to have the *H*-plane arm also of the reduced dimensions at the junction. Over a band of wavelengths from 3.05 cm

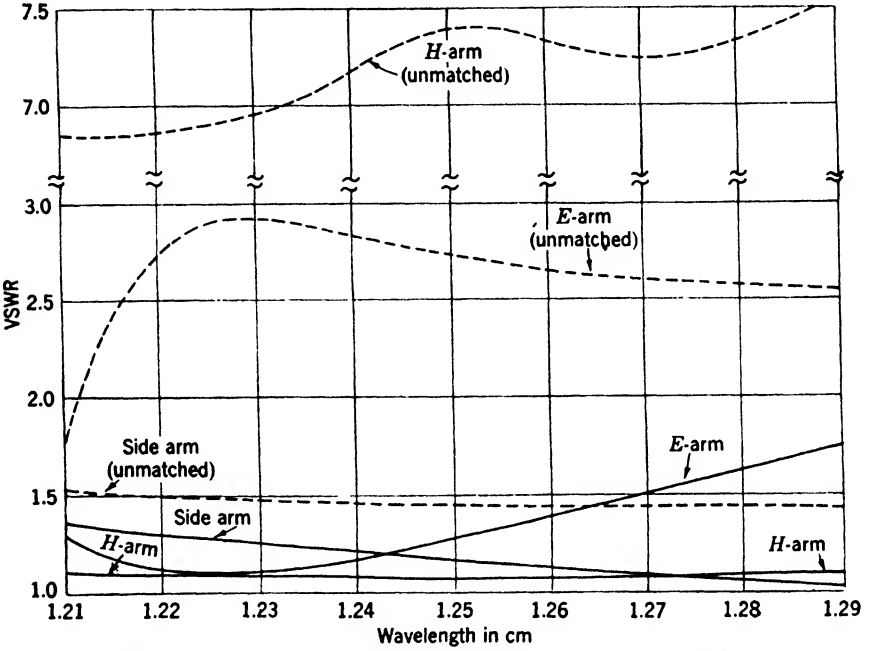

FIG. 8·39.—Effects of a post and iris for matching a magic T in ¼-in. by ½-in. waveguide.

to 3.30 cm, an unmatched magic T constructed of guides having inside dimensions 0.9 in. by 0.4 in. and 0.9 in. by 0.2 in. had a voltage standing-wave ratio in the *E*-plane arm of about 1.16, in the *H*-plane arm of 3.3, and in the side arm of 1.61. If these figures are compared with the curves in Fig. 8·38, it is apparent that the match of the series arm is greatly improved, with no effect on the shunt arm and without too drastic an effect on the side arms. Final matching was accomplished by matching the series arm with a large post and then matching the shunt arm with a small post, Fig. 8·40. The resulting curve of voltage standing-wave ratio vs. wavelength for the magic T, which includes the quarter-wavelength transformers, is shown in Fig. 8·41 for an experimental model.

[1] Private communication from P. R. Tunnicliffe, TRE, Jan. 16, 1946.

Considerable care must also be taken in matching the ring-circuit magic T. In the discussion in Sec. 8·11 it was assumed that the junction effects of the *E*-plane T could be neglected. It is seen from the fre-

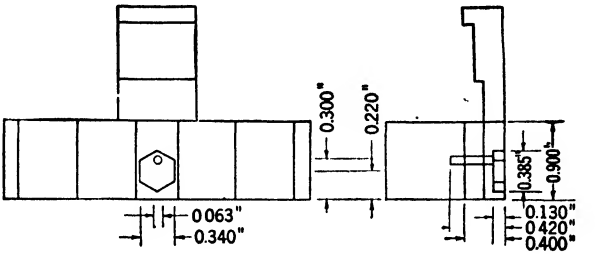

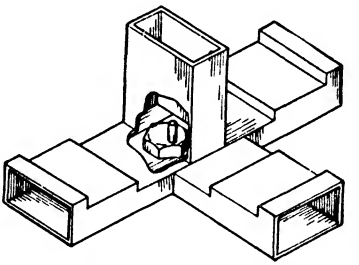

FIG. 8·40.—Modified magic T.

quency-sensitivity curves, Figs. 8·30 and 8·31, that this assumption was allowable for the 3.3-cm band for the 1-in. by ½-in. waveguide. Measurements made on a ring-circuit magic T for the 10.0-cm to 11.2-cm band using 3-in. by 1½-in. waveguide show curves very similar to Figs. 8·30 and 8·31. However, when plungers were put in arms (3) and (4) no position of the plunger could be found which would give a low standing-wave ratio in the remaining arms. Apparently the simple series-circuit assumption cannot be used here. By changing the size of the center post, Fig. 8·29, from 1.972 in., which is the calculated value for 3-in. by 1½-in. waveguide, to 2.100 in., the plunger position can be found and a curve similar to Fig. 8·32 is obtained. However, the standing-wave ratios when the short circuits are replaced by matched loads are high and the cross attenuation is much lower.

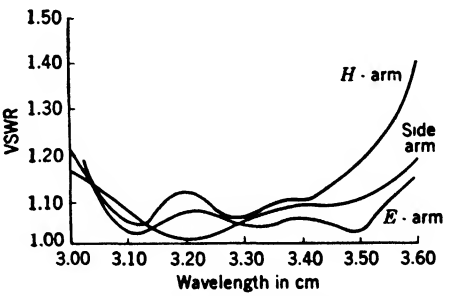

FIG. 8·41.—Frequency sensitivity of the modified magic T.

Some of these difficulties arise from the failure of the assumption that the junction effects are unimportant, and some from the very close spacing of the *E*-plane T's. With the equivalent circuit of the *E*-plane T available, the junction effects may be included in the design. The second difficulty may be removed by adding correct line lengths between the various arms. Although the argument stated in Sec. 8·11 is not applicable when sufficient symmetry is lacking, it can be shown that the magic-T properties are retained if any number of guide wavelengths are inserted between any of the arms provided that the total number of half wavelengths added to the entire ring is even. If this rule is followed a great many alterations on the simple ring circuit can be made.

For a wavelength of 3.3 cm and a waveguide size of 1 in. by $\frac{1}{2}$ in. by 0.050 in. wall, neither of these considerations is of importance. At a wavelength of 1.25 cm and a guide size of $\frac{1}{2}$ in. by $\frac{1}{4}$ in. by 0.040 in. wall, it is easily seen that the arms must be spaced so closely that they run into each other. Here obviously it is necessary to apply the rule just stated. Each addition of length increases the frequency sensitivity considerably, and therefore the addition of line lengths should be avoided if possible. It is not certain if the junction effects must be considered. To the author's knowledge, no ring circuits based on these considerations have been constructed.

The alteration of the line length between the arms is not the only transformation that can be made on the ring-circuit magic T. From the discussion in Sec. 8·11, the scattering matrix of the ring-circuit magic T is seen to be

$$\mathsf{S} = j\frac{1}{\sqrt{2}}\begin{pmatrix} 0 & 0 & 1 & 1 \\ 0 & 0 & -1 & 1 \\ 1 & -1 & 0 & 0 \\ 1 & 1 & 0 & 0 \end{pmatrix}.$$

The solution for Z in Eq. (4) is

$$\mathsf{Z} = (\mathsf{I} + \mathsf{S})(\mathsf{I} - \mathsf{S})^{-1}$$

or

$$\mathsf{Z} = (\mathsf{I} + 2\mathsf{S} + \mathsf{S}^2)(\mathsf{I} - \mathsf{S}^2)^{-1}.$$

Since $\mathsf{S}^2 = -\mathsf{I}$, $\mathsf{Z} = \mathsf{S}$,

$$\mathsf{Z} = j\frac{1}{\sqrt{2}}\begin{pmatrix} 0 & 0 & 1 & 1 \\ 0 & 0 & -1 & 1 \\ 1 & -1 & 0 & 0 \\ 1 & 1 & 0 & 0 \end{pmatrix}.$$

If a transformer with a turn ratio of n:1 is placed on one arm of the magic T, the impedance matrix of the new structure is found by multiplying the corresponding row and column by n or by $\sqrt{Z}$ where Z is the relative

characteristic impedance of the new transmission line compared with the old line. If transformers are put on each arm, the new impedance matrix will then be

$$\mathsf{Z}_n = \mathsf{MZM},$$

where

$$\mathsf{M} = \begin{pmatrix} \sqrt{Z_1} & 0 & 0 & 0 \\ 0 & \sqrt{Z_2} & 0 & 0 \\ 0 & 0 & \sqrt{Z_3} & 0 \\ 0 & 0 & 0 & \sqrt{Z_4} \end{pmatrix}.$$

As an example, let $Z_1 = Z_2 = 1$, $Z_3 = Z_4 = 2$. Then the product MZM results in

$$\mathsf{Z}_n = j \begin{pmatrix} 0 & 0 & 1 & 1 \\ 0 & 0 & -1 & 1 \\ 1 & -1 & 0 & 0 \\ 1 & 1 & 0 & 0 \end{pmatrix}.$$

This matrix may be considered as the sum of four matrices. Three of these matrices are one-quarter-wavelength lines and one is a three-quarter-wavelength line, all of a characteristic impedance of 1,

$$\mathsf{Z}_n = j \begin{pmatrix} 0 & 0 & 0 & 1 \\ 0 & 0 & 0 & 0 \\ 0 & 0 & 0 & 0 \\ 1 & 0 & 0 & 0 \end{pmatrix} + j \begin{pmatrix} 0 & 0 & 1 & 0 \\ 0 & 0 & 0 & 0 \\ 1 & 0 & 0 & 0 \\ 0 & 0 & 0 & 0 \end{pmatrix} + \cdots.$$

Thus, there is a new magic T which is shown in Fig. 8·42. With other choices of the Z_i's a great many variations are possible.

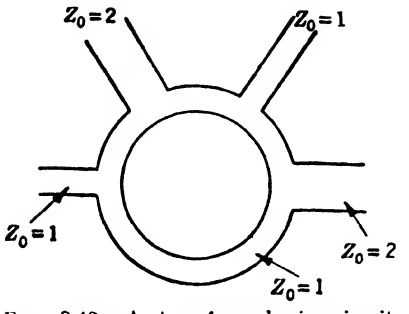

FIG. 8·42.—A transformed ring-circuit magic T.

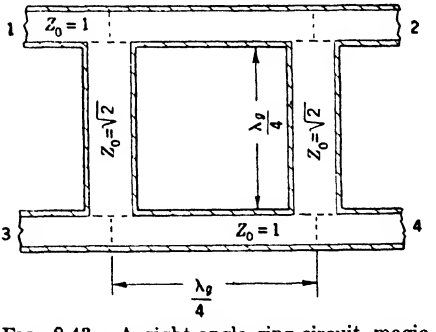

FIG. 8·43.—A right-angle ring-circuit magic T.

These considerations are also applicable to a magic T of another type. This is called the right-angle ring circuit. This ring circuit consists of four one-quarter-wavelength lines, two with a characteristic impedance of 1, and two with a characteristic impedance of $\sqrt{2}$, which connect four

terminal pairs, Fig. 8·43. By applying the method used on the ordinary ring circuit, the scattering matrix and the impedance matrix may be found,

$$S = \frac{1}{\sqrt{2}} \begin{pmatrix} 0 & 0 & 1 & j \\ 0 & 0 & j & 1 \\ 1 & j & 0 & 0 \\ j & 1 & 0 & 0 \end{pmatrix},$$

and

$$Z = j \begin{pmatrix} 0 & 1 & 0 & \sqrt{2} \\ 1 & 0 & \sqrt{2} & 0 \\ 0 & \sqrt{2} & 0 & 1 \\ \sqrt{2} & 0 & 1 & 0 \end{pmatrix}.$$

The same rule for adding line lengths between the various arms applies here, and new structures may be found by adding transformers to the

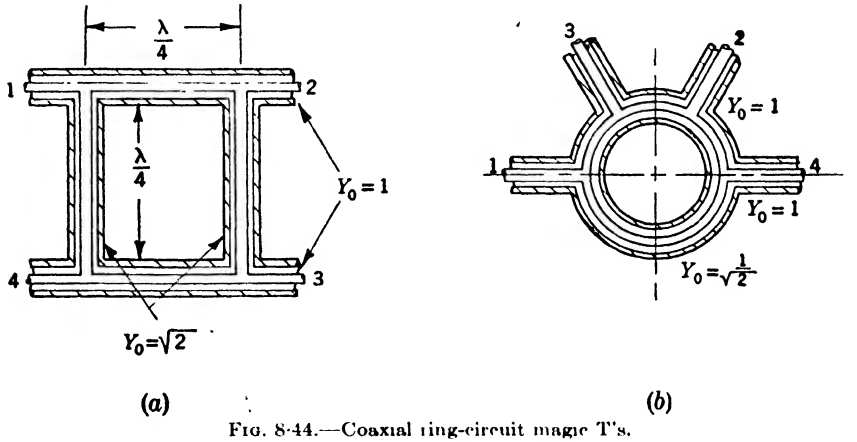

FIG. 8·44.—Coaxial ring-circuit magic T's.

arms as is done for the ordinary ring circuit. It will be observed from the scattering matrix, however, that the voltage coupled from arm (1) to arm (4), or from arm (2) to arm (3), is now 90° out of phase with the wave coupled from arm (1) to arm (3), or from arm (2) to arm (4). If a balanced duplexer were made with a ring circuit of this type, the TR switches would have to be placed at equal distances from the ring circuits.

The construction of magic T's is not limited to rectangular waveguide. A variety of magic T's may be made from coaxial lines and from combinations of waveguide and coaxial line. The discussion presented in Sec. 8·8 was based on the series and parallel natures of the *E*-plane T and the *H*-plane T, Fig. 8·22. It is easy to repeat the symmetry arguments with the *E*-plane T replaced with a coaxial probe, or the *H*-plane T replaced with a coaxial loop, or both substitutions made at once. As has been

pointed out, matching must be accomplished in the series and in the parallel arms.

Coaxial lines may be used in both types of ring-circuit constructions as indicated in Fig. 8·44. The coaxial T shown is a parallel circuit and, therefore, admittances are easier to handle. The scattering and admittance matrices may be found as in the series cases. Although several coaxial ring circuits of the type shown in Fig. 8·44*b* have been constructed, no performance data are available.

8·13. Circular-polarization Duplexer.—A third variation in the design of a balanced duplexer uses magic T's which involve a round waveguide. As an example of such a magic T, consider the construction indicated in Fig. 8·45. The two symmetrical arms of the magic T, arms

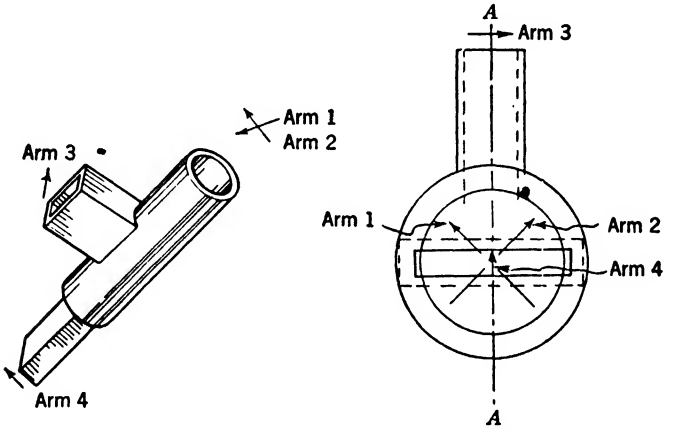

FIG. 8·45.—A magic T using round waveguide.

(1) and (2), are the two perpendicular polarizations in the round waveguide. The analysis of the junction proceeds in exactly the same manner as in Sec. 8·8. For the ordinary magic T of Fig. 8·22, in order to obtain a matched magic T, the matching must be accomplished in arms (3) and (4). Arm (4) can be matched to arms (1) and (2) by using a quarter-wavelength transformer between the rectangular and the cylindrical guides. The transformer shown in Fig. 8·46 is approximately a quarter-wavelength long, and its impedance is approximately correct for a transition between transmission lines of different characteristic impedances. End effects and the change in cross section alter both the length and the Z_0 of the transformer. At 1.25 cm the choice of dimensions of the rectangular and the cylindrical guide is such that a match can be obtained in arm (3) by simply adjusting the distance between arms (3) and (4). At 3.3 cm a matching iris is necessary.

The advantage of using a magic T with round guide in a duplexer becomes apparent if the magnetron and antenna are visualized as placed

on arms (4) and (3), for then the two TR switches are in the same guide. The two switches can, in fact, be made into a single tube. The difference in the electrical path length from the magic T to the TR switch for the two arms, arm (1) and arm (2), must be a quarter of a guide wavelength, as in the previous duplexers. Now, however, the physical distance between the magic T and the TR switch is the same for the two arms since they are in one waveguide. The guide wavelengths in arms (1)

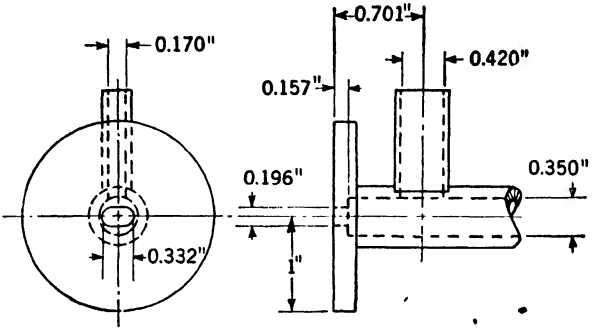

FIG. 8·46.—Dimensions of 1.25-cm-band circular magic T.

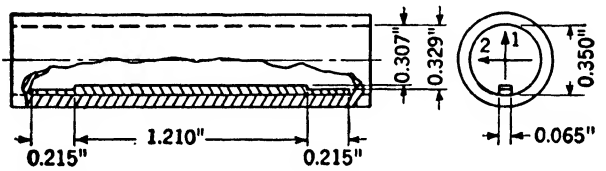

FIG. 8·47.—A quarter-wavelength plate. Dimensions are for 1.25-cm wavelength.

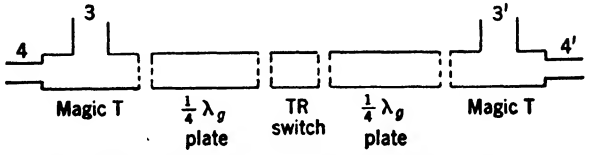

FIG. 8·48.—Diagram of circular-polarization duplexer.

and (2) between the TR and the magic T must, therefore, be altered to result in a quarter-wavelength difference in electrical path length. In other words, if λ_g' and λ_g'' are the wavelengths in arms (1) and (2) respectively, then

$$l = \frac{\frac{\pi}{2}}{\frac{2\pi}{\lambda_g'} - \frac{2\pi}{\lambda_g''}},$$

where l is the length of the section of the cylindrical guide in which the guide wavelengths differ. The change in guide wavelengths may be

accomplished by using an elliptical section of guide, by inserting a fin into a circular guide, by using lumped constants such as a number of capacitive posts, or by using a dielectric slab in circular guide. The second method is illustrated in Fig. 8·47. The stepped construction on each end of the fin is a quarter-wavelength transformer to match into and out of the phase-shifting section.

The waves in arm (1) and arm (2) are thus in phase with each other when they enter the section of guide containing the fin, and are 90° out of phase with each other as they leave the section. Before entering the section containing the fin, the combined wave will thus be a linearly polarized wave whose electric vector is either parallel to or perpendicular to the symmetry plane of the magic T. After leaving the fin, the combined wave is either a right-hand or a left-hand circularly polarized wave. The section of waveguide containing the fin is thus the microwave equivalent to the quarter-wavelength plate used at optical frequencies.

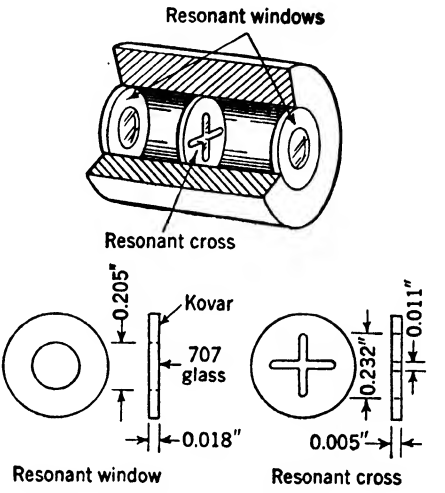

FIG. 8·49.—TR switch.

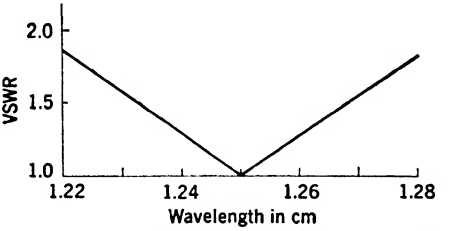

FIG. 8·50.—Bandwidth of TR switch of Fig. 8·49.

The circular-polarization duplexer will, therefore, consist of two magic T's in cylindrical guide, two quarter-wavelength plates, and a TR switch in cylindrical guide, Fig. 8·48. The operation on both low and high power is identical to that of the balanced duplexers previously described.

The TR switch must transmit two perpendicular polarizations, for example, the waves in arms (1) and (2). Figure 8·49 indicates a possible construction. The orientation of the resonant cross is not important since a circularly polarized wave is symmetric about the direction of

propagation. Figure 8·50 shows the voltage standing-wave ratio which the TR switch presents to the quarter-wave plate. It is seen that over the frequency band shown the maximum loss is 0.5 db. Figure 8·51 is

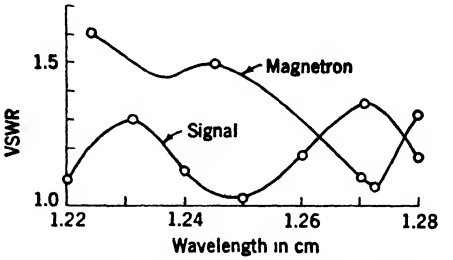

FIG. 8·51.—Standing-wave ratio as seen by the magnetron and signal.

the over-all voltage standing-wave ratio of the duplexer as seen by the magnetron and the antenna of an experimental circular-polarization duplexer shown in Fig. 8·52.

When the leakage pulse is observed on a fast oscilloscope, the energy appears to be almost entirely in the spike. The total energy transmitted by the TR switch, for example, the amount of energy per pulse entering the matched absorber in arm (4), is 9 ergs. The energy per pulse absorbed by the crystal is 0.06 erg. The decrease in leakage energy accomplished by the magic T and the quarter-wavelength plate is thus 22 db. This measurement was made only at the center of the 1.25-cm band. The maximum amount of power which the duplexer will transmit at atmospheric pressure is 87 kw at 0.3 μsec pulse width, 550 pps repetition frequency.

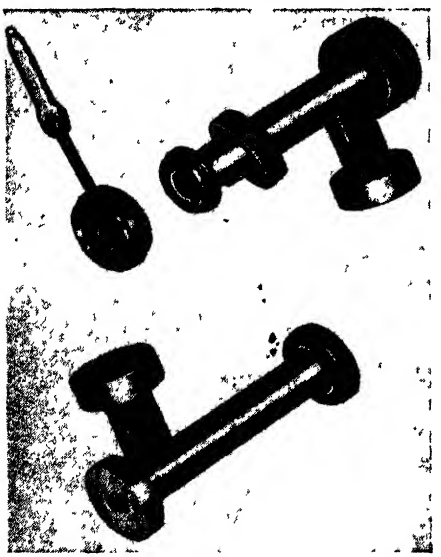

FIG. 8 52.—Duplexer for 1.25 cm employing circular polarization.

8·14. Turnstile Duplexer.—A balanced duplexer that employs a circularly polarized wave but does not use a quarter-wavelength plate can be constructed with a six-terminal-pair network called "the turnstile," Fig. 8·53. Let us consider three experiments performed with matched terminations on 5 arms, and with a matched generator on the remaining arm of the turnstile.

1. With the generator on arm (6), Fig. 8·54*a*, in the cylindrical guide, make an adjustment of two parameters, such as a post diameter and length indicated in Fig. 8·55, until there is no reflected wave. Since the device is symmetrical about a plane through arms (3), (4), and the cylindrical guide, no power will be coupled to arms (3) and (4). The electric field of the wave in arm (6) is odd about the plane of symmetry. Such a field will not propagate in arms (3) and (4). The waves in arms (1) and (2) are equal in amplitude and are 180° out of phase with each other. If unit power is incident in arm (6), the voltages in arms (1) and (2) may be characterized by $+1/\sqrt{2}$ and $-1/\sqrt{2}$.

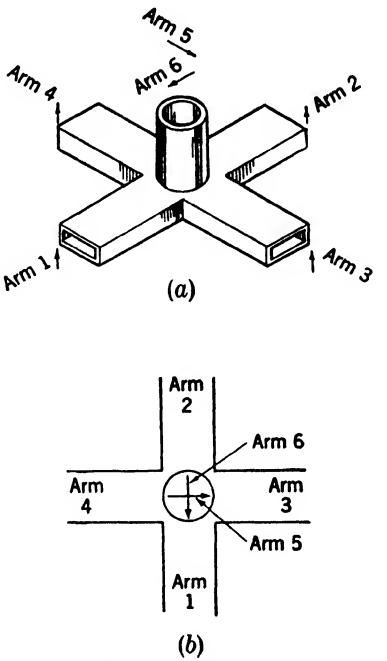

FIG. 8·53.—A turnstile junction.

2. From Experiment (1) it must be concluded that if unit power is incident in arms (1) and (2), Fig. 8·54*b*, such that their respective voltages are 180° out of phase, no power will be coupled to arms (3), (4), and (5) while the amplitude of the wave in arm (6) will be $\sqrt{2}$. There will be no reflected wave in either arm (1) or arm (2).

3. If a generator is placed on arm (1) only, Fig. 8·54*c*, there will be, in general, a reflected wave and a wave which is coupled to each

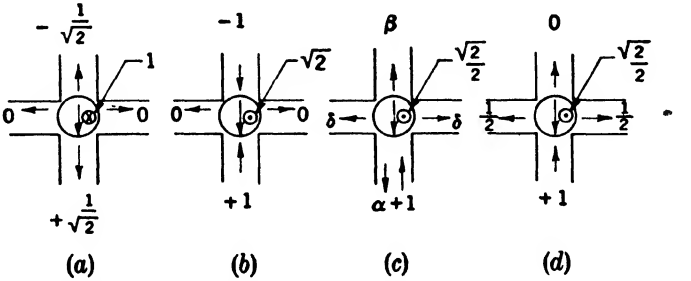

FIG. 8·54.—Diagram to illustrate the matching of a turnstile junction. In (*a*) the direction of the incident wave is into the paper; in (*b*), (*c*), and (*d*) the waves emerge from the plane of the paper.

of the remaining arms except arm (5). From the symmetry of the turnstile the power coupled to arms (3) and (4) will be equal and the waves in phase with each other. When unit power is incident in arm (1), the

amplitude of the wave coupled to arm (6) will be $\sqrt{2}/2$ as indicated by Experiment (2). Comparing Experiments (2) and (3), it is observed that for consistency it is necessary that the reflected wave in arm (1) be equal to the transmitted wave in arm (2), $\alpha = \beta$. If now by a second adjustment $\alpha = 0$, then $\beta = 0$, and necessarily, $\delta = \frac{1}{2}$. This is a device whose properties are indicated in Fig. 8·54*d*. If a wave is incident in any one of the rectangular waveguides when the remaining guides are terminated in their characteristic impedances, one-half the incident power will couple to one polarization in the cylindrical guide, and one-fourth the power will couple to each of the adjacent rectangular guides.

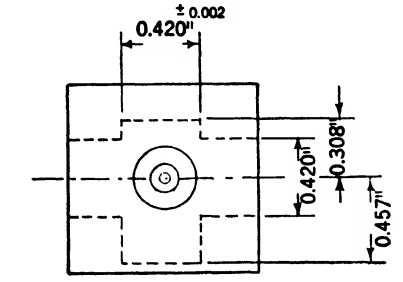

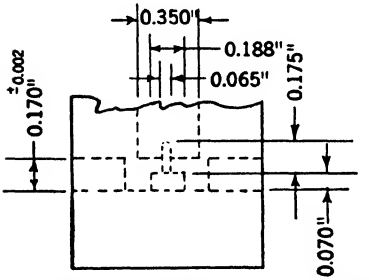

FIG. 8·55.—Dimensions for a matched turnstile junction at 1.25 cm.

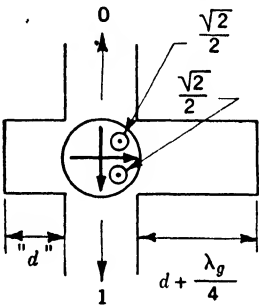

FIG. 8·56.—Turnstile with short circuits on two arms.

No power will be reflected, and no power will be coupled either to the opposite rectangular arm or to the perpendicular polarization in the cylindrical guide.

For duplexing purposes a short circuit is placed in arm (3) and one in arm (4), Fig. 8·56. If the short circuits are placed so that one of them is one-quarter guide wavelength farther from the plane of symmetry than the other, the two reflected waves will arrive at the cylindrical waveguide 180° out of phase with respect to each other. This condition is equivalent to Experiment (2). The two waves, therefore, will couple to arm (5) in the cylindrical guide and no power will be coupled either to arm (1) or to arm (2). The resultant wave in the cylindrical guide will depend upon the relative phases of the two perpendicularly polarized waves in arms (5) and (6). If the positions of the two short circuits are adjusted, maintaining the one-quarter guide wavelength relative displacement, the phase of the wave in arm (5) may be varied without changing

the match of the modified turnstile or the coupling from arm (1) to arm (2). In particular the phase may be made just 90° different from the wave in arm (6). The resultant wave will then be circularly polarized. Critical dimensions are shown in Fig. 8·55 for the 1.25-cm band.

It is clear that the modified turnstile accomplishes everything that the round magic T and the quarter-wavelength plate accomplished in the previous duplexer. Two such turnstiles and a TR switch for round

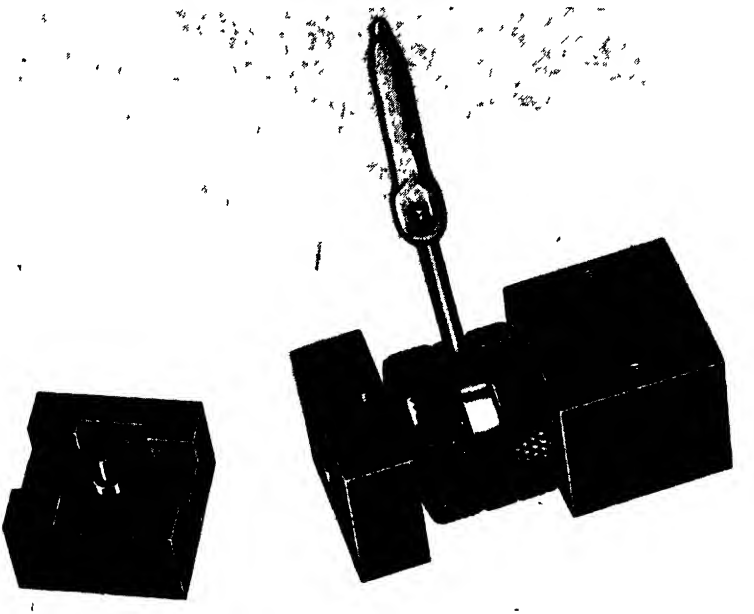

FIG. 8 57.—Balanced duplexer employing turnstile junctions.

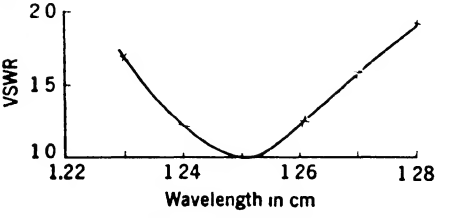

FIG. 8 58.—Frequency sensitivity of turnstile duplexer at high powers.

guide, Fig. 8 57, form a balanced duplexer which functions in a manner identical with the circular-polarization duplexer of Sec. 8·13. The frequency sensitivity at high power level is shown in Fig. 8 58. At low power level the modified turnstile has a voltage standing-wave ratio of less than 1.1 over the band of wavelengths from 1.22 to 1.28 cm. The over-all frequency sensitivity of the turnstile duplexer is, therefore, approximately that of the TR switch, as shown in Fig. 8·50 of Sec. 8·13.

CHAPTER 9

MEASUREMENT TECHNIQUES

By H. A. Leiter

The measurements of the r-f properties of TR and ATR tubes and of complete duplexers usually involve only standard techniques common to all microwave measurements. The emphasis, however, is not necessarily the same, and in many cases it is desirable to develop more or less specialized test equipment and procedures. One of the most important reasons for the development of specialized test equipment is the necessity for mass-production testing of the tubes by relatively untrained personnel.

Measurements on TR tubes and duplexers may be classified under three headings: (1) low-level r-f measurements, (2) high-level r-f measurements, and (3) d-c measurements. The low-level r-f measurements on TR tubes include tuning, insertion loss, Q_0, Q_{L2}, coupling, and keep-alive interaction. The measurements on ATR tubes include tuning, Q_0 and Q_{L2}, and coupling. Duplexer low-level measurements are concerned with tuning, maximum and minimum insertion loss for various magnetron impedances, and bandwidth. High-level r-f measurements must be made of arc loss, arc leakage power, spike leakage energy, direct-coupling attenuation, harmonic leakage power, high-level standing-wave ratio, and recovery-time characteristics. D-c measurements are concerned with the keep-alive characteristics. They include minimum firing voltage, firing time, oscillations, and volt-ampere characteristics.

For the general background and a fuller description of microwave test equipment and transmission-line components, the reader is referred to the following volumes of this series: "Microwave Transmission Circuits" Vol. 9 and "Technique of Microwave Measurements" Vol. 11.

9·1. Basic Low-level Test Equipment.—The fundamental test setup for low-level measurements from which almost all others are derived, consists of an r-f signal source, suitable level-setting and padding attenuators, a power monitor and wavemeter, a slotted section or standing-wave detector, and the object under test which may or may not be followed in the transmission line by a second slotted section and a matched load or power measuring device. With such a setup, the impedance (magnitude and phase of the standing-wave set up by the test object), loaded and unloaded Q, insertion loss, tuning, and other

properties can be measured. The measurements may be made in coaxial or waveguide transmission lines depending upon the object under test and the particular frequency band. In the 10-cm (3000 Mc/sec) band, waveguide and coaxial lines find almost equal use. At 3 cm and below, almost all measurements are made in waveguide. In fact, almost the only coaxial lines used are flexible dielectric-filled cables. Although it is dangerous to generalize, it is probably true that waveguide test benches are more flexible and accurate than those made of coaxial lines. It is easier to make matched variable attenuators, matched loads, and good slotted sections in waveguide, chiefly because there is no center conductor to support. At wavelengths greater than 10 cm, waveguide finds little use because of its great bulk. A typical 10-cm bench using 1½ in. by 3 in. waveguide which includes two slotted sections, two attenuators, and a matched load may be 5 ft long and weigh 30 lbs.

Signal sources most commonly used are klystrons or parallel-element triodes of the "lighthouse" construction. Reflex klystrons, because they are much more easily tuned, have replaced two-cavity klystrons. With present detecting and measuring techniques a power level of 50 to 100 mw from the tube is ample for most measurements. These power levels may be obtained with the 2K28 and 2K41 klystrons in the 10-cm band, and with the 2K39 tube at 3 cm. The 2K39 and 2K41 tubes have integral cavities and operate at beam potentials of 1200 and 600 volts, respectively, with reflector voltages about −200 volts with respect to the cathode. The 2K41 tube may be turned over a range from about 8.8 cm to 14 cm, but only about a 10 per cent tuning range can be obtained on the main tuning knob. The 2K39 tube may be tuned over a 12 per cent band from 3.1 to 3.5 cm by the tuning control. With 1500 to 2000 volts between anode and cathode, the output power of these tubes may be pushed to 0.5 to 1 watt.

The 2K28 tube is a cell-type tube that is used with an external cavity. It operates at lower voltages than the 2K41 tube and produces 100 mw at a beam voltage of 300 volts. This, however, is almost its maximum output power. The tube may be tuned from about 8.5 to 12 cm in a simple waveguide cavity with two short-circuiting plungers. The 2K25 tube is a low-power tube in the 3-cm band. The output power is about 30 mw at 300 volts. The 2K25 and 2K28 tubes, because they are easily tuned and require smaller power supplies, are usually used in preference to the 2K39 and 2K41 tubes if the lower output power is sufficient.

The 2C43 (lighthouse tube) triode is most useful above about 15 cm wavelength. It too operates on about 200 to 300 volts. It suffers from the fact that it has no electronic tuning as the reflex klystrons have; but it requires a simpler power supply.

The r-f power from each of these tubes is coupled out through some form of coaxial line. All except the 2K25 tube are coupled to the main line by a flexible coaxial cable. The 2K25 tube is arranged to mount directly on the waveguide (1 by ½ in. by 0.050 in. wall) with no intermediate fittings. The use of flexible cable has many advantages; but it must be recalled that the fittings used to join these cables together (type N fittings) may introduce standing waves of as much as 1.5 or 2 in voltage. Therefore, where it can be avoided, measurements should never be made through such connectors.

Lossy cables are used whenever possible between the r-f generator and the other test equipment, in order to isolate the oscillator from effects of mismatch in the unit under test. Transitions from cable to coaxial line usually involve a type N r-f connector and a tapered section, or section of line containing step transformers, to afford a match from the cable into the air-filled coaxial line. Transitions from coaxial line or flexible cable to waveguide are of several types. The most common variety has a probe approximately one-quarter wavelength long, but other devices, such as "door knobs" and crossbar-supported probes, serve equally well and are often less susceptible to mechanical distortion than the simple one-quarter-wavelength probe.

The slotted section is one of the most important items of test-bench equipment. It must be very carefully constructed if accurate work is to be done. If any dimension varies from the value specified, the electrical measurements are affected in some manner. Inner dimensions of slotted sections in guide must be accurate. This is true also of the outer conductor of coaxial slotted sections, with the further requirement that the inner conductor must be accurate in size and very closely coaxial with the outer conductor. It is the presence of the inner conductor which makes coaxial slotted lines so much more difficult to construct than the waveguide slotted sections. In a section of either type the slot should be as narrow as possible and accurately parallel to the axis of the line. The thickness of the wall in which the slot is cut must be held to close limits, so that the projection of the probe into the guide will be uniform along the slotted section. A gradual variation in thickness causes the sensitivity of the device to vary from one end to the other. The same action would occur if the inner conductor of a coaxial section were not accurately centered. The length of the slot should be greater than a full wavelength. A full wavelength would ensure that two voltage minima and one maximum, or one minimum and two maxima, could always be obtained were it not for the fact that "end effects" cause values near the ends of slots to be unreliable.

The pickup probe should be made of fairly small wire and should be inserted into the transmission line as short a distance as possible, in order

that it shall not cause a standing wave. Tunable probes are best because the greater sensitivity permits less insertion. The r-f voltage picked up by the probe is either rectified by a detector mounted in the probe and applied to a galvanometer or amplifier, or is applied directly to a spectrum analyzer which contains a superheterodyne receiver. A probe of the second type, which does not contain a detector, is sometimes called an "r-f probe," because it can be used to pick up r-f power which will be delivered to another instrument by means of a flexible cable.

The choice of the instrument used to indicate the magnitude of the power picked up by the probe depends on the kind of measurements to be made and on whether or not the r-f oscillator is modulated. If the r-f oscillator is square-wave modulated, an amplifier is usually employed. Most amplifiers used for this purpose have tunable selective circuits incorporated in them and, therefore, they amplify only at some desired frequency. This is very useful for eliminating effects of power-supply ripple, or other interferences. The amplifier is tuned to that modulation frequency used with the r-f oscillator. Since the oscillator is modulated with a square wave, the rectified r-f pulse has considerable harmonic content. If the amplifier is tuned to amplify at one of these harmonics, an appreciable error may be introduced, since most of the harmonic component is in the rising and falling edges of the pulse, where the r-f frequency may be quite different from the frequency obtained over the flat top of the pulse. If the modulating voltage does not swing the reflector of the oscillator to a nonoscillating voltage during half of the cycle of the rectangular pulse, erratic results may also be expected, because it is likely that the frequencies obtained in the two halves of a cycle will be considerably different. The presence of two or more frequencies may be checked by inserting an absorption wavemeter into the circuit and observing the "dips" in power level as the wavemeter is tuned over the band. It is sometimes very convenient to apply the output voltage of a crystal to an oscilloscope, so that the envelope of the modulated r-f signal may be observed. Power for this monitoring crystal may be taken out of the line by means of a probe similar to the one used in the standing-wave measurement, or by means of a directional coupler.

When the r-f oscillator is unmodulated, a galvanometer may be used to register the crystal current. The crystal current is very nearly proportional to the power picked up by the probe. Consequently,

$$\text{VSWR} = \frac{E_{max}}{E_{min}} = \sqrt{\frac{P_{max}}{P_{min}}} \approx \sqrt{\frac{I_{max}}{I_{min}}}.$$

where the E's are field-strength values along the guide, the P's are the corresponding values of power into the crystal, and the I's are the corresponding crystal currents.

The equation relating crystal current to the applied voltage is, more accurately,

$$I = E^m,$$

where m expresses the law of the detector, that is, if $m = 2$, the detector is said to have a square law. With this notation,

$$\text{VSWR} = \left(\frac{I_{\max}}{I_{\min}}\right)^{1/m}.$$

The crystal is very nearly a square-law device, but for precise work the value of m should be obtained experimentally. This may be considered a calibration of the crystal and it is necessary to calibrate, as a unit, the crystal with its associated equipment, such as a galvanometer or an amplifier, since output impedance has some effect on the crystal law, and since the amplifier itself may not be quite linear. If the range of crystal currents in use is large, it will be necessary to obtain a continuous calibration curve, but the crystal may be calibrated at only one point if the variation in current is not very large. For voltage standing-wave ratios less than three, calibration at a single point is usually sufficient since the variation in crystal law with crystal current is a slow function. Calibration of a crystal is usually done by short-circuiting a line with a metal plug and comparing the values of crystal current vs. probe position with theoretical values of field strength which may be calculated. In a short-circuited lossless line, the field strength at any point may be calculated from the relation

$$E = \left|\sin \frac{2\pi l}{\lambda_g}\right|.$$

The value of m, the crystal-law parameter, can be determined by making a measurement at any distance l from a minimum, since

$$\frac{I_l}{I_{\max}} = \left(\frac{E_l}{E_{\max}}\right)^m = \left(\left|\sin \frac{2\pi l}{\lambda_g}\right|\right)^m,$$

$$m = \frac{\log (I_l / I_{\max})}{\log \left(\sin \dfrac{2\pi l}{\lambda}\right)}.$$

When a spectrum analyzer is used, the r-f power is applied directly from the probe to a calibrated cutoff attenuator built into the instrument. When standing-wave ratios are measured with this apparatus, the probe is set at the position of a voltage minimum and the height of the pip noted. The probe is then moved to a maximum position and the signal is adjusted, by means of the calibrated attenuator, to the same height as when the probe was set at a minimum in the standing-wave pattern.

Spectrum analyzers are very useful for measuring standing-wave ratios greater than two. The calibrated attenuators can be adjusted to give accuracies of ± 0.2 db if care is taken, and if the drive mechanism is carefully built. The sensitive receiver in the analyzer allows measurement of standing-wave ratios as high as 40 db (100-to-1 voltage ratio).

Matched line terminations, matched pads, and matched variable attenuators should have voltage standing-wave ratios less than 1.05 for rough work and less than 1.02 for accurate measurements. Units usable over a broad band of frequencies can be built to fulfill the requirements stated above. Matched pads are particularly important when direct measure-

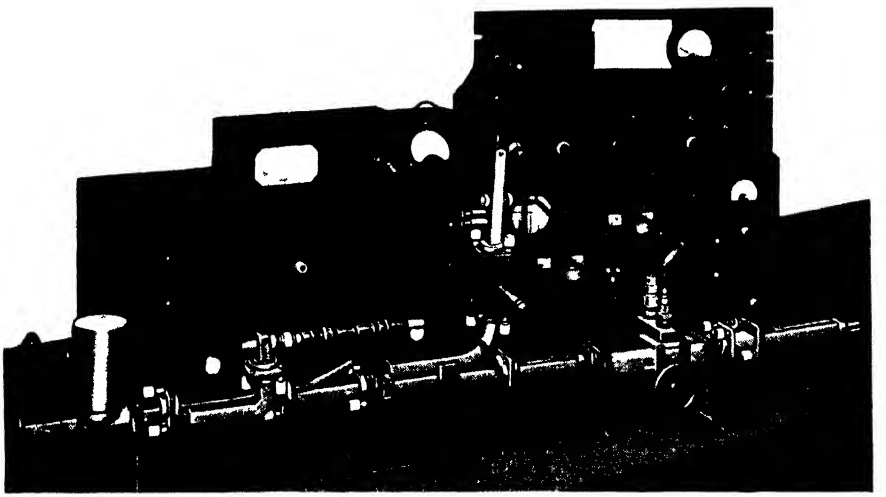

FIG. 9·1.—A typical test bench for use at wavelengths near 3 cm.

ments of insertion loss are to be made. Section 9·2 will discuss this further.

Square-wave modulators are usually condenser-coupled to the reflector circuit of the reflex klystron tube and require only about a 50-volt square wave to throw the tube in and out of oscillation. The square wave should rise sharply and be as flat as possible on top in order to make the frequency modulation small. Experience has shown that a symmetrical square wave, in which the duration of the positive half of the wave is equal to that of negative half of the wave, gives the best results.

Wavemeters are of two types: the coaxial type which is most often used at 10 cm, and the cavity type which is used most frequently at 3 cm. They may be coupled to the source of r-f power in such a manner as to cause a dip in power when they are at resonance (absorption type) or they may be used as transmission meters. The absorption type is more popular since the monitoring device also indicates whether the r-f source

is in oscillation. Measurements of high-Q devices call for greater accuracy than can easily be obtained with ordinary wavemeters. Means for obtaining the required accuracy are discussed in Sec. 9·3.

A typical test bench for use at wavelengths near 3 cm is shown in Fig. 9·1. The oscillator is at the left, then there is a directional coupler for monitoring the power, an attenuator, a directional coupler with a transmission wavemeter and a crystal holder, a second attenuator, the standing-wave detector, a broadband TR tube (1B63), and a matched load terminating the waveguide line. The power supply for the oscillator and a square-wave modulator are contained in the box on the left behind the waveguide. On the lower right is a spectrum analyzer, and above it an audio amplifier.

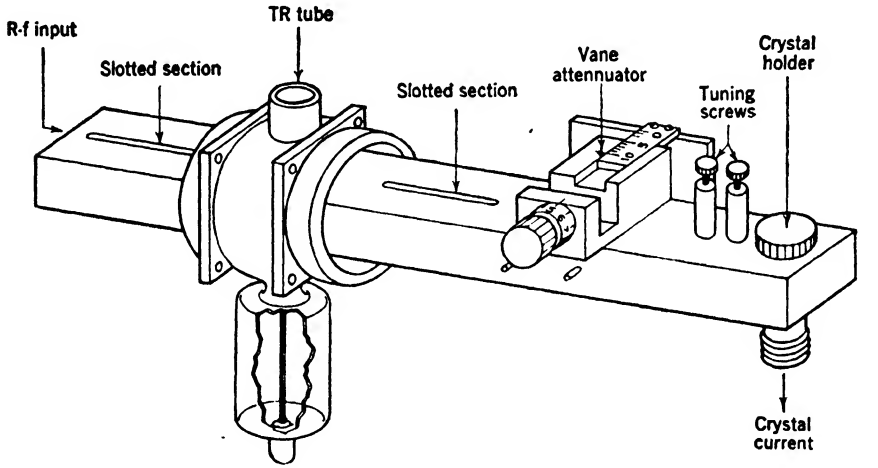

FIG. 9·2.—Determination of insertion loss of 1B24 TR tube.

9·2. Insertion-loss Measurement.—Insertion loss L is defined as

$$L = 10 \log_{10} \frac{P_i}{P_l}, \tag{1}$$

where P_i is the incident power and is the power delivered to a matched load by a matched generator; P_l is the power delivered to a matched load, by the same matched generator, after the unit for which the loss is to be measured has been inserted in the line. Insertion loss is made up of two components—reflection loss and dissipative loss. Reflection loss is caused by an impedance mismatch which reflects part of the incident power back toward the generator. Dissipative loss takes place within the element and is I^2R loss. Dissipative loss is usually determined by subtracting the reflection loss from the total insertion loss.

Insertion loss is determined directly by measuring the power delivered by a matched generator to a matched load and then measuring the power

delivered to the matched load with the unit to be measured in the circuit. A matched calibrated attenuator is very useful in this measurement, since it eliminates the necessity for an accurate power-measuring device. With the unit to be measured inserted between the matched generator and the matched attenuator (Fig. 9·2), the power level into the matched load should be set at some convenient value. The unit being measured is then removed from the circuit and the attenuation increased until the

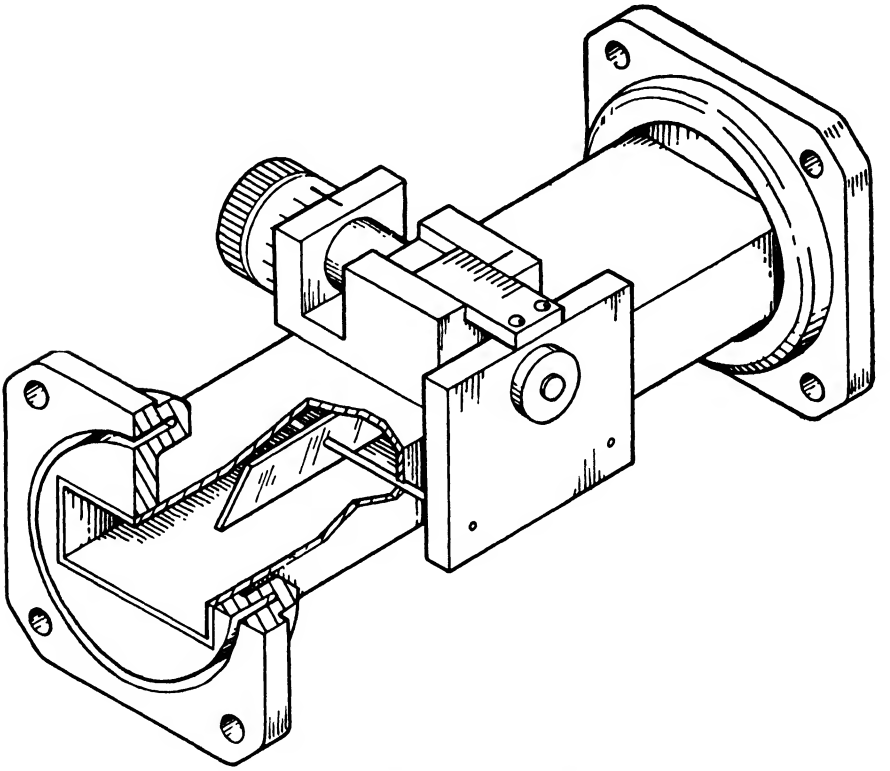

FIG. 9·3.—Sliding-vane attenuator.

power level returns to its former value. The difference between the attenuator readings represents the insertion loss. In general, the platinized-glass type of attentuator, in either coaxial line or waveguide (see Fig. 9·3), is preferred for these measurements, because it holds its calibration well. Resistor-strip attenuators absorb moisture to some extent and, therefore, change calibration.

The tuner shown in the illustration is used to match the crystal detector. Tuners of several varieties are suitable for this purpose. These are all described in Vol. 9, Chap. 9, Radiation Laboratory Series. If the r-f oscillator is capable of delivering sufficient power, a matched pad may be

used in place of the tuner. This pad must have sufficient attenuation to reduce the voltage standing-wave ratio introduced by the crystal to an acceptable value, about 1.05 or less.

When insertion loss is measured directly, it is necessary to ensure that both the generator and the termination are well matched. A termination which has a VSWR of 1.2, if used in the measurement of a TR cavity normally having a loss of 1.5 db, gives values of loss ranging between 1.37 and 1.64 db, depending upon the phase of the impedance: a variation of approximately ± 9 per cent. If, in addition, the generator were mismatched by an equal amount, the range of variation of loss would be about twice that obtained with a mismatched termination alone.

The insertion loss may be determined also by measuring the field strength and the voltage standing-wave ratio in the line, on each side of the unit under test, by means of a probe and slotted section. Let E_1 be the incident electric field, and ΓE_1 the reflected electric field, where Γ is the reflection coefficient of the unit being measured, and let E_2 be the transmitted electric field. Since all fields are measured in lines of the same characteristic impedance, the loss is given by the relation

$$L = 20 \log_{10} \frac{E_1}{E_2}.$$

The maximum field strength in the standing-wave pattern in the first slotted section is given by

$$E_{max} = E_1(1 + |\Gamma|),$$

and the minimum by

$$E_{min} = E_1(1 - |\Gamma|).$$

Hence

$$E_1 = \frac{E_{max} + E_{min}}{2}.$$

The rectified current R from the probe is proportional to the square of the field strength, or

$$R_{max} = k_1 E_{max}^2,$$
$$R_{min} = k_1 E_{min}^2,$$

where k_1 is the constant characteristic of the probe on the generator side of the tube. A similar relation holds for the second slotted section, but with a different constant of proportionality. If no standing wave is present in the second slotted section,

$$R_2 = k_2 E_2^2.$$

The ratio k_1/k_2 may be determined by comparing the probe currents when the unit to be tested is removed from between the slotted sections.

The insertion loss is then

$$L = 20 \log_{10} \frac{\sqrt{R_{max}} + \sqrt{R_{min}}}{2\sqrt{\frac{R_2 k_1}{k_2}}}.$$

The reflection loss L_R, in decibels, is given by

$$L_R = 10 \log_{10} \frac{1}{1 - |\Gamma|^2},$$

or

$$L_R = 10 \log_{10} \frac{(r+1)^2}{4r},$$

where r is the voltage standing-wave ratio. Since

$$r^2 = \left(\frac{E_{max}}{E_{min}}\right)^2 = \frac{R_{max}}{R_{min}},$$

$$L_R = 10 \log_{10} \frac{(\sqrt{R_{max}} + \sqrt{R_{min}})^2}{4\sqrt{R_{max} R_{min}}}.$$

9·3. Pass Band of High-Q TR Switches.—A characteristic of great importance in the performance of a TR tube is the unloaded Q. This is

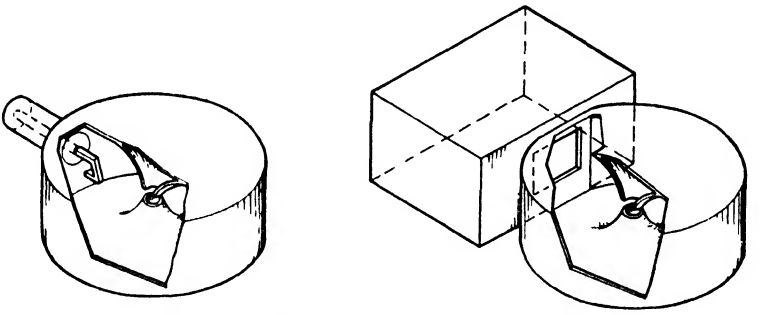

FIG. 9·4.—Methods of coupling to TR cavities.

most easily determined by measuring the Q of a TR tube and its associated cavity, loaded by one window, Q_{L1}. The cavity is mounted so that it terminates a transmission line and the response curve is measured in terms of standing-wave ratio and frequency. Either coaxial line or waveguide may be used, but since the trend in microwave applications has been toward the use of waveguide, the measurements to be described are for the waveguide application.

For a measurement of Q_{L1}, a cavity is mounted on the end of a coaxial line or waveguide as shown in Fig. 9·4. This situation can be represented by the equivalent circuit shown in Fig. 9·5. The coupling of the cavity to the transmission line may be varied by varying the size of the opening

into the cavity. This corresponds to changing the transformer ratio, n_1/n_2, and thus changing the terminating admittance of the line. When the cavity is tuned to resonance, the imaginary part of this terminating admittance is zero and, looking into the cavity from the transmission line, a pure conductance is seen whose magnitude depends on the coupling—that is, the size of the opening—and the unloaded Q of the cavity.

If the coupling iris is very small, a large standing-wave ratio is produced in the transmission line, since the end of the waveguide transmission line is essentially terminated in a very high admittance with a large real component. Thus, a minimum of the standing-wave pattern appears at the window at resonance, and the cavity is said to be "under-coupled." As the opening is increased in size, the real part of the terminating admittance approaches the characteristic admittance of the transmission line, until a size of opening is reached for which, at resonance, $Y = Y_0$, and the cavity is matched to the line. The standing-wave ratio at

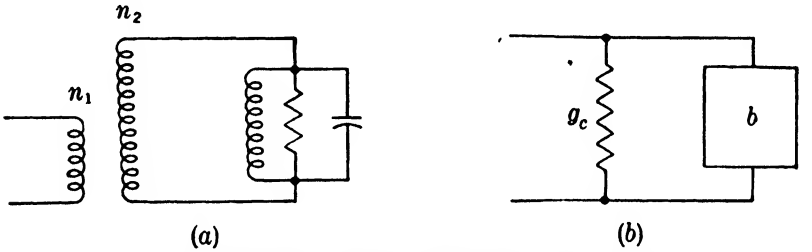

FIG. 9·5.—Equivalent circuit for cavity with input coupling.

resonance will be unity. As the size of the opening is increased still further, the real part of the admittance decreases below Y_0 and, at resonance, a maximum of the standing-wave pattern appears at the opening. When this condition occurs, the cavity is referred to as "over-coupled."

As a result of this behavior, two possibilities are to be distinguished. The voltage standing-wave ratio at resonance is given by

$$r_0 = \frac{1 + \left|\frac{1 - g_c}{1 + g_c}\right|}{1 - \left|\frac{1 - g_c}{1 + g_c}\right|} \tag{2}$$

where g_c is the normalized cavity conductance. If $g_c \leqq 1$, $r_0 = 1/g_c$. This case is of principal interest in duplexer design. If $g_c \geqq 1$, $r_0 = g_c$.

In making measurements on a cavity, the information as to whether g_c is greater or less than one is obtained from the phase of the standing waves. For an iris-coupled cavity, it is usually easy to determine whether a maximum or minimum appears at the opening at resonance.

However, a complicated r-f transmission line between the slotted section and the cavity might make this determination difficult. Nevertheless, the information may be obtained by a study of the behavior of the phase of the standing wave. If the position of a minimum in the standing-wave pattern is measured along the slotted section from an arbitrary origin, and if $g_c < 1$, there will be a quarter-wavelength shift from the position of the minimum at resonance to the position of the minimum at frequencies far off resonance. If $g_c > 1$, the position of the minimum will be the same at resonance as for frequencies far from resonance. It is useful to interpret the behavior of the standing-wave pattern as a function of frequency by tracing the variation on an admittance chart. Figure 9·6

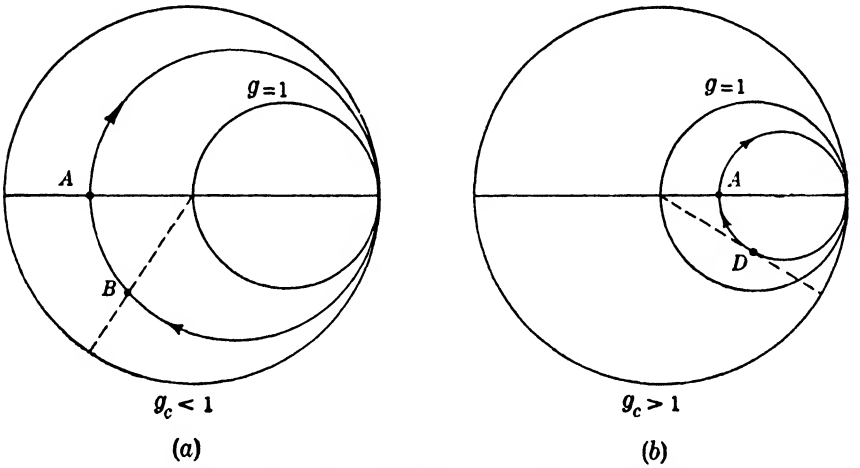

FIG. 9·6.— Circle-diagram explanation of shift of minimum.

shows the circle diagrams for the two cases. For frequencies far from resonance, the cavity acts as a short circuit, and has, therefore, an infinite admittance. As the frequency increases from a value below the resonant frequency to a value above it, the susceptance increases from a large negative value, passes through $b = 0$, and approaches positive infinity. The conductance of the cavity remains constant. The cavity admittance, therefore, traces out a circle whose center is on the line $b = 0$, and at resonance the admittance is represented by point A. If $g_c < 1$, the circle encloses the point $b = 0$, $g = 1$, and the phase of the standing-wave pattern changes through 360° or one-half wavelength, as indicated in Fig. 9·6*a*. If $g_c > 1$, the phase increases to a maximum value at point D in Fig. 9·6*b*, then decreases again with the result that the value at resonance is the same as the value far from resonance; the phase then deviates from zero in the other direction, and finally becomes zero again. The position of the minimum thus varies with frequency in the manner

shown in Fig. 9·7. If the loaded Q of the cavity is high, the circle on the admittance diagram is traversed in a narrow range of frequencies.

The equivalent circuit given in Fig. 9·5 may be generalized to include an output circuit, which can then be interpreted in terms of the cavity coupled by one window by assignment of the proper value to the load.

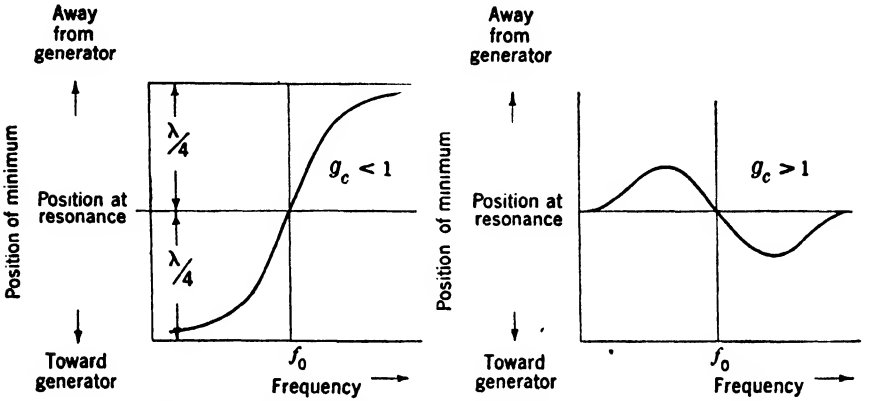

FIG. 9·7.—Variation of minimum position with frequency.

This circuit is shown in Fig. 9·8. All conductances and susceptances are referred to the input line and normalized. At resonance the susceptance terms, lumped together, are zero and the standing wave set up in the input line results from the action of the cavity and load conductance, which are also lumped together. At frequencies off resonance, the susceptance terms contribute to the reflected power and consequently the

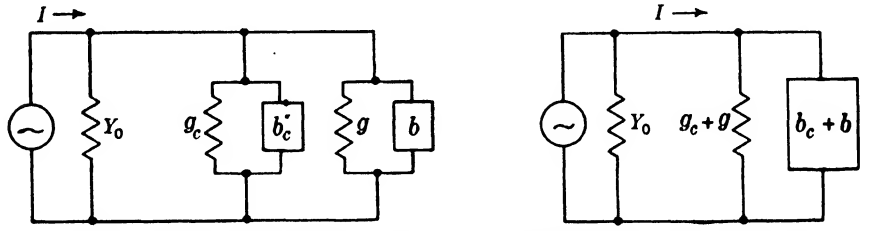

FIG. 9·8.—Equivalent circuit for cavity output loading with matched generator.

standing-wave ratio at resonance is the lowest value obtainable. The loaded Q of the cavity is defined in terms of the resonant frequency and the frequency difference between the half-power points. In order to reduce the power in the load circuit to one half its value at resonance, it is necessary that a value of total load susceptance equal to the total load conductance be added. The loaded Q can be calculated from the equation

$$Q_L = \frac{f_0}{f_2 - f_1} = \frac{\frac{\lambda_1\lambda_2}{\lambda_0}}{\lambda_1 - \lambda_2}, \tag{3}$$

where f_0 and λ_0 are the resonant frequency and wavelength respectively, and f_2 and f_1, λ_2 and λ_1 are the corresponding values at the half-power points. The standing-wave ratio looking into the cavity with an output circuit is given by the equation

$$r = \frac{\sqrt{(1 + g_c + g)^2 + (b_c + b)^2} + \sqrt{(1 - g_c - g)^2 + (b_c + b)^2}}{\sqrt{(1 + g_c + g)^2 + (b_c + b)^2} - \sqrt{(1 - g_c - g)^2 + (b_c + b)^2}}. \tag{4}$$

At the half-power points, $b_c + b = 1 + g_c + g$, so that Eq. (4) reduces to

$$r_{1/2} = \frac{1 + (g_c + g) + \sqrt{1 + (g_c + g)^2}}{1 + (g_c + g) - \sqrt{1 + (g_c + g)^2}}. \tag{5}$$

It is apparent that Eq. (5) gives the same result if $1/(g_c + g)$ is substituted for $g_c + g$. This means that the standing-wave ratio at resonance

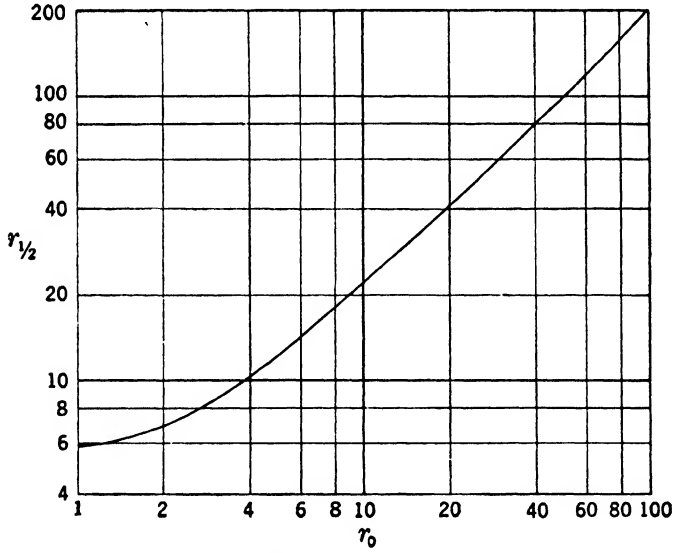

FIG. 9·9.—Plot of $r_{1/2}$ as a function of r_0.

(r_0) can be used in Eq. (5) without regard to the phase of the reflection. A graph of Eq. (5), with $g_c + g$ replaced by r_0, is given in Fig. 9·9. The value of r_0 determines the value of the standing-wave ratio at the half-power points. The frequency difference between these points and the resonant frequency are used to calculate the loaded Q from Eq. (3).

The determination of the unloaded Q of a cavity is particularly simple if the Q of a cavity loaded by only one window is measured. A sample

curve showing a measurement on a 1B27 TR tube in a cavity mounted on the end of a waveguide is shown in Fig. 9·10. Once Q_{L1} is determined, the unloaded Q, Q_0, is calculated from

$$Q_0 = \left(1 + \frac{1}{g_c}\right) Q_{L1} = (1 + r_0) Q_{L1}.$$

When an output circuit is added, it becomes necessary to separate the cavity conductance from the load conductance. Another measurement to determine g_c or the insertion loss must be made in order to calculate Q_0. Two cases are usually of interest: the cavity and the output load are

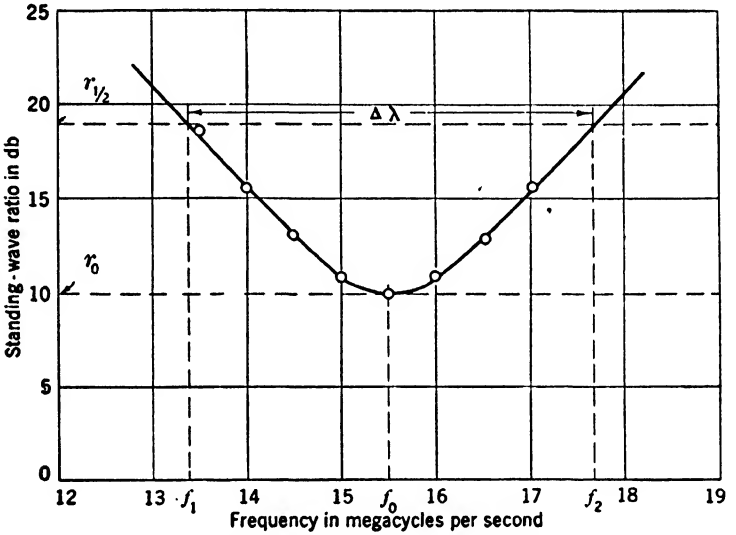

FIG. 9·10.—Typical experimental curve for determining Q_{L1}.

matched at resonance, or the cavity has equal coupling windows. The unloaded Q is given by:

$$Q_0 = \frac{2}{g_c} Q_{L2} \qquad \text{(matched input)}$$

$$Q_0 = \left(\frac{2}{g_c} + 1\right) Q_{L2} \qquad \text{(equal windows)}.$$

As an alternative to the determination of g_c by measurements at resonance with no output circuit, the transmission T of the two-window-coupled cavity and the standing-wave ratio at resonance may be measured. The unloaded Q may be computed from the expression

$$Q_0 = \frac{4(r_0 + 1)}{4r_0 - (r_0 + 1)^2 T} Q_{L2}.$$

If the TR switch is matched at resonance, $r_0 = 1$, and

$$Q_0 = \frac{2}{1 - T} Q_{L2}.$$

It is sometimes more convenient to measure the standing-wave ratio at resonance looking into the TR switch from the two directions than to measure the transmission. Let r_1 and r_2 be two values of the standing-wave ratio. Then

$$Q_0 = \frac{(r_1 + 1)(r_2 + 1)}{r_1 r_2 - 1} Q_{L2}.$$

A check on the accuracy of measurement can often be made using the relation

$$T = \frac{4}{(r_1 + 1)(r_2 + 1)}.$$

In making careful measurements of the Q's of TR tubes in the 3000-Mc/sec frequency range, it is necessary to measure small frequency differences. For example, with a TR tube having an unloaded Q of about 2500 and a Q loaded by one window of 450, it is necessary to determine a wavelength difference of about 0.020 cm. With most coaxial wavemeters, the accuracy of this measurement is hardly better than 10 per cent. A high-Q cavity wavemeter, such as described in Vol. 11, Chap. 5, is necessary.

Another method by which the error can be considerably reduced is by employing a special frequency marker for measuring small frequency differences instead of a wavemeter. The circuit of this device contains a microwave oscillator in conjunction with an oscillator operating in the range of 1 to 20 Mc/sec. The output powers from these two oscillators are mixed together in a crystal mixer. This results in a carrier with sidebands differing from the carrier by multiples of the frequency of the low-frequency oscillator. For example, a carrier frequency of 3000 Mc/sec and a low frequency of 16 Mc/sec give a carrier of 3000 Mc/sec and sidebands of 3000 ± 16 Mc/sec, 3000 ± 32 Mc/sec, and so forth. Thus, with the carrier set at 3000 Mc/sec, a variation of the low frequency from 10 to 20 Mc/sec gives a variation in the first upper sideband over the range from 3010 to 3020 Mc/sec. If the microwave oscillator is stable, the frequency difference can be read to the accuracy with which the 1- to 20-Mc/sec oscillator is calibrated. When this arrangement is used, power from the marker circuit is supplied to one of the input terminals of a spectrum analyzer, and the signal picked up by the probe of the standing-wave detector is supplied to the other input terminal of the spectrum analyzer. The signals are mixed in the crystal in the analyzer. When the two frequencies are brought into coincidence, the signals on

the spectrum-analyzer cathode-ray tube will show interference commonly called "rain," see Fig. 9·11. Since the spectrum analyzer can show two pips from any single microwave frequency, because it contains a superheterodyne receiver, care must be taken to adjust the signals to the same frequency. Two pips on the oscilloscope of apparently equal frequencies might actually differ by twice the intermediate frequency of the receiver. The interference phenomenon will not appear unless the two frequencies are the same. The apparatus is arranged as shown in Fig. 9·12. Suppose that the measurement is to be made of the Q of a TR cavity loaded by one window, at a frequency of 3000 Mc/sec. Oscillator No. 1 is set at 3000 Mc/sec, and the TR cavity is tuned approximately to resonance by adjustment of the tuning mechanism until the standing-wave ratio looking into the cavity is a minimum. The tuning may be accomplished very easily if it is known that the cavity is overcoupled. This is done by

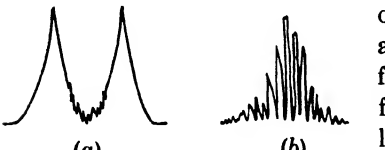

FIG. 9·11.—Interference of signals of two frequencies on spectrum analyzer; (*a*) shows slightly different frequency signals, (*b*) shows signals of equal frequency.

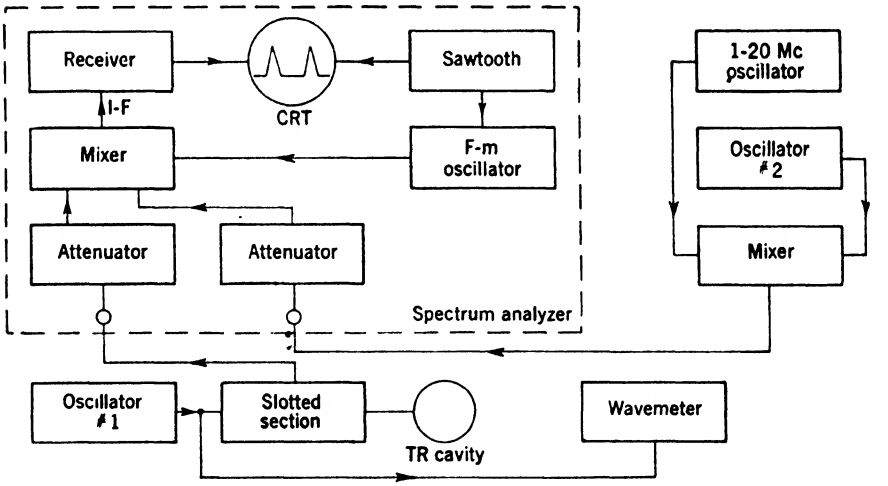

FIG. 9·12.—Schematic diagram of spectrum analyzer, marker circuit, and r-f components arranged for measurement of Q_{L1}.

locating the position of two successive minima in the standing-wave pattern with the cavity completely detuned. The probe of the standing-wave detector is set halfway between these two positions, and the cavity is then tuned until a minimum in the standing-wave pattern appears at this position. Once the cavity is tuned, oscillator No. 2 is adjusted so that with the 1- to 20-Mc/sec oscillator set at some value, say 14 Mc/sec, one of the first sidebands has the same frequency as oscillator No. 1.

This is indicated by the appearance of rain on the oscilloscope. The frequency of oscillator No. 2 *remains fixed* for the rest of the measurement. The marker pip is moved out of coincidence with the main pip by adjustment of the 1- to 20-Mc/sec oscillator, and the standing-wave ratio looking into the cavity is measured. Next the 1- to 20-Mc/sec oscillator is set at some other frequency, for example, 15 Mc/sec. Oscillator No. 1 is tuned until the pips are coincident; the marker pip is moved aside, and the standing-wave ratio at this frequency is measured. This process is continued at the desired frequency intervals over a sufficiently wide band to include the values of $r_{\frac{1}{2}}$ necessary according to the value of r_0.

Some TR tubes, such as the 1B24 and 1B26, are constructed with glass windows and there is no way of actually plugging these windows for Q_{L1} measurements. The cavities can, however, be terminated by means of a short-circuited line. If the short-circuited line is one-quarter guide wavelength long, the glass window will be at a point of maximum field and the loss component of the dielectric constant of the glass adds to the cavity loss. A short-circuited line one-half guide wavelength long does not place a high field at the glass window, but it does cause high currents to flow out of the cavity into the half-wavelength section of line. Unless the coupling between the cavity and the half-wavelength line section is extremely good, there will be loss caused by high currents flowing across poor contacts. Several Q measurements on the same TR tube have shown that the results were more consistent when a quarter-wavelength short-circuited line was used. The values of Q_0 average 2 per cent or 3 per cent higher with the quarter-wavelength line than with the half-wavelength line.

9·4. Pass Band of Broadband TR Tubes.—The principal measurements of interest for bandpass tubes are the measurements of Q and of resonant frequency, for the windows and for the internal elements, as well as for the complete tube. Since the values of Q_{L2} range from 1 to 10, a modulated oscillator and amplifier provide the most accurate means of measuring the standing-wave ratios in the range from one to two in voltage.

To determine the Q of one of these elements, the element is inserted in a section of waveguide between two slotted sections, and the line is terminated in a matched load. The standing-wave ratio as a function of wavelength is then measured for several points and a curve plotted from the data. The resonant wavelength is the wavelength for which the standing-wave ratio is a minimum, and the Q is calculated from the formula

$$Q_{L1} = \frac{b}{2g} \frac{\lambda_0}{\Delta\lambda}, \tag{6}$$

where b is the susceptance at the wavelength $\Delta\lambda$ away from resonance, λ_0 is the resonant wavelength, g is the total loading (equal to $g_L + g_c$), g_L is the terminating conductance (usually unity), and g_c is the shunt conductance of the resonant element. The susceptance b may be calculated for any value of r, the voltage standing-wave ratio, by the formula

$$b = \sqrt{\frac{(r - g)(gr - 1)}{r}}.$$

The conductance g is determined by the standing-wave ratio at resonance, as in the case of a cavity. If g_c can be neglected, and g_L is unity, then Q_{L1} can be written in terms of r and λ alone,

$$Q_{L1} = \left(\frac{r - 1}{2\sqrt{r}}\right)\frac{\lambda_0}{\Delta\lambda}. \tag{7}$$

A second method of evaluating Q_{L1} from measurement employs the fact that the absolute magnitude of the reflection coefficient is a linear function of wavelength near resonance for negligible g_c. By using Eq. (2·13), $d\,|\Gamma|/d\lambda$ is calculated,

$$2\,|\Gamma|\frac{d\,|\Gamma|}{d\lambda} = \frac{8b}{(4 + b^2)^2}\frac{db}{d\lambda}. \tag{8}$$

If this is combined with Eq. (6), and $db/d\lambda$ eliminated, and the value of $|\Gamma|$ is used, then

$$Q_{L1} = \frac{(4 + b^2)^{3/2}}{16}(\lambda_0)\frac{d|\Gamma|}{d\lambda}, \tag{9}$$

or for small b,

$$Q_{L1} = \frac{\lambda_0}{2}\frac{d\,|\Gamma|}{d\lambda}\left[1 + \frac{3}{8}b^2 + \cdots\right] \tag{10}$$

$$\approx \frac{\lambda_0}{2}\frac{d\,|\Gamma|}{d\lambda}. \tag{11}$$

To obtain $d|\Gamma|/d\lambda$, the slope of the curve of $|\Gamma|$ plotted as a function of λ is taken near resonance. If the measurement is made at $b = \frac{1}{2}$, Eq. (11) gives a value for Q_{L1} within 10 per cent of the value obtained from the accurate equation. Care should be taken to measure the slope far enough from λ_0 so that the effect of conductance is negligible, and the linear portion of the resonance curve should be used. Sometimes, for wavelengths on one side of resonance, negative values of $|\Gamma|$ are plotted so $d|\Gamma|/d\lambda$ can be obtained from data on both sides of resonance. Figure 3·5 of Chap. 3 shows some theoretical curves of the variation of $|\Gamma|$ with b, and Fig. 3·6 of Chap. 3 is an example of an experimental determination of Q_{L1}.

The determination of the transmission characteristics of the bandpass TR tube involves essentially only two measurements: (1) the reflection

loss over the band and (2) the dissipation loss. The useful frequency range is determined mainly by the reflection loss, since the insertion loss is small. A measurement of the standing-wave ratio looking toward a TR cavity terminated in a matched line at various points in the frequency band enables the reflection loss to be calculated easily.

Another method of measurement of the bandpass characteristic of low-Q TR tubes utilizes a magic-T impedance bridge. If the magic T is arranged as shown in Fig. 9·13, the power in the output arm (4) is a measure of the magnitude of the voltage reflection coefficient of the unknown impedance, Z_x. The error encountered depends on the match of the detector and generator and the mechanical asymmetry in the

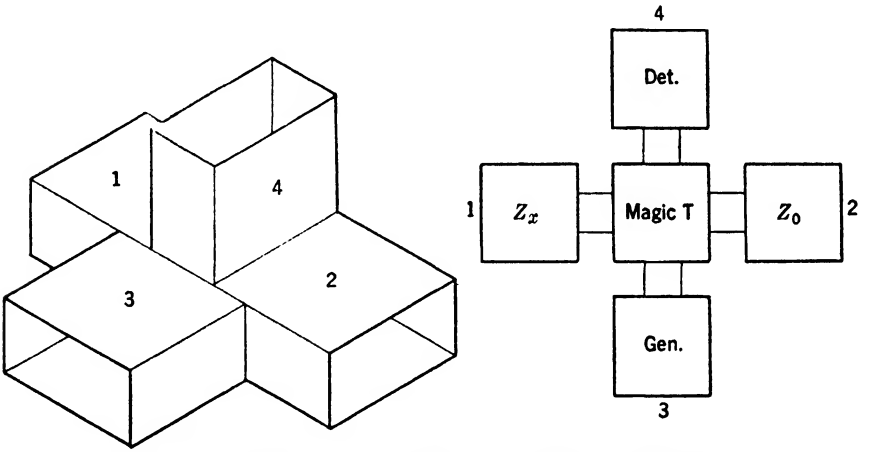

FIG. 9·13.—Arrangement for magic T for impedance-bridge circuit.

magic T. If this magic T is used with a modulated signal source and a crystal detector, the tuning of a device which must be matched at one frequency, or which must have a reflection coefficient less than a certain value at the one frequency, is simple. The tuning of the device is adjusted for minimum power in the output arm. With a perfect magic T, this will be zero for match; otherwise it will depend on the desired reflection coefficient.

With appropriate precautions, it is possible to use a single magic T with several input frequencies. By the use of a corresponding number of local oscillators in a circuit similar to a spectrum analyzer, the power from the output arm may be displayed on an oscilloscope in the form of pips, one pip for each frequency. If three frequencies are used, the behavior of the reflecting element at the midband and band-edge frequencies is easily determined, and may be observed at a glance. If the device is calibrated with a reflection of known magnitude, quantitative data may be obtained. For example, if it is desired to check a resonant

window or a single resonant element, such as is used in a bandpass TR tube, the three frequencies corresponding to midband and the two band-edge frequencies are set on the bridge. The element under test, backed by a matched load, is put on one arm of the magic T. The heights of the pips then give the desired information. The tuning of an element can be accomplished by adjusting for a symmetrical pattern. In addition to a quick examination of the characteristics of single elements, it is also possible to tune two-element bandpass TR tubes and to check the over-all response curve, that is, the standing-wave ratio looking through the tube into a matched load, at three different points in the pass band.

This bridge is excellent for production checking of components, such as the windows of the bandpass TR tube, especially for tuning, since the necessary symmetry of the Q-curve for the proper frequencies can be noted at a glance. Any necessary changes on transmission-resonant elements, such as grinding the glass in the windows or filing metal in other types of elements, may be quickly checked between steps by noting the changes in the pips.

In the preceding discussion it was shown how the bandpass characteristics of TR tubes and filters might be checked, and a method was suggested for tuning the individual elements of one of these devices. The elements of a bandpass TR tube are usually spaced by a quarter wavelength in the guide and they are all tuned to the same frequency. It is not practical, however, to tune the elements of one of these tubes before the tube is assembled, because strains set up in the process of assembly and soldering may seriously detune the resonant elements. The detuning is unpredictable in nature, so it cannot be compensated for by any initial detuning. For this reason the resonant elements of a broadband TR tube, with the exception of the input and output windows which have a very low Q, are made tunable and the tuning is done after assembly.

No single tuning procedure can be outlined which applies to all bandpass TR tubes, but the following procedure applies for most tubes.

1. Mount the tube between a slotted section and a well-matched termination, and use adapter flanges when necessary.
2. Short-circuit all of the elements by turning in the tuning screws until they make contact across the element.
3. Set the oscillator at the proper frequency (usually the center of the desired pass band).
4. Set the probe at a minimum in the standing-wave pattern.
5. Tune the first element until the position of the minimum moves toward the tube a distance equal to the spacing between the elements. If this spacing is one-quarter guide wavelength, as it usually is, the probe may be set halfway between two minima and

the first element tuned until that point becomes a minimum in the standing-wave pattern.

6. Turn the tube end for end and repeat steps (4) and (5), the third element is now nearest the generator.
7. Tune the middle or second element to give minimum reflection. This may be done by first tuning the element for maximum power transmission and then trimming to give the best match. When this is done, however, the generator should be fairly well matched; otherwise there may be considerable difference between the points of maximum power transmission and minimum voltage standing-wave ratio.

If the higher-mode attenuation in the waveguide is not sufficient to eliminate the effects of higher modes, it is necessary to make the element spacing different from a quarter wavelength and to modify the tune-up procedure. It is usually desirable to tune at the midband frequency, in order to assure the best symmetry of the bandpass characteristic. When this is done the position of the minimum is moved a distance different from the element spacing (step 5 of the tuning procedure). This distance is determined experimentally. It is also possible to evolve a tuning procedure which allows tuning at a point which is not the center of the pass band, this point is usually one of the points where a minimum standing-wave ratio is obtained. This method may give satisfactory results, but tuning at the center of the pass band usually gives a more symmetrical characteristic.

9·5. Impedance Measurements of ATR Tubes.—ATR tubes of two different types are of interest. One tube is the high-Q tube and the other

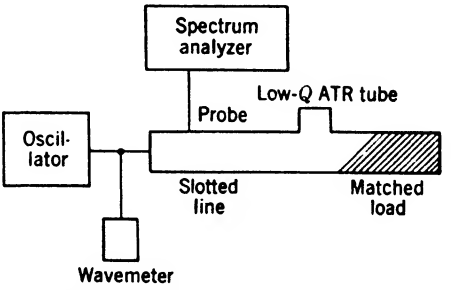

FIG. 9·14.—Measurement of standing waves on low-Q ATR tubes.

is the low-Q tube. The measurements on the high-Q tubes are the same as those discussed in Sec. 9·3 for the TR tube loaded by one window. The measurement of a low-Q ATR tube is made in a different manner from that of a high-Q tube, but again its low-power behavior is determined by making standing-wave measurements. A typical setup is shown in Fig. 9·14.

The ATR tube is mounted in the broad side of the waveguide and, to a first approximation, may be represented by a shunt-resonant circuit in series with the line (Fig. 9·15*a*). The response curve is such that a high standing wave is produced at resonance, while off resonance the impedance of the ATR tube is low (Fig. 9·15*b*).

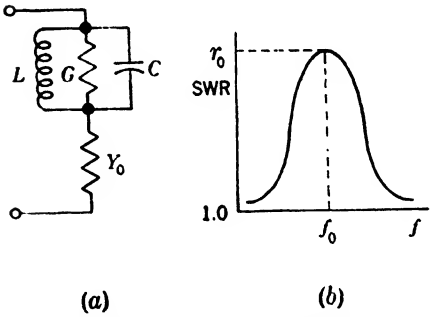

FIG. 9·15.—Equivalent circuits and response curve for low-Q ATR tubes.

If the Q of the tube is sufficiently low, the standing-wave ratio will be large over such a range that a coaxial wavemeter is accurate enough to determine the wavelength readings. A spectrum analyzer is used because the standing-wave ratios are so large. Figure 9·16 shows the type of curve obtained.

The loaded Q of such an ATR tube is defined in terms of the rate of change of susceptance with frequency. If a generator of zero internal impedance and a conductance loading of unity are assumed, then

$$Q_{L1} = \frac{b}{2(g+1)} \frac{f}{\Delta f},$$

where Q_{L1} indicates that the tube is loaded externally by a conductance of unity. The reflection coefficient looking past the tube at a matched load is

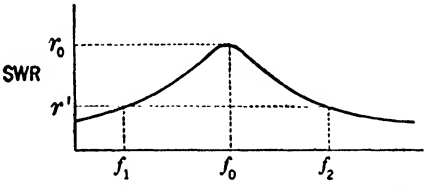

FIG. 9·16.—Standing-wave ratio vs. wavelength for broadband ATR switch.

$$\Gamma = \frac{Z-1}{Z+1},$$

where

$$Z = 1 + \frac{g}{g^2+b^2} - j\frac{b}{g^2+b^2},$$

and

$$|\Gamma| = \frac{|Z-1|}{|Z+1|} = \frac{\sqrt{g^2+b^2}}{\sqrt{(2g^2+g+2b^2)^2+b^2}}.$$

This gives for the standing-wave ratio

$$r = \frac{1+|\Gamma|}{1-|\Gamma|}$$

$$r = \frac{\sqrt{(2g^2+g+2b^2)^2+b^2}+\sqrt{g^2+b^2}}{\sqrt{(2g^2+g+2b^2)^2+b^2}-\sqrt{g^2+b^2}}.$$

At resonance, b is zero and the standing-wave ratio will be

$$r_0 = 1 + \frac{1}{g},$$

or

$$g = \frac{1}{r_0 - 1}. \tag{12}$$

The point at which $b = 1$ is convenient to use for the determination of Q_{L1}. The standing-wave ratio r' at the frequency at which $b = 1$ then depends on the value of g,

$$r' = \frac{\sqrt{(2g^2 + g + 2)^2 + 1} + \sqrt{g^2 + 1}}{\sqrt{(2g^2 + g + 2)^2 + 1} - \sqrt{g^2 + 1}}. \tag{13}$$

From Eqs. (12) and (13), r' can be expressed as a function of r_0, and Fig. 9·17 shows this relation.

A second method for determining the Q of a low-Q ATR tube, which is especially suitable at short wavelengths, makes use of the measurement of the phase shift in the neighborhood of resonance. This is particularly convenient for low-Q devices because the phase varies rapidly while the standing-wave ratio varies by only a very small amount. The two methods have been found to give results agreeing within about 5 per cent at several wavelengths. The position of the minimum is measured in the conventional manner. A high-Q wavemeter or a marker circuit as described in Sec. 9·3 is required, since the range of measurement extends over only a few megacycles. The value of Q is given by

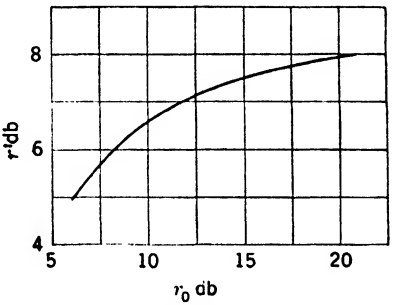

FIG. 9·17.— Standing-wave ratio at points for which $b = 1$ as a function of standing-wave ratio at resonance.

$$Q_{L1} = \frac{\pi c}{\lambda_0 \lambda_g} \left(\frac{1 + 2g}{1 + g} \right) \frac{dl}{df},$$

where c is the velocity of light, λ_0 the resonant wavelength in free space, λ_g the guide wavelength, g is the shunt conductance of the tube, and dl/df is the rate of change of the position of the minimum with frequency. The minimum for which the value of dl/df applies is that which occurs nearest to the plane of symmetry of the tube. Since this is not usually the point at which the measurements are taken, a correction for the

length of line must be made. This is

$$\frac{dl}{df} = \frac{dl'}{df} - n\frac{d\lambda_g}{df},$$

where dl'/df is the measured slope of the line obtained by plotting the observed position of the minimum as a function of frequency and n is the number of wavelengths measured, at resonance, from the minimum nearest the ATR tube to the probe. It is possible to use a magic T in such an arrangement and the correction term is not necessary (see Sec. 9·6). In practice, λ_g is best determined by actual measurement between positions of minima in the standing-wave pattern, but λ_g can be calculated from the known frequency and a careful measurement of the waveguide dimensions. It may happen that the measurements are not centered about the resonant frequency but since dl/df is so nearly independent of frequency. no great precautions are necessary.

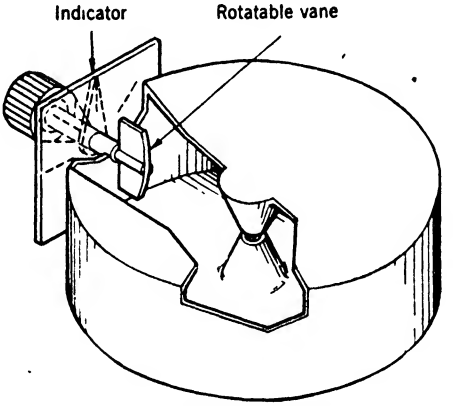

FIG. 9·18.—Tuning check on fixed-tuned TR tubes.

9·6. Low-level Production Testing.—Standing-wave measurements are time-consuming and therefore impractical for production testing if several measurements are necessary. The operator should be able to get the information by a glance at a pattern on an oscilloscope screen or from the reading of a meter. The determination of the important parameters of TR and ATR tubes in production testing is often facilitated by the construction of special apparatus. Some of the quantities which must be measured for each tube are tuning, tuning range (or pass band), unloaded Q, leakage power, keep-alive firing and sustaining voltages, and insertion loss.

Fixed-tuned TR tubes of the 721 type are checked for tuning in a cavity of a given diameter. Owing to variation in construction, the tuning of tubes will scatter about the desired resonant frequency and it is necessary to specify a tolerance. It is impractical to determine the

actual resonant frequency for each tube in a fixed test cavity; therefore, the tuning of the cavity is varied through a desired range and the tube is accepted if resonance occurs in this range. This tuning is accomplished by means of a rotatable vane in the cavity (see Fig. 9·18). The resonant frequency varies from a maximum, when the vane is perpendicular to the axis of the cavity, to a minimum when the vane is parallel to the axis. The amount of tuning depends principally on the vane size and on the clearance in the parallel position. Coupling to the cavity may be either by loop or by iris as convenient. Resonance is determined by noting the occurrence of a maximum in the rectified current of a crystal coupled to the cavity as the vane is turned.

Tunable-gap tubes, such as the 1B27, are checked for tuning range in a cavity of specified diameter at two frequencies, and the tubes are

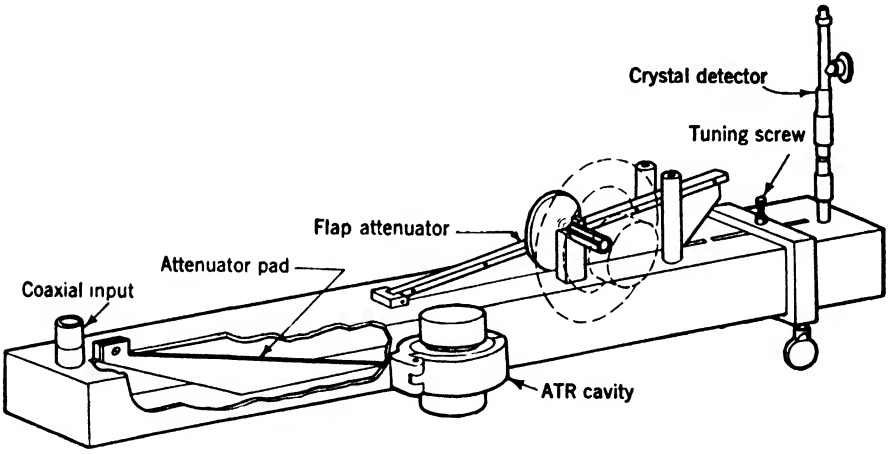

FIG. 9·19. Measurement of Q by power drop in load.

required to resonate at these frequencies within a specified number of turns of the tuning screw. This tuning check is usually done in the same cavity used for other low-level tests (for example, Q_0) by simply plugging in oscillators set at the required frequencies.

The measurement of Q_0 is simplified by the use of the power-drop method. Figure 9·19 shows a sketch of a test bench in which this principle is applied. Since the coupling to the cavity is constant, the loss is inversely proportional to the Q_0 of the TR tube. The loss, or power drop, can consequently be used as a measure of Q_0. In practice, the flap attenuator is calibrated in decibels and is adjusted to keep the detector current constant. The apparatus is calibrated by checking a few tubes of known Q_0.

The detector is a crystal in a special holder designed to give a reasonable match into an average crystal. Final matching is accomplished by

means of a sliding-screw tuner. Figure 9·20 shows a cross section of the crystal holder. The d-c meter on which the crystal current is read is calibrated, by means of the flap attenuator, in terms of decibel drop in power from full scale. A tube is inserted in the cavity, tightly clamped, and tuned far off resonance; the meter is set, by means of the flap attenuator, to read full scale; the tube is tuned to resonance, and the meter reading noted. Tubes of less than a certain power drop are rejected. Keep-alive interaction may also be checked on such a test bench, and, if additional oscillators are provided, tuning ranges may also be determined.

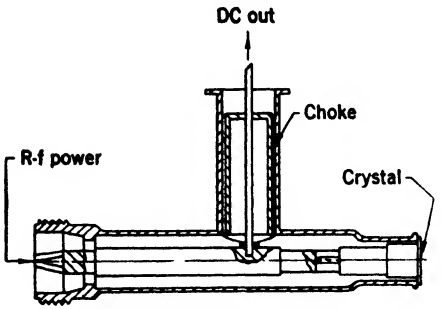

FIG. 9·20.—Crystal holder.

The apparatus shown in Fig. 9·21 is designed for production testing of low-Q ATR tubes in the 10-cm region. The principal feature is a rotatable mount for the tube. The axis of rotation is coincident with the axis of the tube, and therefore, a second measurement with the tube rotated 180° from its initial position affords a correction for lack of symmetry in the position of the resonant window. The instrument is first

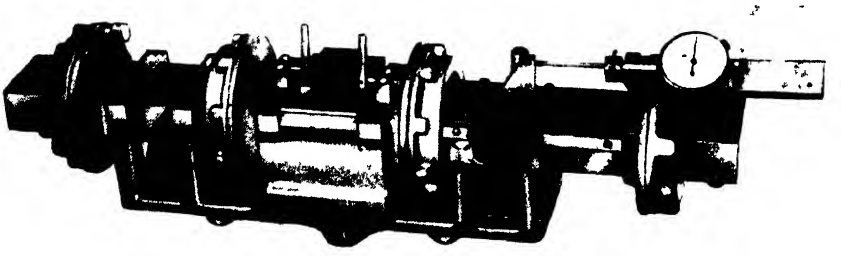

FIG. 9·21.—Production test bench with reversible mount for low-Q ATR tubes.

calibrated with a tube which is tuned to the correct frequency. This tube may be an actual tube, or if several different types are to be checked, a section of waveguide with a window and movable plunger can be used. For a tube of each type, the plunger is adjusted for minimum transmission past the tube at the proper frequency, and the average reference point of the standing-wave minimum for the two positions of the tube is determined. Figure 9·22 gives a schematic view of the apparatus. The points A and A' are choke joints at the ends of the rotatable mount and P is the position of the minimum in the standing-wave pattern when a correctly tuned tube is in the mount. If $\Delta l'$ is the measured value of the

phase shift, Δb may be calculated from the expression

$$\Delta b = (1 + 2g)\frac{2\pi}{\lambda_g}\Delta l'. \tag{14}$$

Once the tolerance in the value of Δb, at the frequency for which the tube is supposedly tuned, is determined, this measurement gives an indication

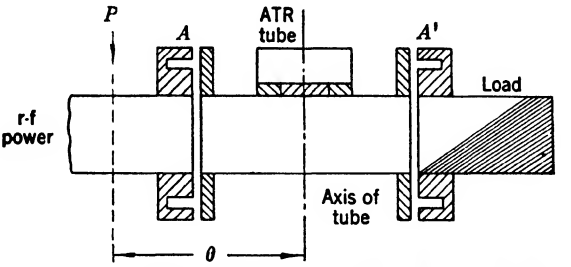

FIG. 9·22.—Schematic diagram of low-Q ATR tubes with reversible mount

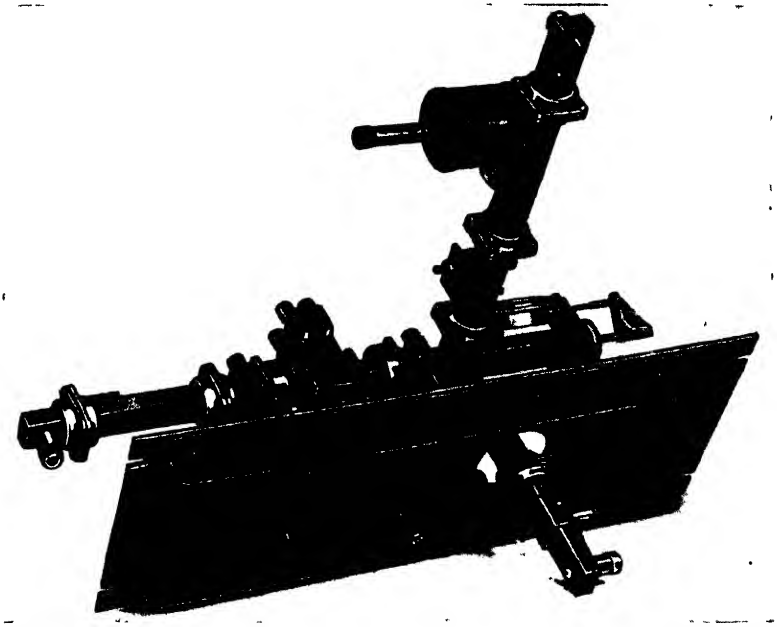

FIG. 9·23.—Magic T and reversible mount combined as impedance bridge for measuring phase shift of low-Q ATR tubes.

of satisfactory performance of the tube. One point to be noted is that the reference point P should be as close as possible to the window. In the 10-cm region it is easy to make the distance three-quarters of a guide wavelength and therefore, the correction for line sensitivity is small. It can always be accounted for in these measurements. At very short

wavelengths, however, the reference point may be several guide wavelengths from the tube, and consequently, the frequency sensitivity of the line may cause serious errors; slight changes in the oscillator frequency are especially troublesome at short wavelengths.

These troubles may be corrected by the use of a reversible mount in conjunction with a magic T. Figure 9·23 shows a photograph of such an arrangement used for measuring 3-cm tubes (1B35 and 1B37 tubes). A schematic diagram of this circuit is shown in Fig. 9·24. If an ATR tube is placed in one arm of the magic T and a short-circuiting plunger in the opposite arm, the plunger may be adjusted to a position where the power into the detector in arm (4) is a minimum. If, at this position, the distance b' from the reference plane of the magic T to the open circuit presented by the plunger (a quarter guide wavelength from the front face of the plunger) is equal to the distance c', the line sensitivity will be a minimum. Any phase shift $\Delta l'$ due to detuning of the tube is compensated by a shift of the plunger of the same amount Δl, and the susceptance Δb introduced by a tube that is slightly off resonance may be calculated from Eq. (14). The determination of Δl is facilitated by using a dial indicator connected to the plunger. Using a tunable tube, a reference point for a correctly tuned tube is determined by setting the indicator to zero for the plunger position for which the power into arm (4) is a minimum. Thus, if a tube inserted in the mount shifts the phase by an amount Δl, the plunger must be moved by an amount Δl and in the same direction relative to the T-junction in order to get minimum power out of arm (4).

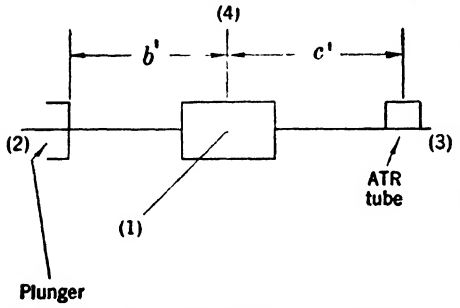

FIG. 9·24.—Schematic diagram of impedance bridge.

The value of the shunt conductance g of the ATR tube may be determined by a measurement of the voltage standing-wave ratio at resonance, or the magic T may be calibrated so that the ratio of power out of arm (4) to the power into arm (1) determines g. This can be done only if the magic T is fairly well matched and not seriously asymmetrical. To calibrate the magic T, it is sufficient to set the power at an arbitrary level and measure the relative power out of arm (4) for various values of voltage standing-wave ratio in the arm which normally holds the tube mount.

Production testing of bandpass TR tubes at low power levels is accomplished with the aid of the triple-frequency impedance bridge. The oscillators are adjusted to midband and band-edge frequencies, after

which it is necessary only to place the tube, backed up with a matched load, on one arm of the magic T and see if the pips show a standing-wave ratio less than a specified value at the three frequencies.

9·7. Leakage-power Measurements.—In addition to the determination of the low-power characteristics of TR and ATR tubes, it is necessary to examine their behavior at high power levels, that is, at transmitter-power levels from a few watts up to powers greater than a megawatt. The principal quantities of interest, in connection with high-power operation, are the leakage power through the TR switch when it has fired, power loss in the tube itself, and recovery time. The complete information about the high-level performance of TR and ATR tubes involves a further subdivision of these quantities and a wide variety of careful measurements of each one.

The leakage power which gets through a TR tube during the transmitter pulse amounts to only a few microwatts average power, for most tubes, and is most conveniently measured by means of a thermistor and thermistor bridge. Wollaston-wire bolometers, thermocouples, and crystals are less rugged than thermistors used at microwave frequencies. The thermistor element mounted in a broadband mount and used with a type TBN-3EV bridge affords a means of measuring the low power which gets through the TR switch. The type of mount depends on the output coupling of the cavity employed for the leakage-power measurement. The cavity may be either iris- or loop-coupled to a coaxial line which is terminated in a coaxial-line thermistor mount. For bandpass TR tubes or for other tubes employed with waveguide, a transition to coaxial line may be used, or the thermistor may be mounted in the waveguide. The output coupling of the TR cavity is adjusted on low-level r-f power, and therefore, a match is seen at the input terminals (see Sec. 9·3). The reflection will vary somewhat among tubes of the same type, because the unloaded Q's are different, but this variation is usually not serious. A drawing of a typical r-f circuit in $\frac{7}{8}$-in. coaxial line, for use at a peak-power level up to 100 kw, is shown in Fig. 9·25.

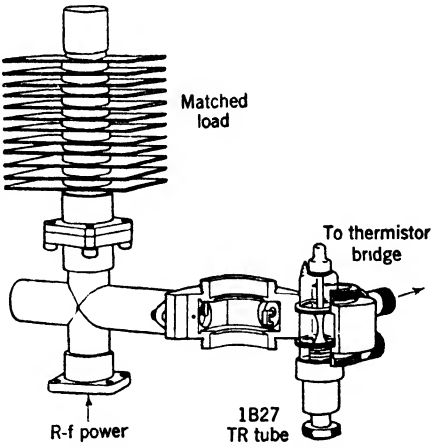

FIG. 9·25. Leakage-power equipment for medium-power level.

At higher power levels a waveguide installation is used (see Fig. 9·26). The cavity is usually shunt-coupled to the waveguide and provided with

a coaxial output line, terminated with the matched thermistor. The cavity output coupling is adjusted for matched input to the cavity. This is accomplished in the following way: a plunger is substituted for the transmitter and a low-level signal is introduced from the load end of the transmission line. A position of the plunger is found for which tuning the TR cavity with no output coupling results in no change in the standing-wave pattern as the cavity is tuned through resonance. This means that the plunger is in the right position to short-circuit the cavity. Next the plunger is moved by a distance of a quarter guide wavelength, and therefore, the low-level signal is effectively introduced directly into the cavity. The output line is added to the cavity, and the coupling is adjusted until the standing waves disappear on the input side of the cavity. The plunger is replaced by the transmitter, and the apparatus is ready to measure leakage power. A directional coupler to monitor the line power facilitates studies of leakage power as a function of line power. For checking the zero setting of the thermistor bridge, a gate, either at the input or output side of the cavity, which will cut the r-f power off entirely from the thermistor, may be used. Figure 9·27 shows the construction of a gate suitable for 3-in. by 1½-in. waveguide.

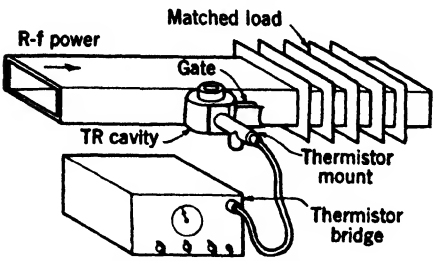

FIG. 9·26.—Waveguide high-power leakage power measurement.

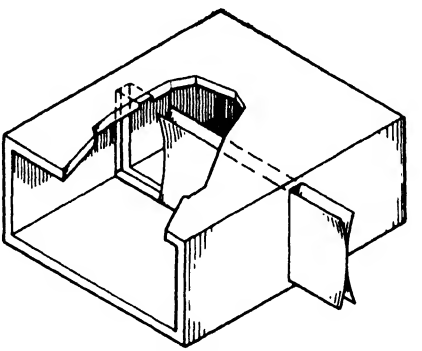

FIG. 9·27.—Gate for large waveguide.

The transition from waveguide to coaxial line may be made by means of a probe coupling, or a doorknob or a crossbar transition may be used. For wavelengths in the 10-cm region, one of the most satisfactory combinations is a thermistor mounted in ⅞-in. coaxial line and a crossbar transition from 3- by 1½-in. guide to ⅞-in. line. It is necessary to check the match in the waveguide portion at the wavelength used. In general, the probe and crossbar transitions are not matched over as broad a band as is the doorknob transition. Figure 9·44 is a sketch of a crystal holder using the crossbar transition. In the 10,000-Mc/sec region the thermistor mount is entirely in waveguide. Built into the unit is a gate which consists of a vane pivoted to swing between a choke-and-flange joint in a

waveguide section (see Fig. 9·28). The temperature sensitivity of the thermistor can be reduced by enclosing the unit in a box filled with rock wool or other insulating material.

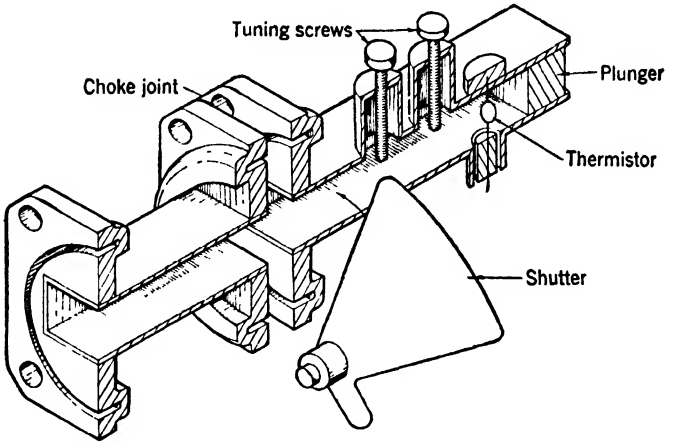

FIG. 9 28.—Thermistor mount and gate for 3-cm measurements.

For measurement of the leakage power of pre-TR tubes, provision for known attenuation between the tube and thermistor must be made, since the leakage power is about 1000 times that of a TR tube. A directional

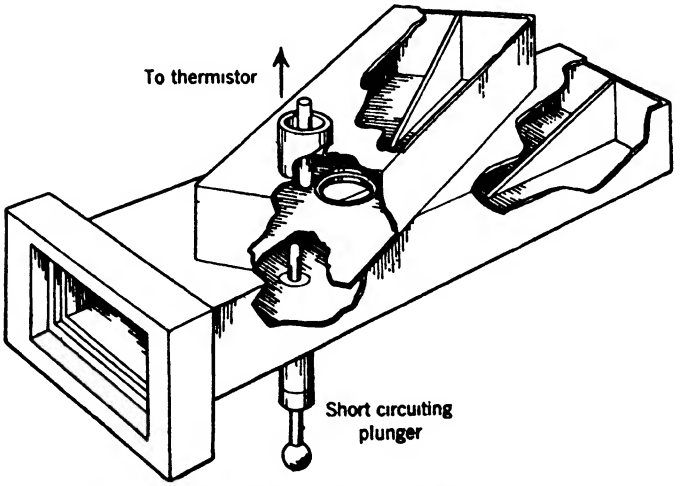

FIG. 9·29.—Termination for use in measuring leakage power of pre-TR tubes.

coupler and matched load accomplish this very well. In addition, a plunger (¼ in.-diameter rod) placed at the proper distance from the pre-TR tube acts as a gate to shut off the power from the thermistor. Figure

9·29 shows this section of waveguide including the termination, plunger, directional coupler, and transition to thermistor mount.

The measurement of the leakage power as described gives the total average leakage power, that is, both flat and spike, and both direct and arc coupling. The thermistor bridge indicates the average power incident on the thermistor, and this value is usually in the range of 10 to 150 μw for line powers up to 100 kw peak power. If P_{ave} is the average power, τ is the pulse length, and ν is the pulse repetition frequency, the average power during the pulse, P_k, is

$$P_k = \frac{P_{ave}}{\tau\nu}. \tag{15}$$

This is, of course, not the peak r-f power in the pulse. Crystal-burnout studies indicate that the quantity of interest is the total energy in the spike. Thus, some separation of energies of spike and flat must be made. The total energy per pulse, W_τ, is given by

$$W_\tau = \frac{P_{ave}}{\nu}. \tag{16}$$

The determination of the spike energy is described in the next section. The flat energy per pulse and, hence, the flat power, is then found by subtracting the spike energy from the total leakage energy.

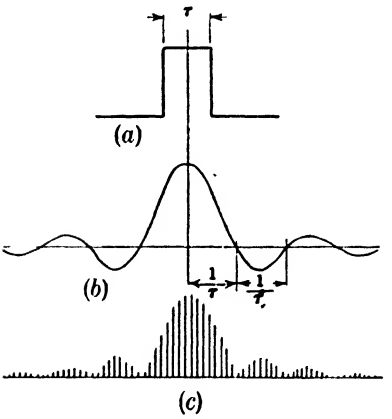

FIG. 9·30.—Characteristics of rectangular pulse: (*a*) single pulse; (*b*) amplitude spectrum; (*c*) appearance of spectrum analyzer scope.

For all these measurements, it is necessary to know both ν and τ accurately. The pulse recurrence frequency ν is easily measured with a calibrated audio oscillator and oscilloscope. Several methods may be used to measure the pulse length. A common method is to use a sine wave, whose frequency is accurately known, to calibrate the sweep speed of a synchroscope or r-f envelope viewer. Once the sweep is calibrated, the pulse length is determined by viewing it on the oscilloscope.

Another method of measuring the pulse length consists of applying a small amount of r-f power to a spectrum analyzer and making use of the characteristic spectrum of the rectangular pulse form. The pulse length can be calculated by measuring the wavelength difference between a known number of zeros of the spectrum. Figure 9·30 shows the spectrum

of a rectangular pulse. If f_m is the frequency corresponding to the m^{th} zero on the right, and f_n is the frequency corresponding to the n^{th} zero on the left, then

$$\tau = \frac{m + n}{f_m - f_n}.$$

9·8. Measurements of Spike Energy.—Once the total average leakage power has been determined, some scheme for measuring the spike energy

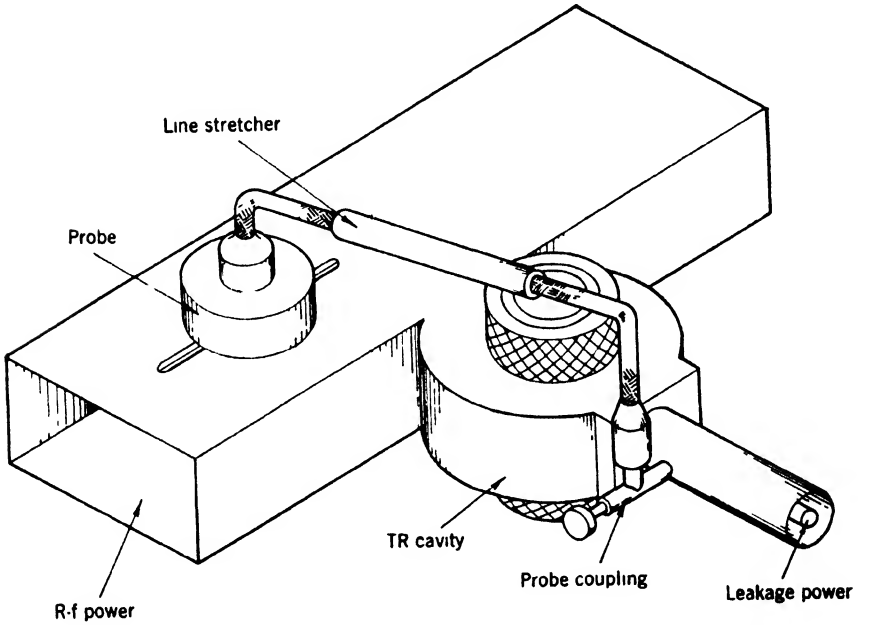

FIG. 9·31.—Cancellation circuit for measurement of spike energy.

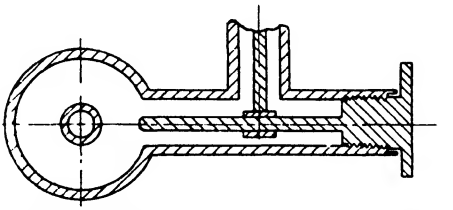

FIG. 9·32.—Adjustable probe coupling to coaxial line.

separately from the flat energy is necessary. One method of measuring the energy in the spike utilizes the cancellation principle. A portion of the r-f energy is coupled out of the main line and into the output line from the TR cavity in the proper phase to cancel out the flat energy and leave only the spike energy. The spike energy can then be measured.

The arrangement for doing this is shown in Fig. 9·31. The magnitude of the bypassed power is varied by means of the adjustable probe at the main line or at the cavity output terminals. A cross section of this coupling is shown in Fig. 9·32.

The proper adjustment of the cancellation circuit for the elimination

FIG. 9·33.—Pulse before and after cancellation of flat.

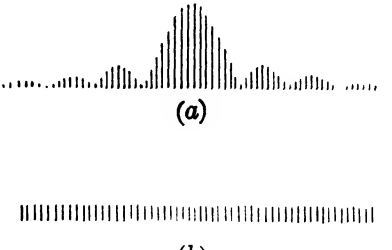

FIG. 9·34.—Spectrum of pulse before and after cancellation of flat.

of the flat energy requires some means of detection by which the adjustment may be checked. Several schemes may be used. One is to replace the thermistor by a reasonably well-matched crystal and to view the output voltage on an r-f envelope indicator. On a fast sweep, the spike energy and the flat energy are easily visible and the circuit is adjusted until the flat energy is canceled (see Fig. 9·33). When the crystal has been replaced by the thermistor, the power in the spike alone is measured. Subtraction of spike power from the total power then gives the flat power. Conversion to spike energy is made as just described [Eq. (16)]. Another

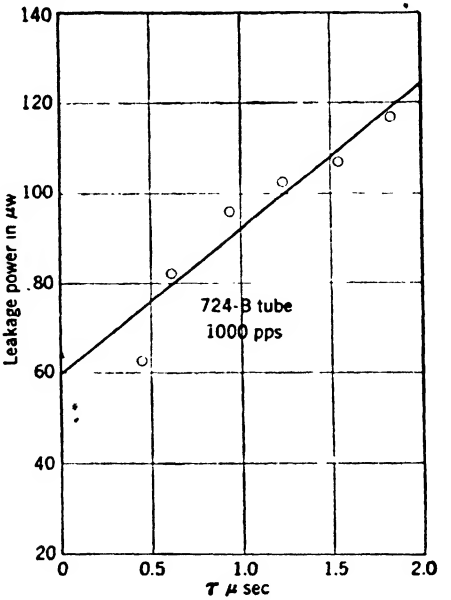

FIG. 9·35.—Total leakage power vs. pulse length. Level at $\tau = 0$ gives spike energy.

method is to use a rapidly acting thermistor bridge and to adjust the circuit for minimum power into the thermistor. This assumes that the flat is really flat and that no harmonic frequencies are present. The adjustment may also be made by picking off a portion of the energy from the slotted section and viewing it on a spectrum analyzer as the coupling is varied. The spectrum of a rectangular pulse is shown in Fig. 9·34. As the flat is canceled out, the spectrum changes to a series of pips of very nearly equal height.

A method that requires less equipment but is capable of giving good results is that of using different pulse lengths at one peak power. If the spike is assumed to be the same for all pulse lengths, a plot of the energy in

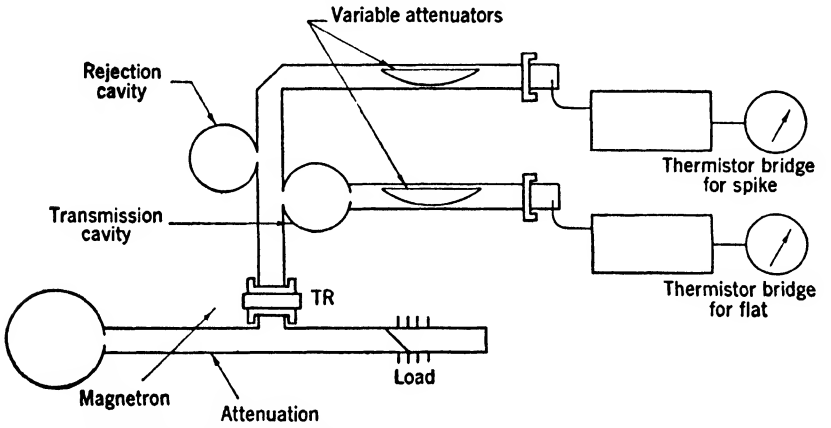

FIG. 9·36.—Separation of spike and flat power by pass and rejection cavities.

the pulse as a function of pulse length, extrapolated to zero pulse length, gives a value for the spike energy. Figure 9·35 shows some data[1] taken in this manner with a 724B tube.

Another method for the separation of the spike and the flat energy has been used by Fiske.[2] Advantage may be taken of the difference in the frequency spectra of the spike and the flat by the use of filters. A transmission cavity placed at the side of the waveguide which leads from the TR tube, see Fig. 9·36, allows the flat power to fall on a thermistor and this power can be measured. Since the spike has such a wide distribution of energy in frequency, only a small fraction of it passes through the transmission cavity if the Q is near 1000. The flat power is forced to enter the transmission cavity by means of a rejection cavity on the side of the waveguide a quarter of a wavelength from the transmission cavity.

[1] J. W. Clarke, "A Method of Analyzing Leakage Power Data," BTL MM-43-140-50, Oct. 11, 1943.

[2] M. D. Fiske, H. N. Wallace, and A. D. Warner, "Final Technical Report on Contract OEMsr-1306," GE, Schenectady, Nov. 7, 1945.

The rejection cavity acts as a high-Q ATR tube. The flat energy passes both the transmission and rejection cavities and enters a second thermistor and the power can be measured. The method may be difficult to use in practice since the cavities must be precisely tuned. With proper care the losses in the cavities need not be excessive.

9·9. Direct-coupling Measurements.—The direct-coupling power is the power which is coupled through a TR cavity by fields other than those of the normal mode. It is the power which is coupled through when the arc is replaced by a perfect short circuit. The equipment and technique for measuring this power are the same as those used for measuring total leakage power, except that the TR tube is replaced by a dummy tube, in which a metallic short circuit is substituted for the discharge gap. With high-Q tubes such as the 1B27, 1B24, 721, or 724, an old tube with the cones soldered together is quite satisfactory as a dummy tube. The power then measured by the thermistor is the direct-coupling power.

The direct-coupling attenuation for a given tube may also be measured at low power levels by using a spectrum analyzer. The TR switch is adjusted in the same way as for the measurement of Q_{L2} (see Sec. 9·3) with a matched output line and with coupling adjusted for matched input to the cavity. The output line is connected to a spectrum analyzer and the attenuator is adjusted to a convenient height of signal on the cathode-ray-tube screen. The TR tube is replaced in the cavity by a tube with a short-circuited gap and the attenuator is readjusted to bring the signal back to the same height. The difference in attenuator readings then gives the direct-coupling attenuation in decibels.

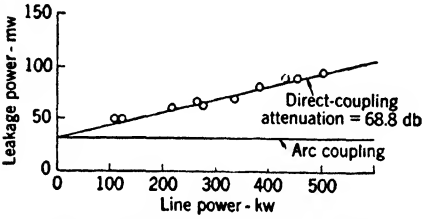

FIG. 9·37.—Variation of direct-coupling and arc-coupling power with line power.

Another, although not so accurate, method of procedure is to measure the leakage power from the TR switch as a function of the line power incident upon the tube. It has been demonstrated (Chap. 5) that the arc leakage power is independent of the incident power over a large range of values, provided that the incident power is sufficiently high. Thus, by extrapolating the leakage-power variation to zero incident power, the arc leakage power is obtained. The slope of the line is the direct-coupling attenuation. Figure 9·37 shows the results of a series of measurements on a 721A tube in a cavity. The arc leakage is 30 mw and the direct-coupling attenuation is 68.8 db.

9·10. Attenuation at Harmonic Frequencies.—An important problem is that of the transmission of harmonic frequencies through the TR switch.

In high-Q TR tubes this transmission may be extremely serious if the power in the harmonics is appreciable, since coupling is possible which transmits the harmonics through the cavity with practically no attenuation. If the power in these harmonics is sufficiently high, the receiver crystal may be burned out. The harmonics may be located by means of a spectrum analyzer. This involves searching over a wide range of frequencies and so requires a very-wide-range analyzer or a series of analyzers. It is more convenient to use some other means of locating the harmonics. One way to locate the harmonic is to use a coaxial wavemeter as a transmission cavity between the TR output terminals and a crystal detector. The measurement of the actual power contained in these harmonics, once the frequency has been determined, requires a thermistor matched at the harmonic frequency and a selective filter device such as a high-Q cavity, resonant at the harmonic frequency, to remove the components of other frequencies. The fundamental frequency and frequencies near it can be attenuated effectively by 60 db or more by using a short-circuited-gap tube as in the measurement of direct-coupling attenuation.

When a discharge occurs across a resonant window as in bandpass TR tubes and pre-TR tubes, a measurement of the attenuation of the fundamental frequency probably gives the attenuation factor for the harmonics also, since the discharge covers the entire window with a conducting screen of ionized gas. This characteristic attenuation of harmonic frequencies has been emphasized as an additional advantage of bandpass TR tubes over high-Q tubes.

9·11. Measurement of Arc Losses.—When a TR tube fires, some power is dissipated in the gaseous discharge of the arc. Since this dissipation may be a function of the shape of the electrodes and especially of the gas filling, complete information about a TR tube requires a measurement of the power lost in the arc. Because this loss is small, it is rather difficult to measure accurately. A simple method for measuring this quantity consists of setting up a TR cavity, with or without an output circuit, with a power measurer in the load end of the transmission line, and then comparing the power reading P_0, with a short-circuited tube in place, with the power reading P_1, when a good TR tube is inserted. The ratio $R = P_1/P_0$ gives the fraction of power transmitted, and $1 - R$ gives the fraction of power lost in the arc. This measurement may be made either in coaxial line or in waveguide, with either high- or low-Q tubes. Accurately calibrated directional couplers with thermistors provide an easy way of measuring power.

Since the loss in one tube usually amounts to only a few per cent of the incident power, with a possible error comparable in magnitude with the measurement, it is somewhat more satisfactory to use several tubes

instead of one. The greater loss with several tubes can be measured to within the same limits of error as for one tube, and if it is assumed that the tubes are reasonably alike, the average loss may be measured with more accuracy than for a single tube. Figure 9·38 shows a waveguide line with two directional couplers, set up for measuring arc loss of several tubes. With this arrangement "dummy" tubes are used to secure the zero readings P_1 and P_2 at the two couplers. The tubes to be measured are inserted in place of the dummy tubes, and the power readings P_1' and P_2' are taken. The fractional loss of power is $1 - P_2'P_1/P_1'P_2$. If the attenuation of either directional coupler is known, the absolute power loss can be calculated.

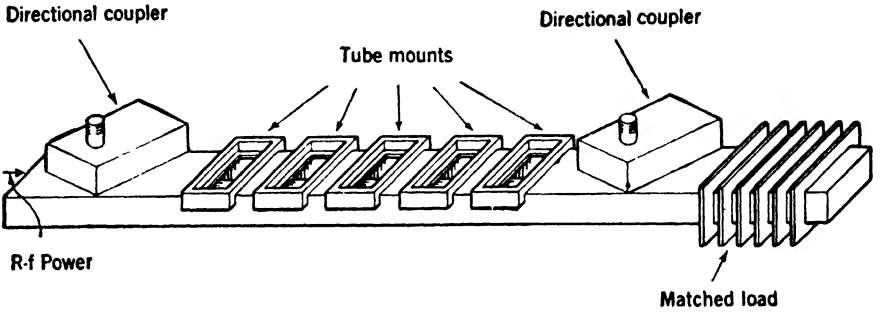

FIG. 9·38.—Equipment for measurement of arc loss on several bandpass tubes.

9·12. Minimum Firing Power.—This quantity is of little interest for most practical applications, since the power level of the transmitter is usually very much in excess of that required to inaugurate the discharge. The minimum firing power is used as a test to determine the quality of some tubes. The measurement is extremely simple, the necessary equipment consists of an r-f oscillator which has a continuously variable output power, a transmission line with mounting for the tube under test, and a power-measuring device which indicates the power level in the line. The arrangement is very compact if waveguide is used. The firing point is determined by increasing the power level until the discharge can be seen (or otherwise indicated) through a small hole in the TR cavity or in the waveguide opposite the tube, and by noting the reading on the power monitor. The power may then be decreased until the arc goes out, thus giving the extinguishing power for the tube.

If a pulsed magnetron is used as a power source, some means of attenuating the incident power must be provided. The most convenient form of attenuator for high power levels is known as a power divider. Figure 9·39 shows a schematic diagram of this device in a coaxial transmission line. Two stubs, each a quarter wavelength from the input terminals, are provided with plungers. The motions of these plungers

are ganged together so that the stub lengths always differ by a quarter of a wavelength. As the plungers are moved in and out, the ratio of the powers delivered to loads (1) and (2) changes over all values from zero to infinity. This can easily be seen from a simple calculation. The susceptance of the stub, with the plunger a distance x from the line, is

$$jb_1 = -j \cot kx,$$

where

$$k = \frac{2\pi}{\lambda}.$$

The admittance of load (1) plus the stub admittance y_1 as seen from the input T-injunction is, therefore,

$$y_1 = \frac{1}{1 - j \cot kx}.$$

Similarly, the admittance of the second branch is

$$y_2 = \frac{1}{1 + j \tan kx}.$$

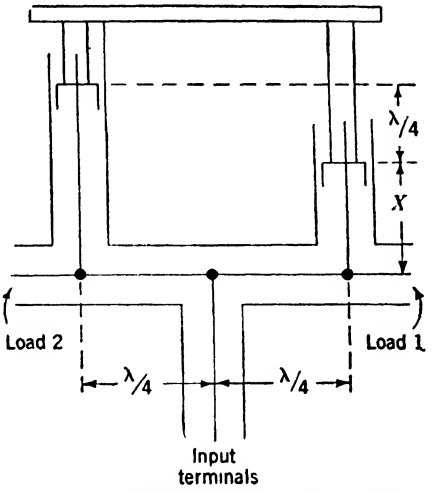

FIG. 9·39.—Diagram of a power divider.

The currents divide in the ratio of these admittances, and the ratio of the powers, R, equals the ratio of the squares of the absolute magnitudes of the currents. Thus

$$R = \left|\frac{1 - j \cot kx}{1 + j \tan kx}\right|^2 = \cot^2 kx,$$

which takes all values from 0 to ∞ as kx varies from $\pi/2$ to 0. The input admittance is equal to unity for all plunger positions, since

$$y_{in} = \frac{1}{1 - j \cot kx} + \frac{1}{1 + j \tan kx} = 1.$$

The admittance looking back from either of the loads, however, varies as the positions of the plungers vary. If load (2) is a matched dummy load, the power from the other terminals can be varied and used for the test bench. It should be remembered that the generator is not matched, and it delivers maximum power when the load is reactive.

9·13. An R-f Pressure Gauge.—The characteristics of any TR, ATR, or pre-TR tube depend on the pressure of the gas with which the tube is filled as well as on its composition. Within certain limits, it is possible to judge the quality of a TR, ATR, or pre-TR tube by measuring the

pressure of the gas inside it. One method of doing this utilizes the electrodeless discharge of a gas at radio frequencies. The gas is excited by the application of a radio-frequency potential. The voltage at which the glow is first excited is a function of pressure, and can serve as a measure of pressure.

A study of the breakdown voltage for an electrodeless discharge, for various gas pressures, yields the typical Paschen curve, very similar to the d-c voltage-breakdown characteristic, or to the variation of leakage power with pressure (Fig. 5·28). The question of interest for pressure measurements is whether reproducible curves can be obtained with slopes of such values that they are useful for pressure measurements. The change of slope of the curve with the frequency of the applied voltage, and the effect of electrode shape, are matters for experimental determination. The structure of the electrodes should be such that pressure determinations are independent of slight variations in position and irregularities in the tubes under test.

An oscillator of conventional design with a built-in, shielded, vacuum-tube voltmeter is used. The oscillator operates at a frequency of 6 Mc/sec and produces a voltage across the electrodes which is variable up to more than 3000 volts. For pre-TR tubes (1B38, 1B54) and low-Q ATR tubes (the 1B44 and others) the electrode structure shown in Fig. 9·40, which rests on the glass window of the tube, is satisfactory. With the electrode and tube in place, the applied r-f voltage is slowly increased until the glow discharge in the tube appears. The voltage at this point is compared with the calibration curve and thus indicates the pressure in the tube.

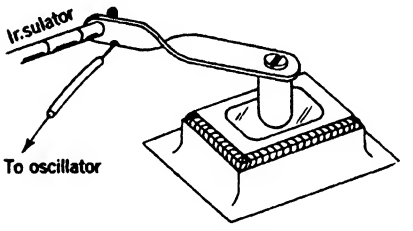

FIG. 9·40.—Electrode structure for testing pre-TR and low-Q ATR tubes.

The calibration curve depends on the gas mixture and the type of tube. A different mixture or a tube of a different type requires a new calibration. A 1B38 tube with the electrode structure illustrated in Fig. 9·40 has a variation of striking-voltage with pressure which is essentially a straight line with a slope of 30 volts/mm of Hg, for argon pressures up to 30 mm of Hg. For air, the slope is 100 volts/mm, up to pressures of 18 mm of Hg. These values are sufficiently accurate for checking low-Q ATR tubes and pre-TR tubes whose gas fillings can vary in pressure by several millimeters without impairing performance. This pressure gauge has been successfully used to check hydrogen thyratrons,[1] (3C45, 4C35). The range of pressures in this case is much lower, and

[1] See Vol. 5.

the pressure region of the Paschen curve below the minimum is employed. The voltage-pressure characteristic has therefore a large negative slope.

Several factors influence the performance of this pressure gauge. The composition of the gas should be the same in all tubes for which the same calibration curve is used. The effect of very small amounts of impurities is serious and usually unpredictable. Each type of tube requires a separate calibration if the structure is appreciably different. If the tube has been in operation, it is possible that a sputtering process has resulted in the deposition of material on the glass. This deposit does not ordinarily affect the calibration unless the deposit is an opaque metallic coating which results in appreciable electrostatic shielding. Temperature effects are quite negligible.

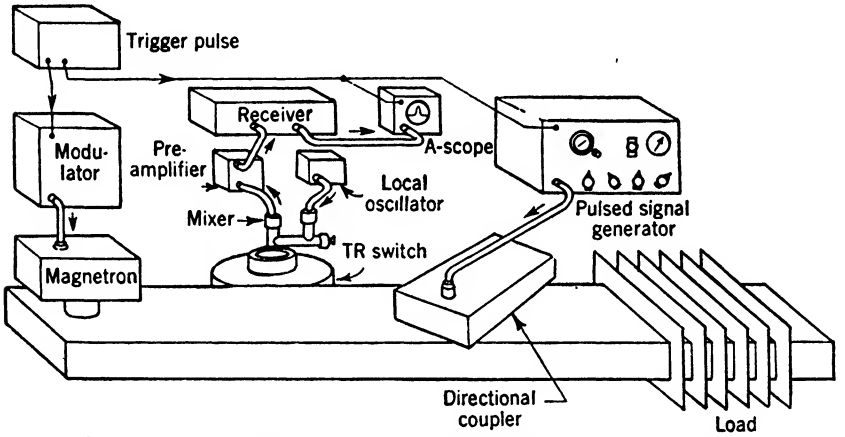

FIG. 9·41.—Arrangement for measuring recovery time of a TR tube.

9·14. Measurements on Recovery Time of TR Tubes.—The determination of the recovery time of a TR tube requires more equipment than any other single measurement. The essential equipment includes a modulator (preferably of the synchronous type), an r-f system, with directional couplers for monitoring the power and introducing a low-level signal, a matched high-power load, a TR cavity, a mixer, a local oscillator, a preamplifier, a receiver, an A-scope, a pulsed signal generator, and a synchronizer or timing unit. The schematic arrangement of these components is shown in Fig. 9·41. This is one of several schemes which have been used for this purpose. The problem is to measure the attenuation of a low-power signal (the "echo" signal) as a function of time after the occurrence of the high-power transmitter pulse. This low-level signal is attenuated because of the presence of electrons around the gap; the attenuation decreases as the number of electrons decreases. Thus, a low-level signal of constant power traces an envelope curve, such as *b*

in Fig. 9·42; as the time of occurrence after the transmitter pulse, a, is varied.

Beginning with the r-f transmission line, the necessary adjustments are straightforward. First of all, in order that the recovery time of the TR tube alone will be measured, no ATR tube is used and the distance from the magnetron to the TR branch is so chosen that the largest possible fraction of a low-level signal coming from the antenna line will be transferred through the TR cavity to the crystal detector. The local oscillator is set at a frequency approximately 30 Mc/sec (that is, the intermediate frequency) from the frequency of the signal generator, which is usually, but not necessarily, close to the magnetron frequency, and the crystal current is adjusted to the operating level of 0.5 ma. When the local oscillator and signal generator are properly tuned, the pulse should appear on the A-scope when the receiver sensitivity is high enough to make the noise visible.

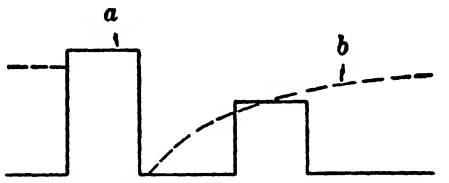

FIG. 9·42.—Recovery-time curve for low-level signal.

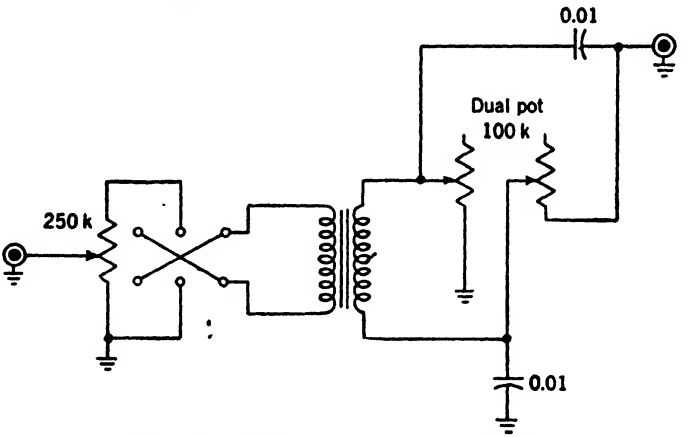

FIG. 9·43.—Phase-control circuit for sine wave.

An essential part of the measurement is the adjustment of the time of occurrence of the low-level pulsed signal with respect to the main transmitter pulse. It is important to be able to adjust the low-level pulse so that it occurs just before the transmitter pulse, in order to provide a reference level at a time when the tube has made as complete a recovery as possible. For one method of timing control, the sine-wave voltage of a master oscillator is used. This voltage is split, by means of a phase-control circuit, Fig. 9·43, into two sine waves having phases that are

variable with respect to each other. Two triggers may be generated from these two sine waves, and their relative times of occurrence will depend on the relative phases of the sine waves. One trigger may be used for the transmitter tube, and the other for the signal generator. A synchroscope[1] is a convenient device to use as an A-scope; it provides the sine wave whose phase may be varied, a fast sweep for viewing the pulses, and one trigger. A trigger generator can form a trigger from the phasable sine wave. An alternative, and somewhat better, method is to use a Model G synchronizer. This device provides two triggers, one with a fixed delay for operating the modulator, and one with a variable delay for operating the pulse signal generator. This gives much more positive operation than the sine-wave phase-control circuit.

The signal generator is an important item of equipment. It must provide a reasonably good rectangular pulse, of approximately 1-μsec duration, in the desired frequency range. If a calibrated attenuator is not built into the r-f output line of the signal generator, such an attenuator must be provided externally. The system may also be designed so that the attenuation may be provided in either the i-f or the video-frequency line. A signal generator such as the type TGS-5BL facilitates a wide variety of measurements (see Vol. 11, Chap. 4). This signal generator uses a wide-range 707B or 2K28 tube and has a variable pulse length, a built-in variable delay for timing control, and an r-f attenuator in the output line. These features make it a very useful instrument in the 10-cm region. Other signal generators are available for the other wavelength regions.

A method for measuring the time scale of the sweep is necessary. This is often accomplished by means of a 1-Mc/sec oscillator which provides a sine wave of accurately known frequency. This sine wave, applied to the signal plates of the A-scope, affords a calibration of the sweep since a complete cycle corresponds to 1 μsec for a 1-Mc/sec wave. When a grid is placed over the face of the cathode-ray tube, time intervals can be estimated to tenths of microseconds. A still better scheme is to use a sweep calibrator which provides a series of equally spaced, very narrow pulses, and to arrange a switch so that these pulses are displayed on the tube. Sweep calibrators are described in Vol. 22 of this series; a suitable one is type B8127.

Once the system is tuned, the measurement is easy. The choice of the origin of the time axis is arbitrary. It is possible either to measure the time interval from the leading edge of the transmitter pulse, since in a great many instances the leading edge of the pulse is sharper and better defined than the trailing edge, or to measure the interval from the

[1] For descriptions of this and other devices mentioned here, the reader is referred to Vol. 22 of this series.

trailing edge, since the recovery of the tube cannot begin until the transmitter has ceased to oscillate. Either of two reference levels for the attenuator setting may be used: the attenuator reading for which the signal level is reduced to noise level, or the reading for a given amplitude of signal immediately preceding the transmitter pulse. The determination of the first reference level is dependent upon the experience of the observer, but with practice a given observer can repeat readings to 0.5 db consistently. In addition, the possibility of saturating the receiver is clearly avoided and irregularities in the sweep base line do not affect the results. The second reference level is easier to set, but care must be taken to avoid the saturation level.

To determine the recovery time of a TR tube, the following procedure is used.

1. The TR cavity is placed at the optimum distance from the transmitter for the operating frequency of the signal generator, which is approximately the same as for the transmitter frequency.
2. The TR cavity is tuned for resonance at the frequency of the signal generator.
3. The local oscillator is tuned until a pip appears on the A-scope. The local oscillator should provide a crystal current of approximately 0.5 ma.
4. The r-f high power is turned on and the signal generator is adjusted until the pip appears immediately ahead of the transmitter pulse.
5. The attenuator reading for a given height of low-level signal (or the reading for which signal disappears into noise) is determined.
6. The signal generator is adjusted until the pip appears at the desired time interval as measured from the leading edge of the transmitter pulse (or from the trailing edge if desired).
7. The attenuator reading for which the signal is the same height as in (5) is determined.
8. From readings (5) and (7), the loss in signal at the particular time interval is calculated.

Essentially this same arrangement is used to measure the recovery time of pre-TR tubes, with a standard TR switch and mixer following the pre-TR tube. The usual arrangement of pre-TR tube and TR tube is employed, with the distance to the magnetron adjusted so that the mixer receives the maximum amount of low-level power from the antenna line. It might be thought that the presence of the TR tube would complicate the determination of the recovery time of the pre-TR tube, but at the power levels at which systems using pre-TR tubes operate, the recovery time of a new TR tube is very short, about 3 db down at 1 μsec, since the leakage power of the pre-TR tube produces a very weak discharge in

the TR tube. An attenuator behind the pre-TR tube, to cut down the power to a level which will not damage crystals, requires a corresponding increase in output power of the pulse signal generator. Consequently, the attenuator method has not been applied for measurement of the recovery time of pre-TR tubes.

Bandpass TR tubes are mounted in much the same way as pre-TR tubes. A waveguide mixer, such as that shown in Fig. 9·44, is used with tubes of this type. The steps just outlined are followed except for tuning of the TR tube which is, of course, unnecessary.

In another method for measuring the recovery time of a TR tube, different frequencies are used for signal generator and transmitter, and

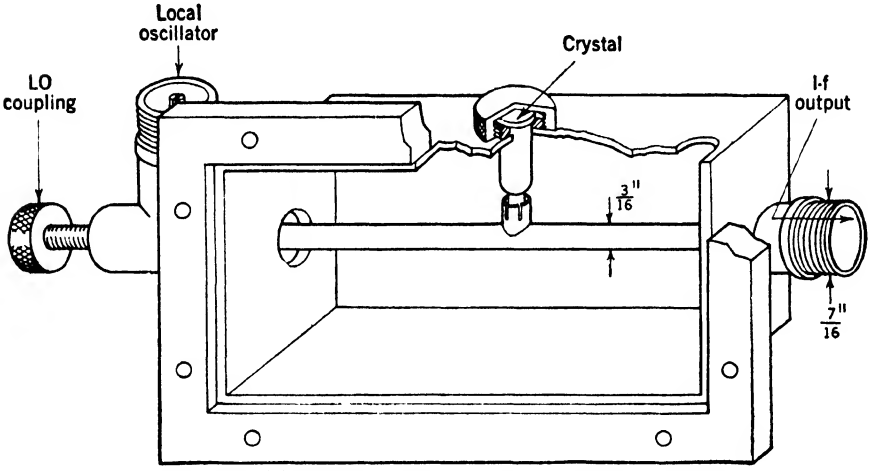

FIG. 9·44.—Waveguide mixer used with bandpass TR tubes.

an additional high-Q TR tube is used as a filter. This arrangement is somewhat simpler since it eliminates the local oscillator and heterodyne receiver, and requires only a video amplifier. Figure 9·45 shows the arrangement of the components. The frequency of the signal generator is different from the transmitter frequency. Both TR tubes are tuned to the signal-generator frequency. The second TR tube reduces the transmitter signal to a value which will not cause undesirable transient effects in the receiver. Enough of the transmitter power gets through, however, to furnish a reference trace on the oscilloscope. A modification of the modulator, to make it pulse the transmitter tube only four times, for example, for every five signal-generator pulses, allows every fifth low-level pulse to come through unattenuated. The trace on the A-scope shows two superimposed pulses, the unattenuated pulse and the pulse affected by the recovery time of the tube. The difference in height of the pulses is a measure of the attenuation due to the recovery time of

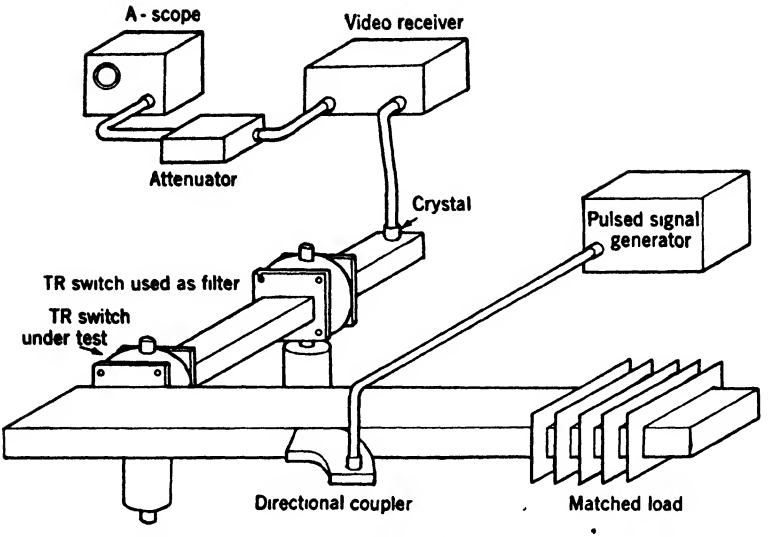

FIG. 9·45.—Two-frequency method for measuring recovery time.

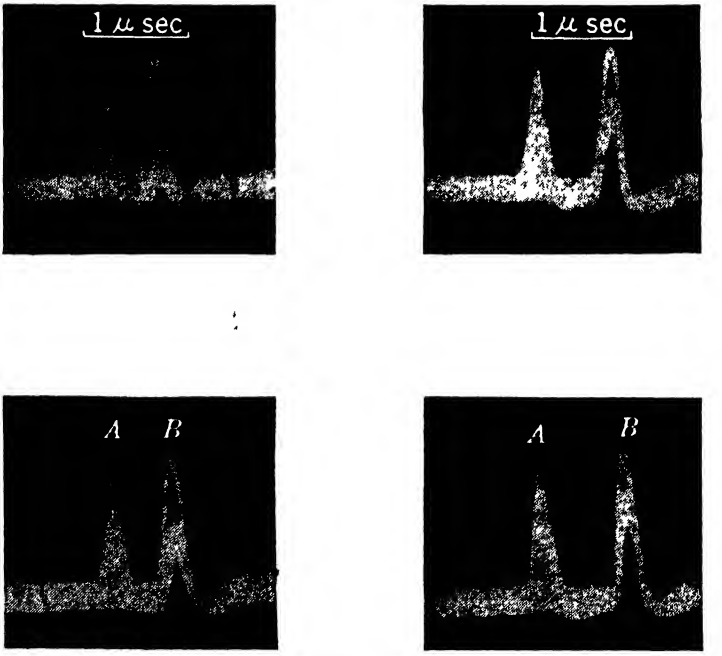

FIG. 9·46.—Oscilloscope photographs of superimposed-pip method of determining recovery time. The transmitter pulse is at *A*, the test-signals at *B*.

the tube. This attenuation is measured by inserting an attenuator in the video circuit. Figure 9·46 shows a photograph of an A-scope trace obtained with this arrangement. A point of interest is the apparent displacement in the maximum of the low-level pulse which is a result of the variation of the recovery time over the length of the pulse.

9·15. Measurements of the Recovery Time of ATR Tubes.—For practical purposes, the recovery time of cell-type tubes, such as the 1B27, the 721, and the 724, is measured by using the tube as a TR tube. The effective recovery time when the tube is used as an ATR tube can then be calculated. The low-Q ATR tubes should behave in very nearly the same manner as pre-TR tubes with the same gas filling. A check of this is sometimes desirable and the following method has been used. For this determination, the arrangement illustrated in Fig. 9·47 is employed. The distance from the TR junction to the transmitter is adjusted to

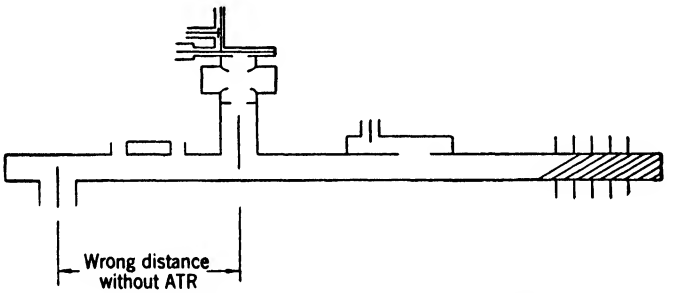

FIG. 9·47.—Relation of components for determination of the effect of ATR tube recovery time.

exactly the wrong length; that is, to such a length that the smallest possible fraction of low-level signal power goes into the TR branch. This adjustment is made with a short-circuiting blank in place of the ATR tube, and its purpose is to place the ATR tube in the position where its recovery time is most effective. The blank is then removed and the ATR tube to be tested is inserted in the mount. With the exception of step (1), the procedure for measuring the recovery time as outlined in Sec. 9·14 is applied. After this measurement is completed, the ATR tube is replaced by the blank, and the distance from the magnetron to the TR branch is adjusted for maximum signal into the TR branch. The recovery time is then measured as before. A comparison of these two measurements then indicates the effect of the recovery time of the ATR tube.

9·16. Life Tests.—A great many factors, which include both mechanical and electrical effects, determine the useful life of TR and ATR tubes. Since a large number of these gas switching tubes contain water vapor in addition to other gases, the life characteristics require careful consideration. In developmental work, the only satisfactory way to determine

the life of these tubes is to set up a sufficient number of tubes to ensure reliable statistical data under conditions approaching actual use. This is easily accomplished with a waveguide line having many TR cavities mounted on the narrow side of the guide. Broadband TR and low-Q ATR tubes may be provided with special mounts on the broad side of the waveguide. A "doorknob" transition, or other suitable device, connects the magnetron to the waveguide section, and a high-power dissipative load terminates the line.

A similar bench can be built in coaxial lines by using T-sections with coupling loops for the individual cavities; the coupling loops are placed

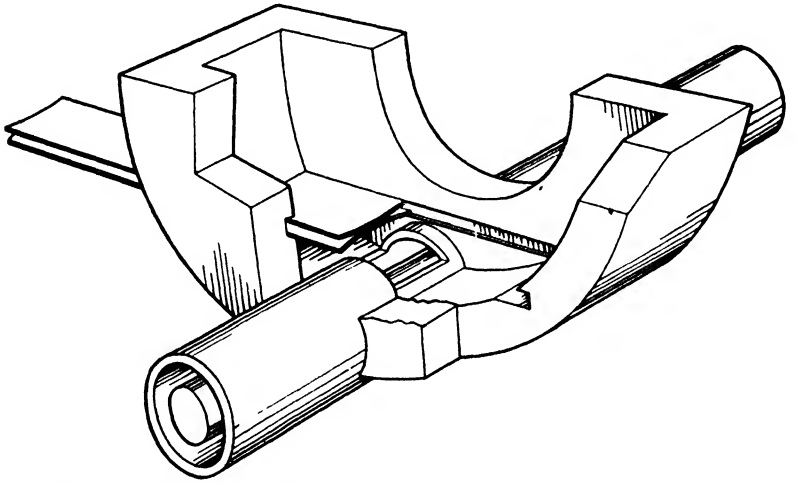

FIG. 9·48.—Illustration of cavity equipped with output gate for crystal protection.

at such a point on the branch line that when the tube fires, the cavity branch, which is a shunt branch, presents an open circuit at the T-section. The waveguide line is preferred because of its simplicity.

This bench provides a good opportunity to study crystal protection as a function of life. The TR cavities or bandpass tubes are provided with mixers of the conventional type which have short-circuited i-f output lines and no local-oscillator connections. To avoid possible damage to the crystal when the r-f power is turned on, output gates (see Fig. 9·48) in front of the mixer coupling iris protect the crystals until it is certain that stable operation has started. For operation it is also necessary to provide a keep-alive power supply.

The gate is removed after the r-f power has been turned on and the character of the discharge between the cones examined through a small hole in the cavity in order to check the operation. The gate is constructed from thin sheets of phosphor bronze, spot-welded together at several points along the center and curved outward in opposite directions. This

provides good contact when the gate slides in the groove cut in the sides of the cavity. The crystals are checked by measurement of the back current at one volt and the front-to-back resistance ratio, by means of a standard crystal-rectifier test set, type TS-268 B/U. Measurements of such quantities as leakage power, recovery time, Q, and keep-alive interaction are best obtained on the special equipment intended for each individual characteristic. Figure 9·49 shows the variation, with time, of recovery time and other parameters of a TR tube.

Certain mechanical tests are closely connected with the useful life of TR tubes. One of the most important of these tests is that of tem-

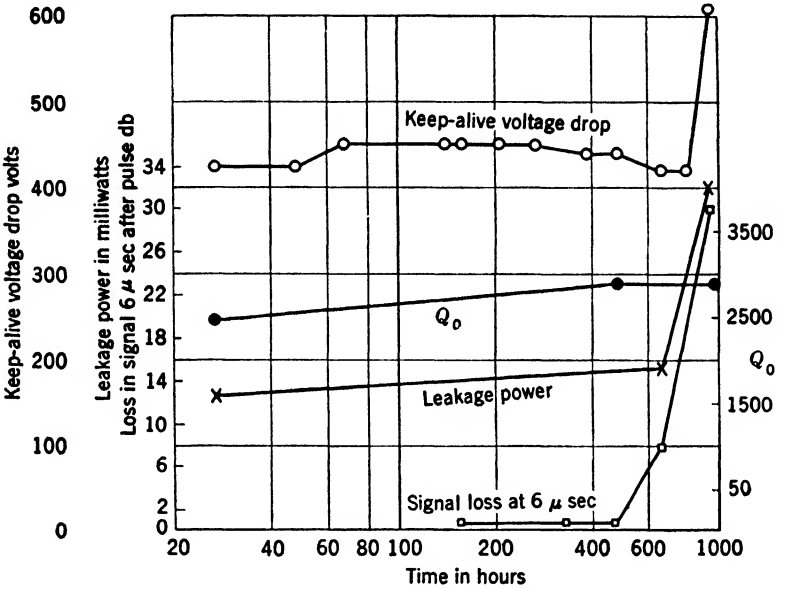

FIG. 9·49.—Typical variation of tube parameters with time.

perature changes because of the multiplicity of metal-to-glass seals involved in the construction of the tubes and of joints between metals with different expansion coefficients. Individual tubes and, when appropriate, tubes such as the 1B27, 721, 724 clamped in the type of cavities in which they will be used, undergo a temperature cycle from room temperature to 100°C, to room temperature, to −40°C, and back to room temperature. After each cycle, or small number of cycles, the tubes are checked to determine whether the extremes of temperature have caused cracks to occur in the seals of the tubes. Measurement of the firing voltage is sufficient to indicate an increase in pressure in the tube. Other mechanical tests, such as vibration and shock tests, are treated in the same manner, and increased firing voltage again indicates tube failure.

9·17. Properties of the Keep-alive.—The function of the keep-alive electrode in a TR tube is to provide a supply of ions near the discharge gap so that the r-f discharge will occur at as low a voltage as possible. This electrode is located near the gap, and a d-c potential is applied between the electrode and the adjacent part of the tube. This potential is high enough to cause a d-c discharge to occur, the initial breakdown potential being a function of the gas filling and the shape of the tube. The voltage characteristic is specified for a given value of current flowing through the keep-alive circuit in terms of the voltage drop between the keep-alive electrode and the adjacent part of the tube. In addition, the initial breakdown voltage should have a reasonable value. A circuit for testing the keep-alive voltage characteristic is shown in Fig. 9·50. When the switch is thrown, the voltage applied to the keep-alive is allowed to build up slowly, by means of a circuit which has a long time constant, so that the striking voltage and then the sustaining voltage at a specified current may be determined.

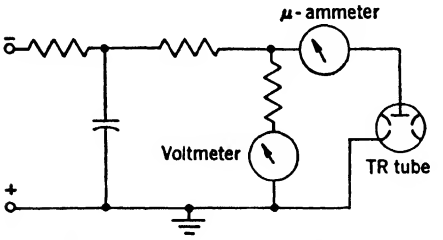

FIG. 9·50.—Circuit for measuring keep-alive voltage characteristics.

Since the d-c keep-alive discharge continues for a time long compared with the duration of the r-f pulse, the life of TR tubes containing H_2O and H_2 depends on the number of hours of operation of the d-c keep-alive. This has been verified and, in some cases, tubes may be life-tested by operating them with a d-c keep-alive and then measuring the sustaining voltage at desired intervals. It is, of course, necessary to correlate this information with the results of actual operation by measurements of recovery time, leakage power, and insertion loss. This d-c-keep-alive life test will not reveal such effects as the sputtering of copper from the cones onto the glass by the r-f discharge, a phenomenon which may occur at sufficiently high r-f power levels. The presence of this metallic film may increase the insertion loss of the tube and greatly impair low-level operating characteristics.

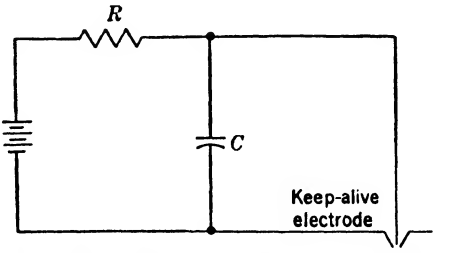

FIG. 9·51.—Circuit for keep-alive electrode.

As can be seen from a consideration of the keep-alive structure and power-supply circuit, the essentials of a relaxation oscillator are present, (Fig. 9·51). These oscillations may be viewed on an oscilloscope if the

keep-alive electrode is coupled through a very small condenser directly to one of the plates on the cathode-ray tube.

9·18. Duplexer Insertion Loss.—The insertion loss of a duplexer is made up of the following components.

1. Reflection loss that results from mismatch. This mismatch will be formed by the combination of the TR switch, ATR switch, and magnetron impedances.
2. The TR-switch loss. This is dissipation loss only.
3. The ATR-switch loss, which may be divided into two parts:
   a. Dissipation loss within the ATR cavity itself.
   b. Power lost into the magnetron because the ATR switch action is not complete. The ATR loss is sometimes called branching loss.

If duplexers employ waveguide mixers, as, for example, at the 3-cm wavelength, the direct measurement of insertion loss (see Sec. 9·2) is quite simple. The mixer may be replaced by a well-matched detector and the magnetron may be replaced by a movable plunger which produces the proper reflection. This reflection will vary somewhat in magnetrons of different types, but a typical value is 20 db. The input side of the duplexer must also be well matched. If the TR and ATR tubes are tunable, they should be tuned for maximum signal into the mixer. The short-circuiting plunger is then moved to the position where the TR signal reaches a minimum value. This is the worst condition that will be encountered in service. After reading the detector-current meter, the duplexer is removed from the matched r-f generator, the detector (or mixer) alone substituted in its place, and the detector-current meter read again. On the assumption that the crystal has a square-law response, the power loss expressed in decibels is ten times the logarithm of the ratio of the crystal currents. If a calibrated attenuator is included in the setup, the meter reading is brought back to its former value and the difference in the attenuator readings is the insertion loss.

Many 10-cm waveguide duplexers have coaxial mixers which are soldered into the TR cavities. Under these conditions, a standard tunable mixer is needed to make the measurement of insertion loss. The crystal detector should be selected so that it is nearly matched in the mixer, since the loss is dependent on the crystal conductance. The TR and ATR tubes are tuned and the plunger adjusted as already described, except that the r-f level should be kept at such a point that the crystal current is 0.5 ma. After this has been done, the duplexer is removed from the matched r-f source and the standard tunable mixer is connected to the r-f source. The standard mixer is tuned until the crystal is matched and the rectified crystal current, in milliamperes, is read. The

loss will be $\frac{20}{m} \log \frac{I}{0.5}$ where m is the crystal law (see Sec. 9·1). The value of m is usually very close to two, as crystals are nearly square-law devices.

It is sometimes desirable to measure the impedances of the TR tube and ATR tube separately, and from these data calculate the losses. This method gives results which check well with those of the more direct method, but it is used only when a careful analysis of a duplexer is being made, since the measurements are more difficult than those in a simple loss determination. Equivalent circuits of duplexers and methods for calculating losses are discussed in Chap. 7.

9·19. Effect of Transmitter Impedance.—In some cases transmitter tubes are consistent enough in cold impedance to enable the duplexer to be preplumbed; that is, the distance from the transmitter tube to the

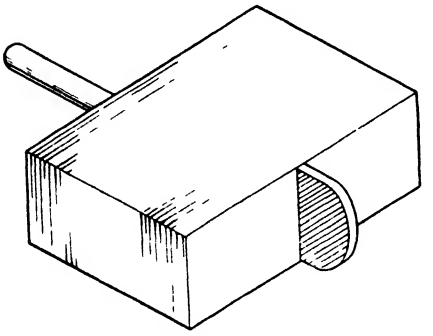

FIG. 9·52.—Waveguide plunger with resistance strip to give lower value of standing-wave ratio than plunger alone.

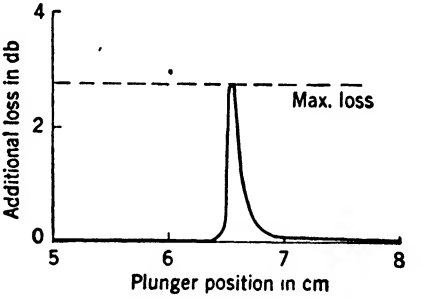

FIG. 9·53.—Variation in low-level signal loss through TR cavity with position of plunger in transmitter line.

TR junction may be so chosen that the largest fraction of the received signal is transmitted into the TR branch. When ATR tubes are used, most, but not all, of the dependence on the transmitter impedance is eliminated. However, variations in the impedance of transmitter tubes cause variations in the duplexer loss (see Chap. 7). The effect of transmitter impedance is measured by replacing the transmitter tube by a plunger and observing the change in received signal, as indicated by the mixer crystal current, when the plunger is moved over a half-wavelength range. This provides a knowledge of the loss for all possible phases of transmitter impedance. The magnitude of this impedance may be varied by means of a piece of resistance strip extending beyond the face of the plunger to reduce the magnitude of the reflection to any desired value, (see Fig. 9·52).

The results of a series of measurements which used two low-Q ATR tubes resonant at 9.03 cm and a bandpass TR tube operating at a wavelength of 9·1 cm are given in Fig. 9·53. A corresponding set of measure-

ments over a band of wavelengths, if the dissipative loss obtained by other methods were taken into consideration, would give the curve shown in Fig. 9·54. (See also Chap. 7.) The area between the curves represents the spread of loss for all possible transmitter impedances.

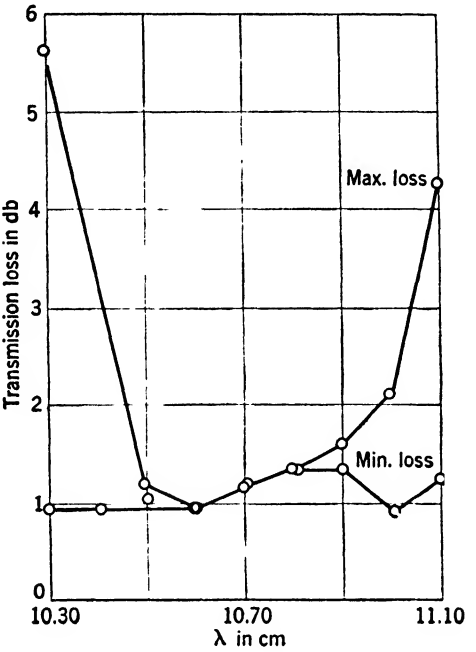

FIG. 9·54.—Effect of transmitter impedance on low-level signal loss over a band of wavelengths.

9·20. High-power Operation of Duplexers.—During the high-power pulse of the transmitter, the function of the TR tube is to disconnect the receiver from the transmission line and to allow most of the power to reach the antenna. The high-power characteristic of the tube must be designed into the duplexer in such a way that, during the transmitter pulse, essentially a continuous transmission line exists between the transmitter and the antenna. The TR tubes of the cell type depend for their high-level action on the properties of the gaseous r-f discharge between the cones of the tube. The cloud of ions and electrons at the gap is equivalent in its action to the insertion of a short circuit in place of the gap. In order to measure the standing-wave ratio introduced during the high-power pulse by the TR and ATR tubes, the tubes are replaced by others which have their cones soldered together. The transmission line which leads to the antenna is terminated in a matched load, and the standing-wave ratio is then measured on a low-power bench.

The low-Q ATR, bandpass TR, and pre-TR tubes during high-power operation also make use of the conducting character of the ionized gas resulting from the r-f discharge. This discharge occurs across the input window of the tube and, therefore, the tubes are mounted on the broad side of the waveguide; consequently, this effective conducting sheet preserves the continuity of the waveguide line through the duplexing section. This condition may be simulated by taking an old tube and covering the inside surface of the window with a layer of Wood's metal. In this way the effects due to the presence of the glass and shape of the input window are preserved. Again, as with the cell-type tubes, all tubes in the duplexer are replaced by these "fired" tubes, and low-level standing-wave measurements are made looking through the duplexer at a matched load in place of the antenna line.

The use of short-circuited tubes does not reproduce the high-power condition exactly, since the gas discharge does not have zero impedance and some power is dissipated in the arc. The exact effect of the power loss is best measured using the individual tubes and not the duplexer itself.

The recovery time of a duplexer can be determined by the procedure described in Sec. 9·14. If the duplexer contains an ATR switch, the recovery time depends upon the recovery of this switch, and also upon the transmitter impedance.

Index